Vol. 66 January, 1962 No. 1

THE JOURNAL OF PHYSICAL CHEMISTRY

(Registered in U. S. Patent Office)

CONTENTS

NOTES

THE JOURNAL OF PHYSICAL CHEMISTRY

(Registered in U. S. Patent Office)

Published monthly by the American Chemical Society at 20th and Northampton Sts., Easton, Pa.

Second-class mail privileges authorized at Easton, Pa. This publication is authorized to be mailed at the special rates of postage prescribed by Section 131.122.

The *Journal of Physical Chemistry* is devoted to the publication of selected symposia in the broad field of physical chemistry and to other contributed papers.

Manuscripts originating in the British Isles, Europe and Africa should be sent to F. C. Tompkins, The Faraday Society, 6 Gray's Inn Square, London W. C. 1, England.

Manuscripts originating elsewhere should be sent to W. Albert Noyes, Jr., Department of Chemistry, University of Rochester, Rochester 20, N. Y.

Correspondence regarding accepted copy, proofs and reprints should be directed to Assistant Editor, Allen D. Bliss, Department of Chemistry, Simmons College, 300 The Fenway, Boston 15, Mass.

Advertising Office: Reinhold Publishing Corporation, 430 Park Avenue, New York 22, N. Y.

Articles must be submitted in duplicate, typed and double spaced. They should have at the beginning a brief Abstract, in no case exceeding 300 words. Original drawings should accompany the manuscript. Lettering at the sides of graphs (black on white or blue) may be pencilled in and will be typeset. Figures and tables should be held to a minimum consistent with adequate presentation of information. Photographs will not be printed on glossy paper except by special arrangement. All footnotes and references to the literature should be numbered consecutively and placed in the manuscript at the proper places. Initials of authors referred to in citations should be given. Nomenclature should conform to that used in *Chemical Abstracts*, mathematical characters be marked for italic, Greek letters carefully made or annotated, and subscripts and superscripts clearly shown. Articles should be written as briefly as possible consistent with clarity and should avoid historical background unnecessary for specialists.

Remittances and orders for subscriptions and for single copies, notices of changes of address and new professional connections, and claims for missing numbers should be sent to the Subscription Service Department, American Chemical Society, 1155 Sixteenth St., N. W., Washington 6, D. C. Changes of address for the *Journal of Physical Chemistry* must be received on or before the 30th of the preceding month. Please include an old address label with the notification.

Claims for missing numbers will not be allowed (1) if received more than sixty days from date of issue (because of delivery hazards, no claims can be honored from subscribers in Central Europe, Asia, or Pacific Islands other than Hawaii), (2) if loss was due to failure of notice of change of address to be received before the date specified in the preceding paragraph, or (3) if the reason for the claim is "missing from files."

Subscription rates (1962): members of American Chemical Society, $12.00 for 1 year; to non-members, $24.00 for 1 year. Postage to countries in the Pan American Union $0.80; Canada, $0.40; all other countries, $1.20. Single copies, current volume, $2.50; foreign postage, $0.15; Canadian postage $0.10; Pan-American Union, $0.10. Back volumes (Vol. 56–65) $30.00 per volume; foreign postage, per volume $1.20, Canadian, $0.40; Pan-American Union, $0.80. Single copies: back issues, $3.00; for current year, $2.50; postage, single copies: foreign, $0.15; Canadian, $0.10; Pan American Union, $0.10.

The American Chemical Society and the Editors of the *Journal of Physical Chemistry* assume no responsibility for the statements and opinions advanced by contributors to THIS JOURNAL.

The American Chemical Society also publishes *Journal of the American Chemical Society, Chemical Abstracts, Industrial and Engineering Chemistry*, International Edition of *Industrial and Engineering Chemistry, Chemical and Engineering News, Analytical Chemistry, Journal of Agricultural and Food Chemistry, Journal of Organic Chemistry, Journal of Chemical and Engineering Data, Chemical Reviews, Chemical Titles, Journal of Chemical Documentation, Journal of Medicinal and Pharmaceutical Chemistry, Inorganic Chemistry, Biochemistry*, and *CA — Biochemical Sections*. Rates on request.

THE JOURNAL OF
PHYSICAL CHEMISTRY

(Registered in U. S. Patent Office) (© Copyright, 1962, by the American Chemical Society)

VOLUME 66 JANUARY 24, 1962 NUMBER 1

STUDY OF MOLECULAR MOTION IN SOME ISOPRENES AND BUTADIENES[1]

BY RAMDAS P. GUPTA[2]

Department of Physics, The Pennsylvania State University, University Park, Pennsylvania

Received December 23, 1960

Experiments on nuclear magnetic resonance and dynamic mechanical measurements have been conducted with samples of *cis*-1,4-polybutadiene, *trans*-1,4-polybutadiene, *cis*-1,4-polyisoprene and *trans*-1,4-polyisoprene, to study the molecular motion. The transition in *cis*-1,4-polybutadiene is observed at 170°K.; for *trans*-1,4-polybutadiene transitions are at 235 and 370°K. Transition for *cis*-1,4-polyisoprene is at 200°K., and for *trans*-1,4-isoprene it is at 235 and 340°K. The main transition in sample B is observed at higher temperature than for sample D and comparatively it is less sharp. The high temperature transition in sample B appears at a higher temperature. The low temperature transition, for all the samples, corresponds to glass transition when the substance changes from solid to rubber. This transition, therefore, probably results from onset of segmental motion. The high temperature transitions for B and D which occur at 370 and 340°K., respectively, may be associated with melting of the crystallites. For samples A and C the onset of segmental motion and the melting of crystallites occur at temperatures very close together; therefore, we observe only one transition. One might be tempted to think that the high temperature transition which arises from melting of the crystallites probably is associated with loosening of the inter-chain-links, but sufficient evidence is needed to be sure of this.

Introduction

Experiments with samples of *cis*-1,4-polybutadiene, *trans*-1,4-polybutadiene, *cis*-1,4-polyisoprene and *trans*-1,4-polyisoprene have been conducted by both nuclear magnetic resonance and dynamic mechanical methods to study molecular motions in these polymers. To my knowledge no one has reported any experimental data on the dynamic mechanical properties of these materials. Nuclear magnetic resonance experiments with natural rubber have been reported by Gutowsky[3] in a temperature range up to 300°K. He has reported two transitions: one at about 150°K. and the other between 200 and 250°K. As he has reported, the temperatures for transitions depend on the cure-time for the sample. Study of rubber samples also has been done by some other workers.[4-8] The aim of the present experiments has been to study the dynamic mechanical properties and to compare these with the n.m.r. results. In certain cases dynamic mechanical measurements have proven easier to detect molecular motions because of the suitability of the frequency range. By comparing dynamic mechanical properties with those of n.m.r., we expect to get a more correct picture of the processes responsible for different transitions and the associated molecular motions.

Experimental

N.m.r. experiments have been performed using a dual purpose 40 Mc. Varian model spectrometer having a 12-in. magnet and a variable temperature probe. An account for the modulation broadening has been taken for the second moment correction. Damping (Q^{-1}) was obtained from the ratio of the width of the resonance curve at the half power points to f_0. $Q^{-1} = \Delta f/f_0$ = half width/resonant frequency. For dynamic mechanical measurements the apparatus used by Kline[9] has been employed. It is a transverse beam apparatus. The specimen rod was suspended by threads inside a Dewar covered with a brass plate. Lead balls were placed inside the Dewar to keep the temperature gradient inside as small as possible. A hot plate was put inside the Dewar in which the flow of current could be monitored to attain a desired temperature. The low temperature runs for the sample were made by allowing the temperature to drift up from liquid nitrogen temperature.

The samples for this experiment were supplied by Dr. A. E. Woodward. The molding of the sample for dynamic measurements was done with great difficulty, using the principle of compression molding under vacuum. The sample used in this experiment has been in the form of a rod of a suitable length and diameter. A very slow and steady drift of temperature was maintained during the course of this ex-

(1) This work was conducted in part with the financial help of the U. S. Atomic Energy Commission.

(2) Institut für Elektrowerkstoffe der Fraunhofer-Gesellschaft, Freiburg, Germany.

(3) H. S. Gutowsky and L. H. Meyer, *J. Chem. Phys.*, **21**, 2122 (1953).

(4) P. J. Flory, "Principles of Polymer Chemistry."

(5) A. A. Morton and L. D. Taylor, *J. Polymer Sci.*, **38**, 7 (1959).

(6) R. E. Cunningham, *ibid.*, **42**, 571 (1960).

(7) A. A. Morton and E. J. Lampher, *ibid.*, **44**, 233 (1960).

(8) G. S. Trick, *ibid.*, **41**, 213 (1959).

(9) D. E. Kline, *ibid.*, **22**, 449 (1956).

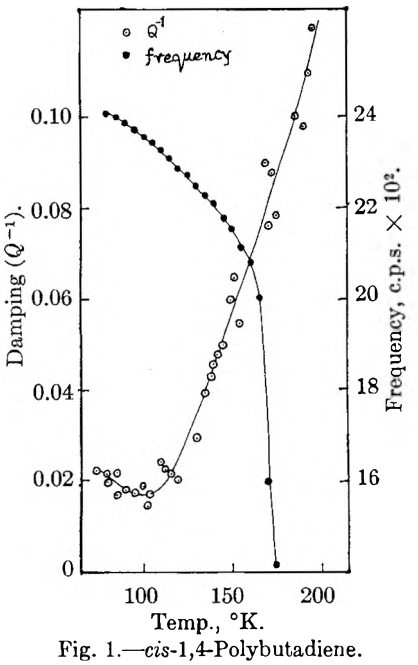

Fig. 1.—*cis*-1,4-Polybutadiene.

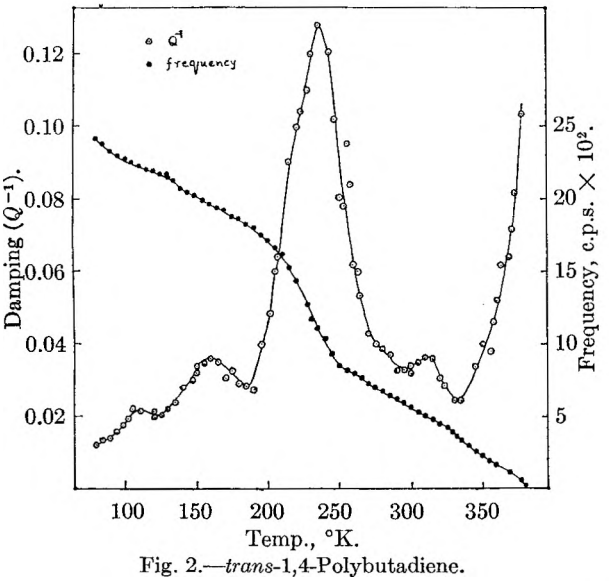

Fig. 2.—*trans*-1,4-Polybutadiene.

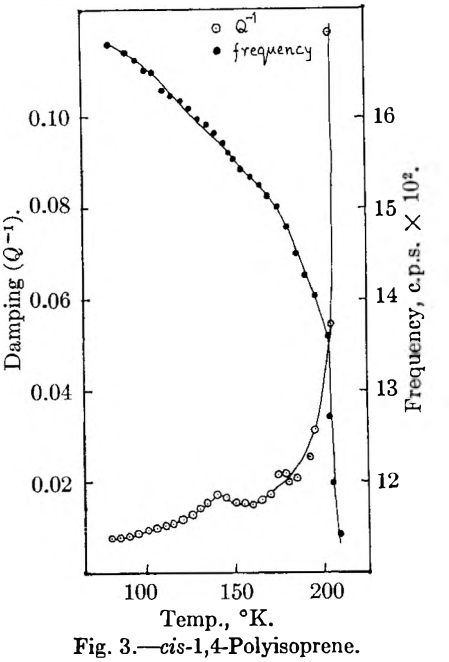

Fig. 3.—*cis*-1,4-Polyisoprene.

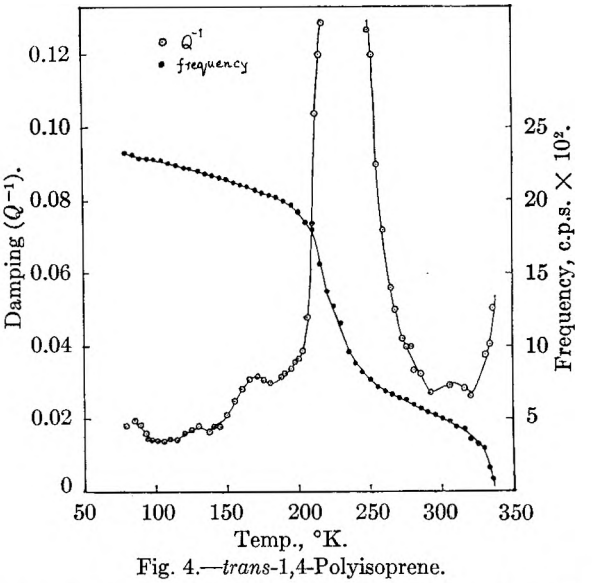

Fig. 4.—*trans*-1,4-Polyisoprene.

periment to be sure that there was no gradient of temperature along the length and breadth of the sample rod. Under the present setup the error in temperature would not be more than a degree.

Results

In Fig. 1, damping (Q^{-1}) and frequency have been plotted against temperature for *cis*-1,4-polybutadiene in a temperature range of 80 to 200°K. We find that damping decreases in the beginning of the temperature range and then it begins to increase at about 110°K. until about 200°K., after which the sample becomes too soft to be used for further experiment. The rise in damping is very abrupt; on the other hand, frequency begins to decrease slowly in the beginning of the temperature range but the decrease becomes abrupt at about 170°K. It shows that the transition at about 170°K. is very much pronounced.

In Fig. 2, damping and frequency plots against temperature have been shown for *trans*-1,4-polybutadiene. In the frequency plot the main transition appears to about 230 and 350°K. There is one more transition at about 150°K., but it is so small that it may be due to scattering itself. For damping plots transition peaks appear at 170, 235, 320 and 370°K., but the peaks at 235 and 370°K. are quite predominant whereas the other peaks may be due to scattering. The maximum (Q^{-1}) value for the peak at 235°K. is about 0.13.

Damping and frequency plots for *cis*-1,4-polyisoprene are shown in Fig. 3. Transition peaks at 140 and 200°K. are observed, but the peak at 200°K. is the main peak.

In Fig. 4, frequency and damping variation against temperature for the sample of *trans*-1,4-polyisoprene has been shown. The frequency plot shows peaks at 225 and 335°K., whereas the damping plot shows peaks at about 235, 340 and 170°K. The peaks at 235 and 340°K. are the

main peaks. The peak at 170°K. has been neglected. The central peak at 235°K. is not a discontinuous peak, rather the upper points fall above the graph on this scale and have not been plotted because it was considered for comparison purposes to be convenient to have the same scale for all the figures. The maximum Q^{-1} value for this peak is about 0.28.

Figure 5 shows a n.m.r. second-moment plot against temperature for *trans*-1,4-polybutadiene and *cis*-1,4-polybutadiene. For *trans*-polybutadiene two transitions are seen, one at about 225°K. and the other at about 350°K. The transition at 225°K. is predominant but the transition at 350°K. is not so obvious and it easily might have been missed. For *cis*-1,4-polybutadiene there is only one transition, which appears at about 175°K.

In Fig. 6, for the samples of *trans*-1,4-polyisoprene and *cis*-1,4-polyisoprene, n.m.r. second moment has been plotted against temperature. In the case of *cis*-1,4-polyisoprene the only transition which is observed is at about 175°K., but in the case of *trans*-isoprene two transitions are observed; one at about 220°K. and the other at about 330°K. The transition at 220°K. is quite sharp, but the transition at 330°K. is not so predominant.

The maximum value of damping (Q^{-1}) for the central peak of *trans*-1,4-isoprene is about double that of the maximum damping value for the corresponding peak of *trans*-1,4-polybutadiene (shown in Figs. 2 and 4). Consequently that transition in *trans*-isoprene is sharper than the corresponding transition in *trans*-butadiene.

The n.m.r. second-moment value for the *cis* samples is lower than the second moment for the *trans* samples. The second moment for *cis*-1,4-polybutadiene at 100°K. is about 18 gauss^2 whereas for the *trans*-1,4-polybutadiene it is about 20 gauss^2 at the same temperature. Similarly in the case of *trans*- and *cis*-isoprene a difference in their second moments has been observed.

Discussion

From the above results one could infer that the low temperature transition, which is at about 235°K. in the case of *trans*-1,4-polyisoprene and *trans*-1,4-polybutadiene, corresponds to glass transition as the substance changes from a solid to a rubber state. This transition is due to the onset of segmental motion. The high temperature transition which appears at about 340°K. in the case of *trans*-1,4-polyisoprene and at about 370°K. for *trans*-1,4-polybutadiene probably is ascribable to melting of the crystallites.

One might be tempted to associate the high temperature transition with melting of the crystallites associated with loosening of inter-chain links, but sufficient evidence is needed to be sure of this.

There is only one transition in the case of the *cis*-1,4-polyisoprene and *cis*-1,4-polybutadiene samples. The onset of segmental motion and the melting of crystallites both take place at almost the same temperature in the case of *cis* samples,

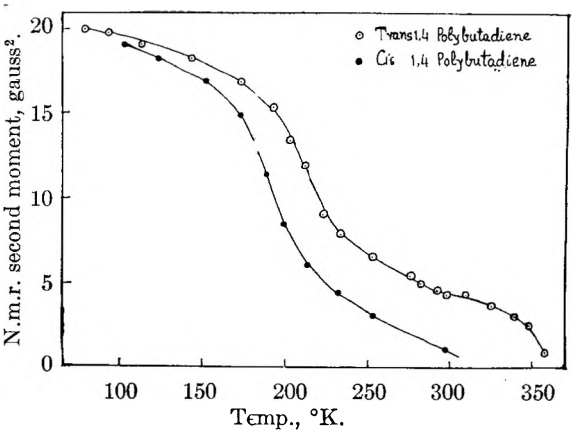

Fig. 5.—*trans*-1,4- and *cis*-1,4-polybutadienes.

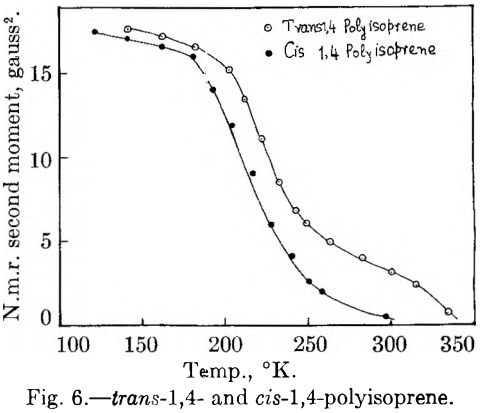

Fig. 6.—*trans*-1,4- and *cis*-1,4-polyisoprene.

and therefore we observe only one peak corresponding to both these processes.

The maximum value of the damping peak (Q^{-1}) for *trans*-1,4-polyisoprene is about 0.28, whereas for the *trans*-1,4-polybutadiene it is about 0.13 (about half the other one). In the case of polyisoprene the transition is also very sharp. This shows that at the corresponding temperatures there is more extensive motion in the case of *trans*-1,4-polyisoprene than for *trans*-1,4-polybutadiene. The middle transition peaks are at about the same temperatures in both *trans* samples, but the high temperature transition in the case of *trans*-1,4-polybutadiene is at a higher temperature than for the *trans*-1,4-polyisoprene sample, because the melting of crystallites takes place at a correspondingly higher temperature in the first case.

Both n.m.r. and dynamic mechanical data show only one peak for *cis* samples, and two main peaks for *trans* samples, though the high temperature transition in the case of *trans* samples is more easily detectable by dynamic mechanical methods than by n.m.r. The processes responsible for these transitions are supported both by dynamic mechanical and n.m.r. methods, as discussed above.

Acknowledgment.—The author is very thankful to Dr. A. E. Woodward for supplying the samples for this experiment and also for taking an interest in this work. Thanks also are due to Miss A. Zweng for helpful discussions.

APPLICATION OF THE ARCHIBALD ULTRACENTRIFUGAL METHOD FOR THE STUDY OF DILUTE POLYMER SOLUTIONS. I. THEORY AND SOME PRELIMINARY DATA ON THE SYSTEM POLYSTYRENE–METHYL ETHYL KETONE

BY HIROSHI FUJITA,[1] HIROSHI INAGAKI,[2] TADAO KOTAKA[2] AND HIROYASU UTIYAMA[3]

Kyoto University, Japan

Received January 17, 1961

The theory of Kegeles, Klainer and Salem for the Archibald ultracentrifugal method for polydisperse macromolecular solutes has been improved and extended. It is shown that the new theory allows determination of the weight-average molecular weight and the light scattering second virial coefficient of a given system from sedimentation experiments performed under conditions appropriate to the Archibald method. The validity of the derived equation has been tested with sedimentation and light scattering experiments on two polystyrenes of different molecular weights in methyl ethyl ketone at 25°. For both the molecular weights and the second virial coefficients fairly good agreements have been obtained between the data from these two different experiments.

Introduction

With its spectacular success demonstrated in recent years for a number of macromolecular solutes of biological interest, the Archibald ultracentrifugal method[4] now is becoming a standard method of the biochemist for the determination of molecular weights of such solutes.[5] The original theory of Archibald[4] dealt with ideal, monodisperse or polydisperse systems, but subsequently Kegeles, Klainer and Salem[6] have extended it to non-ideal, polydisperse systems and indicated that from sedimentation velocity experiments performed under relevant conditions the weight-average molecular weight of a polydisperse solute and the value of a parameter which measures thermodynamic non-ideality of the solution at very low concentrations can be determined.

The purpose of the present article is to develop a treatment of the Archibald method for non-ideal, polydisperse systems in terms of the thermodynamics of irreversible processes and then to report results from some preliminary sedimentation and light scattering experiments performed to verify the theory presented. The system chosen for this purpose was polystyrene in methyl ethyl ketone at 25°.

Theory

Basic Equations.—Consider an ultracentrifugal experiment at constant temperature with an incompressible solution in which q different solutes of non-electrolytes are dissolved in a single solvent. The solvent is labelled as component 0 and the q solutes as components 1, 2, . . , q. For simplicity of the theoretical development it is assumed that the partial specific volumes of all components are independent not only of pressure (thus the solution is incompressible) but also of solute composition. Of course, it is assumed that the usual sector-shaped cell is used for the experiment. We introduce the symbols

r	=	radial distance measured from the center of rotation
ω	=	angular velocity of the rotor
ρ	=	local density of solution
c_k	=	concn. of solute k (k = 1, 2, .., q) expressed in g./ml. of soln.
$\bar{v}_k$	=	partial specific volume of solute k
μ_k	=	chemical potential of solute k per gram
$(J_k)_0$	=	flow (or flux) of solute k relative to the cell-fixed frame of reference

From the theory of isothermal sedimentation in terms of the thermodynamics of irreversible processes it can be shown[7] that for the solution considered here the flow $(J_k)_0$ is represented by

$$(J_k)_0 = \sum_{i=1}^{q} (L_{ki})_v \left[(1 - \bar{v}_i\rho)\omega^2 r - \sum_{j=1}^{q} \mu_{ij}(\partial c_j/\partial r) \right] \quad (1)$$

where $(L_{ki})_v$'s are phenomenological coefficients appearing when linear relations are postulated between the conjugated sets of volume-fixed flows of solutes and thermodynamic forces acting on them.[8] The quantity μ_{ij} stands for

$$\mu_{ij} = (\partial\mu_i/\partial c_j)_{T,P,c_m} \quad (2)$$

Here T is the absolute temperature, P is the pressure at a position and time being considered, and the subscript c_m indicates that concentrations of all solutes other than solute j are fixed while μ_i is differentiated with respect to c_j.

It is physically required that the flow of any solute (that of the solvent as well) must be zero, for all values of time t, at the ends of the ultracentrifuge cell in which a given solution is placed. Application of this condition to equation 1 yields the following set of q equations

$$(1 - \bar{v}_i\rho)\omega^2 r = \sum_{j=1}^{q} \mu_{ij} (\partial c_j/\partial r) \quad (3)$$

$$(i = 1, 2, \ldots, q;\ r = r_1 \text{ and } r_2)$$

where r_1 and r_2 are the radial positions of the men-

(1) Department of Polymer Science, Osaka University, Nakanoshima, Osaka. Formerly at Physical Chemistry Laboratory, Department of Fisheries, Maizuru.

(2) Institute for Chemical Research, Kyoto.

(3) Department of Industrial Chemistry, Kyoto.

(4) W. J. Archibald, *J. Appl. Phys.*, **18**, 362 (1947); *J. Phys. Chem.*, **51**, 1204 (1947).

(5) See, for example, H. K. Schachman, "Ultracentrifugation in Biochemistry," Academic Press, Inc., New York, N. Y., 1959, pp. 181–194.

(6) G. Kegeles, S. M. Klainer and W. J. Salem, *J. Phys. Chem.*, **61**, 1286 (1957).

(7) G. J. Hooyman, "Thermodynamics of Irreversible Processes in Rotating Systems," Leiden, 1955, Chapter III.

(8) The reciprocal relations of Onsager (for example, S. R. de Groot, "Thermodynamics of Irreversible Processes," North Holland Publishing Co., Amsterdam, 1951) are not obeyed by these phenomenological coefficients, *i.e.*, $(L_{ki})_v \neq (L_{ik})_v$ $(i \neq k)$.

iscus and the cell bottom, respectively. This is formally identical with the basis for sedimentation equilibrium of a polydisperse solution in the ultracentrifuge cell. However, the clear distinction should be made here that the term $\partial c_i/\partial r$ in equation 3 is not a function of position r but that of time t, while the corresponding term in the equilibrium equation is a function of r only. This implies that equation 3 is not a differential equation to determine c_i as a function of r but an algebraic relation for the values of $\partial c_1/\partial r$, $\partial c_2/\partial r$, ..., $\partial c_q/\partial r$ at either $r = r_1$ or $r = r_2$. Thus no information can be derived from it about second and higher derivatives of c_i with respect to r. For non-electrolyte solutions μ_i may be written in the form

$$\mu_i = (\mu_i^0)_c + (RT/M_i) \ln (c_i y_i) \qquad (4)$$

where $(\mu_i^0)_c$ is the reference chemical potential per gram of solute i appropriate to the c-concentration scale, M_i and y_i are, respectively, the molecular weight and the activity coefficient on the c-concentration scale of solute i, and finally R is the gas constant. The y_i is chosen here in such a manner that it approaches unity as the concentrations of *all* solutes tend to zero.

With equation 4, equation 3 becomes

$$rc_iM_i(1 - \bar{v}_i\rho)\omega^2/RT = \partial c_i/\partial r + c_i \sum_{j=1}^{q} (\partial \ln y_i/\partial c_j)_{T,P,c_m} (\partial c_j/\partial r) \qquad (5)$$

$$(i = 1, 2, \ldots, q;\ r = r_1 \text{ and } r_2)$$

The specific refractive index increment (at infinite dilution of the solution) of solute i in the given solvent is denoted by R_i. Then to the approximation that terms higher than $0(c_i)$ are neglected, we have

$$\partial n_c/\partial r = \sum_{i=1}^{q} R_i (\partial c_i/\partial r) \qquad (6)$$

where n_c is the excess refractive index of the solution at a position and time concerned. Multiplication of equation 5 by R_i, followed by summation over all solute components and use of equation 6, yields

$$(\omega^2 r/RT) \sum_{i=1}^{q} R_i (1 - \bar{v}_i\rho)M_ic_i = \partial n_c/\partial r + \sum_{i=1}^{q}\sum_{j=1}^{q} R_ic_i (\partial \ln y_i/\partial c_j)_{T,P,c_m} (\partial c_j/\partial r) \qquad (7)$$

$$(r = r_1 \text{ and } r_2)$$

The definition of y_i allows $\ln y_i$ for very low concentrations of all solutes to expand in a form of series as

$$\ln y_i = M_i \sum_{k=1}^{q} B_{ik}c_k + \text{higher terms in } c_1, c_2, \ldots, c_q \qquad (8)$$

where all the expansion coefficients B_{ik} refer to the initial slopes of $\ln y_i$ at $c_1 = c_2 = \ldots = c_q = 0$ and hence are independent of concentration. Solution of equation 5 for $\partial c_i/\partial r$ gives a series expansion

$$\partial c_i/\partial r = (\omega^2 r/RT)(1 - \bar{v}_i\rho)M_ic_i + \text{higher terms in } c_1, c_2, \ldots, c_q \qquad (9)$$

$$(r = r_1 \text{ and } r_2)$$

We now introduce equations 8 and 9 into equation 7, and assume that all solute components have the same partial specific volume $\bar{v}$ and the same specific refractive index increment $\bar{R}$, as is the case with usual synthetic high polymers in a very good approximation. Then we obtain, after some rearrangement of terms

$$RT(\partial n_c/\partial r)/[\omega^2 r(1 - \bar{v}\rho)] = \bar{R} \sum_{i=1}^{q} M_ic_i - \bar{R} \sum_{i=1}^{q}\sum_{j=1}^{q} M_iM_jc_ic_jB_{ij} + \text{higher terms in } c_1, c_2, \ldots, c_q \qquad (10)$$

$$(r = r_1 \text{ and } r_2)$$

To the approximation that terms higher than $0(c_i)$ are neglected, the excess refractive index n_c is represented by

$$n_c = \sum_{i=1}^{q} R_ic_i \qquad (11)$$

which, under the above-mentioned assumption that all solutes have the same refractive index increment, reduces to

$$n_c = \bar{R}c \qquad (12)$$

Here c is the total concentration of the solution at any given position and time. If we divide equation 10 by equation 12 and note that for the solution considered here ρ can be represented by (ρ_0 is the density of the solvent)

$$\rho = \rho_0 + (1 - \bar{v}\rho_0)c \qquad (13)$$

we obtain, after some rearrangement of terms

$$M_{app}(t) = \sum_{i=1}^{q} c_iM_i/c - c \sum_{i=1}^{q}\sum_{j=1}^{q} M_iM_j[B_{ij} + (\bar{v}/M_j)]c_ic_j/c^2 + \text{higher terms in } c \qquad (14)$$

$$(r = r_1 \text{ and } r_2)$$

where $M_{app}(t)$ is a quantity defined by the expression

$$M_{app}(t) = RT(\partial n_c/\partial r)/\omega^2 r(1 - \bar{v}\rho_0)n_c \qquad (15)$$

$$(r = r_1 \text{ and } r_2)$$

and has the dimension of molecular weight.

In the limit when t goes to zero, equation 14 takes the form

$$M_{app} \equiv M_{app}(0) = M_w[1 - M_wBc_0 + 0(c_0^2)] \qquad (16)$$

where c_0 is the value of c for the initial solution (*i.e.*, the solution before centrifugation), M_w is an average molecular weight defined by

$$M_w = \sum_{i=1}^{q} M_if_i \qquad (17)$$

and B is given by

$$B = \sum_{i=1}^{q}\sum_{j=1}^{q} M_iM_j[B_{ij} + (\bar{v}/M_j)]f_if_j/(M_w)^2 \qquad (18)$$

In these equations, f_i denotes the weight fraction of solute i in the *initial* solution. One can see that the M_w defined by equation 17 is nothing but the weight-average molecular weight of the given polydisperse solute. In the present article, the quantity M_{app} appearing on the left-hand side of equation 16 will be termed the apparent molecular weight of the solute. It is important to observe

that the values of M_{app} for both ends of the cell should agree with each other; this is because the right-hand side of equation 16 does not contain terms which depend on r. This theoretical requirement guides the extrapolation to zero time of $M_{app}(t)$ evaluated at the ends of the cell.

Equation 16 may be rewritten to give

$$1/M_{app} = 1/M_w + Bc_0 + 0(c_0^2) \qquad (19)$$

This indicates that a plot for $1/M_{app}$ *vs.* c_0 allows evaluation of M_w from its intercept at $c_0 = 0$ and of B from its *initial* slope.

Comparison with Light Scattering Virial Expansion.—From the statistical thermodynamic theory[9] of the turbidity of polydisperse systems one can show (the proof is omitted here) that the reduced intensity of scattered light at zero angle of incidence, i_0, of a polydisperse solution of the type considered above (in which the partial specific volumes of all components are constant, those of all solutes are the same, and the specific refractive index increments of all solutes are also the same) is represented by a virial form as

$$Kc_0/i_0 = 1/M_w + 2A_2'c_0 + 0(c_0^2) \qquad (20)$$

where c_0 is the total concentration of the solution, A_2' is equal to one-half of B defined above, and K is a light scattering factor defined by

$$K = 2\pi^2 n(c_0)^2(\bar{R})^2/\lambda_0^4 N_A \qquad (21)$$

Here $n(c_0)$ is the refractive index of the solution at a concentration c_0, $\bar{R}$ is the specific refractive index increment of the solute in the given solvent, λ_0 is the wave length of the light (*in vacuo*) used for the experiment, and N_A is Avogadro's number. The A_2', called the light scattering second virial coefficient, is a very basic quantity for the characterization of thermodynamic behavior of dilute polymer solutions.

Comparison of equations 19 and 20 indicates that the intercept and initial tangent of a plot for $1/M_{app}$ *vs.* c_0 yield exactly the same information as do the intercept and initial tangent of the light scattering plot expressed in the form of Kc_0/i_0 *vs.* c_0. It is with this theoretical correlation that the present sedimentation and light scattering measurements on samples of polystyrene in methyl ethyl ketone were concerned. An expansion for $1/M_{app}$ similar in form to equation 19 already has been derived by Kegeles, Klainer and Salem,[6] but the result that the coefficient for c_0 in the expansion is equal to twice the light scattering second virial coefficient appears to be new; and it affords the Archibald method with a distinctive significance in the study of thermodynamic behavior of dilute polymer solutions. The quantity M_{app} appearing in the expansion of Kegeles, *et al.*, did not refer to zero time, and thus their expansion actually corresponds to equation 14 of this paper. From the preceding development it is clear that if the values of M_w and non-ideality factor B are to be determined for the original sample, the extrapolation of $M_{app}(t)$ data to $t = 0$ is essential. This point had been discussed by Archibald[4] in his treatment of ideal, polydisperse systems.

(9) J. G. Kirkwood and R. J. Goldberg, *J. Chem. Phys.*, **18**, 54 (1950); W. H. Stockmayer, *ibid.*, **18**, 58 (1950).

Experimental

Materials.—The system investigated in this preliminary work was polystyrene in methyl ethyl ketone at 25°. Two polystyrene samples having different molecular weights were examined. These polymers were prepared by thermal polymerization at a conversion degree less than 30% and were fractionated with the system benzene–methanol. The intrinsic viscosities, $[\eta]$, of the fractionated materials in benzene at 30° were 1.66 and 0.64 (g./dl.), respectively. For convenience of description, the polymer with high $[\eta]$ is designated as H-PSt and the one with low $[\eta]$ as L-PSt. The methyl ethyl ketone used was of reagent grade, and was distilled before making up each test solution. To obtain complete dissolution each polymer–solvent mixture was heated in a sealed glass tube at about 40° for at least two days.

Ultracentrifugation.—A Phywe ultracentrifuge (Phywe AG., Göttingen, Germany) equipped with a schlieren optical system was used; we used a phase plate as the diaphragm. The centrifuge cell was a conventional 12 mm. one with a 4° sector-shaped centerpiece. To obtain reliable data for the refractive index gradient in the region near the cell bottom, the artificial bottom method was employed according to the technique developed by Ginsburg, *et al.*[10] We used glycerine as the bottom liquid, but it was found that this liquid was not very satisfactory for the present polymer–solvent system, as had been the case with silicone oil for aqueous solutions[10]; the liquid–liquid bottom interface formed gave a somewhat thick line on the photographic plate. Despite this defect, the introduction of this artificial bottom surface made it very easy to investigate boundary gradient curves near the bottom end of the solution column.

The rotor speed was measured on a counter which consisted of a sine-to-pulse converter and a scaler with six decade counter tubes.[11] Its fluctuations were within ±0.4% at speeds lower than 10,000 r.p.m., at which most of the present experiments were performed.

Water from an ultrathermostat of the Haake type was circulated through a jacket fixed around the inner wall of the vacuum chamber for the rotor, and its temperature was automatically regulated by the signal fed back from a thermister thermometer placed close to the rotor. To obtain good heat exchange between the water jacket and the rotor, constant temperature hydrogen was made to pass through the vacuum chamber at a pressure of 2 to 4 mm. With these arrangements the rotor temperature was kept to within ±0.1 of 25° (at which all the sedimentation measurements were performed) during the course of each sedimentation experiment, when it was checked on an electromagnetic thermometer device assembled in the ultracentrifuge.[12]

The optical constants of the ultracentrifuge were determined by using a synthetic boundary cell of the Meyerhoff type.[13] As for the details of these and other necessary procedures we referred mainly to the indications of Klainer[14] and of Schachman.[15]

Partial Specific Volume.—For polystyrene in methyl ethyl ketone (at 25°) it can be shown that its partial specific volume $\bar{v}$ differs from its apparent specific volume $\bar{v}^*$ by the magnitude of the order of 10^{-4} ml./g. in the concentration range from 0 to 1 g./dl. So we assumed, throughout the present calculation, that $\bar{v}$ was equal to 0.907 ml./g., the value of $\bar{v}^*$ for this system reported by Rosen[16] and also by Schulz and Hoffmann.[17] For the density of methyl ethyl ketone we used a literature value of 0.800 g./ml. These

(10) A. Ginsburg, P. Appel and H. K. Schachman, *Arch. Biochem Biophys.*, **65**, 545 (1956).

(11) H. Inagaki and S. Okamoto, *Bull. Inst. Chem. Research, Kyoto University*, **33**, 257 (1955).

(12) At speeds lower than 10,000 r.p.m. this thermometer does not allow direct reading of the true temperature. However, it was possible with it to find out the real temperature of the rotor by determining a calibration curve which gave the difference between the reading on the thermometer and the true temperature as a function of rotor speed.

(13) G. Meyerhoff, *Makromol. Chem.*, **15**, 68 (1955).

(14) S. M. Klainer and G. Kegeles, *J. Phys. Chem.*, **59**, 952 (1955).

(15) H. K. Schachman, in "Methods in Enzymology," Vol. 4, Academic Press, Inc., New York, N. Y., 1957, p. 37.

(16) B. Rosen, *J. Polymer Sci.*, **17**, 559 (1955).

(17) G. V. Schulz and M. Hoffmann, *Makromol. Chem.*, **23**, 220 (1957).

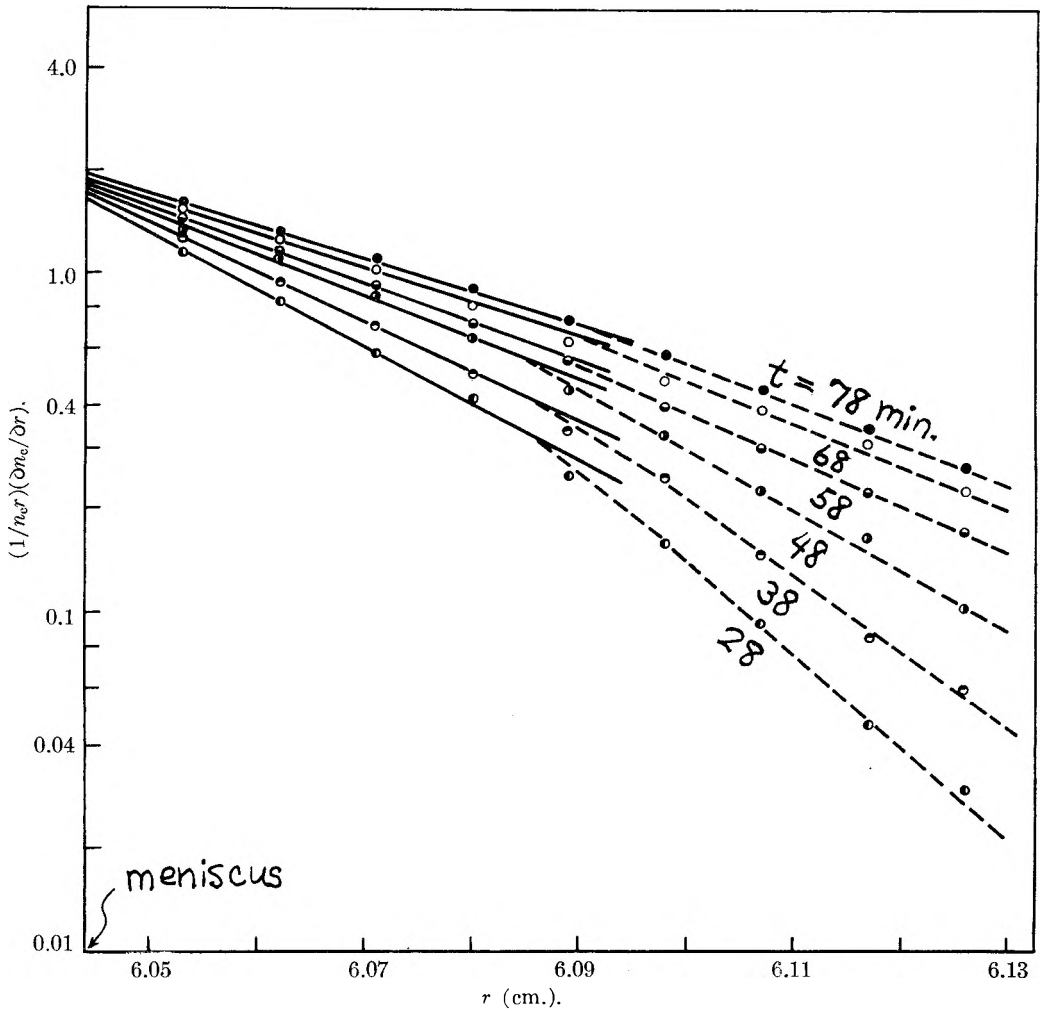

Fig. 1.—Some examples of plots for log $[1/rn_c(r)][\partial n_c(r)/\partial r]$ *vs.* r in the region near the meniscus. The solid lines indicate the existence of a linear region in these plots. H-PSt, c_0 = 0.512 (g./dl.); r.p.m. = 6794.

values of $\bar{v}$ and ρ_0 yield the value 0.274 for the buoyancy factor $1 - \bar{v}\rho_0$.

Light Scattering.—Intensities of the scattered light were measured in a modified photometer[18] of the Brice type[19] equipped with a constant temperature mantle. A cylindrical cell was used to determine the angular variation of the scattered intensity; the range covered from 30 to 150°. For the calibration of the photometer reference was made to the data reported by Carr and Zimm[20] for benzene and carbon tetrachloride. Each test solution of a desired concentration was prepared by heating at 80° for one hour followed by filtration with a No. 5 sintered glass plate. It was directly put into the cell through two sheets of Ultracellafilter of grade m. All measurements were made at 25°. The specific refractive index increment of the solution at 25°, measured with a differential refractometer of the Debye type, was 0.231 ml./g. for a light of the wave length 436 mμ. Required values of Kc_0/i_0, where i_0 is the reduced intensity of the scattered light at zero angle, were obtained by the usual extrapolation on the Zimm plot[21] of the data.

Results and Discussion

Apparent Molecular Weight M_{app}.—Data required for the application of the generalized Archibald method presented above are values of the apparent molecular weight M_{app} as a function of the initial concentration c_0. The required value of M_{app} for a given c_0 may be determined first by evaluating the quantity $M_{app}(t)$ (defined in equation 15) as a function of time from a series of refractive index gradient curves photographed at appropriate intervals of time and then by extrapolating the resulting plot for $M_{app}(t)$ *vs.* t to $t = 0$. According to the theory developed, it is required that this plot for the meniscus $r = r_1$ and that for the cell bottom $r = r_2$ should converge to the same value (which is nothing but M_{app}) at the limit when t goes to zero. In general, as we approach the cell ends, the accuracy of the measurements of refractive index gradient is lowered, and it often is quite difficult, or even impossible, to measure unambiguously the gradient values at the ends directly from the photographic records. Experience indicates that it is essential for a successful investigation of the sedimentation behavior in the regions near the cell ends to choose the rotor speed as appropriately as possible, depending on the initial concentration of a given solution. In this work too, it took a somewhat long time before we were able to discover experimental conditions under which "satisfactory" sedimentation patterns could be obtained. For the majority of the photographic records so obtained we found that the following

(18) H. Inagaki and T. Oyama, *J. Chem. Soc. Japan (Nippon Kagaku Zasshi)*, **78**, 676 (1957).

(19) B. A. Brice, M. Halwer and R. Speiser, *J. Opt. Soc. Am.*, **40**, 768 (1950).

(20) C. I. Carr and B. H. Zimm, *J. Chem. Phys.*, **18**, 1616 (1950).

(21) B. H. Zimm, *ibid.*, **16**, 1099 (1948).

approach worked well for the determination of $M_{app}(t)$. This consisted of calculating, from a given record of gradient curve, the logarithm of the quantity $[1/rn_c(r)][\partial n_c(r)/\partial r]$ as a function of r and then extrapolating the resulting plot for log $(1/rn_c)(\partial n_c/\partial r)$ *vs.* r to both ends of the solution column.[22] It was found that in the early stage of centrifugation in which the maximum gradient remained at the meniscus and no appreciable rise of the gradient occurred at the cell bottom, plots of this type fell on a straight line in the region near either end of the cell. Figure 1 gives some typical examples of such plots. It is of interest to investigate whether or not this *empirical* procedure of extrapolating $(1/rn_c)(\partial n_c/\partial r)$ is theoretically justified.

The values of $M_{app}(t)$ obtained in this way at both ends of the cell for a series of c_0 are shown plotted in Figs. 2 and 3. One can see that, except for some cases, $M_{app}(t)$ for a given c_0 increases with time at the meniscus and decreases at the bottom, following approximately in a linear fashion, but they can be extrapolated to give the same intercept at $t = 0$, which is in agreement with the theoretical requirement mentioned previously. One should observe that the dependence on time of $M_{app}(t)$ is quite small for the low-molecular-weight sample, but it is appreciable for the high-molecular-weight sample; especially, the increase of $M_{app}(t)$ of the latter sample at the meniscus is quite pronounced for almost all concentrations indicated.

It generally is argued that for a polydisperse solute $M_{app}(t)$ decreases with time at the meniscus and increases at the cell bottom, and this usually is interpreted in terms of the fractionation action of the ultracentrifuge. That is, as sedimentation proceeds, the solution at the meniscus contains smaller amounts of higher molecular weight solutes and the solution at the bottom becomes more abundant in such heavier solutes. However, one can show that a dependence on time of $M_{app}(t)$ can be caused by thermodynamic non-ideality of a given solution. To show this it is sufficient if we consider two-component systems. For such a solution equation 14 reduces to

$$M_{app}(t) = M - M^2[B_{11} + (\bar{v}/M)]c + \text{higher terms in } c \qquad (22)$$

where M is the molecular weight of the solute, and c refers to the concentration of the solution at either end of the cell. The value of c at the meniscus is denoted by c_m and that of c at the bottom by c_b. Then, if we write

$$c_m = c_0 - \Delta c_m,\ c_b = c_0 + \Delta c_b \qquad (23)$$

both Δc_m and Δc_b are positive and increase with increasing time. Substitution of equation 23 into equation 22 gives

$$M_{app}(t) = M_{app} + M^2[B_{11} + (\bar{v}/M)]\Delta c_m + \text{higher terms in } \Delta c_m (r = r_1) \qquad (24)$$

$$M_{app}(t) = M_{app} - M^2[B_{11} + (\bar{v}/M)]\Delta c_b + \text{higher terms in } \Delta c_b (r = r_2) \qquad (25)$$

where M_{app} is the apparent molecular weight. From these equations it follows that, as sedimentation proceeds, the value of $M_{app}(t)$ at the meniscus *increases* with time and that of $M_{app}(t)$ at the bottom *decreases*, provided that B_{11} is not negative. Thus we see that the thermodynamic non-ideality of the solution can give rise to $M_{app}(t)$ which varies

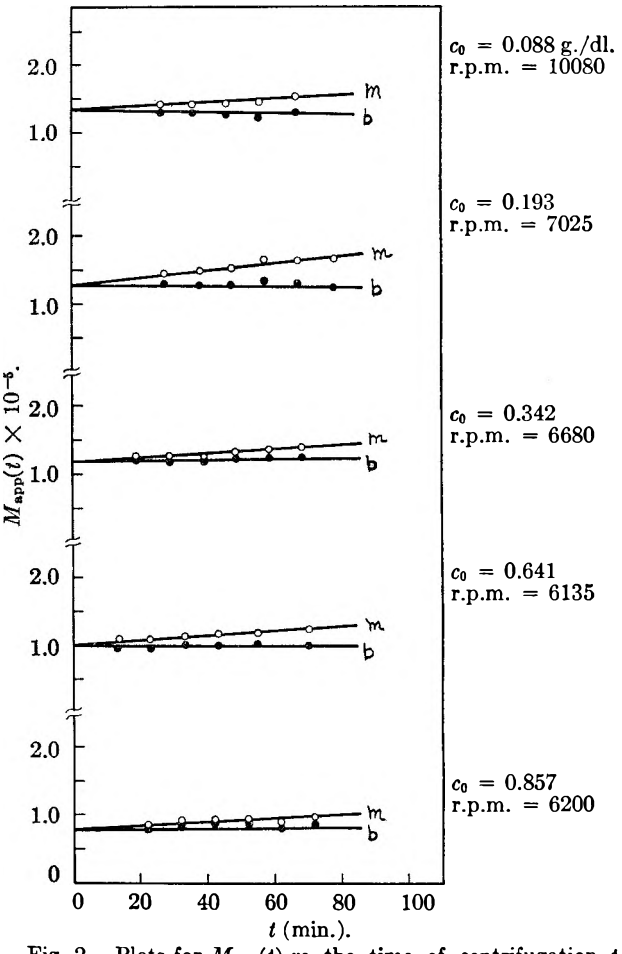

Fig. 2.—Plots for $M_{app}(t)$ *vs.* the time of centrifugation t for the sample L-PSt. The letters m and b indicate the "meniscus" and the "cell bottom," respectively. The rotor speed (in r.p.m.) employed for each value of the initial concentration c_0 is indicated.

(22) The value of $\partial n_c(r)/\partial r$ at each r was directly read off the given curve, and $n_c(r)$ was evaluated by using either of the following two equations

$$n_c(r) = (n_c)_{t=0} - \frac{1}{(r_1)^2}\int_{r_1}^{r_p} r^2\frac{\partial n_c}{\partial r}\,dr - \int_{r_1}^{r}\left[\left(\frac{r}{r_1}\right)^2 - 1\right]\frac{\partial n_c}{\partial r}\,dr$$

(for r near the meniscus)

$$n_c(r) = (n_c)_{t=0} + \frac{1}{(r_2)^2}\int_{r_p}^{r_2} r^2\frac{\partial n_c}{\partial r}\,dr - \int_{r}^{r_2}\left[1 - \left(\frac{r}{r_2}\right)^2\right]\frac{\partial n_c}{\partial r}\,dr$$

(for r near the bottom end of the soln. column)

where r_p is the value of r at a position arbitrarily chosen in the plateau region. These equations can be derived by combining the identity

$$n_c(r) = n_c(r_1) + \int_{r_1}^{r}[\partial n_c(r)/\partial r]dr$$

or

$$n_c(r) = n_c(r_2) - \int_{r}^{r_2}[\partial n_c(r)/\partial r]dr$$

with the equation for $n_c(r_1)$ or $n_c(r_2)$ given previously by Kegeles, *et al.*[9,14]

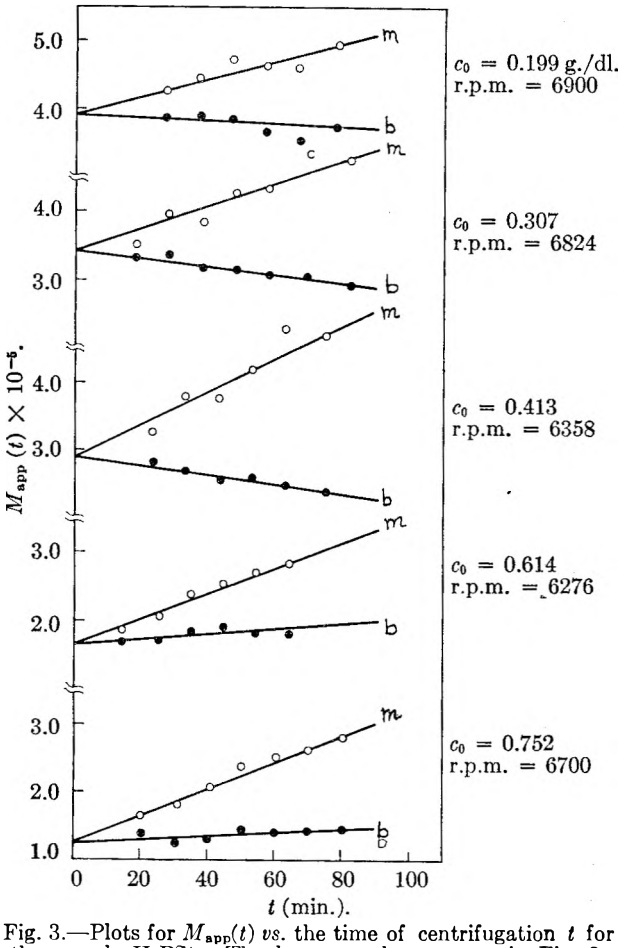

Fig. 3.—Plots for $M_{app}(t)$ *vs.* the time of centrifugation t for the sample H-PSt. The keys are the same as in Fig. 2.

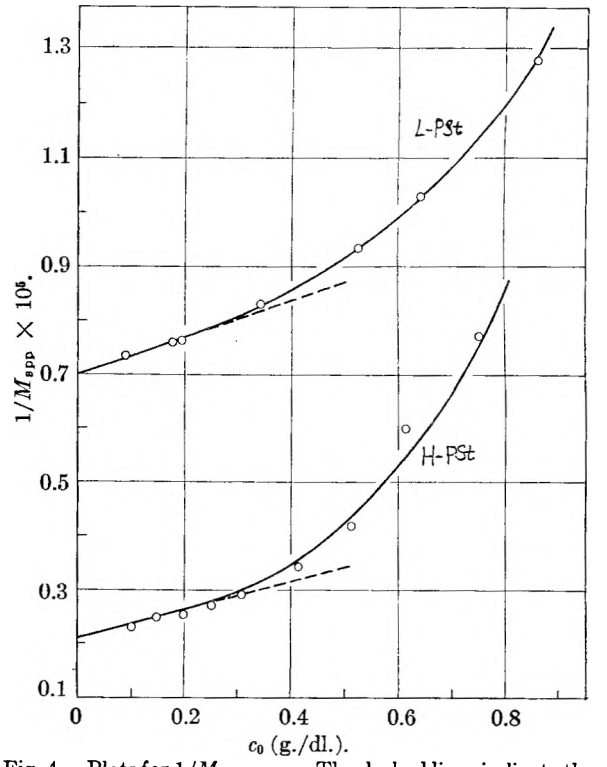

Fig. 4.—Plots for $1/M_{app}$ *vs.* c_0. The dashed lines indicate the initial tangents of respective curves.

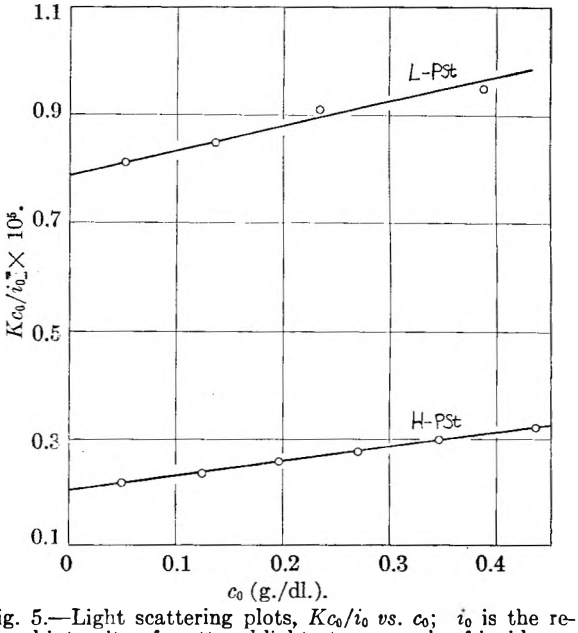

Fig. 5.—Light scattering plots, Kc_0/i_0 *vs.* c_0; i_0 is the reduced intensity of scattered light at zero angle of incidence.

with time in the direction opposite to the dependence produced by the fractionation effect of the centrifuge. Depending upon the relative importance of these two effects, various types of plots for $M_{app}(t)$ *vs.* t may be obtained with actual systems. For the two systems investigated in this work it may be concluded that the non-ideality effect was predominant in most of the cases treated.

Evaluation of the Data for $1/M_{app}$.—Table I gives the values of M_{app} obtained from the intercepts of the plots shown in Figs. 2 and 3. In accordance with equation 19, values of $1/M_{app}$ are plotted against c_0 in Fig. 4. The intercepts of the smooth curves drawn are $0.70_0 \times 10^{-5}$ and $0.21_0 \times 10^{-5}$ for the samples L-PSt and H-PSt, respectively. These figures give $M_w = 1.4_3 \times 10^5$ for L-PSt and $M_w = 4.7_6 \times 10^5$ for H-PSt. As shown in the section "Theory," the initial tangents of these curves should be equal to twice the light scattering second virial coefficients A_2' of respective systems. By drawing the tangent lines as indicated we find that $A_2' = 1.7_5 \times 10^{-4}$ (ml./g. mole) for L-PSt and $A_2' = 1.3_5 \times 10^{-4}$ (ml./g. mole) for H-PSt. It should be noted that these values of M_w and A_2', especially those of A_2', depend to a considerable extent on how we draw a smooth curve through plotted points.

Comparison with Light Scattering Data.—Figure 5 shows plots for Kc_0/i_0 *vs.* c_0 for the two polystyrene solutions studied. The values of M_w and A_2' determined from the intercepts and the initial tangents of these plots are given in Table II, where the corresponding data deduced from the sedimentation studies are included for comparison. It is seen that for both L-PSt and H-PSt the results from the two different experiments are consistent with each other, implying that equation 19 for $1/M_{app}$ is valid. Furthermore, one may remark that the A_2' values derived here are consistent with the literature values, including those of

TABLE I

DATA FOR APPARENT MOLECULAR WEIGHT M_{app} AS A FUNCTION OF INITIAL CONCENTRATION c_0

c_0 (g./100 ml.)	$M_{app} \times 10^{-5}$	R.p.m.	c_0 (g./100 ml.)	$M_{app} \times 10^{-5}$	R.p.m.
	L-PSt			H-PSt	
0.8574	0.78	6200	0.7515	1.29	6700
$.6400$	0.97	6135	$.6135$	1.67	6276
$.5222$	1.07	6819	$.5120$	2.38	6794
$.3415$	1.20	6680	$.4130$	3.01	6358
$.1931$	1.31	7025	$.3074$	3.41	6824
$.1763$	1.32	7980	$.2515$	3.69	6530
$.0882$	1.37	10080	$.1988$	3.92	6900
			$.1495$	4.01	6500
			$.1020$	4.30	7846

Outer, *et al.*,[23] of Oth and Desreux,[24] and of Oyama, *et al.*[25]

TABLE II

COMPARISON OF SEDIMENTATION AND LIGHT SCATTERING DATA[a]

		L-PSt	H-PSt
M_w	Sed.	1.43×10^5	4.76×10^5
	LS	1.27×10^5	4.90×10^5
A_2' (c.g.s.)	Sed.	1.75×10^{-4}	1.35×10^{-4}
	LS	1.92×10^{-4}	1.34×10^{-4}
$\langle s^2 \rangle_z^{1/2}$		.....	315 Å.

[a] $\langle s^2 \rangle_z$ = z-average square radius of gyration of solute.

Finally, we wish to point out one important difference between the plot for $1/M_{app}$ *vs.* c_0 and that for Kc_0/i_0 *vs.* c_0. This is concerned with the upward curvatures of these plots. From Figs. 4 and 5 one can observe that for both L-PSt and H-PSt the plots for $1/M_{app}$ deviate from a straight line at relatively low concentrations and increase sharply with further increase in c_0; this upward curvature is stronger for H-PSt than for L-PSt. On the other hand, although the measurements were limited to lower concentrations than in the sedimentation experiments, the light scattering plots show negligible upward trend in the ranges studied. This difference suggests that the third and higher terms in the expansion 19 would be quite different from those in the expansion 20. It is intriguing to extend the present theoretical treatment to higher terms, with the hope of finding out the real cause of this difference. In connection with this problem, one may remark that Kegeles, *et al.*,[6] have observed a similar and even stronger upward curvature in their $1/M_{app}$ plot for the system polyvinyl chloride ($M_w = 4.8 \times 10^4$)-tetrahydrofuran at 25°. If the strong upward trend of $1/M_{app}$ as seen in these data is the general behavior, it will diminish to some extent the practical value of the Archibald ultracentrifugal method for the study of polymer solutions, since such a property of the plot necessarily leads to a less reliable determination of the intercept and the initial slope.

Acknowledgments.—The authors wish to thank Professor M. Horio, Department of Polymer Chemistry, Kyoto University, Kyoto, for his encouragement and his continued interest in the course of this investigation. Part of this work was supported by a grant-in-aid of research from the Ministry of Education. One of us (H.F.) is indebted to the National Science Foundation (Washington, D. C.) for a fund (G-12477) which made it possible for him to participate in this research project. The assistance of Mr. A. Nakazawa in the sedimentation experiments is gratefully acknowledged.

(23) P. Outer, C. I. Carr and B. H. Zimm, *J. Chem. Phys.*, **18**, 830 (1950).

(24) J. Oth and V. Desreux, *Bull. soc. chim. Belges*, **63**, 285 (1954).

(25) T. Oyama, K. Kawahara and M. Ueda, *J. Chem. Soc. Japan (Nippon Kagaku Zasshi)*, **79**, 727 (1958).

METAL CHELATES OF ADENOSINE TRIPHOSPHATE[1]

BY M. M. TAQUI KHAN AND A. E. MARTELL

Department of Chemistry, Clark University, Worcester, Mass.

Received February 17, 1961

Stability constants of the 1:1 chelates of ATP with divalent metal ions, Cu^{+2}, Ni^{+2}, Co^{+2}, Mn^{+2}, Zn^{+2}, Mg^{+2}, Ca^{+2}, Sr^{+2} and Ba^{+2} are reported at 25° and 0.1 ionic strength. The stabilities increase in the sequence: Ba < Sr < Ca < Mg < Co < Mn < Zn < Ni < Cu. The first and second hydrolysis constants and dimerization constants of copper(II)-ATP chelate are reported.

In view of the participation of metal ions in the biological functions of adenosine phosphates, it was decided to investigate the interaction of these ligands with various metal ions commonly found in biological systems. Recently several investigators[2-4] reported the formation constants of adenosine phosphates with biologically important metals, particularly Ca(II) and Mg(II), by various techniques. The presence of normal and protonic complexes of Ca(II) and of Mg(II) have been reported by Martell and Schwarzenbach[5] and also by Smith and Alberty.[6] Ion-exchange techniques were used by Naninga[7] and Wallas[8] for a number of metals. The important differences between the present and the previous work are the use of a new mathematical treatment of the data and extension of the measurements to metal ions less basic than those of the alkaline earths. In the

(1) This investigation was supported by a research grant, H-3246, from the National Heart Institute, Public Health Service.

(2) K. Burton and H. A. Krebs, *Biochemical J.*, **55**, 94 (1953).

(3) V. DiStefano and W. F. Neuman, *J. Biol. Chem.*, **200**, 759 (1953).

(4) N. Melchior, *ibid.*, **208**, 615 (1954).

(5) A. E. Martell and G. Schwarzenbach, *Helv. Chim. Acta*, **39**, 653 (1956).

(6) R. M. Smith and R. A. Alberty, *J. Am. Chem. Soc.*, **78**, 2376 (1956).

(7) L. B. Naninga, *J. Phys. Chem.*, **61**, 1144 (1957).

(8) E. Wallas, *Acta Chem. Scand.*, **12**, 528 (1958).

present paper the formation constants of normal and protonic complexes of ATP* (adenosine triphosphate) are presented. The formation constants with ADP* (adenosine diphosphate) and adenosine 3- and 5-phosphates are now in progress and will be the subject of a future publication.

Experimental

The experimental method consisted of potentiometric titration of the disodium salt of ATP in the absence and presence of the metal ion being investigated. The ionic strength was maintained approximately constant in a 1:1 titration by use of a medium containing 0.1 *M* potassium nitrate and relatively low concentrations of ligand and metal ion. In 10:1 titrations the ionic strength was adjusted to 0.10 with KNO_3. The experimental technique was essentially the same as the one reported previously.[5] The electrode system was calibrated by direct titration of acetic acid, the observed *p*H meter reading being compared with the actual hydrogen ion concentration calculated from data tabulated by Harned and Owen.[9] The *p*H regions below 3.5 and above 10.5 were calibrated by measurements in HCl and KOH solutions, respectively.

Reagents.—A pure sample of ATP prepared by the Nutritional Biochemicals Corporation was employed in this work. In order to avoid possible hydrolysis prior to potentiometric measurements, each sample was weighed out as a solid and added to the experimental solution just before the addition of base. The metal ion solutions were standardized volumetrically by titration with the disodium salt of EDTA in the presence of suitable indicators as outlined by Schwarzenbach.[10] Carbonate-free KOH was prepared by the method of Schwarzenbach and Biedermann[11] and was standardized by titration with potassium acid phthalate.

Calculations

The acid dissociation constants for the disodium salt of ATP (H_2A) were calculated by a direct algebraic method. The equilibria and the dissociation constants involved are

$$H_2A^{2-} \rightleftharpoons HA^{3-} + H^+$$

$$k_1 = \frac{[HA^{3-}][H^+]}{[H_2A^{2-}]} \quad (1)$$

$$HA^{3-} \rightleftharpoons [A^{4-}] + [H^+]$$

$$k_2 = \frac{[H^+][A^{4-}]}{[HA^{3-}]} \quad (2)$$

If only 1:1 mononuclear complexes form during a titration of a 1:1 mixture of ligand and metal ion, the equilibria may be expressed as

$$M^{2+} + HA^{3-} \rightleftharpoons MHA^-$$

$$K_1 = \frac{[MHA^-]}{[M^{2+}][HA^{3-}]} \quad (3)$$

$$M^{2+} + A^{4-} \rightleftharpoons MA^{2-}$$

$$K_2 = \frac{[MA^{2-}]}{[M^{2+}][A^{4-}]} \quad (4)$$

Two other equilibria may be described as

$$M^{2+} + H_2A^{2-} \rightleftharpoons MHA^- + H^+ \quad (5)$$

$$MHA^- \rightleftharpoons MA^{2-} + H^+ \quad (6)$$

$$K_1' = \frac{[MHA^-][H^+]}{[M^{2+}][H_2A^{2-}]} \qquad K_2' = \frac{[MA^{2-}][H^+]}{[MHA^-]}$$

K_1 and K_2 are related to K_1' and K_2' by the simple relationship

$$K_1 = \frac{K_1'}{k_1} \qquad K_2 = \frac{K_1'K_2'}{k_1k_2} \quad (7)$$

If T_A represents the total concentration of the various ligand species, and T_M that of all the metal species, then

$$T_A = [H_2A^{2-}] + [HA^{3-}] + [A^{4-}] + [MA^{2-}] + [MHA^-] \quad (8)$$

$$T_M = [M^{2+}] + [MA^{2-}] + [MHA^-] \quad (9)$$

The total amount of titratable hydrogen

$$[H^+] = [HA^{3-}] + 2[A^{4-}] + [MHA^-] + 2[MA^{2-}] - aT_A + [OH^-] \quad (10)$$

where "*a*" represents moles of base added per mole of ATP present. From equations 5, 6, 8, 9 and 10 the unknowns $[H_2A^{2-}]$, $[HA^{3-}]$ and $[A^{4-}]$ may be eliminated. $[M^{2+}]$ may be expressed in terms of K_2' as

$$[M^{2+}] = \frac{K_2'[(2-a)T_A - [H^+] + [OH^-]] - [H^+][(a-1)T_A + [H^+] - [OH^-]]}{[H^+](x/y - 1) + K_2'(x/y)} \quad (11)$$

where $x = 2[H^+]^2/k_1k_2$ and $y = [H^+]^2/k_1k_2 + [H^+]/k_2 + 1$. Equation 11 has only two unknowns, K_2' and $[M^{2+}]$; the values of T_A, aT_A, $[H^+]$ and $[OH]^-$ being experimentally measured. A set of values for K_2' was assumed and the corresponding values of $[M^{2+}]$ were calculated for a given point on a titration curve. These values of $[M^{2+}]$ then were substituted in (12) to get the corresponding values of K_1'.

$$K_1' = \frac{[(2-a)T_A - [H^+] - x/y[M^{2+}]k_1k_2y}{[M^{2+}]^2[H^+]} \quad (12)$$

Plotting the various values of K_2' against the corresponding values of K_1' gave a curved line. For each point on the titration curve a different line is obtained. If there is a unique solution for the above equations, plots of K_2' *versus* K_1' give curved lines intersecting at one point. For a particular metal ion the experiment was carried out at three different concentrations and in each case practically the same values of pK_2' and pK_1' were obtained. The average deviation in most of the cases was about ± 0.01 of a *pK* unit. The series of intersecting lines is shown in Fig. 1 for one of the three concentrations studied in the case of the magnesium(II) ion. Similar sets of curves were obtained for other metals. From the values of pK_1' and pK_2' the formation constants K_1 and K_2 were calculated by means of the relationships given by equation 7.

The method of calculation of the formation constants for solutions with ten parts of metal per part of ligand is the same as was carried out for the 1:1 titration. In this case it was assumed that the concentration of free metal ion is the same as the concentration of total metal ion added. This assumption is justified by the fact that the formation constants of the chelate species generally is low, and in the presence of tenfold excess of the metal a very small percentage of metal ion is bound. However, a correction for the metal ion bound was applied with the use of the formation constants obtained from 1:1 titration curves. The various constants obtained are listed in Table I. The equation derived for the calculation of formation constants for the 10:1 titrations is

(9) H. S. Harned and B. B. Owen, "The Physical Chemistry of Electrolytic Solutions," Reinhold Publ. Corp., New York, N. Y., 1958.

(10) G. Schwarzenbach, "Complexometric Titrations," Interscience Publishers, New York, N. Y., 1957.

(11) G. Schwarzenbach and W. Biedermann, *Helv. Chim. Acta*, **31**, 331 (1948).

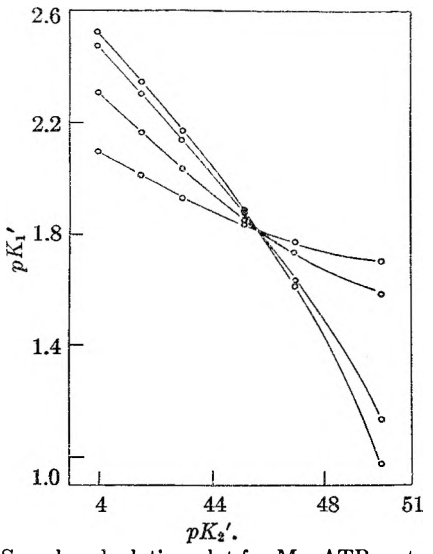

Fig. 1.—Sample calculation plot for Mg–ATP system (1:1) at 5×10^{-3} *M*, 25°, and $\mu = 0.10$ *M* (KNO_3).

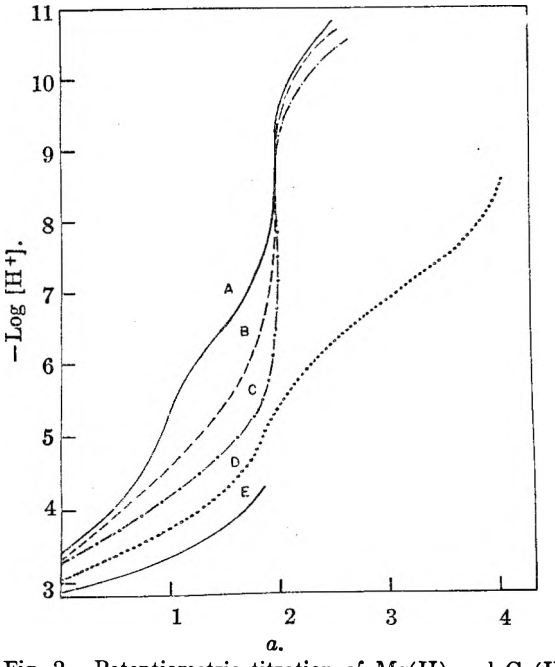

Fig. 2.—Potentiometric titration of Mg(II) and Cu(II) chelates of ATP in 0.1 *M* KNO_3 at 25° with the following molar ratios of ligand to metal ion: A, ligand alone; B, Mg (1:1); C, Mg (1:10); D, Cu (1:1); E, Cu (1:10); a = moles of base added per mole of ligand.

$$[A^{4-}] = \frac{K_2'[(2-a)T_A - [H^+] + [OH^-]] - [H^+][(a-1)T_A + [H^+] - [OH^-]]}{[H^+](x-y) + K_2'x} \quad (13)$$

The value of $[A^{4-}]$, when substituted in the expression for K_1', gives a relationship as before between K_1' and K_2' and the experimentally determined quantities, aT_A, T_M, $[H^+]$ and $[OH^-]$.

$$K_1' = \frac{[(2-a)T_A - [H^+] - [A^{4-}]\,z]}{[M^{2+}][A^{4-}][H^+]/k_1k_2} \quad (14)$$

Values of K_2' were assumed and the corresponding values of K_1' then were calculated.

Solution Equilibria for [CuA].—In the study of the copper–ATP system with equimolar concentration of metal and the ligand ions, it is probable that four species exist: a normal (1:1) chelate $[CuA^{2-}]$, a monohydroxo compound $[Cu(OH)A\cdot H_2O]^{3-}$, a dihydroxo species $[Cu(OH)_2A]^{4-}$ and a dimer $[Cu(OH)A]_2^{6-}$. The solution equilibria may be defined by the equations

$$Cu^{2+} + A^{4-} \rightleftharpoons CuA^{2-}$$

$$K_{MA} = \frac{[CuA^{2-}]}{[Cu^{2+}][A^{4-}]} \quad (15)$$

$$CuA^{2-} + H_2O \rightleftharpoons Cu(OH)A^{3-} + H^+$$

$$K_{M(OH)A} = \frac{(Cu[OH]A^{3-})[H^+]}{[CuA^{2-}]} \quad (16)$$

$$CuA^{2-} + 2H_2O \rightleftharpoons Cu(OH)_2A^{4-} + 2H^+$$

$$K_{M(OH)_2A} = \frac{(Cu[OH]_2A^{4-})[H^+]^2}{[CuA^{2-}]} \quad (17)$$

$$2CuA^{2-} + 2H_2O \rightleftharpoons (Cu[OH]A)_2^{6-} + 2H^+$$

$$K_{(M[OH]A)_2} = \frac{[(Cu[OH]A)_2^{6-}][H^+]^2}{[CuA^{2-}]^2} \quad (18)$$

$$2Cu(OH)A^{3-} \rightleftharpoons (Cu(OH)A)_2^{6-} + 2H_2O$$

$$K_d = \frac{[(Cu[OH]A)_2^{6-}]}{[Cu(OH)A^{3-}]^2} \quad (19)$$

The amount and distribution of the various chelate species present under various conditions of *p*H and total concentration may be calculated from the above equilibria and from the relationship between the total copper content, the value of $-\log[H^+]$ and the amount of hydroxide added. If T_{OH} represents the hydroxide added (in concentration units) to a solution of CuA during the titration, then

$$T_{OH} + [H^+] - [OH^-] = [Cu(OH)A^{3-}] + 2[(Cu[OH]A)_2^{6-}] + 2[Cu(OH)_2A^{4-}] \quad (20)$$

At neutralization values less than $a = 2.5$, *p*H-(5.5–6.5), it was assumed that the concentration of the dihydroxo chelate is negligibly small. Equation 20 then may be simplified to

$$T_{OH} + [H^+] - [OH^-] = [Cu(OH)A^{3-}] + 2[(Cu[OH]A)_2^{6-}] \quad (21)$$

The total concentration of the chelate species T_{CuL} is defined by the relationship

$$T_{CuL} = [CuA^{2-}] + [Cu(OH)A^{3-}] + 2[(Cu[OH]A)_2^{6-}] \quad (22)$$

Combination of equations 16, 18 and 21 gives the expression

$$\frac{T_{OH} + [H^+] - [OH^-]}{[CuA^{2-}]/[H^+]} = K_{M(OH)A} + 2K_{(M[OH]A)_2}\frac{[CuA^{2-}]}{[H^+]} \quad (23)$$

Equation 23 is valid only when a dimer is formed, in which case the plot of $[H^+]\,(T_{OH} + [H^+] - [OH^-])/[CuA^{2-}]$ *versus* $[CuA^{2-}]/[H^+]$ should give a straight line with a slope equal to $2K_{(M[OH]A)_2}$ and the intercept at $[CuA^{2-}]/[H^+] = 0$ equal to $K_{M(OH)A}$. It is of course possible that higher polymers of the type $(Cu[OH]A^{3n-})_n$ may be formed. For instance, if a trimer were formed, a straight line would be obtained when $[H^+]\,(T_{OH} + [H^+] - [OH])/[CuA^{2-}]$ is plotted against $[CuA]^2/[H^+]^2$, the slope of which would be equal to $3K_{(M[OH]A)_3}$. In the Cu–ATP system studied, the presence of a dimer was indicated (Fig. 4). $K_{M(OH)_2A}$

was calculated algebraically from data at high pH with the values of $K_{M(OH)A}$ and $K_{(M[OH]A)_2}$ already determined.

Discussion of Results

The potentiometric titration curve of ATP, shown in Fig. 2A, indicates stepwise dissociation reactions, corresponding to the separate neutralization reactions

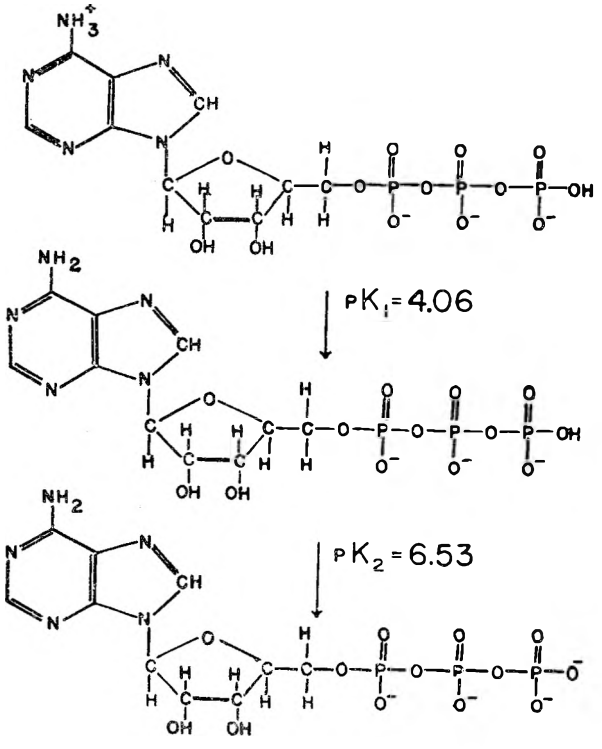

The pK values, 4.06 and 6.53, for 25° are close to the corresponding values, 4.05 and 6.50, obtained for ATP at 20° by Martell and Schwarzenbach.[5] The pK_1 value of ATP is lower than the pK_1 value of adenine ($pK_1 = 4.24$).[12]

Titration curves are illustrated in Fig. 2 (B, C) for ATP chelates of magnesium(II), for 1:1 and 10:1 ratios of metal to ligand ions, and in Fig. 2 (D, E) for 1:1 and 10:1 ratios of copper to ligand ions. In the case of calcium(II), strontium(II), barium(II), manganese(II), cobalt(II), nickel(II) and zinc(II) similar results were obtained.

Mg(II), Ca(II), Sr(II), Ba(II), Zn(II), Mn(II), Co(II), Ni(II) Ions.—Titration of equimolar amounts of ligand and magnesium(II) nitrate, Fig. 2B, resulted in a steep inflection at $a = 2$, corresponding to the formation of a 1:1 chelate. The other ions indicated above also give inflections at $a = 2$ in 1:1 titrations. In the 10:1 titration of magnesium(II) (Fig. 2C), the inflection again is obtained at $a = 2$, but the curve is shifted to lower pH as expected. The formation constants for the normal and acid complexes were calculated from experimental points taken throughout the titration range. The 10:1 titration curves for calcium(II), strontium(II) and barium(II) ions are similar to those of magnesium(II), the inflection occurring at $a = 2$. In the 10:1 titrations of zinc(II), manganese(II), cobalt(II) and nickel(II), a precipitate invariably was formed before the inflection was reached. The formation constants for 10:1 titrations in the case of these metals were calculated over a pH range far below the precipitation point. In the pH range selected, the hydrolysis of the excess metal ion was neglected.

The purpose of doing both 1:1 and 10:1 titrations was to detect the formation of any chelates of the type M_2A or MA_2^{6-}. If such compounds are formed, there should be some difference in the formation constants of the "equivalent" (1:1) and of the "excess" (10:1) titrations. Since such a difference was observed, it seems that the possibility of formation of small amounts of chelates other than those assumed in our equation should be considered. Since the metal ion concentration remains practically constant during an "excess" titration, one would not expect the formation of weak polynuclear complexes to be reflected in a drift of the calculated mononuclear complex constant as a function of neutralization value. However, when the ligand and metal ion are titrated in equivalent amounts, the free metal ion concentration changes rapidly as the metal chelate is formed, and the interference caused by the formation of M_2A (or of MA_2^{6-}) will show up as a drift of the calculated values of MA^{2-} and MHA^{-}. Since no such drift was detected, the possibility of any M_2A or MA_2^{6-} was excluded in 1:1 titrations. A further study of the differences between the 1:1 and 10:1 titrations through the use of model calculations showed that the difference is in the wrong direction for the formation of polynuclear complexes (with more than one metal ion bound per ligand). This fact, plus the lack of a drift of calculated constants with a variation of neutralization values in the equivalent runs, would therefore rule out complex formation as a reason for the differences in the two types of constants listed in Table I. Thus it seems that differences in long-range, ionic forces resulting from differences in charges of supporting electrolyte at constant "ionic strength" are the only factors which would produce the observed effect. Thus the presence of relatively significant concentrations of bivalent metal ion would make the "effective" ionic strength in the 10:1 runs relatively higher than those of the 1:1 titrations, although the calculated ionic strengths are the same. As a result, the dissociation of the complexes into ions would occur to a greater extent than expected in the 10:1 runs, and this is exactly the effect observed.

The stability constants of the metal complexes of ATP, listed in Table I, increase in the order $Ba^{2+} < Sr^{2+} < Ca^{2+} < Mg^{2+} < Co^{2+} < Mn^{2+} < Zn^{2+} < Ni^{2+} < Cu^{2+}$. The order of the stabilities shows the normal sequence except for manganese and cobalt(II), the stability of the manganese(II) chelate being greater than that of cobalt(II), a behavior also observed by Wallas.[8] The higher stabilities of the ATP complexes as compared to those of ADP or AMP are due to the higher basicity and charge of the former as compared to those of the latter, as already has been pointed out.[5]

(12) Results obtained in this Laboratory under the same experimental conditions.

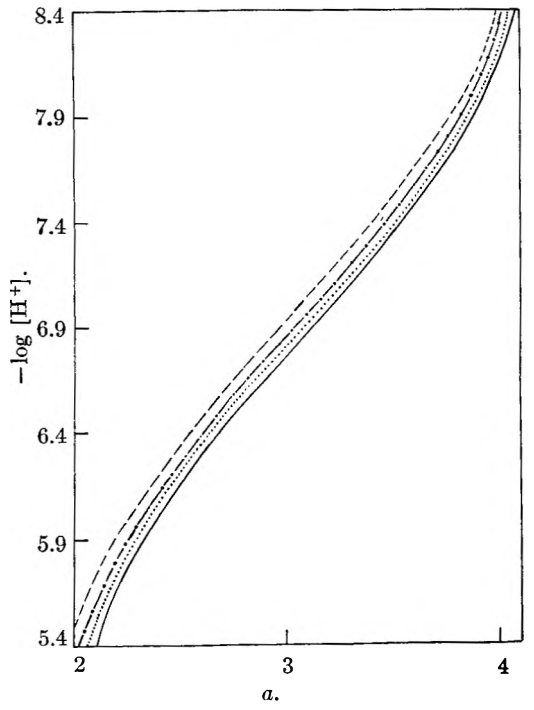

Fig. 3.—Potentiometric titration of 1:1 copper(II)–ATP chelates. Concentrations: ———, 6.00 10^{-3} *M*; ·····, 4.00 10^{-3} *M*; –·–·–, 1.99 10^{-3} *M*; – – –, 1.05 10^{-3} *M*; t = 25°; μ = 0.10 (KNO_3); a = moles of base added per mole of 1:1 chelate compound present.

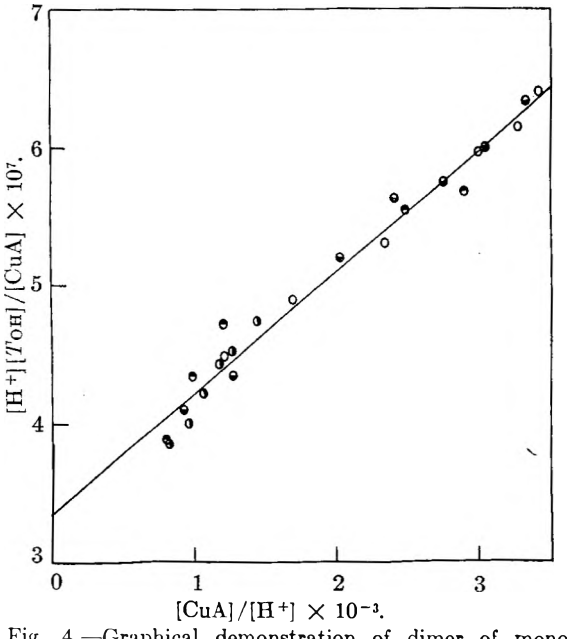

Fig. 4.—Graphical demonstration of dimer of monohydroxocopper(II)–ATP chelate: ○, 6.00 × 10^{-3} *M*; ◒, 4.00 × 10^{-3} *M*; ◓, 1.99 × 10^{-3} *M*; ◑, 1.05 × 10^{-3} *M*.

There are two sites in ATP at which chelation can take place; the amino group at position 6 of the purine ring, or the polyphosphate chain. In order to decide the site at which the metal ion enters, adenosine was titrated with all of the metal ions listed in Table I. There was little or no interaction of metal ions with adenosine, a fact also observed by Martell and Schwarzenbach[5] for the alkaline earths. Therefore, the amino group of the purine ring probably is not involved in chelate

TABLE I

EQUILIBRIUM CONSTANTS FOR THE INTERACTION OF ATP WITH VARIOUS METAL IONS

t = 25.0°, μ = 0.10, pK_1 = 4.06, pK_2 = 6.53

Metal ion	1:1 titrations Log K_1	Log K_2	10:1 titrations Log K_1	Log K_2
Ba(II)	1.85 ± 0.01	3.29 ± 0.01	.....	.....
Sr(II)	2.05 ± .01	3.54 ± .01	.....	.....
Ca(II)	2.13 ± .01	3.97 ± .01	1.78 ± 0.01	3.74 ± 0.02
Mg(II)	2.24 ± .01	4.22 ± .01	1.89 ± .01	3.99 ± .01
Co(II)	2.32 ± .02	4.66 ± .02	2.14 ± .02	4.58 ± .01
Mn(II)	2.39 ± .01	4.78 ± .01	2.18 ± .01	4.70 ± .01
Zn(II)	2.67 ± .01	4.85 ± .02	2.23 ± .01	4.75 ± .02
Ni(II)	2.72 ± .02	5.02 ± .02	2.31 ± .02	4.83 ± .02
Cu(II)	3.12 ± .01	6.13 ± .01	2.78 ± .01	6.01 ± .01

formation of ATP. The conclusion that the polyphosphate chain is the active site is supported by the higher formation constants of ATP as compared to ADP or AMP. Melchior[4] attributed the higher stability to be due to the formation of a terdentate structure of the type

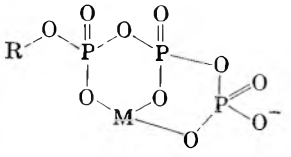

This may be true for metals that form octahedral or tetrahedral bonds, but a different interpretation is offered below for the copper(II) chelate, because of the unique reactions which this compound undergoes at high pH. The acido formation constants of the type MHA^- follow the same trend as indicated for normal complexes. The 10:1 titration results for barium and strontium are not included due to the inconsistent values of the low formation constants.

Copper(II) Ion.—The 1:1 titration curves illustrated in Fig. 3 show a steep inflection at a = 2, corresponding to the formation of a 1:1 chelate compound, followed by an additional concentration-dependent buffer region of the type characteristic of polynuclear metal complex formation. A summary of the equilibrium constants obtained is given in Table II.

TABLE II

EQUILIBRIUM CONSTANTS FOR THE COPPER(II) CHELATES

t = 25.0°, μ = 0.10 (KNO_3)

Log K_{MA}	$pK_{M(OH)A}$	$pK_{M(OH)_2A}$	$pK_{(M[OH]A)_2}$	Log K_d
6.13	6.47	13.49 ± 0.05	10.35	2.59

With the help of these constants it was possible to calculate the distribution of the various chelate species as a function of −log[H+] and total metal chelate concentration. A sample distribution plot is shown in Fig. 5 for a 4.00 millimolar solution of copper(II)–ATP. The plot clearly indicates the successive replacement of CuA^{2-} by $Cu(OH)A^{3-}$, $(Cu[OH]A)_2^{6-}$ and $Cu(OH)_2A^{4-}$ as the principal forms of the metal chelate compounds in solution.

The formation of a dimer and a dihydroxo chelate in the copper(II)–ATP system may be interpreted on the basis that with copper(II), ATP acts primarily as a bidentate ligand. It is sterically difficult for the third phosphate group to bend around and bind

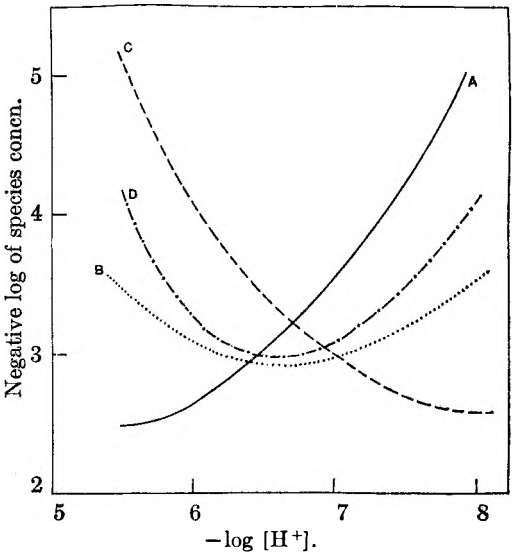

Fig. 5.—Distribution of copper(II)–ATP chelate species as a function of the hydrogen ion concentration: A, diaquo chelate, CuA; B, monohydroxo chelate, $Cu(OH)A^{1-}$; C, dihydroxo chelate, $Cu(OH)_2A^{2-}$; D, dimer, $(Cu[OH]A)_2^{2-}$; $T_A = 4.00\ 10^{-3}\ M$; $t = 25°$; $\mu = 0.10\ M$ (KNO_3).

the third position. Even if there is some weak binding with the third phosphate, the metal ion would have greater affinity for an additional donor group such as hydroxyl ion. Thus the monohydroxo chelate is visualized as being first formed from the diaquo chelate, which then undergoes dimerization or forms a dihydroxo chelate at a higher pH according to the reactions

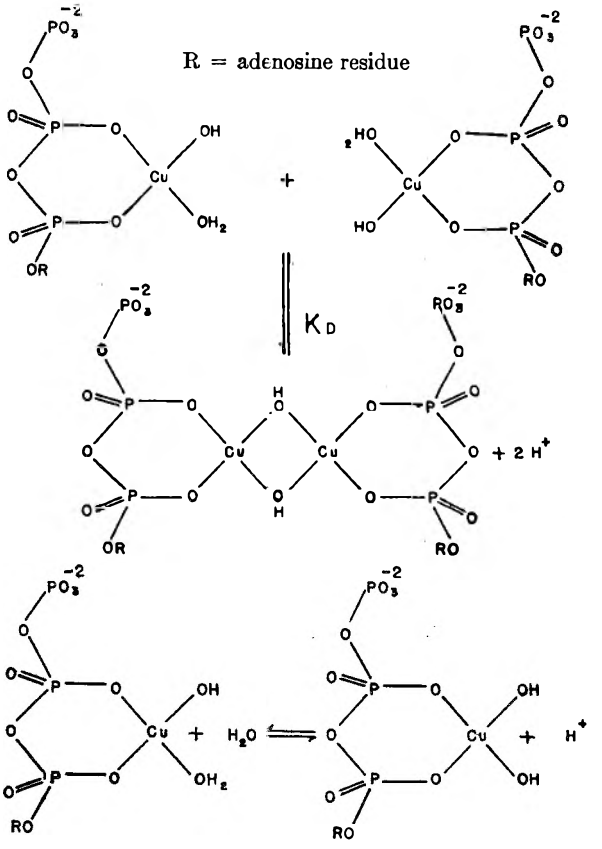

COMPOUND REPETITION IN OXIDE SYSTEMS. SOLID PHASES IN THE SYSTEM Li_2O–Ta_2O_5 AND Na_2O–Ta_2O_5

BY ARNOLD REISMAN

International Business Machines Corporation, Thomas J. Watson Research Center, Yorktown Heights, New York

Received March 4, 1961

The system Li_2O–Ta_2O_5 has been studied in the range 45–100 mole % Ta_2O_5 by X-ray analysis of samples reacted in the solid state at 1350°. Three compounds have been identified and have been assigned the compositions, $Li_2O{\cdot}3Ta_2O_5$, $Li_2O{\cdot}Ta_2O_5$ and $3Li_2O{\cdot}Ta_2O_5$. The system Na_2O–Ta_2O_5 has been similarly studied in the temperature interval 700–1300°. Three compounds have been identified in the highest temperature samples. These have been assigned the compositions $Na_2O{\cdot}3Ta_2O_5$, $Na_2O{\cdot}2Ta_2O_5$ and $Na_2O{\cdot}Ta_2O_5$. Earlier work also has indicated the existence of an $Na_2O{\cdot}3Ta_2O_5$ compound. Analogous lithium and sodium compounds are not isomorphic while the 1:2 sodium compound is isomorphic with the 1:2 potassium analog and the 1:3 sodium salt is isomorphic with a metastable potassium analog. The 1:1 sodium compound has been indexed on the basis of a perovskite-derived orthorhombic unit cell with a two-fold "b" multiplicity. The 1:2 compound exhibits a perovskite-derived bronze structure and has been indexed on the basis of an orthorhombic unit cell with a two-fold "b" multiplicity. The 1:3 sodium salt also has a bronze structure and has been indexed on the basis of an orthorhombic unit cell with two-fold "a" and "b" multiplicities. No solid solution was detected in either system. The results of the sodium system are correlated with those reported in an earlier work, and predictions are made about the melting behavior of the different salts and their repetition in higher weight systems.

Introduction

A number of earlier papers have dealt with stable and metastable equilibrium states in interactions between alkali oxides and the pentoxides of vanadium, niobium and tantalum. Based on observed liquidus characteristics of repeated compounds in the series Li_2O–Nb_2O_5, Na_2O–Nb_2O_5, K_2O–Nb_2O_5 and Rb_2O–Nb_2O_5, working principles have been evolved for predicting stable compound stoichiometries in unknown systems from a knowledge of the equilibrium state in a known related system. A first attempt at applying these principles has been successful in defining the equilibrium compound stoichiometries in the system Cs_2O–Nb_2O_5.[1] In order to determine whether the working principles are generally applicable to oxide–oxide interactions which form compounds, studies of systems involving alkali oxides and V_2O_5 or Ta_2O_5 were initiated. The first of these is

(1) A. Reisman and J. Minec, *J. Phys. Chem.*, **65** 996 (1961).

amenable to precise characterization through the liquidus and is being investigated in the same manner as the niobate series. The tantalate systems, however, exhibit melting temperatures above the range of the available DTA equipment and cannot be characterized as accurately. It was decided, therefore, to attempt resolution of tantalate interactions *via* X-ray analysis of samples prepared by solid state reactions. Since the system K_2O–Ta_2O_5[2] already has been studied through the melting points, it was felt that this system would serve as a reference point for speculating about the melting behavior of tantalate systems which were defined only in subsolidus regions.

Initial choices for investigation were the systems Li_2O–Ta_2O_5 and Na_2O–Ta_2O_5, the latter having been described by King, *et al.*[3] The authors concluded that the system was comprised of three congruently melting compounds having base to acid ratios of 1:2 or 1:3, 1:1 and 3:1. In addition, they reported the existence of solid solution intervals from about 65–75 and 90–100 mole % Ta_2O_5. Since the system K_2O–Ta_2O_5 did not appear to exhibit detectable solid solubility ranges, and such behavior has not been observed in any of the niobate systems previously examined, it was felt that a reinvestigation of the sodium system was necessary in conjunction with the program on compound repetition.

With reference to metastable equilibria in oxide interactions, it was decided that studies of the progress of a reaction at different temperatures might be useful in uncovering transition states. Consequently, the Na_2O–Ta_2O_5 system was investigated by quenching samples reacted at a number of isotherms to see if phases other than the equilibrium ones formed during the course of reaction. Such phases subsequently have been detected in the system K_2O–Ta_2O_5 and were shown to exist in the system K_2O–Nb_2O_5[4,5] as well as in the compound Nb_2O_5.[6,7]

Experimental Procedure

A. The System Li_2O–Ta_2O_5.—Samples for this system were prepared by mixing the powdered reactants, Li_2CO_3 and Ta_2O_5, in a rotating vial for several hours and then reacting them in covered platinum crucibles in air at 1300° for 48 hr. The firing schedule was repeated at 1350°, with intervening grinding, until no further changes were detected in diffraction patterns obtained after successive treatments. Samples representative of each two-phase region were subsequently cooled to room temperature at 1°/min., and also quenched in liquid nitrogen. X-Ray analysis of these samples indicated that the phases detected at room temperature were the same as those existing at 1350°, since the patterns given by analogous compositions in quenched and slowly cooled specimens were indistinguishable. The justification for the assumption that phases existing at 1350° could be quenched in is based on the ability to effect successfully such quenchings in niobate systems.

The starting Ta_2O_5 was obtained from the Fansteel Metallurgical company and was their highest purity grade. Since silica had been observed to have marked effects on the pentoxide, either pure or mixed with alkali metal or other oxides, analyses were performed to determine the silica content which was found to be < 100 p.p.m. The as-received Ta_2O_5 was heated in air at 1000° in covered platinum crucibles. X-Ray examination showed that the ignited material was present in its low temperature, β, form.[2] The carbonate was treated as described in an earlier paper, and samples were prepared at 2.5 mole % intervals.

B. The System Na_2O–Ta_2O_5.—Samples for this system were prepared at 2.5 mole % intervals using Na_2CO_3 dried at 250° in a CO_2 atmosphere, and Ta_2O_5 dried as described above. A second batch of the pentoxide was treated in air at 1410° for 24 hr. and then air-quenched. X-Ray examination of this material indicated that it was present in the high temperature, α, form. Using each of the Ta_2O_5 batches, four duplicate sets of samples were mixed, two containing the α and two containing the β-modification.

Two of these sets, one containing α-Ta_2O_5 and the other β-Ta_2O_5, were used to establish a 1300° equilibrium diagram by consecutive heat treatment at 1300°, with intermediate cooling and grinding, until no further changes were observed in diffraction patterns. This occurred after the first treatment but two additional firings were performed. Upon completion of the firing schedule, the α-set showed complete conversion of Ta_2O_5, in its two phase field, to the β-form. Analogous samples from both sets then were cooled at 1°/min., air-quenched or quenched in liquid nitrogen. As with the lithium tantalate samples, the diffraction patterns of equivalent compositions were indistinguishable, indicating that phases detected at room temperature were representative of those existing at 1300°.

The two remaining unreacted sets each were divided into six parts which were fired at different temperatures in the interval 700–1200° inclusive for 24 hr. The samples were air-quenched at the completion of each treatment, ground and analyzed.

C. X-Ray Examination.—X-Ray studies were conducted in a Debye Scherrer powder camera using Ni filtered Cu radiation generated at 40 Kv. and 20 mamp. Exposure times were 1.5 hr.

Results and their Interpretation

A. The System Li_2O–Ta_2O_5.—Samples were prepared in the range 45–100 mole % Ta_2O_5 at 2.5 mole % intervals. These were air-quenched from 1350° after having been reacted as described in A above. In all, four separate reaction treatments were performed and no detectable differences in diffraction line intensities were observed after the second firing. The final patterns were internally consistent in that each two phase region showed a progressive line intensity variation for each of the coexisting compounds with composition change. Exclusive of a diffraction set attributable to β-Ta_2O_5, three other distinct sets of lines were observed in a total of three two-phase regions. From 100–75 mole % Ta_2O_5, X-rays detected β-Ta_2O_5 + compound I. At 75 mole % only the pattern of I was observed, and from 75 to 50 mole %, the diffraction sets for I and a new phase, II, coexisted. Based on these data, I was assigned a value $Li_2O \cdot 3Ta_2O_5$. At 50 mole % only the pattern of II was observed, and from 50–45 mole %, a mixture of II and a new phase III was present. Consequently, II was assigned the composition $Li_2O \cdot Ta_2O_5$. While not enough data were collected to establish the composition of III, it is likely that this compound has the stoichiometry $3Li_2O \cdot Ta_2O_5$, based on the reported existence of such a ratio in both the K_2O–Ta_2O_5 and Na_2O–Ta_2O_5 systems and the sequential trends discussed in earlier papers. The compound $Li_2O \cdot Ta_2O_5$ has been reported previously by Lapitskii and

(2) A. Reisman, F. Holtzberg, M. Berkenblit and M. Berry, *J. Am. Chem. Soc.*, **78**, 4514 (1956).

(3) B. King, J. Schultz, E. A. Durbin and W. H. Duckworth, U. S. Govt. Report. No. BMI-1106, July 9, 1956.

(4) A. Reisman and F. Holtzberg, *J. Am. Chem. Soc.*, **77**, 2115 (1955).

(5) A. Reisman, F. Holtzberg and M. Berkenblit, *ibid.*, **81**, 1292 (1959).

(6) F. Holtzberg, A. Reisman, M. Berry and M. Berkenblit, *ibid.*, **79**, 2039 (1957).

(7) A. Reisman and F. Holtzberg, *ibid.*, **81**, 3182 (1959).

Simanov,[8] who indexed this meta salt on the basis of a rhombohedral cell. The patterns for the 1:3 and 3:1 compounds are quite complex and could not be indexed from powder photographs. Within the limits of the composition intervals surveyed, 2.5 mole %, regions of solid miscibility as evidenced by single phase patterns in what would be a binary region were not detected. This, coupled with the observation that "*d*" spacing variations were not detected in samples 2.5 mole % to either side of an assigned compound location, and that a second phase made its first appearance in such samples, indicates the absence of appreciable solid solubility.

B. The System Na_2O–Ta_2O_5.—The results obtained at the several isotherms fall into three categories—stable equilibrium, metastable equilibrium and non-equilibrium depending on the following criteria. The results of the repeated 1300° firings starting with either α- or β-Ta_2O_5 were identical, and the data are assumed representative of the stable equilibrium state of the system from room temperature to 1300° at least. These samples never showed more than two phases simultaneously coexisting, and from this it may be concluded that the condensed system behaves as a binary one under a constant oxygen pressure equal to that in the ambient atmosphere. With this as a basis for comparison with samples reacted a single time at lower temperatures, two other situations were detected. In the first of these, regions were observed in which three phases were simultaneously present. Such samples obviously were representative of reactions which had not reached any state of equilibrium, stable or metastable, relative to that defined by the 1300° data. The second situation was one in which although no more than two phases were present simultaneously and the internal consistency of the X-ray data was excellent, the phases present in some regions were not those defined by the 1300° experiments. While such a state of the system is consistent with its being binary, it is obviously metastable relative to the equilibrium system. This is analogous to the case where a system known to generate an intermediate compound shows a metastable extension of the solubility arms of the end members into the fields of the intermediate compound. Such metastable extensions have been observed to eventually intersect in a simple quadruple point to the complete exclusion of the intermediate compound. One such case which will be reported at a later date occurs in the system Li_2O–V_2O_5.

Tables I and II present composite data for the reactions starting with α- and β-Ta_2O_5, respectively. The β-sets were examined at 2.5 mole % intervals in the temperature range 800–1300° inclusive. The 700° β-series was studied at 5 mole % intervals. The α-sets were studied at 5 mole % intervals in the range 700–1200° and at 2.5 mole % intervals in the 1300° series. Excepting the 900° α-series data, the first symbol in each column represents the pure phase whose diffraction intensity is decreasing with decreasing Ta_2O_5 composition. In the 900° α-series, the β-Ta_2O_5 is present in much smaller quantities than the α-phase although both of these phases show a line intensity decrease with decreasing Ta_2O_5 concentration.

The Ta_2O_5 patterns obtained from the 700–900° β-series were indicative of poorer crystallinity than in the higher temperature experiments. Similarly the 700–1000° β-series yielded poorer patterns of compound III than were obtained from samples reacted at higher temperatures. The same was true for compound III in the 700–900° α-series.

1. The 1300° Equilibrium Diagram.—Both the 1300° α- and β-data indicated the presence of three distinct sodium tantalate phases in the range 100–50 mole % Ta_2O_5. Between 100 and 75 mole % Ta_2O_5, β-Ta_2O_5 and compound I were present. At 75 mole % compound I alone was detected, and in the composition interval 75 to 67.5 mole %, a mixture of compounds I and II was observed. Consequently, I was assigned the stoichiometry $Na_2O \cdot 3Ta_2O_5$. From 65 to 50 mole %, mixtures of II and a new phase III were detected and II was assigned the composition $Na_2O \cdot 2Ta_2O_5$ (66 2/3 mole % Ta_2O_5). The 50 mole % samples showed only the pattern for pure compound III, and this material was assigned the composition $Na_2O \cdot Ta_2O_5$. The patterns given by I and II, while exhibiting a great deal of line superposition, are distinctly different, with II giving rise to several non-superimposed inner lines as well as other fainter reflections. A comparison of the patterns for the 1:2 compound and the compound $K_2O \cdot 2Ta_2O_5$ shows them to be almost indistinguishable into the mid-back reflection region excepting a difference in spacing, but not in intensity, between maxima occurring in a quartet of lines and a similar difference in a doublet. Starting in the mid-back reflection region, however, the patterns for the potassium and sodium salt become dissimilar. As a lattice constant difference between the two compounds would become most pronounced in the back reflection region, the sodium and potassium analogs are believed to be isomorphic. The 1:2 sodium salt was indexed on the basis of an orthorhombic unit cell with $a = 6.00$ Å., $b = 2\,(3.83)$Å. and $c = 5.08$ Å. This cell can be thought of as representing a distortion of the perovskite structure.

The 1:3 compound yields a simpler pattern than the 1:2 compound and appears also to represent a tetragonal or orthorhombic distortion of the WO_3 perovskite structure, very similar to that obtained with the sodium–tungsten bronzes. The color of the 1:3 salt, as is the case for the other salt, is white unlike the bronze materials with which it appears to be structurally isomorphic. A comparison of the patterns given by the 1:3 and 1:1 salts shows them to be very similar with all of the major diffraction maxima of the 1:1 salt (excluding lines due to doubling) superimposable on the major diffraction maxima of the 1:3 salt. The remaining 1:3 lines therefore are representative of what are erroneously referred to as superlattice lines in such compounds which represent multiplicities rather than orderings.

(8) A. V. Lapitskii and Y. P. Simanov, *Zhur. Fiz. Khim.*, **29**, 1201 (1955).

TABLE I

X-RAY DERIVED DATA FOR THE SYSTEM Na_2O–Ta_2O_5:α-Ta_2O_5 SERIES

Mole % Ta_2O_5	Phases observed after given firing treatment[a] 1300[b]	1200[c]	1100[c]	1000[c]	900[c]	800[c]	700[c]
100	β	β	β	β	$\alpha + \beta$	α	α
97.5	β + I						
95.0	β + I	β + II	β + II	β + II	$\alpha + \beta$ + II	α + II	α + II
92.5	β + I						
90.0	β + I	β + II	β + II	β + II	$\alpha + \beta$ + II	α + II	α + II + III
87.5	β + I						
85.0	β + I	β + II	β + II	β + II	$\alpha + \beta$ + II	α + II	α + II + III
82.5	β + I						
80.0	β + I	β + II	β + II	β + II	$\alpha + \beta$ + II	α + II	α + II + III
77.5	β + I						
75.0	I	β + II	β + II	β + II	$\alpha + \beta$ + II	α + II	α + II + III
72.5	I + II						
70.0	I + II	β + II	β + II	β + II	$\alpha + \beta$ + II	α + II	α + II + III
67.5	I + II						
65.0	II + III	II + III	II + III	II + III	II + III	II + III	α + II + III
62.5	II + III						
60.0	II + III	II + III	II + III	II + III	II + III	II + III	α + II + III
57.5	II + III						
55.0	II + III	II + III	II + III	II + III	II + III	II + III	α + II + III
52.5	II + III						
50.0	III	III	III	III	III	III	α + II + III

[a] α = α-Ta_2O_5, β = β-Ta_2O_5, I = compound I, II = compound II, III = compound III. [b] Samples fired repeatedly with intermediate cooling and grinding until no further change observed in diffraction patterns. [c] Samples fired once for 24 hours.

TABLE II

X-RAY DERIVED DATA FOR THE SYSTEM Na_2O–Ta_2O_5:β-Ta_2O_5 SERIES

Mole % Ta_2O_5	Phases observed after given firing treatments[a] 1300[b]	1200[c]	1100[c]	1000[c]	900[c]	800[c]	700[c]
100	β	β	β	β	β	β	β
97.5	β + I	β + I	β + II	β + II	β + II	β + II	
95.0	β + I	β + I	β + II	β + II	β + II	β + II	β + II
92.5	β + I	β + I	β + II	β + II	β + II	β + II	
90.0	β + I	β + I	β + II	β + II	β + II	β + II	β + II
87.5	β + I	β + I	β + II	β + II	β + II	β + II	
85.0	β + I	β + I	β + II	β + II	β + II	β + II	β + II
82.5	β + I	β + I	β + II	β + II	β + II	β + II	
80.0	β + I	β + I	β + II	β + II	β + II	β + II	β + II
77.5	β + I	β + I	β + II	β + II	β + II	β + II	
75.0	I	I	β + II	β + II	β + II	β + II	β + II
72.5	I + II	I + II	β + II	β + II	β + II	β + II	
70.0	I + II	I + II	β + II	β + II	β + II	β + II	β + II
67.5	I + II	I + II	β + II	β + II	β + II	II	
65.0	II + III	II + III	II + III	II + III	II + III	II	β + II + III
62.5	II + III	II + III	II + III	II + III	II + III	II + III	
60.0	II + III	II + III	II + III	II + III	II + III	II + III	β + II + III
57.5	II + III	II + III	II + III	II + III	II + III	II + III	
55.0	II + III	II + III	II + III	II + III	II + III	II + III	β + II + III
52.5	II + III	II + III	II + III	II + III	II + III	II + III	
50.0	III	III	III	III	III	III	β + II + III

[a,b,c] Same footnotes as in Table I.

Assuming that the unit cell is orthorhombic, all of the diffraction lines up to 58° (2θ) could be accounted for by the lattice parameters—a = 2 (3.87) Å., b = 2 (5.97) Å. and c = 5.97 Å. Since the pattern becomes complex and somewhat diffuse as the back reflection region is approached, no attempt was made to index the maxima beyond 58°. It is not impossible that the c constant may have a value slightly smaller or larger than 5.97 Å. This question could not be resolved in the absence of single crystal data.

The compound $Na_2O \cdot Ta_2O_5$ yields a simpler diffraction set than either of the other pure phases and was indexed from single crystal and powder data on the basis of an orthorhombic unit cell with a = 5.5237 Å., b = 2(3.8961) and c = 5.4781. The calculated density based on these data is 7.0969 g./cm.^{3} at 25°, and is in good agreement with the powder density value obtained by the method previously described,[2,9] 7.068 g./cm.^{3} at 25°. This compound had been indexed previously by Kay and Miles[10] on the basis of the same unit

(9) A. Reisman and F. Holtzberg, *J. Phys. Chem.*, **64**, 748 (1960).
(10) H. F. Kay and J. L. Miles, *Acta Cryst.*, **10**, 213 (1957).

cell with $a = 5.5130$ Å., $b = 2\ (3.8754)$Å. and $c = 5.4941$ Å.; the calculated density is 7.1272 g./cm.^{3}. From these data it is concluded that while the compounds $Na_2O \cdot Ta_2O_5$ and $Na_2O \cdot Nb_2O_5$[11-13] both are perovskite derived, they are not isomorphic since the tantalate has a two-fold multiplicity in the b direction while the antiferroelectric niobate exhibits a four-fold multiplicity along this axis.

As a $3Na_2O \cdot Ta_2O_5$ compound is one of the phases comprising the 50–25 mole % Ta_2O_5 region,[3] the equilibrium diagram consists of five two-phase regions containing four intermediate sodium tantalate compounds.

An examination of the equilibrium data compiled in the present study reveals further that no extended regions of solid miscibility exist within the composition intervals surveyed. As with the Li_2O–Ta_2O_5 samples, "*d*" spacing variations were not detected to either side of an assigned compound location, and a second phase was observed to either side of such locations.

None of the corresponding lithium and sodium analogs were found to be isomorphic.

2. The Lower Temperature Isotherms.—From Table II it is seen that the 700° β-series yields non-equilibrium samples since regions showing simultaneous coexistence of three phases are present. The corresponding α-set is, in general, similar. Significantly, conversion of the α- to β-modifications of Ta_2O_5 was not effected in these experiments within the time interval allotted. It is evident, however, that even though the α-phase is frozen in at 700°, reaction between the Na_2CO_3 and Ta_2O_5 does commence. Since the lowest eutectic temperature reported for this system[3] is approximately 1000°, a liquid phase reaction is improbable although an intermediate stage in which Na_2O and Na_2CO_3 are simultaneously present is possible. Most interesting about the 700° data, however, is the failure of the compound $Na_2O \cdot 3Ta_2O_5$ to make an appearance, even in a three-phase nonequilibrium mixture. Since such a result might indicate that the 1:3 compound has no stable field of existence at 700°, notwithstanding the results of slow-cooling experiments described in B of the experimental section, the following experiment was performed. A 1:3 reaction mixture was treated continuously at 700° for one week after which time it was analyzed. While the sample did not yield a single phase pattern, it did show the presence of compound I. Thus, it may be concluded that I is stable down to 700° at least and that the 700° series in addition to being non-equilibrium also is metastable with respect to the existence of I.

At 800°, both series exhibit metastable equilibria. The β-set no longer shows a simultaneous three condensed phase region, but again fails to reveal the 1:3 compound. The α-series behaves similarly with respect to the formation of this compound, and in addition shows the metastable presence of α-Ta_2O_5. In the 900–1100° temperature range, in which liquid intermediates are possible, the β-sets are similar to those obtained at 800°. The 900° α-series again is non-equilibrium since a three-phase region involving α- and β-Ta_2O_5 simultaneously is present. The 1000–1200° α-sets are similar and represent metastable equilibria since the 1:3 salt still is undetected. At 1200° the β-set is indistinguishable from that obtained at 1300°.

(11) A. Reisman, F. Holtzberg and E. Banks, *J. Am. Chem. Soc.*, **80**, 37 (1958).

(12) A. Reisman and E. Banks, *ibid.*, **80**, 1877 (1958).

(13) G. Shirane, R. Newnham and R. Pepinsky, *Phys. Rev.*, **96**, 581 (1954).

Discussion

A. General.—In its present state of development, the hypothesis concerning compound repetition in congeneric oxide–oxide interactions may be stated briefly as given below.

1. In an interaction between two non-isomorphic oxides possessing appreciable differences in ionic character, the less ionic oxide will function as the stable or structural determining factor for all intermediate compounds. The more ionic oxide will be structurally labile, functioning to modify the intra-group coördination present in the stable oxide. Thus, where the stable oxide is composed of octahedra (*e.g.*, Ta_2O_5) which are distorted due to a preponderance of edge sharing, the compounds formed by the two oxides will possess octahedra as their basic units, but the latter will exhibit more corner sharing with increasing content of the labile oxide. As a consequence, the structures of compounds formed will be less distorted than the pure stable oxide.

2. The liquidus fields for all analogous compound ratios in a congeneric series will show increasing submergence with increasing molecular weight of the labile oxide. For compounds present in the lowest weight system as incongruently melting phases, it is to be expected that they will repeat for only a few congener interactions depending on the submergence exhibited in the lowest weight system. For congruently melting phases present in the lowest weight system the number of repetitions is, in general, expected to be greater than for incongruently melting phases, but again dependent on the extent of emergence.

B. The System Li_2O–Ta_2O_5.—The compound $K_2O \cdot Ta_2O_5$ is reported as melting at a singular point between congruency and incongruency within the limits of experimental error. In the diagram proposed by King, *et al.*, the compound $Na_2O \cdot Ta_2O_5$ is shown to melt congruently. Consequently, it is postulated that the compound $Li_2O \cdot Ta_2O_5$ melts congruently. This same ratio is expected to reappear in both the Rb_2O–Ta_2O_5 and Cs_2O–Ta_2O_5 systems as incongruently melting phases, greatly submerged in the latter system.

The compound $K_2O \cdot 3Ta_2O_5$ is not believed to be stable in the system K_2O–Ta_2O_5 but such a ratio is detected in the system Na_2O–Ta_2O_5. Since its continuous existence only occurs in two congeneric interactions, it is expected that it is present in the system Li_2O–Ta_2O_5 as an incongruently melting phase which is appreciably submerged, and also is present in the system Na_2O-Ta_2O_5 as an incongruently melting phase with even greater field submergence. The compound $3Li_2O \cdot Ta_2O_5$ is expected to be congruently melting since this compound ratio is congruently melting in both the

Na_2O and K_2O–Ta_2O_5 systems. This ratio should repeat in the Rb_2O and Cs_2O systems.

C. The System Na_2O–Ta_2O_5.—The predicted melting behavior of the compound $Na_2O \cdot 3Ta_2O_5$, as mentioned above, is as an incongruently melting phase. The compound $K_2O \cdot 2Ta_2O_5$ is reported as melting incongruently but exhibits a largely emerged liquidus field. It is postulated that the compound $Na_2O \cdot 2Ta_2O_5$ melts just congruently or just incongruently and that this ratio will repeat in the systems $Rb_2O \cdot Ta_2O_5$ and $Cs_2O \cdot Ta_2O_5$ as incongruently melting phases with progressively greater submerged fields. The compound $K_2O \cdot Ta_2O_5$ melts at a singular point and it is to be expected that the compound $Na_2O \cdot Ta_2O_5$ melts congruently, which is consistent with the observations of King, *et al.* The compound $3K_2O \cdot Ta_2O_5$ melts congruently, which requires that the compound $Na_2O \cdot 3Ta_2O_5$ melt congruently. This also is consistent with the observations of King, *et al.*

The successful indexing of the sodium tantalates provides good confirmation for the belief that the octahedral units comprising the pentoxide persist in each compound. This structural unit gives rise to the lattice parameter around 3.85 Å. The diagram proposed by King, *et al.*, shows the presence of three sodium tantalate phases: a phase Y with an apparent stoichiometry $3Na_2O \cdot Ta_2O_5$, a second phase with an apparent stoichiometry $Na_2O \cdot Ta_2O_5$ and a phase X with a stoichiometry "between $Na_2O \cdot 2Ta_2O_5$ and $Na_2O \cdot 3Ta_2O_5$." The X phase reportedly was observed pure at both 66.7 and 75 mole % Ta_2O_5, indicating that King, *et al.*, detected the 1:2 and 1:3 compounds but were unable to distinguish between them due to the extensive superposition of maxima. This explains their proposal that the 66.7–75 mole % Ta_2O_5 region is one of solid solution rather than a mixture of two phases. A similar explanation accounts for their belief that the region 75–90 mole % Ta_2O_5 is comprised of a phase X solid solution + Ta_2O_5. Since β-Ta_2O_5 and $Na_2O \cdot 3Ta_2O_5$ also exhibit diffraction maxima superposition to some degree, it is assumed that King, *et al.*, failed to detect the 1:3 diffraction lines in the 90–100 mole % Ta_2O_5 region, concluding therefore that this is also a region of solid miscibility. Phase X is depicted as congruently melting. Considering, however, that such a conclusion is based on a possible misinterpretation of the X-ray data and a very few experimental fusion points, the conclusion is suspect.

Two other inconsistencies in the report by King, *et al.*, involve their calculated X-ray densities for α- and β-Ta_2O_5, and a mention of a new phase at the composition $2Na_2O \cdot 3Ta_2O_5$ which is not shown in the proposed diagram but discussed on page 17. They computed densities for α-Ta_2O_5 of 8.41 g./cm.^{3} and β-Ta_2O_5 of 8.63 g./cm.^{3}. The values determined pycnometrically [2] are 8.18 and 8.37 g./cm.^{3}, respectively. In other instances where such disagreements have been noted between calculated and experimentally determined densities, improper indexing has been at fault. The composition $2Na_2O \cdot 3Ta_2O_5$ is reported as exhibiting a perovskite structure other than that of $Na_2O \cdot Ta_2O_5$ and presumably different from that of phase X, whose diffraction characteristics are not mentioned except in noting a similarity to $Na_2O \cdot Ta_2O_5$. No such phase was observed in the present study and since King, *et al.*, do not elaborate on the field of existence of this phase, its status is not understood.

D. Observations on Metastability in the Tantalates.—The β-Ta_2O_5 sets, as noted, achieved the defined equilibrium states at lower temperatures than did the corresponding α-Ta_2O_5 sets. This indicates that the interoctahedral coördination in β-Ta_2O_5 more nearly approximates the sodium tantalate structures than does that of α-Ta_2O_5, requiring less reorganization in the process of forming tantalates than does α.

The difficulty in forming the 1:3 sodium tantalate coupled with the reported absence of this ratio in the system K_2O–Ta_2O_5 indicates that the experimental approach described in this report might be useful in predicting compound repetition, as are studies of liquidus characteristics. In earlier studies,[4,5] it was noted that the system K_2O–Nb_2O_5 could be made to generate a metastable water soluble phase having a composition around $4K_2O \cdot 3Nb_2O_5$. In the next higher system this phase was observed as a stable compound. These observations indicated to the author that: 1. A difficulty in forming a stable phase *via* a low temperature series of solid state reactions might imply that its liquidus field is greatly submerged and that it will not reappear in the next higher interaction; 2. If phases other than the known stable ones can be generated metastably in a given interaction, these phases may be observed in the next higher interaction.

These speculations led to some preliminary rate experiments on the system K_2O–Ta_2O_5 whose stable diagram consists of intermediate phases having compositions of 1:5, 1:2, 1:1 and 3:1, the first exhibiting a greatly emerged incongruent field, the second a more submerged incongruent field, the third melting at a singular point and the fourth melting congruently. When several K_2O–Ta_2O_5 reaction mixtures in the composition interval 100–50 mole % Ta_2O_5 were heat treated at approximately 1000° for 24 hours, they showed the presence of the 1:1 compound, an unknown phase and Ta_2O_5. Neither the 1:2 or 1:5 phases were observed, and the unknown phase appeared pure at the composition $K_2O \cdot 3Ta_2O_5$. A comparison of its diffraction pattern with that of the stable sodium analog showed them to be structurally isomorphic. If the speculations mentioned have any validity these data indicate a reappearance of the 1:3 ratio in the system Rb_2O–Ta_2O_5 as well as a disappearance of the 1:5 and 1:2 ratios. The reappearance of a non-repeated compound has been observed in niobate studies, indicating that such an occurrence is not unusual. Since the disappearance of the 1:2 ratio is not, however, consistent with predications based on liquidus characteristics, and the 1:5 ratio was not detected metastably in the sodium interactions, it is evident that much more detailed investigations are required to determine whether these observations have any

significance. Toward this end extensive studies of the reaction behavior in the remaining tantalate systems have been initiated.

Acknowledgments.—The author wishes to thank Dr. F. Holtzberg for invaluable contributions to the ideas discussed in this and earlier publications, M. Witzen for assisting with X-ray analysis and B. Agule for the preparation of samples.

THE FORMATION CONSTANTS OF THE TANTALUM FLUORIDE SYSTEM. I. POTENTIOMETRIC AND ANION EXCHANGE STUDIES—EVIDENCE FOR SPECIES OF COÖRDINATION NUMBER NINE[1,2]

BY LOUIS P. VARGA AND HARRY FREUND[3]

Department of Chemistry, Oregon State University, Corvallis, Oregon, and the U. S. Bureau of Mines, Albany, Oregon

Received May 22, 1961

Potential measurements with the quinhydrone–calomel cell on perchloric acid solutions containing Ta(V) and hydrofluoric acid were interpreted in terms of the species TaF_6^-, TaF_7^{--}, TaF_8^{---} and TaF_9^{----}. When conditions were defined where the concentrations of hydrolytic, polynuclear and weak acid species of the tantalum fluoride system were negligible, an analytical expression for the average ligand number, $\bar{n}$, in terms of the experimental hydrogen ion concentrations allowed calculation of the formation curve from $\bar{n} = 6$ to 9. The distribution of trace concentrations of TaF_6^- between the perchlorate form of an anion-exchange resin and 1 *M* perchloric acid quantitatively indicated the presence of TaF_4^+ and TaF_5. When combined with the potentiometric data a full sigmoid-shaped formation curve was obtained between the average ligand numbers 4 and 9 suggesting that simple mononuclear species outside these limits were not present. Ranges of values for the stepwise formation constants k_5, k_6, k_7, k_8 and k_9 at 25° were calculated by the ligand number method using a digital computer.

There is considerable qualitative evidence in the literature for the existence of a series of tantalum fluoride complexes of the type $TaF_n^{(5-n)}$ but no studies have described the stepwise formation of these complexes and their simultaneous existence at equilibrium. Solvent extraction distribution data,[4] chromatography on cellulose,[5] anion-exchange distribution,[6] X-ray studies on crystals,[7] and tantalum electrode potential studies discussed in a paper to follow[8] all suggest unhydrolyzed species of one or more varieties at moderate and high acidities. It was the purpose of this study to establish the acid, metal and fluoride ion concentration ranges in which only unmixed mononuclear tantalum fluoride species existed and to calculate the stepwise formation constants of the system. Methods for determining the mixed hydrolytic polymers of metals in this region of the periodic table are under study and will be presented upon satisfactory completion.

Potentiometric H^+ Ion Measurements. Theory.—Several reviews have appeared in recent years which adequately discuss the general methods for studying complex formation[9] and the compilations of stability constants by Bjerrum, Schwarzenbach and Sillen[10] give numerous references to work in the field. It is found that the question of what species exist in solution cannot be separated from the calculation of the stability constants. When the species have been determined in a logical manner the calculation of the constants is straightforward. The procedure in this investigation was to determine the concentration ranges of metal and hydrogen ion which gave values of 0, 1, 0, respectively, to the parameters p, q, r in the general reaction for complex formation in the tantalum fluoride system

$$rH^+ + q\mathrm{TaV} + p\mathrm{OH}^- + j\mathrm{F}^- = H_r\mathrm{Ta}_q(\mathrm{OH})_pF_j \quad (1)$$

The several concentration formation constants at 25° may be written

$$K_{jpqr} = \frac{(H_r\mathrm{Ta}_q(\mathrm{OH})_pF_j)}{(H^+)^r\,(\mathrm{TaV})^q\,(\mathrm{OH}^-)^p\,(F^-)^j} \quad (2)$$

where j, p, q and r may each have a range of integral values. So that the activity coefficients of all species remained approximately constant over the concentration ranges studied, a constant perchlorate ion concentration of 1 *M* was maintained.

If the total analytical concentrations of metal, C_M, and ligand C_A, are known and allowed to vary independently and if the complex species under investigation are relatively stable, then an independent measurement of the free ligand concentration, (A), allows a complete study to be made of the system. Experimental values of the average ligand number, $\bar{n}$, as defined by Bjerrum[11]

(1) Abstracted in part from the Ph.D. thesis of Louis P. Varga, Oregon State University, June, 1960.

(2) Presented at the Symposium on the Determination of Consecutive Formation Constants, N.W. Regional Meeting Am. Chem. Soc., Richland, Wash., June 17, 1960.

(3) To whom communications should be addressed.

(4) J. R. Werning, K. B. Higbie, J. T. Grace, B. F. Speece and H. L. Gilbert, *Ind. Eng. Chem.*, **46**, 644 (1954); R. A. Foos and H. A. Wilhelm, U.S. Atomic Energy Comm., ISC-694 pp. 31–32 (1954).

(5) F. H. Burstall, *et al.*, *J. Chem. Soc.*, 1497 (1952).

(6) K. A. Kraus and G. E. Moore, *J. Am. Chem. Soc.*, **73**, 13, 2900 (1951); J. P. Faris, *Anal. Chem.*, **32**, 520 (1960).

(7) J. L. Hoard and W. J. Martin, *J. Am. Chem. Soc.*, **61**, 1252 (1939); J. L. Hoard, W. J. Martin, M. E. Smith and J. F. Whitney, *ibid.*, **76**, 3820 (1954).

(8) L. P. Varga and H. Freund, *J. Phys. Chem.*, **66**, 187 (1962).

(9) J. C. Sullivan and J. C. Hindman, *J. Am. Chem. Soc.*, **74**, 6091 (1952); L. G. Sillen, *J. Inorg. & Nuclear Chem.*, **8**, 176 (1958); R. S. Tobias, *J. Chem. Educ.*, **35**, 592 (1958); H. M. N. H. Irving, Chapter in "International Conference on Coördination Chemistry," The Chemical Society, London, 1959 (Special publication no. 13); F. J. C. Rossotti and H. S. Rossotti, "The Determination of Stability Constants," McGraw-Hill Book Co., New York, N. Y., 1961.

(10) J. Bjerrum, G. Schwarzenbach and L. G. Sillen, "Stability Constants," I. Organic ligands, The Chemical Society, London, 1957 (Special publication no. 6); II. Inorganic ligands, 1958 (Special publication no. 7).

(11) J. Bjerrum, "Metal Ammine Formation in Aqueous Solution," P. Haase and son, Copenhagen, 1941.

$$\bar{n} = \frac{C_A - (A)}{C_M} \quad (3)$$

were determined by calculating (A) from potentiometric H^+ ion measurements. The quantity (A) in the hydrofluoric acid system is given by

$$(A) = (F^-) + (HF) + 2(HF_2^-) \quad (4)$$

For the calculation of (A) it was determined first that the value of r in equation 1 was zero. With no weak acids other than HF present the sum of the stoichiometric perchloric and hydrofluoric acid concentrations, C_H, is given by

$$C_H = (H^+) + (HF) + (HF_2^-) \quad (5)$$

The dissociation constants of hydrofluoric acid which Ahrland and co-workers[12] determined at $(ClO_4^-) = 1.0\ M$ are the values used here after correction to 25°

$$K_a = \frac{(H^+)(F^-)}{(HF)} = 1.07 \times 10^{-3} \quad (6)$$

$$K_{a2} = \frac{(HF)(F^-)}{(HF_2^-)} = 0.32 \quad (7)$$

From equations 3, 4, 5, 6 and 7 a close approximation to the fluoride ion concentration is

$$(F^-) = \frac{C_A - \bar{n}C_M}{\frac{(H^+)}{K_a} + 1 + \frac{2}{K_{a2}}[C_H - (H^+)]} \quad (8)$$

which when substituted back into equation 3 and solved for $\bar{n}$ gives this quantity in terms of experimental H^+ ion concentrations and the stoichiometric concentrations of total ligand, metal and acid, C_A, C_M and C_H, respectively,

$$\bar{n}C_M = C_A - \frac{C_H - (H)}{1 - \left(\frac{1 + \frac{[C_H - (H^+)]}{K_{a2}}}{\frac{(H^+)}{K_a} + 1 + \frac{2}{K_{a2}}[C_H - (H^+)]}\right)} \quad (9)$$

Writing C_A and C_M as

$$C_A = (A) + \sum_{j=1}\sum_{p=0}\sum_{q=1} j(Ta_q(OH)_pF_j) \quad (10)$$

$$C_M = (TaV) + \sum_{j=1}\sum_{p=0}\sum_{q=1} q(Ta_q(OH)_pF_j) \quad (11)$$

then from equtions 2, 10 and 11 equation 3 becomes

$$\bar{n} = \frac{\sum_{j=1}\sum_{p=0}\sum_{q=1} j(TaV)^q(OH^-)^p(F^-)^iK_{jpq}}{(TaV) + \sum_{j=1}\sum_{p=0}\sum_{q=1} q(TaV)^q(OH^-)^p(F^-)^iK_{jpq}} \quad (12)$$

Equation 12 indicates a powerful method for studying the complex system. Experimental values for $\bar{n}$ calculated from equation 9, when plotted against free ligand concentration, can be interpreted by equation 12. Perturbations brought about in the formation curve by varying the metal and acid concentrations indicate the dependence of $\bar{n}$ upon metal and acid concentrations. In these studies it was determined from the analyses of 12 formation curves[1] that $p, q = 0, 1$ up to a tantalum concentration of 2.0 mM if C_H/C_M were greater than 150. Under these conditions equation 12 reduced to the familar

$$\bar{n} = \frac{\sum_{j=1} j(F^-)^iK_j}{1 + \sum_{j=1}(F^-)^iK_j} \quad (13)$$

the form used in calculation of the constants of the system.

Experimental

Reagent grade hydrofluoric and perchloric acids were standardized with carbonate-free sodium hydroxide using, respectively, phenolphthalein and α-naphthophthalein indicators. All vessels in contact with fluoride containing solutions during make-up and storage were of polyethylene. Standard solutions of sodium perchlorate were made by neutralizing aliquots of standard perchloric acid with sodium hydroxide to pH 6.8 using a glass electrode.

Potassium heptafluorotantalate, K_2TaF_7, was prepared by the method of Brauer[13] from tantalum metal which contained less than 0.001% Cu, 0.001 to 0.01% Fe, 0.001 to 0.01% Mn, 0.01 to 0.1% Nb, 0.01 to 0.1% Ni, 0.001 to 0.01% Si, 0.001 to 0.01% Ti and 0.001 to 0.01 % V. Analysis of the salt for tantalum by the method of Hague and Machlan[14] and for fluoride by the method of Willard and Winter and Armstrong[15] showed the fluoride:tantalum ratio to be 7.03. For solution make-up purposes the composition of the salt was taken as K_2TaF_7.

Titration vessels were of polyethylene or polystyrene, and the buret used in the titrations was constructed entirely of polystyrene. A bright platinum electrode was used as the quinhydrone indicator electrode. The calomel reference electrode was separated from the titration vessel by a salt bridge containing saturated sodium chloride. Liquid junction between the calomel electrode and the salt bridge was through a half-inch length of Corning no. 7930 porous glass rod. The end of the salt bridge which contacted the fluoride-containing solutions in the titration vessel was constructed of polyethylene with an asbestos fiber wick junction sealed into the polyethylene tubing. The calomel electrode, most of the bridge solution and the titration vessel were kept partly submerged in a water-bath at 25 ± 0.1°.

A Leeds and Northrup type K-2 potentiometer was used with an Eppley standard cell and a General Electric mirror galvanometer with a sensitivity of about 0.001 microampere per mm. of scale division.

For each titration the initial known volume of cell solution contained perchloric acid equal to C_H molar, sufficient sodium perchlorate so that $(ClO_4^-) = 1.0$ molar and was saturated with quinhydrone. Potential measurements of this quinhydrone–calomel cell were taken to establish the initial diffusion potential, E_d, in the absence of hydrofluoric acid and tantalum. Sufficient K_2TaF_7 then was added to the cell solution to bring the total metal concentration to the value C_M molar for the particular run. Potentiometric titration of this cell solution was made using a titrant solution containing hydrofluoric acid and perchloric acid such that the sum of the concentrations was C_H molar. Thus C_H was constant in the solution being measured for the entire course of the titration. The titrant also contained C_M molar K_2TaF_7 to maintain C_M constant during the titration. The perchlorate ion concentration was 1.0 M as in the initial cell solution.

To correct for the change in the diffusion potential as the hydrogen ion concentration changed during the course of a titration, diffusion potential curves were plotted.[1] These plots were obtained from titrations made in the absence of tantalum and HF. Increments of 1 M perchloric acid were added to 1 M sodium perchlorate over the same hydrogen ion concentration range covered in an actual titration. The difference between the hydrogen ion concentration as calculated from the dilution factor assuming volumes were additive and that calculated from the Nernst equation was assigned to the correction term E_d. From the titration data taken on solutions containing hydrofluoric acid and

(12) S. Ahrland, R. Larsson and K. Rosengren, *Acta Chem. Scand.*, **10**, 705 (1956).

(13) G. Brauer (ed.) "Handbuch der praparativen anorganischen Chemie," Ferdinand, Stuttgart, 1954, p. 198.

(14) J. L. Hague and L. A. Machlan, *J. Research Natl. Bur. Standards*, **62**, 53 (1959).

(15) H. H. Willard and O. B. Winter, *Ind. Eng. Chem., Anal. Ed.* **5**, 7 (1933); W. D. Armstrong, *ibid.*, **8**, 384 (1936).

TABLE I

THE DETERMINATION OF $\bar{n}$ AS A FUNCTION OF FLUORIDE ION CONCENTRATION

C_M = total tantalum (V) concn.; C_H = total acid concn.; C_A = total fluoride concn.

C_M mM	0.50					1.00					2.00									
C_H mM	154.7					152					200					350				
C_A, mM	E cell, v.	(H^+), mM	$\bar{n}$	(F^-), mM	C_A, mM	E cell, v.	(H^+), mM	$\bar{n}$	(F^-), mM	C_A, mM	E cell, v.	(H^+), mM	$\bar{n}$	(F^-), mM	C_A, mM	E cell, v.	(H^+), mM	$\bar{n}$	(F^-), mM
0	0.40098	154.7			0	0.36520	151.8			0	0.37364	200.0			0	0.42291	350.0		
23.67	.39714	134.1	5.96	0.164	7.00	.36501	150.7	5.93	0.0075	26.72	.37094	180.6	7.22	0.115	122.6	.41299	244.0	7.99	0.464
29.28	.39594	128.3	5.28	.220	10.70	.36430	146.8	5.72	.0360	32.20	.36992	173.7	5.74	.162	130.7	.41205	235.6	7.77	.519
34.43	.39481	123.0	4.90	.275	17.59	.36299	139.9	5.63	.0907	37.24	.36924	169.3	6.34	.194	138.2	.41118	228.2	7.79	.570
39.19	.39396	119.1	6.57	.319	29.60	.36080	128.8	6.55	.190	41.89	.36854	164.9	6.52	.228	145.3	.41045	222.1	8.26	.615
43.60	.39291	114.5	5.98	.375	44.22	.35774	115.1	7.14	.341	46.20	.36785	160.6	6.54	.262	151.9	.40960	215.3	8.12	.668
47.69	.39201	110.7	6.41	.425	57.59	.35461	102.4	7.60	.515	50.19	.36723	156.9	6.79	.293	158.1	.40882	209.2	8.14	.719
51.50	.39113	107.1	6.68	.475	72.04	.35098	89.35	8.74	.746	53.92	.36657	153.0	6.55	.328	169.6	.40714	196.5	7.44	.833
55.05	.39039	104.1	7.76	.519	82.88	.34763	78.85	8.76	.886	59.05	.36575	148.3	6.93	.372	179.8	.40590	187.7	8.06	.922
58.38	.38948	100.6	7.28	.574	91.31	.34481	70.93	8.96	1.22	63.69	.36499	144.1	7.30	.415	189.0	.40466	179.4	8.40	1.02
61.50	.38873	97.80	7.81	.621	100.4	.34128	62.18	8.84	1.53	69.25	.36393	138.4	7.06	.476	197.3	.40341	171.2	8.38	1.11
64.43	.38800	95.14	8.23	.668	108.2	.33792	54.81	8.77	1.88	74.19	.36301	133.6	7.16	.531	208.4	.40169	160.6	8.51	1.26
67.18	.38720	92.29	7.90	.722	115.4	.33442	48.07	8.67	2.29	78.61	.36217	129.5	7.36	.582	218.2	.40006	151.1	8.50	1.40
72.24	.38584	87.67	8.52	.816						84.43	.36099	123.8	7.41	.657	226.7	.39850	142.6	8.39	1.55
76.76	.38447	83.24	8.44	.916						90.99	.35963	117.5	7.59	.749	236.7	.39643	132.0	7.89	1.76
84.51	.38199	75.75	8.43	1.11						97.71	.35814	111.1	7.74	.853	245.4	.39495	124.9	8.49	1.92
93.72	.37878	67.03	8.63	1.39						104.2	.35658	101.9	7.83	.967	254.6	.39294	115.8	8.36	2.15
101.9	.37551	59.15	8.36	1.72						110.2	.35508	99.27	8.03	1.08	264.0	.39092	107.3	8.57	2.40
109.8	.37201	51.74	8.23	2.11						115.0	.35419	95.58	9.03	1.17	273.1	.38872	98.80	8.54	2.70
114.0	.37000	47.90	8.11	2.37						120.4	.35277	90.58	9.24	1.29	281.6	.38654	90.97	8.58	3.02
128.7	.36209	35.34	8.95	3.57						126.4	.35100	84.68	9.06	1.45	290.3	.38423	83.34	8.72	3.39
132.4	.35971	32.23	8.80	4.01											297.3	.38227	77.36	8.90	3.73
136.8	.35685	28.85	9.22	4.20											305.7	.37962	69.94	8.84	4.23

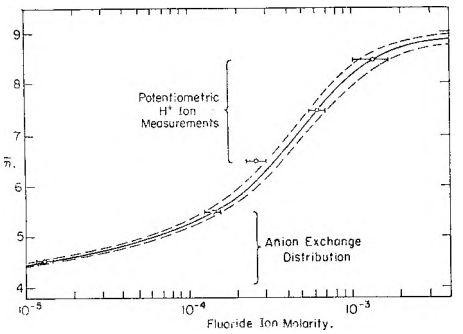

Fig. 1.—The formation curve of the tantalum fluoride system. The experimental fluoride ion concentrations and their standard deviations at half-integral $\bar{n}$'s are given by —o—. The full drawn curve was calculated from the average formation constants and the dashed curves were calculated from the standard deviation limits.

tantalum, corrected values for the hydrogen ion concentrations were calculated.

Results of the Potentiometric Titrations.—Fourteen formation curves which were thought to represent the simple mononuclear tantalum fluoride system were calculated from the titration data by equations 9 and 8. Representative data given in Table I have been presented in full in ref. 1. The molar ratio C_H/C_M ranged from about 151 to 309 in the 14 runs. The average ligand numbers went from about 5.5 to 9 in the fluoride ion concentration range of 1×10^{-5} to 5×10^{-3} M. The fluoride ion concentrations at half-integral $\bar{n}$ values of 6.5, 7.5 and 8.5 which were read from the formation curves plotted in ref. 1 are given in Table II. The mean fluoride ion concentrations for the 14 formation curves at each half-integral $\bar{n}$ value given in Table II are indicated in Fig. 1 along with the standard deviations of the means. As shown below these values were used to determine, in part, the formation constants of the system from equation 13.

It did not appear desirable to use the potentiometric data below $\bar{n} = 6.5$ for quantitative purposes. The decrease of $\bar{n}$ in this region of low excess fluoride ion as the fluoride concentration increased suggested the possibility of hydrolysis occurring even though the free H^+ ion concentrations were at a maximum in this portion of the titration. Release of hydrogen ions by hydrolysis would appear as release of hydrogen ions from HF in the process of complex formation in the theoretical treatment outlined here. In addition, the relative high acidity at the beginning of a titration made small differences in H^+ ion concentrations difficult to measure and the data were scattered. For the low $\bar{n}$ region the distribution of trace levels of anionic tantalum fluoride complexes between molar $HClO_4$ containing known HF concentrations and an anion-exchange resin was used to deduce the formation curve as shown in the next section.

Anion-exchange Distribution. Theory.—In the past, quantitative studies on complex ions using anion-exchange resins usually have employed the ligand form of the anion resin without maintaining a constant ionic strength with $NaClO_4$ or other neutral salt in the outer phase.[16] When trace

TABLE II

FLUORIDE ION CONCENTRATIONS AT HALF-INTEGRAL $\bar{n}$ VALUES

	Fluoride ion molarity		
C_H/C_M	$\bar{n} = 6.5$	$\bar{n} = 7.5$	$\bar{n} = 8.5$
151	2.5×10^{-4}	9.0×10^{-4}	
151	3.5×10^{-4}	10×10^{-4}	
151		2.6×10^{-4}	0.7×10^{-3}
151		5.1×10^{-4}	
152	1.8×10^{-4}	4.75×10^{-4}	0.7×10^{-3}
152	1.45×10^{-4}	6.25×10^{-4}	
152		5.1×10^{-4}	
152		5.6×10^{-4}	
175			2.6×10^{-3}
200	2.5×10^{-4}	7.0×10^{-4}	1.15×10^{-3}
200	2.5×10^{-4}	7.0×10^{-4}	
200		6.4×10^{-4}	
250			2.15×10^{-3}
309	4.45×10^{-4}	6.0×10^{-4}	0.8×10^{-3}
Means	2.67×10^{-4}	6.23×10^{-4}	1.35×10^{-3}
Stand. dev. of means	$\pm 0.38 \times 10^{-4}$	$\pm 0.56 \times 10^{-4}$	$\pm 0.34 \times 10^{-3}$

metal concentrations were used so that low loading of the resin was maintained, the concentration of the ligand in the resin phase remained constant at the exchange capacity of the resin. The resin phase activity coefficients could be assumed constant over the ligand concentration range studied or a small correction determined. When strong complexes were under study it was assumed usually that the outer phase activity coefficients were constant over the small ligand concentration range required to study the system. Distribution studies under such conditions allowed quantitative calculation of the stability constants of the system. It is interesting to note that distribution data may be interpreted easily when the ligand form of the resin is used even if more than one anionic species simultaneously sorb on the resin. When relatively weak complexes were under study, however, the required large variation of ligand concentration in the outer phase necessitated, for quantitative work, extensive and sometimes unreliable determinations of outer phase activity coefficients.

The conditions whereby the neutral salt form of an anion-exchange resin may be used to study complex systems quantitatively when a high constant neutral salt concentration was maintained in the outer phase have not been defined previously. It will be shown below that for systems of strong complexes where only one anionic species is sorbed by the resin over a given ligand concentration range the distribution data may be used to calculate the formation constants of the complex species in the outer phase. These constants, valid for the solution medium used, are comparable then with those obtained by other methods in this medium. At radioactive trace concentrations of tantalum in 1 M perchloric acid polynuclear and hydrolytic species were assumed absent. By comparison with the acid and metal concentrations considered adequate in the potentiometric studies, this assumption appeared justified.

For the case of a positive metal ion M of charge m and a negative monovalent ligand A, the expression

(16) K. A. Kraus and F. Nelson, "Proc. Intern. Conf. Peaceful Uses Atomic Energy," Vol. 7, Geneva, 1956, p. 113, 131; S. Fronaeus, *Svensk Kem. Tidskr.*, **65**, 1 (1953); V. V. Fomin and V. V. Sinkovskii, *Zhur. Neorg. Khim.*, **1**, 2316 (1956) (U. S. Atomic Energy Comm. Transl. no. 3212); Y. Marcus, *J. Inorg. & Nuclear Chem.*, **12**, 287 (1960).

for the anion-exchange equilibrium based on the law of mass action may be written

$$(j - m)\,\mathrm{RClO_4} + \mathrm{MA}_j = \mathrm{RMA}_j + (j - m)\mathrm{ClO_4^-}, \qquad j > m \quad (14)$$

for the case where the perchlorate form of the resin is used. The resin is designated by R and j is the generalized ligand number of the complex. The concentration equilibrium constant for exchange is

$$L_j = \frac{(\mathrm{RMA}_j)\,(\mathrm{ClO_4^-})^{j-m}}{(\mathrm{RClO_4})^{j-m}\,(\mathrm{MA}_j)} \quad (15)$$

and the concentration formation constant of the j complex in the solution phase, K_j, is

$$K_j = \frac{(\mathrm{MA}_j)}{(\mathrm{M})\,(\mathrm{A})^j} \quad (16)$$

At constant perchlorate concentration in the outer phase, low loading of the resin by the complex species and by the ligand, consideration of equations 11, 15 and 16 shows that the distribution ratio, ϕ, of the metal species between the resin and solution phase is

$$\phi = \frac{\sum_{j>m} L_j^*\,(\mathrm{A})^j}{1 + \sum_{j=1} K_j(\mathrm{A})^j} \quad (17)$$

for the case where more than one complex species is sorbed by the resin. The constant L_j^* in equation 17 represents the term

$$L_j^* = L_j K_j \frac{(\mathrm{RClO_4})^{j-m}}{(\mathrm{ClO_4^-})^{j-m}} \quad (18)$$

Equation 17 is considerably complicated by the dependence of ϕ on a different combined exchange equilibrium constant for each species sorbed by the resin. If the special case of only one complex species being sorbed is considered, the summation sign in the numerator of equation 17 may be omitted. Then differentiation of ϕ with respect to (A) and substitution of the expression for $\bar{n}$ from equation 13 gives

$$\bar{n} = j - \frac{\mathrm{d}\log\phi}{\mathrm{d}\log(\mathrm{A})} \quad (19)$$

This relation was given by Bjerrum[11] for the degree of formation function and has been used in various partition studies. If the value of j is known, the ligand number of the species actually sorbed by the resin, equation 19 may be used to derive the formation curve of a system from the slopes of the log ϕ *vs.* log (A) plot. Since in the case of tantalum the ligand number for the neutral species was known to be 5, measurement of the first significant uptake of the metal complex species by the anion resin from low ligand concentrations to higher concentrations may be interpreted in terms of $j = m + 1 = 6$.

Experimental

The anion-exchange resin used was Bio-Rad Laboratories AR grade Dowex 1 × 8, 100–200 mesh, Cl^- form, capacity 3.2 meq. per dry gram. Batches of resin were prepared by repeated washing with 1 *M* perchloric acid until no chloride test was obtained with dilute silver nitrate. The resin then was washed thoroughly with distilled water and dried at 85° for 12 hours.

Radioactive Ta-182 produced at Oak Ridge National Laboratory was received in the form of tantalate in 1.4 *N* KOH solution. The solution concentration was 0.435 mg. Ta per ml. and the specific activity was 7494 mc. per gram. About 60 days elapsed from the assay date to date of first use to allow for decay of the 5.2 day Ta-183. The isotope was characterized by β-absorption and decay measurements using standard techniques. Due to the appearance of some solids in the Oak Ridge tantalate solution, the solution, which was about 1 ml. in volume, was treated with 1.0 ml. of standard 9.91 *M* HF. Effervescence occurred, undoubtedly due to carbonates, leaving a clear solution. From 25 to 40 microliters of this solution was used in each equilibration mixture.

Reagent grade hydrofluoric and perchloric acids were used for solution make-up. The perchloric acid was standardized against sodium hydroxide and solutions containing fluoride were standardized against thorium nitrate.[1] The total HF concentrations of the various solutions used are listed in Table III. The final perchloric acid concentration of all solutions was 1.0 *M*.

TABLE III

ANION EXCHANGE DISTRIBUTION AS A FUNCTION OF FLUORIDE ION CONCENTRATION

All solutions were 1.0 molar in perchloric acid

$(HF)_{stoic.}$, *M*	E_{cell} (H_2–*N* cal.), v	(H^+), *M*	Log (F^-)	Log ϕ
0.0184	...	(1.0)	−4.706	−0.0542
.0290	...	(1.0)	−4.509	.1193
.0396	...	(1.0)	−4.374	.2263
.0715	...	(1.0)	−4.117	.4814
.1141	...	(1.0)	−3.914	.5418
.211	0.3076	1.0	−3.648	.683
.211	...	(1.0)	−3.627	.8102
.396	.3048	1.0	−3.375	.736
.409	.3068	1.0	−3.361	.771
.694	...	(1.02)	−3.140	.753
.694	.3064	1.02	−3.140	.735
.707	.3067	1.01	−3.128	.709
.991	...	(1.08)	−3.011	.725
.991	.3043	1.11	−3.023	.800
1.004	.3059	1.04	−2.989	.644
1.995	.3025	1.19	−2.752	.616
1.98	.3011	1.15	−2.742	.637
1.98	.3014	1.24	−2.772	.737
1.98	.3014	1.24	−2.772	.615
		(Quin–satd. cal.)		
0.0178	0.45138	1.00	−4.721	−0.1896
.0326	.45131	1.00	−4.458	.0445
.0656	.45283	1.06	−4.180	.5328
.1483	.45152	1.01	−3.805	.6717

All of the anion-exchange equilibrations were made with 0.100 g. of the Dowex 1 resin and 15 ml. of solution. The equilibrations were carried out by stirring the solution and resin mixtures in polyethylene centrifuge tubes while immersed in a water-bath at 25° except for the last four equilibrations, which were made by shaking the mixtures in 50-ml. polyethylene bottles. Contact times were mostly in the range of 3 to 4 hours but were nearly 4 days for the last four equilibrations without appreciable difference in uptake noted, so that 3 hours was assumed to be sufficient contact time.

After equilibration the resin–solution mixtures were centrifuged, the solution decanted off and saved for assay, and then the resin was washed rapidly into a filter crucible and repeatedly washed with small portions of distilled water. The resin then was air dried and transferred to tared stainless steel cups in preparation for radioactive assay. The resin samples were weighed and the resin count rate then was corrected to 0.100 g. of resin. Assay of the solutions was made by counting 0.100-ml. aliquots of the solutions on copper planchets after drying under a heat lamp. Duplicate planchets were prepared from each solution assayed.

A Tracerlab G.M. tube type TGC-2 was used for the radioactivity measurements. The detector was used with an Atomic Instrument Co. "Multiscaler" model 105. Counting times varied considerably but the total count

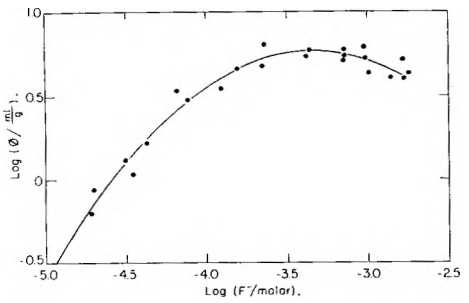

Fig. 2.—The anion-exchange distribution of tantalum fluoride complexes. ϕ = counts per min. per g. resin/counts per min. per ml. solution. The curve follows the least squares equation $\log \phi = -4.6021 - 3.2244 \log(F^-) - 0.4837 \log(F^-)^2$.

taken on the planchets, when feasible, was kept above 10,000 to reduce the random counting error below 1%. Duplicate counts were taken in some cases to improve reliability.

The count rates (see ref. 1) were corrected for background, for daily randomness by a RaD-E reference standard and for radioactive decay. Dead-time corrections were made on all count rates above 10,000 counts/min. Since count rates for resin and solution were in units of c./m. per 0.1 g. and c./m. per 0.1 ml., respectively, the ratio of experimental resin activity to solution activity gave ϕ directly in units of ml./g. in Table III.

Hydrogen ion concentrations were obtained from hydrogen electrode–N calomel electrode potential measurements on most of the solutions after equilibration and from quinhydrone–satd. calomel measurements on the last four solutions. From the stoichiometric HF concentrations and the experimental H^+ ion concentrations, fluoride ion concentrations of Table III were calculated by the relation

$$(F^-) = \frac{(HF)_{stoic.}}{\frac{(H^+)}{K_a} + 1 + \frac{2}{K_{a2}}(HF)_{stoic.}} \qquad (20)$$

Results of the Anion-exchange Studies.—The logarithms of the distribution ratios and fluoride ion concentrations, log ϕ and log (F^-), of Table III were plotted in Fig. 2. A least squares analysis of the data gave the equation for the curve drawn in Fig. 2

$$\log \phi = -4.6021 - 3.2244 \log (F^-) - 0.4837 \log (F^-)^2 \qquad (21)$$

Differentiation of equation 21 with respect to log (F^-) gives

$$\frac{d \log \phi}{d \log (F^-)} = -3.2244 - 0.9674 \log (F^-) \qquad (22)$$

from which the value of log (F^-) at any value of $\bar{n}$ may be calculated from equation 19. Accordingly, log $(F^-) = -4.88$ and -3.85 when d log ϕ/d log (F^-) is 1.5 and 0.5, respectively. Therefore, (F^-) was found to be 1.32×10^{-5} and 1.41×10^{-4} M when $\bar{n} = 4.5$ and 5.5, respectively, assuming that $j = 6$. These values are shown in Fig. 1 and they will be combined with the potentiometric data to calculate several constants of the system. If TaF_6^- is being sorbed in the range where $\bar{n} = 5$, then the presence of TaF_4 must be inferred in this region also. For quantitative interpretation of the anion-exchange data the assumption was made that only TaF_6^- was exchanged by the resin in appreciable concentration up to $\bar{n} = 5.5$, where the slope of the curve of Fig. 2 is 0.5. At higher fluoride ion concentrations, the potentiometric (H^+) studies indicate that the concentration of TaF_7^{--} would rise gradually.

The maximum in the distribution ratio shown in Fig. 2 suggests that the resin was showing some selectivity to an anionic species of low charge. Resin selectivity may be related to ionic radii considerations and by Donnan membrane equilibria to resin and solution phase activity coefficients[17] in effect in the 1 M perchlorate medium used in these studies.

Results of the Combined Data.—The fluoride ion concentrations at half-integral $\bar{n}$ values from the potentiometric and anion-exchange distribution studies are given in Table IV. The data of Table IV are plotted in Fig. 1 and the standard deviation

TABLE IV

FLUORIDE ION CONCENTRATIONS AT HALF-INTEGRAL $\bar{n}$ VALUES

Source	$\bar{n}$	(F^-), M	Standard deviation Absolute	%
Anion ex.	4.5	1.32×10^{-5}	0.12×10^{-6}	9.1
Anion ex.	5.5	1.41×10^{-4}	$.13 \times 10^{-4}$	9.2
Potentiometric	6.5	2.67×10^{-4}	$.38 \times 10^{-4}$	14.2
Potentiometric	7.5	6.23×10^{-4}	$.56 \times 10^{-4}$	9.0
Potentiometric	8.5	1.35×10^{-3}	$.34 \times 10^{-3}$	25

limits of the experimental fluoride ion concentrations are indicated. These results were found for molar ratios C_H/C_M greater than 150 from the potentiometric data and for trace tantalum concentrations in 1 M perchloric acid from the anion-exchange data.

Calculations.—On the basis of the species TaF_4^+, TaF_5, TaF_6^-, TaF_7^{--}, TaF_8^{---} and TaF_9^{----} only existing at equilibrium in the concentration range studied in this investigation we may define the over-all formation constant as

$$TaF_4^+ + F^- = TaF_5,\ \beta_5 = k_5 = \frac{(TaF_5)}{(TaF_4^+)(F^-)}$$

$$TaF_4^+ + 2F^- = TaF_6^-,\ \beta_6 = \frac{(TaF_6^-)}{(TaF_4^+)(F^-)^2}$$

$$TaF_4^+ + 3F^- = TaF_7^{--},\ \beta_7 = \frac{(TaF_7^{--})}{(TaF_4^+)(F^-)^3} \qquad (23)$$

$$TaF_4^+ + 4F^- = TaF_8^{---},\ \beta_8 = \frac{(TaF_8^{---})}{(TaF_4^+)(F^-)^4}$$

$$TaF_4^+ + 5F^- = TaF_9^{----},\ \beta_9 = \frac{(TaF^{----})}{(TaF_4^+)(F^-)^5}$$

The average ligand number becomes from equation 12

$$\bar{n} = \frac{4(TaF_4) + 5(TaF_5) + 6(TaF_6) + 7(TaF_7) + 8(TaF_8) + 9(TaF_9)}{(TaF_4) + (TaF_5) + (TaF_6) + (TaF_7) + (TaF_8) + (TaF_9)} \qquad (24)$$

From equation 13 this may be rearranged to

$$\beta_5(5-\bar{n})(F^-) + \beta_6(6-\bar{n})(F^-)^2 + \beta_7(7-\bar{n})(F^-)^3 + \beta_8(8-\bar{n})(F^-)^4 + \beta_9(9-\bar{n})(F^-)^5 = \bar{n} - 4 \qquad (25)$$

in terms of the over-all formation constants β_j from the equations of (23).

As suggested by Sullivan and Hindman[9] the simultaneous equations of the form of equation 25 were solved by taking (F^-) values at half-integral values of $\bar{n}$. An ALWAC III-E electronic digital computer was used to make the required calcula-

(17) J. E. Salmon, *Rev. Pure and Appl. Chem. (Australia)*, **6**, 25 (1956).

tions in the series of 5 × 5 determinants which were programed. Substituting the data of Table IV into the matrix for equation 25, it was found that positive constants were obtained only when the fluoride ion concentrations were adjusted to give a smooth sigmoid curve between $\bar{n}$ values of 4 and 9. The experimental values of the fluoride ion concentrations for $\bar{n}$ = 4.5, 5.5, 7.5 and 8.5 were held fixed in these calculations. A smooth curve could be drawn through these points as may be seen on inspection of Fig. 1. By iteration procedures the fluoride ion concentration range at $\bar{n}$ = 6.5 which gave positive formation constants was found to be $(3.52 \pm 0.32) \times 10^{-4}$ *M*. Solution of the system using this value at $\bar{n}$ = 6.5 yielded the following average values of the over-all formation constants: $\beta_5 = 6.47 \times 10^4$, $\beta_6 = 2.67 \times 10^8$, $\beta_7 = 5.86 \times 10^{11}$, $\beta_8 = 5.50 \times 10^{14}$ and $\beta_9 = 2.05 \times 10^{18}$. These constants were used to calculate the relative concentrations of the individual species as shown in Fig. 3. The over-all formation constants at the ± limits of the fluoride ion concentrations were calculated similarly to give the standard deviation range of the constants.

From the relations $k_5 = \beta_5$, $k_5k_6 = \beta_6$, $k_5k_6k_7 = \beta_7$, $k_5k_6k_7k_8 = \beta_8$ and $k_5k_6k_7k_8k_9 = \beta_9$ the stepwise formation constants of tantalum fluoride were calculated from the over-all formation constants shown above. These stepwise constants, shown in Table V, apply to a 1 molar perchlorate ion medium at 25°.

TABLE V

THE STEPWISE FORMATION CONSTANTS OF THE TANTALUM FLUORIDE SYSTEM

	Average	One standard deviation limit[a]
k_5	6.47×10^4	$(5.7$ to $7.3) \times 10^4$
k_6	4.13×10^3	$(3.7$ to $4.9) \times 10^3$
k_7	2.20×10^3	$(0.64$ to $4.1) \times 10^3$
k_8	9.39×10^2	10^2 to 5×10^3
k_9	3.73×10^3	10^3 to 4×10^4

[a] One standard deviation of the measured fluoride ion concentrations.

Discussion

Inspection of Fig. 1 shows that the formation function of the simple mononuclear tantalum fluoride complexes exhibits a full sigmoid shaped curve between the average ligand numbers of 4 and 9. These results indicate strongly that fluoride ligand numbers below 4 will not be found in the unmixed fluoride complexes because of the increased ability of OH^- to compete with F^- in complex formation when the fluoride ion concentration becomes small.

Ligand numbers above 9 are unlikely because of radius ratio considerations. Pauling[18] gives the minimum radius ratio for stability of the polyhedron of coördination number 9 as 0.732. This compares with 0.643 for the radius ratio of TaF_8^{---} from the X-ray data of Hoard.[7] In a crystal such as K_2SiF_6 illustrated by Pauling[18], each K^+ ion is surrounded by twelve F^- ions and the ability of the K^+ ions to attract F^- ions away from Si^{+4} is severely limited. It is reasonable to assume that in aqueous solutions containing *M* sodium perchlorate

(18) L. Pauling, "The Nature of the Chemical Bond," Cornell Univ. Press, Ithaca, N. Y., 1948, p. 382.

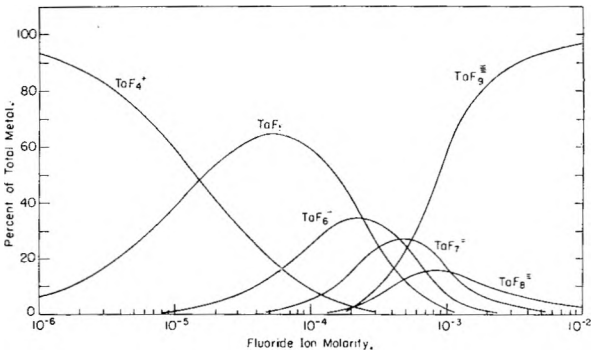

Fig. 3.—The distribution of tantalum between the various complexes as a function of fluoride ion concentration.

anionic species are enlarged compared to the species in a crystal. This may take place by competitive attraction of the fluoride ions of the complex by sodium ions and by the positive dipoles of the water molecules. In a comparable case[19] a decrease in the stability of the cadmium chloride complexes as the salt medium was changed from RbCl to LiCl showed that the stronger the electrostatic field of the cation, the more it weakened and so lengthened the bond between the central and coördinating ions. If the TaF_9^{----} ion indicated in these studies actually exits it may be assumed to have a radius ratio of at least 0.732, which is required for stability of the group. Confirmatory evidence for the existence of TaF_9^{----} from tantalum electrode potential measurements is given in a following paper.[8] Solvent extraction studies to be presented at a later date should give further information on this point.

The nature of the bonding in complexes of this type has been discussed by Duffey[20] in connection with OsF_9^-. In complexes where the central metal has no unshared electrons, the usual spd hybridization gives a maximum covalence of 9. However, Kimball[21] points out that bonds of this nature may be so ionic that the directed nature of covalent bonds and the covalency rules may not apply.

A distinguishing feature of the tantalum fluoride system, shown clearly in Fig. 3, is the high relative concentration of the solvated neutral TaF_5 species throughout almost the entire fluoride concentration range studied. The high extractability of tantalum from acid fluoride media into organic ketones[4] is due likely to a high relative concentration of this TaF_5 species over a wide acid, metal and fluoride concentration range.

It must be recognized that the method for assigning a measure of confidence to the calculated constants was, of necessity, arbitrary due to the two entirely different types of experiments combined to calculate the one set of results. In addition, the ranges of values given for the calculated constants still are highly dependent on the correctness of the several assumptions made in the treatment of the data. The ranges of values given in

(19) Ya. A. Fialkov and V. B. Spivakovskii, *Russ. J. Inorg. Chem.*, **4**, 675 (1959).

(20) G. H. Duffey, *J. Chem. Phys.*, **19**, 553 (1951).

(21) G. E. Kimball, *ibid.*, **8**, 188 (1940).

Table V for the stepwise formation constants appear large but they only reflect the extreme sensitivity of polynomials such as equation 25 to small changes in the experimental ligand concentration. In terms of the formation function the range of constants listed describes the complex system over a quite narrow band indicated by the pair of broken lines in Fig. 1.

Acknowledgments.—This work was made possible through a fellowship authorized in a cooperative agreement between the U.S. Bureau of Mines, Albany, Oregon and Oregon State University.

Assisting in some of the analyses were Howard F. Griffin and personnel of the spectrographic laboratory at the Bureau of Mines. Assistance in the statistical treatment of data was given by Dr. R. G. Petersen of Oregon State University and computer programing assistance was given by Robert N. Brenne. Research paper No. 412, Oregon State University, School of Science, Department of Chemistry.

THE BISMUTH–BISMUTH TRIBROMIDE AND BISMUTH–BISMUTH TRIIODIDE SYSTEMS[1]

BY S. J. YOSIM, L. D. RANSOM, R. A. SALLACH AND L. E. TOPOL

Atomics International, A Division of North American Aviation, Inc., Canoga Park, California

Received June 3, 1961

The phase diagrams of the Bi–$BiBr_3$ and Bi–BiI_3 systems have been determined. The experimental techniques included sampling at temperature, visual observations, conventional thermal analyses and differential thermal analyses. The consolute temperatures (538° at 62 mole % Bi and 458° at 78 mole % Bi for the $BiBr_3$ and BiI_3 systems, respectively) are considerably lower than that of the $BiCl_3$ system (780° at 51 mole % Bi). The freezing point depressions of the metal-rich and salt-rich regions were analyzed. The salts dissolved in molten bismuth were found to have a cryoscopic number of 3. As in the $BiCl_3$ case, this effect can be explained by dissociation of BiX_3 solute or by reaction of BiX_3 with Bi to form the monohalide. In the case of the salt-rich regions the data did not fit a curve corresponding to one single mechanism over the entire liquidus.

Introduction

In a previous report[2] the phase diagram of the Bi–$BiCl_3$ system was described. A retrograde solubility was found, and the two components became completely miscible at 780°. In order to see the effect of varying the anion on the miscibility gap, the liquid–liquid regions of the Bi–$BiBr_3$ and the Bi–BiI_3 systems were determined. Since there are considerable discrepancies in the liquid–solid portions of the phase diagram of the Bi–$BiBr_3$ system[3–5] and the Bi–BiI_3 system,[6–8] these regions were investigated also. Finally, the freezing point depressions of the bismuth trihalide by bismuth and those of bismuth metal by the salts were examined in order to see what could be learned about the species in these solutions.

Experimental

Materials.—The purification of bismuth is described elsewhere.[2] Bismuth tribromide and bismuth triiodide were synthesized by direct combination of the elements. In the $BiBr_3$ case, the molten bismuth was exposed to bromine vapor supplied by a bromine reservoir. The starting materials were contained in a sealed, evacuated Vycor system. In the case of the iodide, finely ground bismuth metal was intimately mixed with a slight excess of iodine and the mixture was heated in a sealed, evacuated Pyrex tube at 175° for 24 hr. Both salts were sublimed under reduced pressure after the excess halogen was removed from them. The melting points of the bromide and iodide were 218.5 and 407.7°, respectively. Chemical analysis of the bromide showed a 46.5 wt. % bismuth as compared to 46.57% theoretical, while that of the iodide showed a 35.9 wt. % bismuth as compared to 35.44% theoretical.

Experimental Methods and Procedure.—The techniques used in this work have been described previously.[2,9] The miscibility gaps were studied by decanting the salt-rich phase at temperature, by differential thermal analyses and by the visual method. The solid–liquid equilibrium curve between the salt-rich eutectic and the base of the miscibility gap in the Bi–$BiBr_3$ case was determined by decantation. All other transitions involving the solid phases were determined by conventional thermal analysis or by differential thermal analysis.

Results

(A) The Bi–$BiBr_3$ System.—The phase diagram of the Bi–$BiBr_3$ system under its own pressure is shown in Fig. 1. The consolute temperature was found to be 538°, considerably lower than that of the Bi–$BiCl_3$ system (780°). A plot of the mean values of the bismuth metal compositions of the two conjugate solutions *vs.* temperature was linear and the composition corresponding to the consolute temperature was 62 mole % Bi. Just as in the Bi–$BiCl_3$ case,[2] a retrograde solubility was observed in the salt-rich region (from 57 mole % at 294° to 45% at 430°) while the solubility of the salt in the metal continues to increase with increasing temperature.

The results of the liqiud–solid portion of the system are compared in Table I with the results re-

(1) This work was supported by the Research Division of the U. S. Atomic Energy Commission. It has been presented in part before the Division of Physical Chemistry at the National Meeting of the A.C.S. in New York, September, 1960.

(2) S. J. Yosim, A. J. Darnell, W. G. Gehman and S. W. Mayer, *J. Phys. Chem.*, **63**, 230 (1959).

(3) B. G. Eggink, *Z. physik. Chem.*, **64**, 449 (1908).

(4) L. Marino and R. Becarelli, *Atti accad. naz. Lincei*, **24**, 625 (1915); **25**, 105 (1916); **25**, 171 (1916).

(5) G. G. Urazov and M. A. Sokolova, *Akad. Nauk S.S.S.R., Inst. Gen. Inorg. Chem.*, **24**, 151 (1954).

(6) L. Marino and R. Becarelli, *Atti accad. naz. Lincei*, **21**, 695 (1912).

(7) H. S. van Klooster, *Z. uanorg. allgem. Chem.*, **80**, 104 (1913).

(8) G. G. Urazov and M. A. Sokolova, *Akad. Nauk S.S.S.R., Inst. Gen. Inorg. Chem.*, **25**, 117 (1954).

(9) L. E. Topol and A. L. Landis, *J. Am. Chem. Soc.*, **82**, 6291 (1960).

TABLE I

COMPARISON OF RESULTS FOR Bi–$BiBr_3$ SYSTEM

	This work		Eggink[3]		Urazov and Sokolova[5]		Marino and Becarelli[4]	
	Mole % Bi	Temp., °C.	Mole % Bi	Temp., °C.	Mole % Bi	Temp., °C.	Mole % Bi	Temp., °C.
1. Melting point								
(a) $BiBr_3$	0.0	218.5	0.0	217.5	0.0	217	0.0	210
(b) Bi	100.0	272.0	100.0	271.5	100.0	272	100.0	272
2. Eutectics								
(a) Salt-rich	21.0	205.0	22.2	204.0	33.0	200	29.2	200
(b) Metal-rich	98.7	263.0	99	262.0	99	255	95	250
3. Base of miscibility gap	57.4–98.0	294.0	46–96	287.0	38–99	262	...	305

TABLE II

COMPARISON OF RESULTS FOR Bi–BiI_3 SYSTEM

	This work		Urazov and Sokolova[8]		van Klooster[7]		Marino and Becarelli[6]	
	Mole % Bi	Temp., °C.	Mole % Bi	Temp., °C.	Mole % Bi	Temp., °C.	Mole % Bi	Temp., °C.
1. Melting point								
(a) BiI_3	0	407.7	0	405	0	408	0	412
(b) Bi	100	272	100	272	100	272	100	285
2. Eutectics								
(a) Metal-rich	99.5	270	99.9	266	99	270	99	284
(b) Salt-rich	..	...	42.2	321	....	..	....	..
3. Base of miscibility gap	47.5–99.0	336	46–99	327	46–98	339	59–97	340
4. Disproportionation of solid BiI		298(?)		..		281		..
Phase transformation of BiI		285(?)		281				..

ported by Eggink,[3] Marino and Becarelli,[4] and Urazov and Sokolova.[5] In agreement with Eggink and with Urazov and Sokolova, it is concluded that a solid subhalide exists. Since the general features of the phase diagram of this system are so similar to those of the Bi–$BiCl_3$ system, it is assumed that the composition of subbromide is the same as that of bismuth subchloride, *i.e.*, of the form BiX. This assumption is consistent with the observation that the duration of the syntectic halt was longest with the sample containing 70 mole % Bi. The solid–liquid results reported in this work are in relatively good agreement with those of Eggink but are in poor agreement with those of Urazov and Sokolova and those of Marino and Becarelli. One of the main reasons for this disagreement is the fact that both Urazov and Sokolova and Marino and Becarelli used only thermal analysis to determine the phase diagram. It has been shown, at least in the chloride case,[2] that for the salt-rich subhalide "liquidus" thermal analysis does not yield accurate results—presumably because of the metastable nature of the system. The fact that the bromide system tends to be metastable is shown by the eutectic halts beyond the composition corresponding to BiBr.

(B) **The Bi-BiI_3 System.**—The phase diagram of the Bi–BiI_3 system under its own pressure is shown in Fig. 2. The consolute temperature was found to be 458°, the lowest of any metal–salt system to date. A plot of the mean values of the bismuth metal compositions *vs.* temperature for the liquid–liquid region again was linear, and the composition corresponding to the consolute temperature was 78 mole % Bi. In contrast to the chloride and bromide systems, there does not appear to be any retrograde solubility in this system.

The results of the liquid–solid portion of this system are compared in Table II with the data reported by Marino and Becarelli,[6] van Klooster[7] and Urazov and Sokolova.[8] The results of this work, in general, are in better agreement with those of van Klooster than with those of Marino and Becarelli or

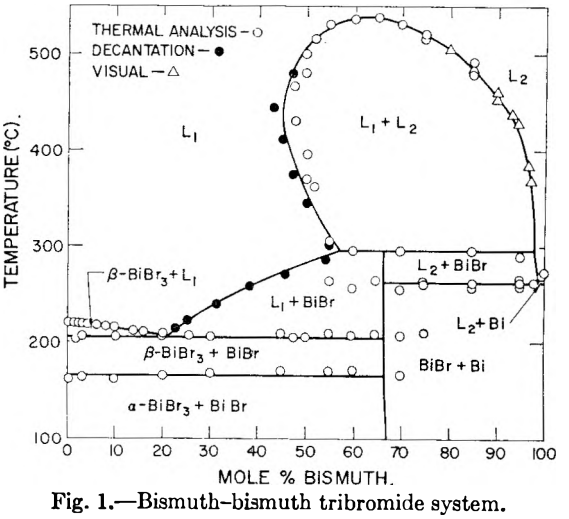

Fig. 1.—Bismuth–bismuth tribromide system.

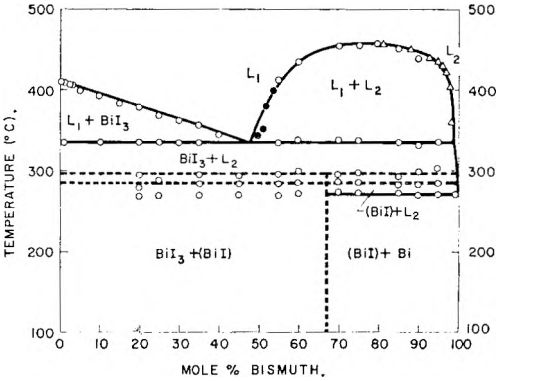

Fig. 2.—Bismuth–bismuth triiodide system: ○, thermal analysis; ●, decantation; △, visual.

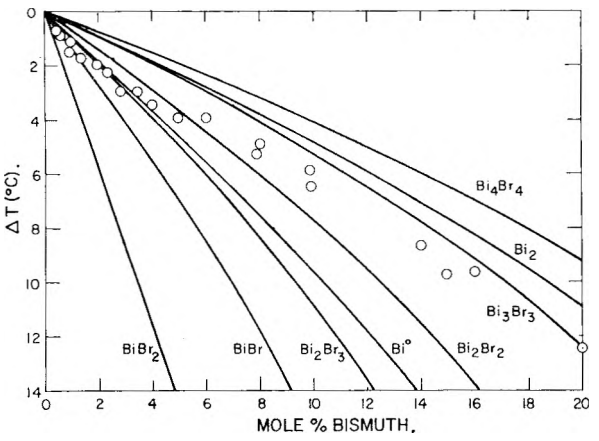

Fig. 3.—Comparison of experimental freezing point depressions of $BiBr_3$ with those calculated for various bismuth species.

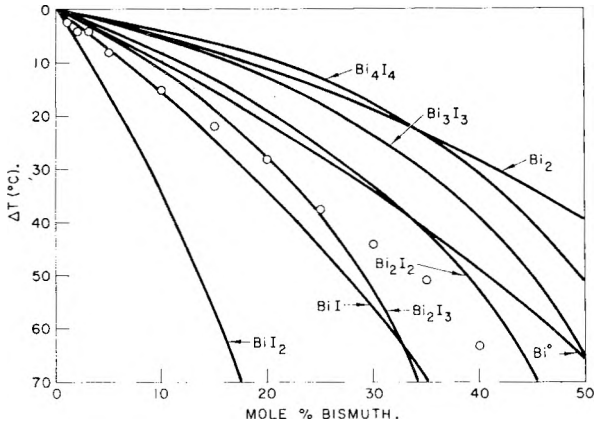

Fig. 4.—Comparison of experimental freezing point depressions of BiI_3 with those calculated for various bismuth species.

Urazov and Sokolova. In addition to the thermal arrests corresponding to the melting points of the components, four thermal halts were found in the liquid–solid region of the phase diagram. These were at 270, 285, 298 and 336°. The halt at 270° corresponds to the metal-rich eutectic. Since the temperature of the base of the miscibility gap is, within experimental error, the same as that of the first halt below the BiI_3 liquidus (336°), it is concluded in agreement with van Klooster that this halt is a monotectic. Thus, in the zone directly below this halt no solid subhalide exists, in contrast to the results of Urazov and Sokolova who found two halts in this temperature region (at 321 and 327°). They concluded, therefore, that a salt-rich eutectic was present and that the subhalide was stable at temperatures up to that of the base of the miscibility gap. Additional evidence for the absence of the subhalide just below the miscibility gap is that a chemical analysis of the upper portion of a 66% bismuth metal sample, quenched from 312°, yielded an I/Bi ratio of 2.95. Also, the duration of the thermal halt at 336° was greatest for samples in the region of the monotectic composition. Thus, this portion of the phase diagram is in contrast to the bromide and chloride cases, where the base of the miscibility gap is a syntectic and the halt below the trihalide liquidus is a eutectic.

The remaining halts at 285 and 298° cannot be unambiguously assigned to definite transitions. Since pure BiI_3 undergoes no phase transition at these temperatures, it is probable that these halts are due to transitions involving an intermediate compound, *i.e.*, a subhalide. At 285°, the durations of the thermal halts were greatest near the composition corresponding to BiI. At 298°, however, the magnitudes of all the halts were too small to permit a corresponding evaluation. In an attempt to confirm the presence of the subhalide, a sample similar to one described in the preceding paragraph was quenched from 219°, and a chemical and X-ray analysis was carried out on the upper layer. The I/Bi ratio was 1.70, which suggested that a subhalide was present; however, the X-ray analysis revealed BiI_3 lines only. Nevertheless, on the basis of the thermal analysis results, it is assumed that a solid subhalide exists. The subhalide is designated in Fig. 2 as BiI although the composition of the subhalide has not been established. If one assumes the existence of the solid subhalide, then the two thermal halts at 285 and 298° suggest that a phase change of the subhalide takes place at the lower temperature and that disproportionation occurs at the higher temperature. More conclusive evidence such as X-ray diffraction measurements of the subhalide taken at temperature would be desirable to test these conclusions further.

Discussion of Results

Considerable doubt as to both the species and the nature of the chemical bonding, particularly at higher temperatures, exists for bromide and iodide as well as chloride solutions containing dissolved bismuth. As in the chloride case, the mechanisms which can be considered for the solution of Bi in $BiBr_3$ and in BiI_3 fall into two classes. The first is solution as Bi atoms, dimers or higher polymers, and the second is solution by reaction of Bi with the trihalide to form a lower-valent compound. In the case of metal-rich solutions, less is known about the species and bonding.

The salt-rich and metal-rich liquidus curves of both the bromide and iodide systems were analyzed as described in the Bi–$BiCl_3$ study[10] in order to see whether information on the mechanism of solution could be obtained. The cryoscopic number n (the number of foreign particles formed in molten bismuth per molecule of solute) was calculated with the Raoult–van't Hoff equation. In both the bromide and iodide systems, as in the $BiCl_3$ case, a cryoscopic number n of 3 was obtained. Thus, the salts do not dissolve in a molecular form. As in the $BiCl_3$ case there are at least 3 mechanisms which would correspond to an n of 3. (1) The BiX_3 dissociates into 4 particles upon dissolving and the bismuth from BiX_3 becomes indistinguishable from the bismuth particles of the molten metal. (2) The BiX_3 reacts with the Bi solvent to form undissociated BiX molecules and (3) the BiX dissociates to yield Bi entities indistinguishable from the bismuth metal particles. Actually the first and third mechanisms cannot be differentiated cryoscopically since the final compositions are identical.

(10) S. W. Mayer, S. J. Yosim and L. E. Topol, *J. Phys. Chem.*, **64**, 238 (1960).

The method for analysis of the salt-rich liquidus is also the same as that described previously,[10] with the exception that the heats of fusion of the salts were not assumed to be independent of temperature. The heats of fusion of $BiBr_3$ and BiI_3 used in the analysis are 5.19[11] and 9.41[12] kcal./mole, respectively, and the ΔCp values are 11.7[11] and 16.0[12] cal./mole-degree, respectively.

The results of the analyses of the salt-rich liquidus curves are shown in Figs. 3–4. Unlike the results of the $BiCl_3$ case, the freezing point depression data do not fit a curve corresponding to one single mechanism over the entire liquidus for either system. This may be due to deviation of the solvent from ideality or to an equilibrium between 2 or more lower-valent bismuth species. Spectrophotometric[13] and e.m.f.[14] studies on the Bi–$BiCl_3$ system have shown that indeed more than one species exists in these solutions. The e.m.f. results suggest that at the melting point of $BiCl_3$, BiCl is the predominate lower-valent Bi species only in very dilute concentrations of dissolved metal (< 0.1 mole %). (Thus, BiCl would not be detected cryoscopically at such low concentrations.)

From an acid–base standpoint, the monomer subhalide should become more stabilized as the acidity of the system increases. Thus, it would be reasonable that the Bi^+ entity becomes increasingly stabilized as one goes from Cl^- to Br^- to I^-. E.m.f.[15] studies have shown that the monomer is indeed more important in the Bi–$BiBr_3$ system than in Bi–$BiCl_3$ melts. The data of Fig. 3 which fit most closely to the BiBr curve at concentrations up to 2 mole % Bi are in accord with this. The data of Fig. 4 suggest that BiI is the most important species up to about 10 mole % Bi. However, while the activities of $BiBr_3$ calculated from the Bi–$BiBr_3$ vapor pressure data[16] are in agreement with those calculated from this work, the activities of BiI_3 calculated from the Bi–BiI_3 vapor pressure results[17] are not, but follow Raoult's law up to about 30 mole % bismuth. If one plots the ideal vapor pressure *vs.* BiI_3 concentration for various species, it can be seen that the experimental pressure data follow much more closely the curves for Bi atoms or for Bi_2I_2 rather than BiI. Further, whereas the solubility of Bi in $BiCl_3$ is increased by the addition of the acid $AlCl_3$,[18] the solubility of Bi in BiI_3 was found to decrease when AlI_3 was added. This would suggest that Bi dissolves in BiI_3 by a mechanism other than subhalide formation, since one would expect the relatively basic subhalide to be stabilized by the acid. Thus, it would appear that the Bi–$BiCl_3$ and Bi–$BiBr_3$ systems are rather similar in nature, but the behavior of the Bi–BiI_3 system is quite different. Perhaps this is not too surprising in view of the greater similarity in physical and chemical properties of pure $BiCl_3$ and $BiBr_3$ (*e.g.*, melting and boiling points and reactivity with water) as compared to pure BiI_3.

(11) L. E. Topol and L. D. Ransom, *J. Phys. Chem.* **64**, 1339 (1960).
(12) M. A. Bredig and A. Dworkin, private communication.
(13) C. R. Boston and G. P. Smith, Annual Progress Report, Metallurgy Division, Oak Ridge National Laboratory, ORNL-2988 p. 9–10 (July 1960).
(14) L. E. Topol, S. J. Yosim and R. A. Osteryoung, *J. Phys. Chem.*, **65**, 1511 (1961).
(15) L. E. Topol and R. A. Osteryoung, "E.M.F., Polarographic & Chronopotentiometric Measurements in Molten Bi–$BiBr_3$ Solutions," to be published.
(16) D. Cubicciotti and F. J. Keneshea, Jr., *J. Phys. Chem.*, **62**, 999 (1958).
(17) D. Cubicciotti and F. J. Keneshea, Jr., *ibid.*, **63**, 295 (1959).
(18) J. D. Corbett and R. E. McMullan, *J. Am. Chem. Soc.*, **78**, 2906 (1956).

INTERCRYSTALLINE ENERGIES IN THE ALKALI HALIDES[1]

By Donald P. Spitzer[2]

Institute for the Study of Metals, The University of Chicago, Chicago 37, Illinois

Received June 5, 1961

Because of the basic importance of intercrystalline energies in determining properties of polycrystalline bodies, relative intercrystalline interfacial energies were determined in many alkali halide systems by measurement of the angles at which intercrystalline boundaries meet one another at equilibrium. The energies of boundaries between two crystals of the same phase were found to vary from 0.2 to 1.3, relative to the NaF intercrystalline energy. The relative energies of boundaries between two dissimilar crystals varied only from 0.7 to 1.0. From the equilibrium angles and the liquid–liquid interfacial energy in the system NaF(solid)–Te(liquid)–CsCl(liquid), the absolute energy of the average NaF grain boundary was determined to be 306 ± 15 ergs/cm.^{2}. Generally, no correlation was found between intercrystalline energies and other basic parameters.

Introduction

The recognition that solid interfaces are not always immobile is fairly recent. Several surface tensions of solid metals have been obtained[3] from the weight on a vertical wire which is necessary to just keep the wire from contracting under the influence of surface tension.

It also has been shown[4] that solid–solid and solid–liquid interfaces may have sufficient mobility to establish equilibrium among their free energies and that the energies are of basic importance in determining the actual distribution of phases and the properties of polycrystalline bodies.

In a polycrystalline solid, the crystals (or grains)

(1) Based on a dissertation submitted to the faculty of the University of Chicago in partial fulfillment of the requirements for the degree of Doctor of Philosophy, December, 1960.
(2) American Cyanamid Company, Stamford, Connecticut.
(3) See, *e.g.*, H. Udin, A. J. Shaler and J. Wulff, *Trans. Am. Inst. Mining Metal. Engrs.*, **186**, 185 (1949); E. R. Hayward and A. P. Greenough, *J. Inst. Metals*, **88**, 217 (1960); A. J. Shaler, "The Mechanical Properties of Crystalline Metal Surfaces," in "Structure and Properties of Solid Surfaces," edited by R. Gomer and C. S. Smith, University of Chicago Press, 1953.
(4) C. S. Smith, *Trans. Am. Inst. Mining Metal Engrs.*, **175**, 15 (1948).

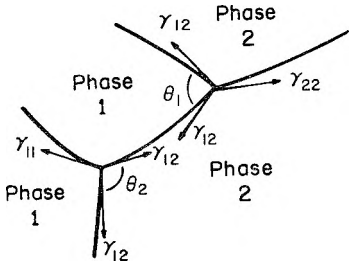

Fig. 1.—Boundary junctions in a binary system.

decrease in number and increase in size as the boundaries between crystals (grain boundaries) change both shape and position, at a rate dependent on the temperature. In the absence of mechanical strains, only the free energy of the boundaries is responsible for their movement and the growth of the grains.

Since three boundaries generally meet one another in a polycrystalline solid, the angle between any two boundaries[5] in a single phase material (where all grain boundary energies are nearly equal[6]) is near to 120° at equilibrium. This was experimentally demonstrated in 1945.[7] In a polyphase polycrystalline solid each type of solid–solid interface present may have a different free energy, but the equilibrium angle between any two types of boundaries is nevertheless constant and reproducible, determined by the free energies of the three interfaces. Measurement of the equilibrium angles at boundary junctions is, in fact a convenient method for the determination of relative free energies of solid–solid interfaces.

In 1929 it was suggested[8] that for each angle of intersection of two crystals, a definite pattern of arrangement of atoms exists, which corresponds to the lowest possible energy in the circumstances. This crystalline nature of small-angle grain boundaries (*i.e.*, where the orientation difference across the boundary is small) is supported by the experiments of Aust and Chalmers[9] and subsequent experiments,[10] and the dislocation model[11,12] seems to provide a realistic picture of a small-angle boundary.

(5) It should be realized that the boundaries we speak of are actually not merely lines, but planes. Hence the angle is an angle between two planes; this angle usually is obtained from measurements on a polycrystalline surface, which is equivalent to measuring angles on random planes through the three dimensional angle. The angles measured on these two dimensional surfaces are statistically related to the true angle, as described later.

(6) We are ignoring possible variation of solid–solid interfacial energies with the orientation difference of the crystals on the two sides of the boundary. C. Herring ("The Use of Classical Macroscopic Concepts in Surface Energy Problems," in "Structure and Properties of Solid Surfaces," University of Chicago Press, 1953, p. 5) treats the general case when there is an effect of the boundary direction on the boundary free energy.

(7) D. Harker and E. Parker, *Trans. Am. Soc. Metals*, **34**, 156 (1945).

(8) F. Hargreaves and R. J. Hills, *J. Inst. Metals*, **41**, 257 (1929).

(9) K. T. Aust and B. Chalmers, *Proc. Roy. Soc.* (London), **201A**, 210 (1950); "Energies and Structure of Grain Boundaries," in "Metal Interfaces," American Society for Metals, Cleveland, 1951, p. 153; *Proc. Roy. Soc.* (London), **204A**, 359 (1950).

(10) Reviewed by F. Weinberg, *Prog. Metal Phys.*, **8**, 105 (1958).

(11) J. M. Burgers, *Proc. Phys. Soc.* (London), **52**, 23 (1940); W. L. Bragg, *ibid.*, **52**, 54 (1940).

(12) W. T. Read and W. Shockley, *Phys. Rev.*, **78**, 275 (1950); "Dislocation Models of Grain Boundaries," in "Imperfections in Nearly Perfect Crystals," John Wiley and Sons, New York, N. Y., 1952, p. 352.

Small-angle boundaries are, however, generally rare in polycrystalline samples with randomly oriented grains. To learn more about the structures and energies of the large-angle boundaries present in ordinary polycrystalline materials, the relative energies of a large number of members of a homologous series of compounds, the alkali halides, were determined by measurement of equilibrium angles at boundary junctions in binary systems.

Relations between Interfacial Energies in Solid and Solid–Liquid Systems.—It is convenient to restrict the term grain boundary to a boundary between two crystals of the same phase and the term interphase boundary to a boundary between two crystals of different phases.

In a two-component polycrystalline solid, the equilibrium dihedral angle between two interphase boundaries, along the line where two interphase boundaries and one grain boundary meet, is determined by the relative energies of the interphase boundary and the grain boundary. The relation between the angle θ_1, the interphase energy γ_{12} and the grain boundary energy γ_{22} (Fig. 1) is obtained by equating the tensions acting along the direction of the grain boundary

$$\gamma_{22} = 2\ \gamma_{12} \cos \theta_1/2 \qquad (1)$$

Hence, when equilibrium is attained between the interfacial energies in a binary polycrystalline system, the relative values of the interphase energy and the two grain boundary energies may be obtained from the measurement of the two dihedral angles.

Equation 1 also is applicable when phase 1 is a liquid. If θ is equal to zero, it can only be said that the solid–liquid interfacial energy is less than or equal to one-half of the grain boundary energy.

In a three-phase solid system there are six different dihedral angles and also junctions of the three interphase boundaries. Three basic relations valid at a three-phase junction (phases 1, 2 and 3) at equilibrium may be obtained from the triangle of forces and the trigonometric formula: $a = b \cos C + c \cos B$, where a, b and c are the sides of the triangle and A, B and C are the angles opposite to these sides. These relations are

$$\gamma_{23} = -\gamma_{13} \cos \theta_3 - \gamma_{12} \cos \theta_2 \qquad (2)$$
$$\gamma_{13} = -\gamma_{12} \cos \theta_1 - \gamma_{23} \cos \theta_3 \qquad (3)$$
$$\gamma_{12} = -\gamma_{13} \cos \theta_1 - \gamma_{23} \cos \theta_3 \qquad (4)$$

In the case where phases 1 and 2 are liquids and and phase 3 is a solid, there is the interesting possibility of determining the absolute value of the grain boundary energy by relating it to the liquid–liquid interfacial energy, which is easy to measure absolutely. This principle was used by Van Vlack.[13] Three relations (equations 7–9) between γ_{33} and γ_{12} (Fig. 2) may be obtained by division of each of the equations 2, 3 and 4 by γ_{23} and use of the relations

$$\gamma_{13}/\gamma_{23} = \sin \theta_2/\sin \theta_1 \qquad (5)$$
$$\gamma_{33} = 2\ \gamma_{13} \cos (\theta_5/2) \qquad (6)$$

and

$$\gamma_{33} = 2\ \gamma_{12} \cos (\theta_5/2)/(-\cos \theta_1 - \sin \theta_1 \cot \theta_2) \qquad (7)$$

(13) L. H. Van Vlack, *Trans. Am. Inst. Mining Metal. Engrs.*, **191**, 251 (1951).

$$\gamma_{33} = -2\,\gamma_{12}\cos\theta_2\cos(\theta_5/2)/\left(\frac{\sin\theta_1}{\sin\theta_2} + \cos\theta_3\right) \quad (8)$$

$$\gamma_{33} = -2\,\gamma_{12}\cos\theta_1\cos(\theta_5/2)/\left(1 + \frac{\sin\theta_1}{\sin\theta_2}\cos\theta_3\right) \quad (9)$$

Three similar relations (equations 10–12, not shown) are obtained from equations 7–9, respectively, by replacing $\sin\theta_2/\sin\theta_1$ by the equivalent $\cos(\theta_4/2)/\cos(\theta_5/2)$. A seventh relation (equation 13) is obtained directly from the triangle of forces at the three-phase junction

$$\gamma_{33} = 2\gamma_{12}\left(\frac{\sin\theta_2}{\sin\theta_3}\right)\cos\left(\frac{\theta_5}{2}\right) \quad (13)$$

Division of equations 2, 3 and 4 by γ_{13} instead of γ_{23} and use of the relation $\gamma_{33} = 2\gamma_{13}\cos(\theta_4/2)$ instead of equation 6 gives seven similar equations (7′ through 13′); these may be obtained from equations 7 through 13 by an interchange of subscripts 4 and 5, and of subscripts 1 and 2.

Experimental

Relative Intercrystalline Energies.—The components of a binary system to be used for dihedral angle measurements must not dissolve in one another extensively and the minimum melting point in the system must be high enough to permit attainment of equilibrium within a reasonable length of time.

Binary systems with limited solid solubility are in general those which form a eutectic. In the case of the alkali halides, NaF and LiF form eutectics with nearly every other alkali halide. Lattice constants in all of the systems studied except the NaF–LiF, NaF–Na halides, NaF–KF and NaF–RbF systems are known[14] and show no detectable solid solubility. In the system LiF–NaF, lattice constants[15] indicate that LiF is soluble in NaF to the extent of about 3 mole % and LiF dissolves about 1.6 mole % of NaF. In the system NaF–KF,[16] KF dissolves in NaF to the extent of 4 mole % and NaF dissolves in KF to the extent of 10 mole %. X-Ray lattice parameters were newly measured for mixtures of NaF and KCl, NaF and KBr, LiF and KCl, and LiF and KBr which had been powdered, compressed into a pellet and heated for five days at 600° (below all of the eutectic melting points) and quenched. No change of lattice parameters indicating solid solubility was found in any of these systems.

The rate of boundary movements in solids is roughly an exponential function of temperature. It was found to be practical to use only those alkali halide systems which had a eutectic melting point of about 550° or higher. Such samples attained equilibrium and a fair grain size (0.02 to 0.05 mm.) within reasonable annealing times (5 to 10 days).

The heats of activation required for grain growth (ΔH) for NaCl and for LiF (analytical reagent grades) were determined from the rate of change in average grain size of pressed compacts as a function of time at three different temperatures, following the method of Burke[17] (with the exceptions that a separate sample was used for each measurement and no preliminary heat treatment was used). ΔH for grain growth was found to be 30 ± 1 and 27 ± 1 kcal./mole for NaCl and for LiF, respectively. The rates of grain growth were much slower in the binary salt systems studied than in binary metal systems, even though the heats of activation for grain growth and for diffusion are of the same order of magnitude as for metals.

The samples used for the dihedral angle measurements generally were prepared from ordinary "analytical reagent" grade salts; a few of the measurements were duplicated, as noted later, with salts of higher purity. Two salts were mixed together and powdered in a mullite mortar to a grain size of about five to ten μ. Deliquescent salts were dried at 120°, both before and after being mixed and powdered. Two mixtures generally were made—90/10 and 10/90 by weight. The powders were pressed in an evacuated stainless steel die, 0.65 cm. in diameter, at a pressure of about 50,000 p.s.i., to form a pellet which then was sealed in an evacuated Vycor tube. The tube usually was heated while being evacuated, to remove water. The fluorides KF, RbF and CsF tended to react with the Vycor tubes and, therefore, samples which contained these salts were placed in graphite thimbles before being sealed in the tubes.

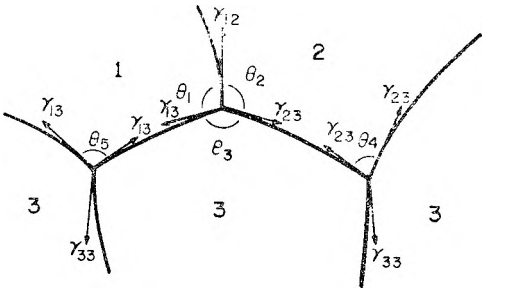

Fig. 2.—Boundary junctions in a three-phase system.

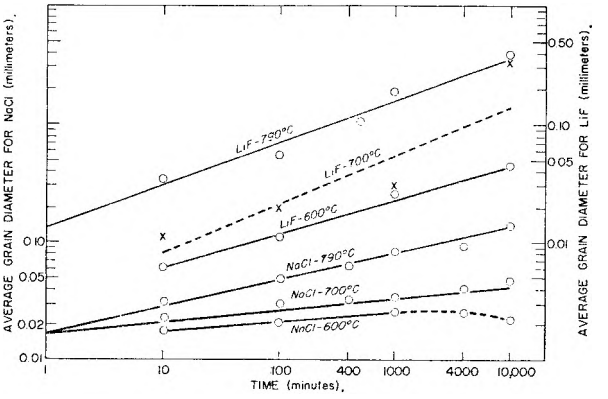

Fig. 3.—Average grain diameters of LiF and NaCl as a function of time at the temperature indicated.

Each sample was annealed in a tube furnace at a temperature below the eutectic melting point (550–650°) for five to ten days. At the end of the annealing period, the sample was cooled to room temperature, usually by quenching in carbon tetrachloride, but sometimes by cooling slowly in the air. The rate of cooling had no detectable influence on the microstructure except in the LiF–NaF system, where a slowly cooled sample showed precipitation of LiF at the NaF grain boundaries.

The annealed pellets were sectioned and polished for microscopic examination. At least one millimeter was ground off one end of the sample, to avoid possible influence of the free surface on the angle statistics, and the surface was polished by methods similar to those used on metals, beginning with graded emery papers. Although no completely satisfactory method of final polishing was found, polishing on a silk-covered lap[18] with alumina as the abrasive and xylene as lubricant gave fair to good polishes, but the results depended greatly on the hardness, solubility and deliquescence of the salts. Absolute alcohol was sometimes a better lubricant than xylene. The deliquescent fluorides were polished in a dry box and kept dry under the microscope by the passage of dry nitrogen through an enclosure around the sample.

With a metallurgical microscope (using normally reflected light) the various components in a sample usually could be distinguished either because of differences in the refractive indexes or because one phase was partly etched away during the polishing.

The usual metallurgical technique used to make boundaries visible is to etch the sample in some solution in which the substance is slightly soluble. This technique worked for single component salt systems, but was not successful in the

(14) E. B. Thomas and L. J. Wood, *J. Am. Chem. Soc.*, **58**, 1341 (1936).

(15) M. K. Slattery, *Proc. Natl. Acad. Sci.*, **14**, 177 (1928).

(16) F. P. Platonov, *Trudy Moskov. Sel'sko-Khoz. Akad. im. K. A. Timeryazeva*, **36**, 42 (1946).

(17) J. E. Burke, *Trans. Am. Inst. Mining Metal. Engrs.*, **180**, 73 (1949).

(18) A standard metallurgical bronze lap, 20.3 cm. in diameter, covered with a silk cloth and motor-driven at 250 r.p.m.

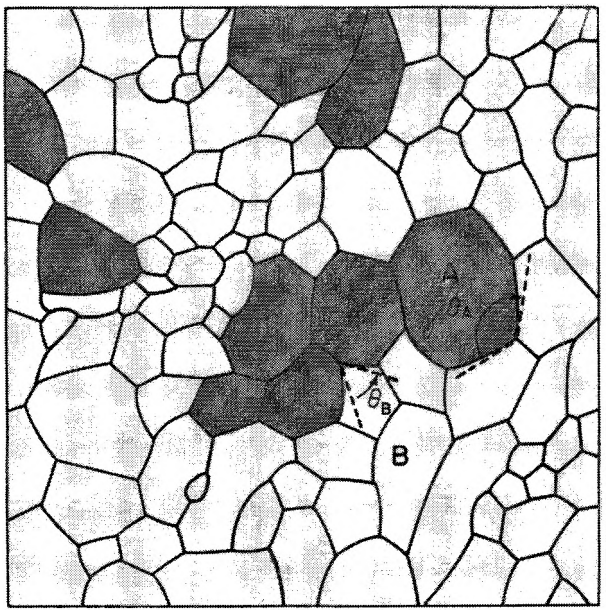

Fig. 4.—Sketch of a binary solid system at equilibrium. θ_A and θ_B are the dihedral angles. About 1000 times actual size.

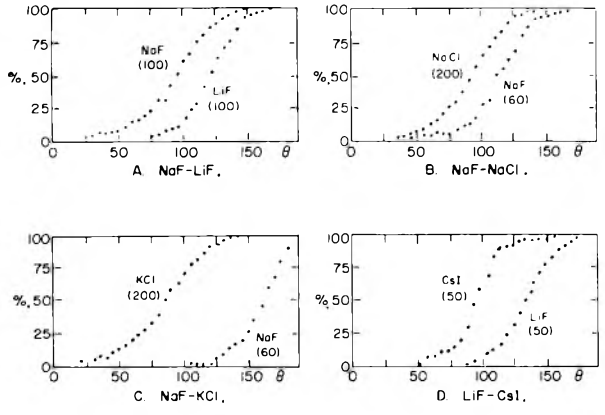

Fig. 5.—Distributions of the angles measured on two-dimensional sections such as shown in Fig. 4. In each graph the ordinate is the percentage of the observed angles which are less than or equal to the angle θ and the abcissa is the angle θ. The angle at the point where a curve crosses the 50% line is the desired true dihedral angle. The curves are labelled with the phase in which the angle was measured (*e.g.*, in A, the curve labelled NaF is for the angle θ_{NaF}). The number in parentheses is the number of observed angles on which the curve is based.

ease of binary systems; because of differences in solubility of the two phases it was not possible to obtain both clear grain boundaries and clear interphase boundaries on any sample either by immersion in various mixtures of water, methanol, ethanol, acetone and saturated solutions of the salts, or by exposure of the sample to the vapors above these mixtures. In a few cases, samples were nicely etched accidentally by the atmospheric moisture. The best etching method, however, was a thermal etching technique. After the surface had been polished, the sample was heated in an open Vycor tube at a temperature of 500–600° for 60–120 sec. This treatment made both grain boundaries and interphase boundaries visible as a narrow groove resulting perhaps from preferential evaporation at the boundaries or perhaps from the establishment of local equilibrium between the intercrystalline energy and the surface energy. A good polished surface before heat treatment was necessary.

Measurements of the dihedral angles were made on the polished and etched surfaces of the specimens at a magnification of 600X or 1400X with a microscope having a rotatable eyepiece containing a reticle with ruled parallel lines and an electrical counting device as described by C. S. Smith.[19]

A maximum error of only one degree is introduced by taking the median observed angle as the true dihedral angle. Using the method of Riegger and Van Vlack,[20] the percentage of observations less than a given angle was plotted as a function of angle in five-degree groups. Fifty observations are sufficient to establish any dihedral angle within five degrees, with a probability of at least 90%. More than fifty observations did not appear to increase the accuracy significantly since the small grain size and the difficulty of judging the position of a tangent to a curved boundary limited the precision of the measurement of individual angles to about five degrees.

For dihedral angles less than about 60°, an error of 5° in the dihedral angle means only a 2–3% error in the interfacial energy ratio (equation 1). At 100°, the error in the ratio due to a 5° error in the dihedral angle has risen to 5%; at 120, 140, 150 and 160°, the error is about 7, 12, 16 and 24%, respectively, and at angles approaching 180°, the error is so great that dihedral angle measurements are valueless. In the present experiments the errors in the interfacial energies are usually 10–15%.

A few characteristic angle–distribution curves are shown in Fig. 5. The interfacial energies obtained from measurements of dihedral angles in binary alkali halide systems are summarized in Table I.

For some of the systems, measurements were made on samples of different composition, samples annealed at different temperatures and for different lengths of time, and samples of different purity.

In the case of the systems LiF–NaF, KCl–NaF, NaF–KBr and NaF–KI, dihedral angle measurements repeated on samples of different percentage compositions were in agreement in every case, within experimental error.

Different annealing times and temperatures produced the same dihedral angles in the systems NaF–LiF, NaF–NaCl, NaF–KF, NaF–KCl and NaF–KI.

Some samples were made from optical quality salts (obtained from Harshaw Chemical Company, Cleveland, Ohio), stated to have impurities of not greater than a few parts per million. Measurements on these salts in the systems NaF–LiF, NaF–NaCl, NaF–KCl, NaF–KBr and NaF–KI were all in agreement with the results of the measurements on the "analytical reagent" grade materials.

From the data in Table I, Table II is constructed, showing the relative grain boundary energies of the alkali halides found by direct comparison to the NaF and LiF grain boundary energies. Similarly, Table III gives the relative energies of the interphase boundaries with NaF and LiF.

Some dihedral angles for liquid phases against the NaF grain boundary are given in Table IV. The temperature of the annealing in each case was 10–25° above the eutectic melting point, so that the liquid present in each sample had a composition near to that of the eutectic, which is shown in Table V.

A Three-Phase Solid System.—A three-phase system provides a convincing proof of equilibrium among solid–solid interfaces (*cf.*, Smith[4]). There are various combinations of angles that permit the same ratio of interface energies to be obtained; some are useless in the particular system used (NaF–LiF–KCl), but measurement of the three angles at the junction of the three interphase boundaries gives ratios of interphase boundary energies which also can be calculated from the six dihedral angles, as a proof of equilibrium. The sample of 40% NaF–30% LiF–30% KCl (by weight) was annealed for seven days at 550°.

The Absolute Energy of the Sodium Fluoride Grain Boundary.—Only a few absolute values of grain boundary energies have been measured,[21] all of metals. The methods of Gjostein and Rhines[22] and of Cohen, Hilliard and Averbach[23] relate the grain boundary energy to the solid surface

(19) C. S. Smith, *Trans. Am. Inst. Mining Metal. Engrs.*, **218**, 58 (1960).

(20) O. K. Riegger and L. H. Van Vlack, *ibid.*, **218**, 933 (1960).

(21) Reviewed by: J. B. Hess, "Measurement of Solid:Solid Interfacial Energies," in "Metal Interfaces," Am. Soc. for Metals, Cleveland, 1952, p. 134; J. W. Taylor, *J. Inst. Metals*, **86**, 456 (1958).

(22) N. A. Gjostein and F. N. Rhines, *Acta Met.*, **7**, 319 (1959).

(23) M. Cohen, J. E. Hilliard and B. L. Averbach, *ibid.*, **8**, 26 (1960).

TABLE I

DIHEDRAL ANGLES AND INTERFACIAL ENERGIES IN BINARY ALKALI HALIDE SYSTEMS

	System[a] A–B	Annealing[b] treatment temp. °C.; time, days	Dihedral angles, degree θ_A	Dihedral angles, degree θ_B	γ_{AB}/γ_{BB}	γ_{AB}/γ_{AA}	γ_{BB}/γ_{AA}	Probable error in γ_{BB}/γ_{AA}
1	NaF–LiF	550–580; 7	95[c]	117.5[c]	0.74	0.96	1.30	0.07
2	NaF–NaCl	500–660; 2–7	112.5[c]	100	0.90	.78	0.87	.05
3	NaF–NaBr	625; 7	135	97.5	1.31	.76	.58	.06
4	NaF–NaI	590; 7	130	95	1.18	.74	.63	.07
5	NaF–KF	600–620; 4–8	122.5	90	1.04	.71	.68	.06
6	NaF–KCl	580–625; 7	162.5	87.5	3.26	.69	.21	.05
7	NaF–KBr	550–625; 7–14	152.5	95	2.11	.74	.35	.06
8	NaF–KI	550; 7–11	130	107.5	1.18	.85	.72	.08
9	NaF–RbF	620; 4	140	100	1.46	.78	.53	.07
10	NaF–RbCl	560; 7	127.5	90	1.13	.71	.63	.06
11	NaF–RbBr	560; 7	150	100	1.93	.78	.40	.06
12	NaF–RbI	560; 7	145	95	1.66	.74	.45	.07
13	LiF–NaCl	600; 7	127.5	97.5	1.13	.76	.67	.07
14	LiF–NaBr	550; 7	137.5	85	1.38	.68	.49	.05
15	LiF–NaI	550; 7	135	95	1.31	.74	.56	.06
16	LiF–KCl	550–650; 5–7	160	82.5	2.88	.67	.23	.06
17	LiF–KBr	550–650; 5–6	152.5	87.5	2.11	.69	.33	.05
18	LiF–KI	550–590; 7–9	135	92.5	1.31	.72	.55	.06
19	LiF–RbCl	550–590; 7	135	92.5	1.31	.72	.55	.06
20	LiF–RbBr	550–590; 7	150	92.5	1.93	.72	.37	.06
21	LiF–CsCl	550; 7	137.5	80	1.38	.65	.47	.05
22	LiF–CsBr	550; 7	125	85	1.08	.68	.63	.06
23	LiF–CsI	550; 7	135	95	1.31	.74	.56	.06
24	NaCl–NaI	550; 7	125	100	1.08	.78	.72	.07
25	NaF–NaCl, Br[d]	550; 8	120	90	1.00	.71	.71	.06
26	NaF–KCl, Br[d]	550; 8	125	97.5	1.08	.76	.70	.07

[a] In general, the dihedral angle θ_A was measured in the system 10% A–90% B (by weight) and θ_B was measured in the system 90% A–10% B. In the case of systems 1 and 6, both angles were measured on each of these two compositions. In systems 7 and 8, both angles also were measured on a 50–50% (by wt.) sample. In system 9, both angles were measured on the 90% NaF–10% RbF sample. Where more than one measurement of a particular angle was made, the results agreed within the precision of the measurements and an average value is given. [b] Generally, the higher annealing temperatures correspond to the shorter times, except in the NaF–NaCl system, where a sample was annealed at 500° for only two days. [c] Angles marked with a "*c*" have an estimated error of ±2.5°; all other angles have an estimated error of ±5°. [d] 50–50 mole % solid solution.

TABLE II

RELATIVE GRAIN BOUNDARY ENERGIES OF THE ALKALI HALIDES (LiF = 1.00)

	F		Cl		Br		I	
	a	*b*	*a*	*b*	*a*	*b*	*a*	*b*
Li	1.00	1.00	*c*	*d*	*c*	*d*	*c*	*d*
Na	0.77	0.77	0.67	0.67	0.49	0.45	0.56	0.48
K	*c*	0.52	.23	.16	.33	.27	.55	.55
Rb	*c*	.41	.55	.48	.37	.31	*c*	.35
Cs	*c*	*c*	.47	*c*	.63	*c*	.56	*c*

[a] Derived from binary systems with LiF. [b] Derived from binary systems with NaF. [c] Melting point of eutectic too low for reliable measurements. [d] The system NaF–LiCl reacts to form the stable pair LiF–NaCl. The NaF–LiBr and NaF–LiI systems behave similarly.

TABLE III

RELATIVE LiF–MX AND NaF–MX INTERPHASE BOUNDARY ENERGIES

(LiF grain boundary energy = 1.00)

	F		Cl		Br		I	
M	LiF–MX[a]	NaF–MX[b]	LiF–MX	NaF–MX	LiF–MX	NaF–MX	LiF–MX	NaF–MX
Li	..	0.74	*c*	*d*	*c*	*d*	*c*	*d*
Na	0.74	..	0.76	0.60	0.68	0.58	0.74	0.57
K	*c*	.55	.67	.53	.69	.57	.72	.65
Rb	*c*	.60	.72	.55	.72	.60	*c*	.57
Cs	*c*	*c*	.65	*c*	.68	*c*	0.74	*c*

[a] Relative LiF–MX interphase boundary energies are from binary LiF–MX systems. [b] Relative NaF–MX interphase boundary energies are from binary NaF–MX systems. [c] Melting point of eutectic too low for reliable measurements. [d] Unstable pair.

TABLE IV

DIHEDRAL ANGLE OF THE LIQUID (WHOSE MAJOR COMPONENT IS MX) AGAINST THE NaF GRAIN BOUNDARY

X / M	F	Cl	Br	I
Li	10°	...	...	...
Na	...	0°	20°	45°
K	10°	15°	20°	55°
Rb	10°	10°	10°	20°
Cs	35°	45°	55°	...
Ag	...	40°	60°	...

TABLE V

MOLE PERCENTAGE OF NaF IN THE EUTECTIC FOR THE BINARY SYSTEM NaF–MX

X / M	F	Cl	Br	I
Li	39	..	..	..
Na	..	33.5	23	18
K	40	26.5	21	12
Rb	33	..	..	..

energy. Bailey and Watkins[24] and also Sears[25] related the grain boundary energy of copper to the surface tension of liquid lead, by slightly different methods.

The grain boundary energy of NaF was measured by Van Vlack's method.[13] This method involves two separate experiments: measurement of the angles in a solid–liquid–

(24) G. J. Bailey and H. C. Watkins, *Proc. Phys. Soc.* (London), **63B** 350 (1950).

(25) G. W. Sears, *J. Appl. Phys.*, **21**, 721 (1950).

TABLE VI

BOUNDARY ENERGIES IN THE SYSTEM NaF–LiF–KCl

	Angle		Ratio of interphase to grain boundary energy
θ_1	KCl *vs.* NaF/NaF	90°	0.71
θ_2	NaF *vs.* KCl/KCl	164°	3.6
θ_3	KCl *vs.* LiF/LiF	90°	0.71
θ_4	LiF *vs.* KCl/KCl	162°	3.2
θ_5	NaF *vs.* LiF/LiF	100°	0.78
θ_6	LiF *vs.* NaF/NaF	117.5°	0.96
θ_7	KCl *vs.* NaF/LiF	106°	..
θ_8	NaF *vs.* KCl/LiF	122°	..
θ_9	LiF *vs.* NaF/KCl	135°	..

TABLE VII

Interphase energy ratio calcd.	Angles used	Ratio obtained
$\frac{\text{NaF–KCl}}{\text{NaF–LiF}}$	7,9	0.74
	1,6	0.74
$\frac{\text{NaF–KCl}}{\text{LiF–KCl}}$	1, 3, 5, 6	0.81
	8, 9	0.83
$\frac{\text{LiF–KCl}}{\text{NaF–LiF}}$	3, 5, 6	0.91
	7, 8	0.88

liquid system as indicated in Fig. 2, to obtain the ratio of the grain boundary energy to the liquid–liquid interfacial energy, and a conventional measurement of the liquid–liquid interfacial energy.

The Solid–Liquid–Liquid System.—Besides the obvious requirement of non-reactivity of the two liquids, it is seen by inspection of equations 7 through 13 that θ_4 and θ_5 (see Fig. 2) must not be extremely large and θ_1 and θ_2 must not both be near to 90° (this would make probable large errors in the cosines of these angles).

The empirical method of trying reasonable pairs of liquids was used to find a suitable pair of immiscible liquids for use with NaF. After numerous trials, the system Te–CsCl was found to satisfy the requirements.[26]

A sample of 30% Te–30% CsCl–40% NaF (by wt.) was made by mixing powders of these materials and compressing them into a pellet, which was annealed for 40 hr. in an evacuated Vycor tube at 600°. At the annealing temperature the system was NaF(solid)–Te(liquid)–CsCl(liquid). The sample was quenched from the annealing temperature in carbon tetrachloride, then sectioned and polished. Final polishing on a silk cloth with alumina as abrasive and xylene as lubricant gave a good polish. The two dihedral angles and the angles at the three-phase junction were measured to obtain the ratio of the NaF grain boundary energy to the Te(l)–CsCl(l) interfacial energy.

The average of the ratios in Table IX, weighted inversely proportional to the square of their probable errors, is 3.15 ± 0.13.

TABLE VIII

EQUILIBRIUM ANGLES IN THE NaF(s)–Te(l)–CsCl(l) SYSTEM AT 600°

θ_1	CsCl *vs.* Te/NaF	36 ± 2°
θ_2	Te *vs.* CsCl/NaF	157 ± 2°
θ_3	NaF *vs.* Te/CsCl	169 ± 2°
θ_4	Te *vs.* NaF/NaF	104 ± 4°
θ_5	CsCl *vs.* NaF/NaF	40 ± 4°

The Liquid–Liquid Interfacial Energy.—A new method which combines features of the maximum bubble pressure method with the capillary height method was used to measure the liquid–liquid interfacial tension. Details of the method will be published elsewhere.[27] It differs from the maximum bubble pressure method only in that here the source of pressure which balances the pressure difference across the curved surface of the bubble is the hydrostatic pressure of the liquid itself instead of an outside source of a gas pressure. The experimental procedure is to measure the height or depth at which a bubble breaks away from a sharp-edged circular hole. The corrections are standard (*cf.*, Adam,[28] Sugden[29] and Harkins[30]).

TABLE IX

Equation used	Ratio of grain boundary energy to liquid–liquid interfacial energy
7	3.26
8	3.31
9	3.17
10	3.15
11	3.18
12	3.05
7′	3.22
8′	3.15
9′	3.27
10′	3.15
11′	3.05
12′	3.18

Measurements were made conveniently in the dark interior of a furnace by observation of the interface through a hole in the top of the furnace as a tube and disc was pushed by a micrometer drive down into the lower liquid until a bubble of it broke through the hole in the disc into the upper liquid.

Measurement on the system Te–CsCl when saturated with NaF was complicated by the fact that the NaF reacts with glassware and Te reacts with metals. Sodium fluoride itself was the only construction material which could confidently be used for the apparatus, which was fabricated by tamping slightly dampened NaF powder into a brass mold, drying and sintering at 900° for one to two hr. Crucibles and tubes up to 5 cm. in length prepared in this way were quite dense and very strong. Discs of NaF were pressed in a steel die from the dry salt. A hole was drilled in a disc and the disc was heated at 900° for one to two hr., then polished on emery papers and finally on a silk cloth with alumina abrasive. It was not possible to obtain perfectly sharp-edged holes, but the best ones had chips of a size only about 1% of the diameter. A disc was attached to a tube by setting the tube on top of the disc and sintering at 800° for one hr. The final diameter of the hole was measured microscopically.

Because the dihedral angle of CsCl against the NaF grain boundary is only about 40°, the liquid spreads along the grain edges of the NaF and seeps slowly through the crucible, but this was minimized by previously saturating with NaF, and eventually a layer of CsCl about 3 mm. thick of constant thickness was obtained over the tellurium. The contact angle of the CsCl on NaF was less than 90° and the contact angle of the Te–CsCl interface on NaF was greater than 90°. Two different tube and disc assemblies made of NaF were used. Only the first observation with each tube was considered reliable because of the possible dissolution of NaF in the CsCl, which would change the diameter of the hole.

TABLE X

THE INTERFACIAL TENSION OF THE SYSTEM Te–CsCl SATURATED WITH NaF AT 600°

Radius of hole (cm.)	Depth (cm.) of breakthrough (cor.[a])	Density[b] (g./cc.)	Interfacial tension (ergs/cm.²)
0.0693	0.567	5.53	97.5
0.0745	0.531	5.53	96.6
			Av. 97.1

[a] Corrected for increase of the liquid level as the tube is lowered, for the thickness of the disc and for the volume of liquid in the hole in the disc. [b] Determined from the variation of bubble pressure with depth, using nitrogen.

(26) The pair Te–$SnCl_2$ was equally good, but gave difficulties in the measurement of the liquid–liquid interfacial energy.

(27) C. S. Smith and D. P. Spitzer, to be published.

(28) N. K. Adam, "The Physics and Chemistry of Surfaces," Oxford Press, London, 1941, p. 374.

(29) S. Sugden, *J. Chem. Soc.*, **121**, 858 (1922).

(30) W. D. Harkins, "Determination of Surface and Interfacial Tensions," in "Technique of Organic Chemistry," Edition III, edited by A. Weissberger, Interscience Press, New York, N. Y., 1959.

Since the grain boundary energy of NaF had been found to be 3.15 times this interfacial tension, the grain boundary energy of NaF is 306 ± 15 ergs/cm.^{2}.

From the relative grain boundary energies given in Table II and the absolute grain boundary energy of NaF, a table of absolute grain boundary energies is prepared (Table XI). The values for the cesium salts are obtained indirectly *via* the LiF grain boundary energy; all other values are based on the ratios obtained against NaF directly. The values given all have uncertainties of 10–20% (probable errors may be obtained from Table I).

TABLE XI

ABSOLUTE GRAIN BOUNDARY ENERGIES OF THE ALKALI HALIDES (ERGS/CM.^{2})

	F	Cl	Br	I
Li	398	...	...	...
Na	306	266	177	193
K	208	64	108	220
Rb	162	193	123	138
Cs	...	187	251	223

To determine whether materials with intermediate lattice constants would have grain boundary energies intermediate to those in Table XI, the grain boundary energies of two solid solutions were obtained from systems with NaF. The grain boundary energy of a 50–50 mole % solid solution of NaCl and NaBr is 217 ergs/cm.^{2}, midway between the grain boundary energies of NaCl and NaBr. The grain boundary energy of a 50–50 mole % solid solution of KCl and KBr is 214 ergs/cm.^{2}, however, much greater than the grain boundary energy of either KCl or KBr.

Discussion

The assumptions involved in the determination of a true dihedral angle from measurements of angles on a two-dimensional plane section have been discussed by Harker and Parker[7] and by Smith.[4] It is necessary that the measured angles represent plane sections at random angles through a representative random sample of all angles in the specimen. Randomality was obtained in the present measurements by the use of a compressed polycrystalline powder, measurements being taken at many places over the entire surface of a plane section.

It is assumed that there is a unique dihedral angle for each type of interface junction, *i.e.*, that the energy of a boundary is independent of the orientation of either of the crystals forming it and of the direction of the boundary itself. This is far from the case when one solid phase has nucleated in or against another, or for boundaries between grains inclined at a very small angle to each other, when the energy is a very steep function of orientation. However, as Shockley and Read[12] have shown, such critical angular relationships are rare in a randomly oriented aggregate, and the experimental distribution curves for the angles are only slightly less sharply peaked than required by theory. The fact that there is some spread does, however, indicate some variation of energy with orientation superimposed on some experimental uncertainty in angle measurement.

Measurements on two-phase mixtures showed that the dihedral angles were independent of the volume fraction of the two phases, as of course they should be. Both "analytical reagent" and high purity optical grade salts gave the same results in the systems studied. The inevitable contamination of one boundary by the other component of the binary system may, of course, already have ob-

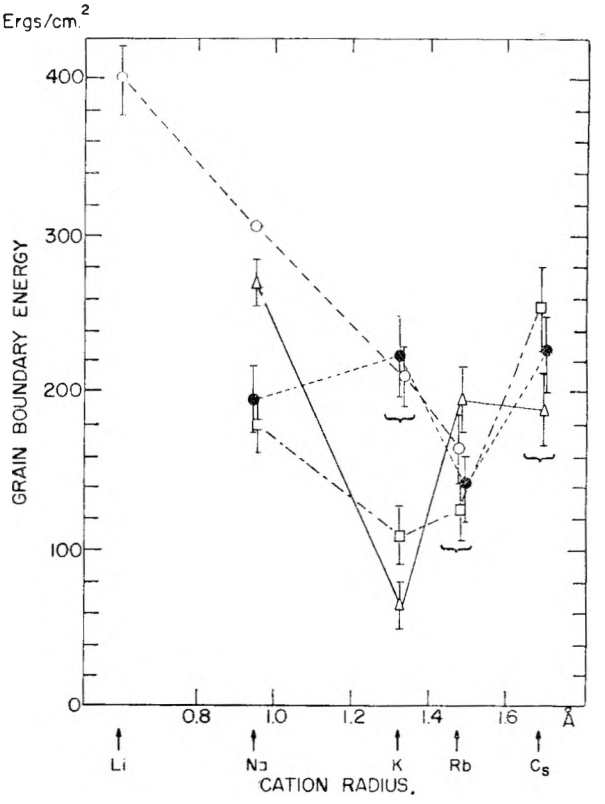

Fig. 6.—Grain boundary energies of the alkali halides as a function of cation radius. The errors indicated are the probable errors arising from the dihedral angle measurements and do not include the error in the absolute value of the NaF grain boundary energy or the error due to contamination. ○, fluorides; △, chlorides; □, bromides; ●, iodides.

scured the effect of other impurities. Measurements on samples annealed less thoroughly than usual (for example, two days at 500° for the NaF–NaCl system) showed that equilibrium angles were achieved in a short time, but the longer times and higher temperatures were used to produce a large enough grain size for reliable measurements of the angles.

No detectable change of angle with temperature was found. McLean[31] shows the temperature coefficient of grain boundary energy in copper to be about 0.001 per degree: the ratio of interface energies would be expected to be even less temperature dependent unless a composition change occurred with temperature.

According to any simple model of a grain boundary (such as the supercooled layer model of McLean[32] or the model of Friedel, *et al.*[33]) it would be expected that the grain boundary energies of the alkali halides would decrease monotonically with decreasing lattice energy, or, what amounts to the same thing in the alkali halides, with increasing ionic radii, just as the surface tensions of the fused salts do.[34] The present measurements follow no such simple rule.

The grain boundary energies of the fluorides will

(31) D. McLean, "Grain Boundaries in Metals," Oxford University Press, London, 1957, p. 72.

(32) D. McLean, ref. 31, p. 73.

(33) J. Friedel, B. D. Cullity and C. Crussard, *Acta Met.*, **1**, 79 (1953).

(34) O. A. Osipov, *Doklady Akad. Nauk S.S.S.R.*, **102**, 1171 (1955).

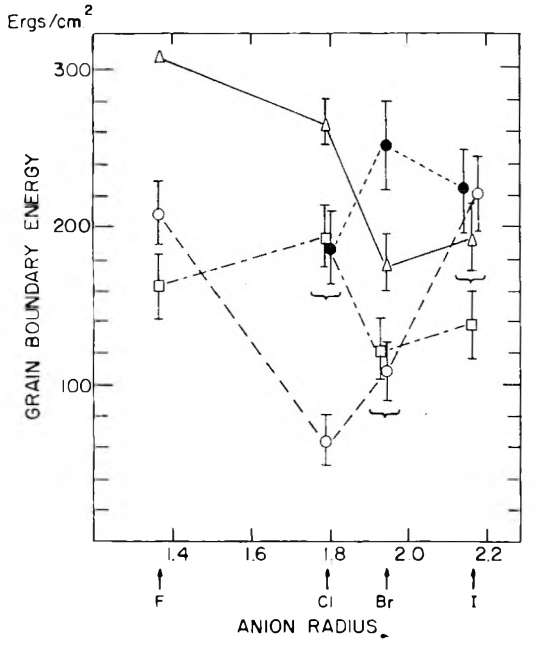

Fig. 7.—Grain boundary energies of the alkali halides as a function of anion radius. The errors indicated are the probable errors arising from the dihedral angle measurements and do not include the error in the absolute value of the NaF grain boundary energy or the error due to contamination. △, Na halides; ○, K halides; □, Rb halides; ●, Cs halides.

be seen to vary linearly with cation radius (Fig. 6) and the energies of the various halides of sodium (Fig. 7) are nearly linear with anion size, but there is no over-all regularity.

It must be emphasized that all of the measurements involve an inevitable contamination with other elements—tellurium, cesium and chlorine in the absolute measurement of the NaF grain boundary energy, and the other alkali metal and/or halogen ions that were in equilibrium with NaF or LiF in the other measurements. No comparison is possible, however, without assuming that the standard boundary was the same throughout, and the departure from simple behavior easily could be due to the fallacy of this assumption. An indication of the magnitude of this error may be given by comparing the ratio of the LiF and NaF boundary energies as they appear in the binary systems with other alkali halides (Table XII), but such errors due to contamination may well cancel out.

TABLE XII

RATIO OF THE LiF AND NaF GRAIN BOUNDARY ENERGIES OBTAINED FROM BINARY SYSTEMS CONTAINING THE SALT MX

X	Cl	Br	I
M			
Na	1.30	1.18	1.12
K	0.91	1.06	1.31
Rb	1.15	1.08	...

In the case of the interphase boundaries between dissimilar alkali halide crystals (Table III), there is considerably less energy variation than in the case of the single phase boundaries. In binary metallic systems the interphase interface energies are frequently lower than the grain boundary energy in either phase,[35] but in the alkali halides the interphase boundary energy is amost invariably intermediate between the grain boundary energies of the pure salts.

In samples annealed just above the eutectic temperature, the energy of the interface between the liquid phase and the sodium fluoride crystal decreases as the amount of sodium fluoride in the eutectic increases (Table IV–V), assuming that the NaF grain boundary energy is the same in all of the systems. The interface energy, therefore, is apparently determined largely by composition, just as in the case of interfaces between two liquids. The solid–liquid interface energy was never far from one-half of the grain boundary energy, even in experiments with the wide variety of liquids (mainly salts) used in the search for a system to be used for the absolute grain boundary energy measurements. This suggests that the interfacial energy is due mainly to the orderliness of the solid: if it were melted, the liquids would be completely miscible.

Although the grain boundary energies of the alkali fluorides and of the sodium halides decreased lineally with increasing lattice parameter, no general correlation has been found between intercrystalline energies and other basic properties of the alkali halides.

Acknowledgment.—The author is most grateful to Professor Cyril Stanley Smith for countless helpful discussions and suggestions during the entire course of this work.

(35) C. S. Smith, "Interphase Interfaces," in "Imperfections in Nearly Perfect Crystals," John Wiley and Sons, New York, N. Y., 1952.

ION-EXCHANGE KINETICS.[1] III. EXPERIMENTAL TEST OF THE THEORY OF PARTICLE-DIFFUSION CONTROLLED ION EXCHANGE

BY F. HELFFERICH

Shell Development Company, Emeryville, California

Received June 12, 1961

Experiments were designed to test the validity of the theory of particle-diffusion controlled ion exchange presented in previous publications. Ion-exchange rates and intra-resin concentration profiles were measured with phenolsulfonic acid cation exchangers and H^+ and Na^+ as the exchanging counterions. The experimental results are in very satisfactory agreement with theoretical predictions based on individual intra-resin diffusion coefficients that were determined by independent conductivity measurements. In particular, the predicted characteristic differences in rates and concentration profiles between forward and reverse exchange of two given ions having different mobilities were confirmed experimentally. The results thus establish the importance of electric potential gradients that were neglected in earlier theories. It is shown by qualitative arguments that the electric potential gradient also should cause transient changes in the co-ion and solvent contents of the resin in the course of ion exchange. These additional predictions also were confirmed by measurements.

Introduction

It long has been established that the rate of exchange of counterions between ion-exchange resins and electrolyte solutions is controlled by diffusion of the counterions either in the resin particle ("particle-diffusion control") or in an adherent liquid diffusion layer ("film-diffusion control").[2] The present study deals exclusively with particle-diffusion controlled ion exchange.

In earlier theories of particle-diffusion controlled ion exchange, it was assumed that interdiffusion can be described in terms of one constant interdiffusion coefficient, and the well-known mathematical solutions for diffusion with a constant diffusion coefficient into, or out of, a sphere were applied.[3] However, in a more recent theoretical treatment[4] based on the Nernst–Planck flux equations it was shown that interdiffusion gives rise to an electric potential gradient which acts on the diffusing ions and results in a variable interdiffusion coefficient and quite different rate laws. In particular, the new and the older theories differ in the following points. In the exchange of two counterions A and B, of which A has the higher mobility, the new theory predicts: (1) Exchange of B (initially in the solution) for A (initially in the resin) is faster than the reverse exchange of A for B (see Fig. 3 in Part I); (2) In the exchange of B for A, a comparatively sharp concentration "front" moves in toward the center of the bead, whereas, in the reverse exchange, the beads are much more uniformly converted (see Fig. 4 in Part I). In marked contrast, the earlier theories predict equal rates and concentration profiles for forward and reverse exchange of two such ions.

Experimental results published so far are inadequate for a quantitative test of the new theory. Therefore the present study was undertaken to provide such a test by a minimum of crucial experiments. For this purpose, ion-exchange rates and concentration profiles were determined experimentally and were compared with theoretical predictions based on independent measurements of the individual diffusion coefficients of the exchanging ions. To establish the superiority of the new theory unambiguously, it was necessary to choose a system for which the new and the older theories predict drastically different rates and concentration profiles, and to measure these accurately. Drastic differences between the theories are obtained with counterions having markedly different mobilities. H^+ and Na^+ (mobility ratio about 6:1) were chosen as two such ions. Accurate rate measurements with the usual spherical ion-exchanger beads of 1 mm. diameter or less are difficult because of the short conversion time (half time, as a rule, less than a minute), and the task of measuring non-stationary concentration profiles in such beads is almost hopeless. Therefore the measurements were made with stacks of ion-exchanger discs which gave much longer conversion times and could be taken apart to determine the concentration profiles.

Beyond the calculation of counterion exchange rates and concentration profiles, as discussed in Part I, the Nernst–Planck equations can be used to predict transient changes in the co-ion and solvent contents of the resin in the course of ion exchange. Separate experiments were made to verify these additional predictions.

Experiments

Disc Preparation.—Cation-exchanger discs were prepared as described by Manecke,[5] with modifications as previously reported.[6] This procedure is essentially as follows. Phenol is sulfonated with concentrated H_2SO_4 at 110°. A mixture of the obtained phenolsulfonic acid solution with aqueous formaldehyde is left standing at room temperature until viscous and then is poured into inert plastic moulds (Mylar plastic sheets with circular holes) which are sandwiched between glass plates. Condensation is carried out in the moulds at 70° (about 3 hours). The properties of the discs are listed in Table I. The limits given are deviations between the individual discs. These deviations are greater than the experimental errors.

Ion-exchange Capacity of the Discs.—The discs were converted to the H^+ form by repeated batch equilibration with 1 *N* HCl and were washed with deionized water to remove sorbed HCl. H^+ then was displaced by successive batch equilibrations with 1 *N* NaCl and was determined in the combined decanted solutions by titration with 0.1 *N* NaOH.

Co-ion Content of the Discs.—Co-ion contents of the discs were measured in equilibrium with 0.1 and 1 *N* solutions of HCl, NaCl and HCl–NaCl mixtures at 25°. After equilibration with the respective solution in a thermostat, ad-

(1) Part I, *J. Chem. Phys.*, **28**, 418 (1958); Part II, *ibid.*, **29**, 1064 (1958).

(2) G. E. Boyd, A. W. Adamson and L. S. Myers, Jr., *J. Am. Chem. Soc.*, **69**, 2836 (1947).

(3) See, for example, T. R. E. Kressman and J. A. Kitchener, *Discussions Faraday Soc.*, **7**, 90 (1949); D. Reichenberg, *J. Am. Chem. Soc.*, **75**, 589 (1953).

(4) F. Helfferich and M. S. Plesset, *J. Chem. Phys.*, **28**, 418 (1958).

(5) G. Manecke, *Z. physik. Chem.* (Leipzig), **201**, 193 (1952).

(6) F. Helfferich and H. D. Oeker, *Z. physik. Chem.* (Frankfurt), **10**, 213 (1957).

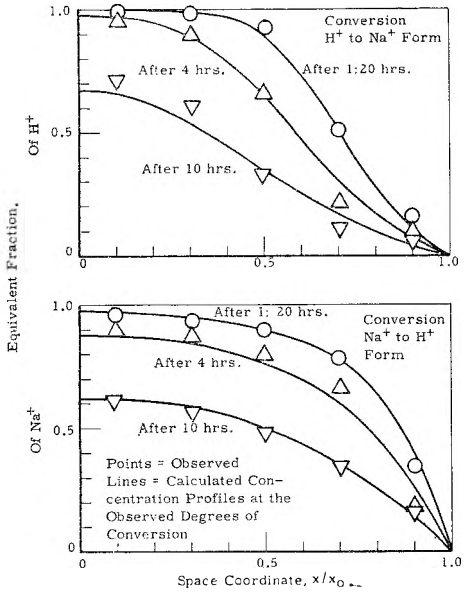

Fig. 1.—Observed and predicted concentration profiles, 25°.

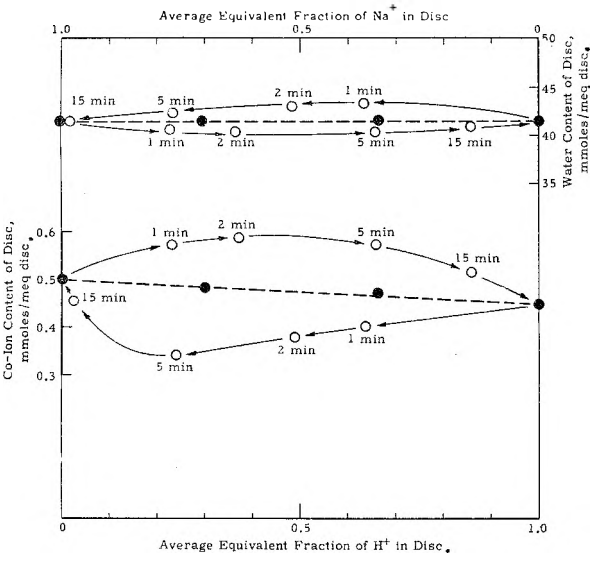

Fig. 2.—Non-equilibrium co-ion and water contents of disc in forward and reverse ion exchange. Equilibrium co-ion and water contents (solid circles, broken lines) are given for comparison (1 *M* solutions, 25°).

herent liquid was wiped off with filter paper and sorbed electrolyte was leached out by successive batch equilibrations with deionized water. Cl^- was determined in the combined decanted solution by Volhard titration with 0.1 *N* $AgNO_3$ and 0.05 *N* NH_4SCN.

Water Content of the Discs.—Water contents of the discs were determined at 25° in equilibrium with water and with 0.1 and 1 *N* solutions of HCl, NaCl and HCl–NaCl mixtures. After equilibration and removal of adherent liquid as described above, the discs were weighed in a stoppered weighing bottle. The water content of the water-washed H^+ form was determined directly by drying the disc to constant weight *in vacuo* over P_2O_5 at 45° (9 days). The water contents of the other forms were calculated from their wet weight, the water content and wet weight of the water-washed H^+ form, the ion-exchange capacity, and the H^+, Na^+ and Cl^- contents.

Electric Conductivity of the Discs.—The conductivities of the discs in the H^+ and Na^+ forms at 25° in equilibrium with 0.1 *N* HCl and NaCl solutions, respectively, were measured. A conventional lucite conductivity cell with platinized platinum electrodes, as described by Manecke[7] and Lorimer,[8] was used. The cell consists of two half-cells between which the disc is clamped. During the measurements, the cell is immersed in the equilibrating solution kept in a thermostat. The resistance of the disc is determined by subtracting the blank resistance of the cell (without disc) from the resistance measured with the disc in place. The resistances were measured with a Jones Bridge (Leads and Northrup, Research Model) in combination with a Tuned Audio Frequency Amplifier, a telephone receiver, and a decade condensor (10^{-3} to 1 μF.) with 1000 cycles alternating current. The average of three readings for every disc was taken; the cell was taken apart and reassembled for every reading. The specific conductivity was calculated from the resistance and the known thickness and cross-section of the disc.

Ion-exchange Rate and Concentration Profile Measurements.—Rates and intra-resin concentration profiles were measured at 25° for complete conversion of the discs from the Na^+ form to the H^+ form with 0.1 *N* HCl, and from the H^+ form to the Na^+ form with 0.1 *N* NaCl. Prior to the experiments, the discs were converted to the monoionic Na^+ form (or H^+ form) and extensively washed with deionized water. A stack of five discs and one inert Mylar disc of the same size were placed in a finger cot of thin rubber, with the inert disc at the far end of the cot. The open end of the cot then was attached to a lucite cell in such a way that the surface of the first disc was exposed to the solution in the cell. The cell was immersed in a thermostat, and the solution was rapidly circulated (flow rate about 10 to 20 ml./sec.) through a Hastelloy-B heat exchanger in the thermostat, the cell, and a 1-liter reservoir bottle. A nozzle in the cell directed a violet jet of solution against the exposed surface of the first disc. The solution was renewed repeatedly, as required to keep the Na^+ (or H^+) concentration below 0.001 *N*. Experiments were made with contact times between the resin and the solution of 1:20, 4 and 10 hr. Thereafter, the disc stack was disassembled, and the individual discs were analyzed for both H^+ and Na^+. For this purpose, both these ions were displaced by successive batch equilibrations with 0.25 *M* $MgCl_2$. In the combined decanted solutions, H^+ was titrated with 0.1 *N* NaOH, and Na^+ was determined in the flame photometer. All measurements were made with the same five discs in the same sequence. Difficulties were encountered in the conversion from the Na^+ to the H^+ form; here, voids between the discs tend to develop because of solvent depletion of the discs, and it was necessary to compress the stack repeatedly by pressing it gently against the lucite cell.

Measurements of Transient Changes in the Co-ion and Water Contents.—The transient behavior of the co-ion and water contents of the resin was studied at 25° for complete conversion from the Na^+ to the H^+ form with 1 *N* HCl, and from the H^+ to the Na^+ form with 1 *N* NaCl. Single discs rather than stacks were used. The disc was equilibrated with 1 *M* NaCl (or HCl), was wiped with filter paper, and then was attached to a glass stirring rod in the following way. A Tygon strip (obtained by splitting a Tygon tube lengthwise in half) was wrapped around the perimeter of the disc, and both ends of the strip were secured to the glass rod by elastics. This "lollipop" was attached to a stirring motor and was immersed in 1 *M* HCl (or NaCl) in a thermostat, the disc serving as the stirrer. Measurements were made with 1, 2, 5 and 15 min. contact time between the disc and the solution. After removal from the solution, the disc was analyzed for its counterion, co-ion, and water contents as described before.

Reagents.—Standard analytical-grade laboratory reagents were used throughout.

Results and Discussion

The experimental results are given in Tables I through III and Figs. 1 and 2.

The foremost aim of this study was a quantitative test of the theory by comparison of observed and predicted ion-exchange rates and intra-resin concentration profiles. The theoretical predictions

(7) G. Manecke and K. F. Bonhoeffer, *Z. Elektrochem.*, **55**, 475 (1951).

(8) J. W. Lorimer, E. I. Boterenbrood and J. J. Hermans, *Discussions Faraday Soc.*, **21**, 141 (1956).

TABLE I

DISC PROPERTIES

Dimensions			
(Swollen in 0.1 *M* soln.)		Diameter	2.7 ± 0.05 cm.
		Thickness	0.18 ± 0.005 cm.
Ion-exchange capacity		1.10 ± 0.035 meq./disc	
		2.08 ± 0.18 meq./g. dry H^+ form	
		1.10 ± 0.06 meq./cm.^{3} when swollen in 0.1 *M* soln.	
Water content	H^+ form	Water washed	49 ± 2 mmoles/meq. disc (71% wt.)
		In 0.1 *M* HCl	43.6 ± 2
		In 1 *M* HCl	43.0[a]
	Na^+ form	Water washed	48.4 ± 2
		In 0.1 *M* NaCl	44.5 ± 2
		In 1 *M* NaCl	43.3[a]
Cl^- content	H^+ form	In 0.1 *M* HCl	0.011 ± 0.004 mmole/meq. disc
		In 1 *M* HCl	.450[a]
	Na^+ form	In 0.1 *M* NaCl	.010 ± 0.004
		In 1 *M* NaCl	.50
Specific conductivity	H^+ form	In 0.1 *M* HCl	.132 ± 0.014 Ω^{-1} cm.$^{-1}$
	Na^+ form	In 0.1 *M* NaCl	.0195 ± 0.0015 Ω^{-1} cm.$^{-1}$
Intraresin diffusion constants	H^+	Uncor.	3.0×10^{-5} cm.^{2}/sec. ±10%
		Cor.	2.4×10^{-5}
	Na^+	Uncor.	4.4×10^{-6} ±10%
		Cor.	3.5×10^{-6}

[a] Measured with one disc only.

TABLE II

OBSERVED AND PREDICTED RATES OF ION EXCHANGE

Experiments with disc stacks and 0.1 *M* solutions at 25°

	Degree of conversion		
		Predicted	
Time	Obsd.	Uncor.	Cor.[a]
Conversion from H^+ form to Na^+ form			
1 hr. 20 min.	0.29	0.30	0.27
4 hr.	.43	.53	.47
10 hr.	.64	.83	.75
Conversion from Na^+ form to H^+ form			
1 hr. 20 min.	0.21	0.24	0.21
4 hr.	.36	.41	.36
10 hr.	.56	.62	.56

[a] Correction for convection conductivity is applied in calculation of diffusion constants.

TABLE III

OBSERVED ION-EXCHANGE RATES

	Degree of conversion	
Time, min.	H^+ form to Na^+ form	Na^+ form to H^+ form
1	0.36	0.23
2	.51	.37
5	.86	.66
15	.97	.86

require the knowledge of the individual intra-resin diffusion coefficients of the two exchanging ions. These coefficients were calculated from the conductivity measurements with the discs in the monoionic H^+ and Na^+ forms. Calculation of counter-ion diffusion coefficients from conductivity measurements is a standard procedure.[9-11] Unfortunately, a correction for "convection conductivity"[10-12] must be applied. Calculation of this correction requires difficult additional measurements which were not made in the present study. Instead, two sets of diffusion coefficients were calculated; the first without correction for convection conductivity, and the second assuming 20% convection conductivity as estimated by Schlögl and Schödel[13] for an almost identical ion exchanger. Both these sets of coefficients were used for calculating theoretical rates and concentration profiles. Fortunately, errors in estimating the correction for convection conductivity have little effect on the predicted rates and hardly any of the predicted concentration profiles. The calculated intra-resin diffusion coefficients of Na^+ and H^+ are included in Table I.

The theoretical rates and concentration profiles presented in Parts I and II are for spherical beads and thus do not apply to the experiments in the present study. Numerical solutions were calculated for one-dimensional geometry, as in the present experiments, on an IBM-704 electronic computer using the procedure described in Part II. The results obtained for the parameter values as in the experiments are included in Fig. 1 and Table II. Numerical results for other conditions are given in dimensionless form in Fig. 3 and Table IV.

The comparison of the observed ion-exchange rates and concentration profiles with the predicted ones in Table II and Fig. 1 shows that the theory is remarkably successful. Qualitatively, the predicted differences in rates and concentration profiles between forward and reverse exchange are confirmed experimentally. The most striking features in which the new theory differs from the previous ones thus are verified experimentally. Exact quantitative agreement cannot be expected

(9) G. Manecke, *et al.*, *Z. Elektrochem.*, **55**, 475 and 672 (1951); *Z. physik. Chem.* (Leipzig), **201**, 193 (1952); *Z. physik. Chem.* (Frankfurt), **2**, 336 (1954).

(10) G. J. Hills, *et al.*, *Trans. Faraday Soc.*, **51**, 719 and 1260 (1956).

(11) K. S. Spiegler and C. D. Coryell, *J. Phys. Chem.*, **56**, 196 (1952); **57**, 687 (1953).

(12) G. Schmid, *Z. Elektrochem.*, **56**, 181 (1952).

(13) R. Schlögl and U. Schödel, *Z. physik. Chem.* (Frankfurt), **5**, 372 (1955).

TABLE IV

CALCULATED DEGREES OF CONVERSION $F(\tau)$, DIMENSIONLESS TIMES $\tau = D_A t/x_0^2$, AND DIMENSIONLESS RATES $dF(\tau)/d\tau$ FOR VARIOUS VALUES OF THE MOBILITY RATIO D_A/D_B[a]

$F(\tau)$	$D_A/D_B = 10$ τ	$dF/d\tau$	$D_A/D_B = 4$ τ	$dF/d\tau$	$D_A/D_B = 2$ τ	$dF/d\tau$	$D_A/D_B = 1/2$ τ	$dF/d\tau$	$D_A/D_B = 1/4$ τ	$dF/d\tau$	$D_A/D_B = 1/10$ τ	$dF/d\tau$
0.05	0.006248	4.103	0.003640	6.938	0.002594	9.715	0.001563	16.10	0.001320	19.07	0.001121	22.55
.1	.02447	2.645	.01449	3.463	.01038	4.827	.006264	7.991	.005258	9.517	.004456	11.26
.15	.05512	1.373	.03261	2.308	.02334	3.222	.01409	5.336	.01183	6.358	.01001	7.532
.2	.09758	1.032	.05793	1.730	.04150	2.414	.02505	4.000	.02100	4.786	.01774	5.677
.25	.1519	0.8267	.09047	1.384	.06485	1.930	.03910	3.213	.03273	3.846	.02764	4.550
.3	.2185	.6892	.1302	1.154	.09335	1.616	.05619	2.691	.04701	3.215	.03976	3.769
.35	.2971	.5912	.1772	0.9910	.1269	1.386	.07629	2.314	.06388	2.749	.05424	3.178
.4	.3876	.5181	.2311	.8709	.1655	1.220	.09945	2.022	.08348	2.377	.07134	2.702
.45	.4900	.4624	.2919	.7789	.2089	1.190	.1258	1.781	.1061	2.063	.09141	2.304
.5	.6038	.4188	.3595	.7052	.2573	0.9830	.1558	1.568	.1322	1.786	.1149	1.963
.55	.7267	.3908	.4321	.6589	.3095	.9115	.1892	1.404	.1618	1.571	.1422	1.698
.6	.8596	.3626	.5115	.6043	.3673	.8241	.2274	1.220	.1963	1.343	.1743	1.436
.65	1.003	.3365	.5981	.5512	.4314	.7373	.2718	1.044	.2368	1.132	.2125	1.194
.7	1.157	.3104	.6937	.4964	.5038	.6481	.3241	0.8763	.2859	0.9347	.2589	0.9776
.75	1.326	.2825	.8008	.4376	.5871	.5550	.3872	.7153	.3450	.7542	.3161	.7803
.8	1.514	.2509	.9244	.3728	.6862	.4570	.4662	.5607	.4203	.5842	.3693	.5995
.85	1.729	.2130	1.074	.2997	.8103	.3533	.5700	.4125	.5206	.4249	.4874	.4327
.9	1.994	.1650	1.269	.2159	.9798	.2431	.7191	.2698	.6662	.2750	.6302	.2788
.95	2.374	.09989	1.576	.1177	1.260	.1256	.9790	.1324	.9227	.1336	.8852	.1344

[a] Calculated for counterions of equal valence, complete particle-diffusion control, one-dimensional geometry, and with the initial and boundary conditions $t = 0$, $0 \leq x \leq x_0$, $C_B = 0$; and $t \geq 0$, $x > x_0$, $C_A = 0$. (x_0 = thickness of resin slab.)

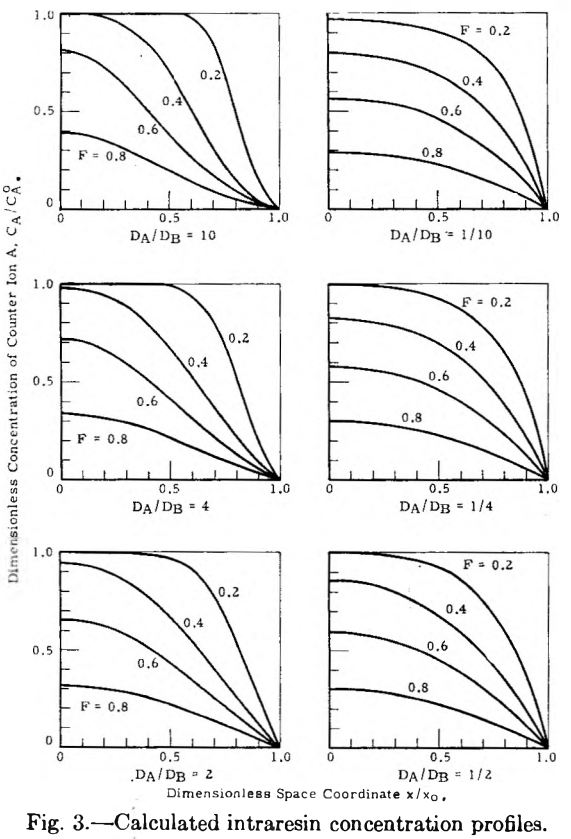

Fig. 3.—Calculated intraresin concentration profiles.

since the simplifying assumptions of the theory—namely, constant individual diffusion coefficients, absence of co-ions in the resin, negligible swelling changes, absence of gradients of counterion activity coefficients—are not completely met and since the correction for convection conductivity is somewhat uncertain. In view of these facts, the complete quantitative agreement for conversion from the Na^+ to the H^+ form must be considered as fortuitous. The agreement for the (faster) reverse process is, indeed, not as good. The deviations, though minor, are considerably larger than the analytical error and show definite trends; the predicted rate is too high, and the predicted concentration profiles are slightly too smooth. It would be highly speculative to attribute these deviations to specific physical causes. Possibly, a systematic experimental error is responsible; in the experiments, water is transferred into the disc stack (see farther below), and liquid films with high diffusion resistance might have formed between the individual discs, thus slowing down the exchange. This explanation is consistent with the observation that the difference between forward and reverse exchange rates is greater in the experiments with single discs (see Table III) where, of course, no such retarding films can form.

The agreement between experiments and theory is very gratifying. However, it should be kept in mind that the experiments were designed in such a way that the simplifying assumptions of the theory are approximately met. In particular, the following points were considered. The measurements were made with 0.1 N solutions because this concentration is low enough to keep the co-ion content small (at or below 1% of the counterion content, see Table I), and yet is high enough to guarantee complete particle-diffusion control. Furthermore, with H^+ and Na^+ in the type of resin used, the resin swells or shrinks very little when being converted from one ionic form to the other (see Table I). Also, the ion-exchange selectivity coefficient is practically independent of ionic composition, so that possible gradients of ionic activity coefficients balance one another and thus have little effect on the ionic fluxes.[6] In more complicated systems, much larger deviations between experiment and theory must be expected.

The measurements of the transient behavior of the co-ion and water contents of the resin during ion exchange were made with 1 M solutions, in order to obtain co-ion contents that are sufficiently high to be measured accurately. The purpose of these measurements was to test the following qualitative predictions.

As discussed in detail in Part I, interdiffusion of counterions in the resin gives rise to an electric potential gradient which slows down the faster counterion and speeds up the slower one and, in this way, enforces the equivalence of the ionic fluxes as required to preserve electroneutrality. In other words, the unbalance of the purely diffusional fluxes of the two ions is automatically corrected by a superimposed electric transference of both counterions in the direction of diffusion of the slower counterion. The electric potential gradient, of course, also acts on any co-ions in the resin. The sign of the gradient is such that co-ions are transferred in the direction in which the *faster* counterion diffuses. Hence, if a fast counterion enters the resin in exchange for a slower one which goes out into the solution, then co-ions are sucked into the resin by electric transference. Of course, the electric potential gradient decays as ion exchange approaches completion, and sorption equilibrium of the co-ion eventually is re-established. The resulting effect thus is a temporary co-ion accumulation in the resin. On the other hand, in the reverse exchange where the faster counterion goes out into the solution, co-ions are sucked out of the resin, and the resulting effect is a temporary co-ion depletion of the resin.

A similar argument can be advanced for the solvent. Electric transference of counterions under the influence of an electric potential gradient is known to cause a cocurrent convection of the solvent; it is this effect which gives rise to "convection conductivity"[9-11] and to "anomalous osmosis."[14] In interdiffusion of counterions (in the absence of an electric current), the automatically superimposed electric transference of counterions is, as pointed out before, in the direction in which the *slower* counterion diffuses. The solvent thus is transferred in this direction. Accordingly, when a fast counterion enters the resin in exchange for a slower one which goes out into the solution, solvent is sucked out of the resin until ion exchange approaches completion, the electric potential gradient decays, and sorption equilibrium is re-established. The resulting effect is a temporary solvent depletion of the resin. In the reverse exchange, on the other hand, the resulting effect is a temporary solvent accumulation in the resin. Co-ion depletion thus is accompanied by solvent accumulation, and *vice versa*.

The experimental results are shown in Fig. 2. For comparison, the equilibrium co-ion and water contents of partially converted discs in equilibrium with mixed HCl–NaCl solutions (total concentration 1 *N*) are included in this figure. The experimental results are in complete qualitative agreement with the theoretical predictions.

It is tempting to use the intra-resin diffusion coefficients of H^+ and Na^+, determined in resins in equilibrium with 0.1 *M* solutions, for predicting the ion-exchange rates with 1 *M* solutions also.

(14) (a) R. Schlögl, *Z. physik. Chem.* (Frankfurt), **3**, 73 (1955); (b) it is irrelevant whether the electric potential gradient is caused by an external voltage source (as in conductivity measurements) or by a diffusion process within the system in the absence of an electric current (as an anomalous osmosis and ion exchange); the individual ion has no means of knowing the cause of the electric potential gradient in its environment.

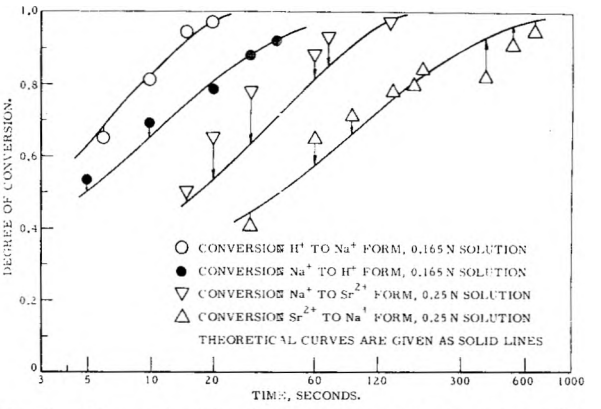

Fig. 4.—Observed and calculated ion-exchange rates with KU-2 resin.

Here, however the results are disappointing. The observed rates are listed in Table III. The difference between forward and reverse exchange rates is as predicted, but the observed rates are throughout only little more than half as high as the predicted ones. The magnitude of this deviation is not surprising since the diffusion coefficients must be expected to be concentration-dependent, and since, contrary to the assumption of the theory, the internal co-ion concentration is high. The direction of the deviation was unexpected since, in most cases, the counterion diffusion coefficients are found to increase rather than decrease with increasing concentration of the external solution.[15] However, a more detailed mathematical analysis shows that, indeed, the presence of substantial amounts of co-ions in the resin should delay ion exchange. The physical cause is that the electric driving force generated by diffusion of the faster counterion is spent in part for transferring co-ions rather than for accelerating the slower counterion.

The results of the present study are interesting in still another respect. Results of self-diffusion measurements by Schlögl and Stein[16] in a similar resin have been interpreted to indicate that (non-stationary) effusion out of a slab may occur with a higher effective diffusion coefficient than steady-state diffusion across the same slab. Such an effect may arise from particular pore geometries. In the present study, no such effect was found. On the contrary, the rates of non-stationary ion-exchange processes have been predicted correctly on the basis of diffusion coefficients determined by conductivity measurements under conditions which essentially correspond to a steady-state process. The deviations, where existing, are minor and in the opposite direction, *i.e.*, the non-stationary process was found to occur with slightly lower diffusion coefficients than the steady-state process.

(15) R. Schlögl, *Z. Elektrochem.*, **57**, 195 (1953); M. Tetenbaum and H. P. Gregor, *J. Phys. Chem.*, **58**, 1056 (1954); N. Ishibashi, T. Seiyama and W. Sakai, *J. Electrochem. Soc. Japan*, **23**, 182 (1955); D. Richman and H. C. Thomas, *J. Phys. Chem.*, **60**, 237 (1956). Decrease of counterion diffusion coefficients with increasing solution concentration was observed only with strong-base anion exchangers by F. Nelson, *J. Polymer Sci.*, **40**, 563 (1959).

(16) R. Schlögl and B. Stein, *Z. physik. Chem.* (Frankfurt), **13**, 111 (1957); *Z. Elektrochem.*, **62**, 340 (1958); see also Erratum, *ibid.*, **63**, 341 (1959).

Conclusions

The good agreement between experiments and theory shows that the latter is essentially sound and, within the limits given by the simplifying assumptions, is able to account quantitatively for observed ion-exchange rates and intra-resin concentration profiles. In particular, the predicted characteristic differences in rates and concentration profiles between forward and reverse exchange of two given counterions have been verified experimentally. Since this is the point in which the new theory differs strikingly from the older ones, the superiority of the new theory is clearly established by experimental results. In terms of physical forces, the new theory differs from the older ones by including the effect of intra-resin electric potential gradients. As qualitatively predicted, these gradients also were found to cause characteristic transient changes in the co-ion and water contents of the resin in the course of ion exchange. This additional confirmation of theoretical predictions is further evidence for the importance of the electric potential gradients and thus, indirectly, for the soundness of the theory. Nevertheless, one should not forget that even the new theory gives only limiting laws for ideal systems and is likely to fail when its simplifying assumptions are not met.

Note Added in Proof.—After this paper had been submitted, experimental results obtained by Fedoseeva, *et al.*,[17] came to my attention. These authors have measured various forward and reverse exchange rates with a strong-acid resin (KU-2) in bead form and also give individual counterion diffusion coefficients determined independently by a tracer technique. These results provide an additional possibility of testing the theory by comparing observed and predicted rates. Such comparisons are shown in Fig. 4 for four cases. (The theoretical rates were calculated as described in Parts I and II; since D_H was not measured, it was assumed that $D_H/D_{Na} \cong 7$, as found in aqueous solutions and in most strong-acid resins.) The agreement is very satisfactory, except for the conversion from Na^+ to Sr^{2+} form. This deviation, however, may arise in part from experimental errors, since the experimental points of the exchanges involving Sr^{2+} scatter considerably. In any event, the predicted striking differences in rate between forward and reverse exchange are confirmed qualitatively by the experiments in Fig. 4. The same is true for additional experiments with Na^+ and Ca^{2+} and with H^+ and Sr^{2+}, for which quantitative comparisons could not be made for lack of data.

Acknowledgments.—The help of D. Dere, F. D. Lozano, J. J. Parker, J. E. Fortado, J. Edvalson and E. J. Agazzi in carrying out the experiments, and of Mrs. E. B. Harris in programming the numerical calculations is gratefully acknowledged.

(17) O. P. Fedoseeva, E. P. Cherneva and N. N. Tunitskii, *Zhur. Fiz. Khim.*, **33**, 936 and 1140 (1959).

THE ELECTRICAL CONDUCTIVITY OF SOLUTIONS OF METALS IN THEIR MOLTEN HALIDES. III. CERIUM–CERIUM TRICHLORIDE[1]

BY H. R. BRONSTEIN, A. S. DWORKIN AND M. A. BREDIG

Chemistry Division, Oak Ridge National Laboratory, Oak Ridge, Tennessee

Received June 16, 1961

The specific conductivity of solutions of cerium metal in molten cerium trichloride has been redetermined by a method which avoids contact with ceramic material. The measurements were performed with two rigidly mounted parallel molybdenum electrodes immersed in the melt, which was contained in a molybdenum cup. The electrical conductivity of solutions of Cd metal in molten $CdCl_2$ was redetermined employing a capillary cell technique. These solutions were used as standards to obtain the cell constant of the "parallel electrode cell." The conductivity of the Ce–$CeCl_3$ solutions at 855° was found to rise from 1.20 for the pure salt to 5.35 ohm^{-1} cm.$^{-1}$ at saturation (9.0 mole % Ce). This increase is ascribed to the presence of mobile electrons which may be in equilibrium ($Ce^{3+} + e^- \rightleftarrows Ce^{2+}$) with divalent metal ions known to exist in other rare earth systems. Low conductivity results reported by previous investigators are attributed to a reaction between melt and ceramic container.

Introduction

Several aspects of the behavior of solutions of cerium in cerium trichloride have been examined in recent years. Phase behavior[2,3] and density–composition relationships[4] as functions of temperature on the Ce–$CeCl_3$ system have been investigated by Senderoff and Mellors. These investigators also have examined electrical conductance[4] and half-cell potentials[5] for solutions of cerium in cerium trichloride. From these investigations, in assemblies which required contact of the metal–salt solution with ceramic materials, a strange dependence of electrical conductivity on metal concentration and the existence of a novel, monovalent rare earth ion (Ce^+) have been reported.[4,5] On the other hand, the recent discovery[6–8] of the solid, non-conductive dichloride and diiodide of Nd and of the metal-like diiodides of La, Ce and Pr does not tend to support the assumption that cerium dissolves in molten $CeCl_3$ as Ce^+.

In view of the apparently anomalous behavior of the Ce–$CeCl_3$ system, a re-examination of this system was undertaken in our general program of study of electrical conductivity in molten metal–metal halide systems.

In a preliminary phase of this study, it was observed that Ce–$CeCl_3$ solutions are quite stable in vessels of molybdenum, but that these solutions

(1) Work performed for the U. S. Atomic Energy Commission at the Oak Ridge National Laboratory, operated by the Union Carbide Corporation, Oak Ridge, Tennessee.

(2) G. W. Mellors and S. Senderoff, *J. Phys. Chem.*, **63**, 1111 (1959).

(3) D. Cubicciotti, *J. Am. Chem. Soc.*, **71**, 4119 (1949).

(4) G. W. Mellors and S. Senderoff, *J. Phys. Chem.*, **64**, 294 (1960).

(5) S. Senderoff and G. W. Mellors, *J. Electrochem. Soc.*, **105**, 224 (1958).

(6) L. F. Druding and J. D. Corbett, *J. Am. Chem. Soc.*, **81**, 5512 (1959).

(7) L. F. Druding and J. D. Corbett, *ibid.*, **83**, 2462 (1961).

(8) J. D. Corbett, L. F. Druding and C. B. Lindahl, *J. Inorg. & Nuclear Chem.*, **17**, 176 (1961).

react extensively with ceramic materials such as Al_2O_3, MgO and ThO_2 to form cerium oxychloride.[9] Therefore, while the published information regarding the solubility[2] of Ce in $CeCl_3$ and the density of the metal solutions,[4] where the solutions were only in contact with inert metals such as molybdenum and tungsten, is not in question, the data from electrical conductivity[4] and e.m.f. measurements[5] performed in ceramic vessels must have been adversely affected by such a reaction.

Unfortunately, accurate determination of half-cell potentials must await demonstration of a nonreactive and refractory insulating material. Electrical conductivity measurements, however, can be made with accuracy in systems in which no contact between the solutions and ceramic insulators occurs. The conductivity apparatus developed in this study employed two rigidly mounted parallel electrodes of molybdenum immersed in a melt which was contained in a molybdenum cup. This parallel electrode assembly yielded data of excellent quality with metal–metal halide systems and was employed for all measurements made on the Ce–$CeCl_3$ solutions; excessive polarization at the electrodes precluded use of this apparatus with pure salts. Accordingly, a sapphire cell[10] was used to confirm the previously established conductivity behavior of Cd–$CdCl_2$ solutions[11] and these solutions were used to determine the cell constant for the parallel electrode assembly. In addition, the cell of synthetic sapphire[10] to which $CeCl_3$ is inert in the absence of Ce was used to establish the conductance of pure $CeCl_3$. This parallel electrode assembly, which permits measurement of electrical conductance without contact between the melt and insulating materials, should generally be applicable to many metal–metal halide systems which are not inert to ceramics at elevated temperatures.

Experimental

Apparatus.—The apparatus used for measuring the conductivity of molten Ce–$CeCl_3$ solutions is illustrated elsewhere.[12] The rotatable turret and entry port, which permit entry into and exit from a metal tank without exposing the melt to the atmosphere, and the auxiliary heater operation have been described for a somewhat similar apparatus.[10] The solution was contained in a molybdenum cup, 1 in. diameter by 3 in. in height, insulated from the metal tank by an alumina cup. The electrode arrangement consisted of two parallel molybdenum rods, 0.070 in. in diameter, extending three inches beyond the end of a metal tube. The electrodes were firmly positioned on 0.265 in. centers and insulated from the metal tube by means of a ceramic plug of prefired lavite. Fastened to the top of each rod were two molybdenum wire leads insulated from each other by ceramic tubing and brought out at the top of the tube by means of lead-out seals. The upper portion of this tube was threaded into a Teflon plug positioned in a metal tube of somewhat larger diameter than that of the electrode assembly tube. This arrangement permitted the raising and lowering of the electrodes to various depths in the melt. The depths were measured accurately with a micrometer mounted on the outer tube.

The Marshall furnace in which the tank was placed and the internal heater were controlled so that the temperature gradient and fluctuation in the melt was limited to ±1°. The temperatures measured during the experiments with the Chromel–Alumel thermocouples in the tank wall were corrected to the true melt temperature by comparing them with a stainless steel-sheathed, swaged MgO Chromel–Alumel couple which could be placed directly in the melt. The latter thermocouple also was used to measure the melting point of the pure $CeCl_3$.

The thermocouple was introduced into the melt with the following device: To one end of a stainless steel tube was welded a connecting flange, to which was bolted a pressure-vacuum seal housing. Through this seal, made similarly as described previously,[10] the 1/8 in. o.d. stainless steel-sheathed thermocouple was placed into the tube. The tube was introduced into the tank in a manner previously described.[10] The sheathed thermocouple then could be lowered or raised through the pressure seal to any desired depth in the melt.

For addition of metal and for stirring, the thermocouple was replaced by a 1/8 in. stainless steel rod joined by gold brazing to a 3.5 in. length of molybdenum rod of the same diameter. Attached to the molybdenum rod by molybdenum brads were two molybdenum blades. The metal to be added was fastened to the stirrer blades by molybdenum wire threaded through holes in both the metal and the blades. This assembly was placed in the melt in the same manner as described for the thermocouple. The melt was stirred by loosening the pressure seal slightly and rotating the metal rod.

For the parallel electrode cell, the resistance measurements were made with a four-terminal type transformer bridge.[13,14] A Jones bridge was used with the sapphire capillary cell assembly previously described.[10]

The Parallel Electrode Cell.—The resistance of a solution measured by immersing two rigidly mounted parallel electrodes is a function of the depth of immersion. The difference in the conductance, $1/R$, per unit depth of immersion of the electrodes, s, is a constant

$$(1/R_2 - 1/R_1)/(d_2 - d_1) = s \text{ ohm}^{-1} \text{ cm.}^{-1} \quad (1)$$

where R_1 and R_2 are the resistances at depths d_1 and d_2. R_1 and R_2 are obtained after subtracting both the resistance of the electrodes above the solution and one-half the resistance of the electrodes immersed in the solution. The resistance of the molybdenum electrode rods was accurately measured at the temperature of the experiment by shorting them at various heights by a heavy copper bar clamp. The four-terminal type transformer bridge eliminates the resistance of the leads above the contact with the molybdenum electrodes. For a metal electrode of uniform cross section and a potential drop along the immersed length, small compared with the drop in the melt, the effective resistance can be taken to be one-half of the total resistance of the immersed length. In this consideration, the area of the bottom of the electrode is negligible compared with the total immersed area.

For an ideally rigid and completely reproducible electrode-crucible geometry of the chosen configuration, the *relative* contribution of a partial short circuit through the metallic crucible wall to the total resistance would be a *constant* fraction of that resistance, *i.e.*, independent of the conductivity of the melt and thus simply included in the calibration, *i.e.*, the determination of the cell constant. Such rigidity or reproducibility of geometry cannot be expected in practice. However, since with electrodes of small diameter the bulk potential drop occurs in the small volume element surrounding each electrode, wall effects are negligible if the distance from each electrode to the metal wall of the container is as great or greater than the distance between electrodes. The position of the electrodes in relation to the wall of the metal container is so fixed to be well within the area where the potential is uninfluenced by the metal wall of the container. In agreement with this, the slight lateral motion of the electrodes allowed by the assembly was found to produce no significant effect on the measured resistance in the melt.

Procedure.—The molybdenum electrodes and stirrer were blasted with abrasive before each entry into the solution to remove any slight traces of surface oxidation. Suffi-

(9) H. R. Bronstein, A. S. Dworkin and M. A. Bredig, *J. Phys. Chem.*, **64**, 1344 (1960).

(10) H. R. Bronstein and M. A. Bredig, *J. Am. Chem. Soc.*, **80**, 2077 (1958).

(11) A. H. W. Aten, *Z. physik. Chem.*, **73**, 578 (1910).

(12) A. S. Dworkin, H. R. Bronstein and M. A. Bredig, *Discussions Faraday Soc.*, in press.

(13) H. R. Bronstein and M. A. Bredig, *J. Phys Chem.*, **65**, 1220 (1961).

(14) E. Fairstein, "An AC Bridge for Measuring Low Resistances," ORNL Instrumentation and Controls Division Semiannual Progress Report, ORNL-1997, 9 (July 31, 1955).

cient anhydrous salt, accurately weighed, was placed in the molybdenum cup, under argon, to give a depth of 2 in. of liquid. The salt was further vacuum-dried in the apparatus and then melted under an argon atmosphere of approximately 24 p.s.i.a.

The sapphire capillary cell assembly was introduced into the melt and measurement of the electrical conductivity of the pure salt made as previously described.[10] After withdrawal of the sapphire cell assembly from the apparatus, an accurately weighed piece of metal was introduced into the melt as described above. (In the case of cerium metal, all manipulations were done under argon.) The solution was stirred intermittently for approximately one hr. at temperature (600° for Cd solutions, 855° for Ce solutions). Composition of the solutions was defined by the weights of the components.

The parallel electrode cell assembly was introduced in the same manner as the sapphire cell. The position of contact with the surface of the melt, as indicated by current flow in the bridge circuit, was determined on carefully lowering the electrode tube by means of the screw arrangement. In order to avoid end effects of the electrodes close to the surface, resistance measurements were commenced in all cases 0.5 in. below the surface of the melt. Resistance readings were made every 0.1 in. to a total depth of 1.3 in. At this depth of immersion, the crucible bottom does not affect the resistance. A plot of the conductance *vs.* depth of immersion in centimeters yields a straight line, the slope of which, "*s*," is the conductance per unit length as expressed by equation 1.

Cell Constant.—Since equation 1 is linear, it follows that

$$\kappa_{unkown} = \frac{s_{unknown}}{s_{known}} \kappa_{known}$$

and

$$\frac{\kappa_{known}}{s_{known}} = C, \text{ "cell constant"}$$

of this parallel electrode arrangement. Attempts to determine this cell constant using pure molten salts were unsuccessful due to excessive polarization at the electrodes. A means of overcoming this polarization effect was to introduce a reducing agent into the salt, *i.e.*, a metal dissolved in its molten salt. While the alkali–alkali halide solutions[10,13] could not be used in the present apparatus due to the high vapor pressure of the alkali metal, Cd–$CdCl_2$[14] solutions were quite suitable. As the latter solutions are non-reactive with sapphire (Al_2O_3),[15] their conductivities were obtained by the capillary cell method, and they then were used as standards for calibrating the "parallel electrode cell." Also, the relatively small concentration dependence of the specific conductance of this system,[11] 1.968 ohm^{-1} cm.$^{-1}$ for pure $CdCl_2$ to 1.906 ohm^{-1} cm.$^{-1}$ for 10 mole % Cd at 600°, minimized any error due to small changes in concentration. Our measured values of the specific conductivity of these solutions from 0 to 15 mole % (saturation)[16] Cd metal agree with Aten's[11] values to better than 1.0%. The cell constant of the sapphire cell was obtained using a 1-Demal KCl solution at 25.0°, the thermal expansion of less than 0.5% being within the error of the high-temperature measurements.

Measurements were made with the parallel electrode cell at 2.7 and 15 mole % (saturation) Cd. No polarization effects were noted as the resistance was independent of frequency in the range of 2 to 10 Kc. The actual resistances measured were of the order of 0.1 to 0.2 ohm, while the resistance corrections of the electrodes were of the order of 0.02 ohm. These resistances were measured with the transformer bridge to ±0.0001 ohm. The error in the determination of the slope, "*s*," was approximately ±1%.

The cell constant, *C*, of the parallel electrode cell was calculated from the result at saturation, namely, from the conductivity κ measured by means of the sapphire cell and the slope "*s*" obtained with the parallel electrodes.

$$C = \frac{\kappa_{(sapphire\ cell)}}{s} = \frac{1.88 \text{ ohm}^{-1} \text{ cm.}^{-1}}{3.32 \text{ ohm}^{-1} \text{ cm.}^{-1}} = 0.566$$

The specific conductivity of the 2.7 mole % Cd solution was calculated from the "cell constant," *C*, and slope $s = 3.46$ ohm^{-1} cm.$^{-1}$, obtained with the parallel electrode cell for this concentration. ($\kappa = (0.566)(3.46)$ ohm^{-1} cm.$^{-1}$ = 1.96 ohm^{-1} cm.$^{-1}$) This value is in excellent agreement with that taken from a plot of specific conductivity *vs.* mole % Cd based on measurements by Aten[11] and with our sapphire cell (1.960).

Materials.—The anhydrous $CeCl_3$ was prepared from $CeCl_3 \cdot 7H_2O$ obtained from two different sources. The material from the first source was used in the first two series of runs while that from the second source was used in a third series. The hydrate was partially dehydrated in a vacuum desiccator over P_2O_5 for four days. It then was heated with NH_4Cl in an evaporating dish and thereafter *in vacuo* at 300°. The anhydrous $CeCl_3$ finally was sublimed under vacuum at 950°. Spectrographic analysis indicated no foreign metals present. No material insoluble in water or alcohol was found. An analysis for cerium and chloride gave an over-all purity of 99.6%. The melting point of $CeCl_3$ was 817°, in agreement with that found by F. H. Spedding and A. H. Daane,[17] and 5° higher than that found by Mellors and Senderoff.[2] Analysis of the Ce metal gave a purity of 99.7%. Spectrographically, no other metals were found.

Anhydrous $CdCl_2$ was prepared from $CdCl_2 \cdot 2.5\ H_2O$. The hydrate was vacuum dried over P_2O_5 at room temperature followed by gradual raising of the temperature to 400° over a three-day period. The salt was treated with HCl + Cl_2 while held molten at 600°. After removing these gases by a flow of argon, the melt was filtered through sintered quartz.

The cadmium metal was "Baker analyzed, assay 100% Cd."

Results and Discussion

Table I contains the results of measurements of the specific conductivity of three separate samples of pure $CeCl_3$ over the temperature range 830 to 930°. Measurements were made in a manner previously described[10] employing a synthetic sapphire cell having a cell constant of 129 cm.$^{-1}$. The resistance measured was independent of frequency within 0.1% in the interval 2 to 10 Kc. Our values for the specific conductivity of $CeCl_3$ are approximately 25% higher than those reported by Mellors and Senderoff.[4] In the evaluation of this discrepancy, as well as of the strange sharp drop in the density of the salt on addition of as little as 0.25 mole % metal, which yielded the enormous value of 500 cc. per mole for the volume of the electron,[2] the lower melting point of the salt reported by Mellors and Senderoff[2] may be of significance.

TABLE I

ELECTRICAL CONDUCTIVITY OF $CeCl_3$

Series no.	Temp., °C.	κ, ohm^{-1} cm.$^{-1}$	$\Lambda = \kappa \cdot V_{equiv}$,[a] ohm^{-1} cm.^{2} equiv^{-1}
1	828	1.12	28.9
1	844	1.17	30.3
3	854	1.19	30.9
2	858	1.21	31.5
1	868	1.23	32.1
2	886	1.29	33.8
1	895	1.30	34.1
1	931	1.38	36.6

[a] V_{equiv} was obtained by extrapolation of the molar volumes of the solutions reported by Mellors and Senderoff[4] to 0% Ce and interpolation for respective temperatures.

Table II lists the specific conductivity of Ce–$CeCl_3$ solutions measured at 855° with the "parallel electrode cell" for three independent series of measurements starting with pure $CeCl_3$ for each series.

(15) Exposure of the sapphire cell to pure $CdCl_2$, $CeCl_3$ and to solutions of Cd–$CdCl_2$ did not result in any weight change. The cell constant also remained unchanged.

(16) L. E. Topol and A. L. Landis, *J. Am. Chem. Soc.*, **82**, 6291 (1960).

(17) F. H. Spedding and A. H. Daane, *Metallurgical Rev.*, **5**, 297 (1960).

With the addition of as little as 0.13 mole % Ce, the frequency effect found in attempts to measure the conductivity of the pure salt by this arrangement was no longer present. At the end of each series, the contents of the molybdenum cup were analyzed for CeOCl.[9] Only trace quantities were ever found.

TABLE II

SPECIFIC CONDUCTIVITY OF SOLUTIONS OF CERIUM IN MOLTEN CERIUM TRICHLORIDE AT 855°

Series no.	Mole % Ce	κ, ohm^{-1} cm.$^{-1}$	
	0	1.20 (sapphire cell value)	
	0	1.20 (extrapolated, parallel electrode cell)	
3	0.13	1.22	
2	.24	1.23	
3	.31	1.28	
2	.58	1.31	
2	1.00	1.38	
1	1.73	1.56	
2	2.50	1.78	
3	3.10	2.02	
1	3.35	2.12	
2	4.75	2.59	
3	5.87	3.26	
1	6.70	3.81	
1	7.90	4.45	
1	Satn. (9.0)[a]	5.44	5.35
1	Satn. (9.0)[a]	5.26	
1	Satn. (9.0)[a]	5.35	

[a] The total amounts of Ce present in cup for the points designated "saturation" were 9.4, 11.9 and 17.3 mole % Ce.

As shown in Fig. 1, a short extrapolation of the Ce–$CeCl_3$ conductivities to that of pure $CeCl_3$ yields a specific conductivity of 1.20 ohm^{-1} cm.$^{-1}$ at 855°, in exact agreement with the value determined using the sapphire cell. This constitutes an excellent verification of the cell constant obtained from the Cd–$CdCl_2$ solutions.

Three conductivity points obtained when the total amount of Ce in the crucible was 9.4, 11.9 and 17.3 mole % Ce resulted in a constant value of 5.35 ± 0.06 ohm^{-1} cm.$^{-1}$. The concentration of Ce (9.0 mole %) at which the conductivity *vs.* mole % Ce curve intersects this value, 5.35 ohm^{-1} cm.$^{-1}$, is the saturation concentration and is in good agreement with that obtained by Mellors and Senderoff[2] in an all-molybdenum apparatus.

Our conductivity results, however, differ strikingly from those of Mellors and Senderoff,[4] who found the specific conductivity to increase from below 1.0 to 1.4 ohm^{-1} cm.$^{-1}$ in the concentration range 0–0.65 mole % Ce, followed by a further increase to only 1.8 ohm^{-1} cm.$^{-1}$ at 8 mole % Ce. As discussed previously,[9] the large discrepancy in the conductivity of the cerium metal solutions is explained by the removal of Ce metal, in the measurements of Mellors and Senderoff, by reaction with the container material, Al_2O_3, to form CeOCl.

The rapid increase, Fig. 1 and Tables II and III, in both the specific and equivalent conductances of the solutions with metal concentration, the rate of which also increases, indicates a large

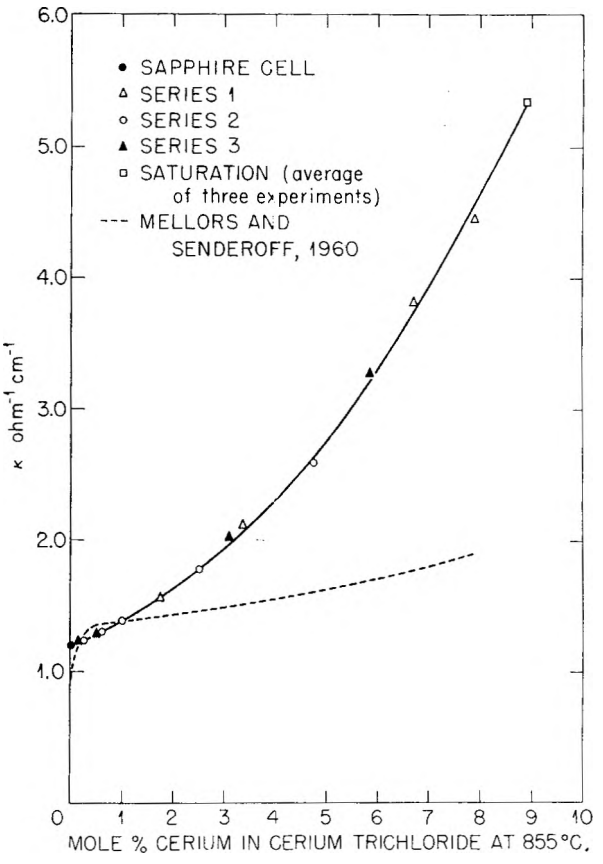

Fig. 1.—Specific conductivity of solutions of Ce in $CeCl_3$ at 855°.

proportion of conductance by electrons. No solute species conducting solely by ion transport would produce, in an amount corresponding to only 9 mole % Ce metal, an increase to a value 4 to 5 times that of the trichloride. No solid phase containing Ce in a valence state lower than 3 was found in the Ce–$CeCl_3$ system.[2,3] Whether a lower valent ionic Ce species such as Ce^{2+} exists at all in the molten solution or, in other words, what the extent of the equilibrium $Ce^{2+} \rightleftarrows Ce^{3+} + e^-$ is, cannot be deduced from the present data. The electronic conductance could be due entirely to the presence of mobile electrons from the re-

TABLE III

EQUIVALENT CONDUCTANCE AT 855°

Mole % Ce	Λ_{soln} (Ce solute), ohm^{-1} cm.^{2}	Λ_{soln} ($CeCl_2$ solute),[a] ohm^{-1} cm.^{2}
0.0	31.2	31.2
1.0	36.1	36.5
2.0	42.2	43.1
3.0	50.0	51.6
4.0	59.2	61.7
5.0	69.9	73.6
6.0	82.8	88.0
7.0	97.3	105
8.0	113	123
9.0 (sat.)	127	140

[a] $\Lambda_{soln} = \dfrac{f_{solute}E_{solute} + (1 - f_{solute})E_{CeCl_3}}{\rho}\kappa$ where f_{solute} is the equivalent fraction of Ce/3 or $CeCl_2$ and E the equivalent weight. The density, ρ, was taken from the measurements by Mellors and Senderoff,[4] with the value for pure $CeCl_3$ extrapolated from those of the solutions.

action $Ce \rightarrow Ce^{3+} + 3e^-$. However, Ce^{2+} ions could be assumed to contribute electronic conductance at a rate increasing with concentration due to overlap of their electronic orbitals, as discussed previously[10,13] for alkali metal atoms or molecule ions. An additional contribution might result from an exchange of electrons between two adjacent valence states, Ce^{2+} and Ce^{3+}. Recent results with Nd–$NdCl_3$ solutions to be reported in detail elsewhere[12] suggest the possibility of such an exchange.

Acknowledgment.—The authors gratefully acknowledge the many helpful suggestions of Dr. M. J. Kelly of this Laboratory concerning the design of the electrode arrangement used in these measurements. We also wish to acknowledge the assistance of D. E. Lavalle of this Laboratory in preparing the anhydrous salts.

CHEMISORPTION STUDIES ON SUPPORTED PLATINUM

BY HANS L. GRUBER

Research and Development Department, The Atlantic Refining Company, Philadelphia, Penna.

Received June 19, 1961

The adsorption of hydrogen, oxygen and carbon monoxide on platinum-on-alumina re-forming catalysts and on the alumina base was investigated. By means of hydrogen adsorption the platinum surface area of freshly prepared samples was found to be 200 to 270 m.²/g. of platinum. The decrease of platinum dispersion due to heat treatment of catalysts is shown. Several catalysts were subjected to complete oxidation–reduction cycles and the amount of hydrogen and oxygen taken up in the different steps of such a cycle was measured. A probable mechanism for the oxidation–reduction cycle was established. The mechanism of CO adsorption on supported platinum was found to depend not only on the nature of the support but also on the degree of dispersion of the metal. The fraction of CO adsorbed in the bridged structure decreases with decreasing metal dispersion.

Introduction

With the increasing commercial importance of supported metal catalysts of low metal concentration, the physical structure of such catalysts has become of considerable interest. In most cases the metal crystallite size is too small to be measured by X-ray techniques and therefore chemisorption seems to be the only approach to the measurement of metal dispersion.

Chemisorption has been used in the past for surface area determinations. However, due to the experimental difficulties of obtaining clean surfaces and the theoretical difficulties of defining a monolayer, chemisorption was later completely displaced by the BET method. Only for samples of very small surface area (metal wires and films) and for multicomponent systems, where one wanted to discriminate between the surfaces of different components, was chemisorption still very useful. In their extensive studies of iron synthetic ammonia catalysts, Emmett and co-workers[1,2] developed a low temperature chemisorption method to determine the surface concentration of the different components in the catalyst. The procedure later was successfully applied to Fischer–Tropsch and other catalysts.[3–5] In all these cases the metal concentration was high enough to represent a substantial part of the surface. For metal concentrations in the order of 1% or less the low temperature chemisorption procedure is not applicable.

High temperature adsorption on supported metal catalysts was studied by several workers.[6–8] Their results gave mainly qualitative information, allowed comparisons of catalysts of similar nature but did not allow quantitative interpretations as to the surface area of the metals. Very recently, the chemisorption at room temperature or above has been employed successfully in several laboratories[9–13] to study the metal dispersion of reforming catalysts.

In the present work we have investigated the adsorption of hydrogen, oxygen and carbon monoxide on platinum-on-alumina catalysts and on the alumina base itself, in order to study metal dispersion, to correlate results obtained with different adsorbates, and to elucidate reduction–oxidation mechanism of such catalysts.

Procedure.—The basic principle of measuring the specific adsorption on a supported metal surface, as it was first utilized by Boreskov,[14] is to select adsorbate and adsorption parameters in such a way as to avoid or minimize adsorption on the support and to facilitate full monolayer coverage or maximize adsorption on the metal. If under the chosen optimum conditions adsorption on the support material still occurs to an extent which makes it advisable to correct for it, it is possible to do so by measuring adsorption on the non-metallized support and by subtracting this value from the total adsorption on the catalyst. This procedure gives what we will call the "net adsorption" on the supported metal.

This net adsorption (V), in cc. of gas adsorbed per g. of catalyst, is by itself a measure of the metal dispersion for a given metal content. It is more convenient to express net

(1) P. H. Emmett and S. Brunauer, *J. Am. Chem. Soc.*, **59**, 310 (1937).

(2) P. H. Emmett and N. Skau, *ibid.*, **65**, 1029 (1943).

(3) R. B. Anderson, W. K. Hall and L. J. E. Hofer, *ibid.*, **70**, 2465 (1948).

(4) P. Y. Butyagin and S. Y. Elovich, *Zhur. Fiz. Khim.*, **26**, 692 (1952).

(5) L. D'Or and A. Orzechowski, *J. Chem. Phys.*, **51**, 467 (1954).

(6) W. W. Russel and H. S. Taylor, *J. Phys. Chem.*, **29**, 1325 (1925).

(7) L. H. Reyerson and L. E. Swearingen, *ibid.*, **31**, 88 (1927).

(8) R. Burshtein and A. Frumkin, *Trans. Faraday Soc.*, **28**, 273 (1932).

(9) T. R. Hughes, R. J. Houston and R. P. Sieg, 135th Natl. Meeting, Am. Chem. Soc., Div. Petrol. Chem., Preprints 4, C-33 (Apr. 1959).

(10) L. Spenadel and M. Boudart, *J. Phys. Chem.*, **64**, 204 (1960).

(11) S. F. Adler and J. J. Keavney, *ibid.*, **64**, 208 (1960).

(12) G. A. Mills, S. Weller and E. B. Cornelius, Preprint No. 113, Second Intern. Congr. on Catalysis, Paris, 1960.

(13) H. L. Gruber and J. H. Ramser, presented at 136th Natl. Meeting, Am. Chem. Soc., Atlantic City, Sept. 1959.

(14) G. K. Boreskov and A. P. Karnaukhov, *Zhur. Fiz. Khim.*, **26**, 1814 (1952).

adsorption per g. of metal, independent of metal concentration, by using the ratio of number of atoms or molecules of gas adsorbed per metal atom (G/M). Knowing the adsorption mechanism one can convert G/M into the ratio of the number of accessible metal atoms to the total number of metal atoms (M^*/M). M^*/M can vary from 0 to 1, corresponding to "zero dispersion" (bulk metal) and "complete dispersion" (monolayer or particles with no interior atoms), respectively. It also is possible to calculate from this data surface area or average particle size of the metal, but not without making a few rather arbitrary assumptions. This point will be discussed in detail later.

Selection of Adsorbate.—From the considerations outlined above, it follows that physisorption must be avoided as far as possible. The amount of physisorption on a given adsorbent will decrease with decreasing boiling point of the adsorbate, with decreasing pressure and with increasing temperature. In general, therefore, one should work at the highest possible temperature and the lowest possible pressure with a low boiling adsorbate which is chemisorbed readily by the metal with very little or no chemisorption occurring on the support. The gases most likely to meet these requirements are hydrogen, oxygen and carbon monoxide.

Oxygen, which was used as an adsorbate by Webb[15] and by Mills,[12] is known to form surface oxide films which can be more than 1 layer thick and of undefined stoichiometry. We have used oxygen therefore only to study the oxidation mechanism but not to determine the metal dispersion.

Carbon monoxide, which was used by Hughes[9] and Mills,[12] is physisorbed to about 1% coverage at room temperature and 100 mm. It therefore should be used only at low pressures (<1 mm.). At higher pressures, physisorption would lead to sizable correction terms in a volumetric procedure and could cause substantial errors. We have used carbon monoxide primarily in a flow procedure, where by using a "slug technique"[16] physisorption is avoided.

Hydrogen, which was used as adsorbate by several workers, shows no measurable physisorption at room temperature or above. With some metals (*e.g.*, Pd), absorption or solid solution might occur to an extent which would complicate or even prohibit its use. With platinum, absorption below 400° is not measurable,[17] and extrapolation of high temperature data indicates absorption of less than 0.01 vol. % at 250°. This value, being several orders of magnitude smaller than the amount adsorbed, can be safely neglected and hydrogen thus appears very well suited for volumetric adsorption measurements.

Selection of Adsorption Parameters.—The optimum temperature for the adsorption measurements with a given system of adsorbent and adsorbate is the one at which the difference in adsorption on the two components (metal and support) is a maximum. Such a maximum can best be located from the corresponding adsorption isobars. As to the hydrogen isobar on platinum, quite a few data are available in the literature.[17-19] At pressures >100 mm. and in the temperature range of interest, the data show a slight and steady decrease of adsorption. For hydrogen adsorption on alumina, the few data available[20,21] indicate poor reproducibility, even with identical samples. This is not surprising in view of the fact that the surface properties of alumina will not only depend on the specific type of alumina used and its purity, but also on the previous history of the sample (method of preparation, calcination time and temperature, degree of dehydration, etc.). We therefore have taken great care to determine adsorption isobars for hydrogen on our alumina at several pressures, in order to establish a reliable correction value for the catalyst support.

Experimental

Two different experimental procedures were used. Most of the CO-adsorption measurements were obtained by a new slug flow technique described in detail elsewhere.[16] Adsorption of hydrogen and oxygen was measured by standard volumetric methods. The glass apparatus used was of conventional design.[22] The sample size could be varied between 5 and 40 g. The gas buret and the constant volume manometer were temperature controlled to 0.1°. The manometer (precision bore tube of 16 mm. i.d.) was read with a cathetometer to 0.05 mm. Low pressures were measured by means of a McLeod gage or an ionization gauge.

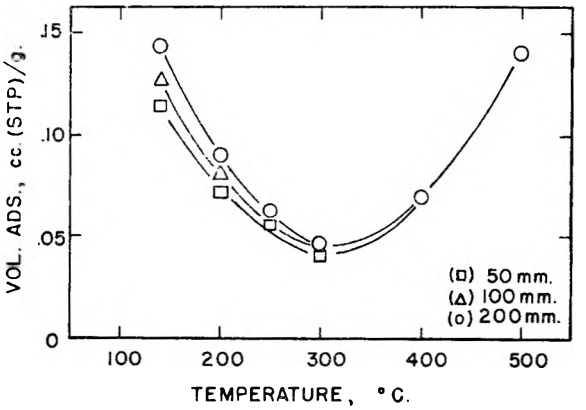

Fig. 1.—H_2 adsorption isobars on η-alumina: 50, 100 and 200 mm.

The system and the samples were evacuated by an oil diffusion pump, which was backed by a mechanical forepump. The samples were protected from oil and mercury vapors by means of cold traps at liquid nitrogen or Dry Ice temperatures.

The prepurified and dried gases were introduced into the gas storage flasks through a purification train, consisting of a liquid nitrogen cold trap and of a silica gel trap at liquid nitrogen temperature. All dead space calibrations were obtained with helium. BET surface areas were determined with nitrogen.

The η-alumina used as support material in this work was calcined at 600° and had the properties

BET surface area, m.²/g.	210
Pore volume, cc./g.	0.55
Skeletal density, g./cc. (determined with helium)	3.31
Impurities, p.p.m.:	
Alkali (Na_2O)	20
Alkaline earths	110
Silicon	33
Iron	55

The catalyst samples were prepared by impregnation of the support with platinum salt solutions in conventional ways. The purity of the platinum salts used was better than 99.9%. The alumina blank for the adsorption measurements was treated identically to the catalyst preparations, except that the platinum salt solution was replaced by water of corresponding *p*H value. After calcination all samples were reduced in flowing hydrogen for 2 hr. at 500°.

Evacuation of the samples overnight (16 hours) at 500° and at a pressure of less than 10^{-5} mm. was adopted as standard pretreatment. This resulted in good reproducibility of the adsorption measurements on the alumina, whereas less severe conditions (a temperature of 450° or lower, and a time of 6 hr. or less) were not satisfactory. The reproducibility of the hydrogen adsorption measurements was ±1% using a 40-g. sample of the blank and a 5-g. sample of platinized catalyst.

Results and Discussion

Adsorption of H on η-Al_2O_3.—Hydrogen adsorption isotherms on the η-alumina support (without metal) were measured at several temperatures. At temperatures higher than 250° saturation occurred at a pressure of 50 to 100 mm. At lower temperatures no such saturation was found in the

(15) See ref. (8) in A. N. Webb and T. T. Mitchell, *J. Phys. Chem.*, **63**, 1880 (1959).

(16) H. L. Gruber, to be published.

(17) Gmelins Handb. d. Anorg. Chemie, Syst. No. 68, "Platin," Part C, Verlag Chemie, Weinheim, 1939, p. 7 ff.

(18) A. F. Benton, *J. Am. Chem. Soc.*, **48**, 1850 (1926).

(19) Takao Kwan, *J. Research Inst. Catalysis*, **1**, 81 (1949).

(20) A. S. Russell and J. J. Stokes, Jr., *J. Am. Chem. Soc.*, **69**, 1316 (1947).

(21) H. W. Guenther, *Dissertation Abstr.*, **15**, 507 (1955).

(22) G. L. Joyner, "Scientific Glass Blowing," Instruments Publishing Co., Pittsburgh, Pa., 1949.

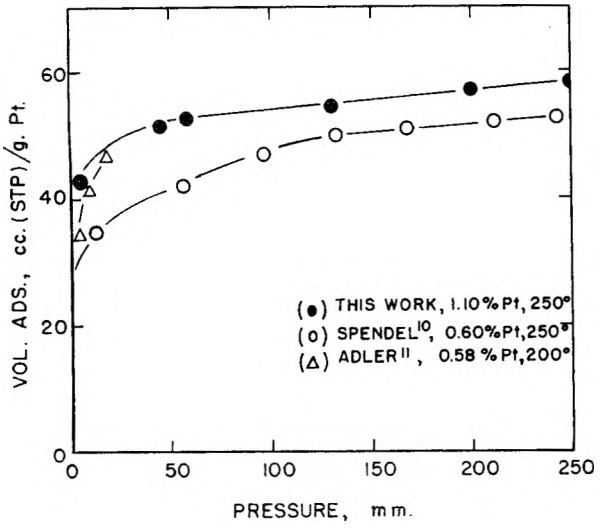

Fig. 2.—H_2 adsorption isotherms on platinum-on-alumina.

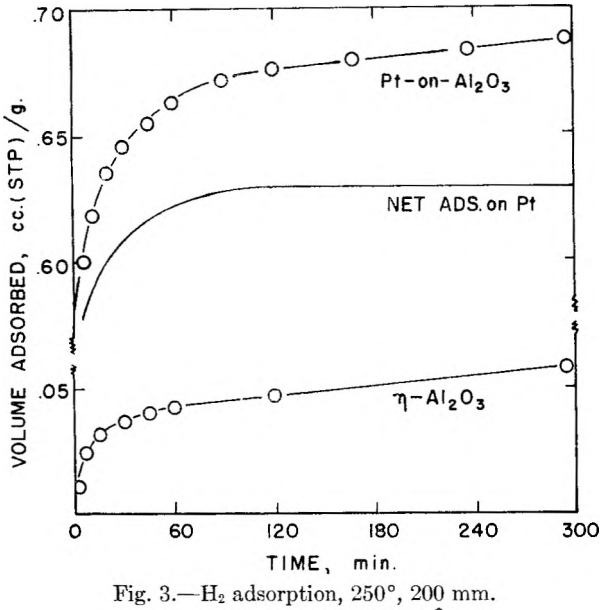

Fig. 3.—H_2 adsorption, 250°, 200 mm.

pressure range studied (up to 200 mm.). The data are plotted in the form of an isobar in Fig. 1. The minimum in the isobar indicates two types of hydrogen adsorption which we call Type A (high temperature) and Type B (low temperature). Type B cannot be ascribed to physisorption for two reasons: (a) the amount is too large to be accounted for by physical adsorption at that temperature; (b) the rate is slow. Due to the appreciable pressure changes in the volumetric system during adsorption, we did not attempt any quantitative evaluation of the rate data accumulated in the course of the determination of the different isotherms. Qualitative information on rates and heats of adsorption is summarized in Table I.

From this data one has to conclude that both Type A and Type B are chemisorption. Type B, having the smaller activation energy, may represent chemisorption on aluminum ions, A on oxygen ions.[23,24] However, our data do not

TABLE I

	Type B (descending branch of isobar)	Type A (ascending branch of isobar)
Temp. range, °C.	140–300	300–500
Rate	Slow	Very slow
Amt. adsorbed after 2 hr. (% of equilibrium), %	80	25
Time required for complete equilibrium, hr.	20–24	100–120
Estimated heats of adsorption, kcal.	7–12	12–18

suffice to draw final conclusions on the mechanism involved.

The minimum in the isobar certainly suggests the temperature range of 250 to 300° as the optimum range for measuring specific adsorption on the alumina-supported platinum and therefore 250° was selected as the temperature for all hydrogen adsorption measurements on the platinum-on-alumina catalyst.

Adsorption of H on Pt-on-Al_2O_3.—An adsorption isotherm of hydrogen on a sample of 1.1% Pt on η-Al_2O_3 was measured at 250° up to a pressure of 250 mm. The results, in terms of cc. (STP) of hydrogen adsorbed per g. of platinum, are shown in Fig. 2 in comparison with data obtained by Spenadel[10] and by Adler[11] for catalysts containing 0.6 and 0.58% Pt, respectively. Plotting adsorption per gram of platinum does not imply that this adsorption is due to the platinum alone but facilitates comparison of data for catalysts of different Pt content. Considering the difference in catalyst preparation as well as the fact that corrections for the support have not been applied, the agreement between the three isotherms, measured in different laboratories, is quite satisfactory.

In the pressure range which we studied, adsorption did not reach a true saturation value. However, at pressures above 100 mm. the slope of the isotherm is very small and constant. For surface area determinations, the hydrogen adsorption therefore is measured between 100 and 200 mm.

The rate of hydrogen adsorption on the catalyst was quite fast initially, about 90% of the total amount being taken up in the first 5 min., but fell off appreciably during the first hour. Complete equilibration at 100 mm. and 250° took about 20 hr. Since as shown previously, adsorption on the support was slow, taking 20 to 24 hr. for equilibration at 250° (see Table I) and since hydrogen adsorption on a clean platinum surface is very fast, it was thought that the slow uptake found with the catalyst might be due to the support only.

A close comparison of the adsorption *vs.* time curves for a platinum catalyst and for the corresponding support (see Fig. 3, note break in ordinate scale), shows this to be true. If the adsorption on the support at any given time is subtracted from the adsorption on the catalyst, the net adsorption *vs.* time curve is obtained. This curve levels out completely at 2 hr. proving that any gas uptake beyond this time is due to adsorption on the

(23) R. M. W. Trapnell, "Chemisorption," Academic Press, New York, N. Y., 1955, p. 76.

(24) E. Wicke, *Z. Elektrochem.*, **53**, 279 (1949).

support only. In all the adsorption measurements for surface area determination a time of 2 hr. therefore was allowed for equilibration.

The nearly instantaneous adsorption on the platinum of about 90% of the final amount also indicates that our reducing and pretreating conditions are satisfactory and result in a relatively clean surface. The slow rate of uptake of the remaining 10% which is adsorbed over the first two hours could be due to impurities as suggested by Adler[11] or due to the high surface coverage on the platinum as suggested by Spenadel.[10] Since in our work repeating the hydrogen adsorption up to 4 times on the same sample gave adsorption *vs.* time curves identical within experimental error, and since several adsorption runs on a platinum black under similar conditions showed an instantaneous uptake of 98% of the total amount, neither one of the two above explanations seems satisfactory. We suggest that the slow adsorption on a fresh catalyst is due specifically to the supported nature of the metal in the following sense: Whereas the bulk of the adsorbed hydrogen molecules will find two platinum sites on the same patch or crystallite of platinum, some of the H molecules adsorbed at rather high coverage will find single isolated platinum sites, which will adsorb one of the two H atoms only. Whether the second H atom then is adsorbed by adjacent oxygen ions of the support, or whether it migrates over the oxide surface to another patch or crystallite of platinum, in both cases we are dealing with a slow, activated process. This hypothesis is supported further by the experimental finding that the relative amount of slow adsorption decreases as the platinum dispersion decreases.

Net Adsorption on Pt.—The difference between the total adsorption on the catalyst and the adsorption on the corresponding support under identical conditions is taken as the net adsorption of hydrogen on the metal. This procedure implies the assumption that the adsorption properties of the carrier toward hydrogen are not affected by the presence of up to 1% platinum on the carrier surface. Since the BET area of the alumina is in the order of 200 m.²/g. and does not change due to the impregnation, calcination and reduction steps employed, the metal, even at maximum dispersion, cannot cover more than 1.5% of the support surface. Therefore, in the case where there is on the carrier surface an independent and random distribution of sites active in hydrogen adsorption and of sites active in platinum adsorption, the above assumption is correct.

It is possible, however, that the same sites which are active in H adsorption preferentially adsorb platinum ions during impregnation. Since the total H adsorption on the carrier is far below a coverage of 1%, impregnation in this case might completely deactivate the carrier for hydrogen adsorption. Such an identity between H and Pt adsorption sites is very unlikely. There is strong experimental evidence for its non-existence in the fact that the impregnated catalyst shows exactly the same rate of slow H_2 uptake over 20 hr. as found for the support. It appears, therefore, that applying the correction for adsorption on the support is well justified. The same conclusion was reached previously by Spenadel[10] on the basis of a different argument.

Metal Dispersion and Surface Area.—The net adsorption per gram of catalyst (see Table II, col. 2) can be converted to a ratio of number of H atoms adsorbed per Pt atom present in the sample, as given in the 3rd column of Table II. We consider this ratio as the physically most significant measure of metal dispersion, since it can be obtained without specific knowledge of surface coverage or adsorption mechanism and without any assumptions concerning these two points. The hydrogen-to-platinum ratio of most of the fresh catalysts studied was in the range of 0.8 to 1.0, in agreement with values reported by Spenadel[10] and by Mills.[12] In no case did we find ratios higher than one after proper reduction of the catalyst, as was reported by Adler.[11] The variation of metal dispersion in the range of 0.8 to 1.0 is attributed to minor variations in the preparation procedure. Sintered and deactivated catalysts showed substantially lower H/Pt ratios, in the order of 0.4 to 0.1.

TABLE II

HYDROGEN ADSORPTION AND METAL DISPERSION

Catalyst	Net ads., cc./g. Pt	Ratio $R = \frac{G}{M}$	S.A., m.²/g. Pt	Part. size, Å.
1.1% Pt on η-Al_2O_3				
TPH,[a] reduced 2 hr. 120° and 2 hr. 510°	0.615	0.97	268	<10
CPA,[b] reduced 2 hr. 510°	.523	.83	229	<10
TPH, reduced 2 hr. 510°	.535	.85	235	<10
TPH, deactivated by severe lab. regeneration	.109	.17	47	50
1.1% Pt (TPH) on η-Al_2O_3				
Sintered in H_2, 500°, 0 hr.	.515	.82	226	<10
72 hr.	.326	.52	144	16
200 hr.	.273	.43	119	20
1200 hr.	.203	.32	88	27
4% Pt on Alon-C[f]	.927	.40	110	21
Pt black, 99.0% Pt (J. Bishop & Co., Malvern, Pa.)	.461	.008	2.2[c]	1000[e]
			2.4[d]	800[e]

[a] TPH = Tetramminoplatinum hydroxide impregnation. [b] CPA = Chloroplatinic acid impregnation. [c] Calculated from H_2 adsorption data after 250° evac. [d] BET surface area. [e] X-Ray line broadening. [f] Alon-C is a high purity, non-porous γ-Al_2O_3 of 100 m.²/g. BET area and is obtainable from Godfrey L. Cabot, Inc., Boston, Mass.

The metal dispersion also can be characterized in terms of metal surface area and average metal particle size. The calculation of these terms requires a number of assumptions as discussed in detail by Hughes,[9] Spenadel[10] and Adler.[11] In order to calculate the surface area, the amount adsorbed in a complete monolayer (V_m) or the coverage $\theta = V/V_m$ must be known. From the shape of the isotherm (see Fig. 2) we have decided to take the amount of hydrogen adsorbed at 100 mm. as representative of a full monolayer. The pressure of 100 mm. corresponds to the classical "Point B" where the slope of the isotherm becomes constant. This is an empirical and somewhat arbitrary choice but it is supported by results on Pt black and Pt films which indicate that under the chosen experimental conditions (250°, 100 mm.) saturation is at least closely approached. If we

further assume that each platinum surface atom adsorbs one H atom and if we take the cross-sectional area (σ) of one Pt atom as equal to 8.9 Å.^{2}, which is an average value of the 3 low index planes (100), (110) and (111), then the surface area (S) per gram platinum can be calculated according to the equation

$$S = \frac{N_A \sigma}{M} \times R$$

where N_A is Avogadro's number, M is the molecular weight of platinum and R is the ratio of H atoms adsorbed per Pt atom. Values of S calculated in this way are given in Table II.

In addition the table lists average Pt particle sizes which were estimated on the basis of Hughes' model: all particles being ideal cubes of uniform size with one face in contact with the support and the remaining 5 faces exposed. The length of one edge (d) of the cube then is related to surface area (S) and volume (V) or density (ρ) by

$$d = \frac{5V}{S} = \frac{5}{S\rho}$$

Since information about the particle shape cannot be obtained from the adsorption data, other models such as semi-spheres or pyramids[11] would serve our purpose as well. It should be emphasized that although all the assumptions made to calculate surface area and particle size are reasonable, the characterization of the metal dispersion of supported platinum by the use of the ratio R (number of H atoms adsorbed per Pt atom in the sample), which does not involve these assumptions, is to be preferred.

Adsorption of Oxygen.—A series of experiments with oxygen was carried out (a) to establish whether oxygen adsorption can serve as a measure of metal dispersion and (b) to obtain information about the oxidation–reduction mechanism. The adsorption of oxygen was measured at 350° and 150 mm. and was corrected for adsorption on the support (0.04 cc. per g. under the given conditions).

Several fresh catalysts after standard reduction and a series of catalysts sintered at 500° in hydrogen were subjected to complete cycles of reduction–oxidation, consisting of 2 hydrogen adsorptions followed by 2 oxygen adsorptions, followed by 2 hydrogen adsorptions. In between each of the adsorption runs the samples were evacuated 16 hr. at 500°. The results are given in Table III.

A comparison between oxygen adsorption (column 3) and hydrogen adsorption (columns 1 and 2) shows identical amounts of both gases being taken up by catalysts of high metal dispersion ($R \geq 0.8$ as measured by H_2 adsorption, columns 1 and 2). With catalysts of lower metal dispersion ($R \leq 0.5$) the amount of oxygen taken up substantially exceeds the amount of hydrogen adsorbed, the ratio of oxygen to hydrogen being close to 2. This difference can be explained in the following way: Whereas hydrogen is only adsorbed on the surface, oxygen at 350° seems able to penetrate the Pt lattice to some extent, forming surface films which are more than one layer thick. If the metal dispersion is extremely high, so that essentially all the platinum is accessible on the surface, then this difference between hydrogen and oxygen cannot become apparent. However, with catalysts having only 50% or less of all the Pt atoms exposed on the surface, more oxygen atoms than hydrogen atoms can be taken up. Our experimental oxygen-to-hydrogen ratio of about 2 suggests formation of oxide films, approximately 2 layers thick. It is for this reason that adsorption of oxygen at elevated temperatures cannot serve as a reliable measure of platinum dispersion.

TABLE III

REDUCTION–OXIDATION RESULTS

Catalyst (1.1% Pt on η-alumina)		Gas atoms adsorbed per Pt atom: H_2		O_2		H_2	
		1	2	3	4	5	6
Fresh, TPH[a]		0.97	0.96	0.98	..	1.96	0.94
TPH		.92	..	.95	..	1.78	.97
CPA[b]		.84	.83	.81	0.26	1.88	..
CPA[c]		.43	.42	.76	..	1.16	.68
Sintered, TPH							
500°, 1 atm. H_2,	0 hr.	.82	.81	.81	.42	1.62	.85
	72 hr.	.52	..	.99	..	1.38	.77
	200 hr.	.43	.44	.78	.33	.95	.53
	1200 hr.	.32	.32	.69	.27	.50	..

[a] Tetramminoplatinum hydroxide impregnation. [b] Chloroplatinic acid impregnation. [c] Chloroplatinic acid impregnation, sulfided, 0.6% Pt.

In several cases the catalysts were evacuated after the first oxygen uptake and oxygen then was readsorbed on the same sample. The second oxygen adsorption values, as given in column 4 of Table III, were always lower and amounted to only $1/2$ to $1/3$ of the first oxygen adsorption values. This shows that under the given outgassing conditions, namely 16 hr. at 500°, 30 to 50% of the oxygen is desorbed. As expected, the actual amount desorbed depended strongly on time and temperature.

Columns 5 and 6 in Table III give 2 subsequent hydrogen adsorption runs after oxygen treatment. The first hydrogen uptake of the oxidized catalyst (column 5) was about twice as high as the second hydrogen uptake (column 6) or hydrogen adsorption before oxidation (columns 1 and 2). At least for fresh catalysts of high metal dispersion, the data indicate that there is a definite ratio in the quantities of hydrogen and oxygen adsorbed during one full cycle. If we take for example the first catalyst in the table, the full cycle can be represented by the reaction scheme shown in Fig. 4.

Structure I is the one present after proper reduction and evacuation at the beginning of the cycle. (I) takes up one H atom per Pt atom forming II. Evacuation of II gives I. The adsorption and desorption of hydrogen according to (I) $\rightleftarrows$ (II) was repeated up to 4 times with practically identical results. (I) also can adsorb 1 oxygen atom per platinum leading to structure III. Evacuation of III causes desorption of part of the oxygen upon formation of IV. Structure IV is not supposed to represent a true stoichiometric compound Pt_2O but a surface oxide film of 0.5 coverage. It can readsorb about 0.5 oxygen atoms per Pt atom. If hydrogen is adsorbed by IV, two H atoms are taken up per Pt atom upon formation of H_2O and II. Evacuation of II leads back to I, which must be identical with the original state of the sample, since the whole cycle now can be repeated.

Additional confirmation of this reaction scheme

was obtained by adsorbing hydrogen on III after short evacuation at the adsorption temperature. In this case no oxygen can be removed and thus going from III to II directly, 3 H atoms per Pt atom should be taken up. The experimental value found was 2.9, in excellent agreement with the predicted 3.0.

The reaction scheme of Fig. 4 holds primarily for catalysts of extremely high platinum dispersion. Samples of lower dispersion deviate from the scheme in two ways. First, in step (I) → (III) more oxygen is taken up than required by the scheme. This was discussed earlier and ascribed to the fact that the oxygen can, to some extent, penetrate the platinum lattice. Second, in step (IV) → (II), less hydrogen is taken up than the amount corresponding to the scheme. This means that hydrogen under the given experimental conditions (2 hr. at 200 mm. and 250°) is not able to reduce all the oxide present in the second layer, and although the surface is properly reduced, some oxygen remains trapped in the interior of the platinum crystallites. If the uptake of hydrogen was measured at 500°, at which temperature the reduction is complete in 2 hr., the higher values required by the reaction scheme were found.

The last column in Table V gives the hydrogen adsorption after the oxidation–reduction cycle. It serves as a measure of the effect of the cycle on the metal dispersion. With catalysts of high dispersion no significant effect was found. All other catalysts showed a distinct increase in the platinum dispersion. In the case of the sintered catalysts, which are tetramminoplatinum hydroxide preparations and do not contain halogen, this increase in dispersion must be due to the reaction with oxygen. Catalysts which are chloroplatinic acid preparations do contain halogen. This halogen may be at least partly responsible for the regeneration mechanism of these catalysts.

Adsorption of Carbon Monoxide.—The apparatus and the experimental procedure used to determine metal dispersion by adsorption of carbon monoxide in a flow system are described in detail elsewhere.[16] Here, we will only discuss CO adsorption on several catalysts of different metal dispersion in comparison with the H_2 adsorption on the same catalyst samples.

Chemisorption of CO on platinum metals at room temperature is non-dissociative and can occur in two different forms according to the structures

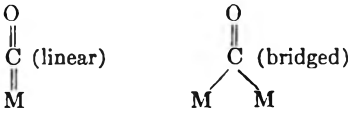

For unsupported platinum the volume of CO adsorbed (V_{CO}) is twice that of hydrogen (V_{H_2}).[25] Adsorption must, therefore, occur in the linear form. For supported platinum, however, Eischens,[26] in his infrared studies, found both forms to be present in varying degrees, depending on the nature of the carrier. On silica-supported platinum up to 15% of the CO is in the bridged structure, whereas on alumina-supported platinum about half of the CO is bridged. Eischens suggests that the alumina carrier makes it easier for the platinum to donate electrons for bond formation, thereby favoring the bridged structure.

Figure 5 shows a comparison of CO and H_2 adsorption for a series of catalysts of different metal dispersion. The net CO adsorption on the metal at 25°, expressed in terms of number of molecules adsorbed per Pt-atom (CO/Pt) is plotted as ordi-

(25) M. A. H. Lanyon and B. M. W. Trapnell, *Proc. Roy. Soc.* (London), **A227**, 387 (1955).

(26) R. P. Eischens, "Advances in Catalysis," Vol. X, Academic Press, Inc., New York, N. Y., 1958, p. 18.

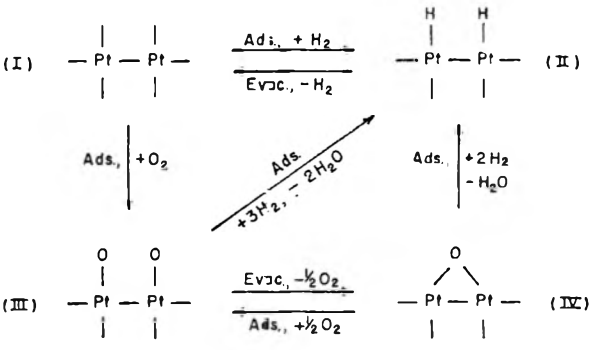

Fig. 4.—Reaction scheme for oxidation–reduction cycle.

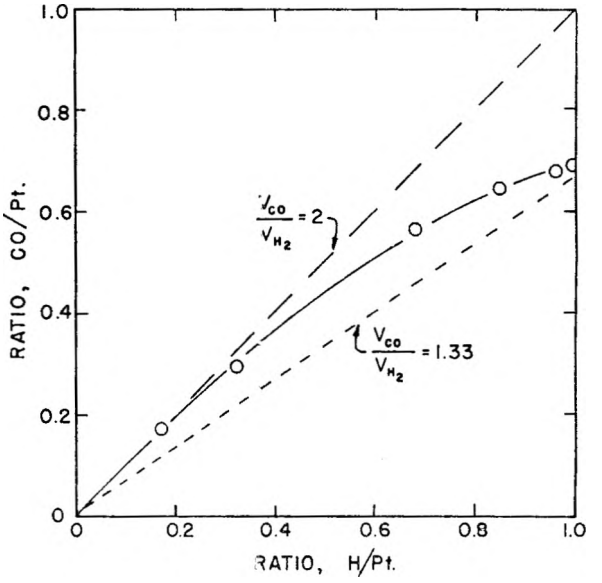

Fig. 5.—Comparison of CO and H_2 adsorption on Pt-on-alumina with varying Pt dispersion.

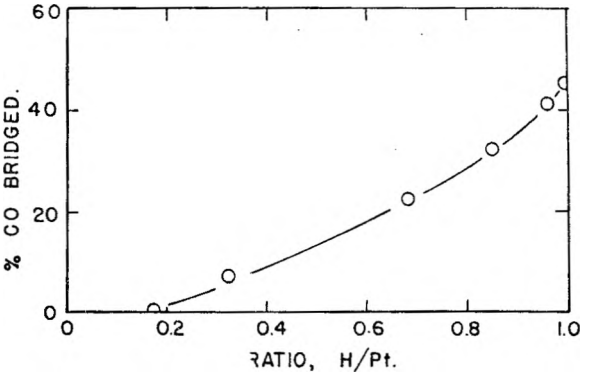

Fig. 6.—Contribution of bridged CO as a function of metal dispersion.

nate and the number of H atoms adsorbed per Pt atom (H/Pt), which is also a measure of metal dispersion, is plotted along the abscissa. The two dotted lines indicate the relations which would result: (a) if all the CO were present in linear form ($V_{CO}/V_{H_2} = 2$) and (b) if 50% were present in the linear and 50% in the bridge structure ($V_{CO}/V_{H_2} = 1.33$).

For catalysts of very high dispersion (H/Pt > 0.8) the ratio V_{CO}/V_{H_2} was found to be 1.4 to 1.5, confirming the infrared data on alumina-supported platinum. However, as the metal dispersion decreases, V_{CO}/V_{H_2} increases and approaches the value 2 for catalysts of relatively small metal surface area. Apparently the CO to H_2 ratio depends not only on the nature of the carrier but also on the degree of metal dispersion. If the nature of the support does affect the properties of a metal dispersed on this support, then such an effect certainly should diminish with decreasing dispersion and a constant V_{CO}/V_{H_2} ratio cannot be expected. We think that this diminishing effect is clearly demonstrated by the data in Fig. 5.

From the V_{CO}/V_{H_2} ratio one can calculate the distribution of CO between the linear and the bridged structure. If x is the fraction of linear, and y the fraction of bridged CO, then

$$\frac{V_{CO}}{V_{H_2}} = \frac{2(x + y)}{x + 2y}$$

and since $x = 1 - y$

$$y = \frac{2 - V_{CO}/V_{H_2}}{V_{CO}/V_{H_2}}$$

The per cent. of CO in the bridged structure, calculated in this way, is plotted against dispersion in Fig. 6. The effect of the support on the CO adsorption mechanism seems to disappear at H/Pt = 0.2, or at an average particle size of about 50 Å. Concerning the structure of the highly dispersed platinum, one additional conclusion can be drawn from the CO data. Since a substantial part of the CO is bridged, the platinum, even at dispersions close to H/Pt = 1.0, is present not in the form of single isolated Pt atoms but in the form of a discontinuous monolayer or as small "crystallites" with essentially no interior Pt atoms.

Acknowledgment.—The author is indebted to many members of the department for assistance in preparation of materials and execution of experiments and wishes to express his appreciation to Dr. J. H. Ramser for many helpful discussions and to Dr. J. E. Connor for his constant encouragement and advice.

EFFECT OF LIGHT ON HYDROGEN CHEMISORPTION ON ZINC OXIDE

BY V. KESAVULU AND H. AUSTIN TAYLOR

Wm. H. Nichols Laboratory, New York University, New York 53, N. Y.

Received June 28, 1961

Illumination of zinc oxide with light from a low-pressure mercury arc lamp leads to a retardation of hydrogen chemisorption at 300° (type-B). This photo-effect is correlated with the photo-conductive property of zinc oxide and a tentative mechanism in terms of the equilibrium between ionized and un-ionized H-donors at the surface is proposed.

It has been known for some time that oxygen can either desorb or adsorb on zinc oxide under the influence of light in the fundamental absorption region. Photodesorption takes place from a reduced sample containing adsorbed oxygen while photosorption is observed on an oxidized sample.[1,2] No such photo-effect has, however, been reported for hydrogen on zinc oxide. The occurrence of two types of hydrogen chemisorption on zinc oxide has been demonstrated,[3] type-A involving an interaction of hydrogen molecules with free polarized zinc atoms (type-A sites) on the surface and type-B being an interaction of hydrogen atoms (from type-A sites) with $O^=$ ions of the oxide surface. In this work, it is shown that light has an inhibitory action on the type-B reaction, thus providing further evidence for the electronic nature of this chemisorption.

Experimental

Apparatus and Procedure.—The reaction chamber, shown in Fig. 1, consisted of a hollow, double-walled, quartz tube A, having an annular space G, of width 1 mm. In the annular space was placed zinc oxide powder (15.41 g.) made by heating zinc oxalate at 420° in a current of dry air. The oxide could be illuminated from both sides of the annular space by means of a spiral, Hanovia low-pressure mercury arc lamp B. The reaction chamber and the mercury lamp were enclosed in an electric furnace E, by means of which the reaction vessel could be maintained at any desired temperature. The entire system then was enclosed in an insulated box F. When necessary, the system could be cooled by means of a stream of cold nitrogen gas through H, H'.

A constant volume apparatus was used. Three U-tubes containing sponge gold were included in the vacuum system to protect the zinc oxide from mercury vapor. The gas space in the catalyst chamber had a volume around 45 ml. However, before each run the volume of gas required to occupy this space at the given temperature and pressure was measured by introducing a known volume of helium. The temperature in the catalyst chamber was measured with a Chromel–Alumel thermocouple C, correct to ±1°. A dibutyl phthalate (DBP) manometer made of a constant bore tube (4 mm. i.d.) was employed to follow pressure changes in the system. The pressure could be read with an error of ±0.1 mm.

After pretreatment of the oxide and evacuation, the catalyst chamber was maintained at constant temperature for about an hour. Then it was calibrated with helium and evacuated for 15 min., 10 min. being sufficient to reach a pressure of 10^{-5} mm. Then a known volume of hydrogen, purified by passing through a heated palladium thimble, was introduced into the chamber and pressure changes followed. The experiment was repeated several times at the same catalyst temperature and gas pressure, alternately with and

(1) Y. Fujita and T. Kwan, *Bull. Chem. Soc. Japan*, **31**, 380 (1958).

(2) A. Terenin and Yu. Solonitzin, *Discussions Faraday Soc.*, **28**, 28 (1959).

(3) V. Kesavulu and H. Austin Taylor, *J. Phys. Chem.*, **64**, 1124 (1960).

without light, each time preceded by calibration with helium. Before commencing an experiment with light, the catalyst was allowed to come to temperature equilibrium in the presence of light. Between runs the oxide was degassed overnight by evacuation at 350–360° and flushing twice with helium. From previous experience this treatment was known to be sufficient to remove hydrogen completely. All experiments were conducted at 300° since type-B chemisorption occurs quite rapidly at 300°, while type-A adsorption is absent.

Pretreatment.—It was shown[3] that the oxide surface undergoes irreversible changes as a result of treatment with hydrogen at elevated temperatures. These changes are associated with the formation of type-A sites on the surface. It was felt desirable to "activate" the oxide fully by several treatments with hydrogen at 300–350°. The extent of "activation" was checked at intervals by q–T curves, shown in Fig. 2. These curves were obtained as follows: a known volume of hydrogen was introduced into the oxide chamber and after an interval of 30 min. the temperature was raised gradually at the rate of one degree per minute. Volumes of hydrogen adsorbed at definite temperatures were determined. The volume of hydrogen in ml. S.T.P. (q) is plotted as a function of temperature. All four q–T heating curves were obtained under identical conditions. Therefore, the increase in the height of the low-temperature maximum is an indication of the increase in the number of type-A sites. Curve 4 represents the state of the oxide surface before the photoexperiments were commenced.

The oxidized sample used in some experiments was obtained by treating the above oxide with dry oxygen (700 mm.) at about 500° for 24 hr. Before making runs, this sample was evacuated thoroughly at 350–360° and the catalyst chamber flushed several times with helium.

Results

Table I presents some typical results obtained with the "activated" zinc oxide. The amounts of gas adsorbed definitely are lower in the presence of light than in the dark. The retarding effect of light is pronounced in the initial stages. Slight irreversible changes taking place in the adsorptive capacity of the oxide also are noticeable.

TABLE I

EFFECT OF LIGHT ON TYPE-B CHEMISORPTION OF H_2 ON ZnO

P_0 = 50.11 mm.; catalyst temp. = 300°

Time, min.	Volume adsorbed in ml. S.T.P. 1 Light	2 Dark	3 Light	4 Dark	5 Light	6 Dark
0.5	0.77	0.92	0.74	0.97	0.80	0.94
1	0.95	1.11	0.93	1.15	0.97	1.18
2	1.13	1.30	1.10	1.35	1.20	1.38
3	1.32[a]	1.41	1.20	1.46	1.31	1.51
5	1.45[b]	1.54	1.36	1.58	1.51	1.68
7	...	1.61	...	1.65	1.64	1.80
10	1.59	1.68	1.58	1.73	1.78	1.92
15	...	1.77	1.72	1.85	1.91	2.07
20	1.85	1.81	1.80	1.92	2.05	2.18
30	1.95	1.93	1.91	2.04	2.18	2.31

[a] 4 min. [b] 6 min.

Figure 3 gives the results of a set of three runs made on the "oxidized" sample. Runs 1 and 3 were made in the dark while run 2 was made in light. The irreversible change is quite pronounced in this case, but the inhibitory effect of light still is unmistakable. The adsorptive capacity of the oxide has decreased from run 1 to run 3. Assuming for all the runs the same trend in this irreversible change, it can be said that, if the second run had been made in the dark instead of in light, one should have obtained a curve which would roughly correspond to the dashed curve 2′. Hence, the

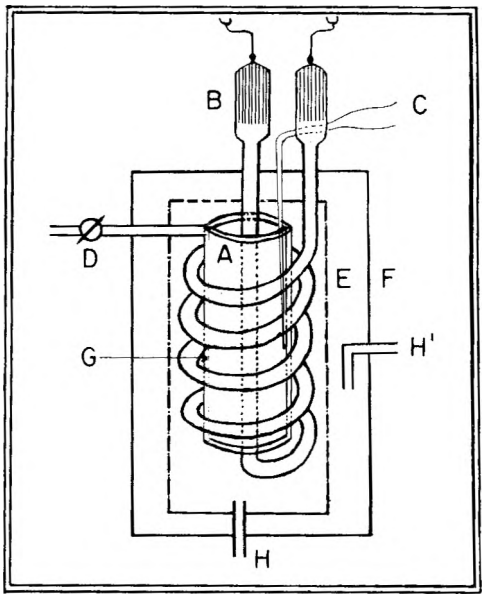

Fig. 1.—Reaction chamber and mercury lamp: A, quartz reaction vessel; B, mercury lamp; C, thermocouple; D, stopcock to vacuum system; E, furnace; F, outer insulated box; G, ZnO in the annular space; H, H′, inlet and outlet for N_2.

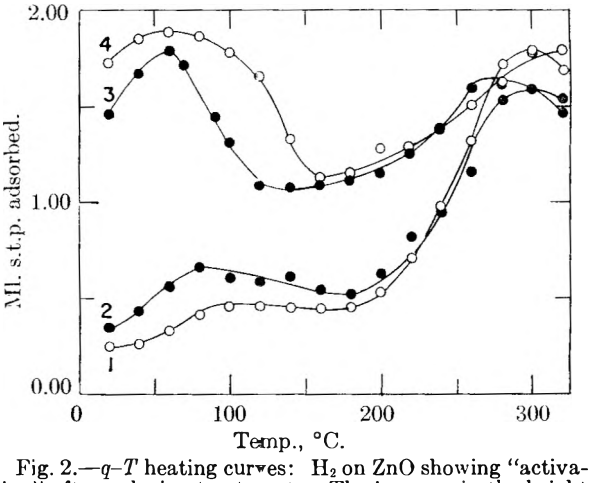

Fig. 2.—q–T heating curves: H_2 on ZnO showing "activation" after reducing treatments. The increase in the height of low-temperature maximum is an indication of the increase in the number of type-A sites. P_0 = 50.11 mm.; rate of heating = 1 degree per minute.

effect of light on chemisorption (under the conditions of the second run) should be at least the difference between the dashed and the solid curves, 2′ and 2, respectively.

Figure 4 compares the results at two different pressures of hydrogen, 50.11 and 9.23 mm., for the "activated" oxide. A comparison of the amounts of hydrogen adsorbed in one minute shows that, at 50.11 mm., light suppresses chemisorption by 17%, while at 9.23 mm., the amount chemisorbed in the presence of light is only 8% lower than in the dark.

Discussion

The above results can be correlated with other surface effects in zinc oxide, and an explanation can be sought in terms of the model previously proposed for type-B chemisorption. Type-B chemisorption

involves the interaction of hydrogen atoms from type-A sites with the lattice O^- ions of the oxide surface.[3] The electrons formed by the thermal ionization of these surface donors, (O^- + H) complexes, enter the empty levels in the conduction band generating a "diffusion potential"[4] which, in turn, opposes further flow of electrons into the conduction band. When equilibrium is reached, a stable electron-rich space charge region is established at the surface. The un-ionized H-donors forming the surface OH^- complexes may be removed from the surface by combination with more H-atoms from type-A sites to form H_2 molecules. Symbolically, one may write

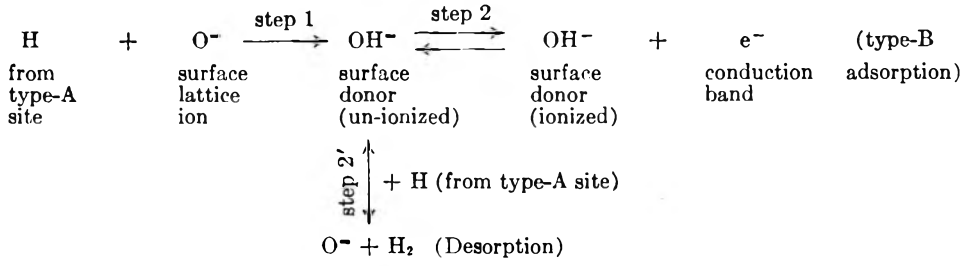

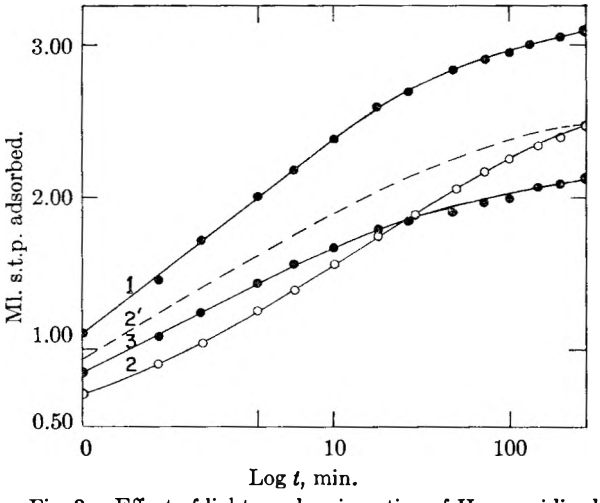

Fig. 3.—Effect of light on chemisorption of H_2 on oxidized ZnO at 300°. Curves 1 and 3 are for the reaction in the dark; curve 2, for the reaction in light; curve 2′ is the expected curve if light had no effect. The numbers indicate the order of performance. P_0 = 50.11 mm.

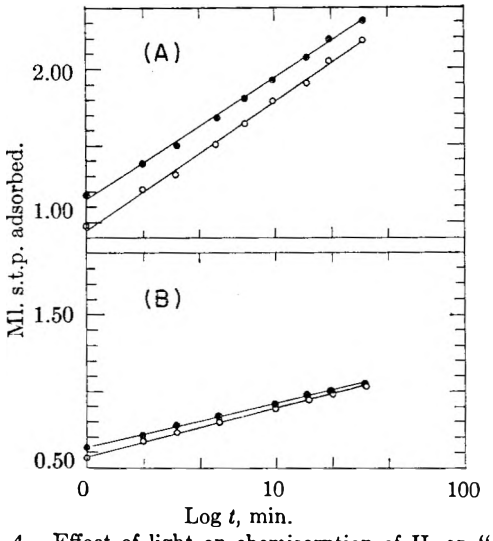

Fig. 4.—Effect of light on chemisorption of H_2 on "activated" ZnO at 300°: (A) P_0 = 50.11 mm.; (B) P_0 = 9.23 mm. Filled circles refer to runs in the dark. Open circles refer to runs in light.

Step 2 represents the equilibrium between the surface donor levels and the conduction band. The dominance of the electronic factor in the chemisorption will depend on the extent to which this step becomes rate determining. The activation energy for this step would consist of two parts—the ionization energy of OH^- and the barrier height of the space charge region. The former may be assumed to be a small constant, while the latter would increase from zero to the steady-state value.

Zinc oxide absorbs strongly light of wave length shorter than about 3850 Å.[5] (fundamental absorption). Illumination of the oxide with light in this fundamental absorption region leads to photoconduction which is shown to be purely a surface effect in zinc oxide.[6] Coincidence of the onset of photoconduction with the fundamental absorption edge shows that the photoconduction results from excitation of electrons from valence band to conduction band.[7,8] However, the charge carriers in photoconduction are electrons,[9,10] and so it is supposed that the holes are trapped immediately after excitation. The physical nature of these traps is not certain. From these facts, it is concluded that illumination with light of wave length shorter than about 3850 Å. leads to the formation of an enrichment-type space charge region at the surface, which is responsible for photoconduction in zinc oxide.[8]

Heiland[11,12] showed that treating single crystals of zinc oxide with atomic hydrogen produces surface conduction. From the saturation values of this surface conductivity, he calculated the surface density of conduction electrons to be 6×10^{12} cm.$^{-2}$. Assuming all the surface donors to be ionized and applying the neutrality condition, he deduced the surface density of H-donors to be also 6×10^{12} cm.$^{-2}$. He considered this to be a reasonable number since a charge density of about 10^{13} cm.$^{-2}$ would correspond to the breakdown potential at the surface. According to Heiland, the H-donors

(4) E. Spenke, "Electronic Semiconductors," McGraw-Hill Book Co., New York, N. Y., 1958.

(5) E. Mollwo, *Reichsber. Physik*, **1**, 1 (1943).

(6) G. Heiland, E. Mollwo and F. Stockmann, "Solid State Physics," Vol. 8, Academic Press, Inc., New York, N. Y., 1959, edited by F. Seitz and D. Turnbull, p. 291.

(7) H. Weiss, *Z. Physik*, **132**, 335 (1952).

(8) R. J. Collins and D. G. Thomas, *Phys. Rev.*, **112**, 388 (1958).

(9) K. Intemann and F. Stockmann, *Z. Physik*, **131**, 10 (1951).

(10) G. Heiland, *Discussions Faraday Soc.*, **28**, 168 (1959).

(11) G. Heiland, *Z. Physik*, **148**, 15 (1957).

(12) See reference 6, p. 311.

are present as OH^- species at the surface. Now, from measurements on type-B adsorption, one can independently calculate the number of H-atoms per cm.^{2} adsorbed on zinc oxide. In a typical experiment, a sample with a surface area of 62.4 m.^{2} adsorbed 0.78 ml. of hydrogen in 100 min. This would correspond to 6.7×10^{13} H-atoms per cm.^{2}. The equilibrium value should be much higher. A comparison with Heiland's figure shows that, at or near equilibrium, only a fraction of the H-donors at the surface is ionized. In the initial stages of adsorption most of the H-donors at the surface may be expected to be ionized as the barrier height due to the space charge region is absent or negligible. As the space charge barrier increases with the progress in adsorption, the ionization process will be retarded. Hence, though both the number of ionized and un-ionized donors would increase with the progress of adsorption, their relative proportion would vary considerably. The fraction of the total H-atoms ionized would decrease steadily as chemisorption progresses.

Now the reason for the negative light effect on hydrogen chemisorption on zinc oxide becomes clear. It may be assumed that initially, in light as well as in the dark, the same number of OH^- complexes is formed from H-atoms from the type-A sites. In the absence of light, most of these would be thermally ionized to form the surface OH^- ions and the freed electrons would go to build the accumulation layer. However, in the presence of light, since there is already an accumulation layer present at the surface, the ionization would be retarded and many of the un-ionized H-donors would be removed from the surface by step 2′. This would have a retarding effect on chemisorption. This effect would be most marked at the initial stages of adsorption; and at higher coverages, since the number of ionized donors is only a small fraction of the total number adsorbed, it may be masked by other processes. Probably then the migration of H-atoms from type-A sites to $O^=$ sites becomes the controlling factor.

ABSORPTION SPECTRA OF THE II, III, IV AND V OXIDATION STATES OF VANADIUM IN LiCl–KCl EUTECTIC. OCTAHEDRAL–TETRAHEDRAL TRANSFORMATIONS OF V(II) AND V(III)[1]

BY D. M. GRUEN AND R. L. MCBETH

Chemistry Division, Argonne National Laboratory, Argonne, Illinois

Received June 30, 1961

The II, III, IV and V oxidation states of vanadium have been characterized spectrophotometrically in LiCl–KCl eutectic in the range 300–2500 mμ and as a function of temperature from 400–1000°. The spectra can be interpreted as arising from electronic transitions within the unfilled 3d shells of the ions. Ligand field considerations show that the low temperature (400°) spectra of V(II) and V(III) can be understood in terms of octahedral VCl_6^{-4} and VCl_6^{-3} complexes. At temperatures higher than 400°, the spectra of V(II) and V(III) undergo changes which can be interpreted in terms of octahedral–tetrahedral transformations involving the equilibria $VCl_6^{-4} = VCl_4^{-2} + 2Cl^-$ and $VCl_6^{-3} = VCl_4^- + 2Cl^-$. The V(IV) spectrum is not strongly affected by temperature. The V(V) spectrum is characterized by a single charge transfer band.

Introduction

As part of a continuing study of the oxidation states and ionic species of metal ions dissolved in fused salts,[2] solutions of vanadium in LiCl–KCl eutectic were investigated by spectrophotometric means.

The lowest electronic state of monatomic neutral vanadium is $3d^34s^2$ ($^4F_{3/2}$), and the five valence electrons are responsible for the relatively complex chemistry of vanadium. Of chemical interest are the II, III, IV and V oxidation states corresponding to the electronic configurations $3d^3$-$3d^0$, all of which have been observed and characterized in aqueous solutions and in crystals.[3]

We set out to learn whether vanadium can exhibit its full spectrum of oxidation states in fused salt solutions, to inquire into the relative stability of the oxidation states, and to study the nature of the ionic species in the melt.

A description of the apparatus and techniques developed for obtaining quantitative absorption spectra on melts up to 1000° is given in the Experimental section of the paper.

Results and Discussion

1. Preparation of Vanadium Solutions in LiCl–KCl Eutectic.—The general procedure for preparing solutions of air and moisture sensitive substances in LiCl–KCl eutectic or in pyridinium chloride has been described previously.[2a]

The basic approach used in the present study was to prepare solutions of vanadium in various oxidation states by dissolution of anhydrous vanadium compounds of known composition. Absorption spectra of the solutions were obtained using 1-cm. fused silica cells. The solidified melts were analyzed for total V content so that molar absorbancies could be calculated. On other similarly prepared melts chemical analyses were performed to determine both the total vanadium content and the oxidation state of vanadium. In general, solutions of higher vanadium concentration were required for oxidation state analyses than for the observation of the absorption spectra.

(1) Based on work performed under the auspices of the U. S. Atomic Energy Commission.

(2) (a) D. M. Gruen and R. L. McBeth, *J. Inorg. & Nuclear Chem.*, **9**, 290 (1959); (b) D. M. Gruen, R. L. McBeth, J. Kooi and W. T. Carnall, *Ann. N. Y. Acad. Sci.*, **79**, 941 (1960).

(3) W. M. Latimer, "Oxidation Potentials," Second Edition, Prentice-Hall, Inc., New York, N. Y., 1952, p. 258.

Since the identification of a spectrum with a particular vanadium oxidation state rests primarily on the oxidation state analyses, the detailed analytical procedures developed for this study are given in the next section.

Vanadium(II) Solutions.—The primary method used to prepare V(II) solutions was to dissolve VCl_2 in LiCl–KCl eutectic. The compound VCl_2 was prepared by treating V metal with HCl gas at 950°.[4] Analysis of the compound by precipitation of V with cupferron and ignition to V_2O_5 gave 40.4% V (calcd. 41.8%). Vanadium metal for this work was obtained from the Vanadium Corporation of America and was found to be 99.3% V by chemical analysis.

Vanadium(II) solutions also were prepared by anodization of V metal in a compartment separated from the 1-cm. silica absorption cell by a fritted disc. After anodization, the solution was filtered through the disc by pressurizing the upper compartment with argon. This procedure was adopted to obtain in the absorption cell solutions free of colloidal material which was always a by-product of the anodization of V metal. The black colloidal matter probably was V metal rather than oxide since the vanadium foil used in these experiments previously had been cleaned in a 1 *M* nitric acid solution and heated *in vacuo* at 400°.

The third method for preparing V(II) solutions was to reduce V(III) solutions with V metal.

V(III) solutions in LiCl–KCl eutectic were prepared by dissolution of VCl_3. The VCl_3 was prepared by refluxing V_2O_5 with S_2Cl_2 according to the method of Funk and Weiss.[5] The product then was heated in a bomb at 240° for 6 hr. to increase the crystallite size. Analysis for Cl^- gave 66.9% found (calcd. 67.6%).

Solutions of V(III) in molten pyridinium chloride were prepared by reaction of V metal with the solvent. In this acidic medium the (II) state is unstable and is oxidized to (III) with reduction of pyridinium ion to hydrogen and free pyridine.

V(IV) solutions were prepared either by dissolution of $VOCl_2$ (Fisher Scientific Co., C.P. grade) or by bubbling dry air through a V(III) solution. Care had to be taken in the latter procedure to terminate the oxidation at the (IV) state. It was found that the (IV)–(V) oxidation with air at 400° was slow, so that by interrupting the air flow every few minutes and taking spectra the oxidation could be halted conveniently when the solution had been quantitatively converted to V(IV).

V(V) solutions were prepared either by continuing the air oxidation procedure used to convert V(III) to V(IV) solutions or by dissolving V_2O_5 (E. H. Sargent Co., C.P. grade) in the eutectic. Solutions prepared by dissolving V_2O_5 always contained a small amount of the V(IV) state which then was oxidized by treating the solutions with an air stream.

V_2O_5 volatilizes slowly out of a LiCl–KCl melt even at 400°.

2. Vanadium Analyses.—(The analytical methods and results described in this section were perfected and carried out by R. Bane, K. Jensen and I. Fox of the Analytical Chemistry Section.)

Since the analyses of the fused salt solutions for total vanadium concentration and for vanadium oxidation state represent the primary data on which certain conclusions of this paper are based, the analytical procedures and results are given in some detail.

A. The total V concentration was determined colorimetrically at 450 mμ using the peroxide complex method.[6]

The peroxide method, while less sensitive than the phosphotungstate method, has the advantage of a much smaller and more reproducible reagent blank. It was found convenient to take aliquots of the samples to fumes of sulfuric acid and then oxidize V to the +5 state by the addition of a few drops of perchloric acid to the fuming sulfuric acid solution. With V in the +5 state, the peroxide color developed rapidly. Fuming with sulfuric acid was made a part of the standard procedure to remove chloride ion, organic matter (*e.g.*, pyridinium chloride) or nitric acid which was used when the samples were put into solution.

The peroxide method was standardized with a series of spike solutions containing known amounts of V and was found to be accurate to within ± 2%.

B. The oxidation state of V was determined by a modification of standard titrimetric procedures.[7,8] Since the Cl^- concentration of the samples was very high, conditions had to be found for titrating Fe(II) without at the same time titrating Cl^-. The following procedure was found to give the desired results.

Solidified samples of LiCl–KCl eutectic containing V in various oxidation states were dissolved in a solution of ferric ammonium sulfate in 10 *N* H_2SO_4. Prior to and during the dissolution argon was bubbled through the solution to remove and exclude oxygen. After the dissolution was complete, 10 ml. of 85% H_3PO_4 was added to complex the remaining Fe(III). The Fe(II) produced was titrated with standardized 0.1 *N* Ce(IV) solution using a Ferroin indicator. The normal color change of Ferroin is from pink to colorless, but in the presence of VO^{++} the change is from pink to blue.

Under the conditions described above, the only reactions occurring are

$$V(II) + 2Fe(III) = V(IV) + 2Fe(II)$$
$$V(III) + Fe(III) = V(IV) + Fe(II)$$
$$Fe(II) + Ce(IV) = Fe(III) + Ce(III)$$

The procedure was tested by running a standard vanadium solution through a Jones reductor (where it was reduced to V(II)) into a receiver containing a solution of ferric ammonium sulfate and 5 g. of LiCl–KCl eutectic in 10 *N* H_2SO_4. This analytical procedure gives the V content to within ±0.5%. Ceric titrations on solutions containing only the dissolved eutectic or pyridine hydrochloride gave negligible blanks.

(4) J. Villadsen, *Acta Chem. Scand.*, **13**, 2146 (1959).

(5) H. Funk and W. Weiss, *Z. anorg. u. allgem. Chem.*, **295**, 327 (1958).

(6) E. B. Sandell, "Colorimetric Determination of Traces of Metals, Third Edition, Interscience Publishers, Inc., New York, N. Y., 1959, p. 929.

(7) I. M. Kolthoff and R. Belcher, "Volumetric Analysis," Vol. III, Interscience Publishers, Inc., New York, N. Y., 1957, p. 146.

(8) H. H. Willard and P. Young, *J. Am. Chem. Soc.*, **51**, 139 (1929).

TABLE I

ANALYTICAL RESULTS FOR VANADIUM IN VARIOUS OXIDATION STATES IN FUSED CHLORIDES

Exp. no.	Oxid. state	Method of preparation	Solvent (A) = LiCl–KCl eutectic B = pyridine HCl	Purpose of experiment	Vanadium mg./g. sample	Ml. 0.09654 *N* Ce^{+4}/g. sample	Electron change V(II) – V(IV) = 2 V(III) – V(IV) = 1	Note
40B	II	Dissolution of weighed amt. of VCl_2	A	Quantitative dissolution study	8.63			
46B	II	Dissolution of weighed amt. of VCl_2	A	Quantitative dissolution study	8.54			
48B	II	Dissolution of weighed amt. of VCl_2	A	Quantitative dissolution study	8.91			
50B	II	VCl_3 + V metal	A	Ab. spectra and temp. study	1.04			
63B	II	VCl_3 + V metal	A	Oxid. state detmn.	6.01	2.52	2.06	
57B	II	Anodization of V electrode	A	Ab. spectra	0.93			*a*
65B	II	Anodization of V electrode	A	Oxid. state detmn.	4.31	1.70	1.94	*b*
71B	III	Dissolution of VCl_3	A	Oxid. state detmn.	4.58	0.91	0.98	
73B	III	Dissolution of VCl_3	A	Ab. spectra and temp. study	1.44			
66B	III	Dissolution of V metal	B	Oxid. state detmn.	7.35	1.53	1.02	
67B	III	Dissolution of V metal	B	Oxid. state detmn.	10.55	2.18	1.02	
14B	III	Dissolution of V metal	B	Ab. spectra	1.45			
15B	III	Dissolution of V metal	B	Ab. spectra	0.84			
16B	III	Dissolution of V metal	B	Ab. spectra	0.40			
17B	III	Dissolution of V metal	B	Ab. spectra	1.15			
14B	IV	Air oxidation of 14B(III)	B	Ab. spectra	1.45			
15B	IV	Air oxidation of 15B(III)	B	Ab. spectra	0.84			
16B	IV	Air oxidation of 16B(III)	B	Ab. spectra	0.40			
17B	IV	Air oxidation of 17B(III)	B	Ab. spectra	1.15			
64B	IV	Dissolution of $VOCl_2$ crystals	A	Oxid. state detn.	~74 mg. V total sample	None		
74B	IV	Dissolution of $VOCl_2$ crystals	A	Ab. spectra and temp. study	1.48			
72B	V	Dissolution of V_2O_5	A	Ab. spectra	2.92			

[a] 12.5 milliamp. × 2000 sec. = 25 coulombs = 6.60 mg. V anodized assuming eq. wt. of 25.48 for vanadium (V^0–V(II)). Total vanadium found was 5.76 mg. but all of the eutectic used in the anodization experiment was not recovered for the vanadium analysis. [b] Coulometrically 71.8 mg. of vanadium was generated and about 73 mg. was found in the entire sample. This value is not too accurate since the total amount of eutectic used was known only approximately. [c] Addition of the sample to Fe^{+3} solution and consequent addition of the indicator showed no Fe^{+2} produced. Thus, no V(II) or V(III) was present since $V^{+2} + 2Fe^{+3} \rightarrow V(IV) + 2Fe^{+2}$.

Electron changes were calculated from the expressions

$$\text{meq. wt. of V} = \frac{\text{grams V present}}{\text{ml. Ce(IV)} \times N\ \text{Ce(IV)}}$$

$$\text{electron change} = \frac{\text{atomic weight V}}{\text{meq. wt. V} \times 1000}$$

Grams V present were found in a separate experiment on a portion of the sample by determining the total V concentration. In Table I, the analytical results on a number of sample preparations are presented.

3. Calculation of Molar Absorptivities.—The absorption spectra data are presented in the form of curves of molar absorptivities *vs.* wave lengths in mμ. To calculate the molar absorptivities of the solutions, the densities of the melts were required.

The density of pyridinium hydrochloride was found to be 1.142 g./cc. at 155°.

For the densities of the LiCl–KCl eutectic melts, the measurements of Van Artsdalen and Yaffe were employed.[9] Their equation $\rho = a - bt$ ($a = 1.8851$, $b \times 10^3 = 0.5275$, t = temp., °C.) is based on data obtained in the range 456–602°. For temperatures outside this range, the densities used in the present calculations were found from a straight line extrapolation of this equation.

4. Absorption Spectra of Vanadium in Various Oxidation States.—A. The V(II) spectrum in LiCl–KCl eutectic at 400° (Fig. 1A) is characterized by three broad bands with maxima at 525 mμ (19,050 cm.$^{-1}$), 832 mμ (12,020 cm.$^{-1}$) and 1390 mμ (7200 cm.$^{-1}$). Some other representative data concerning the spectrum including the half-widths of the bands and their oscillator strengths, are given in Table II. The oscillator strength, f, of an absorption band is given by the equation

$$f = 4.32 \times 10^{-9} \int \epsilon_\nu \, d\nu$$

where ϵ_ν is the molar absorptivity at wave length ν cm.$^{-1}$. Since the three bands in V(II) overlap to some extent, no attempt was made to calculate the f's of individual transitions. Rather, the entire area under the absorption curve from 23,000 cm.$^{-1}$ (435 mμ) to 5000 cm.$^{-1}$ (2 μ) was integrated.

(9) E. R. Van Artsdalen and I. S. Yaffe, *J. Phys. Chem.*, **59**, 118 (1955).

TABLE II

SPECTRAL CHARACTERISTICS OF VANADIUM IN VARIOUS OXIDATION STATES

Ion	System	ϵ	En. max., mμ	En. max., cm.$^{-1}$	Band width at half max. (cm.$^{-1}$)	$f \times 10^4$	Ref.
V(II) $3d^3$ ^4F	LiCl–KCl eut. 400°	17.5	525	19050	3500		
		12.4	832	12020	4000	4.3[a]	b
		8.1	1390	7200	4000		
	Aqueous soln.	0.65	572	17500	5000	0.2	12
	R.T.	0.45	848	11800	4000	0.1	
	$(NH_4)_2[Zn, V(H_2O)_6](SO_4)_2$		358	27900			
	Reflection spectrum		541	18500			13
	R.T.		810	12350			
	LiCl–KCl eut. 400°	35.8	555	18020	4000	6.4	b
		13.0	911	11000	3000	2.0	
	Pyridinium chloride 160°	30.5	545	18350	3950	5.8	b
V(III) $3d^2$ ^3F		13.2	860	11630	3750	2.2	
	$NH_4V(SO_4)_2 \cdot 12H_2O$	6.6	389	25700	3300	1.1	23
	R.T.	3.5	561	17800	3200	0.6	
	Aqueous perchloric acid soln.	8.3	400	25000	5300	2.0	24
		5.5	580	17250	3800	0.9	
	LiCl–KCl eut. 400°	24.5	739	13530	4300	5.9	b
V(IV)	LiCl–KCl eut. 800°	29.7	717	13950	5000	6.5	b
$3d^1$ ^2D	Pyridinium chloride 160°	40.0	742	13500	4500	7.9	b
	Perchloric acid R.T.	17	750	13350	4050	3.3	24
		(15.9)					(28)

[a] Total oscillator strength in region 23000–5000 cm.$^{-1}$. [b] Present work.

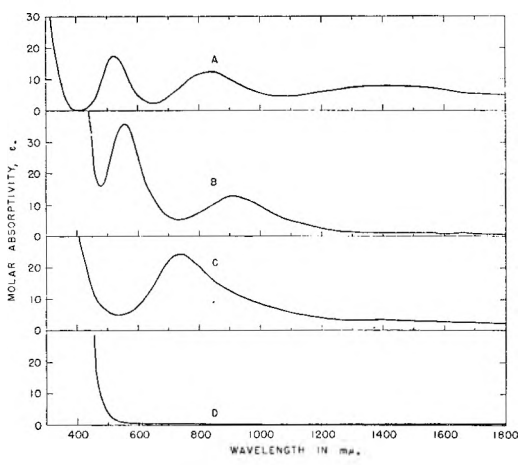

Fig. 1.—Oxidation states of vanadium in LiCl–KCl eutectic at 400°: A = V(II); B = V(III); C = V(IV); D = V(V).

The sum of the oscillator strengths for all three bands thus was found to be equal to 4.3×10^{-4}.

Vanadium in the (II) oxidation state is representative of a $3d^3$ electron system. The splitting of the energy levels of the d^3 configuration in an electric field of octahedral symmetry has been given, for example, by Tanabe and Sugano[10] and by Orgel.[11] Recently, A.D. Liehr has improved these earlier calculations by including the spin-orbit coupling perturbation [private communication of unpublished work]. The observed spectrum of V^{+2} can be fitted to the Liehr diagram with Dq = 700 cm.$^{-1}$. The theoretical energies of the transitions from the $^4A_{2g}$ ground state to the excited states, are: 20,000 cm.$^{-1}$ ($^4T_{1g}$); 11,600 cm.$^{-1}$ ($^4T_{1g}$); 7000 cm.$^{-1}$ ($^4T_{2g}$).

(10) Y. Tanabe and S. Sugano, *J. Phys. Soc. Japan*, **9**, 753, 766 (1954).

(11) L. E. Orgel, *J. Chem. Phys.*, **23**, 1819 (1955).

Holmes and McClure[12] obtained Dq = 1180 cm.$^{-1}$ from spectral studies of V(II) in 1 *M* H_2SO_4. A somewhat higher value (Dq = 1230 cm.$^{-1}$) was found by Jørgensen[13] from reflection spectra of $(NH_4)_2[Zn(H_2O)_6](SO_4)_2$ with small amounts of V(II) isomorphously replacing Zn(II).

In the crystal and in aqueous solution, the V(II) ion presumably is surrounded by an octahedron of water molecules. In the melt, on the other hand, the electric field is due to six surrounding chloride ions. It has been suggested on the basis of experimental data based primarily on aqueous solution studies that Dq for Cl^- is about 75% that of water.[14] The data presented here indicate that in chloride melts, the Dq_{oct} is only about 60–65% as large as in water surroundings. [The decrease of Dq in going from oxygen to chlorine coördination seems to hold true in tetrahedral symmetry also. Thus, the Dq for Ni(II) is 465 and 300 cm.$^{-1}$, respectively, in the tetrahedral ZnO and Cs_2ZnCl_4 lattices.[15,16]] Of all the divalent ions of the first transition metal series, V(II) would be expected to show the strongest tendency toward hexacoördination. The situation arises from the fact that: (1) among the d^1-d^9 configurations, the d^3[V(II)] and d^8[Ni(II)] configurations have the largest octahedral site preference energies and (2) the experimentally determined Dq_{oct} of V(II) is some 30% larger than that of Ni(II).[15] Elementary considerations of crystal field stabilization energies therefore favor the interpretation of the

(12) O. G. Holmes and D. S. McClure, *ibid.*, **26**, 1686 (1957).

(13) Chr. K. Jørgensen, "Absorption Spectra of Complexes of Heavy Metals," European Research Office, U. S. Dept. of the Army. Contr. No. DA-91-508-EUC-247, Oct. 1958.

(14) Chr. K. Jørgensen, *Proc. Tenth Solvay Conf.*, 355 (1956).

(15) D. S. McClure, *J. Phys. and Chem. Solids*, **3**, 311 (1957).

(16) D. M. Gruen and R. L. McBeth, *J. Phys. Chem.*, **63**, 393 (1959). Also, recent unpublished results.

400° spectrum of V(II) as being due to an octahedrally coördinated species.

The absorption spectrum of Ni(II) in a variety of chloride melts has received a good deal of attention.[16–19] The spectrum is markedly affected by temperature and by the size of the alkali metal ion of the solvent. More work is needed to decide whether the spectral changes are due to tetragonal distortion of a tetrahedral $NiCl_4^=$ complex or to an octahedral–tetrahedral transformation. Spectral changes similar to those observed with Ni(II) now have been found with V(II) as revealed in Fig. 2. We will anticipate a forthcoming paper with a detailed discussion of these results by remarking that the high temperature (1000°) spectrum of V(II) indicates the formation of a **tetrahedral $VCl_4^=$ species.**

The problem of the intensity of the V(II) spectrum remains to be discussed. It will be noted from Table II that the total intensity of the V(II) spectrum in LiCl–KCl is greater by a factor of ≈ 10 than the aqueous solution spectrum. It is not likely that the major cause of this increase is temperature change. Holmes and McClure[12] showed that oscillator strengths of d-d transitions in octahedral fields obey an equation of the form $f = f_0 (1 + \exp(-\theta/T))$ where θ is the frequency of the non-totally symmetric vibration in temperature units ($\theta/1.44 = \omega \mathrm{cm.}^{-1}$) and f_0 is the value of the oscillator strength at 0°K. If one assumes 150–300 $\mathrm{cm.}^{-1}$ as a reasonable spread of frequencies for a T_{1u} vibration of MX_6 groupings where X = H_2O or Cl^-, then one would expect a 10–30% increase in intensity from room temperature to 400°. The fact that the half-widths of the bands in the melt are not larger than in aqueous solution further illustrates the relatively minor effect of temperature on the spectrum. The temperature or "vibronic" mechanism therefore cannot account for the increased intensity of the V(II) spectrum in LiCl–KCl eutectic as compared with the aqueous solution spectrum. The additional intensity could, however, arise from a number of alternative mechanisms acting singly or in concert.[20] Thus, a distortion of the octahedral VCl_6^{-4} complex would destroy the **center of symmetry** and provide an intensity mechanism by allowing mixing of orbitals of opposite parity. Detailed calculations would have to be made to decide whether the observed intensity can result from the mixing of 3d and 4p-metal orbitals or whether mixing of ligand orbitals with the 3d orbitals must be included. The importance of the latter possibility must be seriously considered in view of the decrease in the energy of the charge transfer band quite generally observed for transition metal ion spectra in chloride melts as compared with spectra of the same ions in aqueous solution. Additional experimental and theoretical work is required to elucidate these questions.

(17) C. R. Boston and G. P. Smith, *J. Phys. Chem.* **62**, 409 (1958).
(18) Chr. K. Jørgensen, *Molecular Phys.*, **1**, 410 (1958).
(19) G. Harrington and B. R. Sundheim, *Ann. N. Y. Acad. Sci.*, **79**, 950 (1960).
(20) C. J. Ballhausen and A. D. Liehr, *J. Mol. Spectroscopy*, **2**, 342 (1958); Errata, *ibid.*, **4**, 190 (1960); *Phys. Rev.*, **106**, 1161 (1957); R. Englman, *Mol. Phys.*, **3**, 48 (1960).

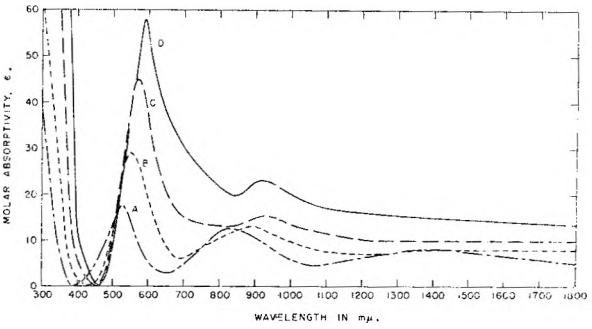

Fig. 2.—Temperature variation of the absorption spectrum of V(II) in LiCl–KCl eutectic: A = 400°, B = 600°, C = 800°, D = 1000°.

B. The V(III) spectrum in LiCl–KCl eutectic at 400° (Fig. 1B) is characterized by two bands with maxima at 555 mμ (18,020 $\mathrm{cm.}^{-1}$) and 911 mμ (11,000 $\mathrm{cm.}^{-1}$). The similarity of the V(II) and V(III) spectra both with respect to the molar absorptivities and the positions of the first two absorption bands is quite marked. In principle there is, of course, no reason why the two spectra should be so much alike, and careful supplementary analytical work was required to determine the particular oxidation state under investigation. This aspect of the work already has been discussed.

The edges of the charge transfer bands of the V(II) and V(III) spectra occur at 380 mμ (26,400 $\mathrm{cm.}^{-1}$) and 460 mμ (20,600 $\mathrm{cm.}^{-1}$), respectively. Identifying the shifts in the edges of the charge transfer bands with equivalent shifts of the band maxima one finds that the charge transfer process is favored energetically by 0.72 volt in the V(III) compared with the V(II) spectrum. It is tempting to correlate this shift with a recent determination of the V(III)–V(II) potential in LiCl–KCl eutectic which was found by Laitinen and Pankey[21] to be −0.748 volt at 450°. The V(III) spectrum in LiCl–KCl eutectic can be fitted to the energy level diagram of Liehr and Ballhausen[22] for a d^2 electronic system in a field of octahedral symmetry. Assigning the long wave length band to the transition from the $^3T_{1g}$ ground state to the $^3T_{2g}$ excited state, one obtains a value for Dq = 1200 $\mathrm{cm.}^{-1}$. With this value of the field splitting parameter, the next triplet–triplet transition ($^3T_{1g} - {}^3T_{1g}$) is predicted to be at 18,700 $\mathrm{cm.}^{-1}$ and clearly corresponds to the observed absorption band centered at 18,020 $\mathrm{cm.}^{-1}$.

The spectrum of V(III) in hydrated crystals[23] and in aqueous perchloric acid solutions[24] also is characterized by two absorption bands (Table II). In the compound $NH_4V(SO_4)_2 \cdot 12H_2O$ these bands are at 25,700 and 17,800 $\mathrm{cm.}^{-1}$, respectively, and can be fitted to the energy level diagram with Dq = 1860 $\mathrm{cm.}^{-1}$.

It will be noted that both absorption bands of V(III) experience about the same wave length shift (7280 ± 440 $\mathrm{cm.}^{-1}$) in going from Dq = 1860 $\mathrm{cm.}^{-1}$ to Dq = 1200 $\mathrm{cm.}^{-1}$, so that the entire

(21) H. A. Laitinen and J. W. Pankey, *J. Am. Chem. Soc.*, **81**, 1053 (1959).
(22) A. D. Liehr and C. J. Ballhausen, *Ann. Phys.*, **6**, 134 (1959).
(23) H. Hartmann and L. Schlaefer, *Z. Naturforsch.*, **6a**, 754, 760 (1951).
(24) S. C. Furman and C. S. Garner, *J. Am. Chem. Soc.*, **72**, 1785 (1950).

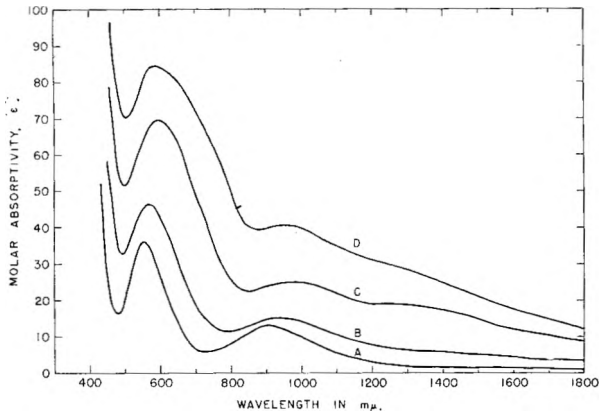

Fig. 3.—Temperature variation of the absorption spectrum of V(III) in LiCl–KCl eutectic: A = 400°, B = 600°, C = 800°, D = 1000°.

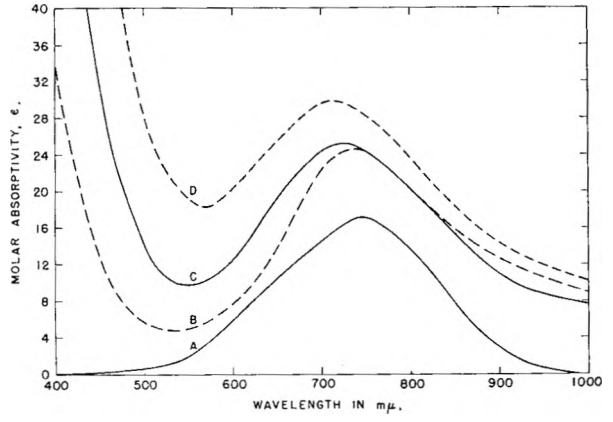

Fig. 4.—Absorption spectra of V(IV): A = 1.1 *M* $HClO_4$ at 25° (ref. 24); B, C, D = LiCl–KCl eutectic at 400, 800 and 1000°, respectively.

spectrum appears shifted to longer wave lengths to the same extent. The reason for this is to be found in the fact that the separation between the $^3T_{2g}$ and $^3T_{1g}$ energy levels is essentially independent of *Dq* as can be seen from an examination of the energy level diagram.[22]

Using an energy level diagram based on calculations which neglect spin–orbit coupling, Harrington and Sundheim derived a $Dq = 800$ cm.$^{-1}$ for V(III) in LiCl–KCl eutectic.[19] The newer energy level calculations which include spin–orbit coupling effects bring the *Dq* value in a chloride environment into better agreement with results already known on other similar systems. Thus, as in the case of V(II) discussed above, the *Dq* value for V(III) in an octahedral chloride environment is about 65% of the *Dq* value in water or oxygen surroundings.

It is of interest to note (Table II) that the half-widths of the V(III) bands are actually less at 400° in the eutectic than at room temperature in aqueous solution. Undoubtedly, the smaller field of the chloride ions compared with the water dipoles is responsible for the narrower bands. The oscillator strengths in the eutectic are larger by a factor of 2–3 compared with the analogous transitions in an aqueous medium. Temperature does not appear to be the cause of the increase in intensity since very similar *f*-numbers are found in molten pyridinium chloride at 160°, as in LiCl–KCl eutectic at 400°. A distortion of the VCl_6^{-3} ion which destroys the center of symmetry of the complex could account for the increase in intensity. Alternatively, a mechanism involving the charge transfer energy states (which occur in chloride melts at energies much lower than in aqueous solution) could account for the greater intensity as discussed above.

It already has been noted that good agreement is obtained when the V(III) spectrum at 400° is compared with calculations for two unpaired d electrons in octahedral surroundings. One therefore feels justified in picturing the V(III) ion as being surrounded by six chloride ions in the melt at 400°. At higher temperatures, however, pronounced spectral changes are observed (Fig. 3) which can be interpreted as being due to an octahedral–tetrahedral transformation, the 1000° spectrum being very similar to the tetrahedral VCl_4^- spectrum in the $CsAlCl_4$ lattice.[25] The V(III) ion appears to be extremely well suited for studying this transformation since its octahedral site preference energy (about 10 kcal. in chloride lattices[26]) is just large enough to stabilize the VCl_6^{-3} complex at low temperatures but too small to compete with chloride ion repulsions which favor tetrahedral VCl_4^- complexes at high temperatures. A detailed investigation of the energetics of this transformation in a variety of fused salt solvents has been carried out recently.[26]

C. The V(IV) spectrum in LiCl–KCl eutectic at 400° (Fig. 1C) is characterized by one band centered at 739 mμ (13,530 cm.$^{-1}$) with a shoulder at ≈650 mμ (≈15,400 cm.$^{-1}$). The half-width of the band is 4300 cm.$^{-1}$ and its *f*-number 5.9×10^{-4}. The spectrum in LiCl–KCl is very similar to that reported for the vanadyl ion, VO^{++}, in aqueous perchloric acid solution by Furman and Garner[24] and by LaSalle and Cobble.[27] The manner of preparation of the V(IV) solutions (Section 1 above) by air oxidation of V(III) solutions or by dissolution of $VOCl_2$ is further evidence that one also is dealing with an oxygenated ionic species in the fused salt solutions.

The VO^{++} spectrum has been discussed theoretically by Jorgensen[28] and by Furlani.[29] The vanadium atom possesses 5 electrons beyond the argon core. In the VO^{++} ion two of these are removed and two others presumably join in a covalent double bond with the oxygen leaving one unpaired electron which gives rise to the observed absorption bands. In the $C_{\infty v}$ electrostatic field of the VO^{++} molecule ion, the 3d orbitals split into three energy states $A_1(d_{z^2})$, $E_1(d_{xz}, d_{yz})$ and $E_2(d_{xy}, d_{x^2-y^2})$. The $A_1(d_{z^2})$ orbital is filled by the σ bonding electrons of the metal–oxygen bond, so that a single band should be observed in the absorption spectrum due to a transition from the E_2 ground state to the E_1 excited state. A splitting of the excited E_1 state, however, is observed both in the aqueous solution

(25) D. M. Gruen and R. Gut, *Nature*, **190**, 713 (1961).
(26) R. Gut, R. L. McBeth and D. M. Gruen, in preparation.
(27) M. J. LaSalle and J. W. Cobble, *J. Phys. Chem.*, **59**, 519 (1955).
(28) Chr. K. Jorgensen, *Acta Chem. Scand.*, **11**, 73 (1957).
(29) C. Furlani, *Ricerca Sci.*, **27**, 1141 (1957).

spectrum and in the melt spectrum, although it is more pronounced in the former. Such a splitting could occur if the electric field symmetry were lowered from $C_{\infty v} \rightarrow C_{2v}$. In a chloride melt one might postulate the existence of an ion $VOCl_3^-$ which would distort from C_{3v} to C_{2v} symmetry under the influence of Jahn–Teller forces.[30] The experimentally observed splitting of the absorption band could be accounted for in this manner.

In contradistinction to the spectra of V(II) and V(III) in LiCl–KCl eutectic which are very temperature dependent, the V(IV) spectrum is quite temperature insensitive (Fig. 4). The peak positions and band intensities remain essentially unaltered in the range 400–1000°. It therefore would appear that the spectrum is determined in first order by the electric field due to the V–O bond and that any change with temperature in the number of coördinating chloride ions has only a negligible effect on the spectrum.

D. The V(V) spectrum in LiCl–KCl eutectic at 400° is characterized by a strong absorption band with leading edge at about 480 mμ and a molar absorptivity in excess of 5000. In aqueous perchloric acid solutions of VO_2^+ an intense band is observed with maximum at 225 mμ having a molar absorptivity of 2240.[28] The leading edge of the band is at ≈380 mμ. Molina[31] recently has studied solutions of V_2O_5 and $NaVO_3$ in LiCl–KCl eutectic and finds that the band edge shifts about 3000 cm.$^{-1}$ to shorter wave lengths in going from the former to the latter solute. He attributes the shift as due to the equilibrium

$$2VO_3^- \rightleftharpoons V_2O_5 + O^{-2}$$

and gives the value 10^{-4} for the dissociation constant.

Since vanadium in the (V) oxidation state has no 3d electrons, the absorption band cannot be attributed to electronic transitions within the inner d shell. The high intensity of the band suggests that its origin is to be sought in a charge transfer mechanism.

Experimental

Spectrophotometer.—Several modifications of commercially available spectrophotometers have been described for measuring absorption spectra at elevated temperatures.[2,17,32–34]

A general problem encountered in making such measurements is due to black-body radiation from the sample. In most commercially available instruments the phototube is located in such a position as to detect all of the black-body radiation emitted by the sample in addition to the transmitted monochromatic beam. The blackbody radiation (noise) increases rapidly with temperature while the intensity of the transmitted monochromatic beam (signal) is essentially unaffected. In practice, the signal-to-noise ratio limits the upper temperature for quantitative spectrophotometric measurements to about 500°.

In previous work,[2] this problem was ameliorated by reversing the positions of light source and phototube on a Beckman DU spectrophotometer. This procedure reverses the light path and eliminates most of the black-body radiation from the light radiation measured by the phototube detectors.

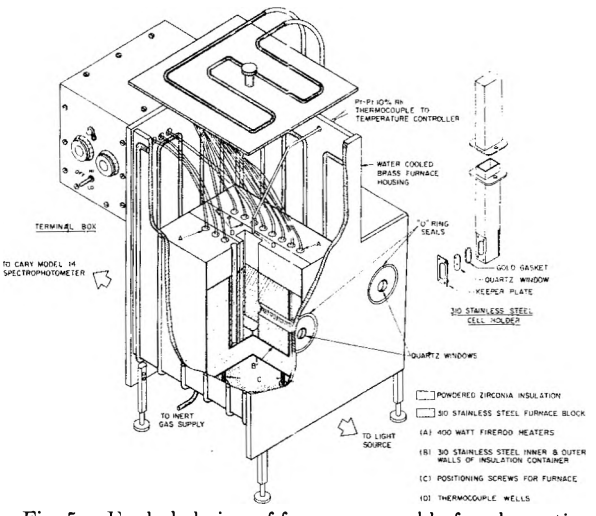

Fig. 5.—Exploded view of furnace assembly for absorption spectra measurements at temperatures up to 1000° with the Cary Model 14 spectrophotometer.

In order to extend the wave length range over which spectra could be measured and to gain the advantages of automation, a Cary Model 14 spectrophotometer similarly was adapted for studies at temperatures up to 1000°. In order to reverse the light path for the ultraviolet and visible regions (200–600 mμ), the phototube compartment was placed in the position normally occupied by the "visible" tungsten lamp compartment. (Provisions for making this replacement exist on the standard Model 14 since the instrument is used in just this way for measuring fluorescence spectra.) The infrared detector (600–2600 mμ) normally is located in the "reverse" position on the standard Model 14. With the Model 14, therefore, it is a simple matter to arrange the light path for all wave lengths in such a way that it traverses the sample first, then the monochromator before finally reaching the detectors.

A hydrogen and a tungsten lamp were used for light sources. These were housed in a light source compartment designed and built by the Applied Physics Corporation, Monrovia, California. The lamps were mounted on a sliding platform so that either could be brought into proper position by means of a shift lever. With the instrument used as described above, the contribution of black-body radiation to the total measured radiation intensity was greatly reduced and in fact did not constitute a serious problem even at 1000°, the upper limit of our temperature range. (See Section 5.)

Furnace.—An exploded view of the furnace and auxiliary parts is shown in Fig. 5. The water-cooled furnace compartment (22.9 × 26.7 × 40.7 cm.) is made of 0.64 cm. brass with 0.64 cm. copper coils silver soldered on to the sides through which the cooling water flows. The light ports in the furnace compartment have quartz discs sealed into the openings. A lucite box (not shown) fits onto the top of the furnace compartment and is connected to a laboratory exhaust duct, thus providing a leak-proof system for obtaining spectral measurements on radioactive samples.

The furnace itself is constructed of 310 stainless steel and is made in 3 parts. The two outside sections each contain eight 400-watt Firerod heaters while the center section is machined to accommodate a cell holder for 1 cm. square absorption cells. The furnace is so designed that the center section can be removed and replaced with other sections designed to hold cells of 2, 5 or 10 cm. light path. These three parts of the furnace are contained in a double-walled 310 stainless steel container filled with powdered zirconia insulation. Insulation on top of the furnace is provided by three sealed 310 stainless steel cans also filled with zirconia insulation.

Because of space limitations inherent in the Model 14, only the sample chamber can be maintained at the high temperature. Since the reference chamber is at room temperature, correction curves for black-body radiation and solvent absorption were obtained (see Section 5).

(30) C. J. Ballhausen and A. D. Liehr, *Acta Chem. Scand.*, (in press).

(31) R. Molina, *Bull. soc. chim. France*, 301 (1961).

(32) B. R. Sundheim and J. Greenberg, *Rev. Sci. Instr.*, **27**, 703 (1956).

(33) J. P. Young and J. C. White, *Anal. Chem.*, **31**, 1892 (1959).

(34) J. R. Morrey and A. W. Madsen, *Rev. Sci. Instr.*, **32**, 799 (1961).

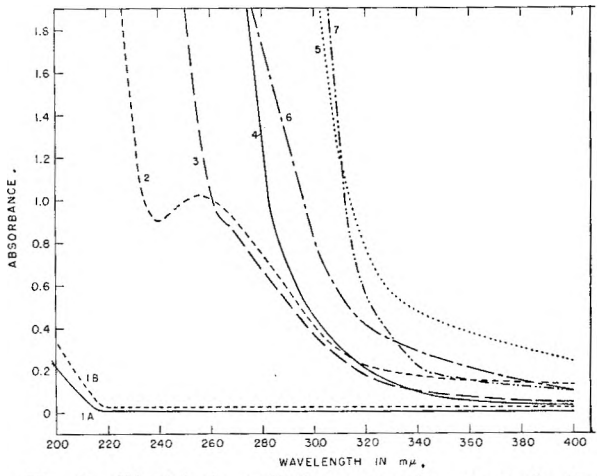

Fig. 6.—Black-body radiation correction curves in the 200–400 mμ region (all curves obtained against a reference path of air at 25°): 1A = air at 400°; 1B = air at 1000°; 2, 3, 4, 5 = LiCl–KCl eutectic at 400, 600, 800 and 1000°, respectively; 6 = LiCl at 900°; 7 = KCl at 900°.

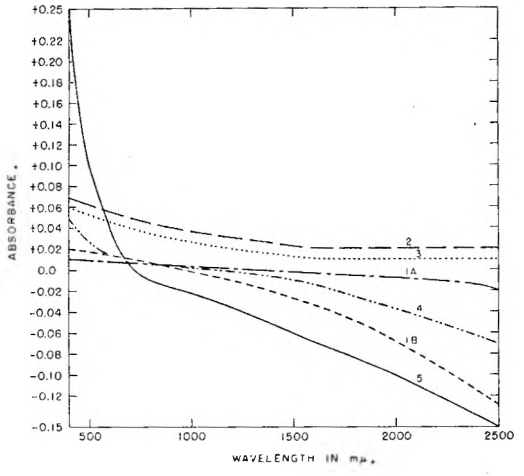

Fig. 7.—Black-body radiation correction curves in the 400–2500 mμ region (all curves obtained against a reference path of air at 25°): 1A = air at 400°; 1B = air at 1000°; 2, 3, 4, 5 = LiCl–KCl eutectic at 400, 600, 800 and 1000°, respectively.

Temperature Controller.—The temperature controller was designed and built by J. Brewer of the Electronics Division, Argonne National Laboratory. Power is controlled through a self-saturating saturable reactor with a chopper amplifier. A Pt–Pt 10% Rh thermocouple is used as a sensing element bucked against a reference source which is a 12 mv. manganin wound helipot. An anti-oscillation control on the amplifier prevents hunting and large overshoots. Provisions exist for pre-heating the furnace rapidly with an automatic switchover to the temperature controller as the temperature approaches a predetermined point. A waterflow interlock system controlled by a solenoid valve turns off the power to the heaters, reactor, light and water sources should a leak develop anywhere within the system. The heater block is connected so that only 12 heaters are controlled and 4 heaters are available for auxiliary heat.

The excellent stability of the controller coupled with the high heat capacity of the furnace resulted in temperatures which were constant to ±0.1° for periods of several hours over the entire temperature range.

Temperature Measurement.—Temperature of the molten salt inside the cell was determined and controlled in the following way: A Pt–Pt–10% Rh thermocouple was calibrated according to the method reported by Roeser and Wensel[35] of the National Bureau of Standards using standard samples of tin, lead, zinc, aluminum and copper metals, and a secondary standard of silver metal. This thermocouple was inserted in a thin wall quartz tube immersed in molten salt in a cell in the operating position of the furnace. The e.m.f. of this thermocouple was measured on a Leeds and Northrup Double Range Potentiometer, Model No. 8662, against a number of settings of the helipot on the temperature controller. After applying the corrections to the e.m.f., a graph was constructed showing the temperature of the molten salt *vs.* helipot settings. Although any temperature setting is maintained within 0.1° by the controller, it is calculated that the temperature within the cell is ±1° from any desired temperature. The apparatus for calibration of the thermocouples was kindly made available to us by R. Thorn and R. Ackermann.

Black-body Radiation.—As mentioned earlier, only the sample compartment was heated while the reference compartment was at room temperature. It was necessary therefore to determine correction curves for black-body radiation (b.b.r.) as well as cell and solvent absorption at various temperatures. The data are displayed graphically in Fig. 6 (200–400 mμ) and Fig. 7 (400–2500 mμ). Curves 1A and 1B represent the absorption of air at 400 and 1000° *vs.* air at room temperature. In the 200–700 mμ region the contribution of black-body radiation at 1000° is apparently smaller than over-all transmission losses. This statement follows from the fact that in this wave length region curve 1B lies above curve 1A by about 0.02 O.D. units while the reverse would be true if the only change in radiation intensity were due to increased emission of b.b.r. at the higher temperature.

Transmission losses could arise either because of small dimensional changes of the furnace block with increasing temperature or because of a possible temperature dependence of the absorptivity of air.

The crossover of curves 1A and 1B occurs at ≈800 and at 2500 mμ, the b.b.r. contribution is about 0.1 absorbance unit.

The effect of introducing into the sample path a 1 cm. square quartz cell filled with LiCl–KCl eutectic was studied as a function of temperature. The results are given in curves 2, 3, 4 and 5 of Figs. 6 and 7. In the infrared and visible regions at 400° (curve 2) the absorption due to the cell plus eutectic amounts to 0.04–0.1 absorbance unit if one takes curve 1A (air *vs.* air at 400°) as the baseline. The decreased transmission in this spectral region presumably is due primarily to reflection and scattering losses from the quartz cell surfaces. In the ultraviolet region, curve 2 exhibits an absorption maximum with a peak at 256 mμ followed by a steep rise in absorption. The first absorption band is almost certainly due to heavy metal ion impurities like Pb^{+2} since it can be virtually eliminated by treating the molten LiCl–KCl eutectic with Mg metal. The second rise in absorption which begins at 240 mμ apparently is due to the fundamental absorption bands of the alkali halide constituents of the melt. This point will be discussed in greater detail in the following section. Curve 2 shows that at 400° b.b.r. effects over the entire spectral range are smaller even than the small transmission losses due to the cell plus eutectic. It should be noted that the 256 mμ absorption band present in most of the eutectic melts decreases the accuracy with which molar absorptivities of added substances can be determined in the ultraviolet region. Rigorous purification of the solvent is required in order to obtain quantitative results in this spectral region. Curve 3, the 600° run lies below curve 2 throughout the infrared and visible region by about 0.01 O.D. units due to b.b.r. In the ultraviolet region the 256 mμ absorption band at 600° appears only as a shoulder on the tail of the fundamental absorption band, which has been shifted toward longer wave lengths. The pattern of spectral changes just described for a temperature of 600° essentially repeats itself at 800° (curve 4) and at 1000° (curve 5). At 1000°, the contribution of b.b.r. is 0.16 absorbance unit at 2500 mμ and 0.08 absorbance unit at 1500 mμ, amounting to 44 and 20% of the measured radiation intensities at these two wave lengths. The correction for the b.b.r. contribution is of course a function of the absorbance of the solution. The correction curves presented here are applicable only to cells filled with pure LiCl–KCl eutectic. A eutectic solution

(35) W. F. Roeser and H. T. Wensel, in "Temperature—Its Measurement and Control in Science and Industry," American Institute of Physics, Vol. 1, Reinhold Publ. Corp., New York, N. Y., 1941, pp. 284–314.

of a transition metal ion with an absorption band will reduce the intensity of the transmitted radiation but will not markedly change the intensity of the b.b.r. In such a case the b.b.r. correction will be larger than in the pure solvent. The additional correction was found to be only 0.020 O.D. units in the range 1300–2100 mμ at 900° with a 1 O.D. neutral density screen in the light path. The magnitude of this effect, though small, must be taken into account for quantitative measurements.

A calculation was made of the ratio of energies emitted per cubic centimeter by two black-bodies at temperatures T_1 and T_2, respectively. From Planck's equation[36] one easily obtains for this ratio at a particular wave length λ

$$\frac{E_{\lambda T_1}}{E_{\lambda T_2}} = \frac{e^{1.43/\lambda T_2} - 1}{e^{1.43/\lambda T_1} - 1} \qquad (1)$$

The temperature of the tungsten lamp filament was determined with an optical pyrometer and found to be ≈2400°. Using the values 2700°K. for T_1 and 1273°K. for T_2 (the temperature of the furnace and sample), the ratio given by eq. 1 is 11 at 2500 mμ and 45 at 1500 mμ. The calculated b.b.r. contributions therefore are 9% at 2500 mμ and 2% at 1500 mμ. The discrepancy between the calculated and experimentally determined values undoubtedly is due to the fact that the assumption of equal emitting volumes made in eq. 1 is a very poor one for our particular experimental setup. Apparently and reasonably, the furnace and sample present a much larger effective emitting volume to the slit of the spectrophotometer than does the tungsten filament.

Fundamental Absorption Bands in Alkali Halides.—In addition to the ultraviolet absorption spectra of alkali halide mixtures given in Fig. 6, the spectra of pure LiCl (curve 6) and pure KCl (curve 7) at 900° also are presented. The characteristic common to the mixtures and the pure substances is that the fundamental absorption bands are shifted to longer wave lengths compared to crystals at room temperature. In melts of KCl at 900° the fundamental absorption band edge is at 320 mμ, whereas in crystalline KCl at room temperature it is at 190 mμ for a 1 cm. path length. Similar shifts of the absorption edges of alkali halide salts have been observed previously by various investigators.[37-40]

From the viewpoint of the present study we are only concerned with the location of the edges of these fundamental bands, since the ultraviolet cut-off places a lower limit on the wave length at which meaningful measurements can be made of the absorption bands of transition metal ions added to the alkali halide melts. In this connection it will be remembered that the molar absorbancies of the "forbidden" transitions of the transition metal ions are of the order 10^{-1}–10^{2} compared with 10^{5} for the fundamental bands in alkali halides.

Acknowledgments.—We are indebted to R. Gut for the preparation of VCl_3 and to S. Bruckenstein for help with the vanadium anodization experiments. The aid of the Analytical group in performing the vanadium analyses once more is gratefully acknowledged.

(36) E. Hausmann and E. P. Slack, Third Edition, "Physics," D. Van Nostrand Co., Inc., New York, N. Y., 1948, p. 336.

(37) E. Mollwo, *Z. Physik*, **124**, 118 (1947).

(38) W. Martienssen, *J. Phys. and Chem. Solids*, **2**, 257 (1957).

(39) B. R. Sundheim and J. Greenberg, *J. Chem. Phys.*, **28**, 439 (1958).

(40) E. Rhodes and A. R. Ubbe ohde, *Proc. Roy. Soc.* (London), **251**, 156 (1959).

THE NICKEL CHLORIDE–CESIUM CHLORIDE PHASE DIAGRAM. TETRAHEDRAL $NiCl_4^{=}$ ION IN THE NEW COMPOUND Cs_3NiCl_5[1]

BY E. IBERSON, R. GUT[2] AND D. M. GRUEN

Chemistry Division, Argonne National Laboratory, Argonne, Illinois

Received June 30, 1961

The phase diagram of the nickel chloride–cesium chloride binary system has been investigated by differential thermal analysis. The system exhibits two congruently melting compounds, $CsNiCl_3$ (m.p. 758°) and Cs_3NiCl_5 (m.p. 547°) as well as three eutectic points at 522, 541 and 747°. These correspond to the compositions 19, 27 and 55 mole % $NiCl_2$. The blue compound Cs_3NiCl_5 is isomorphous with Cs_3CoCl_5.[20] In these 3:1 compounds the transition metal ion is surrounded by four chloride ions in a tetrahedral arrangement. At 417°, Cs_3NiCl_5 decomposes in the solid state to CsCl and yellow $CsNiCl_3$ in which nickel is coördinated octahedrally. Qualitative considerations show that octahedral crystal field stabilization energies play an important role in determining phase stability in the CsCl–$NiCl_2$ system as well as in the other known CsCl–MCl_2 systems. The stereochemistry of the chlorine coördination polyhedra in complex chlorides of the transition elements is discussed in the light of crystal field theory and Jahn–Teller distortions.

Introduction

The application of crystal field theory to problems of structure and bonding has brought about a renewed interest in the stereochemistry of ionic solids.[3,4] One of the important factors governing the arrangements of anions about transition metal cations is the crystal field stabilization energy. In particular, the stability of octahedral *versus* tetrahedral coördination is strongly determined by the octahedral site preference energy which is zero for d^0 and d^{10} configurations, but can be of the order of 15–50 kcal. in the case of d^3, d^4, d^8 and d^9 configurations.[4]

The Ni^{+2} ion with a d^8 configuration has a large octahedral site preference energy and it therefore is not surprising that to date only very few tetrahedral nickel compounds have been prepared. Aside from dilute solutions of Ni^{+2} substituted isomorphously for Zn^{+2} in the compound Cs_2ZnCl_4,[5] the only other known occurrences of the tetrahedral $NiCl_4^{-2}$ grouping are in the compounds $[(C_2H_5)_4N]_2NiCl_4$ and $[(C_6H_5)_3MeAs]_2NiCl_4$ prepared by Nyholm and Gill.[6] The crystal structure of these compounds has been determined recently by Pauling.[7] It was of interest to investigate the phase diagram of CsCl and $NiCl_2$ particularly in view of a number of qualitative observations in the literature concerning the occurrence in $NiCl_2$–alkali halide mix-

(1) Based on work performed under the auspices of the U. S. Atomic Energy Commission.

(2) On leave, Department of Inorganic Chemistry, E.T.H. Zurich.

(3) J. D. Dunitz and L. E. Orgel, Chapter I, "Stereochemistry of Ionic Solids" in "Advances in Inorganic Chemistry and Radiochemistry," Vol. 2, Academic Press, New York, N. Y., 1960.

(4) D. S. McClure, *J. Phys. and Chem. Solids*, **3**, 311 (1957).

(5) D. M. Gruen and R. L. McBeth, *J. Phys. Chem.*, **63**, 393 (1959).

(6) R. S. Nyholm and N. S. Gill, *J. Chem. Soc.*, 3997 (1959).

(7) P. Pauling, Ph.D. dissertation, University of London, 1959.

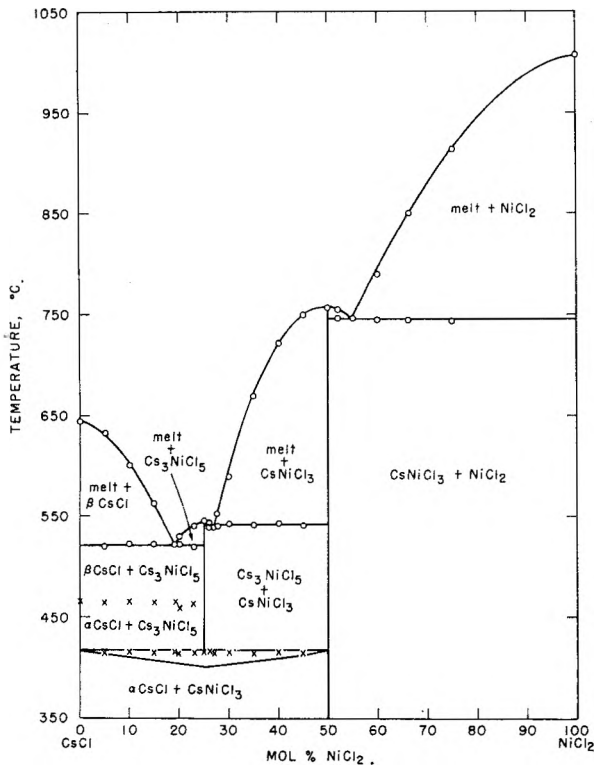

Fig. 1.—$CsCl$–$NiCl_2$ phase diagram.

tures of solids having the blue color indicative of tetrahedral Ni^{+2}.[6,8,9]

A number of other $CsCl$–MCl_2 phase diagrams have been obtained in the last few years by various workers. The discussion given in the present paper correlates all of the available information on these systems and demonstrates clearly the important role of crystal field stabilization (c.f.s.) energies in determining stereochemical and phase behavior in certain instances. It should be made clear at the outset, however, that although they are not considered in this paper, other factors such as radius ratio and specific bonding are of importance and must be taken into account in a definitive discussion of stereochemical and phase behavior.

Results and Discussion

I. The $NiCl_2$–$CsCl$ Phase Diagram.—The phase diagram of this binary system was determined by means of differential thermal analysis as described in the Experimental Section. Figure 1 shows the phase diagram constructed from the data given in Table I. Before discussing the phase diagram in detail, it will be worthwhile to summarize certain observations which have a bearing on the interpretation of the data. (a) A sharp color change from a blue melt to a yellow solid was observed at the liquidus–solid temperatures for compositions greater than 50 mole % $NiCl_2$. (b) In the region 0–50 mole % $NiCl_2$ a similar color transition was observed, not at the liquidus–solid temperatures, but in the solid at 417°. Above 417° the solid was blue; below 417° it was yellow. (c) The color change in the solid was reversible at the transformation temperature and was associated with a heat effect, the heat effect being a maximum at a composition corresponding to 25 mole % $NiCl_2$. The bent line below the 417° halt indicates, as usual, the magnitude of the heat effect.

The outstanding features of the phase diagram are seen to be the 1:1 compound $CsNiCl_3$ (m.p. 758°) and the congruent melting 3:1 compound Cs_3NiCl_5 (m.p. 547°), which has a transformation point at 417°. (The nature of the transformation will be discussed in detail below.) In addition there are three eutectic points at 522, 541 and 747° corresponding to compositions 19, 27 and 55 mole % $NiCl_2$, respectively. The $\alpha \rightarrow \beta$ phase transformation of $CsCl$ was observed to occur at 466°.

II. The New Compound Cs_3NiCl_5.—Of particular stereochemical interest is the occurrence of the blue Cs_3NiCl_5 compound. Not only was it important to obtain crystal structure data on the compound itself, but it also was necessary to determine whether the heat effect at 417° involved a phase transformation or a solid state decomposition reaction. It was found that Cs_3NiCl_5 could be quenched from a temperature above 417° to room temperature without undergoing the decomposition. X-Ray diffraction powder patterns on such quenched samples were found to be essentially identical with patterns of Cs_3CoCl_5, which had been prepared either from the melt or from aqueous solution. It therefore may be said with considerable certainty that the cobalt and the nickel compounds are isostructural. No diffraction lines due to either $CsCl$ or $CsNiCl_3$ were observed in the Cs_3NiCl_5 pattern.

TABLE I

$NiCl_2$, mole %	Obsd. temperatures, °C.			
	[a]	[b]	[c]	[d]
0.0	644		466	
5.0	633	521	465	415
10.0	601	523	466	417
15.0	562	522	466	416
19.1	522	522	466	416
20.0	530	522	461	416
23.0	541	521	464	417
25.0	547			418
26.0	544	541		418
27.0	541	541		416
27.5	552	542		415
30.0	590	542		417
35.0	670	542		416
40.0	723	543		417
45.0	750	541		416
50.0	758			
52.0	756	747		
55.0	747	747		
60.0	790	745		
66.7	850	747		
75.0	915	746		
100.0	1009			

[a] Temp., °C., liquidus. [b] Temp., °C., eutectic. [c] Temp., °C., $CsCl$ $\alpha \rightarrow \beta$ transformation. [d] Temp., °C., Cs_3NiCl_5 solid state decomposition.

X-Ray patterns also were obtained on samples prepared by slow cooling of the Cs_3NiCl_5 compound through its transformation temperature. A melt of the exact composition was cooled to 400°, allowed to equilibrate at this temperature for several hours

(8) F. Meyer and H. Remy, *Ber. deut. chem. Ges.*, **77**, 679 (1944).
(9) F. M. Hornyak, *J. Am. Chem. Soc.*, **79**, 5435 (1957).

TABLE II

COMPOUNDS IN THE $CsCl–MCl_2$ BINARY SYSTEMS

No. of unpaired "d" electrons	Ion	Oct.[b] cryst. radii, Å.	Oct. site pref. energy units of *Dq*	Octahedral $CsMCl_3$	Tetrahedral Cs_2MCl_4	Tetrahedral Cs_3MCl_5	Remarks	Ref.
0	Mg^{+2}	0.65	0	610[a] C	545 C	527 C		14
2	Ti^{+2}	.90	0.7	932 C	747 I			15
3	V^{+2}	.88	9.3	1090 C				12
4	Cr^{+2}	.84	4.2	C			[e,g]	
5	Mn^{+2}	.80	0	593 C	538 C	511 C		16
6	Fe^{+2}	.76	1.3	556 C	558 C			17
7	Co^{+2}	.74	0.7	547 C	597 C	549 C		13
8	Ni^{+2}	.72	9.3	758 C		547 C	[f]	
9	Cu^{+2}	.72[c]	4.2	443 C	498 C	491 C	[g]	10, 18
10	Zn^{+2}	.74[d]	0		601 C	560 I		19

[a] M.p. in °C.; C, congruently melting compound; I, incongruently melting compound. [b] Values taken from L. Pauling, "The Nature of the Chemical Bond," 3rd edition, Cornell University Press, Ithaca, N. Y., Chapter 13, p. 518. [c] Data taken from L. H. Ahrens, *Geochim. et Cosmochim. Acta*, 2, 155, 169 (1952). [d] Data taken from L. Pauling, *J. Am. Chem. Soc.*, 49, 765 (1927). [e] Phase diagram not investigated. [f] Compound stable above 417°. Decomposes into CsCl and $CsNiCl_3$ below this temp. [g] E. Iberson, R. Gut and D. Gruen, unpublished work.

TABLE III

CRYSTAL STRUCTURES OF COMPOUNDS IN $CsCl–MCl_2$ BINARY SYSTEMS

Compound	Crystal class	Space group	Unit cell, Å. *a*	*b*	*c*	*Z*	Coördination around central ion	M–Cl dist., Å.	Remarks	Ref.
Cs_3MgCl_5										
Cs_3MnCl_5										
Cs_3CoCl_5	Tetrag	$I4/mcm, D_{4h}^{18}$	9.18		14.47	4	Tetrahedral	2.34	[a]	20
Cs_3NiCl_5	Tetrag								Isostructural with Cs_3CoCl_5	
Cs_3CuCl_5									[b,c]	
Cs_3ZnCl_5							Tetrahedral		Discussed in 10	
Cs_2MgCl_4										
Cs_2TiCl_4										
Cs_2MnCl_4										
Cs_2FeCl_4										
Cs_2CoCl_4	Orth	$Pnma, D_{2h}^{16}$	9.737	12.972	7.932	4	Tetrahedral	2.26	[a]	21
Cs_2CuCl_4	Orth	$Pnam, D_{2h}^{16}$	9.70	7.60	12.35	4	Tetrahedral distorted	2.22	[a]	18, 23
Cs_2ZnCl_4	Orth	$Pnam, D_{2h}^{16}$	9.737	12.972	7.932	4	Tetrahedral		[a]	22
									Isostructural with Cs_2CoCl_4	
$CsMgCl_3$	Hex	$c/mmc, D_{6h}^{4}$							Isostructural with $CsNiCl_3$	12, 13
$CsTiCl_3$										
$CsVCl_3$	Hex	$c/mmc, D_{6h}^{4}$	7.23		6.03	2	Octahedral		[b]	12
									Isostructural with $CsNiCl_3$	
$CsCrCl_3$	Hex	$P6_12, D_6^2$					Octahedral		[c]	
									Isostructural with $CsCuCl_3$	
$CsMnCl_3$										
$CsFeCl_3$										
$CsCoCl_3$	Hex	$c/mmc, D_{6h}^{4}$	7.194		6.033	2	Octahedral		[b]	13
									Isostructural with $CsNiCl_3$	
$CsNiCl_3$	Hex	$c/mmc, D_{6h}^{4}$	7.18		5.93	2	Octahedral	2.43	[a]	23, 11
$CsCuCl_3$	Hex	$P6_12, D_6^2$	7.20		18.0	6	Octahedral distorted	Mean val. 2.29	[a]	10

[a] Crystal structure data complete. [b] Crystal structure data incomplete. [c] E. Iberson, R. Gut and D. Gruen, unpublished work.

and then cooled to room temperature. X-Ray patterns on samples prepared in this way could be interpreted as due to a mixture of CsCl and $CsNiCl_3$. All the lines observed in these patterns could be indexed assuming the presence of only these two compounds. The conclusion to be derived from these studies is that the solid state transformation of Cs_3NiCl_5 involves in fact a decomposition to CsCl and $CsNiCl_3$ according to the equation

$$Cs_3NiCl_5 \xrightarrow[\text{above } 417^\circ]{\text{below } 417^\circ} 2CsCl + CsNiCl_3$$

blue yellow

III. Comparison of the $CsCl–NiCl_2$ Binary System with Other $CsCl–MCl_2$ Systems.—A search of the literature shows that all the $CsCl–MCl_2$ (M = iron group transition metal) binary systems with the exception of the chromium and copper systems

(10) A. F. Wells, *J. Chem. Soc.*, 1662 (1947).
(11) G. N. Tishchenko, *Trudy Inst. Krist. Akad. Nauk S.S.S.R.*, **11**, 93–96 (1955).
(12) H. J. Seifert and P. Ehrlich, *Z. anorg. u. allgem. Chem.*, **302**, 284 (1959).
(13) H. J. Seifert, *ibid.*, **307**, 137 (1961).
(14) B. F. Markov and I. D. Panchenko, *Zhur. Obshcheii Khim.*, **25** 2042 (1955).
(15) P. Ehrlich and R. Schmitt, *Z. anorg. u. allgem. Chem.*, **308**, 94 (1961).
(16) B. F. Markov and R. V. Chernov, *Ukrain. Khim. Zhur.*, **24**, 641 (1958).
(17) I. S. Morozov, V. I. Ionov and B. G. Korshunov, *Zhur. Neorg. Khim.*, **5** (No. 6), 602 (1960) English translation.
(18) L. Helmholz and R. F. Kruh, *J. Am. Chem. Soc.*, **74**, 1176 (1952).
(19) B. F. Markov, I. D. Panchenko and T. G. Kostenko, *Ukrain. Khim. Zhur.*, **22**, 290 (1956).
(20) H. M. Powell and A. F. Wells, *J. Chem. Soc.*, **1**, 359 (1935).
(21) M. A. Porai-Koshits, *Kristallografiya*, **1**, 291 (1956).
(22) B. Brehler, *Z. Krist.*, **109**, 68 (1957).
(23) B. Morosin and E. C. Lingafelter, *J. Phys. Chem.*, **65**, 50 (1961).

have been studied. For the purposes of this paper a detailed discussion of the various phase diagrams will not be given. We wish rather to focus attention on the most commonly occurring compounds in these systems, namely, the $CsMCl_3$, Cs_2MCl_4 and Cs_3MCl_5 compounds which are listed in Table II together with their melting points. The symbols C or I signify that the compound melts congruently or incongruently. In Table III the available crystal structure data are given.

The $CsMCl_3$ compounds are found in all of the systems investigated with the exception of Zn and occur in one of two different structures, either the $CsCuCl_3$[10] or the $CsNiCl_3$ structure.[11] In both structures the transition metal ion is surrounded by six chloride ions. However, in the $CsNiCl_3$ structure the Cl^- ions are in an essentially perfect octahedral arrangement while in the $CsCuCl_3$ structure the octahedra are severely distorted. The Cu–Cl distances are: $2Cl^-$ at 2.30 Å., $2Cl^-$ at 2.27 Å., and $2Cl^-$ at 2.65 Å., giving the appearance of planar $CuCl_4^{-2}$ groupings with two chlorines at larger distances from the Cu^{+2} ion. In $CsNiCl_3$ as indicated above only one Ni–Cl distance is found and given as 2.43 Å. The $CsVCl_3$[12] and $CsCoCl_3$[13] compounds are reported to be isostructural with $CsNiCl_3$.

The Cs_2MCl_4 compounds are found in all of the systems investigated, with the exception of V and Ni. The structures of the Cs_2MCl_4 compounds with M = Co, Cu or Zn[18,21,22] have been determined. The compounds are isostructural and display tetrahedral coördination of the transition metal ion with chloride ion. In the cobalt compound the Co–Cl distance is 2.26 Å., which is close to the sum of the covalent radii of Co^{+2} and Cl^-. In the copper compound the chlorine tetrahedra are somewhat distorted and the Cu–Cl distances are 2.22 Å.

Six compounds of the type Cs_3MCl_5 have been found so far. (See Table II.) The crystal structure of Cs_3CoCl_5 was determined by Powell and Wells[20] and Cs_3NiCl_5 now has been found to be isostructural with it. Powell and Wells suggested that Cs_3CoCl_5 should be formulated as $Cs_3[CoCl_4]Cl$ since the structure contains tetrahedral $CoCl_4^{-2}$ groupings (Co–Cl distance = 2.34 Å.), with the fifth Cl^- very much further away. The same situation presumably prevails in Cs_3NiCl_5.

IV. The Effect of Crystal Field Stabilization Energies in Determining the Stability and Structures of Compounds in $CsCl$–MCl_2 Systems.—Following the discussions of Dunitz and Orgel[3] and of McClure,[4] an important factor determining the relative stability of various coördination polyhedra about a transition metal ion is the number of electrons in the 3d shell. It can be shown that in an octahedral crystal field, the octahedral stabilization energies in units of Dq are 4 for d^1, d^6; 6 for d^2, d^4, d^7, d^9; 12 for d^3, d^8. In tetrahedral crystal fields the energies are 4 for d^4, d^9; 6 for d^1, d^3, d^6, d^8; and 12 for d^2, d^7. Theoretically, for a point charge model

$$Dq_{\text{tetrahedral}} = \frac{4}{9} Dq_{\text{octahedral}}.$$

By multiplying the tetrahedral energies by the factor 4/9 and subtracting these numbers from the corresponding octahedral energies, the octahedral preference energies in units of Dq are found to be 0.7 for d^2, d^7; 1.3 for d^1, d^6; 4.2 for d^4, d^9; 9.3 for d^3, d^8. These numbers are derived on the basis of the weak field theory which would appear to be the appropriate model for dipositive ions in a ligand field due to chloride ions.

This completely theoretical analysis shows that *octahedral* coördination is most strongly stabilized for d^3 and d^8 configurations. Conversely, tetrahedral coördination is most strongly *destabilized* for the d^3 and d^8 configurations.

The $CsCl$–MCl_2 systems represent an excellent series in which to test the predictions of the theory in a qualitative way. An examination of Tables II and III reveals the remarkable fact that the tetrahedral Cs_2MCl_4 and Cs_3MCl_5 compounds are *unstable* in the vanadium (d^3) and nickel (d^8) systems, while stable tetrahedral phases exist for the d^0, d^2, d^5, d^6, d^7, d^9 and d^{10} systems. The chromium (d^4) system which has not yet been investigated is expected to have stable tetrahedral phases. If this turns out to be the case, then the statement can be made that *stable $CsCl$–MCl_2 compounds with tetrahedral configuration around the metal ion exist at room temperature for all 3d elements except vanadium and nickel.* Thus, in the $CsCl$–VCl_2 phase diagram the only compound found is octahedrally coördinated $CsVCl_3$.[12] In the $CsCl$–$NiCl_2$ system, Cs_2NiCl_4 does not exist at all, while the tetrahedral Cs_3NiCl_5 decomposes in the solid state to CsCl and octahedral $CsNiCl_3$. In all other systems tetrahedrally coördinated Cs_3MCl_5 and/or Cs_2MCl_4 compounds have been found. It would appear therefore that c.f.s. energies can determine phase stability in certain cases. In addition to the large c.f.s. energies discussed above, the Jahn–Teller effect remains to be examined since it is important for the distortions of the coördination polyhedra and the crystal structure.

In octahedral fields, the d^3, d^5, d^8 and d^{10} configurations are stable against distortion and only small distortions connected with degeneracies in the t_{2g} orbitals are expected for the d^1, d^2, d^6 and d^7 configurations. However, large distortions involving degeneracies in the e_g orbitals are expected for d^4 and d^9 configurations. Öpik and Pryce[24] have concluded that in these cases distortions from octahedral symmetry favoring an arrangement with four near neighbors and two distant ones always should be the most stable. It is of interest to compare these theoretical predictions with the crystal structure data on the $CsMCl_3$ compounds.

As pointed out above, these compounds crystallize either in the $CsNiCl_3$ structure with perfect octahedral coördination or in the $CsCuCl_3$ structure which displays exactly the kind of distortion toward a square planar arrangement expected for a d^9 configuration. On theoretical grounds one would expect all other $CsMCl_3$ compounds to have the $CsNiCl_3$ structure, with the exception of $CsCrCl_3$ (d^4 configuration) for which the Jahn–Teller distortion should be large, and which therefore would

(24) U. Öpik and M. H. L. Pryce, *Proc. Roy. Soc.* (London), **A238**, 425 (1957).

be expected to have the $CsCuCl_3$ structure. The compound $CsCrCl_3$ now has been prepared in these laboratories (Iberson, Gruen and Gut, unpublished work) and has been found to be isomorphous with $CsCuCl_3$. The situation with respect to the $CsMCl_3$ compounds therefore is exactly analogous to that found with the iron group transition metal difluorides and KMF_3 compounds. The difluorides crystallize in the tetragonal structure having regular or slightly distorted octahedral environments with the exception of CuF_2 and CrF_2, which are monoclinic with strong tetragonal distortion of the octahedra.[3] The KMF_3 (M = iron group transition metal) series of compounds recently have been found to possess the ideal perovskite structure with the exception of $KCuF_3$ and $KCrF_3$, which are tetragonal.[25]

In tetrahedral crystal fields, large distortions from regular tetrahedral symmetry are to be anticipated only for the high-spin configurations d^3, d^4, d^8 and d^9. However, the theory predicts an elongation of the tetrahedron ($c/a > 1$) for d^3 and d^8 systems and a flattening of the tetrahedron ($c/a < 1$) for d^4 and d^9 systems. Detailed crystal structure studies on Cs_2CuCl_4[18] show that the $CuCl_4^{-2}$ grouping is a flattened tetrahedron as required by theory for a d^9 configuration. On the other hand, the MCl_4^{-2} groupings in Cs_2CoCl_4, Cs_3CoCl_5 and Cs_2ZnCl_4 are nearly perfect tetrahedra.[20-22] Very small or zero distortions are to be expected in these systems.

An example of a compound in which an elongation of the MCl_4^{-2} tetrahedron is to be expected is Cs_3NiCl_5. The powder data available for the substance at present cannot give information on this point and an effort is being made to obtain single crystals of the compound for detailed crystal structure determinations.

In conclusion it may be pointed out that the (hypothetical) compounds Cs_2CrCl_4 and Cs_3CrCl_5 which have not yet been observed should show a flattening of the coördination tetrahedron similar to the situation found in Cs_2CuCl_4.

(25) K. Knox, *Acta Cryst.*, **14**, 583 (1961).

Experimental

Anhydrous nickel chloride was prepared from analytical reagent grade $NiCl_2 \cdot 6H_2O$ according to the method of Johnson, *et al.*[26] The $NiCl_2 \cdot 6H_2O$ was dehydrated by heating in a quartz tube at 550° under a stream of dry HCl gas for several hours. The final product, consisting of golden yellow mica-like crystals of $NiCl_2$, was obtained by sublimation in a stream of dry argon at 1000°, the product being cooled to room temperature and stored in a desiccator for future use. The HCl and argon gas streams were dried by passage through magnesium perchlorate.

Analytical reagent grade CsCl was dried by melting and the cesium chloride–nickel chloride melts were prepared and handled in quartz tubes under an atmosphere of dry argon. The clear blue melts did not wet the silica surface. (Wetting of the silica surface by molten chlorides usually is due to traces of oxide or hydroxide formed by hydrolysis of the melt.[27]) A thermocouple in a thin walled silica container was placed in the melt. A second silica tube was filled with dry zirconia and also contained a thermocouple. Both silica tubes were inserted in a massive nickel block surrounded by a tubular furnace. The differential thermocouple voltage was registered on an electronic recorder during the cooling of the melt. The temperature of the cell containing the salt was measured at short intervals of time (1 to 3 min.) and the cooling rate kept below 3°/min. (usually 1.5–2.5°/min.), the cold junction of the Chromel–Alumel thermocouple being immersed in melting ice at 0°.

To reduce errors due to the sublimation of nickel chloride, the largest mole fraction used was 75 mole % $NiCl_2$. The melting point of the pure compound was taken to be 1007° as reported by Johnson, *et al.*[26]

Acknowledgments.—The authors wish to express their thanks to Dr. S. Siegel and Mrs. Elizabeth Sherry (Chemistry Division, Argonne National Laboratory) for the X-ray diffraction studies of the compounds CsCl, Cs_3CoCl_5, Cs_3NiCl_5, $CsNiCl_3$ and $CsCrCl_3$, as well as for helpful discussions on certain aspects of the crystal structures of the $CsCl–MCl_2$ compounds.

(26) J. W. Johnson, D. D. Cubicciotti and C. M. Kelley. *J. Phys. Chem.*, **62**, 1107 (1958).

(27) A. H. V. Wartenberg, *Angew. Chem.*, **69**, 258 (1957).

RADIATION CHEMISTRY OF WATER WITH PULSED HIGH INTENSITY ELECTRON BEAMS[1]

BY A. R. ANDERSON AND EDWIN J. HART

Chemistry Division, Argonne National Laboratory, Argonne, Illinois

Received July 5, 1961

The radiation chemistry of water, aqueous ferrous sulfate, hydrogen peroxide and formic acid has been studied using pulsed electron beams from the Argonne linear electron accelerator. With a pulse length of ~1.4 μsec. and an electron energy of ~15 Mev., the dose rate received by the solutions during a pulse is equivalent to $\sim 2 \times 10^{23}$ e.v. ml.$^{-1}$ sec.$^{-1}$. Under these conditions, $\sim 10^{-5}$ *M* hydrogen atoms (and hydroxyl radicals) are generated throughout the irradiated volume. All irradiations are monitored with the Fricke dosimeter, for which $G(Fe^{3+})$ is 11.4 ± 0.5 under these irradiation conditions. Preliminary studies with neutral water and with 0.8 *N* sulfuric acid solutions show that the initial yields of both hydrogen and hydrogen peroxide are about 80% higher in the acid solution but that, in each case, $G(H_2) = G(H_2O_2)$. Oxygen is not an initial product. Yields of hydrogen have been measured in 0.8 *N* sulfuric acid up to 8 *M* hydrogen peroxide and up to 0.1 *M* in neutral solution. Hydrogen peroxide exerts a much stronger scavenging action in neutral than in acid solution. In each case, but at different concentrations of hydrogen peroxide, the scavenging curves eventually coincide with those determined using Co^{60} γ-radiation at a dose rate of $\sim 10^{17}$ e.v. ml.$^{-1}$ sec.$^{-1}$. Although difficulties remain, these data are consistent with the transient existence of two reducing species designated as the solvated electron, e^-_{aq}, predominant in neutral solutions, and the H atom, predominant in acid solution. Hydrogen peroxide is 50 times more effective in suppressing hydrogen formation in neutral solutions than in 0.8 *N* sulfuric acid solutions. Some relative hydrogen atom (or e^-_{aq}) and hydroxyl radical rate constants consistent with the $G(H_2)$ and $G(H_2O_2)$ are reported. In contrast to the lower $G(Fe^{3+})$ obtained with ferrous sulfate, measurements with the formic acid dosimeter (0.01 *M* HCOOH, 0.001 *N* H_2SO_4, 0.001 *M* O_2) give the same yields as with Co^{60} γ-radiation at much lower dose rates. $G(H_2O_2)$ for oxygen saturated neutral water is higher than that for γ-rays. This greater yield can be explained on the basis of competing radical–radical reactions.

Introduction

Current theory holds that the molecular products, hydrogen and hydrogen peroxide, formed in the radiolysis of water originate from H and OH radicals produced initially in high local concentrations along the track of the ionizing radiation. With γ-radiation or with fast electrons the radicals form in localized clusters or spurs, with the inter-radical or radical-solute reaction taking place during the expansion of the spurs. At the dose rates presently available from γ-ray sources or from X-ray and van de Graaff machines, alteration of the dose rate produces no quantitative chemical changes as the distance between individual spurs is so large that the radicals formed in any one spur react with solute molecules before they diffuse to the reaction zone of a neighboring spur. With electron linear accelerators, however, the dose rate during a pulse can be as much as 10^6 greater than that from the most powerful γ-ray source and a condition is produced in the solution where inter-track reactions can be observed. The general chemical manifestation of the higher dose rate will be the enhancement of products from inter-spur reactions at the expense of the radical–solute reactions. Previous observations of such effects have been made by Brasch, Huber and Waly,[2] by Hutchinson,[3] by Rotblat and Sutton[4] and by Glazunov and Pikayev.[5]

In our work we have investigated the radiolysis of pure water, of 0.8 *N* H_2SO_4, and of solutions containing oxygen, formic acid, hydrogen and hydrogen peroxide, at dose rates during a pulse corresponding to 2×10^{23} e.v. ml.$^{-1}$ sec.$^{-1}$. The irradiations were carried out with the Argonne electron linear accelerator, using 1.4 μsec. pulses of 15 Mev. electrons. Under these conditions we generate throughout the irradiated volume a uniform concentration of 12 to 15 μ*M* of hydrogen atoms and of hydroxyl radicals in a time that is short compared to appreciable radical–radical reaction, which is assumed to proceed with a rate constant of 6×10^9 l. mole^{-1} sec.$^{-1}$ (10^{-11} cc. molecule^{-1} sec.$^{-1}$).[6] Spur reactions, on the other hand, are substantially over in 10^{-9} second,[7] so they are complete at the end of the pulse.

Experimental

Preparation of Solution.—A modification of the "syringe technique" described previously[8] was used in our irradiations. Syringe A of Fig. 1 containing the degassed solution was the actual irradiation cell. After evacuation, the solution from chamber "B" was forced by argon pressure into the syringe which previously had been flushed with argon. By this technique the concentration of oxygen in solution could be maintained readily at less than 1 μ*M*. Solutions equilibrated with oxygen or hydrogen in the evacuation chamber were forced into the syringe using a pressure of the same gas.

Triply distilled water was used for all the solutions; hydrogen peroxide solutions were made from 98% H_2O_2 (Buffalo Electro Chem. Corp.) without further purification; formic acid was purified as described elsewhere[9]; oxygen was purified by a partial fractional distillation while high purity hydrogen and argon were used directly from the gas cylinders after passage through a liquid nitrogen trap. The solutions for dosimetry all were aerated (0.001 *M* $FeSO_4$, 0.001 *M* NaCl in 0.8 *N* H_2SO_4).

Analysis.—Hydrogen was analyzed chromatographically on a Molecular Sieve column (No. 13X, Wilkens Instrument and Research Co., Walnut Creek, California), using a technique developed in this Laboratory.[10] The gas was extracted from solution in a Van Slyke gas analysis apparatus, argon added and the gas mixture forced into a reservoir from where it was carried in a stream of argon to the column. This technique was checked using the mass spectrometer and the two methods agreed to within 2%. Oxygen also could be estimated in a similar way although the sensitivity of the

(1) Based on work performed under the auspices of the U. S. Atomic Energy Commission.

(2) A. Brasch, W. Huber and A. Waly, *Arch. Biochem. Biophys.*, **39**, 245 (1952); A. Brasch and W. Huber, *Science*, **105**, 112 (1947).

(3) F. Hutchinson, *Radiation Research*, **9**, 13 (1957).

(4) (a) J. Rotblat and H. C. Sutton, *Nature*, **180**, 1332 (1957); (b) *Proc. Roy. Soc.* (London), **A 255**, 490 (1960).

(5) P. Ya. Glazunov and A. K. Pikayev, *Doklady Akad. Nauk S.S.S.R.*, **130**, 1051 (1960).

(6) H. Fricke, *Ann. N. Y. Acad. Sci.*, **59**, 567 (1955).

(7) P. J. Dyne and J. M. Kennedy, *Can. J. Chem.*, **36**, 1518 (1958).

(8) E. J. Hart, S. Gordon and D. A. Hutchinson, *J. Am. Chem. Soc.*, **75**, 6165 (1953).

(9) E. J. Hart, *ibid.*, **76**, 4312 (1954).

(10) S. Gordon and G. E. Adams, private communication.

method using argon as a carrier gas was only about 10% of that for hydrogen. Hydrogen calibrations were carried out periodically during each series of hydrogen analyses and the sensitivity, expressed in terms of recorder peak area, was 200 cm.^{2} per micromole. Thus 0.025 micromole of hydrogen could be analyzed readily. At concentrations of H_2O_2 greater than 0.1 M, the gas was extracted from solution on a vacuum line, without the solution contacting mercury, and toeppled into an evacuated gas bulb. The oxygen was extracted by absorption in alkaline sodium hydrosulfite in the van Slyke apparatus and the hydrogen determined as described above.

Gas analysis for formic acid solutions was carried out by extracting the gas in the van Slyke apparatus, absorbing the CO_2 in potassium hydroxide solution, absorbing the oxygen in alkaline sodium hydrosulfite and determining the residual hydrogen by gas chromatography.

Hydrogen peroxide in neutral solution and in weakly acid formic acid solution was analyzed using the triiodide method[11]; the molar extinction coefficient at a wave length of 3500 Å. is taken as 2.59×10^4, at 25°. In acid solution the hydrogen peroxide was analyzed by oxidizing a 3 mM $FeSO_4$ solution and determining the ferric ion produced by its absorption at 304 mμ; the molar extinction coefficient is 2225 at 25° and the temperature coefficient of 0.7% per degree. For hydrogen peroxide concentrations <0.5 mM, analyses were carried out by titration against standard ceric sulfate using ferrous *o*-phenanthroline as an indicator.

Ferric ion analyses from the dosimetry solutions were carried out spectrophotometrically as described above.

Irradiation Technique.—The 100-cc. syringe, shown in Fig. 1, was held horizontally in a brass holder which was mounted on an optical bench, arranged so that the long axis of the syringe was parallel to the axis of the accelerator tube. Previous measurements, described elsewhere,[12] showed that if the volume of solution was restricted to 25 ml. an energy averaged dose rate[5b] could be defined for an effective irradiated volume of 15.3 ml. Our energy averaged instantaneous dose rates are defined simply as: total energy absorbed per pulse (e.v.)/effective irradiated volume (ml.) x duration of pulse (sec.) and are those pertaining to a pulse assumed to rectangular. Under these conditions the beam had been degraded by a $^3/_8$" thick polystyrene disc before it reached the solution. The absorption of Bremsstrahlung radiation produced in the window of the accelerator, in the polystyrene block and in the glass window of the syringe (2 mm. thick) contributed <1% to the total energy absorbed in solution. All irradiations were monitored with the Fricke dosimeter (0.001 M $FeSO_4$, 0.001 M NaCl, 0.8 N H_2SO_4, aerated) in a similar syringe, for which the ferric yield had been determined ealorimetrically[12] over the range of dose rate from 1.3 to 2.3×10^{23} e.v. ml.$^{-1}$ sec.$^{-1}$ used in the present work. Uniform energy absorption in the irradiated volume of 15.3 ml. also is assumed. By using a radical–radical rate constant of 6×10^9 l. mole^{-1} sec.$^{-1}$,[6] one finds that the half life of the 15 micromolar radicals generated is 5 μsec. compared to the 1.4 μsec. electron pulse. Uniform free radical concentration also obtains during the pulse since radicals diffuse of the order of 1000 Å. per μsec., a distance of the same order as radical–radical separation for 15 μM concentration.

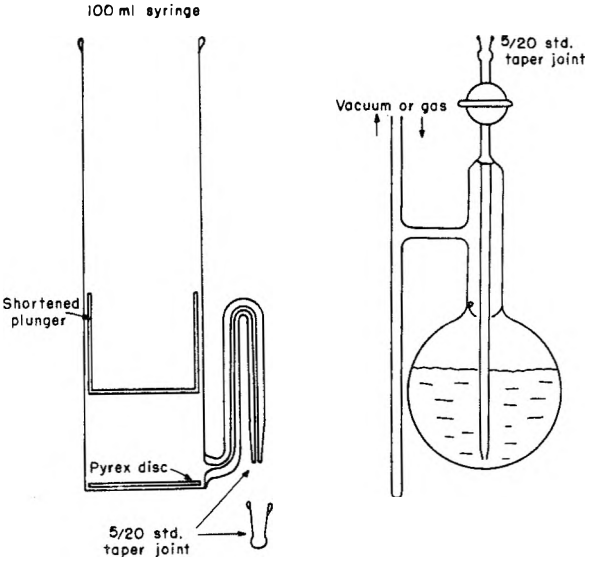

Fig. 1.—Syringe and evacuation chamber.

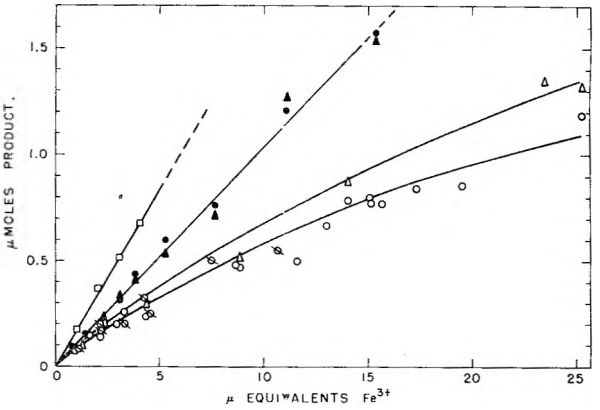

Fig. 2.—Yields from linac irradiation of neutral water and 0.8 N H_2SO_4:

Solute		Product	
—	○	H_2O_2	Neutral in H_2O
—	△	H_2	
600 μM H_2	◎	H_2O_2	
10^{-3} M O_2	□	H_2O_2	
—	●	H_2O_2	0.8 N H_2SO_4
—	▲	H_2	0.8 N H_2SO_4

Irradiated volume ~25 ml.; instantaneous dose rate ~2×10^{23} e.v. ml.$^{-1}$ sec.$^{-1}$.

Results

Striking differences exist between the hydrogen (and hydrogen peroxide) yields obtained from the radiolysis of oxygen-free neutral water and 0.8 N sulfuric acid. Oxygen is not an initial product. $G(H_2)$ is 0.71 ± 0.04 and 1.23 ± 0.12 in neutral water and 0.8 N sulfuric acid, respectively. A similar difference is found for $G(H_2O_2)$ between these two media. Typical results appear in Fig. 2. Micromoles of product are plotted as a function of microequivalents of ferric ions produced by the same radiation dose under identical conditions. These data were obtained over a period of several weeks at dose rates ranging from (1.6–2.3) × 10^{23} e.v. ml.$^{-1}$ sec.$^{-1}$. As the change in $G(Fe^{3+})$ over this range of dose rate is within the experimental limits of the calorimetric determination[12] our yields are based on a mean $G(Fe^{3+})$ equals 11.4 ± 0.5. In neutral water at this dose rate the amounts of hydrogen peroxide and hydrogen deviate more than 5% from linearity at hydrogen peroxide concentrations greater than 10 μM. However, in 0.8 N H_2SO_4 no deviation from linearity occurs at hydrogen peroxide concentrations up to 100 μM. Where the hydrogen and hydrogen peroxide yields diverge from each other in neutral water the differences are approximately equivalent to the oxygen formed, in the cases where oxygen was determined. The addition of ~600 μM of hydrogen to neutral water had no effect on $G(H_2O_2)$ within experimental error (Fig. 2).

Yields of hydrogen measured over a wide range of hydrogen peroxide concentrations in both neutral and 0.8 N H_2SO_4 solutions are given in Table I

(11) C. J. Hochanadel, *J. Phys. Chem.*, **56**, 587 (1952).
(12) A. R. Anderson, *ibid.*, **66**, 180 (1962).

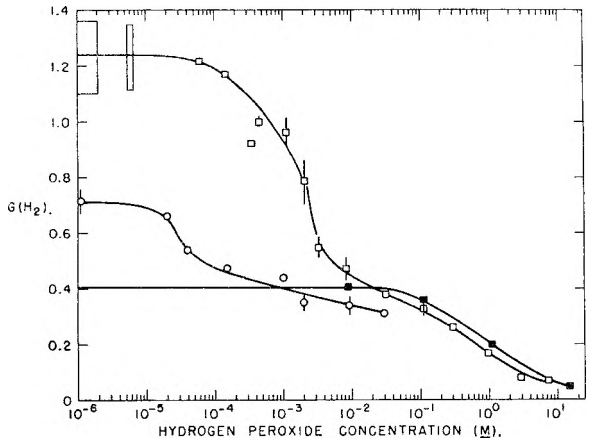

Fig. 3.—Hydrogen yields from linac and γ-ray irradiated hydrogen peroxide solutions. □, measurements in deaerated 0.8 N H_2SO_4. Linac data: □, deaerated 0.8 N H_2SO_4; ○, neutral water. Co^{60} γ-ray data: ■, deaerated 0.8 N H_2SO_4.

and in Fig. 3.[13] Note that the scavenging effect of hydrogen peroxide is much greater in neutral than in acid solutions. This effect accounts for the curvature of the dosage curves in neutral solutions.

TABLE I

EFFECT OF HYDROGEN PEROXIDE ON $G(H_2)$ FOR 15 MEV. PULSED ELECTRON AND γ-RAY IRRADIATION OF WATER AND 0.8 N SULFURIC ACID

Solvent, 0.8 N H_2SO_4		Solvent, neutral water	
15 Mev. electrons			
(H_2O_2), M	$G(H_2)$	(H_2O_2), M	$G(H_2)$
....	1.23 ± 0.12[a]		
0.00006	1.22	...	0.71 ± 0.04[b]
.00015	1.17	0.00002	0.66 } From tangents
.00034	0.92	.00004	.54 } to curve
.000444	1.00 ± .01	.00014	.47[c]
.00108	0.96 ± .05	.00036	.48 ± .04
.00208	.79 ± .07	.0011	.44
.00317	.55 ± .03	.0029	.35 ± .02
.00815	.47 ± .04	.0096	.34 ± .03
.0325	.38 ± .01	.029	.31 ± .01
.108	.33 ± .02		
.3	.26		
1.0	.17		
3.0	.085		
7.8	.068		
	Co^{60} γ-Rays		
0.00	.407	0.001	0.40
0.11	.36	.0056	.40
1.1	.20	.0081	.34
11.6	.049		

[a] $G(H_2O_2)$ = 1.24 ± 0.07. [b] $G(H_2)$ = 0.76 ± 0.09. [c] Single measurement.

In each case, but at different concentrations of hydrogen peroxide, the scavenging curves flatten off at $G(H_2)$ ~0.45 and then they coincide with those determined for Co^{60} γ-radiation at a dose rate of 10^{17} e.v. ml.$^{-1}$ sec.$^{-1}$.[14] This is more clearly demonstrated in 0.8 N H_2SO_4 solution where hydrogen yields were determined at concentrations of hydrogen peroxide up to 8 M. The centering of inflection points close to the accepted values for molecular hydrogen yields in the γ-radiolysis of water and the subsequent coincidence of $G(H_2)$ with the scavenging curves measured at a much lower dose rate lend added confidence to our dosimetry techniques.[12] In neutral water containing 10^{-3} M oxygen, however, the initial yield of hydrogen peroxide was increased to 1.98 ± 0.06 molecules per 100 e.v., and it remained constant up to 30 μM, the highest concentration of hydrogen peroxide measured (Fig. 2).

Results of measurements with the formic acid dosimeter (0.01 M HCOOH, 0.001 N H_2SO_4, 0.001 M O_2) are given in Table II. Linear yield *vs.* dose curves were obtained for each product and product yields agree within experimental error with those determined for Co^{60} γ-radiation at a much lower dose rate.[9]

TABLE II

YIELDS FROM THE FORMIC ACID DOSIMETER

(0.01 M HCOOH, 0.001 N H_2SO_4, 0.001 M O_2)

Product	Yield from Linac irradiation G	Yield from Co^{60} γ-ray irradiation[9] G
H_2O_2	3.25 ± 0.16	3.39 ± 0.22
CO_2	2.69 ± .12	2.75 ± .10
$-O_2$	2.72 ± .10	2.82 ± .06
H_2	0.43 ± .02	0.43 ± .03

Discussion

Figure 3 reveals several interesting features about the radiation chemistry of water. It supplies information relating to (a) two reducing species, and (b) $k_{H+H}/k_{H+H_2O_2}$ and relative radical–radical rate constants.

Two Reducing Species.—In the scavenging of molecular hydrogen, hydrogen peroxide has been shown to be less effective in γ-ray irradiated 0.8 N sulfuric acid than in neutral solution.[14] The data presented in Fig. 3 show the effect of added hydrogen peroxide on hydrogen yields in neutral and 0.8 N H_2SO_4 solutions irradiated by 15 Mev. electrons. In each case the addition of hydrogen peroxide decreases $G(H_2)$ rapidly until the γ-ray molecular yield is reached. At higher hydrogen peroxide concentrations $G(H_2)$ then follows the scavenging curve for γ-ray radiolysis. At $G(H_2)$ of 0.4, the concentration of hydrogen peroxide is high enough to suppress all radical–radical reactions in the bulk of the fluid outside the spur. Any further reduction in the hydrogen yield at higher concentrations of hydrogen peroxide is due to the penetration of scavenger into the expanding spur, before the intraspur H + H reactions are complete.

The divergent yields of hydrogen in neutral and in acid solution and the different reactivities of hydrogen peroxide indicate that the reactive reducing species are different in the two media. There is an increasing amount of evidence accumulating in radiation chemistry[14-16] to suggest the existence of two reducing species in the radioly-

(13) Later work has shown that the $G(H_2)$ *vs.* (H_2O_2)/dose rate is not completely independent of dose rate as is assumed in the theoretical treatment below.

(14) A. R. Anderson and E. J. Hart, *J. Phys. Chem.*, **65**, 804 (1961).

(15) (a) D. Armstrong, *et al.*, *Proc. 2nd Intern. Conf. Peaceful Uses Atomic Energy*, P/1517, **29**, 80 (1958); (b) A. O. Allen and H. Schwarz, *ibid.*, P/1403, **29**, 30(1958).

(16) F. S. Dainton and D. B. Peterson, *Nature*, **186**, 878 (1960).

sis of water. The general conclusion is that the solvated electron, e^-_{aq}, is converted to the H atom in acid solution by reaction

$$e^-_{aq} + H_3O^+ \longrightarrow H + H_2O \qquad (1)$$

Our data are consistent with this postulate although some difficulties remain especially in the interpretation of our recent dose rate results.[17]

Relative Effectiveness of the Two Reducing Species in Diminishing Hydrogen Formation.—The marked difference in the shape of the $G(H_2)$ *vs.* dose curves in Fig. 2 for acid and neutral solution is related in some complex manner with the different reactivity of the two reducing species with hydrogen peroxide as well as with other transient species such as the hydroxyl radical. In 0.8 *N* sulfuric acid we assume that the concentration of hydrogen ions is high enough under our conditions of irradiation to convert all e^-_{aq} to hydrogen atoms. Then the gross competition reactions may be expressed by (2) and (3).

$$e^-_{aq} + H_2O_2 \longrightarrow OH^- + OH \qquad (2)$$
$$H + H_2O_2 \longrightarrow H_2O + OH \qquad (3)$$

The relative effectiveness of reactions 2 and 3 in reducing hydrogen formation can be deduced as 50 to 1 by calculating the concentration of hydrogen peroxide needed to lower the initial hydrogen yield by the same proportionate amount in neutral and acid solution. This ratio compares with the ratio of about 5:1 to 10:1 deduced for γ-ray radiolysis.[14] Possible reasons for this divergence will be discussed below.

In contrast to the striking effect of hydrogen peroxide in suppressing hydrogen formation, added hydrogen at a concentration of 600 μM has no effect on $G(H_2O_2)$. Our observations on the effects of added hydrogen and hydrogen peroxide on $G(H_2)$ and $G(H_2O_2)$ from neutral solutions indicate that the rate constant for reaction 2 is at least 100 times greater than that for reaction 4

$$OH + H_2 = H_2O + H \qquad (4)$$

based on reasonable assumptions regarding the rate constants for competing reactions.

Relative H + H and H + H_2O_2 Rate Constants.—An analysis of the hydrogen suppression curves of Fig. 3 enables one to calculate the relative rate constants of the hydrogen forming reaction

$$H + H \longrightarrow H_2 \qquad (5)$$

to scavenging reactions 2 and 3. In reaction 5, and in the following discussion H represents the H atom of the acid solution or e^-_{aq} assumed to be effective in neutral solutions. Let α be the rate constant of reaction 5 and β the rate constant for the pertinent scavenging reaction, either 2 or 3. Then neglecting reactions of the hydroxyl radicals and assuming homogeneous kinetics, we have

$$\frac{\partial(H)}{\partial t} = -2\alpha(H)^2 - \beta(H)(H_2O_2)$$

$$(H) = \frac{\beta(H_2O_2)(H)_0}{[2\alpha(H)_0 + \beta(H_2O_2)]e^{\beta(H_2O_2)t}} - 2\alpha(H)_0$$

and the fractional number of H atoms combining with (H_2O_2) is

(17) J. K. Thomas and E. J. Hart, unpublished results.

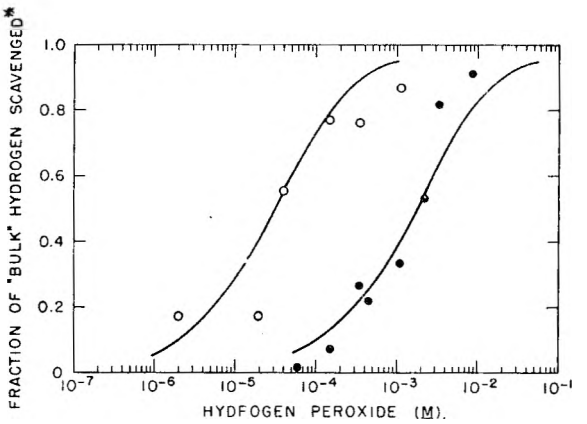

Fig. 4.—Effect of hydrogen peroxide on the suppression of "bulk" hydrogen in linac irradiated water and 0.8 *N* sulfuric acid. ○, water; ●, 0.8 *N* H_2SO_4; solid line, theoretical curves from equation 6: $*1 - \left[\frac{G(H_2) - 0.4}{H(H_2)_0}\right]$.

$$\int_0^\infty \alpha(H)^2 dt = \frac{\beta(H_2O_2)}{2\alpha(H)_0} \log_e\left[1 + \frac{2\alpha(H)_0}{\beta(H_2O_2)}\right] \qquad (6)$$

where (H_2O_2) is the concentration of hydrogen peroxide in moles/liter (assumed to remain constant) and $(H)_0$ is the initial concentration of reducing species developed during the pulse assumed to be infinitely short. A comparison of the experimental data with the fraction of H reacting with hydrogen peroxide calculated from equation 6 is shown in Fig. 4. In spite of this crude treatment, satisfactory agreement with experiment is found until penetration of the spurs occurs. Table III gives the conditions prevailing in the solution during the pulse and the ratio β/α is calculated from equation 6. The large difference in this ratio in neutral and 0.8 *N* sulfuric acid supports the conclusion that different hydrogen forming species are involved in these two media. β/α, computed from equations derived from the Flanders–Fricke one radical model[13,18] for hydrogen suppression by hydrogen peroxide in γ-ray spurs also appears in Table III. This ratio is nearly the same for electrons and γ-rays in neutral water but it is appreciably different in 0.8 *N* sulfuric acid. We suggest that the low ratio of 0.007 obtained in 0.8 *N* sulfuric acid with electrons represents reaction of the hydrogen atom (reaction 3) whereas 0.1 obtained for suppression in the γ-ray spur consists mainly of reaction with e^-_{aq} as represented by reaction 2. This means that in the spur, reaction 1 is incomplete while in the bulk and the suppression reaction is controlled by hydrogen atoms formed from (1).

Ratios of Radical–Radical Rate Constants.—The primary radical reactions in the radiolysis of water are 5, 7 and 8

$$OH + OH \longrightarrow H_2O_2 \qquad (7)$$
$$H + OH \longrightarrow H_2O \qquad (8)$$

and the observed yield of water decomposition is equal to

$$g(-H_2O) = 2g(H_2) + g(H) = 2g(H_2O_2) + g(OH)$$

If we assume that the rate constants for reactions 5, 7 and 8 are equal except for the statistical factor

(18) D. A. Flanders and H. Fricke, *J. Chem. Phys.*, **28**, 1126 (1958).

TABLE III

RELATIVE $H + H$ AND $H + H_2O_2$ RATE CONSTANTS IN WATER AND 0.8 N H_2SO_4 FROM PULSED ELECTRON BEAM IRRADIATIONS[a]

	Water	0.8 N H_2SO_4
Postulated reducing species	e^-_{aq}	H
g(reducing species)	3.05[23]	3.66[21b]
$(H)_0$ initial concn. of reducing species (M)	1.18×10^{-5}	1.54×10^{-5}
H_2O_2 for 50% suppression (M)	3.3×10^{-5}	170×10^{-5}
$(H_2O_2)_{50\%}/(H)_0$	2.8	110
β/α (electron beam)	0.3	0.007
β/α (γ-ray)[14]	0.5	0.1

[a] 1.4×10^{-6} sec. 15 Mev. electron pulse at an input dosage of 1.64×10^{23} e.v. ml.$^{-1}$ sec.$^{-1}$.

of two in reaction 8, the amount of water re-formed in reaction 8 is equal to $g(H_2) + g(H_2O_2)$ and the yield for total decomposition of water is

$$g(-H_2O)_T = g(-H_2O) + g(H_2) + g(H_2O_2)$$

Experimental data indicate that, over a wide range of ionization density, $g(-H_2O)_T = 4.50$ in neutral solutions[14,19,20] while in 0.8 N H_2SO_4, $g(-H_2O)_T = 5.8$.[21]

At the low dose rates available from Co^{60} γ-ray sources the concentration of molecular products, hydrogen and hydrogen peroxide, produced from intra-spur radical reactions builds up quickly to a low steady state value of the order of one micromolar in the absence of scavengers. Recombination of hydrogen and hydrogen peroxide in the bulk of the solution then occurs by reactions 3 and 4. At higher dose rates, however, where the adjacent spurs overlap before the intra-spur radical–radical reactions are complete, reactions 5, 7 and 8 compete with the back reactions 3 and 4. Under these conditions, an increase of molecular products is observed demonstrating that the rate constants k_5, $k_7 > k_2$, k_3, k_4. The initial slope of the hydrogen and hydrogen peroxide dose curves will be independent of dose rate, but the concentration of molecular products built up before deviation from linearity is observed will depend not only on the relative concentration of radicals and molecular products in the bulk of the solution but also on the relative rate constants for reactions 2, 3, 4, 5, 7 and 8. As the concentration of radicals is proportional to dose rate, increasing the dose rate will simply extend the linear part of the product–dose curve to higher concentrations of molecular products. This argument implies that the linear part of the dose curve exists at the low γ-ray dose rates but this linearity cannot be observed for γ-rays as deviation occurs at molecular product concentrations less than 1 μM. At very high dose rates, however, the important initial linear portion of the curve is extended so that reliable initial yields can be measured.

Table IV gives the theoretical yields obtained by solving the simultaneous equations applicable to free radical reactions 5, 7 and 8.

$$\frac{d(H)}{dt} = -2k_5(H)^2 - k_8(H)(OH) + e_1(t)$$

$$\frac{d(OH)}{dt} = -2k_7(OH)^2 - k_8(H)(OH) + e_2(t)$$

In these equations,[22] $e_1(t)$ and $e_2(t)$ represent the rate of H and OH radical generation during an electron pulse assumed to be rectangular.

$$(H_2) = \int_0^\infty k_5(H)^2$$

and

$$(H_2O_2) = \int_0^\infty k_7(OH)^2$$

These equations have been solved on the analog computer for the radiation yields[21b,23] $g(H)$, $g(OH)$, $g(H_2)$ and $g(H_2O_2)$, given in Table IV applying to neutral and acid solutions. The free radical rate constants used vary about the zero diffusion controlled activation energy rate constant of 10^{-11} cc. molecule^{-1} sec.$^{-1}$ calculated by Fricke.[6] The agreement between experiment and theory is close enough to conclude that the relative rate constants selected for k_5, k_7 and k_8 are satisfactory for acid solution. In neutral solution, however, the large divergence between experimental and calculated yields indicates that the pertinent hydrogen forming reactions represented by (5) are very slow or that reaction 8 specifically written as

$$e^-_{aq} + OH \longrightarrow OH^- \qquad (8')$$

is very high. This conclusion is derived from results in Table IV. Here the low experimental yields in neutral solutions can be approximated by assuming k_5 equal to zero and k_8' equal to $6k_7$. Alternatively if k_8' is $10k_5$, $G(H_2)_{calcd.}$ approaches $G(H_2)_{exp.}$

Measurements with neutral solutions of 0.001 M O_2 give $G(H_2O_2) = 1.98$ compared to 1.23 for Co^{60} γ-rays at much lower dose rates. In the presence of oxygen and low hydrogen peroxide we have reactions 9, 10 and 11

$$H + O_2 \longrightarrow HO_2 \qquad (9)$$

$$OH + HO_2 \longrightarrow H_2O + O_2 \qquad (10)$$

$$2HO_2 \longrightarrow H_2O_2 \qquad (11)$$

in addition to 7 and 8. By assuming that all H disappears by (9), reaction 5 can be eliminated and the equations for hydrogen peroxide formation become:

$$\frac{d(OH)}{dt} = -2k_7(OH)^2 - k_{10}(HO_2)(OH) + e_2(t)$$

$$\frac{d(HO_2)}{dt} = -k_{10}(HO_2)(OH) - 2k_{11}(HO_2)^2 + e_1(t)$$

and

$$(H_2O_2) = \int_0^\infty [k_7(OH)^2 + k_{11}(HO_2)^2]dt$$

Since the dosage curves are linear, secondary reactions of hydrogen peroxide are unimportant.

(19) H. A. Schwarz, J. M. Caffrey, Jr., and G. Scholes, *J. Am. Chem. Soc.*, **81**, 1801 (1959).

(20) A. R. Anderson and E. J. Hart, *Radiation Research*, **14**, 689 (1961).

(21) (a) N. F. Barr and R. H. Schuler, *ibid.*, **7**, 302 (1957); (b) *J. Phys. Chem.*, **63**, 808 (1959).

(22) D. L. Phillips, Argonne National Laboratory, has developed an analytical solution for these equations for an infinitely short pulse. Applied Mathematics Division Memorandum No. 17, Feb. 3, 1961.

(23) (a) P. V. Phung and M. Burton, *Radiation Research*, **7**, 199 (1957); (b) E. J. Hart, *J. Am. Chem. Soc.*, **76**, 4198 (1954).

TABLE IV

COMPARISON OF EXPERIMENTAL AND CALCULATED $G(H_2O_2)$ AND $G(H_2)$ FOR PULSED ELECTRON IRRADIATIONS IN WATER AND 0.8 N SULFURIC ACID

	$g(H)$	$g(OH)$	$g(H_2)$	$g(H_2O_2)$	k_5[b]	k_7[b]	k_8[b]	$G(H_2)_{exp}$	$G(H_2)_{calcd.}$[a]	$G(H_2O_2)_{exp}$
0.8 N H_2SO_4	3.65	2.95	0.45	0.80[21b]	6	6	12	1.23 ± 0.12	1.45	1.24 ± 0.07
	3.65	2.95	.45	.80	6	3	12	1.23 ± .12	1.36	1.24 ± .07
O_2-free water	3.16	2.64	.39	.65[22]	6	6	12	0.71 ± .04	1.23	0.76 ± .09
	3.16	2.64	.39	.65	6	3	12	.71 ± .04	1.13	.76 ± .09
	3.05	2.91	.41	.48[23]	6	6	12	.71 ± .04	1.18	.76 ± .09
	3.05	2.91	.41	.48	0.6	6	12	.71 ± .04	1.01	.76 ± .09
	3.05	2.91	.41	.48	0	6	12	.71 ± .04	0.99	.76 ± .09
	3.05	2.91	.41	.48	6	6	36	.71 ± .04	.82	.76 ± .09
	3.05	2.91	.41	.48	0	6	36	.71 ± .04	.74	.76 ± .09
	3.05	2.91	.41	.48	6	6	120	.71 ± .04	.60	.76 ± .09
Water + oxygen	3.16	2.64	.39	.65	6	6	12		1.70[c]	1.98
	3.05	2.91	.41	.48	6	6	12		1.58[c]	1.98

[a] $G(H_2)_{calcd.} = G(H_2O_2)_{calcd.}$ [b] k's in units of l. mole^{-1} sec.$^{-1}$ $\times 10^{-9}$. [c] $G(H_2O_2)_{calcd.}$ for $k_3 = k_9 = k_{10}$ and $k_{11} << k_8$.

Solving these six equations for $G(H_2O_2)$ on the analog computer gives a value of 1.70 and 1.58 for the conditions detailed in Table IV. In this calculation we arbitrarily assume $k_8 = k_9 = k_{10}$ and that $k_{11} << k_8$. At a concentration of 0.001 M O_2 only the molecular hydrogen yield, $g(H_2)$, is found with our electron irradiations. Therefore all the hydrogen atoms and electrons escaping spur reactions produce hydroperoxy radicals or the equivalent O_2^-. Since reaction 11 is slow compared to 7 and 10,[24] $G(H_2O_2)$ is determined in the main by the relative rate constant ratio, k_7/k_{10}, all remaining hydroperoxy radicals are assumed to form hydrogen peroxide *via* 11. Some additional adjustment of the rate constants is needed but in view of the uncertainty of parameters the agreement is satisfactory for these preliminary measurements.

Formic Acid Dosimeter.—In contrast to the simple case of ferrous sulfate and oxygen-saturated water, product yields obtained with the formic acid dosimeter (0.01 M HCOOH, 0.001 M O_2, 0.001 N H_2SO_4) are identical with the results from Co^{60} radiolysis.[9] See Table II. With the formic acid dosimeter, reaction 9 and

$$OH + HCOOH \longrightarrow H_2O + HCOO$$

efficiently remove all the radicals escaping from the spur so that the resulting reaction mechanism is identical to that pertaining at lower dose rates.

Acknowledgments.—The authors are indebted to Dr. H. Fricke for the mathematical treatment of results, to Miss V. Meyers and Mr. J. Hennings for experimental assistance and to Mr. K. Johnson for his willing coöperation in the operation of the linear accelerator. One of the authors (A. R. A.) wishes to express his thanks to the U.K.A.E.A. for his support on an exchange scheme during the course of this work.

(24) H. A. Schwarz, private communication.

METAL–AMINE COMPLEXES IN ION EXCHANGE. II. 2-AMINOETHANOL AND ETHYLENEDIAMINE COMPLEXES[1]

BY LEONE COCKERELL AND HAROLD F. WALTON

University of Colorado, Boulder, Colorado

Received July 5, 1961

The stabilities of complexes of 2-aminoethanol with Ag(I), Ni(II) and Cu(II), and of ethylenediamine with Ni(II), Cu(II) and Zn(II), have been measured in a cation-exchange resin and compared with the stabilities in aqueous solution. The ethylenediamine complexes are much more stable in the resin than in solution. Formation constants are given for Ni(II)–2-aminoethanol complexes in aqueous solution.

Some years ago we reported on the stability of certain metal–ammonia and metal–amine complex ions in cation-exchange resins.[1] In sulfonated polystyrene resins the ratio of combined ammonia to metal ion was the same in the resin as in a solution in equilibrium with the resin. This was true over a wide range of ammonia activities, metal ion concentrations in solution and equivalent fractions of metal ions in the resin. Butylamine likewise was held equally strongly in the resin and in the solution. Other amines were held more or less strongly in the resin; for example, benzylamine was bound more tightly by silver ions in the resin than in the solution, and this was ascribed to a reinforcement of the coördinating tendency by π-bonding with the benzene rings of the resin. This conclusion has been substantiated by studies of non-ionic absorption of aromatic amines by polystyrene-type resins.[2]

(1) Part I: R. H. Stokes and H. F. Walton, *J. Am. Chem. Soc.*, **76**, 3327 (1954).

(2) S. R. Watkins and H. F. Walton, *Anal. Chim. Acta*, **24**, 334 (1961).

The behavior of ethylenediamine was of special interest. This amine was held much more strongly by silver ions in the resin than by silver ions in the solution, for a given concentration of free amine, provided the ratio of bound amine to silver was less than unity.

This paper compares the stabilities of complexes of ethylenediamine with Ni^{++}, Cu^{++} and Zn^{++} in the solution and resin phases, and for comparison, the stabilities of complexes of 2-aminoethanol with Ag^+, Ni^{++} and Cu^{++}. The coördination of ethylenediamine with Ag^+ will be the subject of a separate paper.

Experimental

Materials.—The resin used was Permutit Q, kindly supplied by the Permutit division of Ionac Chemical Company. It was a sulfonated polystyrene, 30–50 mesh, with nominal crosslinking of 10%. The exchange capacity was 5.11 meq./g. (dry basis) in the hydrogen form, and the water uptake, determined pycnometrically, was 0.19 ml./meq. It was washed in the usual way.

The amines were Eastman White Label grades, distilled from fresh quicklime before use. The ethylenediamine boiled at 115° (628 mm.), the 2-aminoethanol at 168° (625 mm.) (corr.).

Equilibration.—Weighed amounts of air-dried resin, usually in the hydrogen form but sometimes saturated with metal ions, were placed in flasks with 100 ml. of solutions containing known quantities of amine, metal nitrate and nitric acid. They were shaken at 30 ± 1° for at least 8 hours. Attainment of equilibrium was verified by comparing results found by starting with hydrogen-form resins with those found by starting with metal-saturated resins.

Analytical.—After equilibration, samples of solution were withdrawn and their *p*H immediately determined with a Beckman Model G *p*H meter, using Beckman *p*H 7 buffer as a standard. For solutions containing silver ions the potassium chloride in the reference electrode was replaced by saturated potassium nitrate solution. Their total base content was found by potentiometric titration to the inflections at about *p*H 5. The metal-ion concentrations also were determined: Ag by titration with thiocyanate, Cu by iodide–thiosulfate titration, Ni gravimetrically with dimethylglyoxime, Zn gravimetrically as $Zn_2P_2O_7$.

Ionization Constants.—To calculate the amount of amine bound to the metal ions, "practical" ionization constants were used which were found by potentiometric titrations of the bases at various ionic strengths, using a Beckman Type E glass electrode. The "practical" ionization constant of an acid BH^+ is defined as

$$K'_a = \frac{(H^+)[B]}{[BH^+]}$$

the square brackets denoting molar concentrations, (H^+) the "hydrogen-ion activity" as read on the *p*H meter.

In determining complex ion stabilities in aqueous solution it is customary to provide a uniform ionic environment and constant ionic strength by adding an excess of an electrolyte such as sodium perchlorate. This cannot be done here as the sodium ions would enter the ion exchanger. Where cations of double charge are involved, such as Ni^{++} or enH_2^{++} (en = ethylenediamine), it is impossible to keep the ionic strength constant during the experiments unless one works at tracer levels. Thus the proper "practical" ionization constant to use in the calculations is in some cases uncertain within several hundredths of a logarithmic unit. Since the object of this work was to compare stabilities in the resin with those in the solution, rather than to evaluate individual stability constants, this uncertainty was less serious than it might have been. Furthermore, the ionic strength did not usually exceed 0.15.

The enH^+–enH_2^{++} Ion-exchange Distribution.—In evaluating the ethylenediamine experiments one had to know how the two cations, enH^+ and enH_2^{++}, were distributed between the solution and the resin. The distribution quotient used was that evaluated earlier.[1] The distribution is so one-sided that the resins always contained much more enH_2^{++} than enH^+.

Results

(a) **Calculation of Bound Base.**—In calculating the amounts of base coördinated to the metal ions in the solution and in the resin it was considered that the total equivalent concentration and the total volume of the solution were the same after shaking with the resin as they were before. In other words, the absorption of water and electrolyte by the resin was ignored. Since only 1 g. of resin was used to 100 ml. of solution this was reasonable.

The calculation then proceeded as follows for the monofunctional base, 2-aminoethanol.

Subtracting the metal ion concentration in solution from the total electrolyte concentration gave the concentration of the cation BH^+. From this, the *p*H and K_a' the concentration of free base, B, was calculated. Subtracting this from the total base concentration, found by titration, gave the concentration of bound base in solution.

The quantity of metal ions in the resin was the difference between that originally added and that found in the solution. Subtracting this from the exchange capacity of the resin, on an equivalent basis, gave the BH^+ in the resin. The total amine (BH^+ plus B) in the resin was the difference between the amine added and that found in the solution. The quantity of free B in the resin was negligibly small, so the difference between the total B in the resin and the BH^+ gave the quantity of B bound by the resin.

For the case of ethylenediamine the calculation was complicated by the presence of two cations, enH^+ and enH_2^{++}. The equivalent concentration of base cations in solution equals $[enH^+] + 2[enH_2^{++}]$; the total titratable base equals $[enH^+] + 2$ [free and bound en]. The free en in the solution could be calculated from the *p*H but was always very small. The ratio $[enH^+]/[enH_2^{++}]$ was calculated from the *p*H and K_1 for enH_2^{++}, and by solving simple simultaneous equations the concentrations of enH_2^{++}, enH^+ and en were found. A sample calculation is given in reference 1.

(b) **2-Aminoethanol Complexes.**—For the cation $C_2H_7NOH^+$ we found, by titrating 5×10^{-3} *M* base with 0.1 *M* HCl in the presence of potassium nitrate, $pK'_a = 9.45$ at ionic strength 0.05, 9.50 at ionic strength 0.10, both at 25°. These values agree with the value 9.74 at ionic strength 0.50 found by Bruehlman and Verhoek.[3]

(i) **2-Aminoethanol and Nickel.**—In this case, and in no other case reported in this paper, the concentration of nickel ions left in solution after ion exchange was too small to allow any accurate estimate of the binding of the base by nickel ions in the solution. The binding in the resin could, however, be calculated with fair certainty.

Since no data on the formation constants in solution could be found in the literature, a series of tests was made in which different amounts of 2-aminoethanol were added to solutions 0.071 *M* in nitric acid and 0.012 *M* in nickel nitrate, giving a constant ionic strength of 0.107. In addition, solutions 0.025 *M* in $C_2H_7NOHNO_3$,

(3) R. J. Bruehlman and F. H. Verhoek, *J. Am. Chem. Soc.*, **70**, 1401 (1948).

0.005 and 0.010 M in $Ni(NO_3)_2$, and containing enough potassium nitrate to make the ionic strength 0.10 were titrated with sodium hydroxide. The concentration of Ni^{++} did not affect the formation curve, showing that polynuclear complexes are absent. For brevity's sake the formation curve is not shown. Standard curve-fitting procedures gave

$$K_1 = 950 \pm 50;\ K_2 \doteq 125;\ K_3 \doteq 100;\ \beta_3 = 1.15 \times 10^7$$

The notation is that of Bjerrum, Schwarzenbach and Sillén.[4]

We found no marked difference in stability between the complexes in the resin and the complexes in the solution. There is a slight stabilization in the resin at low $\bar{n}$, a slight destabilization at high $\bar{n}$.

(ii) **2-Aminoethanol with Silver and Copper.**—Here the concentrations of metal left in solution after ion exchange were large enough that $\bar{n}$, the ratio of bound amine to total metal, could be determined in the solution at the same time that it was determined in the resin. The solution data gave log $\beta_2 = 6.56$ for silver, agreeing with the value 6.68 found by Bruehlman and Verhoek. The stabilities in the resin and in the solution are compared in Fig. 1. To save space the free base concentration is not given. The complexes with silver and copper are both less stable in the resin than in the solution.

(c) **Ethylenediamine Complexes.**—For the cation enH_2^{++} the following values of pK_1' were found by titration (at 25°): $\mu = 0.04$, 7.05; $\mu = 0.08$, 7.09; $\mu = 0.15$, 7.22. At $\mu = 0.10$, $pK_2' = 10.03$. The medium in each case contained ethylenediammonium ions and nitrate ions with no added salt. Our constants agree with those found by Schwarzenbach[5] at 20° and $\mu = 0.1$; $pK_1' = 7.22$, $pK_2' = 10.03$.

The equilibrium quotient for the ion-exchange reaction was taken as 5.0, with units millimoles/g.

$$enH_2^{++} + 2enH.R \rightleftharpoons 2enH^+ + enH_2.R_2$$

dry resin and millimoles/ml. solution.[1] As explained previously, this value has little influence on the calculation of $\bar{n}$ for the resin, since the cation enH_2^{++} predominates overwhelmingly in the resin.

The calculated $\bar{n}$ values are compared for the resin and the solution in Figs. 1 and 2. Two curves are drawn for each of the ions Cu^{++} and Ni^{++}, representing different proportions of added metal salts. The effect of the degree of loading of the resin by metal is seen clearly with the nickel complexes (see also Table I).

(d) **Other Complexes.**—Tests also were made with ammonia and Ni^{++} and with pyridine and Ag^+ and Cu^{++}. All these complexes were equally stable in the resin and the solution. Pyridine complexes are not stabilized in the resin environment, unlike benzylamine complexes,[1] and this finding parallels our observations on the absorption of uncharged aromatic amines by sulfonated polystyrene resins.

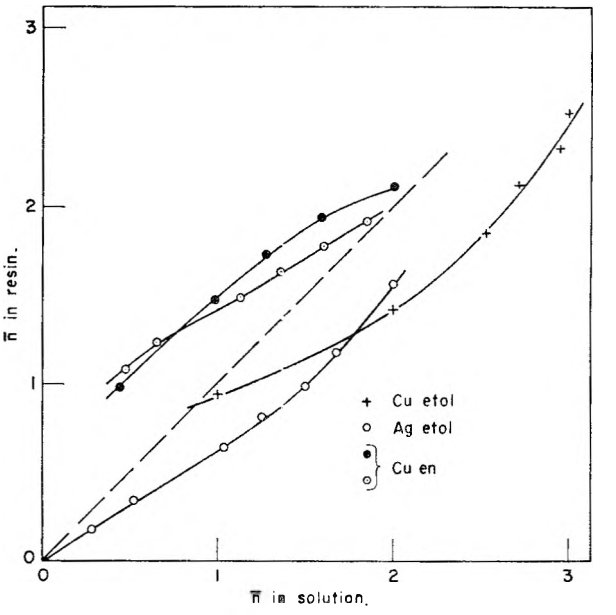

Fig. 1.—Formation of complexes with 2-aminoethanol ("etol") and ethylenediamine ("en"). The Cu–en complexes are more stable in the resin; filled circles, 2.0 meq. total Cu/g. resin; open circles, 5.0 meq. Cu/g. resin; about 50–80% of Cu was in resin at equilibrium; the proportion in the resin increased with proportion of "en".

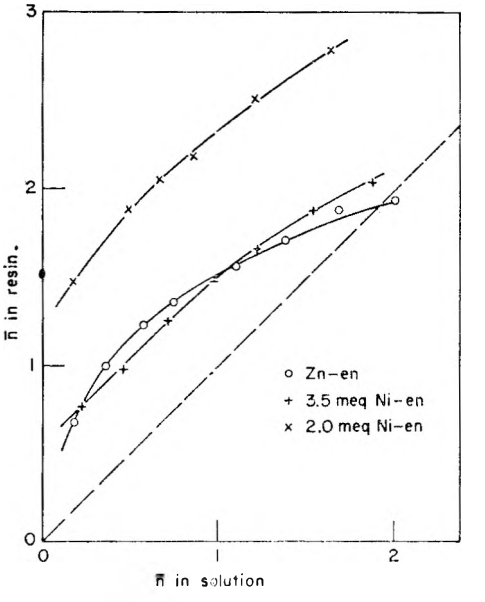

Fig. 2.—Formation of complexes with ethylenediamine. The total meq. of Ni in the system is indicated in the graph; for meq. Ni in resin at equilibrium, see Table I.

(e) **Amine Binding and Cation Exchange.**—Addition of amine changes the distribution of metal ions between the resin and the solution. With 2-aminoethanol the change is not large and may be in either direction; increasing the free amine concentration shifts silver ions from the resin into the solution (where the complex is more stable), but shifts nickel ions from the solution into the resin unless a large excess is added, when the reverse change occurs. Ethylenediamine, on the other hand, definitely drives the metal ions into the

(4) J. Bjerrum, G. Schwarzenbach and L. G. Sillén, "Stability Constants," Chemical Society, London, 1957.

(5) G. Schwarzenbach, H. Ackermann, B. Maissen and G. Anderegg, *Helv. Chim. Acta*, **35**, 2337 (1952).

TABLE I

METAL ION CONTENT OF RESINS

Metal ion	Amine[a]	Equivalent fraction of metal in resin
Ag	etol	0.75–0.65
Ni	etol	.54– .64
	en (1)	.03– .24
	en (2)	.40– .74
Cu	etol	.48– .53
	en (1)	.46– .80
	en (2)	.51– .77
Zn	en	.38– .69

[a] etol = 2-aminoethanol; en = ethylenediamine. The equivalent fraction for the lowest amine concentration is placed first.

resin as its concentration is increased. The effect is shown in summary form in Table I, which also shows, for nickel, the effect of resin loading on the complex stability.

Discussion

The main conclusion to be drawn from these data is that the resin environment stabilizes metal–ethylenediamine complexes. In the light of additional evidence to be presented in a subsequent paper, it is thought probable that the diamine acts as a "cross-linking ligand," binding metal ions together in a chain or network, and that this cross-linking occurs much more readily in a cation-exchange resin, where the metal ions are close together, than it does in dilute solutions.

Acknowledgments.—Most of this work was described in the Ph.D. thesis of Leone Cockerell (University of Colorado, 1954), and some of it was presented at the 138th National Meeting of the American Chemical Society, New York, 1960. Part was supported by the U. S. Atomic Energy Commission, Contract AT-(11-1)-499.

METAL–AMINE COMPLEXES IN ION EXCHANGE. III. DIAMINE COMPLEXES OF SILVER(I) AND NICKEL(II)[1]

BY M. G. SURYARAMAN AND HAROLD F. WALTON

Department of Chemistry, University of Colorado, Boulder, Colorado

Received July 5, 1961

The stabilities of complexes of silver ions with ethylenediamine and 1,3-propanediamine have been measured in sulfonated polystyrene cation-exchange resins having different degrees of crosslinking and functional-group content. Preliminary measurements also have been made with nickel(II) and hydrazine. In every case the complexes were more stable in the resin than in solution, the stabilization being greatest with ethylenediamine and silver ions, but the maximum degree of coördination was less in the resin. The stability was independent of crosslinking and silver ion concentration. Internal polymerization of the metal–amine complexes is suggested as a partial explanation.

Introduction

In measuring the stability of metal–amine complexes in cation-exchange resins we found[2] that the silver–ethylenediamine complex is much more stable within a sulfonated polystyrene resin than in aqueous solution. There were indications that a silver ion added only one molecule of ethylenediamine in the resin as compared to two molecules in aqueous solution. The tentative explanation was offered that the species in the resin was a doubly charged complex ion, $^{+}AgH_2NC_2H_4NH_3^{+}$. That such an ion exists in solution was shown by Schwarzenbach.[3] He also found strong evidence for a dimer, $Ag_2(en)_2^{++}$ (en = ethylenediamine), and suggested to us that this dimer might be formed in the resin.

That the formation of $Ag(enH)^{++}$ could not alone account for the complexing in the resin was easily shown by loading the resin with silver ions to more than half its exchange capacity. The Ag^{+}:en coördination was still in the ratio 1:1.

This paper describes a detailed study of the coördination of ethylenediamine with silver ions in cation-exchange resins. The variables studied included crosslinking of the resin and the degree of sulfonation of the resin. Tests also were made with 1,3-propanediamine (pn) as the ligand. As it seemed very likely that these diamines were acting as crosslinking ligands to bind two or more silver ions together, the coördination of hydrazine also was studied in a preliminary way. Since hydrazine reduces silver ions, these tests were made with nickel ions.

Experimental

Materials.—The resins were all of the sulfonated polystyrene type, Dowex 50-W, kindly supplied by the Dow Chemical Co., Midland, Michigan. They were of "white" grade, pale yellow in color, and very uniform in crosslinking and sulfonation, as shown by the flotation method.[4] The particle size was 100–200 mesh. Three degrees of crosslinking were used: 2, 4 and 8% nominal divinylbenzene. The capacities on a dry basis were, respectively, 5.245, 5.176 and 5.153 meq./g. (H-form). In addition, two "special capacity" resins were used; these were made from crosslinked polystyrene by partial sulfonation and were kindly provided by Robert M. Wheaton. These had 2% crosslinking and exchange capacities of 1.629 and 2.322 meq./g. dry H-resin; they were designated A and B, respectively. All resins were washed and air-dried before use. **Ethylenediamine** and **1,3-propanediamine** were Eastman White Label grades redistilled from barium hydroxide. The ethylenediamine boiled at 114° (628 mm.) (corr.), 1,3-propanediamine at 131° (623 mm.). **Hydrazine** was obtained as 85% hydrazine hydrate from Arapahoe Chemicals, Inc. and diluted for use without further purification. **Nickel fluoborate**, used in the experiments with hydrazine, was made from Baker and Adamson

(1) Part II, *J. Phys. Chem.*, **66**, 750 (1962).

(2) R. H. Stokes and H. F. Walton, *J. Am. Chem. Soc.*, **76**, 3327 (1954).

(3) G. Schwarzenbach, H. Ackermann, B. Maissen and G. Anderegg. *Helv. Chim. Acta*. **35**, 2237 (1952).

(4) M. G. Suryaraman and H. F. Walton, *Science*, **131**, 829 (1960).

fluoboric acid (48% solution) and basic nickel carbonate; its solutions had *p*H 5.5.

Equilibration.—Weighed portions of air-dried resin, H-form, of known moisture content were placed in flasks with measured amounts of nitric acid, silver nitrate and amine (in the hydrazine experiments, fluoboric acid, nickel fluoborate and amine). Water was added to give a convenient volume. Usually 4 meq. of resin was used with 50 ml. of solution of total normality 0.1. The flasks then were shaken or stirred at 25 ± 1° (in one series of tests, 50 ± 1°) for at least 8 hr., preferably 24 hr. The solution then was withdrawn and its *p*H immediately determined using a Beckman Model G *p*H meter and a reference electrode with saturated potassium nitrate solution as the salt bridge. The total base was determined by potentiometric titration to the inflection at *p*H 4.5–5. Silver was determined by potentiometric titration with chloride after acidification; nickel by titration with EDTA using murexide indicator.

To interpret the data with ethylenediamine and 1,3-propanediamine one must know the distribution of singly and doubly charged cations between the solution and the resin. This was measured for each resin by shaking weighed amounts of air-dried hydrogen-form resin with nitric acid solution and enough diamine to give a mixture of the two ions, enH^+ and enH_2^{++}. Four to six different proportions of amine were used in every case. After equilibration the enH^+ in the solution was found by titration with standard acid, and the enH_2^{++} by difference, with checks made by titration with standard base to the poor inflection at *p*H 8.5. The total amine in the resin was found by difference, and its ionic composition calculated from this value and the known ionic capacity of the resin.

Water Uptake.—The amount of water taken up by the resins on swelling was determined for the different cationic forms by a modification of the "blotting" method of Bonner, *et al.*[5] About 0.5–1 g. of moist resin was placed in a small weighing bottle and blotted dry with strips of close-textured filter paper. As each strip was withdrawn, any adhering resin was scraped back into the bottle with a metal microspatula. Blotting was continued until a strip became only barely wet at the edges or corners after thorough "working" in the resin. The bottle then was stoppered and weighed. Then about 0.1 ml. of water was added and the blotting and weighing repeated. The weighed, blotted resin then was analyzed for metal ion and base contents and total exchange capacity. This rather crude technique gave results reproducible within 0.01 g. H_2O/meq. resin, and seems to us the best way of determining water uptake, short of elaborate isopiestic vapor pressure measurements.

For the silver–ethylenediamine and nickel–hydrazine complexes the resins were wetted with 0.1 *M* amine solution instead of water.

Results and Discussion

The **ionization constants** used in the calculations all were determined by titration under as nearly as possible the same ionic strength as that used in the test solutions, although, as explained in the previous paper,[1] it is impossible to keep the ionic strength constant in all the experiments. The *pK'* values used were (see also ref. 1)

enH_2^{++}, $pK_1' = 7.22$, $pK_2' = 10.03$; pnH_2^{++}, $pK_1' = 8.88$, $pK_2' = 10.64$; $N_2H_5^+$, $K_a' = 8.12$

Ion Exchange of Diamine Cations.—Values of *K*, the equilibrium quotient for the reaction

$$enH_2^{++}\ (\text{solution}) + 2enH^+R^- \rightleftharpoons 2enH^+\ (\text{solution}) + enH_2^{++}R_2^-$$

are given in Table I. The units are equivalents of resin/liter of solution. The probable error is ±0.05 to 0.1 in log *K*, which is not very good, but more than adequate for the purpose, as will be seen from Table II.

Silver and Ethylenediamine.—Table II gives some typical data obtained in the equilibrations as

(5) O. D. Bonner, W. J. Argersinger and A. W. Davidson, *J. Am. Chem. Soc.* **74**, 1044 (1952).

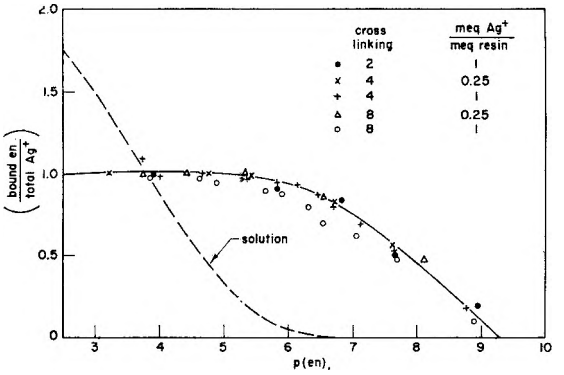

Fig. 1.—Silver–ethylenediamine complexes in Dowex-50 resins. The ratio Ag:resin indicated is the ratio of *total* silver to resin. The amount of silver in the resin varied greatly; typical data are shown in Table I for 1 meq. Ag: 1 meq. resin.

TABLE I

DISTRIBUTION QUOTIENTS FOR enH^+–enH_2^{++} AND pnH^+–pnH_2^{++} EXCHANGES[a] AT 25°

Amine	Resin crosslinking	log *K* at *N* = 0.7	log *K* at *N* = 0.9
en	2%	1.1	1.0
	4%	1.4	1.2
	8%	..	1.6
	2%—sp. cap. A	1.2	0.95
	2%—sp. cap. B	0.9	0.8
pn	2%	..	1.65

[a] en = ethylenediamine pn = 1,3-propanediamine; *N* = equivalent fraction of doubly charged ion in the resin.

an indication of the relative magnitudes of the concentrations involved. This table also shows the very marked shift of metal ions from the solution into the resin which occurs as more amine is added, and which qualitatively is to be expected from the greater stability of the complex in the resin.

Figure 1 shows the data of Table II along with all the other data obtained with the commercial Dowex resins. The values of "meq. Ag^+/meq. resin" are the quantities originally added; only a part of the added silver entered the resin, but this portion increased with the amount of added amine. The "solution" curve was drawn from Schwarzenbach's values[3] for the formation constants of $Ag(en)^+$ and $Ag(en)_2^+$. This was done for two reasons; first, the amount of bound amine in solution in our experiments usually was too low to evaluate accurately, and the concentration of dissolved silver ions often was very low too; second, silver and ethylenediamine form several different complex species in solution,[3] and the dashed curve of Fig. 1 focuses attention on only two of these. Analysis of our solutions gave values of $\bar{n}$, the ratio of bound amine to total silver, lying roughly along the lower part of this dashed curve.

From Fig. 1 it is clear that the complex is over a thousand times as stable in the resin as it is in the solution for low values of $\bar{n}$, and that the association in the resin reaches a limiting value of $\bar{n} = 1$. (There is some evidence that $\bar{n}$ in the resin rises above 1 for ethylenediamine concentrations of 0.1 *M* and above.) The formation curve is independent of the crosslinking and of the equivalent fraction of silver in the resin, except that with 8%

TABLE II

BINDING OF ETHYLENEDIAMINE BY SILVER IONS IN DOWEX 50W × 4[a]

Solution composition						Resin composition				
pH	Meq. titratable base	enH$^+$	enH$_2^{++}$	Ag$^+$	p(en)	enH$^+$	enH$_2^{++}$	Bound en	Ag$^+$	$\bar{n}$
5.09	0.092	0.007	1.001	2.931	8.77	...	1.710	0.194	1.093	0.18
5.63	.357	.030	1.148	2.613	7.63	...	1.412	0.751	1.411	.53
5.86	.557	.054	1.246	2.392	7.13	...	1.273	1.127	1.632	.69
6.06	.874	.093	1.347	2.152	6.70	...	1.097	1.491	1.872	.80
6.16	1.048	.131	1.499	1.987	6.45	...	1.116	1.694	2.037	.83
6.31	1.458	.204	1.567	1.777	6.11	...	1.006	1.995	2.247	.89
6.70	2.211	.496	1.643	1.334	5.33	0.014	0.854	2.535	2.690	.94
7.46	3.729	1.865	1.072	1.107	4.00	0.047	0.623	2.871	2.917	.99

[a] All quantities in millimoles except where stated. Solution volume = 50 ml. 4.024 mmole $AgNO_3$ and close to 4 meq. of resin were used in every case.

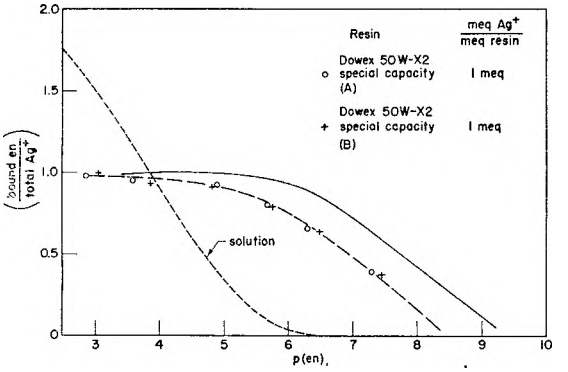

Fig. 2.—Silver–ethylenediamine complexes in special-capacity, partially sulfonated Dowex-50 resins. Resin A, capacity 1.63 meq./g. dry H-resin; resin B, capacity 2.32 meq./g.

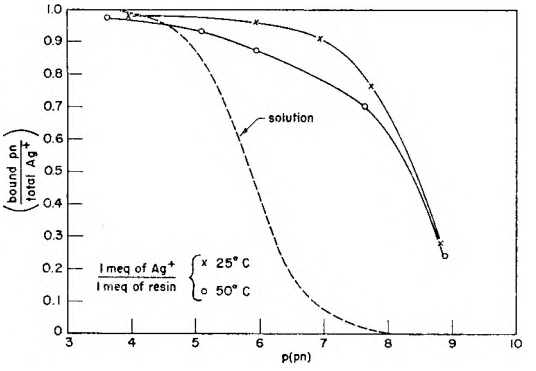

Fig. 3.—Silver–1,3-propanediamine complexes in Dowex-50 resin, 2% crosslinking.

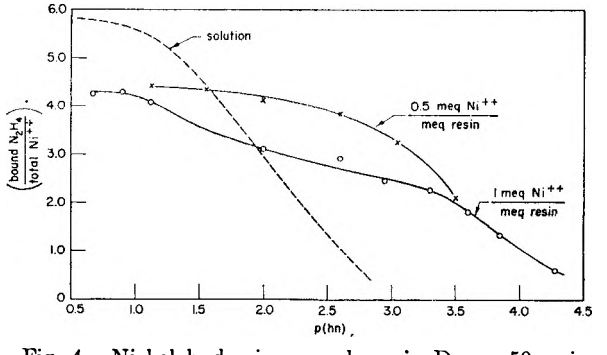

Fig. 4.—Nickel–hydrazine complexes in Dowex-50 resin, 2% crosslinking. The Ni:resin ratios are ratios of *total* nickel to resin; some 80–90% of the nickel was in the resin, the amount increasing with decreasing p(hn).

crosslinking, high silver loading, and $\bar{n}$ above 0.5, a definite drop in stability was observed. This could be due to a steric effect.

As was mentioned in the Introduction, the limiting $\bar{n}$ of unity must be explained by a complex $(Ag\ en^+)_x$, not $(Ag\ enH)^{++}$, for the 1:1 ratio of bound amine to silver is maintained even when the exchange sites of the resin are saturated with silver ions. It is possible that a dimer $(Ag_2en_2)^{++}$ is formed in the resin as it is in solution,[5] but the ring structure attributed to this dimer seems improbable in the restricted solution volume inside the resin. A more likely possibility is a linear polymer

$$(Ag^+ \longleftarrow H_2NCH_2CH_2NH_2 \longrightarrow Ag^+ \longleftarrow H_2NCH_2CH_2NH_2)_x$$

The stability of such a polymer would increase, the more closely the silver ions could be brought together. Increasing the crosslinking of the resin would be expected to stabilize the polymer, yet it does not. A possible explanation for this fact is that the polymer lies *along* the polystyrene chains of the resin, rather than bridging them. The maximum distance between the sulfonate ions of adjacent benzene rings in the polystyrene chain is about 15 Å., the minimum (*cis*-configuration) is 2.8 Å. The Ag–Ag distance in the postulated polymer is an intermediate value, 8.5 Å. One thus may picture the polymer entwined like a vine around the randomly oriented polystyrene chains.

Evidence that the Ag–en complex restricts the swelling of the resin in water is given in Table III. The water uptake on swelling is distinctly less for the complex in the resin than for silver ions in the resin. Perhaps the postulated linear polymer restricts the thermal motion of the polystyrene chains and thereby restricts the volume they occupy. Even with the Ag–en complex present the 2% resin has more than twice as much water as the 8% resin in the swollen state, so it does not appear that the postulated polymer bridges or crosslinks the resin chains to any great extent.

If a linear polymer is formed which lies along the polystyrene chains, its stability should be affected by changing the spacing of the sulfonic acid groups along the chains. The experiments with "special capacity" resins, having less than half the normal degree of sulfonation, showed that this was the case. Figure 2 shows that the complex formed

in these resins is only one-sixth as stable as that in the fully sulfonated resins (for $\bar{n} = 0.5$).

If a polymer of any kind is formed one would expect its stability to depend on the concentration of silver ions in the resin, yet this is not the case, except as noted with the 8% crosslinked resin. A possible explanation is that the silver ions tend to cluster together along the resin chains rather than to be dispersed randomly; this also would help to explain the anomalous increase in affinity for silver ions found with increasing proportion of silver ions in the silver–hydrogen cation-exchange equilibrium.[5]

Another peculiar feature of Figs. 1 and 2 is the slope of the formation curve for $\bar{n} < 1$. The theoretical maximum slope of $\bar{n}$ against log (ligand concn.) for a 1:1 complex is 2.303/4 = 0.82. The slope of these formation curves is about 0.3, considerably less than that expected for a 1:1 complex. This slope could be explained if a complex $Ag(enH)^+$ predominated in the resin in this range, and so could the lack of dependence on the silver ion concentration. One would, however, no longer have an explanation of the extraordinary stability of the complex in the resin, unless it were the rather tenuous explanation offered in our previous paper.[3]

Silver and 1,3-Propanediamine.—The formation curve for this complex in the resin is shown in Fig. 3, which also shows the formation curve for the complex in solution as determined by Schwarzenbach.[6] He reported that only the 1:1 complexes, $Ag(pn)^+$ and $Ag(Hpn)^{++}$, existed (except at high silver ion concentrations), and of these the first was much the more stable.

Again the same relationships are found, with somewhat less stabilization in the resin than with the silver–ethylenediamine complex, namely, a factor of $10^{2.5}$ at $\bar{n} = 0.5$, contrasted to the factor $10^{3.2}$ for ethylenediamine. The slope at $\bar{n} = 0.5$ seems to be greater than with ethylenediamine, which may be significant.

Nickel and Hydrazine.—If the idea of a metal ion–diamine polymerization is correct, we should find that other "crosslinking ligands"[7] form more stable metal complexes in an ion-exchange resin than in solution. Such a "crosslinking ligand" is hydrazine. Nickel and zinc salts are known to form insoluble compounds with hydrazine, apparently of a polymeric nature, which precipitate from aqueous solutions.[8] We therefore made preliminary measurements of the stability of the nickel–hydrazine complex in 2% crosslinked Dowex-50 resin, using solutions of nickel fluoborate, since fluoborate is one of the few anions that does not form a precipitate.

The results are shown in Fig. 4. Again the dashed line represents Schwarzenbach's formation curve for the solution.[8] The association is stronger in the resin than in the solution, except for high $\bar{n}$ and high loading of the resin. (With 1 meq. of Ni^{++} added per meq. of resin, virtually all the nickel went into the resin.) Increasing the proportion of amine displaced nickel ions into the resin from the solution. There are indications that an association of $3N_2H_4$:1 Ni^{++} is preferred in the resin, by contrast with the 6:1 coördination in fluoborate solutions, and this is consistent with the idea of a three-dimensional network of nickel ions crosslinked with hydrazine molecules. The extremely small water uptake of the resin loaded with nickel and hydrazine (Table III) certainly suggests a crosslinked network.

TABLE III

WATER UPTAKE BY DOWEX-50 RESINS[a]

Resin cation	Water uptake, mg. H_2O/meq. resin, for crosslinking 2%	4%	8%
H_3O^+	1020	500	280
Ag^+	470	270	170
$Agen^+$	290	160	140
enH_2^{++}	..	200	140
Ni^{++}	460	..	..
$Nihn_4^{++}$	100	..	..

[a] For the special capacity resins in H_3O^+-form, the uptakes were: resin A, 580 mg./meq.; resin B, 720 mg./meq.

Conclusions

Evidence is presented that ethylenediamine, 1,3-propanediamine and hydrazine form polymeric association complexes with metal ions in cation-exchange resins. The data for silver and ethylenediamine suggest that linear polymers are formed, but the slope of the formation curve for low amine:silver ratios is hard to explain on this view.

Acknowledgment.—One of us (M. G. S.) acknowledges the tenure of a Dow Chemical Company research fellowship 1959–1960.

The work was supported by the U. S. Atomic Energy Commission, Contract AT-(11-1)-499. Part of it was presented at the 138th National Meeting of the American Chemical Society, New York, 1960.

(6) G. Schwarzenbach, B. Maissen and H. Ackermann, *Helv. Chim. Acta*, **35**, 2333 (1952).

(7) G. Schwarzenbach, *Angew. Chem.*, **70**, 451 (1958).

(8) G. Schwarzenbach and A. Zobrist, *Helv. Chim. Acta*, **35**, 1291 (1952).

THE HEAT CAPACITY OF POTASSIUM HEXACHLORORHENATE(IV) FROM 7 TO 320°K. ANOMALIES NEAR 12, 76, 103, AND 111°K. ENTROPY AND FREE ENERGY FUNCTIONS. SOLUBILITY AND HEAT OF SOLUTION OF K_2ReCl_6. ENTROPY OF THE HEXACHLORORHENATE ION[1]

BY R. H. BUSEY, H. H. DEARMAN AND R. B. BEVAN, JR.

Chemistry Division, Oak Ridge National Laboratory, Oak Ridge, Tennessee

Received July 17, 1961

Low temperature heat capacity data on K_2ReCl_6 are presented and the thermodynamic functions are tabulated. Of the four coöperative transitions exhibited by this compound with heat capacity maxima at 11.9, 76.05, 103.4 and 110.9°K., only the one at the lowest temperature is the result of a magnetic transition. It is estimated that an entropy of approximately R ln 2 is associated with each of the three remaining transitions. The solubility of K_2ReCl_6 in 0.01 M HCl is 0.1689 m at 25° and 0.0841 m at 0°. The standard heat of solution is 10,397 cal. mole^{-1} at 25°. The thermodynamic functions at 298.15°K (cal. deg.$^{-1}$ mole^{-1}) are: $C_p^0 = 51.31$, $S^0 = 88.84 \pm 0.18$, $(H^0 - H_0^0)/T = 37.970$ and $-(F^0 - H_0^0)/T = 50.873$. The entropy and entropy of formation at 298.15°K. of the hexachlorohenate ion are: $S^0(ReCl_6^-(aq.)) = 59.8$ cal. deg.$^{-1}$ mole^{-1} and $\Delta S_f^0(ReCl_6^-(aq.)) = -140.2$ cal. deg.$^{-1}$ mole^{-1}.

Introduction

The low temperature heat capacity of potassium hexachlororhenate(IV), K_2ReCl_6, reported here was measured to provide values of the entropy and free energy functions in connection with the study of the chemistry of technetium and rhenium being carried out at this Laboratory.[2,3] Two additional motives may be cited. There is a dearth of low temperature heat capacity data on compounds of the second and third transition series. An increased interest[4-6] in the chemical and physical properties of compounds of these two series has been brought about by the application of ligand field theory and molecular orbital theory to the spectral, magnetic and thermochemical properties of these compounds.

The magnetic susceptibility of K_2ReCl_6 follows the Curie–Weiss law, $\chi'_M = C/(T + \theta)$, from 80 to 400°K., with $\theta = 57°$ and a Curie constant C corresponding to three unpaired electrons in the 5d shell of Re^{+4} with their orbital angular momentum quenched by the crystalline octahedral field of Cl^- surrounding the Re^{+4} but their spins free to be oriented by an external magnetic field. The heat capacity data presented in this paper in conjunction with the magnetic susceptibility data[7] clearly demonstrate that the heat capacity anomaly observed with a maximum at 11.9°K. described below arises from a transition from a paramagnetic state to an ordered antiferromagnetic state below 11.9°K. The unusual and unexpected characteristic of the heat capacity of this compound is, however, that in addition to this antiferromagnetic transition at 11.9°K. three other coöperative transitions appear with heat capacity maxima at 76.05, 103.4 and 110.9°K.

The only other low temperature heat capacity data available on a paramagnetic compound of the second or third transition series are those of Bailey and Smith[8] on $(NH_4)_2IrCl_6$, K_2IrCl_6 and $Na_2IrCl_6 \cdot H_2O$.

Experimental

Potassium Hexachlororhenate Samples.—The measurements were made on two differently prepared samples of K_2ReCl_6. This was done to reduce the probability that the "extra" anomalies might be due to an undetected impurity (for example, an hydrolysis product $K_2Re(OH)Cl_5$) in the samples. It is unlikely that the K_2ReCl_6 samples prepared by different procedures would contain the same concentrations of impurities. Sample I was prepared[9] by KI reduction of $KReO_4$ according to the procedure given in "Inorganic Synthesis."[10] Sample II was prepared by hypophosphorous acid reduction of $KReO_4$ according to the procedure given by Rulfs and Meyer.[11] Both preparations were dried in an evacuated dessicator charged with P_2O_5. The chlorine and rhenium contents determined gravimetrically[12] were, respectively, as follows: sample I, 44.53 and 39.04%; sample II, 44.55 and 39.24%; theoretical values 44.58 and 39.03%. The chloride analyses should be accurate to 0.1% but the rhenium analyses probably are accurate to only 0.3%. A gravimetric silica analysis on sample I gave 0.10% SiO_2. A spectroscopic analysis of the samples indicated that both samples had the same silicon content. If the chloride analyses are corrected for the silica content of the samples the results become 44.57 and 44.59% for samples I and II, respectively, which compare very favorably with the theoretical value. Both samples when dissolved in dilute hydrochloric acid gave clear solutions with no residue. A third sample, III, used for measurements below 15°K., was a sample recrystallized from a 6 M hydrochloric acid solution of K_2ReCl_6 prepared by combining samples I and II. No analysis of sample III was made.

The weight (*in vacuo*[13]) of sample I introduced into the calorimeter was 86.915 g., of sample II, 89.767 g., and of

(1) This paper is based upon work performed for the United States Atomic Energy Commission at the Oak Ridge National Laboratory operated by Union Carbide Corporation.

(2) R. H. Busey, *J. Am. Chem. Soc.*, **78**, 3263 (1956).

(3) J. W. Cobble, G. D. Oliver and W. T. Smith, Jr., *ibid.*, **75**, 5786 (1953), and preceding papers of this series.

(4) Papers presented at the Xth Solvay Council at Brussels, published in "Quelques Problemes de Chimie Minérale," R. Stoops, editor; Codenberg, Bruxelles, 1956.

(5) International Conference on Coördination Chemistry, Rome, 1957. Papers published in "Chemistry of the Co-ordination Compounds," Pergamon Press, New York, N. Y., 1958.

(6) Symposia on "Ligand Field Theory" and "Magnetic Phenomena in Inorganic Chemistry," sponsored by the Division of Inorganic Chemistry of the American Chemical Society, Chicago, Illinois, September, 1961.

(7) R. H. Busey and E. Sonder, *J. Chem. Phys.*, **35**, in press (1962); this paper lists references to magnetic susceptibility measurements made on K_2ReCl_6 by other investigators.

(8) C. A. Bailey and P. L. Smith, *Phys. Rev.*, **114**, 1010 (1959).

(9) By D. E. LaValle of the Analytical Chemistry Division of Oak Ridge National Laboratory.

(10) L. C. Hurd and V. A. Reinders, "Inorganic Synthesis," H. S. Booth (ed.), Vol. 1, McGraw-Hill Book Co., New York, N. Y., 1939, pp. 178–180.

(11) C. L. Rulfs and R. J. Meyer, *J. Am. Chem. Soc.*, **77**, 4505 (1955).

(12) Re as $(C_6H_5)_4AsReO_4$: H. H. Willard and G. M. Smith, *Ind. Eng. Chem., Anal. Ed.*, **11**, 305 (1939); modified by W. T. Smith, Jr., and S. H. Long, *J. Am. Chem. Soc.*, **70**, 354 (1948).

(13) The density of K_2ReCl_6 was determined to be 3.303 g./ml. at 25°.

sample III, 84.699 g. This represents 0.18215, 0.18813 and 0.17751 mole, respectively, based upon 477.16 as the molecular weight.[14] In each case one atmosphere pressure of helium was added to aid rapid thermal equilibrium.

Apparatus and Temperature Scale.—The copper calorimeter and cryostat used for measurements on samples I and II for the temperature range 15 to 320°K. have been described previously.[15,16] Calibration of the gold resistance thermometer–heater was carried out concurrently with the heat capacity measurements by means of a standard copper–constantan thermocouple. The measurements using samples I and II immediately followed those made on Re_2O_7,[15] in which article results of a calibration check on the standard thermocouple are given.

The measurements below 15°K. utilizing sample III were made in an adiabatic calorimeter employing liquid helium as refrigerant for the low temperature range. The calorimeter is similar to that of Westrum, Hatcher and Osborne.[17] A description of this calorimeter will be made in a subsequent paper on the heat capacity of K_2ReBr_6.[18]

Solubility Determination.—The solubility of K_2ReCl_6 (Table III) in 0.0100 and 0.0050 *M* HCl at 25.00 ± .01°, and in .0100 *M* HCl at 0°, was measured by equilibration of the salt with the solution contained in a 200-ml. loosely stoppered flask submerged in a 25.00 ± 0.01° water-bath or ice-bath. The solution was agitated with a magnetic stirrer. A sample of the clear solution for analysis was withdrawn with a slightly warmed pipet, transferred to a weighing bottle and the solution weighed. The weight of the salt in the aliquot was determined by dilution with 0.0100 *M* HCl to a known volume and the concentration of the resulting solution measured spectrophotometrically with a Model 14 Cary spectrophotometer. The concentration was computed by averaging the concentrations calculated from the absorbancy observed at each of the following wave lengths (in Å.) using the molar absorbancy indices given in parentheses: 6500 (2.98), 6990 (2.37), 7060 (4.14), 7135 (3.55) and 7200 (2.34). Equilibration time was varied from 20 to 100 hr. Equilibrium was approached from below saturation in runs 1, 2, 4 and 7; for the remainder the approach to equilibrium was from supersaturation.

Heat of Solution Measurements.—The heat of solution of K_2ReCl_6 was measured in a solution calorimeter similar to that described by Kunzler and Giauque.[19] A 100 ohm combination thermometer–heater of S.W.G. No. 40 double-silk covered enameled copper wire is encased between two concentric platinum cylinders welded together at each end and provided with a 3 mm. o.d. platinum tube for leads and support of the thermometer–heater in the calorimeter. This thermometer–heater encasement, 2.75 cm. in diameter and 7.0 cm. in length, serves as a stirring tube. A Leeds and Northrup type G-2 Mueller bridge is employed for resistance measurements when the thermometer–heater is used as a temperature sensing element. For electrical energy input a White 100,000 microvolt double potentiometer is used with appropriate standard resistors and timing device described previously.[15,16] The calorimeter vessel is a 500-ml. silvered Dewar, which was specially constructed without spacers to reduce heat leak. The calorimeter is operated within a water-bath thermostated to 25.2° and constant to ± 0.001°. A heat of solution run was started at a temperature sufficiently above 25° such that the final temperature resulting from the endothermic reaction was below 25° and gave an average temperature very close to 25°. All solution and electrical calibration runs were performed with the calorimeter temperature below that of the bath to prevent evaporation of water to the top of the calorimeter and its subsequent erratic return to the calorimeter solution. The calorimeter was cooled for ensuing electrical calibration by complete removal by evacuation of a small amount of water (1 to 2 ml.) introduced into a small, thin walled, glass bulb immersed in the calorimeter solution. The calorimeter was allowed to equilibrate for at least an hour after cooling before measurements were made to ensure no detrimental thermal effects resulting from distillation of water from the tube leading to the cooling bulb back to the calorimeter solution. Visual examination of this tube following a cooling and equilibration for an hour showed no water on the tube above the solution.

The calorimeter has a calculated temperature sensitivity of 0.00003° and an observed, reproducible sensitivity of 0.0001°, or is capable of detecting ±0.1 cal. The calorimeter was checked for performance by measuring the heat of solution of KCl to give a final molality of 0.1030. The heat observed, 4198 ± 4 cal. mole^{-1}, is in fortuitously perfect agreement with 4198 cal. mole^{-1} listed in NBS Circular 500[20] for the heat of solution of KCl to form a solution of this molality.

TABLE I

HEAT CAPACITY OF K_2ReCl_6

Sample I—$T_{av.}$, °K.; C_p (cal. deg.$^{-1}$ mole^{-1})

Series 1	292.97	51.08	300.88	51.31	Series 2	15.16	4.874	16.74	5.848
18.96	6.926	21.96	8.590	25.36	10.41	28.76	12.21	31.59	13.74
34.55	15.20	38.16	17.05	41.63	18.81	45.29	20.52	49.61	22.49
54.30	24.40	59.18	26.27	64.33	28.16	69.78	30.03	80.46	33.13
86.08	34.61	91.90	36.20	97.92	37.85	119.17	40.23	126.32	41.12
133.51	42.07	140.47	42.90	147.85	43.57	155.49	44.29	163.21	44.99
171.06	45.66	178.88	46.23	186.90	46.93	195.14	47.27	203.50	47.78
211.94	48.20	220.52	48.60	229.22	49.06	238.06	49.35	246.93	49.67
255.94	49.99	265.09	50.26	274.41	50.63	283.21	50.88	292.81	51.13
301.93	51.43	311.29	51.68	320.77	51.93	Series 3	69.35	29.89	83.18
33.83	87.46	35.03	91.49	36.08	95.00	37.00	97.56	37.71	99.61
38.37	101.59	39.28	102.47	39.75	103.09	40.35	103.40	40.54	103.61
40.50	103.88	40.34	104.24	39.93	104.66	39.86	105.25	39.49	106.03
39.49	107.02	39.65	108.26	39.98	109.62	40.48	110.63	41.08	110.82
41.29	111.02	41.03	111.21	40.90	111.48	40.73	111.78	40.47	112.14
40.12	112.67	40.05	113.52	39.94	114.82	39.97	116.73	40.00	119.53
40.24	Series 4	63.99	28.12	66.03	28.75	68.10	29.43	69.93	30.08
71.55	30.65	72.97	31.18	73.98	31.59	74.60	32.09	75.08	32.50
75.56	33.11	76.02	33.84	76.42	33.02	76.95	32.49	77.42	32.44
77.88	32.49	78.40	32.62	79.11	32.71	80.18	33.03	81.90	33.49
84.53	34.20	Series 5	86.58	34.77	90.13	35.73	93.68	36.67	97.02
37.54	100.02	38.54	102.27	38.69	103.57	40.40	104.21	40.09	104.70
39.70	105.50	39.48	106.71	38.58	108.42	39.95	109.88	40.67	110.61
41.08	111.01	41.20	111.47	40.59	112.00	40.32	112.52	40.09	113.04
40.00	113.70	39.90	114.96	39.91	117.50	40.08	Series 6	108.85	39.97
109.26	40.08	109.66	40.40	110.03	40.63	110.37	40.99	110.70	41.12
111.02	40.99	111.39	40.70	111.84	40.43	112.50	40.07	Series 7	101.77
39.19	102.22	39.47	102.66	39.82	103.06	39.92	103.38	39.96	103.64
39.77	103.85	39.73	104.07	39.79	104.30	39.69	104.61	39.53	105.07
39.50	105.92	39.40	74.34	31.62	74.89	31.85	75.34	32.16	75.76	32.63
76.14	32.75	76.49	32.42	76.84	32.39	77.22	32.36	77.66	32.36	78.23
32.47	79.24	32.76	Series 9	71.01	30.45	72.96	31.15	74.58	31.98	75.65
33.17	76.11	34.00	76.31	33.26	76.49	32.99	76.66	32.79	76.83	32.64
77.04	32.52	77.27	32.46	77.56	32.43	78.18	32.58	79.73	32.90	Series 10
98.21	37.85	99.14	38.14	100.13	38.50	101.11	38.99	101.92	39.47	102.50	40.02	102.86	40.11	103.14	40.27	103.39	40.38	103.61	40.51
103.82	40.32	104.05	40.07	104.31	40.04	104.66	39.74	105.16	39.56	105.86	39.56	106.97	39.62						

Sample II—Series 11 | 85.69 | 34.58 | 93.77 | 36.72 | 123.41 | 40.79 | Series 12 | 65.10 | 28.45 | 67.86 | 29.40 | 70.41 | 30.29 | 72.61 | 31.11 | 74.23 | 31.77 | 75.34 | 32.74 | 76.19 | 33.42 | 77.04 | 32.38 | 77.89 | 32.45 | 78.92 | 32.73 | 80.53 | 33.17 | 83.63 | 34.02 | 88.49 | 35.40 | 94.36 | 36.96 | 98.80 | 38.08 | 101.01 | 38.89 | 102.33 | 39.63 | 102.92 | 40.16 | 103.32 | 40.00 | 103.71 | 39.89 | 104.10 | 39.59 | 104.49 | 39.45 | 104.88 | 39.34 | 105.27 | 39.25 | 105.79 | 39.33 | 106.75 | 39.51 | 108.01 | 39.81 | 109.25 | 40.22 | 110.16 | 40.63 | 110.76 | 41.00 | 111.36 | 40.40 | 111.96 | 39.98 | 112.56 | 39.80 | 113.15 | 39.67 | 113.92 | 39.75 | Series 13 | 96.51 | 37.38 | 99.11 | 38.15 | 101.29 | 38.94 | 102.47 | 39.56 | 102.99 | 40.00 | 103.52 | 39.89 | 104.03 | 39.58 | 104.55 | 39.34 | 105.07 | 39.24 | 105.59 | 39.22 | 106.35 | 39.36 | 107.57 | 39.64 | 108.72 | 39.92 | 109.72 | 40.38 | 110.42 | 40.81 | 110.83 | 41.15 | 111.24 | 40.49 | 111.72 | 40.12 | 112.19 | 39.93 | 112.67 | 39.74 | 113.14 | 39.78 | 113.61 | 39.71 | 114.89 | 39.78 | 117.46 | 40.03 | 121.16 | 40.46 | Series 14 | 182.02 | 46.64 | 190.27 | 47.10 | 198.06 | 47.54 | 206.23 | 48.03 | 214.29 | 48.38 | 220.72 | 48.67 | 228.45 | 49.03 | 236.29 | 49.34 | 243.90 | 49.65 | 251.74 | 49.92 | 259.78 | 50.20 | 267.54 | 50.42 | 275.47 | 50.69 | 283.52 | 50.93 | 291.68 | 51.14 | 299.98 | 51.41 |

Sample III—Series 15 | 7.96 | 1.959 | 9.54 | 3.292 | 10.76 | 5.026 | 12.06 | 6.458 | 13.98 | 4.492 | 16.24 | 5.623 | 18.09 | 6.509 | Series 16 | 7.09 | 1.414 | 8.30 | 2.122 | 9.19 | 2.677 | 10.14 | 3.901 | 11.10 | 5.373 | 11.75 | 8.545 | 12.19 | 6.494 | 12.62 | 3.988 | 13.31 | 4.277 | 14.25 | 4.554 | 15.27 | 5.065 | 16.32 | 5.576 | 17.50 | 6.188 |.

(14) "1956–1957 International Atomic Weights," E. Wichers, *J. Am. Chem. Soc.*, **80**, 4121 (1958).

(15) R. H. Busey, *ibid.*, **78**, 3263 (1956).

(16) R. H. Busey, ORNL-1828, an unclassified A.E.C. document readily available through the Office of Technical Services, Department of Commerce, Washington 25, D. C.

(17) E. F. Westrum, Jr., J. B. Hatcher and D. W. Osborne, *J. Chem. Phys.*, **21**, 419 (1953).

(18) R. H. Busey, R. B. Bevan, Jr., and R. A. Gilbert, to be published.

(19) J. E. Kunzler and W. F. Giauque, *J. Am. Chem. Soc.*, **74**, 3472 (1952).

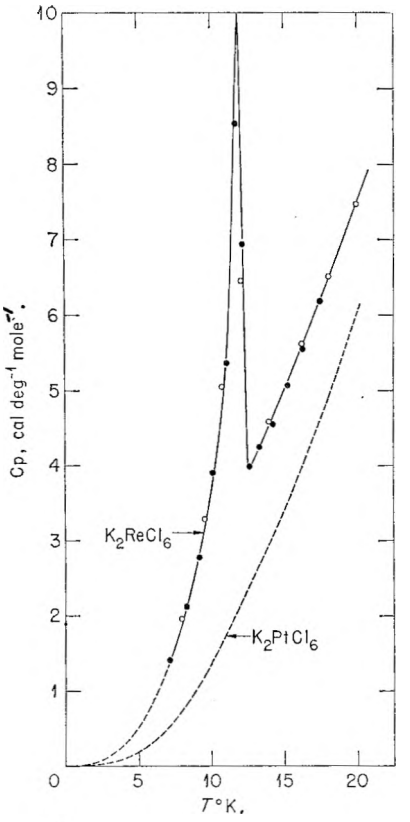

Fig. 1.—Coöperative transition of K_2ReCl_6 with heat capacity maximum at 11.9°K. The transition is from an antiferromagnetic, ordered state below 11.9°K. to the paramagnetic state above this temperature. Open circles are series 15, filled circles Series 16.

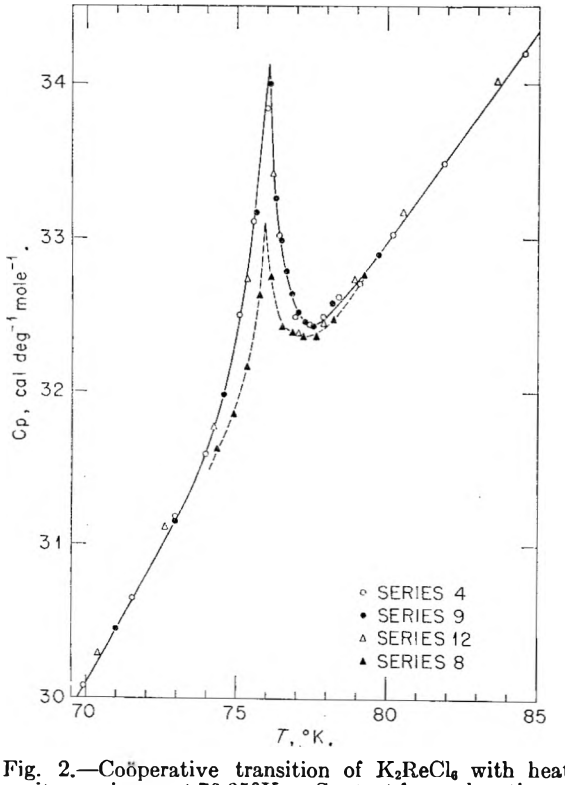

Fig. 2.—Coöperative transition of K_2ReCl_6 with heat capacity maximum at 76.05°K. See text for explanation of series.

Results

Heat Capacity Data.—The heat capacity observations determined by the adiabatic method are given in Tables I and II. The results on samples I and II as given have been corrected for the silica content,[21] assuming it is present in the samples as SiO_2. This correction amounts to −0.06% at 300°, −0.02% at 200°, + 0.02% at 100° and +0.05% at 50°K. Temperature increments of the individual measurements can be inferred from the adjacent mean temperatures. No correction for curvature has been made. The measurements were made in the order of the series given; the measurements in a particular series were continuous in that the calorimeter never cooled overnight by more than one or two degrees. In those series of measurements in which an anomaly in the heat capacity appeared, no interruption in the measurements occurred. The results are expressed in terms of the defined thermochemical calorie equal to 4.1840 absolute joules. The ice point was taken as 273.15°K.

Table II

Total Heat Content through Anomalous Regions

Series	T_1	T_2	ΔH (meas.) (cal./mole)	$\int C_p\,dT$ (cal./mole)	Δ	%
2	72.608	78.471	189.67 (1)	189.48	0.19	0.10
3	71.944	81.065	295.34 (2)	295.44	− .10	− .03
2	101.086	115.714	585.12 (2)	585.44	− .32	− .05
11	69.470	80.713	358.46 (2)	358.83	− .37	− .10
11	96.944	119.471	891.13 (3)	894.03	−2.90	− .32

The measurements given in series 1 were made before the sample was cooled and served to check for any irreversible change that might have occurred upon cooling the sample to low temperatures. Series 2 measurements cover the temperature range 15 to 320°K. and revealed the possible existence of heat capacity anomalies between 72 and 78°K. and between 100 and 115°K. Series 3, 4 and 5 were made to characterize the shape of the heat capacity anomalies. Series 15 and 16 measurements reveal the antiferromagnetic transition at 11.9°K. and are shown graphically in Fig. 1. The remaining series are discussed below.

Reversibility of the Transitions.—Series 6 through 10 were made to test the reversibility of the three second-order transitions characterized by the previous measurements. The reversibility of the transitions was studied in the following manner. The day before the measurements of series 6 were made the sample was cooled from room temperature to 116.5°K. and maintained at this temperature overnight. The following morning the sample was cooled to 108.5°K. as rapidly as possible (0.1°/min.) and measurements immediately were started. Following these measurements the sample was cooled from 113 to 108°K. and again maintained at the lower temperature overnight. The following morning the sample was cooled from 108 to 101.5°K. at the rate of 0.1°/min., and series 7 measurements were begun immediately. Following the series 7 measurements, the sample was

(20) "Selected Values of Chemical Thermodynamic Properties." Circular 500, National Bureau of Standards, Washington, D. C., 1952, p. 487.

(21) C_p of SiO_2 taken from K. K. Kelley, Bureau of Mines Bulletin 477 (1950).

cooled to 90°K., allowed to stand at this temperature overnight and cooled to 73.5°K. the following morning at an average cooling rate of 0.25°/min.; measurements of series 8 then were made.

The object of the cooling technique used for the series 6–8 measurements was to determine whether it is possible to "freeze in" some disorder in cooling rapidly through a particular transition from a temperature a little above to a temperature a little below the maximum in the heat capacity. Figures 2 and 3 present the results of each series of measurements over the temperature ranges of the heat capacity anomalies. It is evident from the measurements of series 6–8 (represented by the dotted curves in Figs. 2 and 3) that there is a certain amount of sluggishness in the rate at which thermal equilibrium is established upon cooling. No evidence of slow thermal equilibrium was observed during the heat capacity measurements, however; for the small temperature rise runs thermal equilibrium was established within 1 to 2 min. following energy input. The anomaly with a maximum at 110.9°K. apparently is more reversible than the other two, because the results of series 6 measurements fall on the smooth curve on the high temperature side of the anomaly.

Series 9 and 10 measurements were carried out to determine whether the results of series 3, 4 and 5 represented true equilibrium values, since measurements of series 6, 7 and 8 indicated a certain amount of irreversibility. For series 3 measurements the sample had been below 76° for only 2 hr., below 100° for 24 hr. and below 108° for 30 hr.; for series 4 the sample had been below 76° for 6 hr.; for series 5 measurements the sample had been below 100° for 20 hr. The sample was cooled from 185° (the temperature to which the sample was warmed following series 8 measurements) to 70° and maintained at this temperature for 42 hr. Measurements of series 9 then were made, and the sample was warmed to 97° and maintained at this temperature for 114 hr. Series 10 measurements were carried out following this period.

The results of series 9 and 10 agree very well with those of series 3, 4 and 5 (Figs. 2 and 3), in which latter series the sample stood below the anomalous regions for shorter periods of time. It now remains to compare the heat content given by the smooth curves drawn through the results of series 3, 4, 5, 9 and 10 with the heat content obtained in the "large temperature rise" determinations of series 2 and 3. This information is given in Table II, in which columns 2 and 3 give the temperature interval covered by one or more heat capacity determinations made in the series given in column 1, column 4 gives the measured heat content over this interval, and column 5 gives the heat content for the same interval obtained by integration of the smooth curves of Figs. 2 and 3. The numbers in parenthesis in column 4 give the number of normal temperature rise runs covering the interval given in columns 2 and 3. The agreement is satisfactory except for the second temperature interval of series 11 made on sample II which will be considered below. The agreement between the two values of the heat contents also indicates that apparently no sluggishness is observed upon heating rapidly through the anomalous regions. The normal temperature rise runs (Series 2 and 3) covered an anomalous region in 10 to 20 min. whereas the time required to cover the same region with small temperature rises required several hr.

Results on Sample II.—Data obtained on sample II are given in Table I, and in Table II as series 11–14. Results in the anomalous regions are given

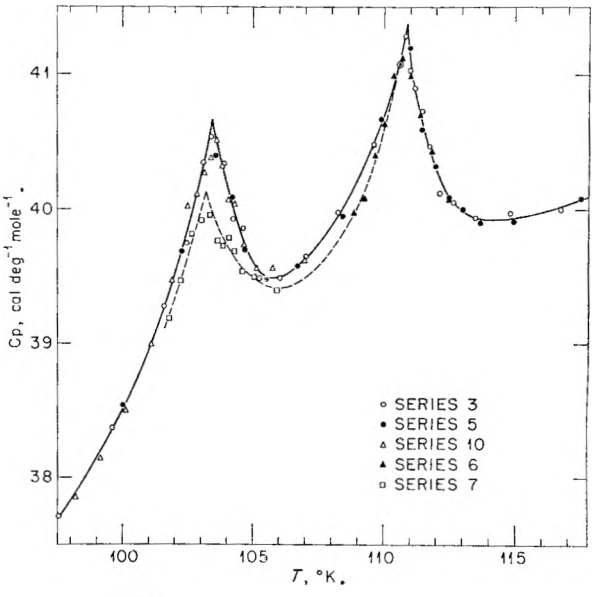

Fig. 3.—Coöperative transitions of K_2ReCl_6 with heat capacity maxima at 103.4 and 110.9°K. See text for explanation of series.

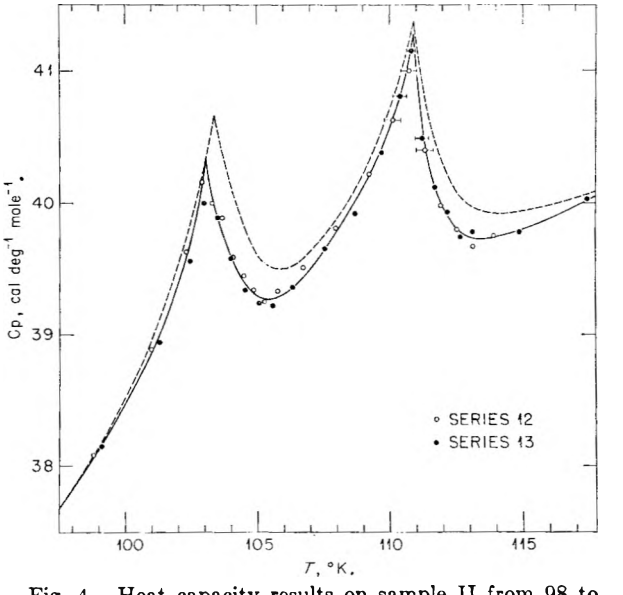

Fig. 4.—Heat capacity results on sample II from 98 to 117°K. Dotted curve represents results obtained on sample I (Fig. 2).

graphically in Figs. 2 and 4. In Fig. 4 the results obtained on sample I are shown as the dotted curve. In the regions of the 76° anomaly fairly good agreement was obtained (Fig. 2 and Table II), but in the vicinity of the 103 and 111° anomalies the second sample gave results definitely lower

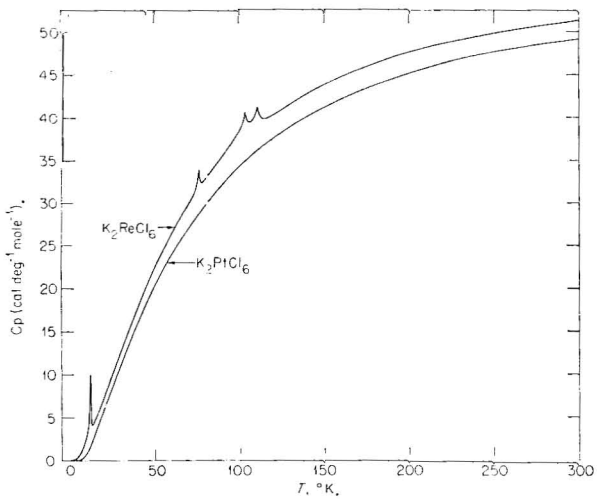

Fig. 5.—Heat capacity of K_2ReCl_6 showing the four anomalies in relation to the remainder of the heat capacity curve. Heat capacity of the isomorphous, diamagnetic K_2PtCl_6 is given for comparison.

than sample I, as can be seen from Fig. 4 and Table II. The greatest divergence appears to be on the high temperature side of each of the anomalies. Outside the anomalous regions the results obtained on sample II are within 0.1 to 0.2% of the results obtained on sample I.

Figure 5 gives the molal heat capacity *vs.* temperature for the temperature region studied showing the anomalies in relation to the rest of the heat capacity curve.

Solubility and Heat of Solution of K_2ReCl_6.—The solubility data are given in Table III. The solubility apparently is independent of the low HCl concentration and should closely approximate the aqueous solubility in the absence of hydrolysis, a conclusion also reached by Rulfs and Meyer.[11] They obtained for the solubility 83.3 g./l. in 0.01 *M* HCl at 25°, which becomes 0.180 mole/1000 g. H_2O using our observed approximate density of 1.054 g./ml. for the saturated solution at 25°. Their determination is 6.5% above the value 0.169 *m* given in Table III. Their concentration also was determined spectrophotometrically, presumably using the absorption maximum at 2810 Å. for which they give a molar absorbancy index of 1.18×10^4 as compared to 1.33×10^4 observed in this Laboratory. Converting their solubility to our molar absorbancy index yields the value 0.160 *m*. No mention is made of an approach to equilibrium from above saturation and it is possible that Rulfs and Meyer's method of stirring by slowly bubbling nitrogen presaturated with solvent through the solution was inadequate.

The temperature coefficient of solubility and heat of solution will be employed later to aid in estimating the mean activity coefficient of K_2ReCl_6 in the saturated solution at 25°.

The heat of solution of K_2ReCl_6 at 25° in 0.0100 *M* HCl as a function of the concentration of the resulting solution is given in Table IV. The standard heat of solution at 25°, $\Delta H^0_{25°} = 10{,}397 \pm 15$ cal. mole^{-1}, was obtained by extrapolation of $(\Delta H_m - \Delta H_{m=0.02602})$ *vs.* $m^{1/2}$ to $m = 0$ with the aid of the Debye–Hückel limiting law, and utilizing the fact that the limiting value of $(\Delta H_m - \Delta H_{m=0.02602})$ at $m = 0$ is equal to $(\Delta H^0 - \Delta H_{m=0.02602})$.

TABLE III

SOLUBILITY OF K_2ReCl_6 AT 0 AND 25°

Run no.	Temp., °C.	Molarity of HCl	Solubility, moles/1000 g. H_2O
1	25.00 ± 0.01	0.0100	0.1690
2	25.00	.0100	.1692
3	25.00	.0100	.1685
4	25.00	.0050	.1690
	Av. for 25°		.1689
5	0.00	0.0100	.0830
6	.00	.0100	.0843
7	.00	.0100	.0850
	Av. for 0°		.0841

TABLE IV

HEAT OF SOLUTION OF K_2ReCl_6 IN 0.0100 *M* HCl AT 25°, CAL. MOLE^{-1}

Sample	Final molality	ΔH
1	0.02602	10637
2	.02472	10627
3	.01197	10580
4	.005144	10535

$\Delta H^0_{25°} = 10{,}397 \pm 15$

Discussion and Thermochemical Calculations

Thermodynamic Properties of K_2ReCl_6.—It is difficult to ascertain the significance of the differences exhibited by samples I and II in the anomalous regions. A cursory search of the literature revealed no compound having a low-temperature heat capacity anomaly which has been the subject of precise duplicate measurements on two different sample preparations, either by one or by different investigators. It is believed, however, that the data on sample II do give strong evidence that the three "extra" anomalies shown by the K_2ReCl_6 samples arise from the K_2ReCl_6 itself and not from an impurity or impurities in the samples.

Smoothed values of the thermodynamic properties obtained from large scale graphs are given in Table V. Because of the coöperative transition with a heat capacity maximum at 11.9°K., extrapolation of the heat capacity to 0°K. utilizing the Debye T^3 law is more uncertain than usual. The estimated entropy at 7°K. is 0.471 ± 0.05 cal. deg.$^{-1}$ mole^{-1}. The smoothed heat capacities are believed to be accurate to 5% below 15°, to 1% at 25°, and to 0.2% above 40°K., except in the anomalous regions where the values may be in error by 2%. The entropy at 298.15°K. should be accurate to 0.2%, *i.e.*, 88.84 ± 0.18 cal. deg.$^{-1}$ mole^{-1}. The values of entropy and free energy do not include the contributions from nuclear spin or isotopic mixing and are therefore the conventional ones to be used in calculations of chemical equilibria.

Comparison of the Entropies of K_2ReCl_6 and K_2PtCl_6.—K_2ReCl_6 is isomorphous[22] with the diamagnetic compound K_2PtCl_6. The small differences[23] in cell size and in mass of these two

(22) B. Aminoff, *Z. Krist.*, **94**, 246 (1936).

(23) Face centered cubics, cell sizes Pt 9.745 Å., Re 9.881 Å. (1.4%); 4 molecules/unit cell, octahedral; densities Pt 3.34 g./ml., Re 3.30 g./ml. (1.2%); mol. wt. K_2PtCl_6 = 486.16, K_2ReCl_6 = 477.16 (1.8%).

TABLE V

THERMODYNAMIC PROPERTIES OF K_2ReCl_6
(CAL. DEG.$^{-1}$ MOLE^{-1})

T, °K.	C_p^0	S^0	$\frac{H^0 - H_0^0}{T}$	$-\frac{F^0 - H_0^0}{T}$
7	1.32	0.471	0.346	0.125
10	3.64	1.271	0.936	.335
11.5	7.40	1.955	1.457	.498
11.9	10.00	2.254	1.702	.552
13	4.10	2.757	2.036	.721
15	5.01	3.406	2.370	1.036
20	7.47	5.171	3.326	1.845
25	10.19	7.133	4.430	2.703
30	12.88	9.231	5.616	3.615
35	15.50	11.415	6.842	4.573
40	18.01	13.650	8.083	5.567
45	20.39	15.910	9.319	6.591
50	22.64	18.176	10.540	7.636
60	26.58	22.661	12.894	9.767
70	30.11	27.028	15.105	11.923
72	30.81	27.885	15.532	12.353
74	31.63	28.739	15.955	12.784
76.05	34.12	29.628	16.402	13.226
77	32.52	30.039	16.607	13.432
78	32.49	30.458	16.810	13.648
80	32.98	31.286	17.209	14.077
90	35.70	35.327	19.112	16.215
100	38.51	39.225	20.903	18.322
102	39.52	39.996	21.256	18.740
103.4	40.66	40.542	21.531	19.011
105	39.61	41.157	21.793	19.364
107	39.64	41.903	22.125	19.778
109	40.22	42.642	22.451	20.191
110.9	41.37	43.345	22.764	20.581
113	39.99	44.102	23.093	21.009
115	39.94	44.803	23.385	21.418
120	40.32	46.509	24.081	22.428
130	41.59	49.785	25.377	24.408
140	42.74	52.911	26.577	26.334
150	43.77	55.896	27.691	28.205
160	44.71	58.750	28.724	30.026
170	45.56	61.486	29.690	31.796
180	46.33	64.112	30.593	33.519
190	47.00	66.638	31.440	35.198
200	47.58	69.064	32.234	36.830
210	48.11	71.398	32.978	38.420
220	48.60	73.647	33.676	39.971
230	49.05	75.817	34.334	41.483
240	49.46	77.913	34.956	42.957
250	49.82	79.939	35.544	44.395
260	50.15	81.899	36.098	45.801
270	50.46	83.797	36.623	47.174
273.15	50.56	84.383	36.784	47.599
280	50.77	85.637	37.123	48.514
290	51.07	87.424	37.599	49.825
298.15	51.31	88.843	37.970	50.873
300	51.36	89.160	38.052	51.108
310	51.64	90.848	38.494	52.354
320	51.90	92.492	38.919	53.573

salts leads one to assume that the lattice heat capacity of K_2ReCl_6 is very nearly equal to the molal heat capacity of K_2PtCl_6, and hence that the lattice entropy of the rhenium compound is equal to the molal entropy of the platinum compound. Lohr, Osborne and Westrum[24] utilized a similar comparison between ThF_4 and UF_4 to conclude that UF_4 might possess appreciable excess entropy (*i.e.*, non-lattice) below 20°K. above that given by a Debye T^3 extrapolation. Later measurements[25,26] showed this to be indeed the case. These authors also utilized the heat capacity of ThO_2 to estimate the magnetic entropy of UO_2, NpO_2 and other actinide oxides.[27] This procedure fails, however, for the first transition series metal fluorides[28] and consequently must be employed with caution. Stout and Catalano employed a corresponding states argument using ZnF_2 thermal data to arrive at an estimate of the lattice heat capacity and lattice entropy of several anhydrous fluorides of the first transition series metals. Their method requires a knowledge of the division of the molal entropy into a lattice entropy and a "non-lattice" entropy (such as the magnetic entropy) at some high temperature. Such a division of the entropy of K_2ReCl_6 at room temperature is not possible, however, because although we know the magnetic entropy (R ln 4) we have no *a priori* knowledge of the entropy associated with the 76.0, 103.4 and 110.9°K. anomalies.

Figure 5 shows that the heat capacity of K_2ReCl_6 exceeds that of K_2PtCl_6[29] over the whole temperature range. The magnetic entropy of K_2ReCl_6 at high temperatures is R ln 4 = 2.75 cal. deg.$^{-1}$ mole^{-1}. The entropy difference between the two compounds reaches this value at approximately 23°K., a temperature considerably below the next heat capacity anomaly of K_2ReCl_6 at 76.0°K. The conclusion is that the heat capacity anomalies at 76.0, 103.4 and 110.9°K. are not magnetic in origin. The magnetic data[7] leave no question that the 11.9°K. anomaly is magnetic in origin, and also show apparently normal behavior over the temperature interval from 60 to 150°K.

The excess entropy of K_2ReCl_6 above that of K_2PtCl_6 is 9.06 cal. deg.$^{-1}$ mole^{-1} at 300°K. This difference becomes 6.31 cal. deg.$^{-1}$ mole^{-1} when the magnetic entropy of R ln 4 is subtracted. A portion of this remaining entropy difference is accounted for by a low energy vibrational state within the $ReCl_6^-$ ion. Two of the crystal field bands observed in the absorption spectrum[30,31] of K_2ReCl_6 in 1 M HCl solution (5000 to 13,800 Å.) show unusually distinct vibrational fine structure. (One band is centered at 7100 Å. and the other at approximately 10,800 Å.; the latter is actually an incompletely resolved electronic doublet band). For each of these two electronic bands the average energy separation of the vibrational fine structure bands is 150 cm.$^{-1}$, a very low vibrational energy. Approximately equal vibrational fre-

(24) H. R. Lohr, D. W. Osborne and E. F. Westrum, Jr., *J. Am. Chem. Soc.*, **76**, 3837 (1954).
(25) D. W. Osborne, E. F. Westrum, Jr., and H. R. Lohr, *ibid.* **77**, 2737 (1955).
(26) J. H. Burns, D. W. Osborne and E. F. Westrum, Jr., *J. Chem. Phys.*, **33**, 387 (1960).
(27) D. W. Osborne and E. F. Westrum, Jr., *ibid.*, **21**, 1884 (1953).
(28) J. W. Stout and E. Catalano, *ibid.*, **23**, 2013 (1955).
(29) L. V. Coulter, K. S. Pitzer and W. M. Latimer, *J. Am. Chem. Soc.*, **62**, 2845 (1940).
(30) R. H. Busey, to be published.
(31) K. Jørgensen, *Acta Chem. Scand.*, **9**, 710 (1955).

quencies in the fine structure would be expected for the absorption bands which are observed in the spectral range 5000 to 13,800 Å. since these bands arise from crystal field energy states that have the same electronic configuration as the electronic ground state, namely a $d\epsilon^3$ configuration in terms of crystal field theory.[32] The curves of internuclear distance would be approximately the same for these states resulting in approximately equal vibrational frequencies for the electronic ground state and all excited electronic states of the same $d\epsilon^3$ configuration. The conclusion is, then, that the vibrational energy separation in the electronic ground state is approximately 150 cm.$^{-1}$, the same as is observed in the two higher electronic states.

This low energy vibrational state of 150 cm.$^{-1}$ gives rise to 2.68 cal. deg.$^{-1}$ mole^{-1} vibrational entropy at 300°K., assuming a simple harmonic oscillator. This leaves an entropy of 3.63 cal. deg.$^{-1}$ mole^{-1} as an estimate of the entropy associated with the anomalies at 76.0, 103.4 and 110.9°K. Assuming equal division of this entropy among the three transitions there results 1.21 cal. deg.$^{-1}$ mole^{-1} for each anomaly, a value reasonably close to R ln 2 = 1.38 cal. deg.$^{-1}$ mole^{-1} considering the uncertainties involved in the lattice and vibrational entropy estimates.

The 76.0° anomaly is a typical coöperative transition. The transitions at 103.4 and 110.9°K. similarly are coöperative transitions but do not have the familiar λ shape because of their proximity to each other. The estimated entropy of R ln 2 associated with each of the transitions is strongly suggestive that these are order–disorder types of coöperative transitions. These transitions may represent successive distortions of the face-centered cubic structure, and/or distortions of the octahedral $ReCl_6^=$ ion. Magnetic susceptibility measurements[7] on a *powdered* sample of K_2ReCl_6 showed no unusual behavior through the temperature interval but similar measurements on a single crystal might reveal anomalous behavior of the magnetic susceptibility along the different crystal axes. The absorption spectrum[30] shows that the octahedral ion is distorted as evidenced by the observed splitting (by fields of lower symmetry) of certain absorption bands that are degenerate for a perfect octahedral field surrounding the Re^{+4}. The interpretation of these coöperative transitions requires more knowledge of any crystal symmetry change and/or change in symmetry of the chloride ions surrounding the Re^{+4}.

Entropy of $ReCl_6^=$ (Aq.).—Calculation of the standard free energy of solution at 25°, $\Delta F^0_{Sol.} = -RT \ln K_{SP} = -1364 \log [4 (\gamma_\pm m_s)^3]$ requires knowledge of the mean molal activity coefficient, $\gamma_\pm$, of the K_2ReCl_6 in the saturated solution in addition to the molal solubility, m_s. Since no activity data are available an estimate must be made of $\gamma_\pm$. The observed mean activity coefficients of 1–2 electrolytic salts[33,34] range in value from 0.343 to 0.407 at m = 0.2. Based upon this information alone one might estimate $\gamma_\pm$ (25°, m = 0.169) = 0.39 ± 0.03 for K_2ReCl_6. A better estimate may be made, however, by utilizing the temperature coefficient of the solubility and the observed heat of solution in the following manner. The standard heat of solution, ΔH^0, is related to the temperature coefficient of solubility by the thermodynamic equation $d \ln K_{SP}/d(1/T) = -\Delta H^0/R$. To integrate this expression an estimate of the temperature coefficient of ΔH^0 is required, *i.e.*, $\Delta C_p = \bar{C}^0_{p_2} - C_p$ is required. ($\bar{C}^0_{p_2}$ is the partial molal heat capacity of K_2ReCl_6 in an infinitely dilute solution and C_p is the molal heat capacity of K_2ReCl_6(c)). Based upon $\bar{C}^0_{p_2}$ equal to −50 and −61 for the 1–2 salts Na_2SO_4 and K_2SO_4, respectively,[35] ΔC_p for the solubility reaction is estimated to be −100 cal. deg.$^{-1}$ mole^{-1} and temperature independent over the temperature range of interest. Substitution into the integrated equation of the values for m_s at 25 and 0°, ΔH^0, and ΔC_p gives for the remaining unknown $\gamma_\pm$(25°, m = 0.169)/$\gamma_\pm$(0°, m = 0.0841) the value 0.80. The temperature variation of $\gamma_\pm$ at m = 0.08 is small (~0.04% deg.$^{-1}$ calculated for K_2SO_4) consequently $\gamma_\pm$(25°, m = 0.169)/$\gamma_\pm$(25°, m = 0.0841) = 0.80 within the accuracy of the calculation. Reference to a graph of $\gamma_\pm$ *vs.* $m^{1/2}$ for several 1–2 salts shows that the above ratio is approximately proportional to $\gamma_\pm$(m = 0.169). It may be inferred from such a graph that $\gamma_\pm$ (25°, m = 0.169) for K_2ReCl_6 is 0.36, which is somewhat below that of K_2SO_4($\gamma_\pm$ = 0.375) and approximately equal to that of $(NH_4)_2SO_4$. $(NH_4)_2SO_4$ gives 0.81 for the above ratio. A 50% uncertainty in the estimate of ΔC_p results in a 3% uncertainty in the estimated $\gamma_\pm$, thus $\gamma_\pm$(25°, m = 0.169) = 0.36 ± 0.01.

The standard free energy of solution at 25° is $\Delta F^0_{Sol.} = -1364 \log [4(\gamma_\pm m_s)^3] = 4150$ cal. mole^{-1}. The entropy of solution becomes $\Delta S^0 = (\Delta H^0 - \Delta F^0)/T = 20.9$ cal. deg.$^{-1}$ mole^{-1}. The entropy of K_2ReCl_6(aq.) at 25° is $S^0(K_2ReCl_6(aq.)) = \Delta S^0 + S^0(K_2ReCl_6(c)) = 108.8$ cal. deg.$^{-1}$ mole^{-1}. Using 24.5[36] cal. deg.$^{-1}$ mole^{-1} for the entropy of K^+(aq.), $S^0(ReCl_6^=(aq.)) = 59.8$ ± 0.2 cal. deg.$^{-1}$ mole^{-1}. This entropy combined with S^0(Re) = 8.89,[37] $S^0(H_2)$ = 31.21,[36] and $S^0(Cl_2)$ = 53.29[36] cal. deg.$^{-1}$ mole^{-1} gives for the entropy of formation of $ReCl_6^=$(aq.): $\Delta S_f^0(ReCl_6^=(aq.)) = -140.2$ cal. deg.$^{-1}$ mole^{-1}.

No thermal measurements are available for obtaining the heat of formation of $ReCl_6^=$(aq.). Kapustinskii and Vasilevskii[38] give an estimate of −282.1 kcal. mole^{-1} for the heat of formation of H_2ReCl_6(aq.) at 25°. Since H_2ReCl_6(aq.) is a strong acid[39] this also represents $\Delta H_f^0(ReCl_6^=(aq.))$. Combined with the above $\Delta S_f^0(ReCl_6^=$

(32) See, for exanple, D. S. McClure, *Solid State Phys.*, **9**, 399 (1959).

(33) H. S. Harned and B. B. Owen, "The Physical Chemistry of Electrolytic Solutions," Third Edition, Reinhold Publ. Corp., New York, N. Y., 1958.

(34) R. A. Robinson and R. H. Stokes, "Electrolyte Solutions," Second Edition, Academic Press, Inc., New York, N. Y., 1959.

(35) H. S. Harned and B. B. Owen, ref. 33, p. 354.

(36) W. M. Latimer, "Oxidation Potentials," Second Edition, Prentice–Hall, Inc., New York, N. Y., 1952.

(37) W. T. Smith, Jr., G. D. Oliver and J. W. Cobble, *J. Am. Chem. Soc.*, **75**, 5785 (1953).

(38) A. F. Kapustinskii and K. I. Vasilevskii, *Zhur. Neorg. Khim.*, **2**, 2031 (1957).

(39) G. E. Boyd and Q. V. Larson, unpublished results of this Laboratory.

(aq.)) and other known thermochemical data,[40] this heat gives −1.62 v. for the potential of the $ReCl_6^{=}$–ReO_4^- couple. This potential is much too negative and the above estimated heat from which it was derived must be in error.

Acknowledgments.—We wish to thank Mr. D. E. LaValle for the preparation of the samples of K_2ReCl_6, and Mr. Q. V. Larson and Dr. R. A. Gilbert for assisting with the heat capacity measurements.

(40) From Latimer[38] $\Delta F_f^0(H_2O(l.)) = -56.69$ kcal. mole^{-1} and $\Delta F_f^0(Cl^-(aq.)) = -31.35$ kcal. mole^{-1}. From J. W. Cobble *et al.*,[3] $\Delta F_f^0(ReO_4^-(aq.)) = 137.1$ kcal. mole^{-1}.

PROPERTIES OF BASES IN ACETONITRILE AS SOLVENT. I. CONDUCTIVITY OF NITROGEN BASES

BY W. S. MUNEY AND J. F. COETZEE[1]

Department of Chemistry, University of Pittsburgh, Pittsburgh 13, Pennsylvania

Received July 18, 1961

The conductivity of the following 6 nitrogen bases has been measured in acetonitrile as solvent: *n*-butylamine, diethylamine, pyrrolidine, 1,1-dimethylguanidine, 1,3-diphenylguanidine and triethylamine. At the same concentration, the degree of ionization of all 6 bases is approximately 4 powers of ten smaller in acetonitrile than in water, and 3 powers of ten smaller than in methanol. The main reason for the extreme weakness of the ionization of these bases in acetonitrile is the fact that the acid properties (proton donating power, as well as the capacity to solvate anions) of acetonitrile are very weak. The concentration dependence of the equivalent conductivity of nitrogen bases in acetonitrile differs markedly from that applying in protogenic solvents, such as water and the alcohols. At concentrations greater than approximately 5×10^{-2} *M*, the predominant over-all ionization reaction of 1,3-diphenylguanidine ($pK_b = 4.00$ in water) involves hydrogen bonding between protonated and free base, as follows: $2B + CH_3CN \rightleftarrows (BH{:}B)^+ + CH_2CN^-$, and the value of the corresponding over-all ionization constant is approximately 4×10^{-10}. At lower concentrations, simple ionization becomes predominant: $B + CH_3CN \rightleftarrows BH^+ + CH_2CN^-$, $K_b \sim 2 \times 10^{-11}$. For the remaining 5 bases, the concentration dependence of the equivalent conductivity is quite different from that described for 1,3-diphenylguanidine. Under certain conditions these bases give log Λ_o *vs.* log *C* plots with unusually large negative slopes of −3/4. The reason for this behavior has not been established with certainty, but it is shown that if these bases are dimerized in acetonitrile, and the over-all ionization reaction is the following: $B_2 + 2\ CH_3CN \rightleftarrows 2\ BH^+ + 2\ CH_2CN^-$, the slopes should be equal to −3/4, as observed. However, a preliminary study of the infrared absorption spectra of these bases in acetonitrile provided no conclusive evidence for either the presence or the absence of dimers. Further study is concerned with the determination of molecular weights of nitrogen bases in acetonitrile. Spectrophotometric titration of *n*-butylamine and pyrrolidine with water in acetonitrile as solvent indicated extensive interaction between these bases and water. However, the increase in the conductivity of nitrogen bases in acetonitrile on addition of small concentrations of water is not large, because the ion pairs produced, BH^+OH^-, are only weakly dissociated.

Introduction

In recent years there has been a renewed interest in the theoretical aspects of the properties of non-aqueous solutions. The majority of the theoretical studies that have been carried out dealt with the polarography and conductivity of salts, and relatively few were concerned with the properties of acids and bases. One reason for the emphasis on salts is undoubtedly the fact that in many non-aqueous solvents serious experimental difficulties are encountered with solutions of acids and bases. Several such difficulties are described in this paper.

Acetonitrile is a very interesting solvent for acid–base studies. It is a considerably weaker base than water, and a much weaker acid. In addition, its dielectric constant (38 at 25°) falls in the intermediate range, where small variations in the concentration of many electrolytes result in striking changes in ion association. Acetonitrile therefore acts as a strongly differentiating solvent for acids and bases, and certain intrinsic properties of such compounds, which are not apparent in a leveling solvent, such as water, can be studied in acetonitrile. Several important theoretical studies have dealt with solutions of Brönsted *acids* in acetonitrile. Conductometric,[2–6] polarographic,[7] spectrophotometric[3,6,8] and various titrimetric[4,6,9] methods have been used for this purpose, and many aspects of the behavior of Brönsted acids in acetonitrile are now understood quantitatively. By comparison, very little theoretical information is available on the behavior of *bases* in acetonitrile. The studies that have been carried out were concerned almost entirely with the titration of amines, either with coulometrically generated hydrogen ions,[10] or by adding a variety of acids, using either the potential of the glass electrode[4,11,12] or the heat of the reaction[13] to indicate the course of the titration. A major problem which complicates the study of bases, as well as acids, in acetonitrile is that conventional hydrogen ion indicator electrodes do not behave reversibly in this solvent. We were unable

(1) Address all correspondence to J. F. C.

(2) F. J. Moore and I. B. Johns, *J. Am. Chem. Soc.*, **63**, 3336 (1941).

(3) C. M. French and I. G. Roe, *Trans. Faraday Soc.*, **49**, 314, 791 (1953).

(4) E. Römberg and K. Cruse, *Z. Elektrochem.*, **63**, 404 (1959).

(5) G. J. Janz and S. S. Danyluk, *J. Am. Chem. Soc.*, **81**, 3846, 3850, 3854 (1959).

(6) M. K. Chantooni, Jr., "Acid–Base Equilibria in Acetonitrile," Ph.D. thesis, University of Minnesota, 1960.

(7) J. F. Coetzee and I. M. Kolthoff, *J. Am. Chem. Soc.*, **79**, 6110 (1957).

(8) M. Kilpatrick, Jr., and M. L. Kilpatrick, *Chem. Revs.*, **13**, 131 (1933).

(9) P. R. Bryant and A. H. Wardrup, *J. Chem. Soc.*, 895 (1957).

(10) C. A. Streuli, *Anal. Chem.*, **28**, 130 (1956).

(11) J. S. Fritz, *ibid.*, **25**, 407 (1953).

(12) H. K. Hall, Jr., *J. Phys. Chem.*, **60**, 63 (1956); *J. Am. Chem. Soc.*, **79**, 5444 (1957).

(13) E. J. Forman and D. N. Hume, *J. Phys. Chem.*, **63**, 1949 (1959).

to obtain constant and reproducible potentials with the *hydrogen electrode* in solutions of Brönsted acids in acetonitrile. There is good reason to believe that the hydrogen electrode cannot be expected to behave reproducibly, let alone reversibly, in acetonitrile. For example, Franklin and Sothern[14] found that adsorbed hydrogen is partly displaced from a platinum electrode by nitriles, and also that the potential of the electrode varies with the amount of hydrogen adsorbed. It also is well known that platinum black catalyzes the hydrogenation of nitriles to amines. However, other authors[4,15] have reported potential values obtained with the hydrogen electrode in solutions of Brönsted acids in acetonitrile. Although *glass electrode* measurements in acetonitrile have been of considerable practical importance, they are of limited theoretical significance, because the electrode does not behave reversibly in this solvent. Finally, the *quinhydrone electrode* does not act as a hydrogen ion indicator electrode in acetonitrile; in any event, it is not applicable in strongly basic solutions in any solvent.

Conductometry, which would appear to be an obvious choice for the study of the ionization of nitrogen bases in acetonitrile, has been largely ignored, possibly because the majority of these bases have extremely low conductivities in acetonitrile, and the experimental difficulties are formidable (*vide infra*). To our knowledge the only conductometric study of solutions of bases in acetonitrile is that of Usanovich and Dulova,[16] which dealt with the variation of the conductivity–viscosity product of picoline–acetonitrile mixtures over the entire range from 0 to 100% picoline. The conductivity of these mixtures was found to be extremely small, but some interaction between the picolines and acetonitrile was indicated.

This paper is concerned with the results of a conductometric study of 6 nitrogen bases in acetonitrile as solvent. The behavior of these bases in acetonitrile was found to be quite different from that in water and other protogenic solvents.

Experimental

Purification of the Solvent.—Eastman practical grade acetonitrile was purified by a modification of a procedure described elsewhere.[6] The solvent first was shaken, for 30–45 min. periods, with, successively (1) 2 batches of silica gel (to remove most of the water present), (2) 2 batches of Fisher 80–200 mesh chromatographic adsorption alumina (to remove acetic acid), and (3) phosphorus pentoxide (to remove most of the remaining water). The product then was distilled from a small amount of fresh phosphorus pentoxide (5–10 g. per liter of solvent) under a high reflux ratio through a 2.5-ft. long column packed with glass helices (b.p. 81.5 ± 0.2°). It was observed that large amounts of phosphorus pentoxide cause polymerization of the solvent during the distillation. Two distillations generally were carried out, although the second distillation usually gave hardly any detectable improvement in the purity of the product. The middle fraction of the distillate was stored in a glass vessel which had been painted black, from which the solvent was dispensed by means of a glass siphon. Contact with the atmosphere was made through a drying tube packed with anhydrous magnesium perchlorate and Caroxite. Carbon dioxide was removed immediately before use of the solvent by bubbling Airco Pre-Purified nitrogen, which first had been passed through Drierite and Caroxite tubes, through the solvent for 45 min.

The water content of the purified solvent (as determined by Karl Fischer titration in methanol as solvent) was always less than 2×10^{-3} M (3.6×10^{-3} % by volume), and often less than 1×10^{-3} M, which is the approximate lower limit of water which can be detected in acetonitrile by Karl Fischer titration. The conductivity of the solvent varied from 4 to 6×10^{-8} ohm^{-1} cm.$^{-1}$. These values agree closely with the lowest values reported in the literature.[5,6]

Purification of the Bases.—Fisher reagent grade *n*-butylamine and diethylamine, Eastman white label triethylamine, and Eastman practical grade pyrrolidine were purified by first drying these bases over sodium hydroxide, and then over sodium metal, followed by refluxing over fresh sodium metal for 2 hr., and finally by fractional distillation. In all cases boiling points agreed closely with those listed in Beilstein. Eastman white label 1,3-diphenylguanidine was recrystallized twice from toluene (m.p. 151.0°). Eastman white label 1,1-dimethylguanidinium sulfate was used to prepare the corresponding free base, by treating an aqueous solution of the former with an excess of sodium hydroxide. The free base was extracted with freshly distilled chloroform, the chloroform phase then was dried over Drierite, and finally the chloroform was evaporated at room temperature by passing dry, carbon dioxide-free nitrogen through the solution. The solubility of the free base in acetonitrile was only approximately 7×10^{-4} M.

In all cases, due precautions were taken to exclude carbon dioxide and moisture.

Conductance Measurements.—Since even the strongest nitrogen bases are only very slightly ionized in aceonitrile, relatively large solvent corrections could not be avoided. Since the magnitude of the solvent corrections undoubtedly accounts for the major uncertainty in the measurements reported in this paper, the use of a highly accurate conductance bridge would not have served any useful purpose. All conductance measurements were made at a frequency of 1,000 cycles with an Industrial Instruments Inc. Model RC 16B2 bridge. Since it was necessary to measure high resistances, the cell capacitance was balanced by means of a 140 $\mu\mu$f. variable capacitor, and special attention was devoted to external leads and bridge grounding to maintain electrical symmetry. The bridge was calibrated by substituting for the conductance cell a series of precision resistors shunted by a 50 $\mu\mu$f. capacitor. The bridge was found to be accurate to within ±1% below 0.5 megohm, ±2% below 1 megohm, and ±5% below 2 megohms.

All conductance measurements were made in a Fisher Scientific Company No. 9-366 "Low Conductivity" cell, immersed in a light mineral oil-bath at 25.0 ± 0.1°. The cell electrodes were lightly platinized (greyed); with shiny electrodes serious polarization effects were encountered. The cell constant (determined in the usual way with standard aqueous potassium chloride solution) remained constant at 0.117 cm.$^{-1}$ during the entire study.

Measurement of Absorption Spectra.—Absorption spectra were recorded with Perkin–Elmer Model 21 and Cary Model 14 recording spectrophotometers, over the full frequency range covered by these instruments, for (1) acetonitrile alone, (2) the bases studied, both in carbon tetrachloride and in acetonitrile, (3) water in acetonitrile, and (4) solutions containing water as well as the bases studied, in acetonitrile as solvent.

Results and Discussion

The Solvent Correction.—In the measurement of the conductivity of an essentially neutral salt solution, it usually is adequate to correct the observed conductivity of the solution by subtracting the conductivity of the pure solvent. However, when the conductivity of an acid or base is measured, the value of the correction which should be applied becomes much more uncertain, unless specific information is available about the nature and concentrations of the impurities present in the solute and especially in the solvent. It is evident that if the solvent contains an impurity which is a

(14) T. C. Franklin and R. D. Sothern, *J. Phys. Chem.*, **58**, 951 (1954).
(15) V. A. Pleskov, *J. Phys. Chem.* (*U.S.S.R.*), **22**, 351 (1948).
(16) M. Usanovich and V. Dulova, *J. Gen. Chem.* (*U.S.S.R.*), **17**, 669 (1947).

weak acid, addition of a base will cause an increase in the ionization of the impurity, with the result that the proper solvent correction will be larger than the conductivity of the "pure" solvent. Likewise, if the solvent contains a weak base impurity, the proper solvent correction will be smaller than the solvent conductivity. Only when the impurity is the salt of a strong acid with a strong base, which does not react in any way with the added acid or base, will the solvent correction be adequately represented by the solvent conductivity.

Although the conductivity of the acetonitrile used in the present study was as low as the smallest value reported for this solvent in the literature, it nevertheless constituted in some measurements a considerable fraction of the total conductivity of the base solutions measured. Although only those nitrogen compounds which are particularly strong bases in water ($pK_a > 10$) have been studied, the conductivities in "dry" acetonitrile were so low that it generally was unavoidable to work with solvent corrections which ranged from 6% for the most concentrated to 50% for the most dilute solutions studied. However, in experiments in which the effect of small concentrations of water was studied, the solvent correction was smaller.

The main impurities which are likely to be present in acetonitrile are water and the various hydrolysis products of acetonitrile, namely acetamide, ammonium acetate, ammonia and acetic acid. It is evident that if any of these impurities (particularly acetic acid) is present in the solvent, the proper solvent correction for solutions of bases will not be the same as the conductivity of the solvent alone. The effect of water was studied in some detail, and is described in subsequent sections of this paper. Ammonia can be detected and determined polarographically at concentrations higher than approximately 5×10^{-5} M in acetonitrile.[7] The solvent used in this study always contained less than this concentration of ammonia, which is sufficiently low to be ignored, since only much more concentrated solutions of compounds which are all stronger bases than ammonia were studied. The presence of acetic acid in the solvent would be much more objectionable, because acetic acid is a much stronger acid than acetonitrile (or water), and reactions such as the following

$$B + HOAc \rightleftarrows BH^+OAc^- \rightleftarrows BH^+ + OAc^- \quad (1)$$

and possibly also

$$B + BH^+OAc^- \rightleftarrows (BH{:}B)^+ + OAc^- \quad (2)$$

would increase the conductivity of solutions of bases. Special attention therefore was devoted to the elimination of acetic acid in the purification of the solvent, by treatment with activated alumina. No evidence was obtained for the presence of acetic acid in the purified solvent. Any traces of acetic acid which might nevertheless have been present would have resulted in an essentially constant "background" conductivity, because in all cases the base would have been present in large excess. We have verified that even when a solvent correction which is 3 times as large as the solvent conductivity is applied, the important features of the relationships obtained do not change sufficiently to compromise the conclusions drawn from the results.

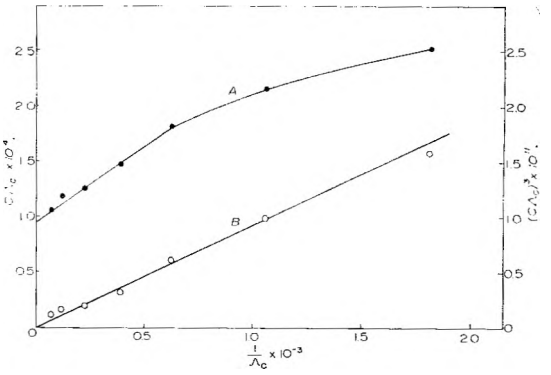

Fig. 1.—Concentration dependence of equivalent conductivity of diethylamine in acetonitrile: A, $1/\Lambda_c$ *vs.* $C\Lambda_c$; B, $1/\Lambda_c$ *vs.* $(C\Lambda_c)$.[3]

Since no unambiguous information was available about the nature of the trace impurities present in the solvent, all conductance values reported in this paper were corrected by subtracting from the measured conductance the conductance of the solvent alone ("dry" acetonitrile, or acetonitrile with water added, where appropriate).

Concentration Dependence of the Equivalent Conductivity.—Since the bases studied ionize as 1:1 ionophores in water (and in other protogenic solvents, SH) according to the following over-all reaction

$$B + SH \rightleftarrows BH^+ + S^- \quad (3)$$

the Ostwald dilution function applies in such solvents in the following form

$$K_b = \frac{\Lambda_c^2 C}{\Lambda_0(\Lambda_0 - \Lambda_c)} \quad (4a)$$

where K_b is the over-all ionization constant of the base, Λ_c is its equivalent conductivity at a concentration C, and Λ_0 that at infinite dilution. Equation 4a can be rearranged to read

$$\frac{1}{\Lambda_c} = \frac{1}{\Lambda_0} + \frac{C\Lambda_c}{K_b\Lambda_0^2} \quad (4b)$$

Hence, a plot of $1/\Lambda_c$ *vs.* $C\Lambda_c$ (a Kraus–Bray plot) gives a straight line with an intercept equal to $1/\Lambda_0$ and a slope equal to $1/K_b\Lambda_0^2$. It therefore is possible to evaluate Λ_0 and K_b simultaneously from the same data. If the measurements are made at sufficiently low ionic strength values, it may be unnecessary to apply corrections for interionic forces.

However, we found that in acetonitrile as solvent, the ionization of several nitrogen bases is not represented by equation 4b. As an illustration, the results for diethylamine are represented by plot A in Fig. 1. It is evident that (1) the plot is not linear at higher (but still moderate) concentrations; and (2) what is more significant, extrapolation of the approximately linear section of the plot (at lower concentrations) cuts the $1/\Lambda_c$ axis at a negative, and therefore unreal, value. The behavior of triethylamine, 1,1-dimethylguanidine and 1,3-diphenylguanidine in acetonitrile also is not represented by equation 4b. On the other hand, the data for *n*-butylamine and pyrrolidine are represented quite well by equation 4b, and the linear plots obtained

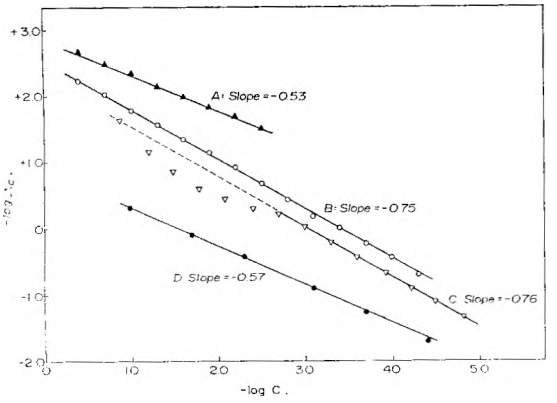

Fig. 2.—Pyrrolidine in acetonitrile: A, no water added; B, C and D, 0.11, 1.1 and 16 M water added, respectively.

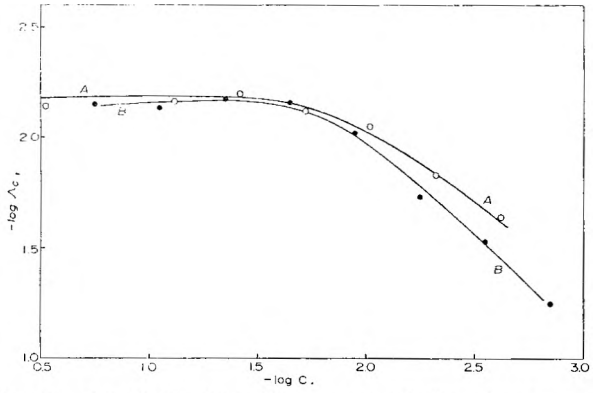

Fig. 3.—1,3-Diphenylguanidine in acetonitrile: A, no water added; B, 0.10 M water added.

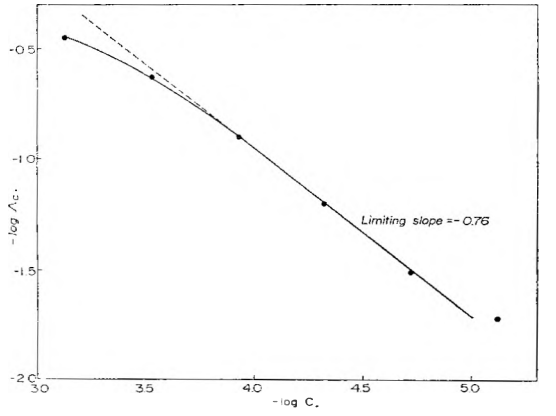

Fig. 4.—1,1-Dimethylguanidine in acetonitrile.

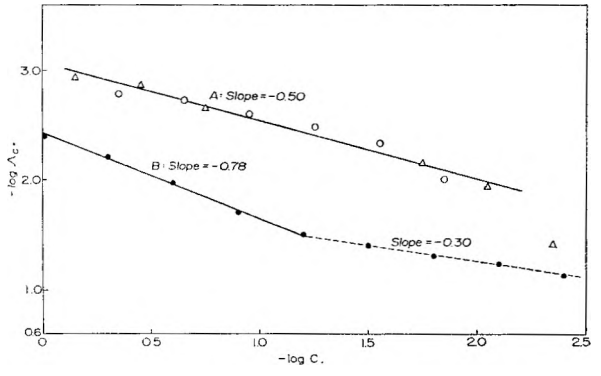

Fig. 5.—n-Butylamine in acetonitrile: A, no water added (0 and Δ: 2 independent runs); B, 1 M water added.

extrapolate properly to small positive values of $1/\Lambda_c$. The situation becomes even more obscure when the effect of small concentrations of water is considered, because addition of 0.1 or 1 M water to solutions of n-butylamine or pyrrolidine gives results similar to those described for diethylamine in the "dry" solvent. In pure water, the conductance behavior of pyrrolidine is represented quite well by equation 4b, and the dissociation constant which we calculated from a Shedlovsky plot (pK_a = 11.1) agrees fairly well with the literature value (11.3) obtained by potentiometric titration.[17]

Information about the possible over-all ionization reactions of nitrogen bases in acetonitrile can be obtained by considering the log Λ_c *vs.* log C plots given in Figs. 2 to 5. Additional information about these plots is given in Table I. The salient features are the following. (1) In the majority of cases, the log Λ_c *vs.* log C plots are linear over wide concentration ranges. (2) The slope of the linear section of the plot usually is equal to one of 3 values: $-3/4$, $-1/2$, or 0. The significance of these different values of the slope will now be discussed.

Slopes of log Λ_c vs. log C Plots.—For an electrolyte which undergoes simple $1 \rightarrow (1 + 1)$ ionization in a given solvent, for example

$$B + CH_3CN \rightleftarrows BH^+ + CH_2CN^- \qquad (5)$$

the log Λ_c *vs.* log C plot is linear, and its slope is equal to $-1/2$, as long as the degree of ionization of the electrolyte is negligible as compared to unity over the concentration range studied. A slope of zero is obtained in cases such as

$$2B + CH_3CN \rightleftarrows (BH{:}B)^+ + CH_2CN^- \qquad (6)$$

where hydrogen bonding occurs between the free base and its cation. Analogous hydrogen bonding of acid anions by the acid itself has been observed with a number of acids in several solvents, including acetonitrile (for example, see ref. 6). It is more difficult to account for a slope which is more negative than $-1/2$. A slope of $-3/4$ requires that the ionization reaction produces 4 ions per mole of solute. Hence the possibility exists that those nitrogen bases which give a slope of $-3/4$ are dimerized. Thus, if the over-all ionization reaction is

$$B_2 + 2CH_3CN \rightleftarrows 2BH^+ + 2CH_2CN^- \qquad (7a)$$

or, if sufficient water is present

$$B_2 + 2H_2O \rightleftarrows 2BH^+ + 2OH^- \qquad (7b)$$

and if α is the fraction of the dimer ionized at a molar concentration C_2 of the dimer, it follows that the over-all ionization constant, K_b', of the base will be given by

$$K_b' = \frac{(2\alpha C_2)^2(2\alpha C_2)^2}{(1 - \alpha)C_2} \qquad (8)$$

If α is given by the conductivity ratio, Λ_c/Λ_0, and if it is negligible as compared to unity over the concentration range studied, it follows from equation 8 that

$$\frac{d \log \Lambda_c}{d \log C_2} = -\frac{3}{4} \qquad (9)$$

(17) S. Searles, M. Tamres, F. Block and L. A. Quarterman, *J. Am. Chem. Soc.*, 78, 4917 (1956).

TABLE I

CONDUCTIVITY OF NITROGEN BASES IN ACETONITRILE

Base	pK_a in water	Water present, M	Slope of log Λ_c vs. log C plot	Concn. range, $M \times 10^{3a}$	$\Lambda_c \times 10^3$ at $C = 0.1$ M	α at $C = 0.1$ M[b]
n-Butylamine	10.61	1.5×10^{-3}	−0.50	9 → 700	2.8	1.7×10^{-5}
		1.1	− .78	60 → 1,000	22	1.0×10^{-4}
Diethylamine	10.98	1.6×10^{-3}	− .77	7 → 900	1.8	9×10^{-6}
Pyrrolidine	11.27	1.0×10^{-3}	− .53	3 → 400	4.7	2.8×10^{-5}
		0.11	− .75	0.05 → 400	17	8.1×10^{-5}
		1.1	− .76	.02 → 2[d]	32	1.5×10^{-4}
		16	− .57	.04 → 100	500	2.4×10^{-3}
1,1-Dimethylguanidine	[c]	2×10^{-3}	− .76	.02 → 0.3[e]	10,000[f]	4.8×10^{-2}[f]
1,3-Diphenylguanidine	10.00	1.0×10^{-3}	0	30 → 300	6	4×10^{-5}
		0.10	0	30 → 200	7	4×10^{-5}
Triethylamine	10.78	1.6×10^{-3}	− .75	20 → 1,000	1.5	7×10^{-6}

[a] Concentration range over which the slope remains constant at the value given in the previous column. [b] Degree of ionization = $\alpha = \Lambda_c/\Lambda_0$; assumed Λ_0 values: 160 for diphenylguanidine, 165 for *n*-butylamine and pyrrolidine in "dry" acetonitrile, and 210 for all other cases (see also text). [c] Virtually a strong base in water. [d] Irregular behavior at higher concentrations. [e] Limited solubility. [f] At $C = 10^{-4}$ M.

Possible over-all ionization reactions corresponding to the 3 different slopes of the log Λ_c *vs.* log C plots observed in this study are summarized in Table II. It should be noted that a slope of $-1/2$ can be obtained with 2 different reactions.

TABLE II

SLOPES OF LOG Λ_c *vs.* LOG C PLOTS FOR DIFFERENT IONIZATION REACTIONS

Possible over-all ionization reaction[a]	Over-all ionization constant[b]	Slope
(1) $B_2 + 2SH \rightleftarrows 2BH^+ + 2S^-$	$2\alpha^4C^3$[c]	$-\frac{3}{4}$
(2) $B_2 + SH \rightleftarrows (BH{:}B)^+ + S^-$	$\frac{\alpha^2C}{2}$[c]	$-\frac{1}{2}$
(3) $B + SH \rightleftarrows BH^+ + S^-$	α^2C	$-\frac{1}{2}$
(4) $2B + SH \rightleftarrows (BH{:}B)^+ + S^-$	$\frac{\alpha^3}{4}$	0

[a] SH = proton donor, either CH_3CN or H_2O, at a constant equilibrium concentration. [b] For values of α that are negligible as compared to unity. [c] For purposes of comparison, in all cases C refers to the molar concentration of base added, calculated for B, not B_2.

It is not possible to decide from only the value of the slope whether the base is protonated by acetonitrile or by water. The lowest water concentrations attained in the purification of the solvent amounted to approximately 1×10^{-3} M (2×10^{-3} % by volume), which is not negligible as compared to the very low ion concentrations produced by even the strongest nitrogen bases studied, which are all only very slightly ionized in acetonitrile. However, conductometric titration of 0.1 M *n*-butylamine in acetonitrile (which already contained 1.5×10^{-3} M water) with water over a concentration range of 0.01 to 1 M water gave a virtually linear increase of conductivity with increasing water concentration over the whole range, and extrapolation to zero water concentration gave a conductivity value only 2% lower than that measured with 1.5×10^{-3} M water present. Hence we conclude that in acetonitrile with a water concentration no greater than a few millimolar, the acetonitrile itself acts as the major proton donor. As the water concentration is increased, the water rapidly takes over the role of proton donor. At 0.08 M water, the conductivity of 0.1 M *n*-butylamine has double the value for the dry solvent.

It follows from equation 8 that for reaction 1 in Table II, a plot of $1/\Lambda_c$ *vs.* $(C_2\Lambda_c)^3$ should be linear, with an intercept of $1/\Lambda_0$ and a slope of $16/K_b'\Lambda_c^4$. Such a plot is shown for the case of diethylamine in "dry" acetonitrile (plot B in Fig. 1). It is to be noted that in all figures shown, for purposes of simplicity and intercomparison, the quantity C refers to the molar concentration of (monomeric) base added; if dimerization occurs, the concentration C_2 of the dimer will be given by $C_2 = C/2$.

The main features of the results listed in Table I and in Figs. 2 to 5 are the following.

1. The conductance behavior of 1,3-diphenylguanidine differs markedly from that of the other bases studied. The log Λ_c *vs.* log C plot given in Fig. 3 for this base in "dry" acetonitrile, and also with 0.10 M water added, has a slope of zero at concentrations above approximately 5×10^{-2} M. For such solutions the predominant ionization reaction therefore must be number 4 in Table II. In more dilute solutions the simple ionization reaction (no. 3) becomes predominant. Formation of the species $(BH{:}B)^+$ has been observed before[18] in the spectrophotometric titration of 1,3-diphenylguanidine with the indicator acid bromophthalein magenta E in benzene as solvent.

2. Perhaps the most striking feature of the results listed for the remaining 5 bases is the frequency with which a slope of approximately $-3/4$ is obtained over wide concentration ranges. It already has been shown that an over-all ionization reaction involving dimers of these bases would produce a slope of $-3/4$. The following mechanisms whereby dimerization of nitrogen bases in acetonitrile could occur were considered. (a) Association of these bases by N–H–N hydrogen bonding

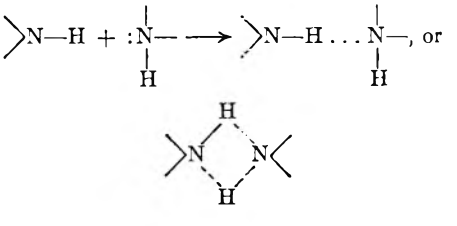

Primary and secondary amines are known to be considerably associated in the pure, liquid state, even at temperatures near the boiling point. However, tertiary amines cannot associate in this way, and yet triethylamine also gives a slope of $-3/4$. Furthermore, it is not to be expected that the association of primary and secondary amines will result in the formation of actual dimers, and particularly not that such dimerization will persist over a wide concentration range. (b) Interaction between the base and acetonitrile. One possible reaction is

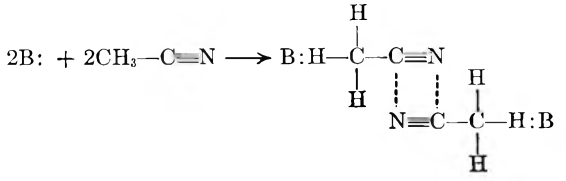

In this connection it is noteworthy that Zhukova,[19] who found from infrared studies that pure acetonitrile is extensively associated, postulated the formation of an analogous dimer in the pure nitrile

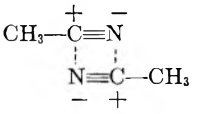

(c) Various possibilities involving what may be termed "effective dimerization" of nitrogen bases in acetonitrile also were considered. For example, the ion pairs produced by reaction of these bases with water in particular would have a highly unsymmetrical charge distribution, and it is conceivable that these ion pairs will "dimerize" to quadrupoles

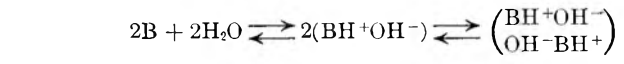

However, it can be shown that in this case the log Λ_c *vs.* log C plot should have a slope of $-1/2$, not $-3/4$. Similarly, formation of a 2:1 adduct between base and added water

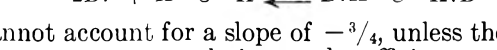

cannot account for a slope of $-3/4$, unless the reaction goes to completion and sufficient water is present to combine with virtually all the base. We obtained no evidence for the formation of such a 2:1 adduct (*vide infra*), and in any event a slope of $-3/4$ was obtained in several experiments in which insufficient water was present to combine with all of the base.

Of the various possible reactions whereby nitrogen bases could conceivably dimerize in acetonitrile, those involving reaction between the base and acetonitrile appear most logical. We carried out a preliminary investigation of the infrared absorption spectra of several of the bases in acetonitrile, but obtained no conclusive evidence for the occurrence of significant reactions between these bases and acetonitrile, although the spectral evidence does not rule out the possibility of such reactions occurring. We therefore present the dimerization hypothesis simply as one which is consistent with the conductance data obtained. It seems desirable to determine the molecular weights of selected nitrogen bases in acetonitrile, and this is the subject of further study in this Laboratory. It is of course also possible that the mechanism of ionization of ionophoric bases in acetonitrile may be entirely different from, and perhaps much more complex than that applying in common protogenic solvents, such as water and the alcohols. In this connection it is interesting to note that Usanovich and Dulova[16] postulated that picolines ionize in acetonitrile by the reactions

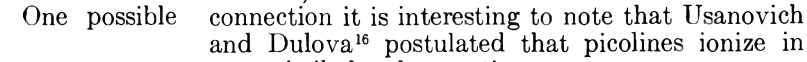

However, such a mechanism seems energetically unfavorable, and in any event would not account for our slopes of $-3/4$.

We also have considered the possibility that the ionization of nitrogen bases in acetonitrile may occur by a simple $1 \rightarrow (1 + 1)$ over-all reaction, and that the increase in the slope of the log Λ_c *vs.* log C plots to values more negative than $-1/2$ is due to one or more of the following factors. (a) The uncertainty in the magnitude of the solvent correction (discussed before). If the proper solvent correction is larger than that which actually is applied (for example, if the solvent contains significant concentrations of acetic acid), the observed slope will indeed be too negative at low concentrations of base. However, at higher concentrations of base (above approximately 0.01 M), the slope is virtually unaffected by even a 3 or 4-fold increase in the solvent correction. Extensive calculations showed that it is impossible to reduce the observed slope of $-3/4$ to $-1/2$ over more than a very restricted concentration range by simply assuming larger solvent corrections. Furthermore, different batches of solvent and bases (which are not likely to contain exactly the same concentrations of impurities) gave a reproducible slope of $-3/4$. (b) Non-equilibrium conditions. It actually was observed that the conductance of all bases studied exhibited in the "dry" solvent a rapid increase of up to 10% within the first few minutes, followed by a much slower further increase, which continued without reaching an equilibrium value for 2 weeks, at which time the conductance was about double its initial value. A somewhat similar "aging" phenomenon occurs with solutions of many weak acids in acetonitrile (see for example, reference 6). It is likely that the slow drift which is still occurring after a few minutes with solutions of nitrogen bases in acetonitrile is due to subsequent reactions involving decomposition of the solvent (base-catalyzed polymerization, amidine formation. etc.). We therefore have made all conductance measurements after 30 min. The reason for the initial drift may be that removal of a proton from acetonitrile by an amine-type base is not a rapid process. The further "aging" process was not studied further. In those experiments in which water was added, drifts were smaller, and virtually stable conductance values were obtained within a few minutes. It was verified that reproducible and equilibrium values were measured by repeating the measure-

(18) M. M. Davis and H. B. Hetzer, *J. Research Natl. Bur. Standards*, **46**, 496 (1951).

(19) E. L. Zhukova, *Optika i. Spektroskopiya*, **4**, 750 (1958).

ments with a new sample of freshly purified pyrrolidine, in a new batch of solvent to which 0.11 *M* water had been added, and making measurements both after 1 hr. and after 24 hrs. In both cases the original slope of $-3/4$ was reproduced. We therefore believe that the slopes of $-3/4$ observed in this study are real, and have definite significance. (c) Changes in dielectric constant, and particularly in viscosity, of the medium at high concentrations of base. The viscosity values of diethylamine (3.67 cp. at 25°) and triethylamine (3.63) are quite close to that of acetonitrile itself (3.45). Hence it is unlikely that the bulk viscosity of the medium will change greatly as the concentration of these bases is varied, particularly in the more dilute solutions studied. Very large variations in viscosity are required to change the slope from $-3/4$ to $-1/2$. The same is true of variations in the dielectric constant of the medium. (d) Changes in the nature of the ion species with changing concentration of the bases. Such changes will cause curvature in the log Λ_c *vs.* log C plots over relatively narrow concentration intervals (see Fig. 3 as an example), and therefore cannot account for the fact that in several cases the slopes remain constant at $-3/4$ over wide concentration ranges.[20]

Primary Hydrogen Bonding Reaction of Nitrogen Bases with Water. Spectrophotometric Titration with Water.—The primary hydrogen bonding reaction of *n*-butylamine and pyrrolidine with small concentrations of water in acetonitrile was studied by using the water band in the infrared first overtone region. The first overtone band was used, rather than the fundamental, because it was much better resolved. Solutions of *n*-butylamine and of pyrrolidine in acetonitrile, containing varying concentrations of water, were scanned over the range from 1290 to 1640 mμ. Several bands were obtained, and the following assignments made: 1410 mμ (O–H stretch of free water), 1465 (O–H stretch due to hydrogen bonding giving H_2O–H_2O association), 1530 (very broad, possibly also H_2O–H_2O polymers), 1528 (N–H stretch of free amine), and 1540 (N–H stretch of amine–water adduct). An unassigned band at 1497 mμ also was observed. The free water band at 1410 mμ was the only completely resolved band useful for quantitative calculations. The absorbance at the wave length of maximum absorption, which remained constant at 1410 mμ with varying water concentration, followed Beer's law. The results are presented in Table III. The slight decrease in molar absorptivity at higher water concentrations may be the result of increasing association of water with itself.

TABLE III

APPLICABILITY OF BEER'S LAW TO FREE WATER BAND AT 1410 mμ IN ACETONITRILE AS SOLVENT

Water concn., *M*	Absorbance[a]	Molar absorptivity[b]
0.100	0.038	0.380
.200	.077	.385
.400	.155	.388
.600	.229	.382
.800	.307	.384
1.60	.583	.364
2.20	.785	.357

[a] Cell length = 1 cm. [b] $\epsilon_{av.} = 0.384$ (for first 5 solutions).

In Table IV the results are presented for the spectrophotometric titration of *n*-butylamine with water. The concentrations of free water were calculated from the absorbance values at 1410 mμ, using a value of $\epsilon = 0.334$ for the first 5 solutions, and $\epsilon = 0.364$ for the sixth. It is evident that it is not possible to decide from the equilibrium constant values obtained which of the 2 mechanisms given in Table IV actually applies. In both cases the equilibrium constant values exhibit a trend to decrease at lower water concentrations. The same trend is evident in the case of pyrrolidine, which gives practically the same equilibrium constant values as those obtained with *n*-butylamine under the same conditions. It is simple to show that this trend cannot be the result of simultaneous formation of a 2:1 adduct (B:H–O–H:B), which on theoretical grounds is possible, but not likely. It seems reasonable to assume that the observed trend is caused by additional interaction between water and the 1:1 adduct, such as hydration of the ion pairs, BH^+OH^-, produced.

TABLE IV

SPECTROPHOTOMETRIC TITRATION OF *n*-BUTYLAMINE WITH WATER IN ACETONITRILE AS SOLVENT

Total [H_2O]	Absorbance[a] (at 1410 mμ)	Free [H_2O]	[H_2O] Reacted	Formation constant of adduct: Mechanism A[b]	Formation constant of adduct: Mechanism B[c]
0.300	0.092	0.240	0.060	0.27	0.13
.500	.158	.412	.088	.24	.10
.600	.181	.472	.128	.31	.17
.900	.267	.695	.205	.38	.22
1.000	.295	.770	.230	.39	.23
2.000	.574	1.610	.390	.40	.20

[a] Experimental conditions: 0.99 *M* *n*-butylamine, in 1-cm. cell, *vs.* blank containing same concentration of base, but without any water added. [b] $B: + H_2O \rightleftarrows B:H—O—H$. [c] $B_2 + 2H_2O \rightleftarrows 2(B:H—O—H)$.

Degree of Ionization of Nitrogen Bases in Acetonitrile.—Nitrogen bases are too weakly ionized in acetonitrile for the evaluation of Λ_0 values from the conductivity data for the bases. However, approximate Λ_0 values can be estimated from values for ion conductivities available in the literature. Walden and Birr[21] reported λ_0 values for a number of substituted ammonium ions in acetonitrile at 25°, including the following: isobutylammonium 89.8, diethylammonium 94.7, triethylammonium 89.2, piperidin-

(20) In this connection it is interesting to note that French and Roe,[3] who obtained log Λ_c *vs.* log C plots with slopes more negative than $-1/2$ for picric acid in acetonitrile, attributed the deviation of the slope from $-1/2$ to more negative values to the fact that the nature of the anion changes from Pi^- to $(Pi:HPi)^-$ at higher concentrations. However, it can be shown by calculation, using a variety of numerical values (within reasonable limits) for the formation constant of the $(Pi:HPi)^-$ complex and for the ratio $\lambda^0_{(Pi:HPi)^-}/\lambda^0_{Pi^-}$ that while it indeed is possible to account on this basis for a slope which is slightly more negative than $-1/2$ (perhaps as negative as -0.55) this is possible only if it is assumed that the value of the ratio $\lambda^0_{(Pi:HPi)^-}/\lambda^0_{Pi^-}$ is considerably smaller than $1/2$ (actually, $1/2$ would be a reasonable value), and even then it is possible only for the very restricted concentration range over which both types of anions are present in significant concentrations. At lower concentrations the slope must have a limiting value of $-1/2$ (as was pointed out by French and Roe), but at higher concentrations it must approach zero (see Table II). It seems quite possible that in the more concentrated solutions of French and Roe picric acid was associated to a certain extent.

(21) P. Walden and E. J. Birr, *Z. physik. Chem.*, **144**, 269 (1929).

ium 93.3, and diisoamylammonium ion 76. With the exception of the last example, these values are all in the vicinity of 90, which will be used as a reasonable average value for the species BH^+ of 5 of the bases in the present study; for the species $(BH:B)^+$, half that value, or 45, wil be used. For diphenylguanidine, a value of 75 will be assumed for the species BH^+, and approximately 40 for the species $(BH:B)^+$. Of the anions studied by Walden and Birr, thiocyanate ion, with a λ_0 value of 123.2, approaches the CH_2CN^- ion closest in size and structure. A λ_0 value of 120 will be used for the CH_2CN^- ion. Since the conductometric titration of *n*-butylamine with water in acetonitrile as solvent indicated (*v.s.*) that the mobility of the OH^- ion in acetonitrile does not differ greatly from that of the CH_2CN^- ion, a λ_0 value of 120 will be adopted for the OH^- ion as well. The possibility that the mobility of the lyate ion, CH_2CN^-, may be enhanced by a "proton-jump" mechanism (as with the OH^- ion in water) seems unlikely, because it is not to be expected that the mobility of the OH^- ion will be similarly enhanced in acetonitrile as solvent.

Hence, the approximate degree of ionization values listed in Table I were calculated by assuming the following Λ_0 values: for diphenylguanidine: (40 + 120) = 160, for *n*-butylamine and pyrrolidine in "dry" acetonitrile (assuming the ionization is represented by reaction 2 in Table II): (45 + 120) = 165, and in all other cases: (90 + 120) = 210. Naturally, these calculations are only very approximate, but the uncertainty in the α-values listed in Table I should not exceed ±25%.

Diphenylguanidine appears to be the only base of those studied for which the actual over-all ionization reaction can be given unambiguously (*v.s.*), and for which a definite ionization constant can therefore be evaluated. At concentrations above approximately 5×10^{-2} *M*, the over-all ionization constant, K_b', corresponding to reaction 4 in Table II, is given by

$$K_b' = \frac{\alpha^2}{4} = 4 \times 10^{-10} \qquad (10)$$

At a concentration of 3×10^{-3} *M*, where $\Lambda_0 = 1.5 \times 10^{-2}$, the simple ionization reaction (number 3 in Table II) predominates, and the over-all ionization constant, K_b, then is given by

$$K_b = \alpha^2 C = \left(\frac{1.5 \times 10^{-2}}{195}\right)^2 \times 3 \times 10^{-3} = 2 \times 10^{-11} \qquad (11)$$

It follows from equations 10 and 11 that the formation constant, K_f, of the species $(BH:B)^+$ for 1,3-diphenylguanidine is given by

$$K_f = \frac{[(BH:B)^+]}{[B][BH^+]} = 20 \qquad (12)$$

It is evident from the α-values listed in Table I that the bases studied are all extremely poorly ionized in acetonitrile, even when up to 16 *M* (29% by volume) of water has been added. It should be noted that a degree of ionization of approximately 1×10^{-5} at a concentration of 0.1 *M*, which applies to *n*-butylamine, diethylamine and pyrrolidine in the "dry" solvent, corresponds to a "conventional" pK_b value of 11, calculated (for purposes of comparison with pK_b values in protogenic solvents) on the basis of simple $1 \rightarrow (1 + 1)$ ionization. This is 8 powers of ten smaller than in water. It is clear that, of the bases studied, 1,1-dimethylguanidine is by far the most extensively ionized in acetonitrile, as it is in water. Its degree of ionization of approximately 5×10^{-2} at a concentration of 1×10^{-4} *M* corresponds to a "conventional" pK_b value of 7 in acetonitrile (also calculated for simple $1 \rightarrow (1 + 1)$ ionization, for purposes of comparison), whereas in water it is virtually a strong base. The differences in the degree of ionization values of *n*-butylamine, diethylamine, pyrrolidine and triethylamine in acetonitrile are not very large, but *n*-butylamine definitely occurs higher in the order of strengths: pyrrolidine > *n*-butylamine > diethylamine ~ triethylamine, whereas in water the order is: pyrrolidine > diethylamine > triethylamine > *n*-butylamine.

It is interesting to note that, although extensive interaction occurs between the bases studied and added water, as described in the previous section, only a moderate increase in conductivity occurs. If the ionization of a nitrogen base in the presence of added water occurs by a series of reactions such as

$$B: + H_2O \overset{K_1}{\rightleftharpoons} B:H{-}O{-}H \overset{K_2}{\rightleftharpoons} BH^+OH^- \overset{K_3}{\rightleftharpoons} BH^+_{solvated} + OH^-_{solvated}$$

then the product K_2K_3 must be very small. Walden and Birr[21] found that the halides, especially the chlorides, of incompletely substituted ammonium salts (for example, ethylammonium chloride) are quite weak electrolytes in acetonitrile. It is to be expected that the corresponding hydroxides will possibly be even weaker, since the hydroxyl ion is very small. Hence K_3 is undoubtedly quite small, and a major cause of the extreme weakness of nitrogen bases as electrolytes in acetonitrile containing even moderate concentrations of water must reside in the stability of the BH^+OH^- ion pairs.

Finally, it is interesting to note that the over-all ionization constants of *n*-butylamine and triethylamine in methanol (dielectric constant = 33; compare acetonitrile = 38) are only 2 or 3 powers of ten smaller than in water.[22] The much weaker ionization of these bases in acetonitrile therefore is mainly the result of the fact that the acid properties (proton donating power, as well as the capacity to solvate anions) of this solvent are very weak.

Acknowledgment.—Financial support by the Research Corporation and by the National Science Foundation (under grant number NSF-G14502) is gratefully acknowledged.

(22) J. R. Schaefgen, M. S. Newman and F. H. Verhoek, *J. Am. Chem. Soc.*, **66**, 1847 (1944).

STANDARD HEATS OF FORMATION OF 2,2-DIMETHOXYPROPANE (l), AND 2,2-DIETHOXYPROPANE (l). GROUP ADDITIVITY THEORY AND CALCULATED HEATS OF FORMATION OF FIVE KETALS

BY J. H. STERN AND F. H. DORER

Department of Chemistry, Long Beach State College, Long Beach 4, California

Received July 24, 1961

The standard heats of formation of 2,2-dimethoxypropane (l) and 2,2-diethoxypropane (l), (−109.92 and −128.15 kcal./mole, respectively), were determined from heats of acid-catalyzed hydrolysis and appropriate heat of mixing corrections. The heat of formation of the new group combination $[C-(O)_2(C)_2]-2[C-(O)(H)_3](g)$ (7.15 ± 0.75 kcal.) was calculated independently from the heats of formation and vaporization of the two ketals and pertinent group additivity theory data. The uncertainty of ±0.75 kcal. indicates that the calculated heats of formation of the ketals deviate less than 1% from the experimental values. Measurements with unpurified 2-methoxy-2-butoxypropane agree within 2.3% of the calculated value. Calculated heats of formation of four additional ketals also are given.

Introduction

This investigation was undertaken to obtain experimental heats of formation of selected aliphatic ketals. With these results, and the group additivity theory of Benson and Buss,[1] the heats of formation of a variety of other ketals were calculated. A search of the literature showed that no heats of formation of any ketals have been reported.

The group additivity theory assumes that thermodynamic properties of gaseous molecules consist of the algebraic sum of individual parts. The additivity of group properties represents a second-order approximation[2] and has been remarkably successful in predicting good values of heats of formation, standard entropies and heat capacities at 298°K.

2,2-Dimethoxypropane,

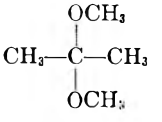

has the following groups:

$$2[C-(H)_3(C)]+[C-(O)_2(C)_2]+2[O-(C)(C)]+2[C-(O)(H)_3].$$

Each group consists of a polyvalent atom in the molecule together with its ligands. For example, the first term represents the contribution of two identical groups made up of the end methyl carbons **C**-, each of which is attached to the three hydrogens (H_3) and the central carbon (C). The second term represents the contribution of the central group, which consists of the central carbon **C**-; this is attached to two oxygens $(O)_2$ and the two methyl carbons $(C)_2$. The succeeding terms are made up in the same way, until all atoms attached to more than one neighbor are accounted for.

The contributions to the heats of formation of all groups except $[\mathbf{C}-(O)_2(C)_2]$ are tabulated independently or in combination with other groups. The $[\mathbf{C}-(O)_2(C)_2]$ group is basic to all ketals and the combination $[C-(O)_2(C)_2]-2[C-(O)(H)_3]$ can be calculated from the heat of formation of any one ketal. The experimental heats of formation of two ketals were determined and used to calculate an average value of the group combination.

The heats of formation of 2,2-dimethoxypropane (l) and 2,2-diethoxypropane (l) were obtained from acid-catalyzed heats of hydrolysis with appropriate heat of mixing corrections.

The acid-catalyzed reaction of ketals with water is[3-5]

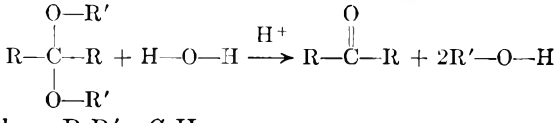

where $R,R' = C_nH_{2n+1}$.

Hydrolyses of some ketals and their qualitative heat effects were studied by Arbusow.[3] He found that the reactions proceeded rapidly and irreversibly to completion and were all endothermic. Only the heat of hydrolysis of 2,2-diethoxypropane was determined quantitatively and reported to be 4.51 kcal./mole.

In order to obtain the heats of formation of the gaseous compounds, the heat of vaporization of 2,2-diethoxypropane was experimentally determined from the variation of its vapor pressure with temperature. Heats of vaporization of closely related ketals were estimated using Trouton's Constant calculated from the above data.

Experimental

Materials.—2,2-Dimethoxypropane (Eastman) and 2,2-diethoxypropane (Dow) were purified by vacuum distillation and examined by GLC (Aerograph) using a Ucon-Polar substrate column. Only peaks of appropriate ketals were observed.

	Boiling point, °C.	Refractive index, 20°
2,2-Dimethoxypropane	33.9–34.8 at 150 ± 2 mm.	1.3777 ± 0.0002
2,2-Diethoxypropane	51.9–52.5 at 103 ± 1 mm.	1.3889 ± 0.0002

Aqueous 1 *N* HCl was prepared from distilled water and concentrated reagent grade acid. Absolute methanol and ethanol were reagent grade

Calorimeter and Experimental Procedure.—The calorimeter has been described elsewhere.[6] The reactions were

(1) S. W. Benson and J. H. Buss, *J. Chem. Phys.*, **29**, 546 (1958).

(2) Atomic and bond property additivities are zeroth and first-order approximations, respectively. In all cases where group contributions are available, calculations based on them have given much closer values than estimates based upon additivity of bond or atomic properties.

(3) A. E. Arbusow, *Z. physik. Chem.*, **121**, 209 (1926).

(4) C. R. Noller, "Chemistry of Organic Compounds," 2nd Edition, W. B. Saunders Co., Philadelphia, Pa., 1957, p. 204.

(5) E. E. Royals, "Advanced Organic Chemistry," Prentice-Hall, Englewood, N. J., 1954, p. 631.

(6) J. H. Stern and A. Passchier, *J. Chem. and Eng. Data*, in press.

carried out in solutions initially consisting of excess dilute aqueous acid (100 ml.), and the product alcohol (100 ml.), so that the exothermic effect of mixing these would be minimized. Large heat of mixing corrections thus were avoided. Four to six g. of freshly distilled ketal was weighed into a thin glass ampoule which was submerged in the reaction solution. After crushing the ampoule, the reaction proceeded very rapidly and thermal equilibrium was attained in less than 60 sec. Completeness of the reaction was shown by the absence of ketal peaks in a GLC analysis of the products.

Heat of mixing corrections were measured similarly. Observed temperature changes were corrected for heat exchange[7] and electrical calibrations were made after each run in the range 26 ± 1°.

Results and Discussion

Heat of Hydrolysis of 2,2-Dimethoxypropane.—The details are given in Table I.

TABLE I

THE HEAT OF HYDROLYSIS (ΔH_h) OF 2,2-DIMETHOXYPROPANE (l)

Moles ketal in ampoule	$-\Delta T$ cor. °C. (±0.002)	Total energy change (cal.)	ΔH_h, kcal./mole ketal
0.04366	1.103	192.7	4.414
.05474	1.367	245.1	4.478
.03785	0.948	166.3	4.394

Av. ΔH_h = 4.429 ± 0.044 kcal./mole

Heat of Hydrolysis (ΔH_h) of 2,2-Diethoxypropane (l).—Details are given in Table II.

TABLE II

THE HEAT OF HYDROLYSIS OF 2,2-DIETHOXYPROPANE (l)

Moles ketal in ampoule	$-\Delta T$ cor. °C. (±0.002)	Total energy change (cal.)	ΔH_h, kcal./mole ketal
0.03031	0.799	144.3	4.762
.02965	.780	143.4	4.836
.02958	.775	140.8	4.759

Av. ΔH_h = 4.786 ± 0.044 kcal./mole

Heat of Mixing Corrections and Reduction to Standard States.—The appropriate heat of mixing corrections (ΔH_m) of acetone and alcohol in their experimental environment were determined in order to correct the calorimetric reaction results of Tables I and II (ΔH_h) to standard states. Tables III and IV list all summarized values. Precision indices in Tables I through IV are standard deviations.

TABLE III

HEAT OF MIXING CORRECTIONS FOR ACETONE AND METHANOL IN HYDROLYSIS OF 2,2-DIMETHOXYPROPANE (l)

Substance	ΔH_m, kcal./mole	No. of determinations
Acetone	−0.22 ± 0.02	2
Methanol	−0.26 ± 0.01	2

TABLE IV

HEAT OF MIXING CORRECTIONS FOR ACETONE AND ETHANOL IN HYDROLYSIS OF 2,2-DIETHOXYPROPANE (l)

Substance	ΔH_m, kcal./mole	No. of determinations
Acetone	+0.13 ± 0.02	2
Ethanol	−0.057 ± 0.005	2

(7) A. Weissberger, "Physical Methods of Organic Chemistry," 3d Edition, Interscience Publishers, Inc., New York, N. Y., 1959, p. 538.

Standard Heats of Formation of 2,2-Dimethoxypropane (l) and 2,2-Diethoxypropane (l).—Standard heats of formation of water, methanol and ethanol were obtained from N.B.S. Circular 500.[8] The heat of formation of acetone was calculated from the thermodynamic properties given by Pennington and Kobe.[9] By combining these with the average ΔH_h (Tables I and II), and heat of mixing corrections ΔH_m (Tables III and IV) the heats of formation shown in Table V are obtained. The heat of formation based on Arbusow's data is given for comparison and is in excellent agreement. The assigned uncertainty is attributed primarily to the estimated errors in the values from the literature. The error resulting from experimental measurements is much lower since the measured heats are comparatively small.

TABLE V

STANDARD HEATS OF FORMATION OF 2,2-DIMETHOXYPROPANE (l) AND 2,2-DIETHOXYPROPANE (l)

	$\Delta H f^0$, kcal./mole
2,2-Dimethoxypropane (l)	−109.92 ± 0.5
2,2-Diethoxypropane (l)	−128.15 ± 0.5 (Arbusow −127.94)

TABLE VI

VAPOR PRESSURES OF 2,2-DIETHOXYPROPANE

T, °K.	V.p., cm.	T, °K.	V.p., cm.
286.9	2.80	297.9	4.42
288.6	3.12	299.0	4.61
292.7	3.63	299.8	4.70
294.4	3.87	301.0	4.95
297.3	4.35	303.3	5.45

TABLE VII

CALCULATED HEATS OF FORMATION OF MISCELLANEOUS KETALS

		$\Delta H f^0$, kcal./mole
2-Methoxy-2-butoxypropane (l)	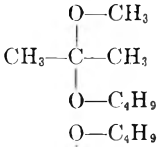	−129.3
2,2-Dibutoxypropane (g)	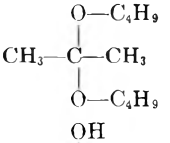	−139.6
2,2-Dihydroxypropane (g)	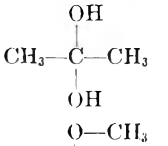	−109.2
2-Methoxy-2-(2-methoxyethoxy)-propane (g)	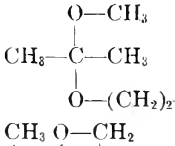	−144.9
2,2-Dimethyl-1,3-dioxacyclopentane (g)	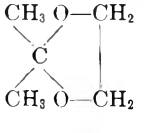	− 99.6

(8) "Selected Values of Chemical Thermodynamic Properties," Circular 500, National Bureau of Standards, U. S. Government Printing Office, Washington, D. C., 1952.

(9) R. E. Pennington and K. A. Kobe, *J. Am. Chem. Soc.*, **79**, 300 (1957).

Heats of Vaporization.—The heat of vaporization of 2,2-diethoxypropane (7.61 kcal./mole) was determined from the variation of its vapor pressure with temperature, using a Smith-Menzies[10] isoteniscope thermoregulated to ±0.01°. The values are shown in Table VI.

Assuming that entropies of vaporization of the two similar ketals are equal, the heat of vaporization of 2,2-dimethoxypropane is 7.03 kcal./mole. The error introduced in this calculation by the above assumption is likely to be very small.[11]

The Additivity Group Theory and Calculated Heats of Formation.—From each of the heats of formation of the two ketals and the available group combinations we obtain the average value of the new combination $[\mathbf{C}-(O)_2(C)_2]-2[\mathbf{C}-(O)(H)_3]$ (g) = 7.15 ± 0.75 kcal. Thus the calculated heats of formation (−109.1 and −127.4 kcal./mole for 2,2-dimethoxypropane (l) and 2,2-diethoxypropane (l), respectively) are within 0.8 kcal. (0.6%) of the experimental heats. The theory is based on data with uncertainties of comparable absolute magnitude.

Calculations for other ketals are useful, particularly in the absence of experimental heats. Table VII includes heats of formation based on the average value of the above group combination.

The calculated heat of 2-methoxy-2-butoxypropane (l) was checked by measurements on an unpurified sample yielding a value of −132.2 kcal./mole. The difference is 2.3% and it is believed that in this case the calculated heat is more reliable.

The group property theory in conjunction with relatively few experimental measurements predicts quite reliable values of thermodynamic properties of many compounds. The theory is valuable when experimental measurements are not feasible. 2,2-Dihydroxypropane of Table VII probably would offer serious calorimetric difficulties, since it is unstable.

Acknowledgment.—We wish to express our gratitude to Mr. Lloyd Peak for carrying out some of the measurements, to Dr. Sidney W. Benson for fruitful discussion, and to the Research Corporation for financial support.

(10) Reference 7, p. 436.

(11) G. N. Lewis and M. Randall, "Thermodynamics," 2nd Edition, McGraw-Hill Book Co., New York, N. Y., 1961, p. 519.

THE INFLUENCE OF CHEMISORPTION OF OXYGEN ON THE ELECTRON SPIN RESONANCE OF ZINC OXIDE

BY R. J. KOKES

Department of Chemistry, The Johns Hopkins University, Baltimore 18, Maryland

Received July 26, 1961

Amounts of oxygen chemisorption have been determined on preparations of zinc oxide prepared by (a) decomposition of zinc oxalate, (b) decomposition of zinc carbonate and (c) oxidation of metallic zinc. The results indicate the existence of two types of oxygen chemisorption, one appearing at room temperature and the other appearing at 200° or above. Zinc oxide, doped or as is, has been shown to have an electron spin resonance signal that reflects the concentration of free electrons. The effect of low and high temperature oxygen adsorption on this signal has been examined as a function of coverage. Interpretation of the results leads to the tentative conclusion that the low temperature form of chemisorption occurs as O^- ions formed by reaction with conduction electrons, and the high temperature form occurs as $O^=$ stabilized by migration of donors to the surface.

Introduction

Many of the chemical and physical properties of zinc oxide are profoundly influenced by the chemisorption of oxygen. When zinc oxide is used for photocatalysis,[1] such as the production of hydrogen peroxide from water and oxygen, the presence of chemisorbed oxygen is an obvious factor. When used as a hydrogenation catalyst[2,3] zinc oxide must be pretreated at elevated temperatures either *in vacuo* or in hydrogen to remove oxygen, a catalytic poison. Other properties such as conductivity,[4] photoconductivity and luminescence,[5] and sintering rate[6] are influenced to some degree by oxygen chemisorption. But in spite of the fact that oxygen chemisorption plays such an important role in determining the properties of zinc oxide, only a few studies have been made in which the amount of oxygen chemisorption has been determined.[7-10] The nature of this chemisorption still is not clear. In this present work the effect of oxygen adsorption on the electronic state of the zinc oxide has been studied by the examination of the electron spin resonance spectra.

Experimental

Catalysts.—ZnO-I was the S.P-500 pigment manufactured by the New Jersey Zinc Company by burning zinc in air. Representative analysis showed that the concentration of paramagnetic ions in this sample was less than 1 p.p.m.; the concentration of aluminum, known to function as a donor, was found to be less than 10 p.p.m. The surface area of this catalyst repeatedly degassed at 550° was 3 m.²/g.[11]

(1) G. M. Schwab, *Advances in Catalysis*, **9**, 229 (1957).

(2) J. F. Woodman and H. S. Taylor, *J. Am. Chem. Soc.*, **62**, 1393 (1940).

(3) E. Molinari and G. Parravano, *ibid.*, **75**, 5233 (1953).

(4) D. J. M. Bevan and J. S. Anderson, *Discussions Faraday Soc.* **8**, 238 (1950).

(5) G. Heiland, E. Mollwo and F. Stockmann, *Solid State Phys.*, **8**, 191 (1959).

(6) T. J. Gray, *J. Am. Ceramic Soc.*, **37**, 534 (1954).

(7) E. R. S. Winter, *Advances in Catalysis*, **10**, 196 (1958).

(8) S. R. Morrison, *ibid.*, **7**, 259 (1955).

(9) T. I. Barry and F. S. Stone, *Proc. Roy. Soc.* (London), **335A**, 124 (1960).

(10) T. I. Barry, Paper No. 70, International Conference on Catalysis, Paris, 1960.

(11) It has been noted by Kesavulu and Taylor [*J. Phys. Chem.*, **64**, 1124 (1960)] that ZnO-I evacuated at 360° for 26 hr. retained large amounts of carbon dioxide and water. They claim that as a result there is no chemisorption of hydrogen between 30 and 360°. We have

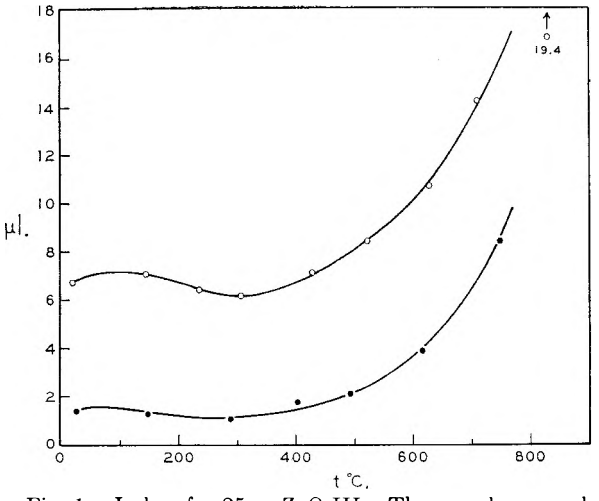

Fig. 1.—Isobar for 25 g. ZnO-III. The sample was calcined in air 16 hr. at 1000°. For the data indicated by the open circles (P = 50 μ) the sample was degassed 16 hr. at 1000°; for the data indicated by the closed circles (P = 20 μ) the sample was degassed 16 hr. at 800°.

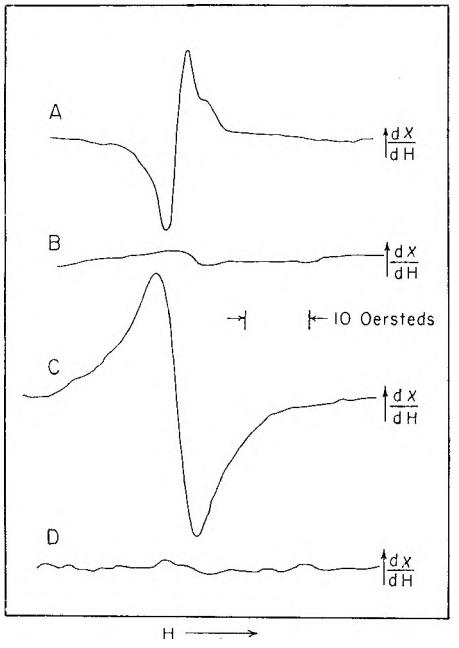

Fig. 2.—Spectra of doped and undoped ZnO-I: A, ZnO-I (0.5 mole % Ga) × 1 scale; B, ZnO-I undoped × 1 scale; C, ZnO-I undoped × 13 scale; D, ZnO-I (0.5 mole % Li) × 13 scale. The ordinate, dχ/dH, is a recorder trace of the derivative of the absorption expressed in arbitrary units. The sweep amplitude was 1.5 gauss.

ZnO-II was prepared by the decomposition of zinc oxalate in air at 500° followed by calcination at 500° for 16 hr. ZnO-III was prepared by the heating of zinc carbonate in oxygen at 500°.

Doped samples with lithia, alumina or gallia were prepared by slurrying 2 g. of zinc oxide with 4 cc. of the appropriate nitrate solution of the ion being added. The resulting slurry was evaporated to dryness and calcined. In every batch prepared, a blank was run in which zinc oxide was slurried with distilled water, evaporated to dryness, and calcined at the same time as the doped catalysts.

Adsorption Experiments.—Adsorption experiments were carried out in a volumetric system equipped with mercury cut-offs and designed for studies at low pressures. The sample container was made of fused silica to permit high temperature studies. Studies of adsorption as a function of temperature were carried out by admitting a measured amount of oxygen to the sample at or below room temperature and measuring the amount adsorbed after one hour at each of a series of higher temperatures.

Spectra studies were carried out on weighed samples of catalysts (about 0.2 g.) in 2 mm. i.d. fused silica tubes that were sealed to the sample container used in adsorption studies. After evacuation or adsorption, these tubes were sealed off and the spectra were determined. In all studies of oxygen adsorption the pressure when the tubes were sealed off was less than 2 μ.

Electron Spin Resonance Measurements.—All Spectra were obtained with the Varian-4500 spectrometer at a frequency of 9200–9525 Mc. This instrument yields a recorder trace of the derivative of the adsorption curve. The center of the signal and the half-width (peak-to-peak distance on the recorder trace) were determined by field measurements with a proton probe. At the power levels used, saturation effects were absent.

The number of spins/g. sample was determined by comparing the integrated intensity of the signal from zinc oxide to that from a known amount of diphenylpicrylhydrazyl diluted 1000:1 with ZnO-I. Initially, this comparison was made by double integration of the recorder trace; it later was established that the same results were obtained by assuming that the integrated intensity was proportional to the height × (peak-to-peak distance).[2] Unless otherwise specified all spectra were obtained at 24°.

Results

Adsorption.—Figure 1 shows an isobar[12] obtained for ZnO-III calcined and degassed at high temperatures. Results for ZnO-II and ZnO-III were similar insofar as they showed a minimum amount of adsorption at 200–300° and the absence of any maximum at the higher temperature. This behavior was observed for catalysts degassed at temperatures as low as 500°.

Other observations that have a bearing on the nature of this chemisorption are the following.

(a) The reproducibility of adsorption for evacuated virgin catalyst samples was fairly good, but if the catalyst was exposed to oxygen for a long time at 550°, the oxygen adsorption was found to be reduced even after evacuation for 16 hr. at 550°.

(b) Adsorption between −100 and +100° was essentially complete in 30 min.; at 400° an initial rapid adsorption was followed by a slower adsorption that continued even after several days.

(c) The presence of pre-adsorbed oxygen put on at 400° has little effect on the oxygen adsorption at 25°. For example, a sample of degassed ZnO-I adsorbed 0.9 μl./g. at room temperature. Adsorption of 2.5 μl. of oxygen/g. at 400° reduced subsequent adsorption at 25° to 0.7 μl./g. Extrapolation of these and other data indicate that it would take 15–20 μl./g. of oxygen adsorption at 400° to block out adsorption (~1 μl./g.) at 25°.

Resonance Spectra of Various Catalysts.—Table I summarizes the results obtained for various catalyst preparations. All spectra were ob-

found that after evacuation at 550° for 16 hr. ZnO-I does adsorb hydrogen in amounts comparable to those observed by Kesavulu and Taylor for zinc oxide from zinc oxalate. (We found ~0.01 cm.³/m.² at 1 mm. compared to their finding of 0.01 cm.³/m.² at 60 mm.) Thus, it would seem that the residual carbon dioxide and water is not a problem under our conditions of pretreatment.

(12) It is apparent from the method of measurement that the data do not truly represent isobars inasmuch as the pressure varied somewhat. Runs wherein the pressure variation was negligible showed that the shape of these curves was little influenced by changes in pressure.

tained at room temperature and the signal observed occurred at $g = 1.96$.

The reproducibility of the runs with ZnO-I degassed at 550° is indicated by the first three rows of Table I. If the catalyst is examined as is or briefly degassed at room temperature (fourth row) no signal is observed, but after prolonged evacuation at room temperature a faint signal is detectable.

The results obtained for the blank in the doping experiments show that slurrying with distilled water has little effect on the signal; hence, changes due to doping are the result of the added ion. For purposes of illustration the spectra obtained with undoped and doped ZnO-I are shown in Fig. 2. The horizontal scale is the same in all cases; the half-width for curve C is 7.1 gauss.

TABLE I

ELECTRON SPIN RESONANCE SPECTRA OF VARIOUS CATALYSTS[a]

Sample	Pretreatment[b]	Spins/g. $\times 10^{-16}$
ZnO-I	Degassed 550°	2.3
ZnO-I	Degassed 550°	2.2
ZnO-I	Degassed 550°	2.4
ZnO-I	Degassed (5 min.) 25°	<0.2[c]
ZnO-I	Slurried with distilled water; dried and degassed 550°	2.1
ZnO-I	Doped 0.5 mole % Li degassed at 550°	<0.3[c]
ZnO-I	Doped 0.5 mole % Ga degassed 550°	11
ZnO-I	Degassed 550° Adsorbed 10 μl. H_2/g. heat treated, 2 hr. 210°	5
ZnO-II	Calcined 550°, degassed 550°	1.5
ZnO-II	Slurried with distilled water calcined 800°, degassed 800°	<0.5[c]
ZnO-II	Doped with 0.05 mole % Al calcined 800°, degassed 800°	68
ZnO-II	Doped with 0.05 mole % Al calcined 1000°, degassed 1000°	134
ZnO-II	Doped with 0.04 mole % Ga calcined 800°, degassed 800°	10

[a] The signals described herein occurred at $g = 1.96$. [b] Unless otherwise specified all calcinations and evacuations were carried out for 16 hr. [c] No definite signal was observed. The values represent an estimate of the maximum the signal could be and be unobservable.

Results for ZnO-II also are shown in Table I. After calcination and evacuation at 550°, ZnO-II gives a signal comparable to that of ZnO-I but after calcination and evacuation at 800° this signal becomes undetectable. Doping with gallia or alumina results in the reappearance of this signal. The strength of the signal obtained with 0.05% added alumina increases with higher calcination temperatures that favor more complete solid solution.

Although the sample of ZnO-II degassed and calcined at 800° showed no signal at room temperature, a signal appeared (at g = 1.96) when the spectra was examined at −195°. (The signal from all samples was stronger by a factor of roughly four at −195°.) The strength of the signal at −195° from ZnO-I or ZnO-II increased by 30 to 50% when the catalyst was irradiated by ultraviolet light while the spectra were being observed. Irradiation at room temperature has no apparent effect on either catalyst.

According to the results in Table I if the catalyst is treated in a manner known to increase its conductivity[5] (irradiated at −195°, evacuated, doped with gallia, alumina, or adsorbed hydrogen at 210°) the signal at $g = 1.96$ increases; if it is treated in a manner known to decrease its conductivity[5] (calcined at high temperature, or doped with lithium) the signal decreases. Other data show that whenever the evacuated catalyst is exposed to air (which decreases the conductivity) the signal decreases.

Effect of Adsorbed Oxygen on the Resonance Spectra.—Figure 3 shows the variation of the integrated intensity and half-width of the signal as a function of the amount of oxygen adsorption at 25°. For the sake of comparison, a dotted line is shown that corresponds to a decrease in intensity of one spin per one half molecule of adsorbed oxygen. In run K53, after adsorption reached a steady value at 1.06 μl./g., a side tube was sealed off for examination of the spectra and the sample was evacuated. In one minute the pressure fell to 10^{-6} mm. After ten minutes evacuation, another side tube was sealed off; later adsorption studies revealed that the ten minute evacuation removed only 0.16 μl. of oxygen, and hence, 0.90 μl./g. remained adsorbed on the catalyst. These data (represented in Fig. 3) show that 85% of the oxygen adsorbed at room temperature is strongly held and that it is this strong adsorption that decreases the signal.

Figure 4 shows the variation of the integrated intensity and half-width of the signal as a function of the amount of oxygen chemisorption at 400°. Once again, the dotted line corresponds to a decrease in intensity of one spin per one half molecule of adsorbed oxygen. Comparison of the data in Fig. 4 to that in Fig. 3 shows that although the adsorption is far less at 25° than at 400°, it is more effective in decreasing the signal intensity.

In both cases the half-width of the signal decreases as the signal intensity decreases. Thus, although the oxygen adsorbed at high and low temperatures vary in effectiveness in neutralizing the signal, they both produce the same over-all effect.

Discussion

Zinc oxide is an n-type semiconductor that is non-stoichiometric due to excess zinc. Conductivity measurements[8] on sintered zinc oxide pellets have shown that oxygen adsorption at room temperature and above decreases the conductivity; this decrease occurs because adsorbed oxygen reacts with conduction electrons to form an ionic species. The observations of Barry and Stone[9] that the gas phase O^{18}–O^{16} exchange in the presence of a zinc oxide catalyst is immeasurably fast at −130° and measurable at −195° indicate that the adsorbed species is probably atomic rather than molecular.

Morrison[8] has postulated that there are two types of oxygen chemisorption, one occurring at room temperature, the other at higher tempera-

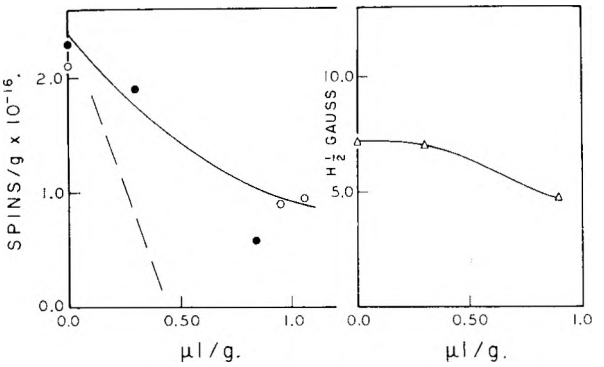

Fig. 3.—Effect of oxygen adsorption at 25°. Electron spin resonance at room temperature: ●, spins/g., Run K27; ○, spins/g., Run K53; Δ, half-width of adsorption signal of K27. Dotted line corresponds to a decrease in the signal of one spin/adsorbed oxygen atom. Solid line for integrated intensity plot is calculated on the basis indicated in the discussion. (The value used for e_0 was 2.4×10^{16}/g.)

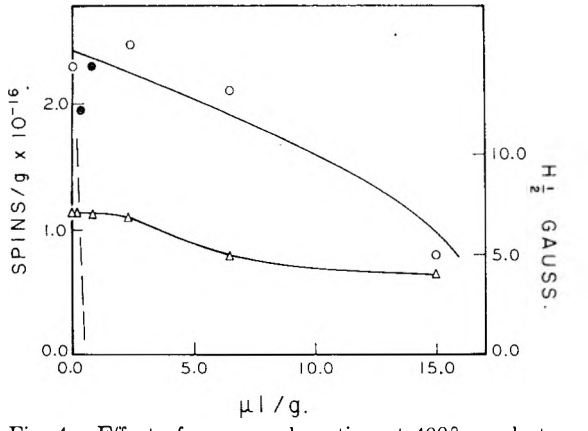

Fig. 4.—Effect of oxygen adsorption at 400° on electron spin resonance at room temperature: ○, spins/g., Run K28; ●, spins/g., Run K27 heat treated at 400°; Δ, half-width of adsorption signal. Dotted line corresponds to a decrease in the signal of one spin/adsorbed oxygen atom. Solid line for integrated intensity plot is calculated on the basis indicated in the discussion. (N_d was assumed to be 9×10^{17}/g.; this corresponds to $K_i = 3.2 \times 10^{19}$/cm.^{3}.)

tures. He assumed that the low temperature variety (henceforth called type A) was adsorbed $O^=$ ions and that the high temperature variety (type B) was adsorbed O^- ions. Barry and Stone,[9] in opposition to Morrison, postulate that type A adsorption occurs as O^- ions and type B adsorption occurs as $O^=$ ions that may be stabilized by the migration of excess zinc to the surface under the influence of the boundary layer potential.[13]

The data in Fig. 1 confirm the existence of type A and B chemisorption. The fact that no maximum in the isobar occurs at high temperatures is consistent with the supposition of Barry and Stone that migration of excess zinc, an activated process, accompanies type B adsorption. The slow adsorption above 400° that persisted for several days and the partial irreversibility of the adsorption also are consistent with a process involving bulk diffusion.

The results of adsorption experiments substantiate the suggestions of Barry and Stone, but little can be said about the charge of these adsorbed species without measurements of the change in the electronic state of the solid. The electron spin resonance signal has been shown to reflect changes in the number of free electrons. On the basis of the data in Table I, there can be little doubt that the signal observed for zinc oxide at $g = 1.96$ is due to un-ionized donors and/or conduction electrons. (Similar observations have been reported for other semiconductors.[14-16])

One cannot rule out the possibility that un-ionized donors contribute to the signal, but the lack of splitting due to the nuclear spin of gallium and aluminum for the doped samples together with the increase in the signal during ultraviolet irradiation of undoped samples are consistent with the interpretation that the signal is due to conduction electrons.

On the above basis the data in Fig. 3 and Fig. 4 can be interpreted in a straightforward fashion. In undoped zinc oxide conduction electrons are assumed to be produced by the following equilibrium

$$Zn_i \rightleftharpoons Zn_i^+ + e^-, \quad \frac{(Zn_i^+)(e^-)}{(Zn_i)} = K$$

where (e^-), (Zn_i) and (Zn_i^+) are the concentrations of conduction electrons, interstitial zinc, and interstitial zinc ions, respectively.[17] The assumed mechanism of oxygen adsorption can be represented as

$$\text{Type A: } {}^1/_2O_2 + e^- \longrightarrow O_s^-$$
$$\text{Type B: } O_s^- + Zn_i^+ \longrightarrow Zn_i^{++}\,O_s^=$$

where O_s^- represents an adsorbed ion and Zn_i^{++} $O_s^=$ represents an adsorbed $O^=$ on stabilized by the migration of an interstitial zinc ion to the surface.

For the degassed catalyst

$$\frac{(e_0^-)(Zn_i^+)}{(Zn_i)} = K = \frac{(e_0^-)^2}{(Zn_i)}$$

Where (e_0^-) is the electron concentration in the absence of adsorbed oxygen. Provided the ionization of Zn_i is only partially complete at 25°, we can write

$$(N_d) \equiv (Zn_i) + (Zn_i^+) \approx (Zn_i)$$

and hence, $(e_0^-)^2 = K(N_d)$. With the same approximation we can indicate the effect of adsorption on the species (Zn_i), (Zn_i^+) and (e^-) as

Type A adsorption:

$$(Zn_i) = (N_d) - (Zn_i^+) \approx (N_d)$$
$$(Zn_i^+) = (e^-) + (O_s^-)$$

Type B adsorption:

$$(Zn_i) = (N_d) - (Zn_i^{++}O_s^=) - (e^-)$$
or $$(Zn_i) \approx (N_d) - (Zn_i^{++}O_s^=)$$
$$(Zn_i^+) = (e^-)$$

In the above, the amounts of adsorption are expressed as adsorbed ions per unit volume of catalyst. When these values are substituted in the equi-

(13) K. Hauffe, *Advances in Catalysis*, **7**, 213 (1955).

(14) G. Feher, *Phys. Rev.*, **114**, 1219 (1959).

(15) G. Feher, D. K. Wilson and E. A. Gere, *Phys. Rev. Letters*, **3**, 25 (1959).

(16) J. Lambe and C. Kikuchi, *J. Phys. Chem. Solids*, **8**, 492 (1959).

(17) Recently, it has been suggested that the conductivity of undoped zinc oxide may be due to donors other than interstitial zinc. [D. G. Thomas, *ibid.*, **3**, 229 (1957).] Clearly, the above discussion would be applicable even if the donors were oxygen vacancies.

librium expression and this is solved for (e^-), we find

Type A adsorption:

$$(e^-) = \frac{-(O_s^-) + \sqrt{(O_s^-)^2 + 4(e_0^-)^2}}{2}$$

Type B adsorption:

$$(e^-) = \sqrt{(e_0^-)^2 - \frac{(e_0^-)^2}{(N_d)}(Zn_i^{++}O_s^=)}$$

wherein we have made use of the relation $KN_d = (e_0^-)^2$.

Since (e^-) and (e_0^-) are presumably determined by the integrated intensity of the signal, the derived expression for type A chemisorption, which contains no adjustable parameters, completely describes the data in Fig. 3. The solid line in Fig. 3 is calculated on this basis. The above expression for type B adsorption specifies the data in Fig. 4 in terms of the adjustable parameter (N_d); the solid line in Fig. 4 is that calculated for $N_d = 9 \times 10^{17}$ electrons/g.

The value of K determined by the above value of N_d is 3.2×10^{15} cm.$^{-3}$. It is possible to check the validity of this value by computing the value of the donor ionization E_d energy from the formula[5]

$$K = \frac{1}{2}\left(\frac{2\pi m^* kT}{h^2}\right)^{3/2} e^{-E_d/kT}$$

where m^* is the effective mass of the electron, h is Planck's constant, T is the absolute temperature and k is Boltzmann's constant. Reported values of m^* range from 0.1 to 0.5.[5] This leads to a value of E_d between 0.1 and 0.2 e.v. Values based on conductivities of powders are roughly 0.1 e.v. or less[5]; hence, the values of K and N_d are not unreasonable.

Finally, it should be noted that the above picture offers an explanation for the small effect of type B adsorption on Type A adsorption. Type A adsorption is an example of depletive chemisorption and as such is governed by the number of free electrons and the boundary layer potential. According to the derived equations type B adsorption affects the number of free electrons far less than type A adsorption; hence, the decrease of type A adsorption by the presence of pre-adsorbed oxygen should be far less if the pre-adsorbed oxygen is put on at 400° than when it is put on at 25°.

Acknowledgment.—We are grateful to Mrs. Olga Shaffer who ran some of the spectra reported herein. Acknowledgment also is made to the donors of the Petroleum Research Fund, administered by the American Chemical Society, for support of this research.

THE VOLUME CHANGE ON MIXING IN SOME BINARY LIQUID ALKALI NITRATES[1a]

BY B. F. POWERS, J. L. KATZ[1b] AND O. J. KLEPPA

Institute for the Study of Metals and the Department of Chemistry, The University of Chicago, Chicago 37, Illinois

Received July 28, 1961

The volume change on mixing has been measured in liquid mixtures of sodium nitrate with lithium, potassium, rubidium and cesium nitrates. It is found that the excess volumes are all *positive*. To a first approximation they may be represented by the empirical relation $\Delta V^E = +2.2 \times 10^4 X(1 - X)[(d_1 - d_2)/(d_1 + d_2)]^4$ cc./mole. Here X is the mole fraction in the mixture, while d_1 and d_2 are the interionic distances characteristic of the two pure salts.

Introduction

In a recent communication[2] the authors have reported some new information on the volume change on mixing in liquid mixtures of sodium nitrate–potassium nitrate. Based on 21 successful experiments at 350 and 425° we found that the excess volumes in this system are *positive* and, within our precision, independent of temperature. The maximum occurs near the 50–50 composition and is $+0.07 \pm 0.02$ cc./mole.

In the present communication we give a more detailed report on our study of the volume change on mixing in binary alkali nitrate systems which have sodium nitrate as a common component. Our results indicate that systems which do not have sodium nitrate or lithium nitrate as one of the components will have volume changes on mixing which are too small to be determined by our technique. Unfortunately, our attempts to study the other systems which have lithium nitrate as a common component so far have been inconclusive due to the thermal instability of this salt.

Experimental and Errors

The equipment used in the present work is a modified and improved version of an apparatus recently developed by one of the authors for determination of the volume change on mixing in liquid alloy systems.[3] The principal features will be readily understood from the schematic diagram given in Fig. 1 of ref. 3. The following modifications were made.

The ball and socket joint (on the axis CC in the earlier version) has been replaced by a standard taper joint. This permits rocking of the U-tube about the standard taper joint.

We also have attached a simple open end manometer to the surge volume bulb, to permit determination of the pressure inside the cell at any time.

The course of a typical experiment is as follows: The pure salts are melted and cast into sticks of a diameter slightly smaller than the inside diameter of the Pyrex U-tube. The two salts are weighed (total amount about $^1/_3$ the gram molecular weight) and placed in the two "legs" of the cell. These then are sealed off and the cell immersed in the salt-bath.

(1) (a) Work supported by the Office of Naval Research at the University of Chicago under Contract No. Nori 2121 (11); (b) American Chemical Society Petroleum Research Fund Predoctoral Fellow.

(2) J. L. Katz, B. F. Powers and O. J. Kleppa, *J. Chem. Phys.*, **35**, 765 (1961).

(3) O. J. Kleppa, *J. Phys. Chem.*, **64**, 1542 (1960).

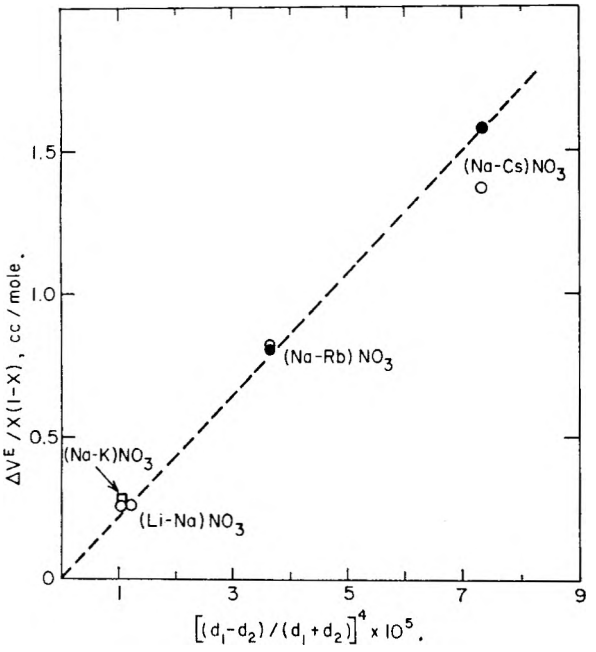

Fig. 1.—Dependence of the excess volume ($\Delta V^E/X(1 - X)$) on the parameter $(d_1 - d_2)/(d_1 + d_2)$. Open symbols, argon atmosphere; closed symbols, helium atmosphere.

To remove dissolved gases from the two molten salts the cell is maintained under a floor pump vacuum overnight. It then is filled with an inert gas (argon, helium) and connected by means of the 3-way stopcock (A) to the octoil-filled 0.1 cc. constant pressure gas "buret." After a constant volume has been achieved in the cell–capillary–buret system the two salts are mixed by gently rocking the cell for about 5 min. One or two additional 1 min. mixing periods were used to check for completeness of mixing. After mixing, a new constant volume is established in the system, and the excess volume is calculated from the volume increment. For further details on procedure and calculation the reader is referred to earlier work.[3] Most of our experiments were carried out with argon as the inert gas, although helium was used in some cases.

The lithium, sodium and potassium nitrates were Mallinckrodt Analytical Reagents, and were used without further purification. The rubidium and cesium nitrates were purchased as "99.9% pure or better" from the Millmaster Chemical Corporation, and were recrystallized once from distilled water before casting. In order to avoid possible thermal decomposition of the lower melting salt we adjusted the operating temperature of each series of experiments to a value slightly higher than the melting point of the higher melting salt (310° for lithium nitrate–sodium nitrate, 340° for sodium nitrate–rubidium nitrate and 425° for sodium nitrate–cesium nitrate).

The experimental results recorded in Table I adequately illustrate the magnitude of the random error in our experiments. However, they of course give no hint as to possible systematic errors. It is believed that the only potentially significant systematic error would arise from the possible difference in the solubility of the inert gas in the pure salts, on the one hand, and in the salt mixture on the other.

Very few data are available for the solubility of rare gases in molten salts and their mixtures. Protsenko and Bergman[4] report a solubility of xenon in the sodium nitrate–potassium nitrate eutectic of about 10^{-7} mole Xe/cc. solvent in the temperature range 260–450° at 1 atmosphere. In observations on fluoride melts Grimes, Smith and Watson[5] found the solubility of argon to be 2–3 times that of xenon, while that of helium is about 13 times that of xenon.

If we assume that these ratios apply also in the nitrate melts, we estimate a maximum total solubility of about 0.8 cc./mole of argon and about 3 cc./mole of helium in our fused salt mixtures. In the course of the present investigation we have been able to confirm that the solubilities are of this order of magnitude. On the other hand, we have been unable to find solubility data for the considered inert gases in the pure fused salts, and to make numerical estimates of differential solubilities.

However, since the actual solubility of helium in our salt melts presumably is about 4 times that of argon, its differential solubility also might be expected to be much larger than that of argon. Fortunately, our experimental results for sodium nitrate–rubidium nitrate and sodium nitrate–cesium nitrate, where we used both argon and helium as inert gases, give no indication of a large difference in differential solubility. Therefore, we conclude that our reported results are not modified significantly by differential solubility of the inert gas.

TABLE I

EXCESS VOLUMES IN BINARY LIQUID NITRATE SYSTEMS INVOLVING SODIUM NITRATE

System	Temp., °C.	Inert gas	Mole fraction, X_{NaNO_3}	$\Delta V^E/X(1 - X)$, cc./mole	
$(Na-K)NO_3$	350	Ar	0.3–0.7	0.26 ± 0.08 (mean of 9 expt.)	
	425	Ar	0.3–0.7	0.28 ± 0.08 (mean of 12 expt.)	
$(Na-Li)NO_3$	310	Ar	0.51	0.26	0.26 ± 0.02
			.51	.25	
			.50	.28	
			.51	.24	
$(Na-Rb)NO_3$	340	Ar	0.80	0.61	0.82 ± 0.10
			.50	.85	
			.50	.92	
			.49	.88	
		He	0.52	0.73	0.81 ± 0.06
			.52	.80	
			.51	.89	
$(Na-Cs)NO_3$	425	Ar	0.66	1.53	1.37 ± 0.12
			.62	1.45	
			.58	1.41	
			.46	1.49	
			.38	1.21	
			.35	1.16	
		He	0.51	1.67	1.58 ± 0.09
			0.51	1.50	

Results and Discussion

Our experimental data for all the four binary systems covered in the present study are presented in Table I. It will be noted that the excess volumes in all cases are *positive*, the values of $\Delta V^E/X(1 - X)$ ranging from about +0.26 cc./mole in sodium nitrate–lithium nitrate and sodium nitrate–potassium nitrate to +0.8 in sodium nitrate–rubidium nitrate and +1.5 in sodium nitrate–cesium nitrate. Thus, it is apparent that the excess volumes increase quite markedly with increasing difference in size between the two participating cations.

It is recalled here that in a recent study of the heats of mixing in the binary alkali nitrates, Kleppa and Hersh[6] found that these systems are all *exothermic*, and that the enthalpies of mixing to a good first approximation obey the semi-empirical relation

$$\Delta H^M = -140X(1 - X)[(d_1 - d_2)/(d_1 + d_2)]^2 \text{ kcal./mole}$$

In this expression d_1 and d_2 are the interionic

(4) P. I. Protsenko and A. G. Bergman, *J. Gen. Chem. U.S.S.R.*, **20**, 1365 (1950).

(5) W. R. Grimes, N. V. Smith and G. M. Watson, *J. Phys. Chem.*, **62**, 862 (1958).

(6) O. J. Kleppa and L. S. Hersh, *J. Chem. Phys.*, **34**, 351 (1961).

distances characteristic of the two pure salts. The numerical factor (140 kcal./mole) is of the order of magnitude of the lattice energies of the salts. The simplicity of this equation has aroused considerable interest. It begs the question whether equally simple relations may apply for the other excess thermodynamic functions, and notably for the excess volumes considered in the present work.

In order to obtain an answer to this question we have plotted our excess volume data against different powers of the parameter $(d_1 - d_2)/(d_1+d_2)$. Figure 1 shows that we obtain a reasonably good straight line that passes through the origin in a plot against the fourth power of this parameter. This suggests for the excess volume an empirical relation of the type

$$\Delta V^E = +V'X(1 - X)[(d_1 - d_2)/(d_1 + d_2)]^4$$

For the considered alkali nitrate mixtures, the value of the numerical constant V' is about 22,000 cc./mole.

It was shown by Longuet-Higgins,[7] in his theory of conformal solutions, that any first-order solution theory will predict the same sign for all the excess thermodynamic functions (ΔF^E, ΔH^E, ΔS^E and ΔV^E). Thus, our volume and enthalpy data for the considered alkali nitrate systems demonstrate that a satisfactory theory for these mixtures must be second order or higher. An attempt has been made recently to account for the observed enthalpies of mixing by means of second-order conformal solution theory.[8] However, no similar attack has been made as yet on the problem of the excess volumes

(7) H. C. Longuet-Higgins, *Proc. Roy. Soc.* (London), **A205**, 247 (1951).

(8) H. Reiss, J. L. Katz and O. J. Kleppa, *J. Chem. Phys.* (in press).

PERTURBATIONS OF THE NICKEL METAL K X-RAY ABSORPTION EDGE DUE TO SMALL CRYSTAL SIZE AND HYDROGEN CHEMISORPTION

BY P. H. LEWIS

Texaco Research Center, Beacon, New York

Received July 31, 1961

The X-ray absorption edge of small nickel crystals (*ca.* 30 A.) has been found to have small perturbations from that of bulk nickel. The perturbation has different characteristics from those observed when gases are adsorbed. The small crystal perturbations have been tentatively associated with the possession of atom-like energy states. The effect of chemisorbed hydrogen on the electron-empty energy levels of the small crystal nickel is qualitatively the same as that of chemisorbed oxygen, but quantitatively about half as small. It is suggested that the changes in catalyst absorption edge spectrum due to gas chemisorption are better correlated with the gas molecules spreading surface atoms apart rather than with an increase in potential field about each atom.

Introduction

Although catalytic reactions on the surfaces of small metal crystals have been studied extensively, the knowledge of many fundamental aspects is still incomplete. Little is known about how the energy levels of these crystals are affected by their crystal size, their contact with support materials or with adsorbed gases. X-Ray spectroscopy can be used to study those energy levels (closely grouped to form bands) that are affected when the metal crystals are small enough (*ca.* 50 Å. or smaller). Then the atoms on the surface form a sufficiently large fraction of the total so that perturbation effects are not diluted beyond observation by large numbers of unaffected interior atoms. The bands that are affected are in an energy region roughly 40 e.v. wide and, for nickel, 8 k.e.v. above the Bohr K-level. Energy levels in the lower 10 e.v. part contain valence electrons. For nickel metal these valence electrons occupy the 3d and the lower part of the 4s band. Since these bands contain electrons, they should be studied using the profiles of X-ray emission lines. The energy bands in the upper 30 e.v. section: the higher energy part of the nickel 4s band and the entire 4p band, can be studied using metal absorption edge[1] measurements since they have no electrons in them. It is with these last bands that this paper will be concerned. The X-ray spectral methods measure the density of energy levels, the extent of electron filling, and their angular momentum quantum number.

The first object of this paper is to show the differences between the K X-ray absorption edge of very small nickel crystals and that of bulk metal. The second object is to compare the catalyst nickel X-ray absorption edge after the chemisorption of hydrogen with that after the chemisorption of oxygen. The similarities found in this comparison tend to lead to a unified picture of the effect of chemisorbed gas on a metal.

Since the mathematical methods used to study the X-ray absorption edge were not conventional, a description of these precedes the experimental results.

Use has been made of X-ray absorption edge spectra to measure solid state characteristics of catalysts. The valence state of supported transition metal oxides[2] has been determined. A study has been made of the absorption spectrum 10–100 e.v. above the edge discontinuity.[3] The problems connected with the observation of small changes in the X-ray absorption spectrum of metals due to chemisorbed gas have been shown to be surmount-

(1) An absorption edge occurs when the X-rays have just sufficient energy to raise an inner electron to the empty levels. A discontinuous change in absorption coefficient as a function of X-ray wave length characterizes the edge.

(2) (a) H. P. Hanson and W. O. Milligan, *J. Phys. Chem.*, **60**, 1144 (1956); (b) R. O. Keeling, Jr., *J. Chem. Phys.*, **31**, 279 (1959).

(3) R. A. Van Nordstrand, *Advances in Catalysis*, **12**, 149 (1960).

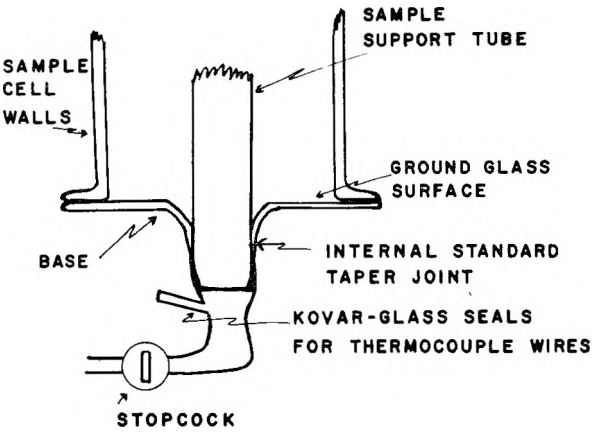

Fig. 1.—Sample support.

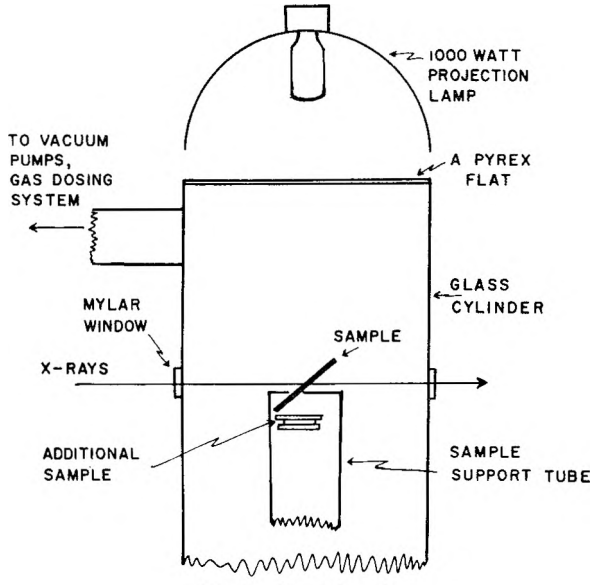

Fig. 2.—Sample cell.

able in a study of the effect of chemisorbed oxygen on nickel.[4]

The chemisorption of hydrogen on nickel has been studied with conductivity,[5] magnetic susceptibility[5] and surface dipole measurements.[6] These investigations have shown that the bond formed is probably covalent and the nickel–hydrogen dipole is small, the hydrogen being negative.

Experimental

A. The X-Ray System and Procedures.—The X-ray apparatus, method of collection of data and analysis of error have been described.[1] Some check runs were made using a Von der Hyde double-crystal attachment to the Philips spectrometer and germanium crystals.

B. Vacuum System.—With the exception of the mechanical pump, the entire vacuum system was mounted on a flat, wooden board (equipped with height adjusting screws) so that the sample could be removed from the X-ray beam. This board was cut so as to fit the angle formed by the diffractometer base and the X-ray tube housing. This permits reproducible positioning of the sample to the X-ray beam. The sample was supported on a glass tube that fits into the internal standard taper joint of a glass base made as shown in Fig. 1.

This glass base was cemented to the sample cell, shown in Fig. 2, with DeKhotinsky cement. The cell's 6.35 cm. diameter glass cylinder has slits cut into it for the passage of X-rays. These were covered with 1 mil mylar that is cemented to the glass with Bonding Agent[7] R-313. These windows were cooled with air jets. Rays from a 1000 watt projection lamp in an ellipsoidal reflector[8] were used to heat the sample.

The sample wafer was mounted in slots cut in the end of an 18 mm. diameter glass tube at an angle of 45° with respect to the tube axis. This position permits the sample to intercept both X-rays and heat rays.

The attachment of the cell to vacuum pumps and gas dosing system was made demountable. The connection was sealed with Apiezon W. The pumping system consisted of a mechanical pump, an oil diffusion pump and a liquid nitrogen trap. Gas, stored in a bulb, was admitted to the sample cell by means of a calibrated, 0.1 cc. dosing stopcock. The gas pressure in the bulb was measured with a mercury manometer.

The temperature of the sample was measured with an iron–constantan thermocouple. Higher gas pressures in the sample cell were measured with a thermocouple gage, RCA 1946; lower pressures with a cold cathode Miller gage.

C. Materials.—The catalyst was prepared by impregnating Davison silica gel 12 with a water solution of Baker's reagent grade nickel nitrate. This silica support was chosen because very small nickel crystals with high hydrogen adsorptive capacity had been obtained.[5a] The powder, after drying, was compressed into sheets 0.02 cm. in thickness. A 2 × 2 cm. square was cut from the sheet and placed in the slots of the 18 mm. glass tube shown in Fig. 2. This sheet attenuates the intensity of the X-rays by a factor of 20 on the high energy side of the absorption edge. Additional catalyst powder was placed just beneath this sheet in the sample support tube. This additional catalyst material helps to improve gas adsorption measurements and reduce contamination. The total sample in the cell weighed about 0.3 g. X-Ray absorption measurements were used to calculate[4] the nickel content of the catalyst to be 6.9%.

The maximum number of hydrogen atoms adsorbed per nickel atom, measured at 25° and 0.1 mm. pressure, was 0.12 (24 cc. (STP)/g. Ni). This capacity compares favorably with that previously reported[5] for Davison silica supported nickel, 40 cc. (STP)/g. Ni, measured at −78° and at 100 mm.

No measurement of the crystallite size of the catalyst nickel was attempted. The apparatus used for the X-ray absorption work is not suited for determination of the catalyst sample nickel crystal size by X-ray diffraction, high resolution electron microscopy, magnetic measurements, or gas adsorption at low temperatures. The work of Schuit and van Reijen[5a] with the same nickel on Davison silica gel catalyst that was used shows that the nickel crystals have a diameter of about 30 Å.

Matheson electrolytic hydrogen, cleaned of residual oxygen by passage through a tube filled with hot (350°) copper and thence through a liquid nitrogen-cooled trap, was used. The results subsequently were checked using palladium-filtered hydrogen. Linde oxygen was used without further purification.

D. Experimental Procedure.—All the work was based on a "bare" nickel catalyst in which the nickel is free of oxygen. The preparation was begun by raising the sample temperature to 350° under a vacuum of 10^{-2} mm. The degassed sample was reduced with hydrogen for 15 hr. at 350°. The cell subsequently was pumped down to a residual pressure of 1×10^{-4} mm. with the sample at 350°. When the sample was cooled to room temperature, the pressure in the cell fell to 1×10^{-5} mm. The entire procedure was repeated before obtaining X-ray data. The effect of hydrogen on this bare nickel was obtained by passing hydrogen over the sample at room temperature, maintaining the pressure at 1 atm.

Analysis of the X-Ray Data.—The raw experimental data of an X-ray absorption edge study are the ratios of the intensity of the monochromatic X-ray beam before passing through the

(4) P. H. Lewis, *J. Phys. Chem.*, **64**, 1103 (1960).

(5) (a) G. C. A. Schuit and L. L. van Reijen, *Advances in Catalysis*, **10**, 242–5 (1958); (b) P. W. Selwood, *ibid*, **9**, 93 (1957).

(6) M. H. Sachtler and G. J. H. Dorgelo, *J. chim. phys.*, **54**, 27 (1957).

(7) Made by Carl H. Biggs Company of Los Angeles.

(8) E. H. Nicollean, G. R. Gunther-Mohr and L. R. Weisberg, *I.B.M. J. Research and Development*, **1**, 349 (1957).

sample, I_0, to those after passage, I. These ratios are related to the mass absorption coefficient of the sample, μ_m, the density of the sample, ρ, and the thickness of the sample, t, by

$$\log (I_0/I) = \mu_m \rho t/2.303$$

It is the measurements of the mass absorption coefficient of the nickel that will show how the energy levels of the metal are affected. One cannot make direct use of catalyst absorption measurements alone to study the state of catalyst nickel. First, the absorption by the support must be subtracted. Second, the change in metal absorption is a very small fraction of the catalyst absorption. Third, because angular settings of the monochromator crystal cannot be determined exactly, there is a need for a continuous calibration as the wave length of the monochromatic X-rays is changed. The basic technique[4] for overcoming these difficulties is based on taking absorption data for the catalyst sample, s, and for a thin, bulk metal foil, f, at each angular position of the monochromator crystal. If the catalyst nickel has the same energy band characteristics as that of the bulk nickel metal, the logarithmic plot of these X-ray absorption edge data will obey the straight line relationship

$$\log (I_0/I)_s = A \log (I_0/I)_f + B$$

Here, the intercept B is equal to $\mu_m\ t/2.303$ for the silica support. It is a constant for the small range of X-ray wave lengths used in studying an absorption edge. The slope A is the ratio of the product, $\mu_m t$, for the catalyst metal to that for the bulk nickel foil. When the two nickel metals are in the same state, the mass absorption coefficients for the two will be equal for X-rays of every wave length, A will be constant, and the linear plot of X-ray absorption data for catalyst *vs.* bulk nickel will be observed. When the catalyst nickel is perturbed, its mass absorption coefficient no longer need equal that for bulk metal for all the wave lengths of the X-rays used in studying the absorption edge. Then A will vary with wave length and a non-linear plot will be observed.

In the previous work,[4] non-linear behavior was noted when individual data points fell off the straight line by more than the experimental error. This method becomes useless when each deviation from the straight line is less than the experimental error calculated for a single point. Small non-linear deviations still can be detected by examining the data for trends. This can be understood by looking at Fig. 3. While the sums of the squared deviations from each line are the same, the data in one scatter randomly and in the other show a sinusoidal trend.

The detection of a non-random data trend can be made in two ways. The first is the method of mean square successive differences.[9] This technique uses two data. The first, Z_i, is the perpendicular distance of each point to the mean square straight line. The second, $Z_{i+1} - Z_i$, is the difference between the perpendicular distances for two adjacent data points. Each of these is squared and then summed using the total number of data points, n. The first sum, called S^2 and equal to $(1/n)\Sigma Z_i^2$, will be larger than the second sum, called δ^2 and equal to $(1/(n-1))\Sigma(Z_{i+1} - Z_i)^2$, if a non-random trend occurs. The actual ratio, δ^2/S^2, called k, has been analyzed statistically[9] to determine the probability that a trend is non-random. For a given n, the smaller k is, the less random the data.

The second technique used to analyze for trends is based on the trite axiom that the slope and intercept of any part of a straight line must be equal to the slope and intercept of the entire line. The slope and intercept determined using a part of the X-ray data must be equal to those determined using all the X-ray data, if the metal in the sample has the same state as the bulk metal. If the catalyst metal is perturbed, the inequality of the appropri-

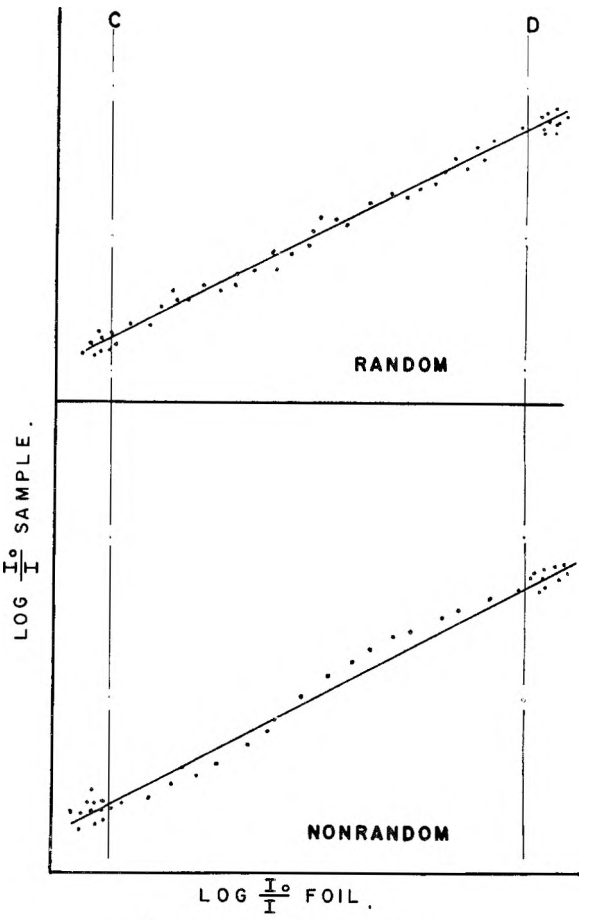

Fig. 3.—Kinds of data scatter.

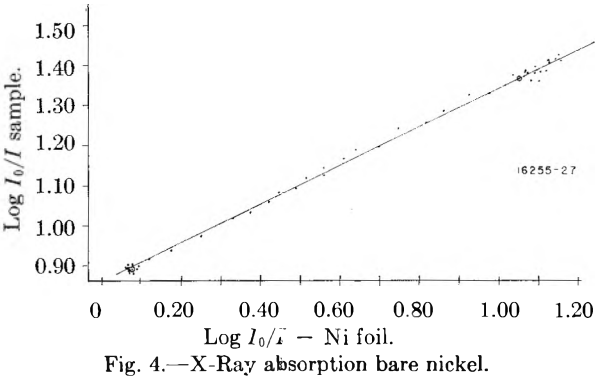

Fig. 4.—X-Ray absorption bare nickel.

(9) C. A. Bennett and N. L. Franklin, "Statistical Analysis in Chemistry and the Chemical Industry," John Wiley and Sons, Inc., New York. N. Y., 1954, pp. 677–684.

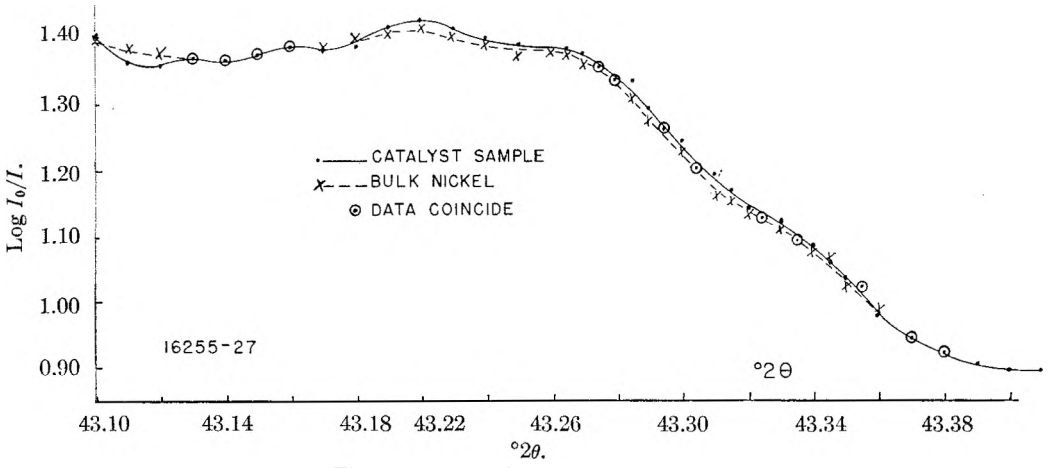

Fig. 5.—X-Ray absorption bare nickel.

ate straight line parameters describes the kind of perturbation and its amount. The method will be called the inequality technique.

A number of considerations must be heeded in this analysis. It is necessary that the number of data points in any given subdivision of the data be large so that the calculated slope and intercept have sufficient precision. Second, the subdivision must be made in the same manner for each run and should have physical significance. Third, the method cannot be used in studies involving the greater perturbations of X-ray absorption data that occur in plots of data for nickel metal *vs.* completely oxidized catalyst nickel. Then the mid-range data can no longer be approximated by a straight line.

Segregation of the data is done as follows. Preexamination of Figs. 4 and 6 shows that the log–log plots consist of two clusters of data connected by a string of data points. Least squares analysis using only the data in the two clusters leads to "end-point" results; the string of data points, "mid-range results"; and all the data, "all data." The clusters of data occur where the metal X-ray absorption is relatively invariant with wave length. The lower cluster is connected with the excitation of nickel L-shell electrons to very high energy bands. The magnitude of X-ray absorption due to this excitation is constant over the absorption edge. Only statistical scatter of the data points is to be expected. The upper cluster is associated with the excitation of nickel K-shell electrons to the high energy boundary of the 4p band and beyond. These points also scatter sufficiently to be considered random. The "mid-range" data are connected with excitation to the 4s and 4p bands of nickel. The number of data points in this mid-region is roughly half of the 56 points taken.

The great advantage of both methods is the great improvement in sensitivity over that of the "one point" type used previously.[4] One oxygen atom per 30 nickel atoms can be detected instead of but one per 10.

Experimental Results

X-Ray Absorption Characteristics of Bare, Small Crystal Nickel.—A log–log plot of observed X-ray absorption data for the bare, small crystal nickel on Davison silica gel-12 *vs.* that for bulk nickel foil is shown in Fig. 4. The straight line was obtained by a least squares treatment of the end-point data. The experimental points having abscissa 0.7–1.0 tend to have high ordinates. A more conventional plot of the X-ray absorption data for both catalyst and bulk nickel foil *vs.* angular setting of the monochromator is in Fig. 5. In Fig. 5 the catalyst data are plotted as observed. The bulk nickel foil data were scaled from observed data by multiplying by the slope, A, and adding the intercept, B, to each product using end-point values for A and B. The plot shows that the general shape of the catalyst nickel X-ray absorption curve is the same as that of bulk metal except for a small increase in absorption coefficient in the central part of the data, 43.18–43.32° (2θ).

The accumulated analytical results for nine runs are listed in Table I.

TABLE I

X-RAY ABSORPTION RESULTS FOR BARE, SMALL CRYSTAL NICKEL

The inequality technique

	Av. slope	Av. intercept
All data	0.492 ± 0.008	0.805 ± 0.005
Mid-range	.503 ± .007	.802 ± .008
End-points	.490 ± .008	.803 ± .005

T-value (Mid-range, end-point slope data) 3.25
Chance of coincidence 1 in 400

The method of mean square successive differences
Typical k values 1.04, 0.90, 1.22
Probability of non-random run 0.999

The table shows the averages of mid-range and end-point slopes to differ by about twice the root mean square error. A Student's Test[10,11] was applied to this difference to show that coincidence of these two slopes has a probability of less than 1 in

(10) The factor T is calculated by

$$T = \frac{\bar{X}_1 - \bar{X}_2}{S_p(N_1^{-1} + N_2^{-1})^{1/2}}$$

where $\bar{X}_1$, $\bar{X}_2$ are the averages of each group, N_1, N_2 are the number of data in each group, and $S_p = \left[\frac{N_1\sigma_1^2 + N_2\sigma_2^2}{N_1 + N_2 - 2}\right]^{1/2}$. The value of T calculated is correlated with the probability that $\bar{X}_1$ and $\bar{X}_2$ be different in reference 11.

(11) W. J. Dixon and F. J. Massey, "Introduction to Statistical Analysis," McGraw-Hill Book Co., New York, N. Y., 1951, p. 101–105.

400. Typical k values correspond to a high probability of a non-random deviation from linearity.

These measurements of non-linear behavior show the small crystal nickel is not in the same electronic state as that of bulk metal. The perturbation due to small crystal size is characterized by differences between slopes calculated using the three methods of collecting data that are not observed in the intercept data.

Some concern was given to the possibility that the small crystal effect might be due to a systematic instrumental factor. To test this, the X-ray absorption data for nickel catalysts having a smaller hydrogen adsorptive capacity as compared to the nickel/Davison silica gel 12 catalyst were run. The smaller hydrogen adsorption was indicative of larger nickel crystals.[12] For these the differences in slope were less than the root mean error. Moreover, a large k value, 1.9, indicated a very low probability of a non-random trend. It was concluded that what had been observed for the small nickel crystals was not due to instrumental factors.

There is still the possibility that the small crystal effect might really be due to contamination. This might occur either through incomplete reduction of the nickel or through incomplete removal of residual gas from the cell. Incomplete reduction does not seem likely because the X-ray absorption characteristics of the small crystal sample do not change after a total of 180 hr. of reduction. Usually 36 hr. is more than adequate to obtain catalyst metal having the X-ray absorption characteristics of bulk metal when the metal crystals are larger. The maximum amount of surface oxygen contamination possible was calculated to be less than 12% of a monolayer.[13] The small crystal effect moreover, will be, shown to be different in X-ray characteristics from that observed when the small metal crystals have adsorbed gas on their surface.

Schuit and van Reijen[5a] have shown that a thin skin of silica can be formed on nickel crystals. The conditions for forming this skin include forming the catalyst by coprecipitation and heating it to temperatures above 400°. Since the sample used in the present X-ray work was made by impregnation and never heated above 350°, it was concluded that the thin silica skin never was formed on the nickel crystals used. The small crystal X-ray effect observed therefore is not to be correlated with the formation of this silica coating.

The Hydrogen Effect on Nickel X-Ray Absorption Characteristics.—The easy observation of the effect of hydrogen on the nickel X-ray edge is a nasty problem in that an optimum crystallite size is required. If the nickel crystals are too big, the small amount of hydrogen adsorbed will produce no measurable X-ray effect. If the crystallites are too small, one is faced with the problem (not insurmountable) that the weak hydrogen effect on the bulk metal state of the catalyst nickel occurs simultaneously with a relatively large small crystal perturbation. For easy observation the nickel crystal size should be such that the perturbations should be of comparable magnitude. The log–log plot of X-ray absorption data for such nickel supported on Davison silica gel-12 exposed to hydrogen *vs.* that of bulk nickel metal is shown in Fig. 6; the more conventional plot in Fig. 7. The sinusoidal distortion of the X-ray absorption edge of the bulk metal state by hydrogen can be observed in these figures. It is characterized in the analytical results of Table II by a slope in the mid-range that is larger than the other slopes calculated; and an intercept that is smaller.

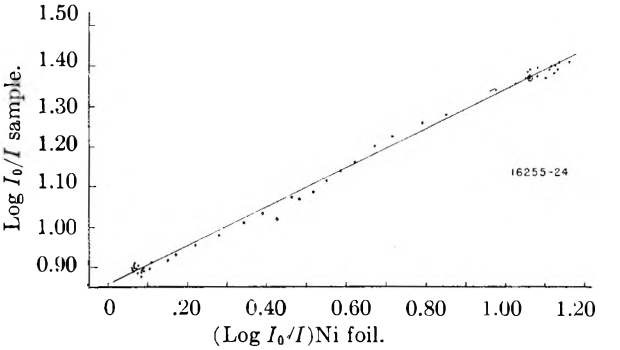

Fig. 6.—X-Ray absorption nickel-hydrogen.

TABLE II

X-RAY ABSORPTION RESULTS FOR NICKEL EXPOSED TO HYDROGEN

	The inequality method	
	Av. slope	Av. intercept
All data	0.494 ± 0.005	0.800 ± 0.004
Mid-range	.518 ± .005	.786 ± .005
End-points	.489 ± .005	.801 ± .006
T-values	7.5	3.3
Chance of coincidence	1 in 400	1 in 400
Method of mean square successive differences		
Typical k values	0.75, 1.13, 1.23	
Probability of non-random run	0.999	

It again is clear that the plot of the X-ray absorption data for catalyst nickel with hydrogen adsorbed on it *vs.* that for bulk foil is not linear.

The perturbation of the nickel X-ray absorption edge is smaller but qualitatively the same as that observed[4] when oxygen is the chemisorbed gas. This raises the possibility that the effect is due to an oxygen impurity that is adsorbed preferentially. A review of the experimental section shows that care was taken to keep the oxygen content of the hydrogen at a very low figure. It is more convincing, however, that the hydrogen effect can be removed by heating the sample to 350° in a high vacuum. It was found that deliberately added oxygen could not be pumped off. It is realized that thermal regeneration of oxidized metal surfaces does occur through incorporation of the oxygen into the bulk of the metal. The X-ray absorption technique is sensitive to gas whether it be on the surface, in the interior of the small metal crystals, or on the surface in small patches. The disappearance of the hydrogen effect on the X-ray data shows that the gas has left the metal. The gas

(12) S. F. Adler and J. J. Keavney, *J. Phys. Chem.*, **64**, 208 (1960); L. Spenadel and M. Boudart, *ibid.*, **64**, 204 (1960).

(13) One oxygen atom per 30 nickel atoms can be detected by the X-ray method. For 30 Å. crystals, 26% of the metal atoms are on the surface.

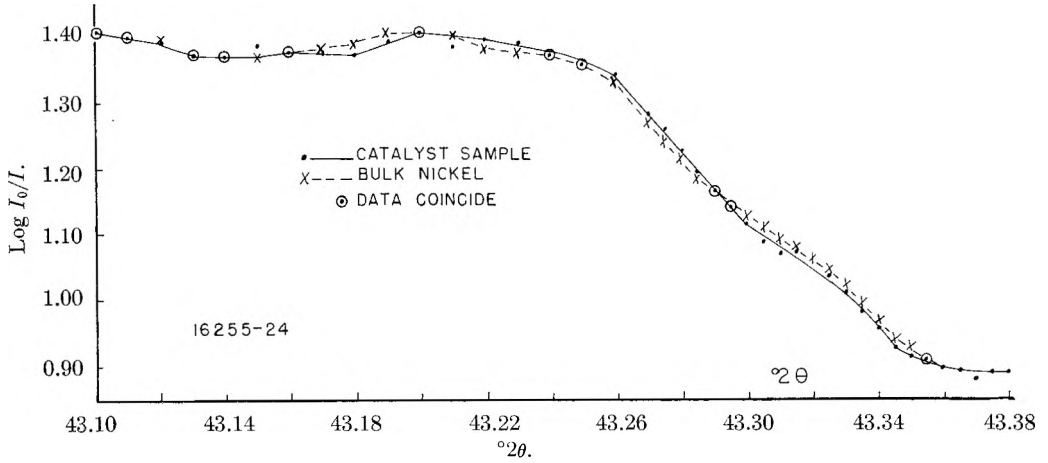

Fig. 7.—X-Ray absorption nickel–hydrogen.

must be, therefore, hydrogen. The work was further checked by using palladium-filtered hydrogen.

Discussion

A picture for interpreting the X-ray results obtained after the chemisorption of oxygen by nickel has been described.[4] To review the fundamentals: (1) The X-ray absorption edge can be divided into two energy sections. The first section, associated with the 4p band, lies between 43.18 and 43.29° (2θ) in Fig. 7. The second section, associated with the 4s band, lies between 43.29 and 43.36° (2θ). (2) The magnitude of an absorption coefficient for X-rays of energy E is governed by the product of the density of empty levels at energy E above the K level (or level of origin of the excited electron) times the probability that the X-rays can excite an electron. (3) This probability is governed by the selection rule that an electron can be excited from one level to another if the resulting change of angular momentum is one. The absorption coefficient measured with K electron excitation is, therefore, a mirror of the amount of p character of the bands. (4) A metal, due to hybridization, has a 4p band with decreased p character and a 4s band with some p character. (5) The effect of gas chemisorption is to reduce the metal's hybridization: the p content of the 4s band is reduced and that of the 4p band increased. (6) The change in the angular momentum makeup of the bands is due to the increase in the depth of the potential well in which the metal atom exists upon transfer of charge.

Since hydrogen affects the absorption edge in much the same way as oxygen does, this same interpretation should be attempted. It generally is successful except for the last statement, (6). Comparing the differences in slope and intercept that are observed when hydrogen is adsorbed with those due to an equal amount of oxygen, the oxygen has 2 times the effect that hydrogen does. The error of this ratio is extremely large, ±1. This ratio should be compared with that obtained by magnetic measurements. The decrease in magnetization was found to be equal for oxygen and hydrogen.[5a] The large error in the X-ray absorption result makes unprofitable any speculation about the discrepancy between the X-ray and magnetic methods, interesting as it may be. It is surprising that hydrogen should exert as much influence on the nickel as it does. The nickel–oxygen bond has a 50% ionic character; the nickel–hydrogen bond but 3%.[14] The X-ray results, at least, do not respond in a way proportional to the charge displacement that the ionic character calculations indicate. To attribute the X-ray effects observed as being due to the deepening of the potential well about the metal atom seems difficult. An alternate explanation might be mentioned. Goodenough[15] has shown that the conductivity of 3d transition metal oxides decreases both with atomic number and distance between atoms. He suggests that this intermetal distance is quite critical. Thus for small distances between metal atoms, electrons are delocalized; for larger distances, localized to each atom site. To put it slightly differently, when the metal atoms are closely spaced the valence electron energy levels are common to the crystal as a whole and are metallic in character (have mixed angular momentum character) and become atomic in character (have pure angular momentum characteristics) when the atoms are further apart. To apply this theory to chemisorption it must be assumed that chemisorbed atoms spread the surface metal atoms apart by situating themselves in the interstices between the atoms of the surface. Some estimate of this deformation of the metal surface may be obtained by examining the lattice parameters, a_0, of nickel compounds.

TABLE III

LATTICE CONSTANTS OF NICKEL COMPOUNDS

	a_0, Å.	Deformation, %
Nickel[16]	3.53	0
Nickel hydride[17]	3.73, 3.83	5.7, 8.5
Nickel oxide[16]	4.18	18.4

(14) Calculated from electronegativity data from L. Pauling, "Nature of the Chemical Bond," Cornell University Press, Ithaca, N.Y. 1939 and from A. L. Allred and E. G. Rochow, *J. Inorg. & Nuclear Chem.*, **5**, 264 (1958).

(15) J. B. Goodenough, *Phys. Rev.*, **117**, 1442 (1960).

(16) H. F. Swanson and E. Tatge, "Standard X-ray Diffraction Powder Patterns," Vol. 1, Natl. Bur. Standards Circular 539, p. 13, 47.

(17) A. Janko and Pierre Michel, *Compt. rend.*, **251**, 1001 (1960). Two nickel hydride phases have been found. Both are face-centered cubic but have different lattice constants.

It is notable that the ratio of deformations, 3.2 to 1, or 2.2 to 1, depending on the lattice constant for nickel hydride, is closer to the X-ray effects observed than that calculated using per cent. ionic character. The placing of the hydrogen (and oxygen) atoms in the interstices of the metal surface layer fits in with the lack of observation of a Ni–H absorption band in the infrared.[18] This negative result was interpreted by these authors as being due to bonding of the hydrogen to two or more metal atoms. The interstitial position of the adsorbed gas atom also has been suggested by Mignolet[19] and Farnsworth.[20]

Sufficient theoretical background has not been developed to enable one to determine from the X-ray absorption data whether a given bond is covalent or ionic. Indeed, if it is the latter, it is not clear from the X-ray data which way the dipole is oriented. It should be noted, however, that the effect of hydrogen on nickel is not confined to an effect on the 3d electrons but further encompasses perturbations of the 4s and 4p bands of the metal.

While a mode has been developed for interpreting the X-ray absorption edge changes that occur after gas adsorption, an interpretation of the small crystal effects is by no means clear. It is not surprising that a perturbation of the X-ray absorption edge should be observed for a sample of metal crystals approaching atoms in size. Mott[21] has, in fact, suggested that the main effect of atomization of a large metal crystal would be that the bands would lose their hybrid symmetry characteristics. While this is a plausible explanation for the enhanced X-ray absorption in the small crystal's 4p band, a decrease in absorption in the 4s band was not observed.

It is conceivable that the enhanced X-ray absorption is due to the additional surface energy levels proposed by Tamm.[22] No firm correlation can be made, however, of the present X-ray observations with the Tamm levels.

One importance of the observation of a small crystal size effect on the X-ray absorption data is the possibility of extending X-ray size measurements below 50 Å. For smaller crystals than this[12] the X-ray diffraction lines become so broad as to become indistinguishable from background. The perturbation of the X-ray absorption edge should be greater (and hence more easily observed) the smaller the crystal size. It is evident that empirical and theoretical work is required before the X-ray absorption edge measurements can be used to make quantitative measurements of crystallite size.

Acknowledgment.—The author would like to thank Mr. McNelly for obtaining the X-ray data and making the mathematical computations. Discussions with members of the Physical Research Section of the Texaco Research Center have been most helpful.

(18) R. P. Eischens and W. A. Pliskin, *Advances in Catalysis*, **10**, 1 (1958).

(19) J. C. P. Mignolet, *Bull. soc. chim. Belges*, **67**, 358 (1958).

(20) T. H. George, H. E. Farnsworth and R. E. Schlier, *J. Chem. Phys.*, **31**, 89 (1959).

(21) N. F. Mott, *Proc. Phys. Soc.*, (London), **62A**, 416 (1949).

(22) See, for example, F. Seitz, "Modern Theory of Solids," McGraw-Hill Book Co., New York, N. Y., 1940, pp. 320–326.

DETECTION OF METAL ION HYDROLYSIS BY COAGULATION. IV.[1] ZINC[2]

BY E. MATIJEVIĆ, J. P. COUCH AND M. KERKER

Department of Chemistry, Clarkson College of Technology, Potsdam, New York

Received August 4, 1961

The coagulation method has been used to determine the charge of zinc ions in aqueous solution at various *p*H's. Coagulation concentrations of zinc nitrate solutions for negative silver bromide sol *in statu nascendi* were obtained over a *p*H range from 2.0 to 8.7. At *p*H <6.7, these indicate simple divalent (hydrated) zinc ions. Above *p*H ~8, there is a hydrolyzed species with a charge of +3. This corresponds to a polynuclear zinc complex with the general formula $[Zn_{2+n}(OH)_{2n+1}]^{+3}$. For a Zn:OH ratio of 1:1, the formula would be $Zn_3(OH)_3^{+3}$, which can be represented structurally as a six-membered ring. The possibility of the existence of Zn_2OH^{3+} also is discussed. Electrophoretic mobility data show that *hydrolyzed* zinc ions adsorb on the AgBr particles strongly and may, above a certain concentration of zinc, reverse the charge of the sol particles.

Introduction

Although the hydrolysis of aqueous solutions of zinc salts has been studied by numerous investigators,[3–16] there is no general agreement among their results. Except for Kullgren,[3] who measured the inversion of sucrose at elevated temperatures, this work has been based upon *p*H measurements and potentiometric titrations of zinc salt solutions

(1) Part III, E. Matijević, K. G. Mathai, R. H. Ottewill and M. Kerker, *J. Phys. Chem.*, **65**, 826 (1961).

(2) Supported by the Office of Ordnance Research Contract No. DA-ORD-10.

(3) C. Kullgren, *Z. physik. Chem.*, **85**, 466 (1913).

(4) F. Achenza, *Ann. chim.* (Rome), **48**, 565 (1958).

(5) L. S. Lilich and Yu. S. Varshavskiĭ, *J. Gen. Chem. U.S.S.R.*, **26**, 337 (1956).

(6) S. DeMende, *Compt. rend.*, **226**, 916 (1948).

(7) H. Guiter, *Ann. chim.* (Paris), **2**, 72 (1947).

(8) É. Carrière, H. Guiter and M. Annouar, *Bull. soc. chim. France*, 72 (1947).

(9) É. Carrière, H. Guiter and M. Annouar, *ibid.*, 405 (1946).

(10) H. F. Brown and J. A. Cranston, *J. Chem. Soc.*, 578 (1940).

(11) H. Hagisawa, *Bull. Inst. Phys. Chem. Research* (Tokyo), **18**, 368 (1939).

(12) J. Guéron, *Compt. rend.*, **195**, 150 (1932).

(13) I. M. Kolthoff and T. Lameda, *J. Am. Chem. Soc.*, **53**, 832 (1931).

(14) V. Čupr, *Z. anorg. u. allgem. Chem.*, **198**, 310 (1931).

(15) H. G. Denham and N. A. Marris, *Trans. Faraday Soc.*, **24**, 510 (1928).

(16) M. Quintin, *Compt. rend.* **184**, 1657 (1927); *J. chim. phys.*, **24**, 712 (1927).

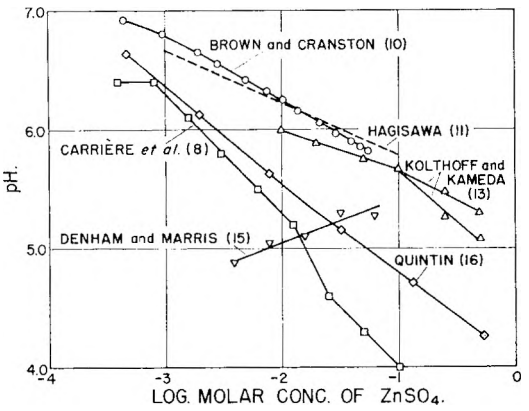

Fig. 1.—Graphical presentation of data available in the literature on *p*H values of aqueous solutions of zinc nitrate in various concentrations. The number in parentheses indicates the reference.

at various concentrations. Because zinc is only very weakly hydrolyzed, the *p*H varies slightly, even over rather wide ranges of concentration, and thus the measurements are rather precarious. It is not too surprising, then, that different investigators disagree markedly. In Fig. 1, we have depicted a number of published *p*H data for solutions of $ZnSO_4$ in order to demonstrate the enormous scatter of results. It is obvious that conclusions regarding the existence of hydrolyzed zinc species, based on such data, are hardly acceptable. Because of these difficulties, it would seem desirable to use another method for the detection of the hydrolyzed zinc species in aqueous solutions.

We already have shown[1,17,18] that coagulation of lyophobic colloids can be utilized successfully to determine ionic charge. For positive ions, the method is based upon the determination of the concentration of a salt solution necessary to coagulate a negative silver halide sol. Since the critical coagulation concentration as a function of ionic charge is well known,[19-21] it is possible to establish the ionic charge of the *counterions* in solution with great certainty. The formation of hydrolyzed species of a coagulating metal ion of a charge different from that of the simple nonhydrolyzed ion can be followed by determining the coagulation concentration at various *p*H values of the medium. In order to formulate the species unambiguously, this information about the ionic charge must be combined with knowledge of the metal to hydroxyl ratio (Me:OH). This can be obtained from potentiometric measurements.

In this work we have applied the coagulation method to the detection of the hydrolysis of zinc. The results indicate that at *p*H ~8, zinc hydrolyzes to form triply charged polymeric ions. In addition, both the coagulation and electrophoresis measurements show that these hydrolyzed species adsorb onto the silver bromide sol particles sufficiently to reverse the particle charge. The simple non-hydrolyzed zinc ions do not exhibit this behavior.

Experimental

All experiments were performed using a AgBr sol *in statu nascendi*. Turbidity changes were followed with time after mixing a solution of $AgNO_3$ (to give a final concentration of 1×10^{-4} *M*) with a solution of KBr (to give a final concentration of 2×10^{-3} *M*). $Zn(NO_3)_2$ was used as the coagulating electrolyte. The *p*H of the solutions was adjusted by addition of HNO_3 or NaOH. When NaOH was used, $AgNO_3$ and $Zn(NO_3)_2$ were in one solution and KBr and NaOH in another before they were mixed for coagulation measurements. A parallel number of systems was prepared without $AgNO_3$ in order to determine whether zinc hydroxide was formed. Only experiments in which the concentration of NaOH was small enough and no formation of zinc hydroxide precipitate ensued were utilized further. When HNO_3 was used, the HNO_3, $Zn(NO_3)_2$ and KBr were in one solution and the $AgNO_3$ in the other prior to mixing.

It has been shown that there is no significant difference between the behavior of silver bromide and silver iodide sols *in statu nascendi* relative to the charge determination and also that aged sols and sols *in statu nascendi* behave identically.[1] For this reason we have used only AgBr sols *in statu nascendi* for this work. Details of the coagulation technique have been described previously.[19,22]

Microelectrophoresis experiments were carried out using the same equipment as before.[1]

All chemicals were of the highest purity grade and water was doubly distilled from an all-Pyrex still. All glassware was carefully cleaned and steamed before use.

Results

Typical results are depicted in Figs. 2 and 3. The turbidity (τ) of the system 10 minutes after mixing the reacting components is plotted (full line) as a function of the concentration of $Zn(NO_3)_2$. Ten minutes has been shown to be critical for AgBr sols and the lower valent (1 to 3) counterions.[22] The corresponding *p*H is given by the dotted lines and the electrophoretic mobility (μ) by the dashed lines. The three examples chosen correspond to (a) addition of HNO_3 to give 1×10^{-3} *M*, *p*H ~ 3; (b) no addition of HNO_3 or NaOH, *p*H ~ 5–6; (c) addition of NaOH to give 1.6×10^{-4} *M*, *p*H ~ 7–8.

The critical coagulation concentration, which is obtained by extrapolation of the steep part of the coagulation curve to zero turbidity, is identical in the first two cases but is much lower at the higher *p*H. In addition, the turbidity curves at higher *p*H's exhibit a typical kink, such as that in Fig. 3, which is quite reproducible.

The electrophoretic mobility curves for the first two cases show that these sols remain negative over the wide range of concentration of added $Zn(NO_3)_2$, approaching zero only at the highest concentrations. The picture is quite different if *p*H $\geq$ 6.7. For example, in Fig. 3, with increasing concentration of $Zn(NO_3)_2$, the sol exhibits a zero electrophoretic mobility point and with still higher concentration the originally negatively charged sol becomes positively charged. We will show that the kink in the coagulation curves at higher *p*H is directly related to this reversal of charge.

A summary of the coagulation results is presented in Fig. 4. The critical coagulation concentration of zinc nitrate (expressed in molarity of the added salt) is plotted against the *p*H of the medium. Small arrows indicate points read from the coagulation curves in Figs. 2 and 3. The coagulation con-

(17) E. Matijević, M. B. Abramson, K. F. Schulz and M. Kerker, *J. Phys. Chem.*, **64**, 1157 (1960).

(18) E. Matijević and B. Težak, *ibid.*, **57**, 951 (1953).

(19) E. Matijević, D. Broadhurst and M. Kerker, *ibid.*, **63**, 1552 (1959).

(20) E. Matijević, K. F. Schulz and B. Težak, *Croat. Chem. Acta*, **28**, 81 (1956).

(21) B. Težak, E. Matijević and K. F. Schulz, *J. Phys. Chem.*, **59**, 769 (1955).

(22) B. Težak, E. Matijević and K. F. Schulz, *ibid.*, **55**, 1557 (1951).

centration remains quite constant up to pH ~6.7. There is a decrease at lowest pH's due to the coagulation effects of hydrogen ions. Above pH ~6.7, the critical coagulation concentration drops sharply over a rather narrow range of pH and then levels off again at a much lower value. It was not possible to extend the measurements to even higher pH because of the formation of insoluble zinc hydroxide.

Discussion

The Schulze–Hardy rule states that the higher the charge of a coagulating counterion, the lower its critical coagulation concentration. Earlier work with silver halide sols has given quantitative results which enable one to relate critical coagulation concentration and ionic charge.[19-21] We will now utilize these results to determine the ionic charge of the zinc ions involved in the coagulation process described above.

It is apparent from Fig. 4 that there are two predominant zinc species acting as coagulating cations; one at low pH for which the critical coagulation concentration of added $Zn(NO_3)_2$ is 1.4×10^{-3} M and the second at higher pH which coagulates at 1.6×10^{-5} M. The higher value corresponds exactly to that of simple doubly-charged counterions.[19-21] In Fig. 4, the critical coagulation concentration of Ba^{++} for the same AgBr sol is depicted by II. Since the value is the same as that for our system at low pH, it can be concluded that up to pH ~6.7 the predominant species in zinc salt solutions is simple (hydrated) zinc, Zn^{+2}.

Above pH ~6.7, the critical coagulation concentration decreases, leveling off at pH ~8, and thus indicating the hydrolysis of the simple zinc ion to give species of charge greater than +2. The critical coagulation concentration of this hydrolyzed species corresponds closely to that expected for a simple triply-charged ion such as Al^{+3} (depicted by III on Fig. 4). It would appear, therefore, that the hydrolyzed zinc species are triply charged and this can be accounted for only if polynuclear complexes are assumed. The above comparison should actually be made on the normality rather than molarity scale. Other factors will lead us to consider the possibility that the hydrolyzed zinc ion is either a dimer or trimer, in which case the critical coagulation concentrations on the normality scale would change accordingly. The possibility of the complex zinc ion having a charge of +4 must be eliminated, since a simple ion of charge +4, such as Th^{+4}, would have a value which is thirty times less than that for Al^{+3} (Al^{+3}—1.1×10^{-4} N; Th^{+4} —4.0×10^{-6} N).[17,19]

Actually this difference between the critical coagulation concentration of Al^{+3} and a triply-charged hydrolyzed zinc species can be easily understood. First, a triply-charged polynuclear zinc complex is a large cation which in turn will have a lower coagulation concentration than a simple, small counterion of the same charge.[21] Secondly, the electrophoretic mobility curves show that the hydrolyzed species adsorb rather strongly on the sol particles and it is well known that such adsorption of a counterion lowers the critical coagulation concentration. The possibility of the zinc species being +4 is further obviated because such a polynuclear ion would have an even lower critical coagulation value than that cited above for Th^{+4}.

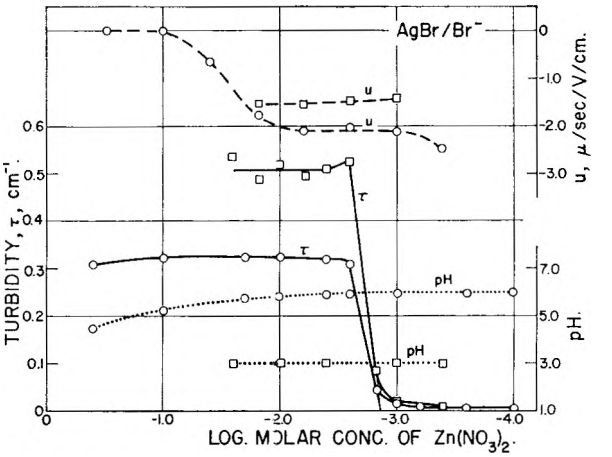

Fig. 2.—Coagulation (τ), mobility (μ) and pH curves of a silver bromide sol *in statu nascendi* in the presence of various amounts of zinc nitrate. Turbidities are for light of 546 mμ and 25°, 10 min. after mixing the reacting components. Concentrations: $AgNO_3$, 1×10^{-4} M; KBr, 2×10^{-3} M; HNO_3, 1×10^{-3} (□); no addition of HNO_3 or NaOH (○).

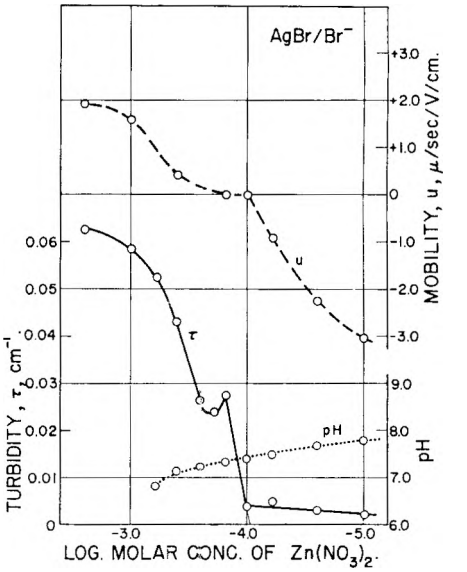

Fig. 3.—Coagulation (τ), mobility (μ) and pH curves of a silver bromide sol *in statu nascendi* in the presence of various amounts of zinc nitrate. Concentrations: $AgNO_3$, 1×10^{-4} M; KBr, 2×10^{-3} M; NaOH, 1.6×10^{-4} M.

A charge of +3 for hydrolyzed zinc ions means that these are present in solution in the form of a polynuclear complex whose formula is $[Zn_{2+n}(OH)_{2n+1}]^{+3}$. Which of several possible complexes actually is formed depends on the Zn:OH ratio. In the case of aluminum ion hydrolysis, this ratio could be established unambiguously by direct potentiometric titration.[1] However, as was pointed out in the introduction, because Zn^{+2} is a very weak acid, titrations and pH measurements with zinc salt solutions are precarious and have not led to a Zn:OH ratio which can be accepted with confidence. Most previous workers favor a 1:1 ratio for Zn:OH, and a formulation of the $ZnOH^+$ for the complex.[4,10,11,13,23] Since none of them actually had de-

(23) J. Besson and W. Eckert, *Bull. soc. chim. France*, 1676 (1959).

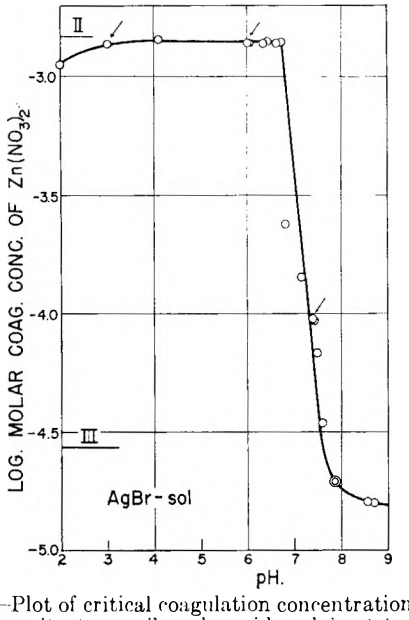

Fig. 4.—Plot of critical coagulation concentrations against *p*H for zinc nitrate on silver bromide sol *in statu nascendi*. Concentrations: $AgNO_3$, 1×10^{-4} *M*; KBr, 2×10^{-3} *M*. Arrows indicate points obtained in Figs. 2 and 3. II and III: Coagulation concentrations (expressed in molarities) for simple di- and tri-valent counterions obtained on the same sol.

termined the charge, this seemed to be the simplest conclusion. However, knowing that the charge of the complex is +3 and accepting, for the moment Zn:OH = 1:1, the hydrolyzed species that follows is $Zn_3(OH)_3^{3+}$. Structurally, this complex can be visualized as a six-membered ring with three zinc tetrahedra linked by oxygens. It is interesting to note that Kakihana and Sillén[24] have suggested the same type of a complex for hydrolyzed beryllium ion based upon entirely different considerations.

Trimeric zinc species also were suggested by Carrière, Guiter and Annouar.[7-9] However, the complex they derived was uncharged since they included the neben ion (Cl^-, NO_3^-) in the structure of the complex. Their conclusions do not seem to be justified for two reasons. First, their experimental data are completely out of line when compared with others (Fig. 1) and secondly, they neglected the activity effects in a concentration range where this cannot possibly be done.

It should be mentioned that the possibility of the existence of Zn_2OH^{+3} as the predominant species cannot be excluded as long as the Zn:OH ratio is not known with certainty. The coagulation results cannot distinguish between Zn_2OH^{3+} and $Zn_3(OH)_3^{3+}$. When the molar coagulation concentration is expressed in normalities, the difference between the values obtained for the two species is too small to justify any distinction. A definite conclusion can be reached only if extremely carefully determined and analyzed *p*H data of zinc salt solutions were to yield an unambiguous Zn:OH ratio. Such an investigation is desirable.

The existence of higher species such as $Zn_4(OH)_5^{3+}$ and $Zn_5(OH)_7^{3+}$ is rather unlikely since it would be difficult to give a reasonable structure for such complexes.

Finally, the shape of the coagulation curve at high *p*H (Fig. 3) remains to be discussed. The kink in the curve is due to a combination of two coagulation processes, each taking place primarily at different concentration ranges. At lower concentrations of $Zn(NO_3)_2$, the negatively charged sol is coagulated by the complex zinc cation, whereas at higher concentrations this complex adsorbs and reverses the charge of the AgBr particles. Were this latter the only process, the recharged sol, stabilized by the adsorbed hydrolyzed zinc ions, would exhibit a sharp decrease in turbidity, and at a still higher concentration of $Zn(NO_3)_2$ the turbidity would be comparable to that for an uncoagulated sol. However, there are sufficient nitrate ions present in the solution to coagulate the sol of reversed charge. The coagulation concentrations of anions for positive sols are much lower than those of cations for negative sols.[19] Furthermore, the concentration of monovalent anions necessary to produce coagulation decreases very sharply with decreasing charge density of the sol particles.[20-22] Since we are concerned with a region near the isoelectric point, there apparently are sufficient nitrate ions present to coagulate these sols, now weakly charged with positive hydrolyzed zinc ions. The kink in the coagulation curve is due, then, to the onset of stabilization upon the adsorption of the hydrolyzed zinc ions, countered at slightly higher concentration by the coagulation of the slightly recharged sol by the nitrate ions. These conclusions are supported by the electrophoretic mobility data since the kink coincides with the electrophoretic zero point.

These results confirm our previous conclusion[1] that hydrolyzed complex ions are responsible for the reversal of charge of lyophobic colloids, whereas simple doubly and triply charged ions do not cause this effect. Kruyt and Troelstra[25] have qualitatively indicated that zinc ions reverse the charge in alkaline solutions, but they have assumed the adsorption of insoluble hydroxides.

(24) H. Kakihana and L. G. Sillén, *Acta Chem. Scand.*, **10**, 985 (1956).

(25) H. R. Kruyt and S. A. Troelstra, *Kolloid-Beih.*, **54**, 262 (1943).

THE BASE STRENGTHS OF 2,2′-BIPYRIDYL AND 1,10-PHENANTHROLINE

BY I. R. BEATTIE AND M. WEBSTER

Department of Chemistry, King's College, Strand, London, W.C. 2

Received August 4, 1961

The interaction of 2,2′-bipyridyl and 1,10-phenanthroline with hydrogen chloride in the presence and in the absence of water has been examined. The "dihydrochloride" of 1,10-phenanthroline is extremely hygroscopic and in moist air reacts to form the monohydrate monohydrochloride. It appears that 2,2′-monohydrochloride is *cisoid* even when anhydrous. 1,10-Phenanthroline monohydrate in solution in benzene is in equilibrium with water and the anhydrous base.

The behavior of 2,2′-bipyridyl and 1,10-phenanthroline as monoprotic bases in aqueous solution down to *p*H values of the order of unity is well established.[1] Thus, the ratio of K_1 to K_2 for the conjugate acids of 2,2′-bipyridyl is about 10^5, and it has been suggested that such behavior is due to hydrogen bonding,[2] inductive effects,[3] and contributions from structures such as (I)[4]

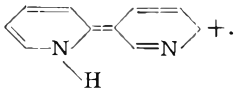

I

These views have been discussed by Westheimer and Benfey.[5] In the case of 1,10-phenanthroline the picture is simplified by the fixed alignment of the rings. The results reported here were obtained during a study of the products of hydrolysis of the addition compounds formed by these bases with antimony and phosphorus pentahalides.

1,10-Phenanthroline crystallizes from water as the monohydrate, with a low vapor pressure.[6] It has been suggested that the water is hydrogen-bonded to the nitrogen, although the frequently quoted experimental evidence for this is slight.[7] According to Nakamoto,[4] if gaseous hydrogen chloride is passed into an ethereal solution of 1,10-phenanthroline (monohydrate ?) and the product dried over phosphoric oxide for five days, the *monohydrate* monohydrochloride is obtained. These results suggest that hydrogen bonding may be of importance in determining the base strength of the monohydrochloride in aqueous solution. Thus, although Nakamoto has pointed out that the N. . . H distance in II is long for adequate hydrogen bonding, this argument does not apply to III.

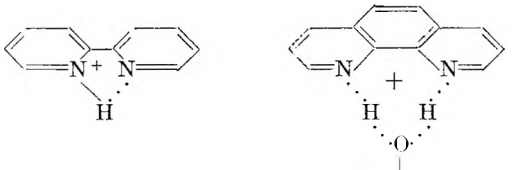

II III

We find that prolonged passage of hydrogen chloride into an ethereal solution of 1,10-phenanthroline monohydrate yields a compound with a chloride content corresponding to more than 2 moles of HCl per mole of monohydrate. However, this compound readily loses hydrogen chloride on warming to 45°, to give the monohydrate monohydrochloride. Passage of hydrogen chloride into a solution of 1,10-phenanthroline in ether under rigidly anhydrous conditions yields a precipitate which, when warmed to 45° in air, analyses for the *monohydrate* monohydrochloride. However, outgassing *in vacuo* for 30 min. gives a compound analyzing as 1,10-phenanthroline·2.7$_8$ HCl. These results can be rationalized in terms of a very hygroscopic dihydrochloride and variable amounts of HCl_2^- ion, depending on the time for which the hydrogen chloride was passed. It is clear that the addition of one molecule of water to the anhydrous hydrochloride involves the effective deprotonation of one nitrogen.

In order that the hydrogen bonding in 1,10-phenanthroline monohydrate could be studied in more detail, this compound was examined in solution in ether and benzene. Figure 1 shows the infrared spectrum of the monohydrate (a) in ether and (b) in benzene. The spectrum of water in these solvents at similar concentrations also is shown. In the case of the ethereal solution the two spectra are virtually identical (anhydrous 1,10-phenanthroline has no peak in this region). However, in benzene the free water peaks in the solution of the monohydrate are considerably smaller than those to be expected from complete dissociation. Further, there is a broad peak centered at about 3410 cm.$^{-1}$ analogous to that found in the monohydrate in the solid state. These results show that in the strongly hydrogen bonding solvent ether the monohydrate dissociates completely, or nearly completely, while in the case of benzene only partial dissociation occurs. Both 1,10-phenanthroline monohydrate and the corresponding monohydrochloride showed negligible weight loss *in vacuo*.

The behavior of 2,2′-bipyridyl contrasts sharply with that of 1,10-phenanthroline. Thus, 2,2′-bipyridyl (which is known to be *trans* in the solid[8] and thought to be *transoid* in solution[9]) may be recrystallized anhydrous from water. Correspondingly we find that the dihydrochloride (which is thought to deviate largely from planarity) crystallizes anhydrous from concentrated hydrochloric acid. However, 2,2′-bipyridyl monohydrochloride (which generally is assumed to be *cisoid* in aqueous solution) crystallizes from water as the dihydrate. 2,2′-Bipyridyl monohydrochloride dihydrate readily

(1) See for example P. Krumholz, *J. Am. Chem. Soc.*, **73**, 3487 (1951); *J. Phys. Chem.*, **60**, 87 (1956).

(2) R. F. Knott and J. G. Breckenridge, *Can. J. Chem.*, **32**, 512 (1954).

(3) See for example F. G. Mann and J. Watson, *J. Org. Chem.*, **13**, 502 (1948).

(4) K. Nakamoto, *J. Phys. Chem.*, **64**, 1420 (1960).

(5) F. H. Westheimer and O. T. Benfey, *J. Am. Chem. Soc.*, **78**, 5309 (1956).

(6) J. S. Fritz, F. W. Cagle and G. F. Smith, *ibid.*, **71**, 2480 (1949).

(7) G. F. Smith and F. P. Richter, "Phenanthroline and Substituted Phenanthroline Indicators," G. F. Smith Chemical Company, Columbus, Ohio, 1944.

(8) L. L. Merritt and E. D. Schroeder, *Acta Cryst.*, **9**, 801 (1956).

(9) P. E. Fielding and R. J. W. Le Fevre, *J. Chem. Soc.*, 1811 (1951).

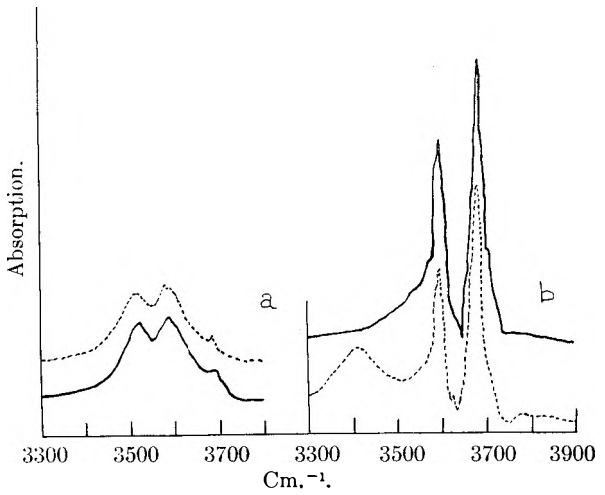

Fig. 1.—(a) The infrared spectra of: water in ether ———; (27.2 mmoles l.$^{-1}$) 1,10-phenanthroline monohydrate in ether ——— (19.4 mmoles l.$^{-1}$). (b) The infrared spectra of: water in benzene ———; (24.4 mmoles l.$^{-1}$) 1,10-phenanthroline monohydrate in benzene -------- (21.1 mmoles l.$^{-1}$).

loses water *in vacuo* to yield the anhydrous compound. The ease with which 1,10-phenanthroline·2.7$_8$HCl gains water and loses hydrogen chloride to give the monohydrate monohydrochloride, coupled with the stability of this compound and the free base monohydrate *in vacuo*, suggests that hydrogen bonding may be of importance in determining the basic behavior of 1,10-phenanthroline. The properties of the analogous 2,2′-bipyridyl compounds show that hydrogen bonding is likely to be less important for these compounds and further indicates, by analogy with monoprotonated 1,10-phenanthroline, that the rings in 2,2′-bipyridyl monohydrochloride are not coplanar.

TABLE I

THE ULTRAVIOLET SPECTRA OF CERTAIN COMPOUNDS OF 2,2′-BIPYRIDYL

Compound[a]	Max. (mμ) (i)	Max. (mμ) (ii)	Method or solvent
Bipy·	285	238	KCl
	285	[b]	$CHCl_3$
Bipy·2HCl	305	[c]	KCl
	302	[b]	$CHCl_3$
Bipy·2H$_2$O·HCl	302	240	KCl
	300	[b]	$CHCl_3$
Bipy·HCl	301	240	KCl
	301	[b]	$CHCl_3$

[a] Bipy· = 2,2′-bipyridyl. [b] Not observed. [c] Very weak if present.

Table I shows the ultraviolet spectra of 2,2′-bipyridyl monohydrochloride under a variety of conditions (the free base and dihydrochloride are included for comparison). The spectra are virtually identical in all cases for the monohydrochloride, and it appears that the compound is *cisoid* even in the absence of water.

Experimental

(All melting points are uncorrected.)

Reagents.—1,10-Phenanthroline monohydrate was an A.R. chemical or recrystallized from water; m.p. 94.5–95.5° (the m.p. depends on the experimental conditions—closed or open tubes, rate of heating, ratio of mass of 1,10-phenanthroline to internal volume in a closed tube). The spread of literature values[10] for the m.p. of 1,10-phenanthroline monohydrate is undoubtedly largely due to loss of water. Our given m.p. is the sharpest value obtained by us. It also is the lowest: anhydrous by vacuum sublimation of the hydrate (the anhydrous material is exceedingly hygroscopic): 2,2′-bipyridyl anhydrous by vacuum sublimation of A.R. material.

1,10-Phenanthroline monohydrate monohydrochloride was obtained from 1,10-phenanthroline monohydrate (about 0.45 g.) in sodium-dried ether (about 100 ml.) by passage of hydrogen chloride for about 1.5 hr. Precipitate weight corresponded to 2.59 moles of HCl per mole of hydrate (Found: Cl, 31.8. Calcd. for $C_{12}H_8N_2\cdot H_2O\cdot 2.5_9HCl$; Cl, 31.7. The precipitate readily lost HCl on warming to 45° and after 2 hr. no further loss in weight was observed (Found: Cl, 14.9. Calcd. for $C_{12}H_8N_2\cdot H_2O\cdot HCl$: Cl, 15.1 %); m.p., 173–176° (sealed tube).

1,10-Phenanthroline hydrochloride was obtained from 1,10-phenanthroline (anhydrous about 0.40 g.) dissolved in ether (about 100 ml.) by passage of hydrogen chloride (from concd. sulfuric acid on sodium chloride and dried by phosphoric oxide) for about 1.75 hr. The solid was collected as a centrifugate, washed with ether and the slurry (a) placed in an oven at 45° for 40 min.; (b) *in vacuo* for 30 min. The solid from (a) corresponded to $C_{12}H_8N_2\cdot H_2O\cdot HCl$ (Found: Cl, 15.3. Calcd. for $C_{12}H_8N_2\cdot H_2O\cdot HCl$: Cl, 15.1); (b) corresponded to $C_{12}H_8N_2\cdot 2.7_8HCl$ (Found: Cl, 35.05).

2,2′-Bipyridyl Dihydrochloride was obtained from ethereal solution by passage of dry hydrogen chloride (Found: Cl, 31.0. Calcd. for $C_{10}H_8N_2\cdot 2HCl$: Cl, 31.0; m.p. 205–225° (sealed tubes)). *Cf.* 150–155° of Nakamoto.[4] Also from concentrated hydrochloric acid (Found: Cl, 30.7. Calcd. for $C_{10}H_8N_2\cdot 2HCl$: Cl, 31.0; m.p. 200–235° (sealed tubes)).

2,2′-Bipyridyl Monohydrochloride Dihydrate was obtained from aqueous solution by treatment of 2,2′-bipyridyl with the calculated quantity of standard approximately molar hydrochloric acid. Long needle-shaped crystals from evaporation on a steam-bath (Found: Cl, 15.4. Calcd. for $C_{10}H_8N_2\cdot 2H_2O\cdot HCl$: Cl, 15.5); m.p. 44–45° (open and sealed tubes).

Analyses—For 2,2′-bipyridyl compounds by determination of chloride gravimetrically as silver chloride. For compounds of 1,10-phenanthroline, the interfering base had to be removed (before precipitation) by use of the cation exchange resin ZeoKarb 225.

Weight loss.—*In vacuo* 1,10-phenanthroline monohydrate, 1,10-phenanthroline monohydrate monohydrochloride and 2,2′-bipyridyl dihydrochloride all lost <1 mg. per hr. on a 50-mg. sample. A 60-mg. sample of 2,2′-bipyridyl monohydrochloride dihydrate lost 10 mg. in 30 min. (Found: Cl, 17.9. Calcd. for $C_{10}H_8N_2\cdot HCl$: Cl, 18.4). The absence of water also was shown by an infrared spectrum of this compound as a mull in Nujol.

Spectra.—Ultraviolet spectra were determined on a Unicam S.P. 500, using *either* 1-cm. vitrous silica cells with chloroform dried over and distilled from calcium hydride, *or* KCl discs. In the case of anhydrous 2,2′-bipyridyl monohydrochloride, where anhydrous conditions were essential, the spectra in solution were determined using a vacuum technique with no taps or joints. For the solid state spectra a dry-box was used. Infrared spectra were determined on a Perkin–Elmer 221.

We thank Dr. C. W. Rees for helpful discussion, the Department of Scientific and Industrial Research for a grant to M.W., and for the purchase of a Perkin–Elmer 221 infrared spectrometer, and the Royal Society for a grant to purchase a Unicam S.P. 500.

(10) I. Heilbron and H. Bunbury, "Dictionary of Organic Compounds," Eyre and Spottiswoode, London, 1953; C. Allen, "The chemistry of Heterocyclic Compounds. Six-Membered Heterocyclic Nitrogen Compounds with Three Condensed Rings," Interscience Publ., New York, N. Y., 1958; R. Belcher, M. Stacey, A. Sykes and J. C. Tatlow, *J. Chem. Soc.*, 3846 (1954).

THE REACTIVITY OF HYDROGEN ATOMS IN THE LIQUID PHASE. II. THE REACTION WITH SOME ORGANIC SOLUTES

BY T. J. HARDWICK

Gulf Research & Development Company, Pittsburgh 30, Pennsylvania

Received August 8, 1961

Using a method developed previously, the reactivity of a number of organic compounds with hydrogen atoms was measured in *n*-hexane solution at room temperature. The following classes of compounds react by addition of hydrogen only: esters, methylbenzenes, disulfides, conjugated or condensed aromatic compounds, vinyl monomers, and stable free radicals. Reacting by both addition and hydrogen abstraction are: aliphatic acids, aldehydes, ketones, alkynes and alkyl (other than methyl) benzenes. Alcohols, ethers and mercaptans are relatively inert. The effect of temperature on these reactions was studied, but the results are not easily interpreted. Absolute values for the rate constants at room temperature were obtained from a comparison with values previously established.

Introduction

A method of measuring the reactivity of hydrogen atoms in solution has been described recently.[1,2] The technique involves dissolving small amounts (up to 2%) of the material in question in a saturated hydrocarbon and, after exposure to relatively low doses of ionizing radiation, measuring the hydrogen gas yield as a function of solute concentration. Hydrogen atoms, produced *in situ* by the absorption of radiation by the solvent, react competitively with solvent and solute. A generalized plot of the radiolytic hydrogen yield (G_{H_2}) as a function of solute concentration is shown in Fig. 1.

The number and type of reactions taking place in such a system during radiolysis are many and varied. In the present case, however, it is necessary to consider only those reactions which influence the formation of hydrogen gas. The pertinent reactions on radiolysis of solvent RH containing solute S are

$$\mathrm{RH} \xrightarrow{G_1} \mathrm{H_2} + \text{products} \qquad (1)$$

$$\mathrm{RH} \xrightarrow{G_2} \mathrm{H} + \mathrm{R} \qquad (2)$$

$$\mathrm{H} + \mathrm{RH} \xrightarrow{k_3} \mathrm{H_2} + \mathrm{R} \qquad (3)$$

$$\mathrm{H} + \mathrm{S} \xrightarrow{k_4} \mathrm{HS} \qquad (4)$$

$$\mathrm{H} + \mathrm{S} \xrightarrow{k_5} \mathrm{H_2} + \mathrm{R}' \qquad (5)$$

Reaction 1 is the so-called "hot hydrogen atom" or "molecular hydrogen" reaction which produces hydrogen gas in yield G_1, unaffected by small concentrations of solute. "Thermal" hydrogen atoms are produced in yield G_2, and react with solvent (reaction 3), or solute by addition (reaction 4) or abstraction of hydrogen (reaction 5).

Using a steady-state treatment for hydrogen atoms, the following kinetic expression is derived

$$\frac{1}{G_{H_{2(0)}} - G_{H_{2(S)}}} = \frac{1}{\Delta G_{H_2}} = \frac{k_3}{k_4} \times \frac{[\mathrm{RH}]}{[\mathrm{S}]} \times \frac{1}{G_2} + \frac{1}{G_2}\left(\frac{k_5}{k_4} + 1\right)$$

where

$G_{H_{2(0)}}$ is the hydrogen gas yield in pure solvent
$G_{H_{2(S)}}$ is the hydrogen gas yield at solute concn. S
ΔG_{H_2} is the decrease in hydrogen gas yield resulting from the addition of solute to the pure solvent

A plot of $1/\Delta G_{H_2}$ *vs.* $[\mathrm{RH}]/[\mathrm{S}]$ gives a straight line of slope $(k_3/k_4)(1/G_2)$ and intercept $(1/G_2)(k_5/k_4 + 1)$. Where hydrogen atoms react with the solute by addition only, *i.e.*, $k_5 = 0$, the intercept is $1/G_2$. Values of G_1 and G_2 have been determined for a number of saturated hydrocarbons.[2]

In the generalized study of hydrogen atoms with various classes of solutes, *n*-hexane has been used as the hydrocarbon solvent. In this case $G_1 = 2.12$, $G_2 = 3.16$. The rate constant k_3 has been measured as 4.9×10^9 cc. mole^{-1} sec.$^{-1}$ at 23°.[2] Relative rate constants obtained from the kinetic plots have been converted to absolute values using this value for k_3.

This paper reports values of the reactivity of hydrogen atoms with organic compounds of several classes, *e.g.*, aliphatic esters, acids, aliphatic alcohols, ethers, aldehydes, ketones, alkyl aromatics, condensed aromatics, etc. A comparison of methanol and *n*-hexane as solvents and sources of hydrogen atoms is made. Preliminary studies have been made on the effect of temperature. Comment is given on the accuracy and precision of the results.

Experimental

Materials.—Pure Grade *n*-hexane was obtained from Phillips Petroleum Company, and was purified further by prolonged stirring with sulfuric acid. In all cases the unsaturation content of the purified solvent was less than 0.2 m*M*/l., as measured by bromination. Baker and Adams' Reagent methanol was purified further by refluxing over alkaline silver oxide and distilling. The measured aldehyde content was less than 0.1 m*M*/l.

There are too many chemicals to list the sources in detail. The purest available were used, and several were freshly distilled before use where deterioration on standing was suspected, *e.g.*, aldehydes. Alcohols, however, were rigorously purified to remove carbonyl compounds. In general, the solutes used were sufficiently reactive that small amounts of impurities would not significantly affect the measured value of the rate constants.

Irradiation and Analysis.—The methods of irradiating degassed solution and measuring the resultant hydrogen yield have been described in detail previously.[1] Briefly a 100-ml. sample of solution was degassed and irradiated to about 20 krad. by X-rays from a Van de Graaff accelerator. The energy absorbed in each sample was monitored by a simultaneous irradiation of a solution of the Fricke dosimeter. Hydrogen gas was determined by isolating it from other gases and measuring the amount in a McLeod gage. In a typical experiment, 5–10 μmoles of radiolytic hydrogen gas was produced. All runs were made at 23 ± 1° unless otherwise stated.

Irradiation at Various Temperatures.—In experiments designed to study the effect of temperature, the irradiation cells were submerged in a constant temperature bath to the

(1) T. J. Hardwick, *J. Phys. Chem.*, **64**, 1623 (1960).
(2) T. J. Hardwick, *ibid.*, **65**, 101 (1961).

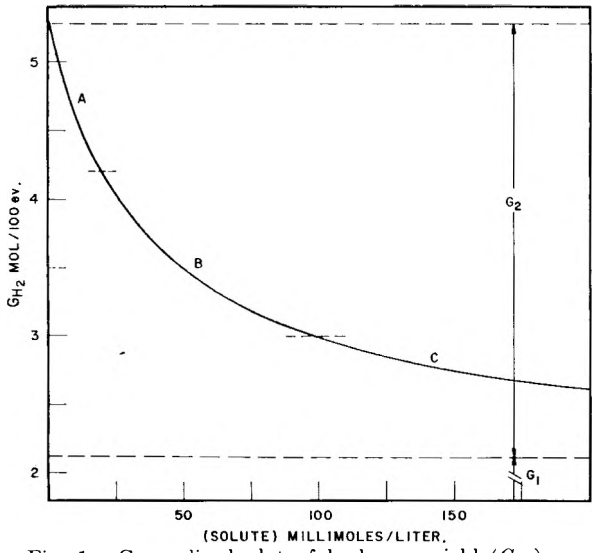

Fig. 1.—Generalized plot of hydrogen yield (G_{H_2}) as a function of solute concentration in *n*-hexane, $k_4 = 10^{12}$ cc. mole^{-1} sec.$^{-1}$. The most reliable results are obtained in region B.

point where the levels of the irradiated liquid and the bath liquid were the same. All samples received the same exposure, for the total electron charge from the accelerator was the same for each run and the energy of the electrons was monitored on an expanded scale, which permitted a voltage setting reproducible to ±10 kv. The results indicated a precision of ±0.6%. The relative hydrogen yields were placed on an absolute basis by taking $G_{H_2(0)} = 5.28$ at 23°.

Concentration of Solutes.—The concentration of solute varied considerably, depending on the reactivity. In general, four to eight different solute concentrations were used, varying over a factor of four. The concentration range was less than this for solutes: (1) where the reactivity is low (a 2%/volume was the maximum solute concentration used) or (2) where the solutes are sparingly soluble, as is the case for some of the solid polyaromatics.

Results and Discussion

Treatment of the Data.—A correction was applied to all results to account for the absorption of energy directly by the solute. For simplicity it was assumed that no hydrogen atoms were produced from the solute (a doubtful assumption), but in most cases low yields of such atoms will have little effect on the final result. The correction, as applied, involved normalizing the energy absorbed by *n*-hexane to 100 ml. of solvent, taking into account the ratio of electron densities of solute and *n*-hexane.

All compounds studied gave a straight line on plotting $1/\Delta G_{H_2}$ *vs.* [*n*-hexane]/[solute]. The value of the intercept in all cases was equal to or greater than 0.316 ($1/G_2$) within an experimental error of ±5%.

As a preliminary step, a modified least squares fit was made on the kinetic plot of the corrected data. For those solutes where the value of the intercept was within ±5% of 0.316, ($1/G_2$), the least squares fit was recalculated assuming the intercept fixed at 0.316.

The relative rate constants (k_3/k_4) were calculated from the slopes of the straight lines in the kinetic plots. The value of k_5/k_4 was determined from the intercept; if k_5/k_4 was less than 0.05, k_5 was taken as zero or negligible. Absolute values of k_4 and k_5 were calculated from the measured ratios.

Esters.—The reactivity of hydrogen atoms with some aliphatic esters is shown in Table I. With the exception of methyl acetate, the rate of hydrogen atom addition to such esters is the same within experimental error, *viz.*, 8.6×10^{10} cc. mole^{-1} sec.$^{-1}$. Hydrogen atom abstraction is less than 5% of this value or $< 4 \times 10^9$ cc. mole^{-1} sec.$^{-1}$. The invariance of k_4 in the series implies that the same reaction is taking place, and we ascribe this to the addition of hydrogen atoms to the carboxyl group. In the kinetic development of the reaction mechanism, one includes some unknown constant relating the effective collision diameter of *n*-hexane and the ester carboxyl group. A variation in rate with increased chain length of either alkyl group of the ester therefore would not be expected. Reduced reactivity might be expected if steric hindrance were a factor, *e.g.*, from a compound such as *t*-butyl pivalate.

TABLE I

REACTIVITY OF HYDROGEN ATOMS WITH ALIPHATIC ESTERS
REACTION BY ADDITION ONLY
$T = 23 \pm 1°$

	Acetate	Propionate	Butyrate	Valerate
		× 10^{10} cc. mole^{-1} sec.$^{-1}$		
Methyl	6.9[a]	8.3	8.6	
Ethyl	8.3	8.3	8.5	8.2
n-Propyl	9.2	9.2		
Isopropyl	8.4	9.0		
n-Butyl	9.0	8.1		
n-Amyl	8.4			

Mean 8.6 ± 0.4 × 10^{10} cc. mole^{-1} sec.$^{-1}$

[a] Not included in calculating mean value.

The rate constant for methyl acetate is low, and was not included in determining the mean value. No satisfactory explanation is apparent at this time, but the discrepancy is not likely to be due to impurities, for possible impurities (acids, aldehydes, etc.) are much more reactive toward hydrogen atoms than are esters. It may be that the unique case of two methyl groups attached to the carboxyl group results in a slightly lowered reactivity.

Acids.—With acids as solutes the intercept of the kinetic plot was always > 0.316, indicating that k_5 has a significant value. The rates of addition (k_4) and abstraction (k_5) are reported in Table II. From these data several factors may be noted: (1) Hydrogen atoms both add to, and abstract from, organic acids. The abstraction of hydrogen from trifluoroacetic acid is particularly significant. (2) For all aliphatic acids the rates of addition and abstraction are about the same. (3) The ratio of k_5/k_4 is constant for all acids despite large changes in individual rates.

It seems clear from the results that hydrogen atoms are attacking the carboxyl part of the organic acid, either adding to this group or abstracting the carboxyl hydrogen. Somewhat surprising is the constancy of the ratio k_5/k_4 despite large changes in reactivity and structure. This may be due either to the requirement of a suitable collision geometry for each type of reaction, and the ratio of 0.27 is about the value expected, or to a transi-

tion complex in which addition to the carboxyl group or abstraction of hydrogen occur with fixed relative probability. As in the case of aliphatic esters the length and structure of the alkyl chain seems to have little or no effect on the rate of reaction.

TABLE II

REACTIVITY OF HYDROGEN ATOMS WITH ORGANIC ACIDS

$T = 23 \pm 1°$

	k_4 (addition) $\times 10^{11}$ cc. mole^{-1} sec.$^{-1}$	k_5 (abstraction)	k_5/k_4
Acetic acid	6.1	1.5	0.24
Propionic acid	6.9	1.6	.23
Butyric acid	5.8	1.6	.27
Valeric acid	5.4	1.6	.29
Isobutyric acid	5.5	1.6	.28
Trifluoroacetic acid	16	4.4	.28
Benzoic acid	29	8.3	.28
			0.27 ± 0.02

Trifluoroacetic acid and benzoic acid were chosen to illustrate that hydrogen indeed is abstracted from the carboxyl position. This of course must be so in the case of trifluoroacetic acid. Studies with other aromatic compounds *vide infra* indicate that abstraction of hydrogen from the benzene ring is an unlikely process when compared to hydrogen atom addition.

If the postulate of a constant value of k_5/k_4 is correct, it follows that hydrogen atoms react with benzoic acid only in the carboxyl position. If reaction with the ring occurred to any significant extent k_5/k_4 would decrease. As will be shown later the rate of addition of hydrogen atoms to benzene rings is about $2\text{–}3.5 \times 10^{11}$ cc. mole^{-1} sec.$^{-1}$, and such a contribution to the rate might not be detected easily in the case of such a reactive compound as benzoic acid.

The rate of addition of hydrogen atoms to aliphatic acids is seven times greater than to aliphatic esters. Apparently the addition takes place on the carboxyl group in both cases. It is suggested that the energy of activation for attack on an ester carboxyl group is larger than for the corresponding attack on an acid carboxyl. It also is possible that the replacement of hydrogen by an alkyl group exhibits a small steric effect.

The absence of reaction 5 in the hydrogen attack on aliphatic esters ($k_5 < 4 \times 10^9$ cc. mole^{-1} sec.$^{-1}$) tends to confirm that hydrogen abstraction in acids occurs at the carboxyl group.

The higher reactivity of hydrogen atoms toward fluorinated acids is unexpected, and little comment can be made at this time.

The results presented here agree qualitatively with gas phase work. Burton[3,4] photolyzed acetic acid vapor and suggested that a hydrogen atom abstraction from the carboxyl group might occur

$$CH_3COOH + H \longrightarrow CH_3COO + H_2 \qquad (6)$$

with an energy of activation in the range 7–11 kcal. In a later paper Henkin and Burton[5] postulated an analogous reaction between hydrogen atoms and propionic acid, with an activation energy between 7.7 and 9.2 kcal., assuming a steric factor of unity.

In view of the preliminary nature of earlier results, it perhaps is not fair to make a quantitative comparison. The values of the rate constants obtained, however, indicate that in the liquid phase the activation energy for hydrogen abstraction is less than 5 kcal.

Alcohols.—The radiolytic hydrogen gas yields for the system 2%/volume aliphatic alcohols in *n*-hexane are shown in Table III. Values range from slightly above to slightly below 5.28 mole/100 e.v. Either the alcohols are relatively inert to hydrogen atoms, or reaction 4 is insignificant compared to reaction 5. Values of $G_{H_2} > 5.28$ probably arise from hydrogen gas derived directly from the alcohol, for in the correction for energy absorbed by the solute, no hydrogen gas formation from this source is postulated. Values below 5.28 probably are due to traces of aldehyde or other reactive impurity which is not easily removed from the alcohol.

TABLE III

RADIOLYTIC HYDROGEN GAS YIELDS FROM THE SYSTEMS *n*-HEXANE–ALIPHATIC ALCOHOLS

$T = 23 \pm 1°$

Solute	G_{H_2} $[C_6H_5CN] = 0$	G_{H_2} $[C_6H_5CN] = 0.5\%$/vol.
None	5.28	3.47
Methyl alcohol 2%/vol.	5.48	3.46
n-Propyl alcohol 2%/vol.	5.24	3.58
Ispropyl alcohol 2%/vol.	5.28	3.33
n-Butyl alcohol 2%/vol.	5.21	3.38
Isobutyl alcohol 2%/vol.	5.33	3.55
n-Amyl alcohol 2%/vol.	5.20	3.50
n-Hexyl alcohol 2%/vol.	5.30	3.56
Mean	5.29	3.48 ± 0.08

To determine whether reaction 5 is significant, the hydrogen yield from solutions of *n*-hexane containing 0.5%/volume of benzonitrile, with and without 2%/volume aliphatic alcohol, was measured. The results are shown in the last column of Table III. If reaction 5 were significant, the value of G_{H_2} should increase on adding alcohol. For example, consider the system 0.5% benzonitrile, 2% *n*-propyl alcohol. If the abstraction of hydrogen from the alcohol occurred at a rate $= 2 \times 10^{10}$ cc. mole^{-1} sec.$^{-1}$, G_{H_2} would be 3.91. As G_{H_2} is not measurably changed on adding alcohols, the reactivity of hydrogen atoms on alcohols must be low.

This raises the possibility of using such alcohols as a source of hydrogen atoms on radiolysis. Adams and Baxendale[6] in effect did this in their studies on the methanol radiolysis. Strong and Burr[7] studied the addition of hydrogen atoms to acetone in isopropyl alcohol solution, where hydrogen atoms came from the radiolysis of the solvent. A comparison of methanol and *n*-hexane as solvents and *in situ* sources of hydrogen atoms appears later in this paper.

Ethers.—Experiments to determine the reactivity of hydrogen atoms on diethyl and diisopropyl

(3) M. Burton, *J. Am. Chem. Soc.*, **58**, 692 (1936).
(4) M. Burton, *ibid.*, **58**, 1645 (1936).
(5) H. Henkin and M. Burton, *ibid.*, **60**, 831 (1938).
(6) G. E. Adams and J. H. Baxendale, *ibid.*, **80**, 4215 (1958).
(7) J. D. Strong and J. G. Burr, *ibid.*, **81**, 775 (1959).

ether were made in the usual manner. No measurable addition of hydrogen atoms was found with either compound.

It is probable that aliphatic ethers are in the same category as aliphatic alcohols and paraffins—solvents producing hydrogen atoms on radiolysis, but relatively inert to attack by them. Evidence for this is found in Newton's work on the radiolysis of a series of pure aliphatic ethers.[8,9] The initial hydrogen yield is of the same order as is found for the corresponding alcohols.[10] Highly branched ethers have lower initial hydrogen yields than those with *n*-alkyl groups (*cf.*, paraffins and alcohols). With increasing dose the hydrogen yield decreases, a result which occurs only when the reactivity of hydrogen atoms with the solvent is low. The hydrogen yield from pure isopropyl alcohol was 2.42 moles/100 e.v.; with added iodine this yield dropped to about 1.6 moles/100 e.v.[9]

Although no pertinent experiments have been carried out in the present study it would appear that aliphatic ethers, like paraffins and aliphatic alcohols, may be used as a solvent and source of hydrogen atoms.

Aldehydes.—The reactivity of hydrogen atoms with several aliphatic aldehydes was measured. Individual yields were less reproducible than in other systems, with a consequent greater deviation in the slope and intercept of the kinetic plot. Among four aldehydes studied, *viz.*, propionaldehyde, *n*-butyraldehyde, isobutyraldehyde and *n*-valeraldehyde, no significant difference in slope or intercept was observable. To obtain the best values, the modified least squares fit was made for all data on all aldehydes. The rate of addition (k_4) is 6.6×10^{11} cc. mole^{-1} sec.$^{-1}$ ($\pm 15\%$); the rate of abstraction (k_5) is 2.8×10^{11} cc. mole^{-1} sec.$^{-1}$ ($\pm 25\%$); $k_5/k_4 = 0.42$.

Deviations greater than usual perhaps are due to the chemical nature of the aldehydes. Some dimers or polymers may be present, perhaps in equilibrium with the monomer. As the normal method of sample preparation includes a rapid cooling (to $-100°$) and a slower thawing, equilibrium between monomer and polymer may not always be fully established before irradiation.

The modes of reaction have been interpreted as addition to the carbonyl group and abstraction of the carbonyl hydrogen, in a manner analogous to the reactions with aliphatic acids. The structure of the alkyl chain apparently does not affect the reactivity of the hydrogen atoms.

Abstraction of hydrogen from the carbonyl group has been suggested previously[11-16] as one step in the gas phase photolysis of aldehydes. The value of 6 kcal. reported for the gas phase at room temperature ($P = 1$)[13] is higher than can be allowed from our results. Curiously, we find no previous suggestion that hydrogen atoms add to the carbonyl group.

Ketones.—Hydrogen atoms both add to, and abstract hydrogen from, aliphatic ketones (Table IV). For dialkyl ketones the rate of addition is in the same general range, but individual values are significantly different. The rates of abstraction vary widely, and attempts to relate the reactivity to chemical structure have not been successful.

In view of the general inertness of alkyl chains to hydrogen atoms, as exemplified by alkanes, alcohols, acids, esters and aldehydes, one is loath to attribute the hydrogen abstraction reaction to simple abstraction from the alkyl group, although such a step has long been considered part of the mechanism for ketone photolysis.[17] Although we know of no data for or against the postulate, it is proposed that hydrogen abstraction takes place from the enol form, *e.g.*

$$\mathrm{R{-}\underset{\displaystyle OH}{\underset{|}{C}}{=}CH_2} + H \longrightarrow \mathrm{R\underset{\displaystyle O}{\underset{|}{C}}{=}CH_2} + H_2 \qquad (7)$$

$$\longrightarrow \mathrm{R\underset{\displaystyle O\\ \displaystyle H}{\underset{|}{C}}{=}\dot{C}H} + H_2 \qquad (8)$$

In the enol form, hydrogens on both the olefinic carbon and on the oxygen are expected to be reactive. Addition of hydrogen to the olefin group of the enol would in one case give the same product as addition to the keto form.

TABLE IV

REACTIVITY OF HYDROGEN ATOMS WITH KETONES

$T = 23 \pm 1°$

Ketone	k_4 (addition) $\times 10^{11}$ cc. mole^{-1} sec.$^{-1}$	k_5 (abstraction)	k_5/k_4
Acetone	3.2	1.6	0.51
Methyl ethyl ketone	3.2	1.5	.47
Diethyl ketone	3.8	1.7	.44
Methyl *n*-propyl ketone	2.8	0.75	.27
Methyl isopropyl ketone	3.9	0.6	.16
Methyl isobutyl ketone	3.0	1.32	.44
Diisopropyl ketone	3.5	0.7	.20
Cyclohexanone	6.8	2.4	.35
Acetophenone	12.0	<0.6	< .05
Benzophenone	27.7	<1.0	< .05
Dichlorotetrafluoroacetone	10	<1.0	< .10

With all these possibilities of varying reactivities and equilibria between the keto and enol form it is understandable why a consistent pattern of rate constants is unlikely.

It would appear that the reactions of hydrogen atoms on ketones differ in the gas and the liquid state. Harris and Steacie,[17] using a Wood's tube as a source of hydrogen atoms, found the main reaction to be hydrogen abstraction. On the other hand Strong and Burr[7] showed that hydrogen atoms, produced by the radiolysis of isopropyl

(8) A. S. Newton, *J. Phys. Chem.*, **61**, 1485 (1957).

(9) A. S. Newton, *ibid.*, **61**, 1490 (1957).

(10) W. R. McDonell and S. Gordon, *J. Chem. Phys.*, **23**, 208 (1955).

(11) J. A. Leermakers, *J. Am. Chem. Soc.*, **56**, 1537 (1934).

(12) F. Patat, *Z. physik. Chem.*, **B32**, 274 (1936).

(13) W. R. Trost, B. de B. Darwent and E. W. R. Steacie, *J. Chem. Phys.*, **5**, 203 (1947).

(14) D. C. Grahame and G. K. Rollefson, *ibid.*, **8**, 98 (1940).

(15) F. E. Blacet and J. N. Pitts, Jr., *J. Am. Chem. Soc.*, **74**, 3382 (1952).

(16) P. A. Leighton, L. D. Levanas, F. E. Blacet and R. D. Rowe, *ibid.*, **59**, 1843 (1937).

(17) G. M. Harris and E. W. R. Steacie, *J. Chem. Phys.*, **13**, 554 (1945).

alcohol as solvent, were scavenged by acetone in an addition reaction. In this same study evidence for hydrogen abstraction was found, for about 3.5% of the hydrogen formed on the radiolysis of isopropyl alcohol containing 5% acetone-d_6 appeared as HD. Such a result is in complete agreement with our findings.

By way of contrast, alkyl radical reactions with ketones, usually occurring as a secondary step in ketone photolysis or pyrolysis in the gas phase, appear to be exclusively hydrogen abstraction reactions.

Methyl-Substituted Benzenes.— The reactivity of hydrogen atoms with a series of methyl-substituted benzenes is given in Table V. In all cases the intercept of the kinetic plot was within ±5% of 0.316. Hydrogen abstraction, if it occurs, must do so with a rate constant of 10^{10} cc. mole^{-1} sec.$^{-1}$ or less.

TABLE V

REACTIVITY OF HYDROGEN ATOMS WITH METHYL-SUBSTITUTED BENZENES

$T = 23 \pm 1°$

Compound	k_4 (addition) cc. mole^{-1} sec.$^{-1}$
Benzene	1.8×10^{11}
Toluene	2.9
o-Xylene	2.7
m-Xylene	2.9
p-Xylene	4.2
1,2,4-Trimethylbenzene	5.4
1,3,5-Trimethylbenzene	5.5
1,2,3,5-Tetramethylbenzene	4.1
1,2,4,5-Tetramethylbenzene	4.0
Pentamethylbenzene	3.7
Hexamethylbenzene	2.7

It is perhaps a virtue of the general method of measuring relative rate constants that there is no inherent correction for the size of the solute molecules. Thus, in the present case where one is dealing only with addition to the benzene ring, the same relative number of collisions of hydrogen atoms with solvent molecules and the benzene ring will occur with all solutes. In practice, however, this concept is modified by a shielding effect owing to the substituted methyl groups.

An examination of the results in Table V shows that on substituting up to three methyl groups on the benzene ring the reactivity is increased. As more methyl groups are added, the rate decreases, perhaps owing to steric hindrance of the methyl groups, preventing collision with the ring nucleus.

With the exception of *p*-xylene, approximately the same rate is found for compounds having the same number of methyl groups. The increased rate with *p*-xylene may be due to increased resonance in the benzene ring when the *para* positions are similarly occupied.

This stepwise change in reaction rate as a function of the number of methyl groups may be considered as the result of two processes. As methyl groups are added, the activation energy of addition decreases, giving rise to a faster rate. In the opposite direction, however, is a decrease in the probability of a hydrogen atom colliding with the ring portion of the molecule. This latter effect of steric hindrance of course will increase with the number of substituted methyl groups.

Even if this picture of opposing factors is correct, it is not possible from the present data to separate them in quantitative fashion. The above interpretation could be checked by a measurement of the temperature coefficients of the hydrogen atom reactions. Unfortunately, however, methods of experimentally determining activation energies for hydrogen atom reactions in solution are not as yet properly developed.

The reactivity of hydrogen atoms with benzene and toluene has been studied in the gas phase by Allen, Melville and Robb.[18] Comparison in the case of benzene is not justified, for benzene was one of the compounds used to establish an absolute value for k_3.[2] The reactivity of hydrogen atoms with toluene, however, is much higher than was reported by Allen.[18] The discrepancy is somewhat puzzling, but as our result for toluene fits into a general pattern of reactivity, more confidence has been placed in the present value.

Alkyl Benzenes.—The rate constants for the reaction of hydrogen atoms with a series of alkyl benzenes are listed in Table VI. Both addition and hydrogen abstraction occur.

From the similarity of the rates of addition to most monosubstituted benzenes, it would appear that the rate of addition of hydrogen atoms to the benzene ring is independent of the nature of the alkyl substituent. With the same relative frequency of collisions with the benzene ring for all monoalkyl benzenes, the close agreement of measured rate constants is considered to represent a true agreement of reactivities by hydrogen atom addition.

TABLE VI

REACTIVITY OF HYDROGEN ATOMS WITH SOME ALKYL BENZENES

$T = 23 \pm 1°$

Compound	k_4 (addition) $\times 10^{11}$ cc. mole^{-1} sec.$^{-1}$	k_5 (abstraction)
Ethylbenzene	3.5	1.1
n-Propylbenzene	3.3	0.6
n-Butylbenzene	3.3	0.5
Isopropylbenzene	3.8	0.2
sec-Butylbenzene	3.5	0.8
t-Butylbenzene	2.7	<0.1
t-Amylbenzene	3.5	<0.2
o-Diethylbenzene	4.6	0.6
m-Diethylbenzene	4.3	1.0
p-Diethylbenzene	4.9	1.9
Hexaethylbenzene	4.1	2.2
p-Diisopropylbenzene	3.0	0.8
1,3,5-Triisopropylbenzene	3.2	0.2

For *t*-butylbenzene, which has a lower rate of hydrogen atom addition than is general, it is perhaps significant that all three substituents on the α-carbon atom are identical. It may be more than coincidental that the rate constant is close to that for toluene (Table V).

As in the case of methyl-substituted benzenes,

(18) P. E. M. Allen, H. W. Melville and J. C. Robb, *Proc. Roy Soc.* (London), **A218**, 311 (1953).

the addition of successive ethyl groups to the benzene ring would appear to reach a maximum value for reactivity and then decrease. The contribution of ethyl groups to steric hindrance of course will be greater and less well defined, and in addition hydrogen abstraction may occur on collision with an ethyl group. The same effect does not appear in the limited results for isopropylbenzenes, but it may be that the opposing factors affecting the rate tend to cancel out.

It is interesting to compare the total rate of reaction (k_4+k_5) of hydrogen atoms with the *o*-, *m*- and *p*-isomers of the dimethyl- and diethylbenzenes. Within each isomer group the rates of reaction of the *o*- and *m*-isomers are equal, while the rate with the *p*-isomer is much greater. A similar result has been observed with *o*-, *m*- and *p*-terphenyl (Table VII).

In contrast to their behavior with methyl-substituted benzenes, hydrogen atoms do abstract from many alkyl-substituted benzenes. Since those showing no hydrogen abstraction have alkyl groups on all three positions of the α-carbon atom, it is reasonable to suppose that hydrogen atoms are abstracted from the α-carbon position exclusively. The results are not sufficiently accurate to justify further comparison among the compounds studied, but on increasing the number of substituted groups a greater rate of hydrogen abstraction usually occurs.

Somewhat surprisingly, the rates of hydrogen atom abstraction from isopropylbenzenes are considerably lower than the rates for the corresponding ethyl compounds. In this case the decrease in rate is not considered to be due entirely to steric effects.

Acetylenes.—The reactivity with only one alkyne has been studied: heptyne-1. The rate of hydrogen atom addition is 8.0×10^{11} cc. mole^{-1} sec.$^{-1}$; the rate of hydrogen atom abstraction is 1.6×10^{11} cc. mole^{-1} sec.$^{-1}$. As it is expected that the alkyl group will be relatively inert, these reactivities are assumed to be general for all alkynes.

Nitriles and Nitroalkanes.—Considerable technical difficulty was encountered with these materials. Some are sparingly soluble in *n*-hexane. With all there appeared evidence that a portion of the solute was being absorbed on the surface of glass, both in the make-up volumetric flasks and in the irradiation cells themselves. The results accordingly are somewhat erratic. However, within the limits of experimental error, the reactivity of hydrogen atoms with all compounds within each group was the same. For aliphatic nitriles $k_4 = 3.0 \times 10^{11}$ cc. mole^{-1} sec.$^{-1}$ ($\pm 25\%$); $k_5 = 1.4 \times 10^{11}$ cc. mole^{-1} sec.$^{-1}$ ($+25, -100\%$). No great confidence is placed in a significant value of k_5. For nitroalkanes $k_4 = 7.0 \times 10^{11}$ cc. mole^{-1} sec.$^{-1}$ ($\pm 25\%$); $k_5 > 10^{11}$ cc. mole^{-1} sec.$^{-1}$.

Sulfur Compounds. (a) **Carbon Disulfide.**—Hydrogen atoms react with carbon disulfide by addition; $k_4 = 26.4 \times 10^{11}$ cc. mole^{-1} sec.$^{-1}$.

(b) **Dimethyl Disulfide.**—Hydrogen atoms react by addition only; $k_4 = 44 \times 10^{11}$ cc. mole^{-1} sec.$^{-1}$. This confirms the known high efficiency of this compound as a radical scavenger.

(c) ***t*-Butyl Mercaptan.**—This compound proved relatively inert, $k_4 < 10^{11}$ cc. mole^{-1} sec.$^{-1}$. Part of this reactivity may be due to disulfide impurities, which would markedly increase the apparent reactivity. Spot checks with other simple mercaptans confirmed a low reactivity with hydrogen atoms.

Free Radicals.—Diphenylpicrylhydrazil (DPPH), a stable free radical, is sparingly soluble in *n*-hexane (~0.5 m*M*/l.). Various concentrations, made up by weight and checked by e.s.r., were irradiated. Although the decrease in G_{H_2} was small, the data were sufficiently reproducible to demonstrate that the kinetic plot gave a straight line of intercept 0.32 ± 0.06. Assuming no hydrogen abstraction, $k_4 = 1.05 \times 10^{13}$ cc. mole^{-1} sec.$^{-1}$ ($\pm 10\%$).

A second free radical

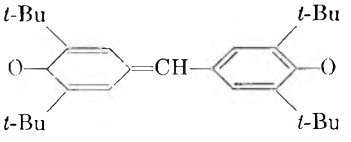

(Coppinger's Radical—CR)[19] was found to be more soluble in *n*-hexane. The hydrogen yields from the system *n*-hexane–CR, plotted kinetically, gave a straight line of intercept 0.320. The rate of hydrogen atom addition was found to be 9.0×10^{12} cc. mole^{-1} sec.$^{-1}$.

The kinetics indicate that these radicals react as true hydrogen atom scavengers. As might be expected the rate of addition is the highest which has been measured in our experimental work.

Miscellaneous Aromatic Compounds.—The reactivity of hydrogen atoms with a number of aromatic compounds is shown in Table VII. All react by addition only. Roughly speaking they can be divided into two classes, the first group having reactivities below 6×10^{11} cc. mole^{-1} sec.$^{-1}$, the other group having reactivities above 10×10^{11} cc. mole^{-1} sec.$^{-1}$. To the first group can be added the alkyl benzenes (Tables V and VI). To the second group can be added acetophenone and benzophenone.

In the first group the compounds are similar to alkyl benzenes in that a relatively inert group is attached to the benzene ring. For comparative purposes one-half the value of the rate constant for bibenzyl and diphenylmethane should be used, for this gives the rate of attack for one benzene ring. Assuming that steric hindrance is the same for monosubstituted groups, the reactivity due to substituents increases in the order $H < C_6H_5 < C_6H_5CH_2 < CH_3 <$ alkyl $< NH_2 < OH < CH_2OH$.

The distinguishing feature of the second group is that all compounds have a reactive group conjugated to the benzene ring. As might be expected this results in greatly increased reactivity. The mode of attack of hydrogen atoms is not known, except that reaction occurs by addition. This uncertainty, coupled with the varying sizes of the compounds, nullified any attempts to assign reactivity to structure in this group.

Normally benzyl acetate would not belong to

(19) G. M. Coppinger, *J. Am. Chem. Soc.*, **79**, 501 (1957).

TABLE VII

REACTIVITY OF HYDROGEN ATOMS WITH SOME AROMATIC COMPOUNDS

$T = 23 \pm 1°$

	k_4 (addition) $\times 10^{11}$ cc. mole^{-1} sec.$^{-1}$
Aniline	4.0
Phenol	4.2
Bibenzyl	4.4
Diphenylmethane	4.6
Benzyl alcohol	6.0
Benzoic anhydride	8.8
Benzonitrile	10.0
Nitrobenzene	12.5
Biphenyl	13.5
Toluonitrile	14
Monoisopropylbiphenyl	14
Naphthalene	14.6
Triphenylene[a]	15
Acenaphthene[a]	15
α-Methylnaphthalene	15.5
Phenanthrene[a]	18
o-Terphenyl	20
m-Terphenyl	20
trans-Stilbene	21.9
5-Butylanthraquinone	23.5
Benzyl acetate	27
Anthracene[a]	31
p-Terphenyl[a]	37
Tetraphenylbutadiene[a]	39

[a] Compounds were insufficiently soluble to give data over a suitably wide concentration range. An intercept of 0.316 was assumed, and a mean value of the slope from several points was used to determine relative rates.

the group, for the structure is not obviously conjugated, nor would the sum of the reactivities of the benzene ring and the ester add up to the experimentally determined rate. It may be that for this compound a hydrogen bond exists between the *ortho* hydrogen and the doubly bound oxygen of the carbonyl group, in effect giving two condensed six-membered rings.

The results in the system *t*-butylanthraquinone (TBA) in *n*-hexane are in contrast to those obtained by Dewhurst.[20] In his system, however, solutions of 1 and 2 mM TBA were irradiated to ~5 Mrad., probably producing 10–15 mM/l. of unsaturated products. It is suggested that for much of the radiolysis hydrogen atoms disappeared by reaction with these unsaturates, rather than by reaction with TBA.

Effect of Temperature.—Radiolytic hydrogen yields from pure *n*-hexane at various temperatures are shown in Table VIII. A slight but steady decrease is observed with decreasing temperatures. The radiolytic hydrogen yields from solutions of methyl methacrylate (MMA) in *n*-hexane were measured in the same temperature range. The results for three temperatures are plotted kinetically (Fig. 2). From the intercept G_2 is obtained, and from the slope and G_2, the relative values k_3/k_4 are obtained. The results are summarized in Table VIII.

Taylor, Mori and Burton[21] found a decrease in $G_{H_2(0)}$ in the radiolysis of liquid neopentane be-

(20) H. A. Dewhurst, *J. Phys. Chem.*, **62**, 15 (1958).

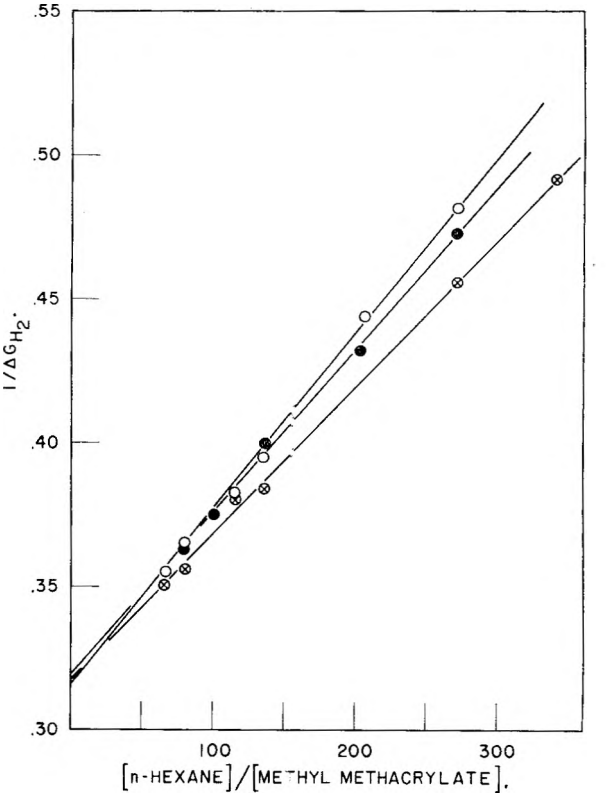

Fig. 2.—Kinetic plot for the reactivity of hydrogen atoms on the system—methyl methacrylate in *n*-hexane solution—as a function of temperature. ○, 23°; ⊗, 0°; ●, −19°.

TABLE VIII

VALUES OF G_1, G_2, $G_{H_2(0)}$ AND k_3/k_4 AT VARIOUS TEMPERATURES

	Temperature			
	23°	0°	−4°	−19°
$G_{H_2(0)}$ (± 0.03)[a]	5.28	5.21	5.17	5.14
G_1	2.12	2.06		2.01
G_2	3.16	3.15		3.13
k_3/k_4	1.92×10^{-3}	1.66×10^{-3}		1.79×10^{-3}

[a] Indicates the reproducibility in at least four runs at each temperature.

tween +50 and −20° Taubman, *et al.*,[22] reported no significant change in the radiolytic hydrogen gas yield from *n*-octane and *n*-decane between −60 and +90°, although no limits of error were given. Dewhurst[20] reported $G_{H_2(0)}$ = 3.5 at −78° for *n*-hexane; in preliminary experiments we find $G_{H_2(0)} = 4.8 \pm 0.2$ at this temperature. Previously we had reported that the change in $G_{H_2(0)}$ for several alkanes was less than 3% between −25 and +40°.[2]

It perhaps is surprising to find the yield of hydrogen atoms unaffected by temperature, while the "molecular" or "hot atom" hydrogen decreases with temperature. No satisfactory explanation has been found.

The ratio k_3/k_4 varies with temperature, but has a minimum value at about 10°. This result is an indication of the complicated nature of the diffusion and competitive reaction processes taking place in solution. Attempts to interpret the data

(21) W. H. Taylor, S. Mori and M. Burton, *J. Am. Chem. Soc.*, **82**, 5817 (1960).

(22) A. B. Taubman, L. P. Ivanova, *et al.*, *Doklady Akad. Nauk. S.S.S.R.*, **134**, No. 2, 397 (1960).

are hindered by a lack of knowledge of certain parameters (*e.g.*, what constitutes a collision between a hydrogen atom and a solvent molecule) and by the general elementary state of the theory of diffusion processes in liquids as applied to a system such as the present one.

An understanding of the effects of temperature on hydrogen atom reactivity in the liquid phase must await further theoretical development. In the meantime it would appear most unwise to assign energies of activation to hydrogen atom processes in solution when measured by this radiolytic method.

Comparison of *n*-Hexane and Methanol as Solvents and Sources of Hydrogen Atoms.—As indicated in the section on alcohols, and as shown by the experiments of Strong[7] and Baxendale,[6] aliphatic alcohols may be used as solvents and *in situ* sources of hydrogen atoms in the same manner as saturated hydrocarbons. In a series of experiments the hydrogen yields from pure methanol and from methanol solutions of (1) methyl methacrylate and (2) benzene were measured. For pure methanol $G_{H_2} = 3.95$, in good agreement with some workers,[6,10] but lower than was found by others.[23,24] The hydrogen yields for the solution, plotted kinetically, gave $G_2 = 2.52$, $G_1 = 1.43$. Data of Adams[6] using benzoquinone as a solute give substantially the same result.

Hydrogen yields were measured using two other solutes, cyclohexene and *cis*-pentene-2. Both addition and hydrogen abstraction were measured. With cyclohexene as solute $k_3/k_4 = 1.32 \times 10^{-3}$, $k_5/k_4 = 0.11$; with *cis*-pentene-2 as solute $k_3/k_4 = 1.53 \times 10^{-3}$, $k_5/k_4 = 0.09$.

In Table IX the ratios of the rate constants $(k_4+k_5)/k_3$ are compared for the solvents methanol and *n*-hexane, using various solutes. The ratio $k_{H + n\text{-hexane}}/k_{H + \text{methanol}}$ (last column) is reasonably constant. It would appear that the same kinds of processes are occurring in methanol solution as in *n*-hexane solution.

The actual value of the ratio does not necessarily mean that the rate of attack of hydrogen atoms on methanol is 1/5.8 of that on *n*-hexane, (*i.e.*, 8.5×10^8 cc. mole^{-1} sec.$^{-1}$). The rate of attack on the solvent is affected by the relative size of the solvent molecules, the extent of association, the rate of various diffusion processes, effect of structure on reactivity, etc. The results confirm those found in the section on aliphatic alcohols, namely, that the hydroxyl hydrogen is relatively inert to abstraction by hydrogen atoms.

Comment on the Accuracy of the Rate Constant Values.—All rate constant values are based on the premise that under our conditions of measurement $k_{(H + n\text{-Hexane})} = 4.9 \times 10^9$ cc. mole^{-1} sec.$^{-1}$ at 23°. This intermediate standard value in turn is derived from other comparative experiments performed by the author[2] and by others.[18] In the course of such a sequence of comparisons, errors accumulate. The values of some of the constants used, *e.g.*, the effective collision diameters of the hydrogen atom in liquids and in gases, are not known accurately. In view of the many correlations it is questionable whether results reported here are known to better than a factor of 2 or 3 or an absolute scale. On the other hand evidence was presented in a previous paper[2] which indicates satisfactory agreement between the rates of H atom reactions in liquid and in gas phase. As more experimental evidence accumulates the uncertainty in absolute values will be less. For the present, we shall continue to obtain relative rate constants (k_3/k_4 and k_5/k_4) with the greatest possible precision.

(23) G. Meshitsuka and M. Burton, *Radiation Research*, **8**, 285 (1958).

(24) N. N. Lichtin, *J. Phys. Chem.*, **63**, 1449 (1959).

TABLE IX

REACTIVITY OF H ATOMS WITH SOLVENTS

COMPARISON OF $k_{H+n\text{-HEXANE}}$ WITH $k_{H+\text{METHANOL}}$

Solute	Rate constant ratio $\frac{(k_4 + k_5)}{k_3}$ Methanol	*n*-Hexane	Ratio $\frac{k_{H+n\text{-Hexane}}}{k_{H+\text{Methanol}}}$
cis-Pentene-2	713	127	5.6
Cyclohexene	822	127	6.8
Benzene	106	25.6	4.1
Methyl methacrylate	3020	520	5.8
			5.6 ± 1.0

It perhaps is more important at this point to designate the extent of systematic and random errors associated with the present experimental method. Systematic errors are (1) those involved in apparatus calibration and operation, and are considered to be low (<1%) and, (2) those involved in relating results from the Fricke dosimeter to the amount of energy absorbed in *n*-hexane (±2%). Since the experimental method requires a comparison of hydrogen yields (G_{H_2}) without and with scavenger, systematic errors have little effect on the final result.

Random errors involve mainly the reproducibility of hydrogen analysis and dosimetry measurements, plus any error arising from variation in handling procedures. These have been considered together and experimentally it has been found that in a given system 95% of the hydrogen yields measured are within ±1% of the mean value; 50% are within ±0.5% of the mean value. The error in $G_{H_{2(0)}}$ is smaller (±0.3%) as a result of a large number of determinations.

The error in k_3/k_4, or more properly, in the slope of the kinetic plot, varies with reactivity and with experimental conditions. The abscissa values, or ratios of concentrations, are known with sufficient accuracy to be considered as constants. Measurable deviations will arise only from the uncertainty of ordinate values.

The generalized plot of hydrogen yield *vs.* solute concentration (Fig. 1) is better used to illustrate the source of error in the determination of hydrogen atom reactivity. At low solute concentrations (region A) one is measuring a small difference of two large numbers, and the error will be a significant fraction of this difference. When converted to a reciprocal, the error is of considerable magnitude.

In region C very little change in hydrogen yield occurs as the solute concentrations increase. Although $1/\Delta G_{H_2}$ is determined with good precision, there is sufficient error to affect the kinetic plot

significantly, for it is these data which most affect the value of the intercept. In this region of high solute concentration a correction must be made for energy absorbed in the solute, and for hydrogen atoms evolving from it. At more than 2% solute concentration such corrections become more uncertain and the error accordingly increases.

The most suitable region for making hydrogen yield measurements is at that in which the solute concentrations give G_{H_2} = 4.2–3.0 (region B). Ideally this should cover at least a three-fold range in solute concentration.

Usually a compromise must be made. In the case of esters the reactivity is so low that G_{H_2} = 4.0 at 2% concentration. With methyl methacrylate ($k_3/k_4 = 2.55 \times 10^{12}$ cc. mole^{-1} sec.$^{-1}$) the reactivity is such that a desirable combination of wide range in G_{H_2} at low solute concentration can be obtained.

The precision with which the rate constants can be measured is considered to be

$<10^{11}$ cc. mole^{-1} sec.$^{-1}$ ± 7%
1–5 × 10^{11} cc. mole^{-1} sec.$^{-1}$ ± 5%
>5 × 10^{11} cc. mole^{-1} sec.$^{-1}$ ± 3%

In some instances (marked with a superscript *a* in Table VII) the solubility of the solute in *n*-hexane is too low to obtain a suitably wide range of solute concentration. The error accordingly is larger.

Acknowledgment.—The author wishes to thank the Nuclear Physics Section for the operation of the Van de Graaff accelerator, and Mr. H. O. Strange for the preparation of Coppinger's radical.

COMPARATIVE STUDIES ON THE DECARBOXYLATION OF PICOLINIC ACID AND MALONIC ACID IN THE MOLTEN STATE AND IN SOLUTION

BY LOUIS WATTS CLARK

Department of Chemistry, Western Carolina College, Cullowhee, North Carolina

Received August 10, 1961

Kinetic data are reported for the decarboxylation of picolinic acid in the molten state and in *p*-cresol, aniline, phenetole, β-chlorophenetole, *p*-dimethoxybenzene and nitrobenzene, as well as for the decarboxylation of malonic acid in *p*-dimethoxybenzene. The parameters of the Eyring equation are calculated and a possible mechanism of the reaction is suggested.

Schenkel and Klein studied the decarboxylation of picolinic acid in the molten state as well as in several polar solvents by means of the loss in weight, allowing the CO_2 to escape.[1] Cantwell and Brown studied the decarboxylation of this acid in acid, basic and neutral media by weighing quantitatively the amount of CO_2 evolved in measured time intervals.[2] Results of these studies led the authors to favor the zwitterion as the initial reacting form, and to propose a unimolecular mechanism for the reaction. They found, nevertheless, that the rate of decomposition of picolinic acid was lowered and the activation energy raised by both acids and bases.

Fraenkel and co-workers have shown that, in the decarboxylation of malonic acid in polar liquids, a bimolecular mechanism is involved, and that, in the rate-determining step, the electrophilic, polarized, carbonyl carbon atom of a carboxyl group unites with an unshared pair of electrons on a nucleophilic atom of solvent.[3] Other unstable acids, including oxalic acid,[4] oxamic acid,[5] and oxanilic acid,[6] as well as the trichloroacetate ion,[7] have been shown to decompose by this same mechanism. It appeared logical to assume, therefore, that other unstable acids, including picolinic acid, should undergo decarboxylation by a mechanism similar to that of malonic acid. In order to test this possibility kinetic studies have been carried out in this Laboratory on the decarboxylation of picolinic acid in the molten state, as well as in the solvents phenetole, *p*-cresol, nitrobenzene, β-chlorophenetole, *p*-dimethoxybenzene and aniline. For the sake of comparison the decarboxylation of malonic acid was studied in *p*-dimethoxybenzene. The results of this investigation are reported herein.

(1) H. Schenkel and A. Klein, *Helv. Chim. Acta*, **28**, 1211 (1945).
(2) N. H. Cantwell and E. V. Brown, *J. Am. Chem. Soc.*, **75**, 4466 (1953).
(3) G. Fraenkel, R. L. Belford and P. E. Yankwich, *ibid.*, **76**, 15 (1954).
(4) L. W. Clark, *J. Phys. Chem.*, **61**, 699 (1957).
(5) L. W. Clark, *ibid.*, **65**, 180 (1961).
(6) L. W. Clark, *ibid.*, **65**, 572 (1961).
(7) L. W. Clark, *ibid.*, **63**, 99 (1959).

Experimental

Reagents.—Picolinic acid 99.5% assay, and malonic acid, 100.0% assay, were used in this research. The solvents used were reagent grade or highest purity chemicals and were freshly distilled immediately before use.

Apparatus and Technique.—The apparatus and technique used in studying the decarboxylation of picolinic acid and malonic acid in polar solvents (involving measuring the volume in ml. of CO_2 evolved at different time intervals) has been described previously.[8] The thermometer used to determine the temperature of the thermostat, as well as the buret in which the CO_2 was collected, were calibrated by the U. S. Bureau of Standards. In each experiment a 0.2212-g. sample of picolinic acid, or a 0.1870-g. sample of malonic acid (the quantities needed, respectively, to furnish 40.0 ml. of CO_2 at STP on complete reaction) was weighed quantitatively into a fragile glass capsule and was introduced in the usual manner into the reaction flask containing approximately 60 ml. of solvent previously saturated with dry CO_2 gas.

In the study of the decarboxylation of molten picolinic acid the same apparatus and technique as was used for studying the reaction in solution was adopted, except that, for the 3-neck flask, there was substituted an L-shaped 10 mm. o.d. Pyrex brand glass tube 30 cm. in length, sealed at one end, and provided with a 19/38 standard taper outer joint at the other end.

Results

The decarboxylation of molten picolinic acid was studied at 5 different temperatures between 167 and 188°, the experiment being performed twice

(8) L. W. Clark, *ibid.*, **60**, 1150 (1956).

at each temperature. The evolved CO_2 (converted to STP) was plotted against time for each experiment. Straight lines resulted when the log $(V_\infty - V_t)$ was plotted against time from representative points on the smoothed experimental plots.

The decarboxylation of picolinic acid in the six solvents studied, as well as the decarboxylation of malonic acid in *p*-dimethoxybenzene, was first order. Reactions in each solvent were carried out two or three times at three or four different temperatures over a 20° temperature range. The average values of the apparent first-order rate constants for the decarboxylation of molten picolinic acid as well as for the reactions of the two acids in the various solvents at the different temperatures studied were obtained from the slopes of the experimental logarithmic plots. The experimental data are reproduced in Table I. The parameters of the Eyring equation, based upon the data in Table I, are shown in Table II, along with supplementary data for malonic acid obtained previously.

TABLE I

APPARENT FIRST-ORDER RATE CONSTANTS FOR THE DECARBOXYLATION OF MOLTEN PICOLINIC ACID, AND OF PICOLINIC ACID AND MALONIC ACID IN SEVERAL SOLVENTS

System	Temp. (°C. cor.)	$k \times 10^4$ (sec.$^{-1}$)	Av. dev.
Molten picolinic acid	167.47	1.28	± 0.02
	173.67	2.46	.02
	180.61	3.73	.02
	184.22	7.05	.04
	188.35	10.57	.04
Picolinic acid + *p*-dimethoxybenzene	170.56	1.64	.02
	180.61	3.74	.03
	191.20	8.71	.02
Picolinic acid + β-chlorophenetole	172.46	1.75	.03
	182.72	4.15	.02
	192.89	11.13	.04
Picolinic acid + phenetole	150.71	0.37	.01
	159.60	0.665	.005
	165.47	1.18	.01
	168.2	1.53	.04
Picolinic acid + nitrobenzene	172.36	1.73	.01
	180.50	3.52	.01
	189.61	6.69	.03
Picolinic acid + aniline	160.37	1.20	.02
	168.35	1.66	.02
	178.90	3.98	.02
Picolinic acid + *p*-cresol	170.45	1.19	.02
	179.70	2.79	.02
	189.61	6.69	.03
Malonic acid + *p*-dimethoxybenzene	128.62	1.54	.02
	141.05	4.38	.02
	147.18	7.19	.03

Discussion of Results

The data in Table II can be indicative that picolinic acid decomposes in polar solvents by a mechanism similar to that of malonic acid. For both malonic acid and picolinic acid a progressive decrease takes place in the $\Delta H^\ddagger$ of the reaction as the nucleophilicity of the solvent increases. Also, for both acids, anticipated steric effects among the different solvents are reflected by parallel changes in the $\Delta S^\ddagger$ of the reaction. For example, on going from phenetole to β-chlorophenetole, the $\Delta S^\ddagger$ of the malonic acid reaction decreases about 2 e.u./mole while that of the picolinic acid reaction decreases by 6.5 e.u./mole—between phenetole and *p*-dimethoxybenzene the $\Delta S^\ddagger$ for the malonic acid reaction decreases by 4.8 e.u./mole, for picolinic acid it decreases 9.1 e.u./mole. Greater steric hindrance would be expected to be encountered in the picolinic acid reaction than in that of malonic acid due to the proximity of the pyridine nucleus to the carboxyl group in the former.

The $\Delta H^\ddagger$ for the malonic acid reaction in each solvent is smaller than it is for that of picolinic acid. This is due to the fact that the effective positive charge on the carbonyl carbon atom of malonic acid is greater than it is on that of the zwitterion of picolinic acid. In malonic acid we have a strongly electron withdrawing carboxyl group attached to the α-carbon atom of a terminal acetic acid moiety. In the zwitterion of picolinic acid we have attached to the α-carbon atom of the carboxylate ion a much more weakly electron withdrawing imino group.

The value of $\Delta S^\ddagger$ in each system is smaller for malonic acid than it is for picolinic acid, a result to be expected in view of the tendency of dicarboxylic acids to associate into "supermolecule" clusters, whereas the zwitterions would have less tendency to associate.

It has been suggested that, in the decarboxylation of molten malonic acid, the transition state consists of a complex between a polarized, electrophilic, carbonyl carbon atom of one molecule of malonic acid with a nucleophilic hydroxyl oxygen atom on a neighboring malonic acid molecule, both the electrophilic and nucleophilic agents existing as associated complexes composed of two or more molecules each.[13] In molten picolinic acid a similar mechanism probably obtains—the electrophilic carbonyl carbon atom of a zwitterion coördinating with the nucleophilic nitrogen atom on the pyridine moiety of a neighboring molecule or ion. The difference in the $\Delta S^\ddagger$ of these two reactions in the molten state is consistent with this interpretation, since the probability of two picolinic acid ions or molecules combining would be considerably greater than that of two supermolecule clusters of malonic acid. It is worth pointing out in this connection that the values of $\Delta H^\ddagger$ and $\Delta S^\ddagger$ which Cantwell and Brown obtained for the decarboxylation of picolinic acid in the *non-polar solvent* *p*-cymene (39.3 kcal./mole, and +12.8 e.u./mole, respectively[2]) agree within a few tenths of a unit each with those obtained in this research for the decarboxylation of molten picolinic acid (see Table II). It would appear in this case that *p*-cymene is serving as an inert solvent, and that the mechanism of the reaction in the non-polar solvent is the same as that for the decarboxylation of picolinic acid in the molten state.

In spite of the fact that all the solvents studied

(9) C. N. Hinshelwood, *J. Chem. Soc.*, **117**, 156 (1920).
(10) L. W. Clark, *J. Phys. Chem.*, **65**, 2271 (1961).
(11) L. W. Clark, *ibid.*, **62**, 368 (1958).
(12) L. W. Clark, *ibid.*, **62**, 79 (1958).
(13) L. W. Clark, *ibid.*, **64**, 692 (1960).

TABLE II

KINETIC DATA FOR THE DECARBOXYLATION OF PICOLINIC ACID AND MALONIC ACID IN THE MOLTEN STATE AND IN SEVERAL POLAR SOLVENTS[a]

Solvent	Picolinic acid $\Delta H^{\ddagger}$ (kcal./mole)	Picolinic acid $\Delta S^{\ddagger}$ (e.u./mole)	Picolinic acid $\Delta F_{180^\circ}{}^{\ddagger}$ (kcal./mole)	Malonic acid $\Delta H^{\ddagger}$ (kcal./mole)	Malonic acid $\Delta S^{\ddagger}$ (e.u./mole)	Malonic acid $\Delta F_{150^\circ}{}^{\ddagger}$ (kcal./mole)
Melt[9]	39.8	+13.2	33.8	33.0	+ 4.5	31.0
p-Cresol	35.8	+ 3.4	34.3			
Phenetole[10]	35.9	+ 4.5	33.8	29.0	− 6.0	29.3
Nitrobenzene[11]	34.4[b]	+ 0.5	34.1	28.1	− 7.15	30.3
β-Chlorophentole[10]	33.1	− 2.0	34.0	27.8	− 7.9	31.4
p-Dimethoxybenzene	32.0[b]	− 4.6	34.0	27.1	−10.8	32.0
Aniline[12]	31.9[b]	− 4.4	33.9	26.9	− 4.5	28.9

[a] The superscript after the name of the solvent refers to the source of the malonic acid data. [b] These results agree fairly closely with those obtained by Cantwell and Brown using these solvents. See ref. 2.

bring about a lowering of the $\Delta H^{\ddagger}$ in the case of picolinic acid, the rate of reaction is faster in the molten state than in solution as shown by the values of $\Delta F_{180}{}^{\circ\ddagger}$ for the reaction. This may be ascribed to the fact that more steric hindrance is encountered by the zwitterion in attacking a nucleophilic atom of solvent than in uniting with a picolinic acid molecule or ion, as a comparison of the $\Delta S^{\ddagger}$ values in Table II indicates.

Acknowledgment.—The support of this research by the National Science Foundation, Washington, D. C., is gratefully acknowledged.

KINETICS OF EXTRACTION OF ZINC DITHIZONATE

BY CARL B. HONAKER AND HENRY FREISER

Department of Chemistry, The University of Arizona, Tucson 25, Arizona

Received August 10, 1961

The rate of extraction of zinc ion from aqueous solution, using organic solutions of dithizone, has been found to be first order with respect to zinc, first order with respect to dithizone, and inverse first order with respect to hydrogen ion. It is possible, from the data obtained in this study, to formulate the rate-controlling step as consisting of the reaction of a dithizonate ion with a hydrated zinc ion in the aqueous phase. The unexpected slowness of the addition of the first ligand is probably due to the fact that the formation of the monodithizonatodiaquo complex involves the breaking of four water–zinc bonds, whereas the addition of the second ligand requires the breaking of only two such bonds. The rate constant for the reaction was found to be on the order of 1×10^9 l. mole^{-1} min.$^{-1}$. The temperature dependence of the extraction rate was determined and the energy and entropy of activation have been calculated.

Introduction

A survey of the literature shows that little attention has been given to the study of solvent extraction under non-equilibrium conditions. Walkley[1] has published a brief study of the extraction of zinc dithizonate and Irving, Andrew and Risdon[2] have reported work on the separation of copper and mercury by extraction with dithizone under non-equilibrium conditions. Geiger[3] has reported the effect of *p*H on the rate of extraction of copper(II) dithizonate.

Under certain conditions dithizone extractions of zinc give rise to a transient, reddish-purple color in the aqueous phase. This observation seemed in sharp contrast to the well-known rapid formation of zinc complexes.

This paper presents the results of a detailed study of the kinetics of the reactions involved in the zinc–dithizone extractions.

The formation constants of zinc dithizonate also were determined for the first time.

Experimental

Apparatus.—All extractions were performed by agitating the samples in separatory funnels mounted on a Burrell model BB Wrist Action Shaker. These funnels, supplied by Eck and Krebs, were jacketed so that the systems could be maintained at constant temperature by means of water circulated from a thermostat. Measurements of radioactivity were made with a Nuclear-Chicago Model DS5-5 Well-Type Scintillation Detector connected to a Model 183B Scaler. For *p*H measurements a Beckman Model G *p*H meter was used. This meter was standardized against *p*H 7 buffer before each set of measurements. Spectrophotometric measurements were made with a Beckman DU spectrophotometer.

Materials.—Specially processed, high activity zinc-65 in the form of $ZnCl_2$ was obtained from Oak Ridge National Laboratories. Reagent grade dithizone was further purified according to the method cited by Welcher.[4] The dithizone solutions were standardized spectrophotometrically immediately before use. All other chemicals were reagent grade. Further purification was found to be superfluous since none of the materials gave a positive test with dithizone. Water was purified by passing it through a column of Deeminite L-10 ion-exchange resin supplied by Crystal Research Laboratories, Inc.

Procedure.—All extractions were made from aqueous solutions having an ionic strength of one produced by the addition of sufficient perchloric acid or sodium perchlorate. With the exception of measurements made to determine the effect of temperature on extraction rates, all extractions were performed at 25 ± 0.05°. Concentration of zinc ion was $2.0 \pm 0.2 \times 10^{-6}$ *M*.

Determination of Equilibrium Constant for the Extraction of Zinc Dithizonate into Carbon Tetrachloride.—The *p*H of the aqueous zinc solution was adjusted to an ap-

(1) A. Walkley, *Proc. Australian Chem. Inst.*, **9**, 29 (1942).
(2) H. Irving, G. Andrew and E. J. Risdon, *J. Chem. Soc.*, 541 (1949).
(3) R. W. Geiger, Ph.D. thesis, University of Minn., 1951.
(4) F. J. Welcher, "Organic Analytical Reagents," Vol. 3, D. Van Nostrand Co., Inc., New York, N. Y., 1953, p. 466.

proximate value; 15-ml. portions were shaken with equal volumes of carbon tetrachloride solutions of dithizone for a period of 12 hr. The concentration of the dithizone solution was on the order of $1 \times 10^{-3} M$. At the end of 12 hr. shaking a 5-ml. aliquot of the aqueous phase was removed and counted. A sample of the original zinc solution, diluted 100-fold to give a reasonable count rate, was counted. Since the count rate is directly proportional to the total concentration of zinc in the sample, the distribution ratio of zinc could be calculated. Sufficient counting time was allowed on each sample to amass a total count of at least 10,000, so that the statistical counting error would be less than 1%. The *p*H of the aqueous phase was measured to the nearest 0.01 *p*H unit. Extractions were made from unbuffered solutions, with the exception of those in the *p*H range of 4.5–6.0. These were buffered with 0.1 *M* acetate.

Partition of Dithizone.—Equal volumes of dithizone in either chloroform or carbon tetrachloride and aqueous Clark and Lubs buffer solution (ionic strength one) were shaken for 15 minutes. The funnels were allowed to stand for 15 minutes to ensure complete separation of the layers. The organic phase was drained into a spectrophotometric cell (after discarding the first few milliliters) and the absorptivity was measured. From a plot of $(A_s \text{ orig} - A_s \text{ final})/A_s \text{ final}$ *vs.* $1/[H^+]$ values were found for K_a/K_{Dr}. The *p*H of the aqueous phase was measured.

Kinetics Studies.—A 15-ml. portion of dithizone solution was placed in a jacketed separatory funnel. The *p*H of the aqueous zinc solution was adjusted and a 15-ml. portion of this solution was pipetted into the funnel in such a way as to produce virtually no mixing and hence no extraction before the shaker was started. The two solutions previously had been brought to the temperature selected for the study. The sample was shaken for a definite time interval on the Burrell shaker, then allowed to stand for five minutes in order to ensure complete separation of the two phases. Preliminary experiments had shown that the rate of extraction during these separation periods was negligible. An aliquot to be counted was removed from the aqueous phase. The aliquots were of 50 λ, 25 λ or 5 ml., depending upon the amount required to give a reasonable count rate. In the case of the micro samples, enough water was added to the aliquot to give a 5-ml. volume of solution to be counted, thus standardizing the geometry and self-absorption of the count sample. In cases where micro volumes of the aqueous phase were removed, the experiment was continued with further samples being taken at suitable intervals until the volume of the aqueous phase had been changed enough to introduce a significant error. The activity of the aliquot was compared with the original activity of the aqueous phase.

Results

Partition of Dithizone.—In order to calculate both the concentration of the dithizonate ion in the aqueous phase and the formation constants for zinc dithizonate, it was necessary to determine the value of the ratio K_a/K_{Dr} for dithizone. It can be shown that

$$1/D_r = \frac{1}{K_{Dr}} + \frac{K_a}{K_{Dr}[H^+]}, \text{ where } D_r = \frac{[HDz]_0}{[HDz]_{aq} + [DZ]_{aq}} \text{ and } K_{Dr} = \frac{[HDz]_0}{[HDz]_{aq}}$$

Thus from the slope of plots of D_r *vs.* $1/[H^+]$, values of the quotient K_a/K_{Dr} for dithizone were calculated to be $2.0 \pm 0.2 \times 10^{-9}$ and $1.3 \pm 0.2 \times 10^{-10}$ for carbon tetrachloride and chloroform, respectively. These values were determined at 25° and with an aqueous phase whose ionic strength was 1.0. At 6° this ratio for the partitioning of dithizone between chloroform and the aqueous phase had a value of $2.5 \pm 0.4 \times 10^{-11}$.

Formation Constants of Zinc Dithizonate.—From a plot of D_x *vs.* $p[Dz]$, stepwise formation constants were calculated using the graphical method of Dyrssen and Sillen.[5] The over-all formation constant was 1.13×10^{15}, while the stepwise constants, k_1 and k_2, had values of 5.6×10^7 and 1.4×10^7, respectively.

Kinetics of Extraction of Zinc Dithizonate.—A preliminary series of experiments was performed to determine the effect on the rate of extraction of varying the shaker speed. It was found that the rate of extraction increased quite rapidly as the shaker speed was increased, up to a maximum value beyond which the increase in agitation had no significant effect on the rate of extraction. In all subsequent determinations a shaking speed within this "plateau" region was used. On this plateau the rate of extraction was chemically controlled, whereas at slower rates of agitation the transfer processes tended to become rate controlling. The "plateau" region using carbon tetrachloride involved more vigorous agitation than when using chloroform. This was to be expected in the light of the greater viscosity of carbon tetrachloride.

In the first runs carbon tetrachloride was used as the organic solvent. Since the extraction was quite rapid, it seemed advisable to shift to chloroform as the extracting medium. Irving[6] had predicted that the rate of extraction of the dithizonates should be much slower with chloroform than with carbon tetrachloride. This choice seemed particularly wise in view of the need to determine rates toward the beginning of the extraction before the magnitude of the reverse reaction became great enough to introduce a serious error into the computations.

Extractions were made using various concentrations of dithizone in the organic phase and varying values of *p*H in the aqueous phase. As a working hypothesis, the reaction was assumed to be first order with respect to concentration of zinc ion in the aqueous phase. This assumption was validated when plots of log $([Zn]_{orig.}/[Zn]_t)$ *vs.* time were made and the points were found to lie on sensibly straight lines. A tabulation of $[H^+]$, $[HDz]_0$ and slope is made in Table I. An inverse first order of the reaction with respect to $[H^+]$ was found from a plot of log slope *vs.* log $[H^+]$, keeping $[HDz]_0$ constant. In similar fashion the order with respect to $[HDz]_0$ at constant *p*H was found to be one.

The four rate determinations made with carbon tetrachloride can be compared with those using chloroform. It is seen from the data in Table I that these extractions are more rapid than the chloroform extractions by a factor of 58.

Extractions were made at various temperatures. At least three samples of different *p*H values were studied at each temperature. Results are given in Table II.

Discussion

The steps involved in the extraction of zinc with dithizone can be delineated as

$$HDz(0) \rightleftharpoons HDz(aq) \quad (1)$$

$$HDz(aq) \rightleftharpoons H^+ + Dz^- \quad (2)$$

$$Zn^{+2} + Dz^- \rightleftharpoons ZnDz^+ \quad (3)$$

$$ZnDz^+ + Dz^- \rightleftharpoons ZnDz_2 \text{ and} \quad (4)$$

$$ZnDz_2(aq) \rightleftharpoons ZnDz_2(0) \quad (5)$$

(5) D. Dyrssen and L. G. Sillen, *Acta Chem. Scand.*, **7**, 663 (1953).
(6) H. Irving and R. J. P. Williams *J. Chem. Soc.*, 1841 (1949).

TABLE I

Run no.	$[HDz]_0 \times 10^4$	$[H^+] \times 10^4$	Slope[a] (min.$^{-1}$)	k',[b] l. mole^{-1} min.$^{-1}$
1	1.10	1.26	1.10	0.32
2	1.31	1.26	0.12	.24
3	1.34	2.14	.12	.43
4	1.34	3.17	.084	.46
5	1.51	0.89	.24	.33
6	1.51	1.59	.19	.46
7	1.51	2.12	.12	.38
8	1.51	0.31	.51	.24
9	1.51	0.58	.33	.29
10	1.51	0.85	.23	.30
11	2.42	1.26	.11	.24
12	3.50	0.81	.63	.34
13	3.91	1.26	.35	.26
14	6.93	0.81	1.65	.45
15	7.92	19.9	0.046	.26
16	7.92	7.95	.088	.20
17	7.92	6.32	.17	.32
18	7.92	1.26	.59	.22
19	7.92	0.80	.68	.16
20	7.92	0.40	.99	.12
21	8.70	0.63	1.10	.18
22	8.70	1.41	0.64	.24
23	10.3	1.26	1.03	.29
24	10.3	1.26	1.03	.29
25	10.4	0.81	2.66	.49
26[c]	0.084	0.71	0.74	14.4
27[c]	.44	1.45	1.98	15.5
28[c]	.44	3.18	1.16	19.3
29[c]	.44	7.42	0.53	20.5

[a] Slope of a plot of log $[Zn]_{orig.}/[Zn]_t$ *vs.* time. [b] $k' = (2.303 \times \text{Slope} \times [H^+])/[HDZ]$. [c] Carbon tetrachloride used as the extracting medium.

The first and last steps can be disregarded as rate controlling, since neither would give rise to a *p*H dependence. Further, Geiger[3] has reported the results of a study of the rate of attainment of partition equilibrium for dithizone between carbon tetrachloride and water. Equilibrium is essentially reached in less than 15 min. This is considerably less time than is needed to attain equilibrium in the zinc dithizonate system. Step 2 can be dismissed as rate controlling on two counts. First, if step 2 were rate controlling, the first-order dependence with respect to zinc would not be explained. Secondly, extractions of other metals (such as Hg^{+2} and Ag^+) with dithizone proceed much more rapidly than that of zinc. This hardly could be the case if the ionization of dithizone were the rate controlling step. Also the rate of partition of HDz is independent of *p*H. If step four were rate controlling, a second-order dependence upon the concentration of dithizonate should be observed. This leaves only step 3 which is first order with respect to both zinc ion and dithizonate ion concentration. The expression representing the observed rate can be written as

$$-\frac{d(Zn^{+2})}{dt} = k' \frac{[Zn^{+2}][HDz]_0}{[H^+]}$$

From a consideration of steps one and two, it is apparent that the concentration of dithizonate ion in the aqueous phase is directly proportional to the concentration of dithizone in the organic phase and inversely proportional to the concentration of

TABLE II

Run no.	Temp., °K.	HDz $\times 10^4$	$H^+ \times 10^4$	Slope (min.$^{-1}$)	k', l. mole^{-1} min.$^{-1}$
30	279	8.7	0.391	0.38	0.020
31	279	8.7	0.195	.62	.023
32	279	8.7	0.048	.84	.011
33	288	7.9	1.20	.10	.035
34	288	7.9	0.514	.28	.042
35	288	7.9	0.289	.47	.040
36	293	10.1	5.76	.11	.14
37	293	10.1	3.47	.23	.18
38	293	10.1	1.82	.41	.17
39	308	9.8	6.77	.31	.50
40	308	9.8	2.34	.85	.47
41	308	9.8	1.00	1.44	.34

TABLE III

Run no.	HDz $\times 10^5$	H $\times 10^5$	Slope $\times 10^3$ (min.$^{-1}$)	$k' \times 10^3$
1	0.81	5 02	0.5	5.8
2	0.81	0 502	15.5	2.2
3	1.88	2 51	2.87	8.8
4	2.18	5 02	1.76	9.3
5	2.18	2 24	3.08	7.3
6	2.18	1 26	4.24	3.1
7[a]	2.18	1 26	4.24	3
8	8.98	2 2	31.3	18
9[b]	2.28	15 9	22.2	354
10[b]	2.24	13 2	28.4	385

[a] Aqueous phase made 0.3 *M* in KCl. [b] Carbon tetrachloride used as the extracting medium. All other extractions were into chloroform.

TABLE IV

Temp., °K.	k', l. mole^{-1} min.$^{-1}$	$K_a/K_{Dr} \times 10^{10}$	$k \times 10^{-9}$, l. mole^{-1} min.$^{-1}$
279	0.019	0.25	0.76
288	.069	0.56	1.23
293	.12	0.81	1.48
298	.25	1.3	1.92
308	.87	2.8	3.11

hydrogen ion in the organic phase and inversely proportional to the concentration of hydrogen ion in the aqueous phase. Therefore, the above rate expression is equivalent to

$$-\frac{d(Zn^{+2})}{dt} = k[Zn^{+2}][Dz^-] = \frac{kK_a}{K_{Dr}} \times \frac{[Zn^{+2}][HDz]_0}{[H^+]}$$

This is the rate equation for step 3, which must be rate controlling.

It is of interest to compare the above results with those obtained by Geiger in the extraction of copper(II) dithizonate. He found that in the PH range of 0.0–2.0 the rate of extraction of copper(II) dithizonate was virtually independent of the acidity. Further, he reported that an increase in concentration of dithizone in the organic phase did increase the rate of extraction somewhat, although he found no quantitative relationship. On the basis of these observations, a mechanism was postulated by Geiger which involved the reaction of molecular dithizone with copper(II) ion at the interface. A probable cause of this variance is Geiger's use of a slower shaker speed (100 shakes/min. compared with 300 shakes/min. in the present study). This could account for the diffusion-controlled mechanism.

On the basis of K_a/K_{Dr} values, it is to be expected

that the extraction should proceed some fifteen times more rapidly when carbon tetrachloride is substituted for chloroform as the extracting medium. The actual change in the rate constant (k') at 25° is from 0.30 to 17.4, a fifty-eight fold change. Further work needs to be done on the role of the solvent in extraction kinetics.

The suggestion that the addition of the first ligand is rate controlling was proposed by Irving and Williams in 1949,[6] on the basis of the differing rates of extraction when chloroform and carbon tetrachloride were used as the organic media. In their article on the extraction of zinc dithizonate, Irving and co-workers[7] presented a variety of kinetic data. They were interested primarily in showing the relative effects of *p*H, dithizone concentration, and aqueous phase composition on the rate of attainment of equilibrium in the extraction. Therefore, only a few measurements were made under each set of conditions and no quantitative conclusions were presented concerning the kinetics. On analysis of the data presented by Irving, *et al.*, it is found that the orders with respect to hydrogen ion, dithizone and zinc ion concentrations are the same as those determined in the present study. These conditions and rate constants are used in Table III. The rate of extraction into carbon tetrachloride appears, at first, to be anomalously fast. However, since these extractions were made from acetate buffered solutions, whereas the other extractions were made from phthalate buffered solutions, no strict comparison can be made. Further, since different methods of agitating the samples were used in the two studies, no comparison of rate constants can be made except to note that, in both the work of Irving and the present study, the results are internally consistent.

From the data in Table II a plot of log k' *vs.* $1/T$ was made and the best straight line was fitted to the points using the method of least squares. From this line and from the values of K_a/K_{Dz} for dithizone at different temperatures, the rate constants of the reaction

$$Zn^{+2} + Dz^- \rightleftharpoons ZnDz^+$$

at different temperatures were calculated. These are given in Table IV. These values are in accord with the well-known rapid rate of formation and lability of zinc complexes. Bjerrum[8] has reported the virtually instantaneous formation of zinc dithizonate in methanol solution at −75°. Taft and co-workers[9] have shown that the reaction of zinc ion with TA must involve a rate constant of at least 1×10^6 l./mole/min. From the data in Table IV the activation energy and the entropy of activation have been calculated. These values are 7.9 kcal./mole and 2.4 e.u./mole.

Although the attachment of the first dithizone is rate controlling, other considerations seem to call for a rapid first step followed by a slower second step. The doubly charged, uncomplexed zinc ion would be expected to react more rapidly than the monodithizonate species. Further, since the first stepwise formation constant is greater than the second, the concept of a rapid first step would appear to be more tenable.

The zinc ion, in water solution, exists as the octahedrally coördinated aquo complex.[10] The present authors propose the following mechanism for the chelation. One of the solvent molecules is lost from the aquo complex. This is followed by the attachment of the first dithizonate ion through a sulfur–metal linkage, the loss of a second solvent molecule, and then the linkage of the other coordinating group of the first dithizone. The ligand then exerts a bond-weakening effect on the two water molecules which are *trans* to it; these are lost and the monodithizonatodiaquo complex rearranges to a tetrahedral configuration. The last two water molecules are lost in stepwise fashion, with the second dithizonate attaching to the zinc. It is probable that the monodentate attachment of the first dithizonate ligand to the metal ion is the rate-controlling step.

The formation constant of zinc dithizonate, 1.13×10^{15}, is far less than that reported by Geiger and Sandell[11] for the copper(II) dithizonate, 1×10^{23}. This conforms to the normal order of chelate stabilities.

Further work in dithizonate formation constant determination is underway and the results should reveal much of interest with regard to the role of sulfur in chelation.

Acknowledgment.—Financial assistance from the Atomic Energy Commission is gratefully acknowledged. Appreciation is expressed to Tennessee Wesleyan College for granting C. B. H. a leave of absence.

(7) H. Irving, C. F. Bell and R. J. P. Williams, *J. Chem. Soc.* 356 (1952).

(8) J. Bjerrum and K. G. Poulson, *Nature*, **169**, 463 (1952).

(9) R. W. Taft, Jr., and E. H. Cook, *J. Am. Chem. Soc.*, **81**, 46 (1959).

(10) L. E. Orgel, "An Introduction to Transition-metal Chemistry Ligand-Field Theory," John Wiley and Sons, New York, N. Y., 1960, p. 83.

(11) R. W. Geiger and E. B. Sandell, *Anal. Chim. Acta*, **8**, 197 (1953).

ORDERING OF THE OCTAHEDRALLY COÖRDINATED CATION POSITION IN THE PEROVSKITE STRUCTURE

BY FRANCIS GALASSO AND WILDA DARBY

United Aircraft Corporation, Research Laboratories, East Hartford, Connecticut

Received August 14, 1961

An X-ray analysis of compounds with the general formula $Ba(M^{3+}_{0.5}Nb^{5+}_{0.5})O_3$, where M^{3+} is a rare earth, indium or iron ion, has shown that the critical percentage difference in radii necessary for ordering of the M^{3+} and niobium ions in the B sites of the perovskite structure lies between 7 and 17%. Of significance, this value found for ordering encompasses the 15% which has been used as an indication of the maximum percentage difference in the sizes of atoms or ions involved in either solid solution formation or isomorphous substitution.

Introduction

Oxides with the perovskite structure are represented by the formula ABO_3 where A is a large metal cation close packed in layers with oxygen ions, and B is a smaller metal ion situated in an octahedrally coördinated hole between the close-packed layers. As postulated in ref. 1, if two ions are present in the B position, an ordered distribution of the B site ions is most probable when large differences exist in either their charges or ionic radii. This hypothesis is validated qualitatively in Table I, which illustrates the arrangement of B ions in some perovskite-type compounds with variations in both size and charge differences. A review of the published literature, however, indicates insufficient data are available to permit a quantitative determination of the critical differences in charges or radii necessary for transition from a random to an ordered arrangement of the B position ions. Consequently, studies have been initiated at the United Aircraft Research Laboratories in an effort to determine these critical size and charge differences. The purpose of this report is to present the results of a study of ordering of the B position in a series of perovskite-type compounds whose difference in ionic radii varied between 0.05 and 0.45 Å., while the charge difference was held constant.

TABLE I

ORDERED AND DISORDERED PEROVSKITE COMPOUNDS

Compound	Diff. in charge of B ions	Diff. in ionic radii of the B ions, Å.[a]	Arrangement of B
$Ba(Mg^{2+}_{0.5}W^{6+}_{0.5})O_3$	4	0.05	Ordered[2]
$Ba(Zn^{2+}_{0.33}Nb^{5+}_{0.67})O_3$	3	0.05	Random[1]
$Ba(Fe^{3+}_{0.5}Ta^{5+}_{0.5})O_3$	2	0.04	Random[1]
$Ba(Sr^{2+}_{0.33}Ta^{5+}_{0.67})O_3$	3	0.44	Ordered[3]
$Ba(La^{3+}_{0.5}Ta^{5+}_{0.5})O_3$	2	0.46	Ordered[4]

[a] Ahrens radii values used.

Experimental Procedure

Preparation of Compounds.—The compounds selected for study are represented by the formula $Ba(M^{3+}_{0.5}Nb^{5+}_{0.5})O_3$ where M^{3+} is a rare earth ion (La^{3+} through Lu^{3+}), In^{3+} or Fe^{3+}. Since the difference in ionic radii of the B ions varied from 0.45 to 0.05 Å. in this series of compounds, a transition from an ordered to a disordered arrangement of the B sites was expected as the ionic radius of M approached that of niobium.

In all cases the compounds were prepared by mixing barium carbonate, niobium pentoxide, and the appropriate indium, iron or rare-earth sesquioxide according to the formula

$$4BaCO_3 + Nb_2O_5 + M_2O_3 \longrightarrow 4Ba(M_{0.5}Nb_{0.5})O_3 + 4CO_2$$

and heating the mixture in Leco boats at 1200° for 24 hours. It should be noted that only those rare earth sesquioxides that are stable in air at the preparation temperatures were used in the mixtures.

X-Ray Analysis.—Powder X-ray diffraction photographs were taken of the compounds formed using a 57.3 mm. radius Phillips X-ray powder camera and high intensity copper Kα radiation with settings of 50 kv. and 40 ma. In order to observe the superstructure lines, the photographs were exposed from 4 to 7 hours and in the case of $Ba(In_{0.5}Nb_{0.5})O_3$, for 24 hours. The X-ray patterns were read, indexed, and the cell sizes determined by extrapolation of a_0 *vs.* $1/2(\cos^2\theta/\sin\theta + \cos^2\theta/\theta)$ to $\theta = 90°$.[5]

High temperature X-ray diffractometer tracings up to 1000° were made of $Ba(Nd_{0.5}Nb_{0.5})O_3$ and $Ba(Lu_{0.5}Nb_{0.5})O_3$ using a Norelco diffractometer with an attached Tem-Pres heater. These specimens were selected for study because they represented the largest and smallest differences in ionic radii of the B ions in the cubic barium–rare earth niobates. Since no order–disorder transformation of the B sites in either of these compounds was found (see Fig. 1), further high temperature X-ray studies of the barium–rare earth niobate compounds with intermediate size differences of the B ions were not attempted at this time.

Discussion of Results

The results of the Research Laboratories' study reveal that there are weak superstructure lines due to ordering in the X-ray photographs of the compounds prepared with the general formula $Ba(M_{0.5}Nb_{0.5})O_3$, when M was a rare earth or indium ion. In some cases, the ordering lines were diffuse; the diffuseness probably was caused by the small size of the ordered domains. A logical ordered structure for these compounds where the

TABLE II

STRUCTURE CALCULATIONS FOR $Ba(Nd_{0.5}Nb_{0.5})O_4$

hkl	$\sin^2\theta$ (obsd.)	$\sin^2\theta$ (calcd.)	$I \times 10^{-6}$ (calcd.	*I* (obsd.)
111	0.0244	0.0243	4.1	W
220	.0647	.0649	122.5	VS
311	.0893	.0892	1.3	W
222	.0972	.0973	3.4	W
400	.1296	.1296	47.0	S
331	.1540	.1541	0.9	VW
422	.1943	.1946	57.1	S
440	.2594	.2595	29.9	M
620	.3241	.3244	29.5	M
444	.3885	.3893	8.8	W
642	.4536	.4542	34.5	M

(1) F. Galasso, L. Katz and R. Ward, *J. Am. Chem. Soc.*, **81**, 820 (1959).

(2) E. G. Steward and H. P. Rooksby, *Acta Cryst.*, **4**, 503 (1951).

(3) F. Galasso and L. Katz, *J. Am. Chem. Soc.*, **83**, 2830 (1961).

(4) L. Brixner, *ibid.*, **80**, 3214 (1958).

(5) J. B. Nelson and D. P. Riley, *Proc. Phys. Soc.* (London), **57**, 160 (1945).

TABLE III

STRUCTURE DATA FOR $Ba(M^{3+}_{0.5}Nb^{5+}_{0.5})O_3$ COMPOUNDS

Compound	Cell size Å.	Cell sizes Å.[a]	Arrangement of B ions	Diff. in ionic radii of B ions, Å.[b]	% Diff. in ionic radii of B ions
	$a = 8.607$	4.298			
$Ba(La_{0.5}Nb_{0.5})O_3$	$c = 8.690$	4.337	Ordered	0.45	65
$Ba(Nd_{0.5}Nb_{0.5})O_3$	8.540	4.277	Ordered	.35	51
$Ba(Sm_{0.5}Nb_{0.5})O_3$	8.518	4.248	Ordered	.31	45
$Ba(Eu_{0.5}Nb_{0.5})O_3$	8.507	4.234	Ordered	.29	42
$Ba(Gd_{0.5}Nb_{0.5})O_3$	8.496	4.242	Ordered	.28	41
$Ba(Dy_{0.5}Nb_{0.5})O_3$	8.437	4.224	Ordered	.23	33
$Ba(Ho_{0.5}Nb_{0.5})O_3$	8.434	4.216	Ordered	.22	32
$Ba(Er_{0.5}Nb_{0.5})O_3$	8.427	4.208	Ordered	.20	29
$Ba(Tm_{0.5}Nb_{0.5})O_3$	8.408	4.201	Ordered	.18	26
$Ba(Yb_{0.5}Nb_{0.5})O_3$	8.374	4.192	Ordered	.17	25
$Ba(Lu_{0.5}Nb_{0.5})O_3$	8.364	4.187	Ordered	.16	23
$Ba(In_{0.5}Nb_{0.5})O_3$	8.279		Ordered	.12	17
$Ba(Fe_{0.5}Nb_{0.5})O_3$	4.057		Random[1]	.05	7

[a] From Brixner.[6] [b] Ahrens radii values used.

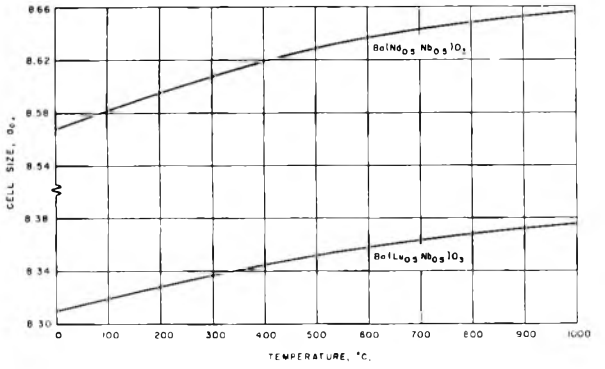

Fig. 1.—Barium–rare earth niobates: thermal expansion.

two B ions are present in equal proportions is one suggested by Steward and Rooksby, in which the two B ions alternate so that the perovskite unit cell edge (~4 Å.) has to be doubled. Therefore, all of the X-ray photographs were indexed using the double cubic perovskite cell parameter, except for $Ba(La_{0.5}Nb_{0.5})O_3$, which also was tetragonally distorted and $Ba(Fe_{0.5}Nb_{0.5})O_3$, in which the iron and niobium ions were not ordered. Table II gives the indexing data as well as observed and calculated intensities; the latter were computed for $Ba(Nd_{0.5}Nb_{0.5})O_3$, assuming an ordered arrangement of Nd and Nb ions. The data indicate the ordered perovskite structure for these compounds is probably a correct one. This is in contrast to the observations which were reported by Brixner[6] while this study was in progress. Brixner indicates that in these barium–rare earth niobates the rare earth and niobioum ions are arranged randomly in the B sites. Since the Research Laboratories' data show that the lines due to ordering in the X-ray photographs are weak, it is conceivable that Brixner may not have observed them in his investigation. It should be noted that his range of exposure times for X-ray photographs (2–4 hr.) is less than that used in this investigation.

In Table III the cell sizes and the differences and percentage differences in the ionic radii of the B ions at room temperature for the prepared compounds are presented. These data indicate that the critical percentage difference in ionic radii between B ions in $Ba(M_{0.5}Nb_{0.5})O_3$ compounds which causes ordering lies between 7 and 17%. The inability to determine more accurately the critical size difference for ordering for these compounds is due to the limitation of available trivalent ions with ionic difference between 0.05 and 0.12 Å. However, the results of this investigation are particularly interesting in view of the observation of Mason[7] that a wide range of isomorphous substitution in ionic compounds is possible if the radii of the substituting and substituted ions do not differ by more than 15%, and Hume–Rothery's rule on atomic size factor which states that atoms which differ in diameter by more than 15% should form limited solid solutions. Although neither Mason's statement nor Hume–Rothery's rule applies directly to order–disorder phenomena, it appears significant that this value of 15% also falls into the critical size range required for the ordering of B ions as found in this study.

(6) L. Brixner, *J. Inorg. & Nuclear Chem.*, **15**, 352 (1960).

(7) B. Mason, "Principles of Geochemistry," John Wiley and Sons, Inc., New York, N. Y., 1958.

THE CHEMISTRY OF URANIUM IN SURFACE IONIZATION SOURCES[1]

BY MARTIN H. STUDIER, ERIC N. SLOTH AND LEON P. MOORE

Argonne National Laboratory, Argonne, Illinois

Received August 14, 1961

Ions emitted from the surface of electrically heated filaments on which solutions of uranium had been evaporated were studied with a modified Bendix time-of-flight mass spectrometer. It was demonstrated that by control of the oxidizing and reducing agents on a heated filament and in the surrounding atmosphere the species of emitted ions can be controlled

$$\text{Oxidizing agents (}e.g.\text{, oxygen)} \rightarrow \quad UC_2^+,\ U^+,\ UO^+,\ UO_2^+,\ UO_3^+ \quad \leftarrow \text{Reducing agents (}e.g.\text{, carbon)}$$

The gaseous species UC_2^+ has been observed.

Introduction

Surface ionization sources are used extensively in mass spectrometry for the isotopic analysis of elements in solid samples.[2] Variation among individual mass determinations, which depend on sample treatment and technique of analysis, have emphasized the need for a better understanding of pertinent chemical effects. In the isotopic analyses of small samples of uranium, especially with single filament sources,[3] both the species and intensity of ions have shown a high degree of variability. In general it is preferable to do a uranium isotopic analysis on U^+ ions rather than on oxide ions to avoid the complications from isotopes of oxygen. Often only oxide ions have been obtained.

Experimental Results and Discussion

A Bendix time-of-flight mass spectrometer[4] was modified to permit the measurement of ions emitted from the surface of electrically heated filaments.[5] This instrument permits continuous monitoring of the entire mass spectrum. As modified, it has proved to be a useful tool for the study of high temperature reactions affecting the species and intensity of ions emitted from heated surfaces. Neutral molecules evaporating from the surfaces can be determined by using the electron gun of the spectrometer to ionize them.

Single filament assemblies were made from 0.001 inch thick tungsten and rhenium ribbons. In the past tungsten was used most extensively in ion sources for production of U^+ ions. Since pure rhenium has become available, it has to a large extent replaced tungsten because of its higher work function and its more desirable physical properties. After it was established that the chemical effects of the two elements were similar, most of the experiments were done with rhenium. Small samples of uranium (10^{-9} to 10^{-5} g.) in dilute acid solutions were evaporated to dryness on the filaments in air. After insertion of the filament into the ion source, the spectrometer was evacuated to less than 10^{-6} mm. As the temperature of the filament was gradually raised, the species of ions emitted from the surface were observed and their intensities were measured. An equimolar standard of U^{235}–U^{238} was used in all experiments as an aid in identifying uranium bearing species. It was demonstrated that by control of the oxidizing and reducing agents on the heated filament and in the surrounding atmosphere the species of emitted ions can be controlled as

$$\text{Oxidizing agents (}e.g.\text{, oxygen)} \rightarrow \quad UC_2^+,\ U^+,\ UO^+,\ UO_2^+,\ UO_3^+ \quad \leftarrow \text{Reducing agents (}e.g.\text{, carbon)}$$

When filaments were free of carbonaceous materials and the hydrocarbon content of the spectrometer vacuum system was low, only the ions of the higher oxides were observed. On several occasions only UO_3^+ ions were obtained with loss of the entire sample below 1000°. Emission of UO_3^+ was enhanced by an air leak.

When the hydrocarbon content of the vacuum system was high (observed by turning on the electron gun of the spectrometer), varying amounts of U^+, UO^+ and UO_2^+ were observed as the oxides were chemically reduced. An air leak increased the relative amount of oxide ions produced. A leak of benzene into the machine eliminated the oxide, and a sustained air leak was required before the oxide ions were observed again.

Carbon was added to the filaments before placing them into the spectrometer. In some cases sucrose was added with the sample. In others, carbon was deposited by letting benzene vapors strike the heated filaments either before or after deposition of the sample. In general, when samples were treated in this way only metal ions were observed. On occasion oxide ions could be observed very briefly during reduction. When sufficient carbon had been added it was difficult to produce the oxide ions again with an air leak.

To control the amount of reducing material on the filaments each assembly first was cleaned of extraneous organic matter by boiling successively in carbon tetrachloride, acetone and alcohol. The filament then was baked out in a vacuum system by slowly raising the temperature to 2200° while the pressure was kept below 5×10^{-6} mm. Samples of uranium deposited on such filaments without further treatment yielded only the higher oxides when analyzed in a spectrometer with low hydrocarbon content. Controlled amounts of carbon were deposited on the filaments by the following procedure: The filament assembly was placed in a 300-cc. vessel with a side arm containing 50 microliters of benzene. The benzene was cooled with a liquid nitrogen bath and the vessel was evacuated to a pressure of less than 10^{-7} mm. The vessel was isolated from the vacuum system with a stopcock and the side arm containing the benzene was immersed in a Dry Ice–acetone bath. After allowing five minutes for the benzene vapors to come to equilibrium with the solid benzene in the Dry Ice bath, the filaments were heated for various periods of time at different temperatures.

Analyses were made on 0.1 microgram samples of uranium deposited on rhenium filaments which had been treated with benzene vapors under different conditions. It was found that a few minutes of "carbonizing" before sample deposition at temperatures between 1200 and 2200° would result in almost exclusive emission of U^+ ions during analysis. However, the degree of carbonizing had a marked effect on the temperature of metal ion emission. (The filament temperature during carbonization seemed more critical than the duration.) Metal ions were observed at temperatures below 1300°. A persistent metal ion beam was obtained frequently at temperatures as high as 2500°. As the temperature of one filament was raised slowly a metal ion beam appeared, passed through a maximum, disappeared completely during a range of temperature of 150°,

---

(1) Based on work performed under the auspices of the U. S. Atomic Energy Commission. Presented in part at the Ninth Annual Meeting (June, 1961) of the A.S.T.M. Committee E14 on Mass Spectrometry.

(2) M. G. Inghram and R. J. Hayden, "A Handbook on Mass Spectroscopy," National Research Council, Washington, D.C., Publication 311, 1954.

(3) L. A. Dietz, *Rev. Sci. Instr.*, **30**, 235 (1959).

(4) D. B. Harrington, "Encyclopedia of Spectroscopy," Reinhold Publ. Corp., New York, N. Y., 1960, pp. 628–647.

(5) M. H. Studier and E. G. Rauh, to be published.

and then reappeared and persisted at much higher temperatures. As a general rule more extensive carbonizing results in metal ion emission at higher temperatures. When filaments were carbonized for 20 min. or longer at 2200°, no U^+ ions were observed until the temperature exceeded about 1800°. Then UC_2^+ ions were observed also but at an intensity factor of 100 below that of the U^+ ions.

It seems that metal ions may arise from several parent molecules. It is probable that they come from uranium metal (low temperature emission) and from one or more refractory carbides (high temperature emission). Positive identification of UC_2^+ ions was made by mass determination and by resolution of the two uranium isotopes in the sample. It is likely that UC and possibly U_2C_3 exist on the filaments also, even though they were not observed as stable gaseous species.[6] The temperature at which metal ions are emitted is consistent with the known physical properties of the metal and carbides.[7]

The oxide ions seem to have a variety of parents also. The trioxide may be present on the filament after evaporation of the sample and be lost at relatively low temperatures. It is formed also from UO_2 by an air leak. As UO_2 is reduced, UO^+ ions are formed. In addition, UO^+ ions are produced when air is leaked into a source which has been emitting metal ions only. Prolific emission of both UO^+ and UO_2^+ ions may be obtained by such an air leak. In one experiment UO^+ ions first appeared. Then UO_2^+ ions appeared and grew to an intensity one hundred times that of the original metal ions. At the same time the metal ion beam increased by a factor of five before it decreased and eventually disappeared. It is probable that the intense oxide beams produced by an air leak are associated with the burning of the highly reactive uranium carbides. Oxide ions produced in this manner can be observed at temperatures far below that at which metal ions can be produced from the same source in the absence of the leak.

Preliminary experiments with 0.1 microgram samples of the alpha emitting U^{233} suggest that well over 90% of the sample may be lost before the temperature for maximum metal ion emission is reached. Apparently, the uranium is lost during reduction before the more refractory carbides are formed. Experiments are under way to devise procedures to minimize these losses. Multiple filament assemblies will be used to investigate the problem. With a multiple filament it should be possible to separate some of the surface effects from the chemical effects. For example, the effect of the carbonizing procedure on the work function of the surface is unknown but is susceptible to study by the multiple filament technique.

(6) H. A. Wilhelm, *et al.*, *J. Chem. Soc.* (Suppl. 2), S318 (1949).

(7) H. Etherington, Ed., "Nuclear Engineering Handbook," 1st Ed., McGraw-Hill Book Co., New York, N. Y., 1958.

Conclusions

Single filament ion sources of tungsten or rhenium will not produce uranium metal ions in the absence of reducing agents other than the filament metals. Deposition of carbon before, during, or after deposition of the sample will ensure subsequent production of metal ions to the exclusion of oxide ions unless the pressure is high. It is probable that the success of single filament sources in the analysis of uranium as metal ions is due to the formation of refractory carbides which decompose at high temperatures.

POLAROGRAPHY OF SOME METAL COMPLEXES WITH TRIETHYLENETETRAMINE

BY E. JACOBSEN AND K. SCHRØDER

Department of Chemistry, University of Oslo, Blindern, Norway

Received August 17, 1961

The complexes of cadmium, copper, lead, zinc, nickel and cobalt with triethylenetetramine have been studied by means of the dropping mercury electrode. The cadmium, copper and lead complex are reversibly reduced to the amalgam at any concentration of the reagent. In alkaline medium the divalent cobalt complex is easily oxidized by air to a red-colored trivalent cobalt complex. The nickel, zinc and trivalent cobalt complex showed an irreversible reduction at the D.M.E. The half-wave potentials and the diffusion current constants of the various complexes are given.

Introduction

Triethylenetetramine (abbreviated "trien") forms stable complexes with certain metals. The composition and stability of the complexes have been determined by potentiometric titration.[1,2] The cadmum complex also has been studied by means of the dropping mercury electrode by Douglas, *et al.*[3] They claim that the complex is irreversibly reduced at trien concentrations less than 0.01 *M*. More recently the polarography of the copper complex has been thoroughly investigated by Jonassen and co-workers.[4]

Hitherto, the polarographic behavior of the complexes formed with other metals has not been investigated. The present paper is an extensive study of the polarography of the cadmium, lead, copper, zinc, nickel and cobalt complexes formed with trien.

Experimental

Materials.—The technical grade triethylenetetramine, obtained from Fluka A. G., Switzerland, was purified as described by Reilley and Schmid.[2] The remaining chemicals were reagent grade and used without further purification. Approximately 0.1 *M* stock solutions of the metal salts were prepared by dissolving 0.1 mole of the corresponding salt in redistilled water and diluting to one liter. The stock solutions were standardized by complexometric titration with EDTA. Standard solutions of trien were prepared and standardized following the procedure given by Reilley and Sheldon.[5] Five-tenths molar phosphate buffer was used as supporting electrolyte. The buffer was prepared by adding potassium hydroxide to phosphoric acid, and its *p*H measured with a *p*H meter. In order to avoid precipitation of metal phosphates, 1 *M* ammonia buffer was used as indifferent electrolyte for the lead, zinc and nickel complexes. The *p*H of the electrolyte was adjusted to the desired value by adding hydrochloric acid to the ammonia solution. Triton X-100, obtained from Rohm and Haas Co., Philadelphia, was found to be effective as maximum suppressor.

Apparatus and Technique.—Polarograms were recorded

(1) G. Schwarzenbach, *Helv. Chim. Acta*, **33**, 974 (1950).

(2) C. N. Reilley and R. W. Schmid, *J. Elisha Mitchell Soc.*, **73**, 279 (1957).

(3) B. E. Douglas, H. A. Laitinen and J. C. Bailar, *J. Am. Chem. Soc.*, **72**, 2484 (1950).

(4) H. B. Jonassen, J. A. Bertrand, F. R. Groves and R. I. Stearns, *ibid.*, **79**, 4279 (1957).

(5) C. N. Reilley and M. V. Sheldon, *Talanta*, **1**, 127 (1958).

with a Tast-Polarograph, Selector D (Atlas Werken, Bremen, Germany). The conventional type of dropping mercury electrode and of electrolysis cell was used. The capillary characteristics, measured in open circuit at a mercury height of 55 cm., were $m = 2.213$ mg./sec., and $t = 3.085$ sec. An external, saturated calomel electrode (S.C.E.) served as reference electrode. The total a.c. resistance of the cell, agar bridge and reference electrode was 800 ohms. Dissolved air was removed from the solutions by bubbling oxygen-free nitrogen through the cell for 10 min. and passing it over the solution during the electrolysis. All experiments were performed at 25 ± 0.1°.

The reversibility of the electrode reactions was tested for each polarogram by determining the slopes of the curves of log $i/(i_d - i)$ *vs.* the potential. Corrections were made for the residual current. Data for the plots were taken by manual operation of the polarograph, measuring the applied potential with a Leeds and Northrup Type K potentiometer. Half-wave potentials were taken from the logarithmic plots and were reproducible to ±1 mv. The trien becomes protonated to varying degrees depending upon the *p*H of the solution, and the concentration, C_x, of the free ligand available for complex formation was calculated at each *p*H value using the following values for the dissociation constants[1]

$$pK_1 = 9.92,\ pK_2 = 9.20,\ pK_3 = 6.67$$

Results and Discussion

The cadmium, lead and copper complexes are reduced directly to the amalgam. Only single waves were observed. The plots of log $i/(i_d - i)$ *vs.* the potentials were straight lines and the slopes indicate that the electrode reactions involve reversible two electron reductions in all cases. The plots of the values of $E_{1/2}$ *vs.* the corresponding values of log C_x resulted in straight lines. The slopes of the lines indicated that only one group is coördinated in each complex. In the concentration range 0.8–40 mmolar trien the half-wave potentials may be expressed by the equations

Cadmium complex: $E_{1/2} = -0.996 - 0.034 \log C_x$
Lead complex: $E_{1/2} = -0.690 - 0.030 \log C_x$
Copper complex: $E_{1/2} = -0.612 - 0.032 \log C_x$

The half-wave potentials of the cadmium and lead complexes are shifted to more negative values with increasing *p*H as shown in Fig. 1. The observed half-wave potentials are linear functions of the *p*H in the *p*H regions 6–9.5 and 6–10.5 for the lead and cadmium complexes, respectively. The slope of both curves is −0.06 volt per *p*H unit, indicating that the reaction takes place at the electrode

$$(\text{Me trien})^{++} + 2H^+ + 2e^- \longrightarrow \text{Me(Hg)} + (H_2\ \text{trien})^{++}$$

where Me represents lead or cadmium, respectively. Above *p*H 11 the slopes of the curves are zero, indicating the reaction

$$(\text{Me trien})^{++} + 2e^- \longrightarrow \text{Me(Hg)} + \text{trien}$$

In the pH region 10–11 the exact value of the slope could not be determined.

The variation of the half-wave potentials of the copper complex with the *p*H of the supporting electrolyte has been studied by Jonassen, *et al.*,[4] and these experiments were not repeated in the present investigation.

The variation of the limiting current with the height of the mercury column above the capillary also was measured. The current varied with the height of mercury; the value $i/\sqrt{h}$, where h is the height of the column after correction for the "back pressure," was fairly constant indicating that the electrode reactions are essentially diffusion-controlled. The diffusion current of the metal complexes in solutions containing excess reagent was measured and found to be proportional to the concentration of the corresponding metal. The diffusion current constants for solutions containing 0.05–2 mmoles of metal complex and excess reagent were 2.58, 3.18 and 2.90 for the cadmium, lead and copper complexes, respectively.

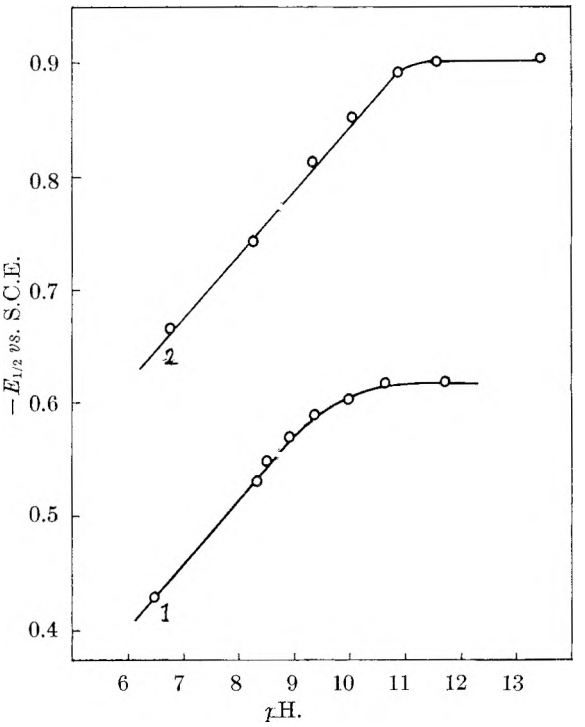

Fig. 1.—Variation of half-wave potentials of lead (curve 1) and cadmium (curve 2) complexes of trien with *p*H of the solution.

In contrast to the results obtained by Douglas, *et al.*,[3] the reduction of the cadmium complex was found to be reversible at all concentrations of the complexing agent. The reagent used in the above investigation was, however, not purified and was probably contaminated with other polyamides. Thus, the apparent irreversible waves at low trien concentrations reported by Douglas (slope of log plot = −0.050) consequently may be due to two or more polyamine complexes being reduced at almost the same potential. At higher concentrations of the reagent, however, the concentration of the polyamine forming the most stable complex with cadmium was great enough to complex all the metal ions present, giving one reversible wave. The complex constant reported by Douglas, $pK_c = 13.9$, also indicates that his reagent was contaminated with other polyamines. The complex constants determined by potentiometric titration, using purified polyamine solutions and the same ionic strength as Douglas, are $pK_c = 10.8$ and 14.0 for the trien[1,2] and tetraethylene pentamine complexes,[6] respectively.

The data obtained for the copper complex are in agreement with the work published by Jonassen.[4]

(6) C. N. Reilley and J. H. Holloway, *J. Am. Chem. Soc.*, **80**, 2917 (1958).

The nickel and zinc complexes with trien showed an irreversible reducion. The plot of $\log i/(i_d - i)$ *vs.* the potential was not a straight line. A maximum on the nickel wave was only suppressed in the presence of 0.008% Triton X-100. The half-wave potentials of both complexes were shifted to more negative values with increasing concentration of the reagent. Because of the irreversible reduction, only a few polarograms were recorded. In solutions containing 4 mmoles of trien the half-wave potentials of the nickel and zinc complexes were −1.20 and −1.38 volts *vs.* S.C.E., respectively.

The divalent cobalt trien complex is not reduced at the dropping mercury electrode. In alkaline medium, however, an anodic wave due to oxidation of the complex was observed. Experiments showed that in alkaline medium the divalent complex is easily oxidized by air to a red-colored complex. Polarograms of partly oxidized cobalt complex showed both an anodic and a cathodic wave. When bubbling air or oxygen followed by pure nitrogen through the cell, the diffusion current of the anodic wave decreased and that of the cathodic wave increased, and after about five minutes bubbling with air only the cathodic wave was observed on the polarogram, indicating that the oxidation was complete.

The cathodic wave of the cobalt complex prepared by oxidation with air was ill-defined and a maximum on the curve was only suppressed in the presence of 0.008% Triton X-100 or 0.005% gelatin. The plot of $\log i/(i_d - i)$ *vs.* the potential does not yield a straight line, indicating an irreversible reduction. The diffusion current constant for the cathodic wave (Table I) indicates, however, a one-electron reduction from the trivalent to the divalent state. The half-wave potential of the cathodic wave of the trivalent complex is shifted to more negative values with increasing *p*H, the shift being about 0.06 volt/*p*H unit.

TABLE I

DIFFUSION CURRENT CONSTANT OF TRIVALENT COBALT TRIEN COMPLEX

3.99 mmoles of trien in 0.5 *M* phosphate buffer, pH 8.1 0.008% Triton X-100 added as maximum suppressor.

Concn., mmolar	$-E_{1/2}$ *vs.* S.C.E.	i_d, μa.	$i_d/Cm^{2/3}t^{1/6}$
0.0504	0.41	0.170	1.62
.1008	.42	0.330	1.57
.504	.43	1.58	1.49
1.008	.45	3.04	1.45

The trivalent complex is easily prepared. It is stable against reducing agents (*i.e.*, ferrous iron, sulfite, etc.) and the reduction wave is well separated from the waves of nickel, lead and cadmium. Because of the drawn-out wave, and the lack of a suitable plateau for measuring the diffusion current, the trien complex is, however, not suitable for the quantitative determination of cobalt in the presence of other metals.

ELECTRON IMPACT SPECTROSCOPY OF THE FOUR- AND FIVE-MEMBERED, SATURATED HETEROCYCLIC COMPOUNDS CONTAINING NITROGEN, OXYGEN AND SULFUR[1]

BY EMILIO J. GALLEGOS AND ROBERT W. KISER

Department of Chemistry, Kansas State University, Manhattan, Kansas

Received August 17, 1961

Appearance potentials and relative abundances are reported for the principal positive ions in the mass spectra of azetidine, trimethylene oxide, trimethylene sulfide, pyrrolidine, tetrahydrofuran and tetrahydrothiophene. Probable ionization and dissociation processes are deduced from the energetics and the heats of formation of the various ions are given. The following ionization potentials were obtained: azetidine, 9.1 ± 0.15 e.v.; trimethylene oxide, 9.85 ± 0.15 e.v.; trimethylene sulfide, 8.9 ± 0.15 e.v.; pyrrolidine, 9.0 ± 0.15 e.v.; tetrahydrofuran, 9.45 ± 0.15 e.v.; and tetrahydrothiophene, 8.57 ± 0.15 e.v.

Introduction

We have determined the mass spectral cracking patterns and the appearance potentials of the principal ions from the four- and five-membered saturated heterocyclic compounds containing nitrogen, oxygen and sulfur. A comparison is made of the various processes and calculated heats of formation obtained in this study with those obtained in previous studies of ethylene oxide and propylene oxide[2] and ethylenimine and ethylene sulfide.[3] Appearance potentials reported in this paper for various ions from tetrahydrofuran and pyrrolidine are in every case higher than the appearance potential reported by Hissel[4] for ions of the same mass, with the exception of the parent-molecule ions in both molecules. In many instances the differences exceed one electron volt and in certain cases the difference in the observed appearance potentials is as great as four electron volts. In many instances the postulated processes,[5] using the appearance potentials reported by Hissel to account for the various ions, require significant rearrangement of the neutral products in order to obtain ΔH_f^+(ion)

(1) This work was supported in part by the U. S. Atomic Energy Commission, under Contract No. AT(11-1)-751 with Kansas State University. A portion of a dissertation presented by E. J. Gallegos to the Graduate School of Kansas State University in partial fulfillment of the requirements for the degree of Doctor of Philosophy in Chemistry.

(2) E. J. Gallegos and R. W. Kiser, *J. Am. Chem. Soc.*, **83**, 773 (1961).

(3) E. J. Gallegos and R. W. Kiser, *J. Phys. Chem.*, **65**, 1177 (1961).

(4) J. Hissel, *Bull. soc. roy. sci. Liège*, **21**, 457 (1952).

(5) F. H. Field and J. L. Franklin, "Electron Impact Phenomena and the Properties of Gaseous Ions," Academic Press, Inc., New York, N. Y. 1957.

which will correspond to those already reported. Processes postulated in this paper, based on the various appearance potentials from tetrahydrofuran and pyrrolidine, are consistent with similar fragmentations of the other heterocyclic compounds we have studied.

Experimental

Mass spectra and appearance potentials were obtained using a Bendix 12–100 time-of-flight mass spectrometer. The instrumentation has been described previously.[2,3] The extrapolated difference method[6] was used to obtain ionization and appearance potentials. Ionization potentials also were determined using the technique of Lossing, Tickner and Bryce.[7]

Azetidine was prepared in our Laboratories. *p*-Toluenesulfonazetidide was prepared first by the slow addition of sodium hydroxide to *p*-toluenesulfonamide in 1,3-bromochloropropane at reflux temperatures, using the method published by Searles, *et al.*[8,9] The azetidide, obtained in about 90% yield, then was recrystallized from 95% ethanol. The melting point of the azetidide was 116–118°. The lithium metal used for the reduction[10] was added slowly to a solution of the azetidide in ethylenediamine contained in a three-necked flask fitted with a reflux condenser. Azetidine was obtained in the fraction collected from 58.5 to 59.0° (uncor.), using a platinum spinning-band column. The refractive index obtained was $n^{25}D = 1.4288$. The azetidine was passed through a Perkin–Elmer model 154 vapor fractometer using a polypropylene glycol column; the resultant chromatogram, showing a short fore-run, indicated only a minor amount of impurities. Infrared information also gave indications of only negligible amounts of impurities and the mass spectral analysis of the azetidine sample showed only traces of impurities of higher molecular weight. It is to be noted that the above physical properties of azetidine agree fairly well with those given by Searles, *et al.*,[8] but only poorly with those reported by Vaughan, *et al.*[11] The refractive index measurements suggest that the azetidine prepared by the latter authors was probably still "wet."

The trimethylene sulfide was obtained from Eastman Organic Chemicals (white label) and was used as received. Gas–liquid partition chromatographic analysis of the trimethylene sulfide at 85° on a tri-*n*-tolylphosphate column revealed no impurity peaks. Mass spectra indicated only negligible traces of impurities of higher molecular weight. The purity was estimated at 99.8 mole%. Both trimethylene oxide and tetrahydrofuran were obtained from the Fisher Scientific Company. Gas–liquid chromatographic analysis and mass spectral analysis of both samples failed to indicate any impurities. Pyrrolidine and tetrahydrothiophene both were obtained from Matheson Coleman & Bell. Gas–liquid chromatographic analysis and mass spectrometric analysis of both samples did not reveal any significant quantities of impurities.

Spectroscopically pure krypton and xenon (obtained from Linde Co.) were used as the calibrating gases by comparing the observed ionization potentials with their known spectroscopic values. The gas used as the calibrating standard (either xenon or krypton) was intimately mixed with the heterocyclic compound during the determination of the appearance and ionization potentials of the various ions formed.

The ionization potentials of carbon dioxide and a number of the rare gases were determined using the Warren method[6] in a preliminary study of our experimental technique. Table I shows that the observed ionization potentials agree, within the quoted error, with the spectroscopic values[12,13] for these gases.

Results

The results of this study on azetidine, oxetane, thietane, pyrrolidine, tetrahydrofuran and tetrahydrothiophene are summarized in Tables II to VII. The principal ions and their relative abundances in the mass spectrum for 70 e.v. electrons are given in columns 1 and 2, respectively, of each table. The appearance potentials of the various ions and the probable process by which each is formed appear in columns 3 and 4. Column 5 gives the determined heat of formation of the ion; ΔH_f^+ was calculated from the appearance potential according to the process shown. (See Discussion, below.)

In the thermochemical calculations for the heats of formation of the gaseous compounds, we have taken −24 kcal./mole for the heat of formation of trimethylene oxide and 15.5 kcal./mole for the heat of formation of azetidine. These values were calculated by the method described by Franklin.[14] Values similarly calculated for the four- and five-membered heterocyclics agreed very closely with the reported literature value heats of formation employed: 14.78 kcal./mole for trimethylene sulfide,[15] −43 kcal./mole for tetrahydrofuran,[16] −2 kcal./mole for pyrrolidine,[4] and −8.1 kcal./mole for tetrahydrothiophene.[17] In the calculations based on Franklin's method a correction factor for the cycloparaffin ring of the same size as the heterocyclic was included. The calculated values substantiated the use of these correction factors.

Discussion

Mass Spectra.—The mass spectra of trimethylene sulfide, pyrrolidine, tetrahydrofuran and tetrahydrothiophene are in agreement with those reported in the A.P.I. table of mass spectral data.[18] The partial mass spectrum for trimethylene oxide is in fair agreement with that found by Beynon[19] by high resolution mass spectrometry. The mass spectrum reported for azetidine is new.

Appearance Potentials. Parent Molecule Ions.—The parent molecule ion is formed by a vertical

TABLE I

PRELIMINARY STUDY OF THE IONIZATION POTENTIAL DETERMINATIONS

Reference	Studied	Δ(I. P.)(e.v.)	Ionization potentials calcd.	(e.v.) Lit.[a]
Ar	Ne	5.75 ± 0.2	21.61 ± 0.2	21.56
Kr	Ne	7.75 ± .3	21.75 ± .3	21.56
	Ar	1.60 ± .2	15.60 ± .2	15.76
	Xe	1.95 ± .1	12.05 ± .1	12.13
	CO_2	0.40 ± .2	13.60 ± .2	13.78[b]
Xe	CO_2	1.90 ± .2	14.03 ± .2	13.78[b]

[a] See ref. 12. [b] See ref. 13.

(6) J. W. Warren, *Nature*, **165**, 811 (1950).

(7) F. P. Lossing, A. W. Tickner and W. A. Bryce, *J. Chem. Phys.*, **19**, 1254 (1951).

(8) S. Searles, M. Tamres, F. Block and L. A. Quarterman, *J. Am. Chem. Soc.*, **78**, 4917 (1956).

(9) S. Searles and S. Nukina, *Chem. Revs.*, **59**, 1077 (1959).

(10) We wish to thank Drs. S. Searles and R. Liepins for their suggestion to use Li metal as the reductant in ethylenediamine solvent.

(11) W. R. Vaughan, R. S. Klonowski, R. S. McElhinney and B. B. Millward, *J. Org. Chem.*, **26**, 138 (1961).

(12) C. E. Moore, "Atomic Energy Levels," Natl. Bur. Standards Circ. 467 Vol. III. 1959.

(13) Y. Tanaka, A. S. Jursa and F. J. LeBlanc, *J. Chem. Phys.*, **28**, 350 (1958).

(14) J. L. Franklin, *Ind. Eng. Chem.*, **41**, 1070 (1949).

(15) W. N. Hubbard, C. Katz and G. Waddington, *J. Phys. Chem.*, **58**, 142 (1954).

(16) P. Gray and A. Williams, *Chem. Revs.*, **59**, 239 (1959).

(17) S. Sunner, *Acta Chem. Scand.*, **9**, 847 (1955).

(18) Mass Spectral Data, American Petroleum Institute Research Project 44, National Bureau of Standards, Washington, D. C.

(19) J. H. Beynon, in "Advances in Mass Spectrometry," edited by J. D. Waldron, Pergamon Press London, 1959, pp. 328–354.

TABLE II

MASS SPECTRUM AND APPEARANCE POTENTIALS OF THE PRINCIPAL IONS OF AZETIDINE

m/e	% relative abundance	Appearance potential (e.v.)	Process	ΔHf^+, kcal./mole
14	0.9			
15	2.2	14.4 ± 1.0	$(CH_2)_3NH \longrightarrow CH_3^+ + C_2H_3N + H$	267
26	14.1	16.6 ± 0.5	$\longrightarrow C_2H_2^+ + CH_3 + NH_2$	327
27	25.8	16.6 ± .5	$\longrightarrow C_2H_3^+ + CH_2 + NH_2$	291
28	100.0	13.1 ± .2	$\longrightarrow CH_2N^+ + C_2H_4 + H$	253
			$\longrightarrow CH_2N^+ + C_2H_3 + H_2$	254
29	63.9	12.5 ± .2	$\longrightarrow C_2H_5^+ + HCN + H$	221
			$\longrightarrow CH_3N^+ + C_2H_2 + H_2$	250
30	46.6	12.3 ± .2	$\longrightarrow CH_4N^+ + C_2H_2 + H$	193
31	2.2			
39	1.7			
40	0.9			
41	1.9			
42	6.4	11.9 ± .2	$\longrightarrow C_2H_4N^+ + CH_3$	258
43	1.4			
44	0.9			
52	0.7			
54	0.9			
56	19.5	11.4 ± .2	$\longrightarrow C_3H_6N^+ + H$	226
57	45.3	9.1 ± .15	$\longrightarrow C_3H_7N^+$	225

TABLE III

MASS SPECTRUM AND APPEARANCE POTENTIALS OF THE PRINCIPAL IONS OF TRIMETHYLENE OXIDE

m/e	% relative abundance	Appearance potential (e.v.)	Process	ΔHf^+, kcal./mole
14	0.9			
15	0.9			
25	3.8			
26	12.1	15.2 ± 0.2	$(CH_2)_3O \longrightarrow C_2H_2^+ + CO + 2H_2$	354
			$\longrightarrow C_2H_2^+ + CH_2O + H_2$	354
27	18.9	14.9 ± .3	$\longrightarrow C_2H_3^+ + CH_2O + H$	295
			$\longrightarrow C_2H_3^+ + CO + H_2 + H$	295
28	100.0	12.4 ± .3	$\longrightarrow C_2H_4^+ + CH_2O$	290
			$\longrightarrow C_2H_4^+ + CO + H_2$	289
29	25.7	12.6 ± .2	$\longrightarrow CHO^+ + C_2H_5$	245
			$\longrightarrow CHO^+ + C_2H_4 + H$	202
			$\longrightarrow C_2H_5^+ + CO + H$	242
30	5.4	10.8 ± .3	$\longrightarrow C_2H_6^+ + CO$	252
31	5.2	13.3 ± .2	$\longrightarrow CH_3O^+ + C_2H_2 + H$	177
37	0.8			
38	1.3			
39	7.4	14.5 ± .2	$\longrightarrow C_3H_3^+ + OH + H_2$	301
40	1.1			
41	9.8	11.8 ± .2	$\longrightarrow C_3H_5^+ + OH$	238
42	1.0			
43	0.4			
57	3.1			
58	29.6	9.85 ± .15	$\longrightarrow C_3H_6O^+$	203

transition process as required by the Frank–Condon rule. A value of 9.1 ± 0.15 e.v. was observed for the ionization potential of azetidine, somewhat higher than the calculated value of 8.35 e.v.[3] An experimental value of 9.0 ± 0.15 e.v. was determined for the ionization potential of pyrrolidine, slightly lower than the value of 9.2 ± 0.2 e.v. previously reported for this molecule by electron impact methods[4]; 8.55 e.v. has been calculated for the ionization potential of pyrrolidine.[3] A value of 9.85 ± 0.15 e.v. is reported here for the ionization potential of trimethylene oxide. This value is somewhat higher than the calculated value of 9.48 e.v. obtained for the ionization potential of this molecule. The ionization potential of trimethylene oxide had not previously been determined experimentally. An ionization potential of 9.45 ± 0.15 e.v. was observed for the tetrahydrofuran. This value is in good agreement with a value of 9.54 e.v. reported using photoionization methods.[20] However, the ionization potential reported here is considerably lower than a

(20) K. Watanabe, T. Nakayama and J. Mottl, Final Report on Ionization Potential of Molecules by a Photo-ionization Method, December, 1959. Dept. Army #5B-99-01, ORD-# TB2-0001-00r-# 1624. Contract No. DA-04-2000 ORD 480 and 737.

TABLE IV

MASS SPECTRUM AND APPEARANCE POTENTIALS OF THE PRINCIPAL IONS OF TRIMETHYLENE SULFIDE

m/e	% relative abundance	Appearance potential (e.v.)	Process	ΔH_f^+, kcal./mole
26	4.9	17.1 ± 0.4	$(CH_2)_3S \longrightarrow C_2H_2^+ + CH_3S + H$ (?)	319
			$\longrightarrow C_2H_2^+ + CH_2S + H_2$ (?)	333
27	9.5	16.7 ± .2	$\longrightarrow C_2H_3^+ + CHS + H_2$ (?)	285
28	3.5	13.6 ± .2	$\longrightarrow C_2H_4^+ + CH_2S$ (?)	253
37	2.0			
38	2.9			
39	13.5	15.3 ± .4	$\longrightarrow C_3H_3^+ + H_2 + H + S$	262
41	11.7	12.2 ± .2	$\longrightarrow C_3H_5^+ + SH$	265
45	25.8	13.9 ± .2	$\longrightarrow CHS^+ + C_2H_4 - H$	271
			$\longrightarrow CHS^+ + C_2H_3 - H_2$	271
46	100.0	11.8 ± .2	$\longrightarrow CH_2S^+ + C_2H_2 + H_2$	233
47	11.3	12.3 ± .15	$\longrightarrow CH_3S^+ + C_2H_3$	235
48	5.9	11.6 ± .15	$\longrightarrow (CH_2S^{34})^+ + C_2H_2 + H_2$	228
59	1.8			
73	2.0			
74	52.3	8.9 ± .15	$\longrightarrow C_3H_6S^+$	220

TABLE V

MASS SPECTRUM AND APPEARANCE POTENTIALS OF THE PRINCIPAL IONS OF PYRROLIDINE

m/e	% relative abundance	Appearance potential (e.v.)	Process	ΔH_f^+, kcal./mole
14	1.1			
15	6.7			
18	1.2			
26	5.9	17.3 ± 1.0	$(CH_2)_4NH \longrightarrow C_2H_2^+ + C_2H_6 + NH_2$	336
			$\longrightarrow C_2H_2^+ + C_2H_6 + NH$	336
27	15.9	16.7 ± 0.3	$\longrightarrow C_2H_3^+ + C_2H_6 + NH$	280
28	51.6	13.9 ± .2	$\longrightarrow CH_2N^+ + C_3H_6 + H$	262
29	10.1	13.2 ± .2	$\longrightarrow C_2H_5^+ + C_2H_3N + H$	222
			$\longrightarrow CH_3N^+ + C_3H_4 + H_2$	257
30	9.2	12.7 ± .2	$\longrightarrow CH_4N^+ + C_3H_4 + H$	193
31	1.2			
38	2.5			
39	15.3	18.9 ± .4	$\longrightarrow C_3H_3^+ + CH_2N + 2H_2$	304
			$\longrightarrow C_3H_3^+ + CH_3N + H_2 + H$	300
41	19.7	15.0 ± .3	$\longrightarrow C_2H_3N^+ + C_2H_2 + 2H_2$	290
			$\longrightarrow C_3H_5^+ + CH_2 + NH_2$	237
42	22.0	13.0 ± .2	$\longrightarrow C_2H_4N^+ + C_2H_6$	276
43	100.0	12.3 ± .2	$\longrightarrow C_2H_5N^+ + C_2H_4$	269
44	4.1			
58	6.1			
68	2.4			
70	32.6	11.0 ± .2	$\longrightarrow C_4H_8N^+ + H$	200
71	26.0	9.0 ± .15	$\longrightarrow C_4H_9N^+$	206
72	1.3			

previously reported value of 10.1 ± 0.2 e.v. obtained from electron impact methods.[4] We calculated a value of 9.88 e.v. for the ionization potential of this molecule using the equivalent orbital method of Hall.[21] The ionization potential of 8.9 ± 0.15 e.v. reported here for trimethylene sulfide is in fair agreement with the photo-ionization value of 8.64 e.v.,[22] although greater than the value of 8.43 e.v. calculated for this cyclic molecule.[3] Our determination of the ionization potential for tetrahydrothiophene gave 8.57 ± 0.15 e.v. in good agreement with both the calculated value[3] of 8.62 e.v. and the value of 8.48 e.v. obtained by photo-ionization.[22]

m/e = **15.**—The ion fragment CH_3^+ for *m/e* = 15 in the azetidine spectrum gives a calculated value of 267 kcal./mole for the $\Delta H_f^+(CH_3)$ if the neutral fragments are C_2H_3N and H. The average of the heat of formation of acetonitrile and acetoisonitrile was used for the heat of formation of the C_2H_3N fragment (28.5 kcal./mole). This value of $\Delta H_f^+(CH_3)$ agrees very well with the value of 262 kcal./mole given for $\Delta H_f^+(CH_3)$ by Field and Franklin.[5]

m/e = **26.**—In the azetidine spectrum the ion fragment at *m/e* = 26 might be either CN^+ or $C_2H_2^+$. Energetics eliminates the former pos-

(21) G. G. Hall, *Trans. Faraday Soc.*, **49**, 113 (1953); **50**, 319 (1954).

(22) L. D. Issacs, W. C. Price and R. G. Ridley, "Vacuum Ultraviolet Spectra and Molecular Ionization Potentials," in "The Threshold of Space," edited by M. Zelikoff, Pergamon Press, Ltd., London, 1957, pp. 143–151.

TABLE VI

MASS SPECTRUM AND APPEARANCE POTENTIALS OF THE PRINCIPAL IONS OF TETRAHYDROFURAN

m/e	% relative abundance	Appearance potential (e.v.)	Process	ΔH_f^+, kcal./mole
18	4.7			
26	4.7	17.3 ± 0.3	$(CH_2)_4O \longrightarrow C_2H_2^+ + H_2 + CH_2O + CH_2$	316
27	23.5	16.1 ± .3	$\longrightarrow C_2H_3^+ + C_2H_2O + H_2 + H$	291
28	5.0			
29	12.4	15.8 ± .2	$\longrightarrow C_2H_5^+ + CO + CH_2 + H$	228
30	2.0			
31	3.8			
37	1.0			
38	1.7			
39	15.7	18.7 ± .6	$\longrightarrow C_3H_3^+ + CH_3O + 2H$	274
			$\longrightarrow C_3H_3^+ + CHO + H_2 + 2H$	287
40	9.6	15.2 ± .3	$\longrightarrow C_3H_4^+ + CH_2 + H_2O$	298
41	44.3	15.5 ± .3	$\longrightarrow C_3H_5^+ + CH_3 + O$	223
			$\longrightarrow C_3H_5^+ + CH_2 + OH$	237
42	100.0	12.7 ± .2	$\longrightarrow C_3H_6^+ + CH_2O$ (?)	278
			$\longrightarrow C_2H_2O^+ + C_2H_4 + H_2$	238
			$\longrightarrow C_2H_2O^+ + C_2H_2 + 2H_2$	196
43	19.6	12.8 ± .2	$\longrightarrow C_2H_3O + C_2H_4 + H$	188
			$\longrightarrow C_2H_3O^+ + C_2H_3 + H_2$	188
44	3.5			
45	0.9			
71	26.1	11.1 ± .2	$\longrightarrow C_4H_7O^+ + H$	161
72	27.4	9.45 ± .15	$\longrightarrow C_4H_8O^+$	175
73	1.0			

sibility. A calculated value of 327 kcal./mole is found for $\Delta H_f^+(C_2H_2)$ considering the neutral fragments to be CH_3 and NH_2. From the appearance potential of $C_2H_2^+$ from pyrrolidine, we calculate a heat of formation for $C_2H_2^+$ of 336 kcal./mole. In this fragmentation the neutral products may be either $C_2H_5 + NH_2$ or $C_2H_6 + NH$ and still satisfy the energetics.

The only ion possible from trimethylene oxide with a $m/e = 26$ is $C_2H_2^+$. A value of 354 kcal./mole is obtained for the heat of formation of $C_2H_2^+$ if the neutral fragments are taken to be either $CO + 2H_2$ or $H_2CO + H_2$. In the tetrahydrofuran spectrum this peak again can be due only to the formation of $C_2H_2^+$ ion. If the un-ionized fragments are considered to be H_2, CH_2O and CH_2, a calculated value for the $\Delta H_f^+(C_2H_2) = 316$ kcal./mole is obtained.

Also, the only possible ion which could be formed from trimethylene sulfide to give $m/e = 26$ is $C_2H_2^+$. A calculated value of $\Delta H_f^+(C_2H_2) = 319$ kcal./mole is obtained if the neutral fragments are taken to be CH_3S and H. A $\Delta H_f^+(C_2H_2) = 333$ kcal./mole is obtained if the neutral fragments are CH_2S and H_2. The heats of formation of CH_3S and CH_2S radicals were estimated using the $\Delta H_f(CH_4S) = -2.97$ kcal./mole[23] and D(C–H) = 94 kcal./mole,[24] giving values of 38 and 76 kcal./mole for the $\Delta H_f(CH_3S)$ and $\Delta H_f(CH_2S)$, respectively. The first process shown in Table IV appears more favorable, although energetics cannot distinguish between the two possibilities.

(23) F. D. Rossini, D. D. Wagman, W. H. Evans, S. Levine and I. Jaffe, "Selected Values of Chemical Thermodynamic Properties," National Bureau of Standards Circular 500, U. S. Government Printing Office, Washington, D. C., 1952.

(24) T. L. Cottrell, "The Strength of Chemical Bonds," 2nd Edition, Butterworths Scientific Publications, London, 1958, pp. 270–271.

The above values agree quite well with $\Delta H_f^+(C_2H_2) = 317$ kcal./mole listed by Field and Franklin,[5] with the singular exception of the case of this ion from trimethylene oxide.

$m/e = 27$.—$C_2H_3^+$ appears to account for the peak at mass 27, in the azetidine spectrum. If the neutral fragments are CH_2 and NH_2, the calculated value for $\Delta H_f^+(C_2H_3)$ is 291 kcal./mole. However it is possible that the ion is HCN, with the accompanying neutral fragments $C_2H_2+2H_2$; this leads to $\Delta H_f^+(HCN) = 355$ kcal./mole. Similarly for pyrrolidine, the thermochemical calculations require that the ion responsible for the peak at $m/e = 27$ be $C_2H_3^+$ along with the neutral fragments C_2H_5 and NH. $\Delta H_f^+(C_2H_3)$ is calculated to be 280 kcal./mole.

$C_2H_3^+$ formed with a loss of CH_2O and H fragments leads to a calculated $\Delta H_f^+(C_2H_3) = 295$ kcal./mole, in the trimethylene oxide spectrum. A $\Delta H_f^+(C_2H_3) = 295$ kcal./mole also is obtained if the neutral fragments are considered to be CO, H_2 and H. In the tetrahydrofuran spectrum, as in the trimethylene oxide case, mass 27 can be only due to the $C_2H_3^+$ ion. Taking the neutral fragments to be C_2H_2O, H_2 and H, a value of 291 kcal./mole is obtained for the heat of formation of $C_2H_3^+$. It should be noted here that our value of 16.1 ± 0.3 e.v. observed for the appearance potential at mass 27 is more than an electron volt higher than that reported by Hissel.[4]

For trimethylene sulfide this ion is necessarily $C_2H_3^+$, formed with the accompanying neutral fragments of CHS + H_2. This leads to a calculated value for the $\Delta H_f^+(C_2H_3) = 285$ kcal./mole. The heat of formation of CHS was estimated to be 115 kcal./mole from the known heat of formation of $CH_4S = -2.97$[23] and D(C–H) = 94 kcal./

TABLE VII

MASS SPECTRUM AND APPEARANCE POTENTIALS OF THE PRINCIPAL IONS OF TETRAHYDROTHIOPHENE

m/e	% relative abundance	Appearance potential (e.v.)	Process	ΔH_f^+, kcal./mole
14	1.2			
15	2.5			
26	6.2			
27	24.5	18.0 ± 0.4	$(CH_2)_4S \longrightarrow C_2H_3^+ + C_2H_3S + H_2$	284
			$\longrightarrow C_2H_3^+ + C_2H_4S + H$	280
28	5.2			
29	3.0			
38	2.8			
39	16.2	17.2 ± .2	$\longrightarrow C_3H_3^+ + CHS + 2H_2$	274
40	2.8			
41	11.1	15.5 ± .2	$\longrightarrow C_3H_5^+ + CH_2S + H$	221
			$\longrightarrow C_3H_5^+ + CHS + H_2$	234
42	2.1			
45	30.0	13.8 ± .2	$\longrightarrow CHS^+ + C_3H_5 + H_2$	278
46	28.9	13.0 ± .2	$\longrightarrow CH_2S^+ + C_3H_4 + H_2$	246
47	24.9	14.0 ± .2	$\longrightarrow CH_3S^+ + C_3H_4 + H$	217
			$\longrightarrow CH_3S^+ + C_3H_3 + H_2$	223
48	2.0			
49	1.6			
50	2.2			
51	2.2			
52	1.0			
53	4.4			
54	11.1	11.9 ± .2	$\longrightarrow C_4H_6^+ + H_2S$	271
55	10.1	12.4 ± .2	$\longrightarrow C_4H_7^+ + SH$	247
56	2.0			
57	3.1			
58	7.9	17.0 ± .3	$\longrightarrow C_2H_2S^+ + C_2H_3 - H_2 + H$	268
59	17.7	15.7 ± .4	$\longrightarrow C_2H_3S^+ + C_2H_2 - H_2 + H$	248
60	100.0	11.7 ± .3	$\longrightarrow C_2H_4S^+ + C_2H_2 - H_2$	208
61	6.1			
62	6.0			
63	1.0			
73	3.0			
85	2.7			
87	16.5	12.4 ± .3	$\longrightarrow C_4H_7S^+ + H$	226
88	50.0	8.57 ± .15	$\longrightarrow C_4H_8S^+$	190
89	3.6			
90	2.5			

mole.[24] Again in the tetrahydrothiophene spectrum, the peak at mass 27 is due only to the formation of $C_2H_3^+$. Considering the fragments to be C_2H_4S and H, a value of 280 kcal./mole is obtained for the heat of formation of $C_2H_3^+$. However, if the neutral fragments are C_2H_3S and H_2, a value of 284 kcal./mole is calculated. The heats of formation of the C_2H_4S fragment and of the C_2H_3S fragment were estimated from the known heat of formation of ethanethiol(g) of −9.1 kcal./mole[23] and the dissociation energy of an S–H and C–H bond given by Cotrell[24] of approximately 90 and 98 kcal./mole, respectively. Values of ΔH_f (C_2H_4S) = 75 kcal./mole and $\Delta H_f(C_2H_3S)$ = 123 kcal./mole were obtained.

The above results for $\Delta H_f^+(C_2H_3)$ compare favorably with the range of values of 275–296 kcal./mole summarized by Field and Franklin.[5]

m/e = 28.—As shown in Table II, this is the largest peak in the azetidine spectrum. Taking either $C_2H_3 + H_2$ or $C_2H_4 + H$ as the neutral fragments, a value for $\Delta H_f^+(CH_2N)$ = 253 or 254 kcal./mole is calculated. Energetics eliminate $C_2H_4^+$ as accounting for *m/e* 28 at electron energies near the appearance potential for this ion. CH_2N^+ is taken as the ion comprising the peak at *m/e* = 28 in the pyrrolidine spectrum. If the neutral fragments are C_3H_6 and H a $\Delta H_f^+(CH_2N)$ = 262 kcal./mole. Hissel[4] reports an appearance potential of 12.5 ± 0.2 e.v. for mass 28 in pyrrolidine, which is substantially less than the value of 13.9 e.v. reported by us. Field and Franklin[5] list $\Delta H_f^+(CH_2N)$ = 250 kcal./mole. We note that CH_2N^+ was not observed in the spectrum of ethylenimine.[3]

The peak at *m/e* 28 is the largest in the trimethylene oxide spectrum. Beynon has indicated in his high resolution mass spectrometric investigation of trimethylene oxide[19] that the ions responsible for *m/e* = 28 are $C_2H_4^+$, with a fractional abundance of 0.9747, and CO, with a fractional abundance of 0.0253. Thermochemical calculation for $C_2H_4^+$ as the ion fragment and CH_2O as the neutral fragment gives $\Delta H_f^+(C_2H_4)$ = 290 kcal./mole.

Taking CO and H_2 as the neutral fragments a value of 289 kcal./mole is obtained for the heat of formation of $C_2H_4^+$. Both of these values are rather high compared to the accepted value of 255 kcal./mole given by Field and Franklin[5] for the heat of formation of $C_2H_4^+$. Fragmentation of trimethylene sulfide gives $C_2H_4^+$ as the ion formed at mass 28. If CH_2S is the neutral fragment, a value for $\Delta H_f^+(C_2H_4)$ = 253 kcal./mole is calculated.

m/e = **29.**—This peak at mass 29 quite likely is due to the $C_2H_5^+$ fragment in the azetidine spectrum. Taking the process as shown in Table II, $\Delta H_f^+(C_2H_5)$ = 221 kcal./mole is calculated, using the heat of formation of hydrogen cyanide for the neutral fragment HCN. However, it should be noted that the process to form $CH_3N^+ + C_2H_2 + H_2$, giving $\Delta H_f^+(CH_3N)$ = 250 kcal./mole, cannot be ruled out on the grounds of energetics. Field and Franklin give 224 kcal./mole for the $\Delta H_f^+(C_2H_5)$.[5] In a study of ethylenimine[3] we previously reported a value of 253 kcal./mole for the heat of formation of CH_3N^+. In the pyrrolidine spectrum energetics again will not allow us to distinguish between $C_2H_5^+$ or CH_3N^+ as the ion of *m/e* 29. If the neutral fragments are C_2H_3N and H, 222 kcal./mole is calculated for the heat of formation of the $C_2H_5^+$ ion. The average of the heats of formation of acetonitrile and acetoisonitrile (28.5 kcal./mole) was used for the heat of formation of C_2H_3N. If the products of ionization and dissociation are $CH_3N^+ + C_3H_4 + H_2$, $\Delta H_f^+(CH_3N)$ = 257 kcal./mole.

Beynon's investigation[19] on *m/e* = 29 for trimethylene oxide reveals a fractional abundance of 0.1836 for CHO^+ and 0.116 for $C_2H_5^+$ for a total fractional abundance of 0.3022, or about 39% CHO^+ and 61% $C_2H_5^+$. Since both ions appear in substantial amounts, a determination of the appearance potential from the ion current at *m/e* = 29 will result in a determination of that ion whose process of formation requires the least amount of energy. Also it would appear that the process is favored which produces the ion present in the larger amount, in that in many cases this process usually requires less energy. However, we cannot distinguish on the basis of energetics between the three possible processes shown in Table III. If CHO^+ is the ion fragment formed and C_2H_4 and H are the neutral products, $\Delta H_f^+(CHO)$ = 202 kcal./mole, in good agreement with the literature.[5] If CHO^+ is formed together with C_2H_5, $\Delta H_f^+(CHO)$ = 245 kcal./mole; if $C_2H_5^+$ is formed and CO and H are the neutral products, $\Delta H_f^+(C_2H_5)$ = 242 kcal./mole.

In the tetrahydrofuran spectrum, two ions could account equally well for the peak at mass 29, $C_2H_5^+$ or CHO^+. Beynon[19] indicates that CHO^+ accounts for 86% of the peak at mass 29. If this is the case and the neutral fragments are $C_2H_4 + CH_2 + H$, the value calculated for the heat of formation of CHO^+ is found to be 192 kcal./mole. $\Delta H_f^+(CHO)$ = 230 kcal./mole is reported in the literature.[25] However, if $C_2H_5^+$ is the ion formed along with the neutral products CO, CH_2 and H, a $\Delta H_f^+(C_2H_5)$ = 228 kcal./mole is calculated, in good agreement with the value of 224 kcal./mole reported for this ion.[5] It appears that the appearance potential determined was for the less abundant ion $C_2H_5^+$, in apparent contradiction to the argument presented above for the more abundant ion. Our observed appearance potential of 15.8 e.v. is about 1 e.v. greater than that reported by Hissel[4] for mass 29 in the tetrahydrofuran spectrum.

m/e = **30.**—Fragmentation of azetidine by electron impact appears to give CH_4N^+ at mass 30. $\Delta H_f(CH_4N)$ = 193 kcal./mole is calculated considering the neutral fragments to be C_2H_2 and H. The values listed by Field and Franklin[5] for the heat of formation of this ion range from 190 to 226 kcal./mole. From pyrrolidine, a value of 193 kcal./mole also is calculated for the heat of formation of the CH_4N^+ ion fragment formed at mass 30, considering the neutral fragments to be C_3H_4 and H. The abundance of CH_3S^+ in thietane and tetrahydrothiophene and CH_3O^+ in oxetane and tetrahydrofuran further indicate that the ion at *m/e* 30 in azetidine and pyrrolidine is CH_4N^+.

Beynon reports 59% $C_2H_6^+$ and 41% CH_2O^+ for *m/e* = 30 in a high resolution investigation of trimethylene oxide.[22] Taking $C_2H_6^+$ as the ion fragment and CO as the neutral fragment, with 10.8 ± 0.3 e.v. as the appearance potential for this process, $\Delta H_f^+(C_2H_6)$ = 252 kcal./mole is calculated, in good agreement with the known value for the $\Delta H_f^+(C_2H_6)$ = 249 kcal./mole.[20] Energetics eliminate CH_2O^+ from consideration.

m/e = **31.**—Practically all of the ions formed at *m/e* = 31 are CH_3O^+ in the trimethylene oxide case according to Beynon.[23] The abundance of this ion is too great to consider it to be $C^{13}CH_6^+$; the appearance potential also eliminates $C^{13}CH_6^+$. A $\Delta H_f^+(CH_3O)$ = 177 kcal./mole is obtained if the neutral fragments are those shown in Table III. Field and Franklin[5] give $\Delta H_f^+(CH_3O)$ = 173 kcal./mole. The value of 177 kcal./mole obtained here also agrees well with the value of 182 kcal./mole for $\Delta H_f^+(CH_3O)$ obtained from our propylene oxide study.[2]

m/e = **39.**—An appearance potential of 18.9 ± 0.4 e.v. was observed for mass 39 in the pyrrolidine spectrum. If the process is $C_4H_9N^+$ fragmenting to $C_3H_3^+ + CH_2N + 2H_2$, $\Delta H_f^+(C_3H_3)$ = 304 kcal./mole; however, if the process involves instead the neutral fragments $CH_3N + H_2 + H$ a value of 300 kcal./mole is obtained for the heat of formation of $C_3H_3^+$. Both of these heats of formation lie within the range of some of the values reported in the literature for $C_3H_3^+$.[5] Our appearance potential again differs significantly from that reported by Hissel.[4]

The only ion of *m/e* 39 which may be obtained from trimethylene oxide is $C_3H_3^+$. The products in addition to $C_3H_3^+$ are OH and H. A calculated $\Delta H_f^+(C_3H_3)$ = 301 kcal./mole is obtained for this process. This value is slightly high, but is within range of a number of values reported for the heat of formation of $C_3H_3^+$.[5] $C_3H_3^+$ also is the ion responsible for the peak at mass 39 in tetrahydrofuran. We have used a value of $\Delta H_f(CH_3O)$ = +10 kcal./mole in calculating $\Delta H_f^+(C_3H_3)$ = 274 kcal./mole.

(25) C. S. Cummings and W. Bleakney, *Phys. Rev.*, **58**, 787 (1940).

If $\Delta H_f(CH_3O)$ = 0.5 kcal./mole, as suggested by Gray and Williams,[16] $\Delta H_f^+(C_3H_3)$ = 285 kcal./mole. $\Delta H_f(CHO)$ = −2.8 kcal./mole[26-28] was used to calculate $\Delta H_f^+(C_3H_3)$ = 287 kcal./mole. Here, the appearance potential of 18.7 ± 0.6 e.v. we report is greater than that reported by Hissel.[4]

The peak at m/e = 39 from trimethylene sulfide also can be only $C_3H_3^+$. If this is formed with the loss of H_2, S and H a value of $\Delta H_f^+(C_3H_3)$ = 262 kcal./mole is calculated. This value is in fair agreement with a number of those reported in the literature for the heat of formation of this ion.[5] In the tetrahydrothiophene as in the previous cases, the ion responsible for the peak at mass 39 is $C_3H_3^+$. Taking the neutral products to be CHS and 2H, $\Delta H_f^+(C_3H_3)$ = 274 kcal./mole is calculated.

m/e = **40.**—According to Beynon's[19] results from high resolution mass spectrometry, the only ion of m/e = 40 from tetrahydrofuran is the $C_3H_4^+$ ion. Considering the neutral fragments to be CH_2 and H_2O the value calculated for $\Delta H_f^+(C_3H_4)$ = 298 kcal./mole. This value lies within the range of values reported for $\Delta H_f^+(C_3H_4)$ in Field and Franklin.[5] Hissel[4] reports a value of 13.0 ± 0.2 e.v. for the appearance potential of m/e = 40 in tetrahydrofuran. This value is substantially lower than our value of 15.2 ± 0.3 e.v.

m/e = **41.**—Energetics alone will not distinguish between the two possible ions $C_2H_3N^+$ and $C_3H_5^+$, either of which could account for the peak at m/e = 41 in the pyrrolidine spectrum. $\Delta H_f^+(C_2H_3N)$ = 290 kcal./mole is calculated taking $C_2H_2 + H_2$ as the neutral products; 297 kcal./mole is reported in the literature for $\Delta H_f^+(C_2H_3N)$. A value of 273 kcal./mole for the $\Delta H_f^+(C_2H_3N)$ was obtained in a study of ethylenimine.[3] $\Delta H_f^+(C_3H_5)$ = 237 kcal./mole is calculated considering $CH_2 + NH_2$ as the neutral fragments. Another process which is possible is the formation of $C_2H_3N^+$ along with two CH_3 radicals leading to $\Delta H_f^+(C_2H_3N)$ = 280 kcal./mole. It is certainly difficult to establish the ion and the process here with certainty; we might well speculate, in view of the next few paragraphs, that the ion is $C_3H_5^+$ and that the neutral fragments therefore are $CH_2 + NH_2$. Hissel's[4] value of 12.6 ± 0.2 e.v. is considerably lower than our value of 15.0 ± 0.3 e.v. for the appearance potential of the ion of m/e = 41.

Beynon[19] reports 0.3 as the total abundance of m/e = 41 in the trimethylene oxide spectrum. His investigation showed 63% $C_3H_5^+$, the remainder due to C_2OH^+. The present work shows a relative abundance of 9.8 for m/e = 41, in sharp contrast to Beynon's results. Considering the ion to be $C_3H_5^+$ accompanied by the neutral product OH, $\Delta H_f^+(C_3H_5)$ = 238 kcal./mole. Beynon indicates that only $C_3H_5^+$ ion is formed in the mass spectrum of tetrahydrofuran.[19] However, the energetics do not conclusively indicate which process is favored as to the neutral fragments formed. If the neutral products are CH_2 and OH, a value of 237 kcal./mole is calculated for the heat of formation of the ion at m/e = 41. There is a second process: $C_4H_8O \rightarrow C_3H_5^+ + CH_3 + O$. For this reaction we calculated $\Delta H_f^+(C_3H_5)$ = 223 kcal/mole. The appearance potential for this process, recorded in Table VI, is 15.5 ± 0.3 e.v., in certain disagreement with the appearance potential of 13.0 ± 0.2 e.v. obtained by Hissel[4] in his investigation of tetrahydrofuran.

The only ion of this mass that can be formed from trimethylene sulfide is $C_3H_5^+$, with the most probable neutral fragment being SH. This process leads to a $\Delta H_f^+(C_3H_5)$ = 265 kcal./mole. This must be regarded as an upper limit, for similar processes in the smaller ring heterocyclics are usually too great. $C_3H_5^+$ accounts for the ions observed at m/e = 41 in the tetrahydrothiophene spectrum. If CH_2S and H are considered the neutral products, a value of 221 kcal./mole is calculated for the heat of formation of $C_3H_5^+$. Taking as the neutral fragments CHS and H_2, a value of 234 kcal./mole is calculated for the heat of formation of $C_3H_5^+$. Both processes appear reasonable. If CH_2 + SH are chosen as the neutral fragments, $\Delta H_f^+(C_3H_5)$ = 250 kcal./mole; if CH_3 and S are the neutral products, 264 kcal./mole is calculated for $\Delta H_f^+(C_3H_5)$.

Field and Franklin[5] list $\Delta H_f^+(C_3H_5)$ = 220–230 kcal./mole. The above results tend to indicate that the $C_3H_5^+$ ion is responsible for the currents observed at m/e = 41.

m/e = **42.**—The ion occurring with m/e = 42 in the fragmentation of azetidine might be due to either $C_2H_4N^+$ or $C_3H_6^+$. Considering the ion fragment to be $C_2H_4N^+$, with CH_3 as the neutral product, $\Delta H_f^+(C_2H_4N)$ = 258 kcal./mole is calculated. This value is in good agreement with the value of 255 kcal./mole given for the heat of formation of $C_2H_4N^+$ from our study of ethylenimine.[3] If we consider the ion of m/e = 42 to be $C_3H_6^+$, formed with the accompanying neutral fragment NH, a value of $\Delta H_f^+(C_3H_6)$ = 209 kcal./mole is calculated. This value is almost certainly too low; we conclude that the process is that shown in Table II.

As indicated in Table V for pyrrolidine, the ion probably formed at m/e = 42 is the $C_2H_4N^+$ ion. A calculated value of 276 kcal./mole is obtained for $\Delta H_f^+(C_2H_4N)$. This value is somewhat high compared to the value given above for the heat of formation of $C_2H_4N^+$, but it is difficult to find another process which will satisfy the energetic requirements. Beynon[19] indicates that nearly 99% of the largest peak of the tetrahydrofuran spectrum is due to $C_3H_6^+$ at mass 42. If the neutral fragment is that indicated in Table VI, a value of 278 kcal./mole is obtained for the heat of formation of $C_3H_6^+$. If CO and H_2 are taken as the neutral fragments, a value of 277 kcal./mole is obtained. Both of these values appear to be too great[5] for the heat of formation of $C_3H_6^+$. Considering the possibility that $C_2H_2O^+$ is the ion, and that C_2H_4 and H_2 are the neutral fragments, a value of 238 kcal./mole is obtained for $\Delta H_f^+(C_2H_2O)$. This value lies within range of a number of the literature values[5] given for the heat of formation of $C_2H_2O^+$. If $C_2H_2O^+$ is formed together with C_2H_2 and $2H_2$, $\Delta H_f^+(C_2H_2O)$ = 196 kcal./mole, a value not in

(26) E. Gorin, *J. Chem. Phys.*, **7**, 256 (1939).
(27) R. Klein and R. J. Schoen, *ibid.*, **24**, 1094 (1956).
(28) T. W. Shannon and A. G. Harrison, *Can. J. Chem.*, **39**, 1392 (1961).

disagreement with the literature.[5] We have here an apparent discrepancy between the decision based upon energetic arguments and the high resolution technique.

m/e = **43.**—In the pyrrolidine spectrum a value of 269 kcal./mole is obtained for the heat of formation of $C_2H_5N^+$, if the neutral product is C_2H_4. There is no previously reported heat of formation for this ion. However, as was the case for the $C_2H_4N^+$ ion fragment in pyrrolidine accounting for mass 42, this value also is considered to be reasonable.

Energetics alone indicate that the ion responsible for m/e = 43 in tetrahydrofuran is due to $C_2H_3O^+$. C_2H_4 and H are considered the neutral fragments, resulting in a calculated value of $\Delta H_f^+(C_2H_3O)$ = 288 kcal./mole. If the neutral fragments here are taken to be C_2H_4 and H, then a value of 188 kcal./mole is obtained for the heat of formation of $C_2H_3O^+$. Either process gives a value which agrees with the values of 171–203 kcal./mole reported for the heat of formation of this ion.[5] It should be noted that Beynon[19] indicates that approximately 75% of the ions at mass 43 are due to C_3H_7 at 70 e.v.

m/e = **45.**—The only ion possible from trimethylene sulfide with m/e = 45 is CHS^+. If the neutral fragments are either C_2H_4 + H or C_2H_3 + H_2, we calculate $\Delta H_f^+(CHS)$ = 271 kcal./mole. This value is in agreement with a calculated value of 271 kcal./mole obtained for $\Delta H_f^+(CHS)$ fragment from our study of ethylene sulfide.[3] This peak at mass 45 in the tetrahydrothiophene spectrum also can be due only to the CHS^+ ion and 278 kcal./mole is calculated for the heat of formation of this ion considering C_3H_5 and H_2 as the neutral fragments. This value is in good agreement with the ΔH_f^+-(CHS) = 271 kcal./mole obtained in both the ethylene sulfide[3] and trimethylene sulfide cases.

m/e = **46.**—The largest peak in the trimethylene sulfide spectrum was observed at m/e = 46. This ion is undoubtedly CH_2S^+. The accompanying neutral products are C_2H_2 and H_2, giving ΔH_f^+ (CH_2S) = 233 kcal./mole again in fair agreement with the value of 245 kcal./mole obtained for ΔH_f^+ (CH_2S) from electron impact studies of ethylene sulfide.[3] The peak at mass 46 in the tetrahydrothiophene study also is due to the CH_2S^+ ion fragment. A value of 246 kcal./mole is obtained for the heat of formation of CH_2S^+ taking the neutral fragments to be C_3H_4 and H_2. This value compares favorably with 233 and 245 kcal./mole obtained in the trimethylene sulfide and ethylene sulfide[3] cases, respectively, for the heat of formation of CH_2S^+.

m/e = **47.**—At m/e = 47 the ion is obviously CH_3S^+ in the electron impact investigation of trimethylene sulfide. $\Delta H_f^+(CH_3S)$ = 235 kcal./mole is obtained if the neutral fragment is C_2H_3. Field and Franklin[5] give a value of 222 kcal./mole for the heat of formation of CH_3S^+. In the tetrahydrothiophene spectrum, as with trimethylene sulfide, the peak at mass 47 is due to CH_3S. If the neutral fragments are C_3H_4 and H a value for $\Delta H_f^+(CH_3S)$ = 217 kcal./mole is calculated. If the neutral fragments are instead C_3H_3 and H_2 a value of 223 kcal./mole is obtained for the heat of formation of CH_3S^+. Both of these values compare well with the literature value[5] of 222 kcal./mole for the heat of formation of CH_3S^+ and allow no distinction to be made in the accompanying neutral fragments.

m/e = **48.**—Only in the case of trimethylene sulfide was an appearance potential determined for an ion of m/e = 48. The abundance of m/e = 48 relative to that for m/e = 46 suggests that this ion is largely $(CH_2S^{34})^+$; also the appearance potentials for m/e = 46 and m/e = 48 are the same within experimental error. If the neutral fragments are C_2H_2 + H_2, we calculate $\Delta H_f^+(CH_2S)$ = 228 kcal./mole, in good agreement with the value of 233 kcal./mole of $\Delta H_f^+(CH_2S)$ from the data of m/e = 46, above, and with the value of 245 kcal./mole from our ethylene sulfide study.[3] However, this ion also may be CH_4S^+. The process involving the radical C_2H_2 leads to a calculated value of 228 kcal./mole for $\Delta H_f^+(CH_4S)$, only somewhat larger than $\Delta H_f^+(CH_4S)$ = 215 kcal./mole calculated using $\Delta H_f(CH_4S)$ = −2.9 kcal./mole and the ionization potential of methanethiol of 9.44 e.v.[22,29]

m/e = **54.**—The peak of m/e = 54 in the study of tetrahydrothiophene apparently is due to the process $C_4H_8S \rightarrow C_4H_6^+ + H_2S$. This gives a value of 271 kcal./mole for the heat of formation of $C_4H_6^+$. This value is in fair agreement with some of the values listed in Field and Franklin[5] for the heat of formation of this ion.

m/e = **55.**—$C_4H_7^+$ is the only possible ion fragment which can account for the peak at mass 55 in the tetrahydrothiophene spectrum. The appearance potential indicates that the neutral fragment is SH.

m/e = **56.**—It is possible that this ion retains its cyclic structure

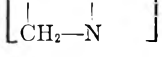

The only possible neutral fragment is H, leading to a calculated heat of formation of $C_3H_6N^+$ of 226 kcal./mole.

m/e = **58.**—In the tetrahydrothiophene spectrum $C_2H_2S^+$ ion is formed with neutral fragments C_2H_3 and H_2 and H, giving rise to the peak at m/e = 58. A calculated value for $\Delta H_f^+(C_2H_2S)$ = 268 kcal./mole is obtained. This value agrees with the value of 261 kcal./mole reported for the heat of formation of $C_2H_2S^+$ from a study of ethylene sulfide.[3]

m/e = **59.**—$C_2H_3S^+$ accounts for the peak at mass 59 for tetrahydrothiophene. If the neutral fragments are C_2H_2, H_2 and H a calculated heat of formation of 248 kcal./mole is obtained for ΔH_f^+ (C_2H_3S). The heat of formation of $C_2H_3S^+$ has not been reported previously in the literature; however, the value reported here appears reasonable in comparison to the known values for $\Delta H_f^+(C_2H_2S)$, although it is somewhat greater than our value of 230 kcal./mole for the heat of formation of $C_2H_3S^+$ obtained from a study of ethylene sulfide.[3]

m/e = **60.**—$C_2H_4S^+$ formation, leaving C_2H_2 +

(29) P. G. Wilkinson, *J. Molecular Spectroscopy* **6**, 1 (1961).

H_2 as the neutral fragments, accounts for the largest peak in the tetrahydrothiophene spectrum; 208 kcal./mole is calculated for the heat of formation of this ion, using the above process. If C_2H_4 is taken as the neutral fragment, $\Delta H_f^+(C_2H_4S)$ = 249 kcal./mole is obtained. A value of 224 kcal./mole was obtained for the heat of formation of $C_2H_4S^+$ in ethylene sulfide.[3] If the value of $\Delta H_f^+(C_2H_4S)$ = 207 kcal./mole is chosen, it would indicate that the $C_2H_4S^+$ ion in the ethylene sulfide spectrum quite possibly retains its cyclic structure.

m/e = **70.**—This ion in the pyrrolidine spectrum can be due only to the $C_4H_8N^+$ ion. As a consequence of the abstraction of a hydrogen from the parent molecule ion, a value of 200 kcal./mole is calculated for $\Delta H_f^+(C_4H_8N)$.

m/e = **71.**—Ionization and dissociation of tetrahydrofuran to $C_4H_7O^+$ and H is responsible for the ion at mass 71; 161 kcal./mole is calculated for the heat of formation of this ion.

m/e = **87.**—Dissociation of the ionized tetrahydrothiophene to $C_4H_7S^+$ and H leads to a heat of formation of $C_4H_7S^+$ of 226 kcal./mole.

Table VIII summarizes the "best values" of heats of formation for a number of ions whose values have not been reported previously. It is quite possible that $C_3H_5O^+$, $C_3H_7N^+$, $C_4H_7S^+$ and $C_4H_8S^+$ retain a cyclic structure and, since each determination of the heats of formation of these ions was obtained from the parent molecule ion or the parent minus a hydrogen ion, the values reported here possibly may differ somewhat from their straight chain counterparts. Combinations of these values of ΔH_f^+ with ΔH_f(radical) allows an estimation of the ionization potentials of the radicals. Table VIII also summarizes a few of these values.

TABLE VIII

HEATS OF FORMATION OF IONS AND IONIZATION POTENTIALS OF RADICALS

Fragment	ΔH_f^+, kcal./mole	I.P. of radical (e.v.)
C_2H_4N	255	7.6
C_2H_5N	255	..
C_3H_7N	225	..
C_3H_5O	193	..
CHS	271	6.8
CH_2S	230	6.7
C_2H_3S	248	9.1
C_2H_4S	207	..
C_4H_7S	226	..
C_4H_8S	190	..

Acknowledgments.—The authors wish to thank Dr. R. N. McDonald for his aid in obtaining the purified azetidine sample with the spinning-band column.

We also gratefully acknowledge the aid given by B. G. Hobrock in obtaining the data presented in Table I.

THE REACTION BETWEEN URANIUM HYDRIDE AND AMMONIA AT ROOM TEMPERATURE[1]

BY MOHAMMED ALEI

University of California, Los Alamos Scientific Laboratory, Los Alamos, New Mexico

Received August 17, 1961

The reaction between NH_3 and UH_3 at room temperature has been found to proceed very rapidly to form essentially a monolayer of nitride. Thereafter, the rate drops off rapidly according to a logarithmic rate law. The kinetic data are quite well interpreted on the basis of the theory of P. T. Landsberg which postulates chemisorption of a reactant as the rate-controlling step.

Introduction

It has been known for some time[2] that UH_3 reacts with NH_3 gas at elevated temperatures to produce mixtures of uranium nitrides. In the reference cited, no reaction was observed at room temperature. At temperatures above 200°, however, a rapid reaction took place to form uranium nitride of composition between UN_2 and U_2N_3. A very stable nitride, UN, also was reported. It was formed by heating the higher nitrides of any composition to temperatures above 1300° *in vacuo*.

The purpose of the present work was to determine whether or not there might be sufficient reaction between UH_3 and NH_3 at room temperature to form a surface layer of nitride. In the previous work, the change in weight of a sample of UH_3 exposed to NH_3 was used as a measure of the amount of reaction which had occurred. It is quite possible, therefore, that a reaction limited to the surface of the UH_3 particles might have gone unnoticed.

Experimental

The apparatus was designed to permit measurement of the surface area and observation of the reaction with NH_3 on a single sample of UH_3. The UH_3 was prepared[3] *in situ* by reaction of H_2 with electropolished uranium metal at ~300°. Surface areas were determined by applying the B.E.T.[4] method to N_2 adsorption isotherms measured at liquid nitrogen temperature. The reaction with NH_3 was studied by admitting a measured amount of pure NH_3 into the system and circulating the gas continuously through the UH_3 sample at room temperature (23°). Since preliminary experiments indicated that NH_3 was being consumed and H_2

(1) This work performed under the auspices of the United States Atomic Energy Commission.

(2) R. E. Rundle, N. C. Baenziger, A. S. Newton, A. H Daane, T. A. Butler, I. B. Jones, W. Tucker and P. Figard, Chemistry of Uranium, Collected Papers, TID-5290, Book 1, paper No. 6, p. 53, August 1945.

(3) J. J. Katz and E. Rabinowitch, "The Chemistry of Uranium," 1st Edition, McGraw–Hill Book Co., New York, N. Y., 1951, pp. 186–207.

(4) S. Brunauer, P. H. Emmett and E. Teller, *J. Am. Chem. Soc.*, **60** 309 (1938).

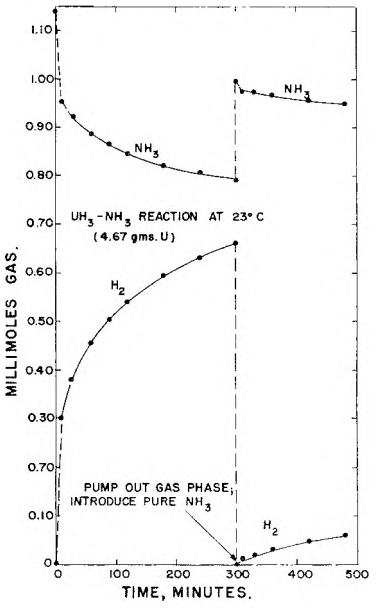

Fig. 1.

formed, the course of the reaction was followed by periodically measuring the total pressure in the system and then freezing out the NH_3 with liquid N_2 to measure the pressure of H_2 in the system. With these pressures and the known volume of the system, it was possible to calculate the amounts of NH_3 and H_2 in the gas phase as a function of time.

The gases used in this work were NH_3, H_2, N_2 and He. The NH_3 was commercial anhydrous material further purified by distillation from sodium. The H_2, N_2 and He were tank gases, purified by passage over hot reduced Cu, Ascarite and $Mg(ClO_4)_2$.

Results and Discussion

Surface Area of UH_3.—Surface areas were determined on 20 different samples of UH_3. In general, the surface areas fell into two categories. UH_3 samples, prepared by simply allowing H_2 to react to completion with uranium metal at temperatures of ~300° or lower, had surface areas ranging from 0.3 to 0.6 m.²/g. Samples prepared by hydriding the metal, decomposing the hydride by pumping, and then rehydriding the finely divided metal, all at ~300°, had surface areas ranging from 0.8 to 1.1 m.²/g. Duplicate determinations on the same sample of UH_3 were in agreement to within 7%.

To determine whether or not additional cycles of decomposing and re-forming would further increase the surface area of UH_3, a sample was subjected to four such cycles. Its surface area was found to be 0.8 m.²/g., indicating that a practical upper limit to the surface area of UH_3 prepared in this way is ~1 m.²/g. Assuming uniform spheres, this corresponds to particles ~0.6 μ in diameter.

Stoichiometry of the UH_3–NH_3 Reaction.—A typical reaction between UH_3 and NH_3 at 23° is depicted in Fig. 1, which shows the composition of the gas phase as a function of time. The break at 300 minutes represents pumping out the NH_3–H_2 mixture present in the gas phase at that time and introducing a fresh sample of pure NH_3. It is apparent from this figure that the reaction is characterized by a very rapid early stage followed by a slower stage in which the rate decreases smoothly with time. Moreover, once the rate has become slow, replacing the gas phase with pure NH_3 does not restore the initial rapid rate. This clearly demonstrates that retardation of the initial rapid reaction is not due to build-up of H_2 in the gas phase. It also is apparent immediately from Fig. 1 and from the fact that the total pressure in the system increases with time that more than one mole of H_2 is formed for each mole of NH_3 consumed. One may, in fact, calculate for each point, on either of the curves in Fig. 1, the mmoles of NH_3 consumed and the mmoles of H_2 formed in the same time interval. If a plot then is made of mmoles H_2 formed *vs.* mmoles NH_3 consumed, a very good straight line is obtained. This indicates that the stoichiometry of the reaction was constant during the time in which experimental points were taken. Moreover, the slope of the line represents the number of mmoles of H_2 formed per mmole of NH_3 consumed. The slopes obtained in seven separate experiments are shown in Table I. In all cases the values reported are least-squares slopes with 95% confidence limits.

TABLE I

STOICHIOMETRY OF THE UH_3–NH_3 REACTION AT ROOM TEMPERATURE

Slope = $\frac{H_2 \text{ formed}}{NH_3 \text{ consumed}}$	$\frac{\text{Total } H_2 \text{ formed}}{\text{Total } NH_3 \text{ consumed}}$
2.44 ± 0.08	2.9
2.19 ± .14	2.8
2.13 ± .19	2.8
2.09 ± .13	2.3
2.21 ± .10	2.5
2.03 ± .10	2.5
1.94 ± .15	2.7

If, at the conclusion of a room temperature reaction experiment, the gas phase is pumped off and the solid product heated to ~300° in the closed system, it is found that a measurable amount of H_2 is liberated. This H_2 is not reabsorbed on cooling the solid to room temperature. If one adds this amount of H_2 to the total H_2 liberated during the room-temperature reaction on the same material and compares this sum with the total NH_3 consumed during the room-temperature reaction, one obtains the ratios listed in the second column of Table I.

As stated earlier, the three known nitrides of uranium are UN_2, U_2N_3 and UN. The formation of each of these compounds by reaction of UH_3 with NH_3 is indicated by the equations below.

Reaction	$\frac{H_2 \text{ formed}}{NH_3 \text{ consumed}}$
$UH_3 + 2NH_3 \longrightarrow UN_2 + 4.5H_2$	2.25
$2UH_3 + 3NH_3 \longrightarrow U_2N_3 + 7.5H_2$	2.50
$UH_3 + NH_3 \longrightarrow UN + 3H_2$	3.00

The experimentally obtained ratios thus indicate that the room temperature reaction between UH_3 and NH_3 generally is forming UN_2, U_2N_3 or nitrides intermediate between these compositions. Furthermore, the process of heating these nitrides to ~300° in the presence of excess UH_3 is tending to bring about conversion to a lower nitride, *e.g.*,

$$3UN_2 + UH_3 \longrightarrow 2U_2N_3 + 1.5H_2$$
$$U_2N_3 + UH_3 \longrightarrow 3UN + 1.5H_2$$

The observed room-temperature stoichiometry thus, in general, agrees with the stoichiometry for formation of known nitrides. There appear, however, to be some real differences in stoichiometry of reactions proceeding on different UH_3 samples. The reason for this is not understood.

Kinetics of the UH_3–NH_3 Reaction.—Data of the type shown in Fig. 1 are fit very well by a kinetic expression of the form

$$[H_2] = k \log \left[\frac{[NH_3]}{[NH_3]_0} (1 + t/t_0) \right]$$

where

k and t_0 = constants
t = time
$[H_2]$ = mmoles H_2 in gas phase at time t
$[NH_3]$ = mmoles NH_3 in gas phase at time t
$[NH_3]_0$ = mmoles NH_3 originally introduced

The data of Fig. 1 and similar data obtained in two other experiments are plotted in the above form in Fig. 2. In each case, the surface area of the UH_3 sample was measured before its reaction with NH_3.

Direct logarithmic rate laws of the type observed here have been encountered frequently in studies of the growth of oxide films on metals.[5] Theoretical mechanisms which lead to such laws generally postulate a reaction whose rate is determined by diffusion through thin films, pores or cavities. A notable exception is the treatment of Landsberg,[6] who derives a direct logarithmic rate law assuming that chemisorption of a reactant is rate controlling. In attempting to decide which of the above mechanisms might conceivably be operative in the present work, it would be important to have an estimate of the thickness of nitride films produced by the observed reaction of NH_3 with UH_3. In the initial rapid reaction (first 10 min.) for the study shown in Fig. 1, ~0.2 mmole of NH_3 was consumed. Assuming a product of composition UN_2, this NH_3 consumption corresponds to formation of 0.1 mmole or 27 mg. of UN_2. The X-ray density[2] of UN_2 is 11.73 g./cm.^{3}. Hence, the volume of nitride formed is $27 \times 10^{-3}/11.73 = 2.3 \times 10^{-3}$ cm.^{3}. The data obtained in Fig. 1 were taken on 4.7 g. of UH_3 having a surface area of 1 sq.m./g. Hence the total surface area of the solid is 4.7×10^4 cm.^{2}. Assuming that the volume of nitride is uniformly distributed over this area, the average thickness of the nitride film is $2.3 \times 10^{-3}/4.7 \times 10^4$ cm., or 5 Å. Since the lattice constant for the face-centered cubic UN_2 is $a_0 = 5.3$ Å^2, such films of nitride can be at most a few atom-layers thick.

With films as thin as these, it seems very unlikely that a diffusion process would be rate controlling. One thus is led to the conclusion that the reaction observed here is one whose rate is controlled by chemisorption of NH_3 on a nitride film. In this connection, it should be noted that the lines in Fig. 2 do not extrapolate to the origin. This indicates that the initial reaction is much more rapid than dictated by the logarithmic law which applies to the data between 10 and 300 min. If one uses the intercepts of these lines as a measure of the amount

(5) U. R. Evans, "The Corrosion and Oxidation of Metals," Edward Arnold Ltd., London, 1960, pp. 829–837.
(6) P. T. Landsberg, *J. Chem. Phys.*, **23**, 1079 (1955).

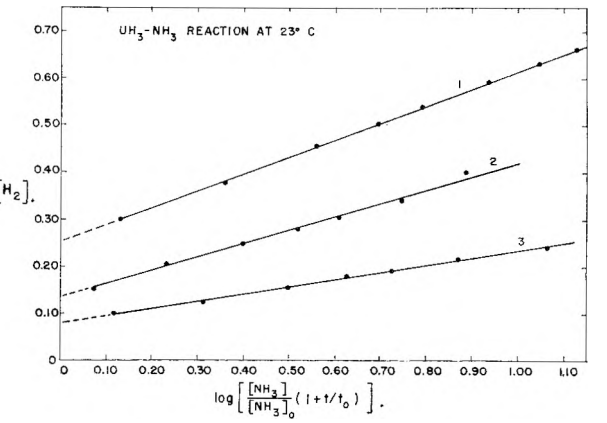

Fig. 2.

of initial rapid reaction and compares this amount of reaction with the surface area of the UH_3 sample, it is quite conceivable that the rapid process represents reaction between NH_3 and bare UH_3 surface to form essentially a monolayer of nitride. Subsequent reaction then involves chemisorption of NH_3 on a nitride surface as the rate-determining step. If such an interpretation is valid, the intercept should, in each case, be proportional to the total surface area of the UH_3 sample. That this is so is shown by the constancy of the ratio, intercept/V_m, in Table II. The intercepts, slopes, and values of t_0 are, in each case, the best values determined by the method of least squares. The limits indicated represent the standard deviation in each case. The quantity V_m is the volume of N_2 required to form a monolayer on the surface in the B.E.T. surface area determination and is therefore a measure of the total surface area of the UH_3 sample.

TABLE II

CORRELATION OF SURFACE AREA WITH KINETIC DATA IN UH_3–NH_3 REACTION AT ROOM TEMPERATURE

Experiment	1	2	3
V_m, cc. N_2 S.T.P.	1.06	0.46	0.71
Specific surface area, σ, m.^{2}/g.	0.99	0.44	0.30
$[NH_3]_0$	1.137	0.979	1.044
Slope	0.364 ± 0.008	0.153 ± 0.014	0.281 ± 0.025
Intercept	0.251 ± 0.006	0.078 ± 0.007	0.134 ± 0.011
t_0	16.4 ± 1.5	23.8 ± 7.3	29.7 ± 7.7
Intercept/V_m	0.24	0.17	0.19
Slope/$V_m[NH_3]_0$	0.30	0.34	0.38
$t_0[NH_3]_0\sigma^{1/2}$	18.6	15.5	17.0

When the theory of Landsberg is applied to the data in Fig. 2, the slope of the line should be given, in each case, by the expression

$$\text{Slope} = \frac{k' V_m (NH_3)_0}{b}$$

where

k' = a constant
b = av. no. of sites invalidated by adsorption of a single NH_3 molecule

If b is constant from one preparation of UH_3 to another, then the ratio, slope/$V_m[NH_3]_0$, should be constant. Table II shows that this condition is met very well.

Finally, in Landsberg's theory applied to the present problem, t_0 is given by

$$t_0 = \frac{1}{C'[NH_3]_0 a s_0}$$

where

C' = a constant
a = effective area of contact between an NH_3 molecule and the surface upon collision
s_0 = sites per unit area at time zero

We already have assumed b constant and found that this correlates well with the observed slopes. Moreover, a ought to be very nearly the cross-sectional area of an NH_3 molecule and independent of the UH_3 surface.

One thus would conclude that t_0 should be proportional to $1/[NH_3]_0 s_0$. From the data in Table II, it can be seen that whereas the slopes and intercepts vary directly with *total* surface area (as measured by V_m), t_0 varies in an inverse fashion with *specific* surface area. This suggests that s_0 is directly related to the specific surface area, σ. In fact, if one arbitrarily assumes $s_0 \propto \sigma^{1/2}$, then the product $t_0[NH_3]_0 \sigma^{1/2}$ should be constant for all experiments. The bottom line in Table II shows that the constancy is indeed quite good. This suggests that the number of sites per unit area is inversely proportional to the square root of the average particle diameter.

Acknowledgment.—The author wishes to express his appreciation to Dr. J. F. Lemons of this Laboratory for his active interest and helpful direction in this work. He also wishes to thank Dr. Walton P. Ellis of this Laboratory for helpful discussions concerning the interpretation of some of the results of this work.

CRYSTAL STRUCTURES OF SOME LANTHANIDE HYDRIDES[1]

BY A. PEBLER AND W. E. WALLACE

Department of Chemistry, University of Pittsburgh, Pittsburgh 13, Pa.

Received August 25, 1961

Hydrides of Pr, Nd, Sm, Tb, Dy, Ho, Er, Tm, Lu and Y have been formed and examined using X-ray diffraction techniques. The dihydrides of the several metals always were observed to be cubic. Appreciable contraction of the lattice occurs when PrH_2, NdH_2 or SmH_2 absorbs extra hydrogen. The PrH_2 and NdH_2 phases remain cubic to the highest hydrogen concentration attainable, whereas the Sm–H system undergoes a transformation such that the Sm ion cores are in a cph arrangement for hydrogen concentrations exceeding that corresponding to the formula $SmH_{2.59}$. Similar transformations are observed for the several heavy lanthanides studied and for yttrium, the range of stability of the dihydride being, however, considerably less than that for the alloys based on SmH_2. The dependence of the lattice spacing on composition is discussed in terms of the presumed electronic nature of the lanthanide hydrides. The observed contraction of the dihydride lattice is consistent with the notion (suggested by their electrical and magnetic behavior) that the lanthanide hydrides are essentially saline in nature and the hydride ion is formed by absorption of electrons from the conduction band of the metal.

Introduction

For many years it has been known that when the lanthanide metals are exposed to an atmosphere of hydrogen at elevated temperatures, reaction occurs and hydrogen is incorporated in the solid, forming what usually are termed "hydrides." Several investigations have been carried out for the purpose of elucidating the structural features of these hydrides. Using conventional X-ray diffraction techniques the arrangement of the metal atoms or ions has been established in several cases and in one instance (the Ce–H system) the hydrogen atoms or ions were located using neutron diffraction data.

To date attention has been focussed largely on the light lanthanides La, Ce, Pr, Nd and Sm. In the elemental state Ce is fcc, Pr and Nd are cph, La is cph with a doubled c spacing and Sm is rhombohedral. However, each of these is observed[2] to form a dihydride MeH_2 in which the arrangement of the metal ion cores is fcc.[2-7] These dihydrides have been found to possess the ability to absorb considerable additional hydrogen without alteration of the structure of the metallic matrix. Also, it was ascertained that to a limited extent hydrogen can be removed from the dihydride. It thus is clear that the phase based on the dihydride stoichiometry embraces a considerable range of composition, which in La-H and Ce-H extends[6,7] to the trihydride composition MeH_3.

Neutron diffraction work on CeH_2 showed[5] the H's to reside in the tetrahedral interstices; thus this material possesses the fluorite structure. A similar study of a sample of composition represented by the formula $CeH_{2.7}$ showed[5] that all the tetrahedral interstices were filled and the additional H's were randomly distributed in the octahedral interstices. Although direct supporting experimental evidence is lacking, it generally is believed that (1) the situation is similar for the La, Pr and Nd dihydrides, with and without additional hydrogen, and (2) in those hydrides in which $H/Ce < 2.0$, the H's are distributed randomly over the tetrahedral sites.

In 1956 Sturdy and Mulford conducted what appears to have been the first and only investigation of a heavy lanthanide–hydrogen system—the Gd–H system.[8] They found by X-ray diffraction, which of course detects only the metal ion

(1) This work was assisted by a contract with the U. S. Atomic Energy Commission.

(2) A. Rossi, *Nature*, **133**, 174 (1934).

(3) B. Dreyfuss-Alain, *Compt. rend.*, **235**, 540, 1295 (1952); **236**, 1265 (1953); **237**, 806 (1953).

(4) R. N. R. Mulford and C. E. Holley, *J. Phys. Chem.*, **59**, 1222 (1955).

(5) C. E. Holley, *et al.*, *ibid.*, **59**, 1226 (1955).

(6) K. Dialer and W. Rothe, *Z. Elektrochem.*, **59**, 970 (1955).

(7) B. Stalinski, *Bull. acad. polon. sci.*, **3**, 613 (1955).

(8) G. E. Sturdy and R. N. R. Mulford, *J. Am. Chem. Soc.*, **78**, 1083 (1956).

cores, the usual fcc dihydride. This phase was observed to exist from $GdH_{1.8}$ to $GdH_{2.3}$. At higher hydrogen concentrations a second phase appeared, in which the Gd ion cores were in a cph arrangement. The two-phase region extended from $GdH_{2.3}$ to $GdH_{2.85}$, above which only the hexagonal phase existed up to $GdH_{2.91}$, the highest hydrogen concentration obtained in their study. Mulford has predicted[9] similar behavior for all the heavy lanthanides except europium and ytterbium.[10]

The present study was undertaken to increase the amount of information available concerning the constitution of heavy lanthanide hydrides, to ascertain whether or not Mulford's prediction is correct and, if so, to locate the several phase boundaries using standard X-ray diffraction techniques. The lanthanides originally included in the study extended from Sm to Lu, with the exception of Eu and Yb. When Sm was observed to form a hexagonal phase, the coverage was extended to Pr and Nd, and, in addition, the chemically similar element Y was included.

Experimental

The lanthanide metals were obtained from the Nuclear Corp. of America, Burbank, Cal. They were analyzed spectroscopically by the supplier and were found to be 99% pure or better. The hydrogen used was obtained from a commercial cylinder and purified by passing through a Deoxo unit, a liquid nitrogen trap and finally a heated palladium tube.

The following procedure was employed in preparing the metal for hydrogen: 0.1 to 0.4-g. samples were cut from the stock supply, the cutting being done under mineral oil. The samples then were polished under mineral oil with progressively finer abrasive papers ending with type 600A. They then were washed successively with CCl_4, acetone and ether. (With the more reactive lighter lanthanons weighing was also under oil.) After weighing, the sample was introduced into the preparation train (vacuum system and appropriate gas metering equipment) and evacuated to high vacuum for at least 4 hr. It then was heated gradually to 500° and hydrogen then was admitted. Hydrides with compositions approximating the dihydride usually formed quite rapidly. For higher hydrogen contents the temperature had to be lowered and higher pressures (up to 1 atm.) had to be applied. After attaining the desired composition, the temperature was reduced and the sample was annealed at 200 to 300° for at least 4 hr. Upon removal the hydrides were placed under oil and kept there to retard oxidation and/or decomposition.

X-Ray diffraction photographs were taken of the samples using a 114.6 mm. diameter camera arranged for Straumanis loading. Filtered $CrK\alpha$ radiation was used. The powder specimens were prepared by crushing the sample under oil and sucking the oil suspension up into a fine capillary which then was sealed off with plastic cement. In the case of the very sensitive Sm trihydride the capillary was filled under helium in a dry box.

Except for some of the higher hydrides, the lines in the diffraction pattern for the single phase materials were quite sharp, permitting accurate determination of the lattice parameters. Extrapolation to 90° Bragg angle was made using Taylor's or Cohen's method.[11]

Results

Experimental effort was largely concentrated on the five metals Sm, Dy, Ho, Tm and Nd. The others were examined only to the extent necessary to establish that their behavior is substantially the same as that of their more thoroughly investigated neighbors in the Periodic Table. In all cases powder diffraction patterns were obtained for the metal containing varying amounts of hydrogen. The patterns were analyzed to ascertain whether the system was single phase or heterogeneous and to determine the structure(s) of the phase or phases present. When the sharpness and intensities of the lines permitted, lattice parameters were evaluated.

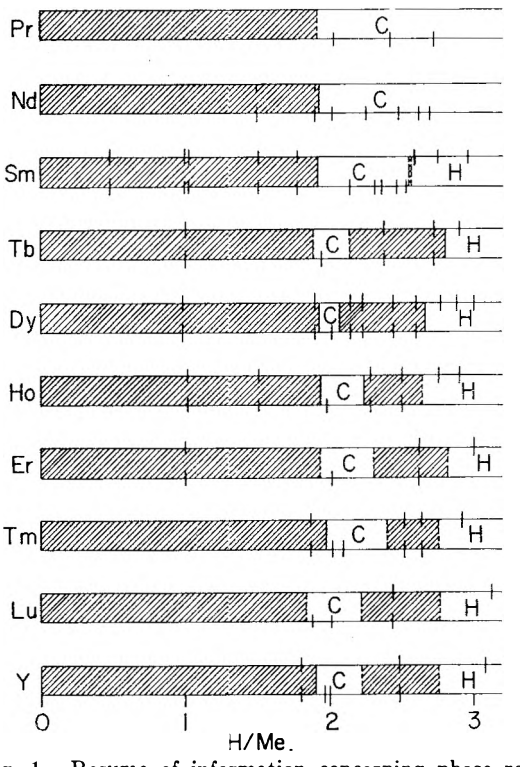

Fig. 1.—Resume of information concerning phase relationships in several lanthanide metal–hydrogen and the Y–H systems. The single phase regions based on the dihydrides (cubic) and trihydrides (hexagonal) are indicated by C and H, respectively. Regions in which two phases coexist are crosshatched. Compositions for which diffraction patterns were obtained are indicated by the vertical line or lines: —|—, two-phase; —|—, single cubic phase; —|—, single hexagonal phase. The phase boundaries whose positions are considered less certain are dashed.

The results obtained are summarized in Fig. 1 and 2 and Table I. In regard to Fig. 1 it is to be noted that no range of primary solubility is indicated. Since earlier work has shown[5,8] that at elevated temperatures several of the metals take appreciable quantities of hydrogen into solid solution, there is undoubtedly some solubility even at room temperature. However, this solubility is probably quite small; at least this seems to be the case for Ho–H, the one system which was examined to ascertain the extent of the primary solubility. The metallic phase coexisting with HoH_2 was examined and its lattice parameters were found to be indistinguishable from those of pure holmium. It also is to be noted regarding Fig. 1 that in some cases (for example, the Dy–H system) a number of compositions were examined and the phase bound-

(9) R. N. R. Mulford, private communication.

(10) Various evidence suggests that these elements are divalent in the metallic state in contrast with the remaining lanthanides, which are trivalent. For Eu and Yb the dihydride is the highest hydride formed. These dihydrides are orthorhombic, possessing the CaH_2 structure. See W. L. Korst and J. C. Warf, *Acta Cryst.*, **9**, 452 (1956).

(11) See, for example, L. V. Azaroff and M. J. Buerger, "The Powder Method in X-Ray Crystallography," McGraw-Hill Book Co., Inc., New York, N. Y. 1958, p. 238 ff.

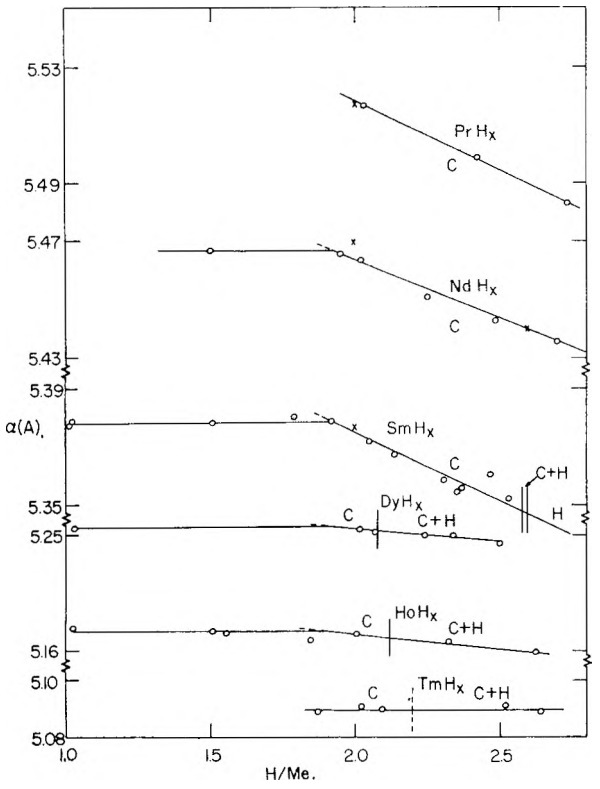

Fig. 2.—Lattice spacing *versus* gross composition for several lanthanide metal–hydrogen systems: O, this study; ×, data from ref. 5.

aries could be located within fairly narrow limits, whereas in other cases (for example, the Lu–H system) the paucity of data introduces large uncertainty into the stated positions of the phase boundaries. In those cases in which the phase boundaries are thought to be fairly precisely located two additional kinds of information were employed, apart from that indicated in Fig. 1: (1) parameter *vs.* composition data as are shown in Fig. 2 and (2) intensities of diffraction lines in the two-phase region.

Discussion of Results

The contraction in lattice parameter for the dihydride phase with increasing hydrogen content, to which attention has been directed previously,[2,4] also is revealed by the results given in Fig. 2. The contraction is quite pronounced for Pr–H, Nd–H and Sm–H but much less so for the other three systems. Actually this difference is more apparent than real due to the variation in the range over which the dihydride phase exists in the several cases (see Fig. 1). In the Dy–H system, for example, the dihydride phase extends only up to about $DyH_{2.08}$. Above this the system is two-phase and the concentration of the cubic form should be fixed. Thus the lattice parameter should be invariant with gross composition when H/Dy > 2.08. The slight dependence on gross composition in the two-phase region for this and the Ho–H system is probably due to slight departures from equilibrium conditions. Thus for the three heaviest lanthanides the permissible contraction is limited by the appearance of the second phase. With Pr, Nd and Sm the range of stability of the cubic phase is much wider and the total contraction of the lattice spacing is increased accordingly.

Table I

Lattice Parameters[a] and X-Ray Densities[b] of Lanthanide Di- and Tri-hydrides

Metal	MeH_2 a_0 (Å.)	MeH_3 a_0 (Å.)	c_0 (Å.)	c_0/a_0	$\rho_{cub.}/\rho_{hex.}$
Pr	5.518 (5.517[c])				
Nd	5.464 (5.470[c])				
Sm	5.374 (5.376[c])	3.782	6.779	1.792	1.082
Gd	(5.303[d])	3.73[d]	6.71[d]	1.80	1.084
Tb	5.246	3.700	6.658	1.799	1.093
Dy	5.201	3.671	6.615	1.802	1.097
Ho	5.165	3.642	6.560	1.801	1.094
Er	5.123	3.621	6.526	1.802	1.102
Tm	5.090	3.599	6.489	1.803	1.104
Lu	5.033	3.558	6.443	1.811	1.108
Y	5.205	3.672	6.659	1.813	1.103

[a] For the dihydride the parameter listed is either measured directly or interpolated to the composition MeH_2. For the "trihydride" the parameters given are for MeH_3 or, if less hydrogen could be introduced into the metal, the parameters are for the most hydrogen-rich sample that could be formed. In no case was the hydrogen–metal ratio less than 2.90. [b] Densities of the cubic form (represented as $\rho_{cub.}$) are those estimated for the hypothetical cubic MeH_3. [c] Data of Holley, *et al.* (ref. 5.). [d] Data of Sturdy and Mulford (ref. 8).

It is of some interest to ascertain the cause of the decrease in lattice dimensions when the dihydrides absorb extra hydrogen. This phenomenon can be rationalized in terms of the concepts held by the present authors concerning the electronic nature of these hydrides. The view is held (1) that the lanthanide hydrides are essentially salt-like in character with the hydrogen of course present as an anion and (2) that the hydrogen acquires its electron upon entry into the metal from the electrons in the conduction band. Support for the first point[12] is provided by such things as the observed heats of hydrogenation,[6] the stoichiometry of the hydrides (trihydride formed with trivalent metals whereas only dihydride can be formed with the divalent metals Eu and Yb) and their positions in the Periodic Table. More recently considerable support for both points has been provided by measurements of the electrical conductivities of certain lanthanide hydrides.[13] Upon complete hydrogenation the conductivity falls by six or more orders of magnitude with Dy, Ho and Yb. Stalinski found a similar behavior for La and Ce and moreover obtained additional evidence for the non-metallic character of these hydrides by noting that their resistivities decreased with increasing temperature.[14] The conductivity behavior is consistent with the notion that the hydride ion is formed using electrons in the conduction band. This also is supported by magnetic work carried out by Trombe[15] for GdH_2, by Stalinski[14,16] for the La–H and Ce–H systems and by Kubota and Wal-

(12) Actually, the presumed saline character of these hydrides should be restricted to the case of the trihydride. Alloys less rich in hydrogen, including the dihydride, exhibit metallic conduction and hence must be regarded as at least partly metallic in nature.

(13) T. Peltz and W. E. Wallace, unpublished.

(14) B. Stalinski, *Bull. acad. polon. sci.*, **5**, 1001 (1957); **7**, 269 (1959).

(15) F. Trombe, *Compt. rend.*, **219**, 182 (1944).

(16) B. Stalinski, *Bull. acad. polon. sci.*, **5**, 997 (1957).

lace[17] for the Ho–H and Tb–H systems. In each case the magneton number is unchanged by hydrogenation, indicating that the electrons used to form the hydride ion are not abstracted from the core.

On the basis of the evidence presented in the preceding paragraph one concludes that as hydrogen is added to the dihydride, electrons are progressively removed from the conduction band. It appears that this would produce a denser structure for two reasons: (a) the conduction electrons in the dihydride screen and hence weaken the interaction between the oppositely charged lanthanide and hydrogen ions; as they are consumed when hydrogen is added, their screening power is reduced, the interactions increase and hence the interionic distances are expected to decrease; (b) as has been discussed in detail by Nabarro and Varley,[18] the quasi-free conduction electrons in a metal due to their Fermi (or kinetic) energy materially contribute to repulsion and hence act to expand the solid; thus as they are absorbed by the dissolving hydrogen this repulsive tendency is decreased, permitting contraction in the lattice.

These considerations make the origin of the contraction of the hydrogen-rich dihydrides clear but do not, of course, clarify why the structure changes to hexagonal for the metals beginning with samarium. The data in column 6 of Table I show that upon changing to the hexagonal form the system achieves a reduction in density of roughly 10%. It is not clear whether the structural change and the concomitant density reduction are merely a matter of reducing the electrostatic energy of the system or whether other factors are involved. Work is under way in this Laboratory at present to evaluate the Madelung number of the hexagonal and cubic forms of the trihydride. This should in time contribute to the elucidation of the factors responsible for the cubic to hexagonal transformation observed for the heavy lanthanides.

The data in Table I show that the axial ratio exceeds the value for the close packing of spheres by about 10%. It appears that the distension along the hexagonal axis develops primarily because of strong repulsion between the hydride ions in certain of the tetrahedral sites; using a model of the undistended hexagonal trihydride, it is noted that

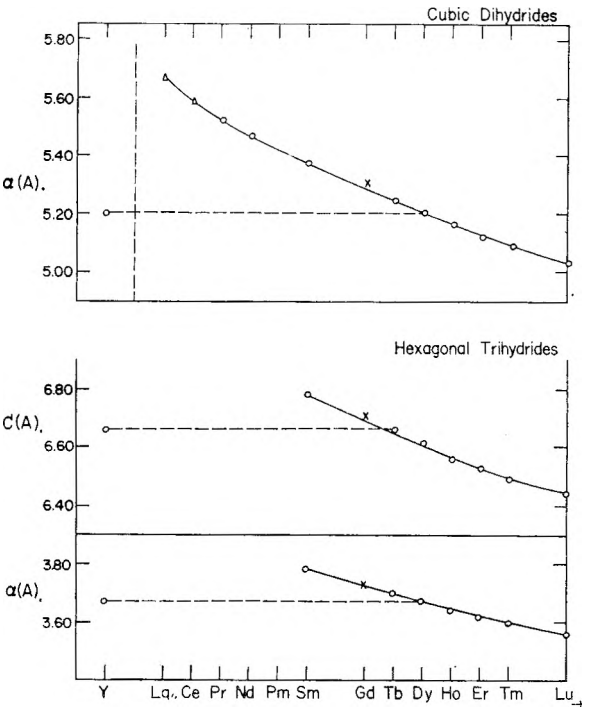

Fig. 3.—Lattice parameters *versus* atomic number for lanthanide dihydrides and samples approaching the composition of the trihydrides: ○, this study; △, ref. 5; ×, ref. 8. Data for YH_2 and YH_3 also are included.

pairs of hydride ions occur separated by a distance of $0.404a_0$ or about 1.5 Å. According to Libowitz and Gibb[19] the ionic radius of H^- is about 1.3 Å. Thus the undistended structure entails too close an approach of the hydride ions and elongation along the hexagonal axis occurs. It is evidently this which produces the abnormally high axial ratio.

In Fig. 3 are plotted lattice parameters for the dihydrides and trihydrides (or nearly so) of the various lanthanides studied to date. These data give clear evidence of the well-known lanthanide contraction.

Acknowledgment.—The authors would like to express their appreciation to Professor R. S. Craig for his generous assistance in connection with many of the experimental aspects of the present work.

(17) Y. Kubota and W. E. Wallace, to be published.

(18) F. R. N. Nabarro and J. H. O. Varley, *Proc. Cambridge Phil. Soc.*, **48**, 316 (1952).

(19) G. G. Libowitz and T. R. P. Gibb, Jr., *J. Phys. Chem.*, **60**, 510 (1956).

CARBON-14-CONTAINING COMPOUNDS PRODUCED BY THE PILE NEUTRON IRRADIATION OF CYANOGUANIDINE[1]

BY THOMAS W. LAPP AND ROBERT W. KISER

Department of Chemistry, Kansas State University, Manhattan, Kansas

Received August 25, 1961

An investigation has been made into the nature and relative amounts of the radiocarbon-labelled products obtained from the dissolution in water of pile-neutron irradiated cyanoguanidine. Liquid scintillation counting was conveniently employed in the radioactivity determinations. Little activity was found in the form of CO, CO_2, CH_4, HCN, CH_3CN, HCHO, HCOOH, urea and methylhydrazine. Acetamidine, guanidine and cyanoguanidine were found to contain 17, 13.5 and 41%, respectively, of the total activity induced in the original sample. A polymeric material, believed to be melamine, was found to contain approximately 13% of the total activity. Possible paths are suggested, in which cyanamide is considered to play an important role, leading from the crystal-stabilized species to the final products observed in solution.

Introduction

In a neutron flux, nitrogen-14 is transformed into carbon-14 by the nuclear reaction N^{14} (n,p) C^{14}. The C^{14} atom recoiling from the transformation carries approximately 40,000 e.v. from the nuclear site. This energy is dissipated to the surroundings in a period of about 10^{-13} seconds. During this "slowing down" period, free radicals and ions are formed within a region near the recoil path of the carbon-14 atom. When the C^{14} recoil atom has been reduced to an energy of about 100 e.v. or less, its state may be stable toward recombination with the free radicals and/or ions produced during the slowing down process.

Yankwich and co-workers[2-4] have shown that this recombination process leads to a variety of C^{14}-labeled compounds. While the various labeled components have been determined for a variety of nitrogen-containing compounds, a clear understanding of the actual processes occurring during the recombination period has not yet been achieved. In order to aid in elucidating these processes, we irradiated cyanoguanidine and subsequently studied the various C^{14}-containing compounds present when the target compound was dissolved in water.

Experimental

Sample Preparation and Irradiation.—Cyanoguanidine (Eastman red label) was dried for one hour at 100° and 4.952 g. of the sample was placed in a quartz ampoule which then was attached to a vacuum line. The ampoule and contents were flushed thoroughly with argon and evacuated to one micron to rigorously exclude oxygen from the sample. The quartz ampoule was sealed off under vacuum with a hand torch. Irradiations were carried out at Oak Ridge National Laboratories in the graphite reactor; pertinent data are as follows: neutron flux of approximately 5×10^{11} cm.$^{-2}$ sec.$^{-1}$; irradiation time of 670 hr.; γ-ray flux of 4.9×10^5 rhr.$^{-1}$; maximum sample temperature of 80°. The sample was allowed to cool for 15 months following irradiation; the ampoule was opened, and the contents were transferred to a Pyrex storage bottle under an argon atmosphere. The sample was maintained under an argon atmosphere during the entire course of the experimental study.

Radioactivity Determinations.—Each carrier isolated was dissolved, either directly or by use of a suitable solvent, into a scintillator solution. All activity measurements were made using a Packard Tri-Carb Liquid Scintillation Spectrometer.[5] The scintillator solution used consisted of a solution of 7.0 g. of PPO (3,5-diphenyloxazole), 50.0 mg. of POPOP (1,4-bis-2-(5-phenyloxazole)-benzene) and 100 g. of naphthalene in one liter of *p*-dioxane. A counting efficiency of (50.0 ± 1.4)% was obtained using samples of benzoic acid-C^{14} from three different sources. Counting efficiency studies were performed on each derivative solute counted in these determinations. The activity of the irradiated cyanoguanidine was $(1.39 \pm 0.05) \times 10^5$ dis. sec.$^{-1}$ g.$^{-1}$.

Preliminary Experiments.—The total carbon-14 activity of the irradiated samples was determined by dissolution of known portions in water. Aliquots were taken and the total activity determined by liquid scintillation counting. The average of four different determinations made over a period of four months was 18.6 ± 0.7 microcuries for the 4.952-g. sample.

In order to establish the distribution of the carbon-14 activity among the species likely to result upon dissolution of the irradiated sample in water, solutions of irradiated cyanoguanidine samples were subjected to analyses for the substances listed in Table I.

TABLE I

CARBON-14 DISTRIBUTION AMONG VARIOUS COMPOUNDS

Fraction	% of total activity: Average	Values obtained
CH_4	0.0	0.0, 0.0
CO	.0	.0, 0.0
CO_2	.0	.0, 0.0
HCN	.0	.0, 0.0
HCHO	.1	.2, 0.1, 0.1
HCO_2H	.4	.4, 0.5, 0.4
CH_3CN	.6	.3, 0.9
CH_3NH_2	3.2	3.3, 3.1
CH_3NHNH_2	1.0	1.3, 0.7
$(NH_2)_2CO$	0.2	0.4, 0.2, 0.1
$(NH_2)_2C{=}NH$	13.5	12.4, 12.9, 14.3, 14.1, 13.9
$CH_3C(NH)NH_2$	16.9	17.0, 17.7, 16.2, 16.6
$NCNHC(NH)NH_2$	41.1	39.6, 42.6
Melamine(?)	13.1	13.5, 12.7

The solution apparatus consisted of an inverted-Y-tube into which a small sample (50–100 mg.) was placed in one arm and distilled water (approximately 5–10 ml.) was placed in the other arm. The Y-tube was placed on the vacuum line and the water degassed by alternately freezing with liquid air and warming while under vacuum. The system was fitted with a cold trap, a 250-ml. bulb for collecting the evolved gases, and a mercury manometer. The Y-tube was closed off from the immediate system and the ice melted. The water then was slowly added in steps to the dry sample while alternately opening the Y-tube to the evacuated system. Upon addition of all of the water to the sample, the pressure change was recorded with the manometer and the collection bulb was closed.

(1) This work was supported in part by the U. S. Atomic Energy Commission, under Contract No. At(11-1)-751 with Kansas State University. Taken in part from a thesis submitted by T. W. Lapp to the Graduate School of Kansas State University in partial fulfillment of the requirements for the M.S. degree, August, 1961. Presented at the 140th National Meeting of the American Chemical Society, Chicago, Ill., September 3–8, 1961.

(2) P. E. Yankwich and J. D. Vaughan, *J. Am. Chem. Soc.*, **76**, 5851 (1954).

(3) P. E. Yankwich and W. R. Corman, Jr., *ibid.*, **77**, 2096 (1955).

(4) P. E. Yankwich and W. R. Corman, Jr., *ibid.*, **78**, 1560 (1956).

(5) Packard Instrument Company, LaGrange, Illinois.

In these analyses, it was necessary to start with a trial group of carriers, hoping to discover other carriers suitable for the separation of the activities found as the study progressed. The principal problem encountered in this type of procedure was the quantitative separation of the various activities free from contamination. Therefore, all compounds and derivatives isolated were purified to constant specific activity in the attempt to achieve radiochemical purity.

Chemical Separations.—Analyses usually were made for one carrier in each solution of the target sample; in a few cases, two or three carriers were added and analyzed per solution of target sample.

Carbon dioxide: direct absorption by sodium hydroxide. **Carbon monoxide**: gas chromatographic radioanalyses using Molecular Sieve 5A (Linde Corp.) as column packing. Radioanalyses were made by passing the effluent from the column, after mixing with a methane–argon mixture, directly through a proportional counter.[6] **Hydrogen cyanide**: direct absorption by sodium hydroxide. **Methane**: Gas chromatographic radioanalysis. **Formaldehyde**: formaldehyde was separated from an aqueous solution of the irradiated sample as the methone (dimedon) derivative.[7,8] **Formic acid**: oxidation with mercuric acetate.[2] **Methylamine**: preparation of the N,N′-methylphenylthiourea derivative.[9] **Urea**: determined by oxidation with jack bean urease.[2] **Cyanoguanidine**: separated by multiple recrystallizations from distilled water. **Guanidine**: after removal of cyanoguanidine, a saturated solution of oxalic acid was added and guanidine oxalate separated by addition of ethanol. **Acetamidine**: base hydrolysis, followed by precipitation of benzylthiuronium acetate.[9] **Methylhydrazine**: 50% sulfuric acid was added to an aqueous sample solution at 0° and methylhydrazine sulfate was precipitated by adding 95% ethanol. **Acetonitrile**: removed by distillation and dissolved directly into the scintillator solution.

Polymeric Material.—Upon dissolution of a sample of the irradiated cyanoguanidine in distilled water, a brown material (about 3.5% by weight of the sample) was found to remain undissolved. The brown solid, separated by centrifugation, was dissolved in sodium hydroxide and added to the scintillator solution. This material was found to contain about 13% of the total activity.

An infrared analysis of a mull of the brown material was obtained using a Perkin–Elmer Model 137 Infracord spectrophotometer; the brown material showed the same absorption bands, particularly the significant 12.25 μ band, as those obtained for pure melamine, suggesting that at least part of this polymeric material is melamine.

Pure melamine shows a sharp ultraviolet absorption at 236 mμ, followed immediately by a very broad, intense absorption band extending to about 200 mμ.[10] A sample of the brown solid was dissolved in 0.1 *N* hydrochloric acid and an ultraviolet analysis obtained using a Cary Model 11 recording spectrophotometer. The analysis of the brown material did not show a sharp absorption at 236 mμ. Very likely other materials are mixed with any possible melamine in the brown solid.

Results of Analyses.—The results obtained by the procedures described above are given in Table I. In all cases the data reported are based on specific activity measurements. The percentage activity is based on the total activity of aliquots of aqueous solutions of the original irradiated cyanoguanidine sample.

The total activity isolated in this study was (90.1 ± 3.9) % of the total carbon-14 activity induced in the cyanoguanidine sample by pile neutron irradiation. Nearly 94% of the total activity isolated in this study occurred in four compounds: cyanoguanidine, acetamidine, guanidine and the polymeric material.

Discussion

The investigation of the system presented in this paper has afforded an interesting insight into the possible solid matrix-stabilized radicals and/or ions produced during the neutron irradiation of solid nitrogen-containing compounds.

In this investigation we have considered only the final chemical form incorporating the recoil carbon-14 atom. It has been suggested previously[3] that many chemical forms of the recoil carbon-14 atom are present within the solid matrix following irradiation and that these matrix-stabilized forms undergo decomposition, rearrangement or further reactions when the solid irradiated compound is dissolved in water. Since only the final form assumed by the recoil carbon-14 actually is determined, these matrix-stabilized species can be arrived at only by a critical analysis of the results obtained from a particular determination and the proposition of reasonable intermediates to yield the products actually observed. From the consideration of a number of studies, a similarity in the final form of the recoil atom may become evident.

The final state of the carbon-14 recoil atom may be considered in terms of three steps, any one of which may have an effect on the final distribution of activity.[11] The first step involves the reduction of the energy of the recoil atom by elastic and inelastic collisions and the final localization of the recoil atom in a reactive site. The second step involves the chemical considerations which may lead to a variety of solid matrix-stabilized chemical species depending upon the structural aspects of the entrapment site and upon the energy available for chemical reactions within the reactive site. The third step considers the collapse of the solid matrix-stabilized species to form stable compounds or the reaction of the stabilized species during subsequent chemical operations carried out on the irradiated material to form stable chemical species.

An important and interesting result of this study is that nearly half of the total activity produced in the pile-neutron irradiation was found in the parent compound, cyanoguanidine. This differs from results previously reported[12] in which only a small amount of the activity has been "retained" in the parent compound. The formation of the cyanoguanidine may be postulated to occur by equations 1 and 2.

$$H_2NC(NH)NHCN \xrightarrow{(n,p)} \text{recoil carbon-14} + \text{molecular fragments} \quad (1)$$

and

$$\text{recoil carbon-14} + H_2NC(NH)NHCN \longrightarrow H_2NC(NH)NHC^{14}N \longrightarrow \cdot NHC^{14}N + H_2NCNH \quad (2)$$

$$\text{recoil carbon-14} + H_2NC(NH)NHCN \longrightarrow H_2NC^{14}(NH)NHCN \longrightarrow H_2NC^{14}NH + \cdot NHCN$$

The carbon-14 containing cyanamide radicals might dimerize subsequently, either with each other or with other inactive cyanamide radicals produced by the fragmentation of the cyanoguanidine molecule, to re-form the parent compound. This possibility becomes more plausible in light of the results obtained by Ma[13] in thermal decomposition studies of guanidine chromate and guanidine

(6) Courtesy of Dr. H. C. Moser and R. D. Shores, Kansas State University.

(7) E. C. Horning and M. G. Horning, *J. Org. Chem.*, **11**, 95 (1946).

(8) W. Weinberger, *Ind. Eng. Chem., Anal. Ed.*, **3**, 365 (1931).

(9) R. L. Shriner, R. C. Fuson and D. Y. Curtin, "The Systematic Identification of Organic Compounds," 4th ed., John Wiley and Sons, New York, N. Y., pp. 202, 207.

(10) I. M. Klotz and T. Askounis, *J. Am. Chem. Soc.*, **69**, 801 (1947).

(11) A. P. Wolf, C. S. Redvanly and R. C. Anderson, *ibid.*, **79**, 3717 (1957).

(12) See, for example, A. P. Wolf, *Angew. Chem.*, **71**, 237 (1959).

(13) C. Ma, *J. Am. Chem. Soc.*, **73**, 1333 (1951).

dichromate. Ma found[13] that at elevated temperatures cyanamide was produced and the major share of the cyanamide dimerized to form cyanoguanidine. By considering the temperatures attained in the local hot spot regions according to the Seitz and Koehler[14] description of the displacement of atoms, it appears reasonable that the high "retention" of the induced carbon-14 activity in the parent compound occurs by the formation of cyanamide, which dimerizes within the local hot spot region to form cyanoguanidine.

The polymeric material observed in this study has been very tentatively identified as melamine. It is speculated that the formation of this compound might occur in much the same manner as the formation of the cyanoguanidine. The formation would involve a trimerization of the cyanamide radicals produced within the local hot spot regions. This speculation is supported by Glasner and Makovsky's[15] studies of the thermal decomposition of guanidine perchlorate in which they report that guanidine perchlorate dissociates in the region of 300–450° to give considerable amounts of cyanamide, which trimerizes at elevated temperatures to form melamine.

$$H_2NC^{14}N + 2H_2NCN \longrightarrow \text{melamine} \quad (3)$$

The formation of other polymeric forms, however, cannot be disregarded due to the fact that very small amounts of the polymeric material were obtained and detailed structural analysis was not possible. If a $-G$ of 4 is assumed for the gamma damage of cyanoguanidine, the radiation damage of the sample would be about 12%. If we assumed that the brown solid is melamine, G(melamine) $\cong$ 0.8, and this would lead to $-G$(cyanoguanidine) $>$ 1.2.

The results of this study have shown that, in addition to the parent compound and the polymeric material, a significant amount of activity ($>$ 10%) was found in only two other compounds, guanidine and acetamidine. A possible method for the formation of guanidine is

$$NH_2C^{14}N + NH_2 \text{ from organic matrix} \longrightarrow HNC^{14}(NH)NH_2 \quad (4)$$

and for acetamidine

$$C^{14}H_3\cdot + NCNH_2 \longrightarrow H_2C^{14}C(NH)NH_2 \quad (5)$$

$$(CH_3\cdot \text{ or } C^{14}H_3\cdot) + NC^{14}NH_2 \longrightarrow \cdot C^{14}H_2C^{14}(NH)NH_2 \text{ or } \cdot CH_2C^{14}(NH)NH_2 \quad (6)$$

Certainly, alternate possibilities for the formation of acetamidine-C^{14} might be written.

The recoiling carbon-14 is a very reactive radical and when its motion becomes essentially diffuse, the carbon-14 can react with its surroundings to produce a variety of molecular species.[11]

$$\cdot\dot{C}^{\cdot 14} + \text{organic matrix} \longrightarrow [:\dot{C}^{\cdot 14}]^-, :C^{14}H_2, \cdot C^{14}H_3 \quad (7)$$

The carbon-14 containing methyl radical then may undergo the reactions postulated in equations 5 and 6. The carbon-14-containing compounds obtained through such a mechanism would contain C^{14} atoms either in the methyl group or at both carbon positions. The production of acetamidine with the carbon-14 atom only in the central carbon position would require the formation of an unlabeled methyl radical, since a methyl group, as such, does not exist in the cyanoguanidine molecule. The formation of this methyl radical might occur by various processes, about which we could only speculate further.

A degradation study, similar to that performed by Wolf and co-workers,[11] of the various compounds produced in this study would determine the activity present at each of the carbon positions and might aid in elucidating the actual processes occurring during the recombination period.

Acknowledgments.—The authors wish to thank Professor H. C. Moser and R. D. Shores for the gas chromatographic radioanalysis of methane and carbon monoxide and D. W. Rathburn for checking some of the procedures.

This research was supported in part by a grant from the Petroleum Research Fund administered by the American Chemical Society. Grateful acknowledgment hereby is made to the donors of said fund.

(14) F. Seitz and J. S. Koehler, *Displacement of Atoms during Irradiation*, in "Solid State Physics," Vol. II, edited by F. Seitz and D. Turnbull, Academic Press, Inc., New York, N. Y., 1956, pp. 305–448.

(15) A. Glasner and A. Makovsky, *J. Chem. Soc.*, 182 (1953).

ELECTRON IMPACT SPECTROSCOPY OF TETRAMETHYLGERMANIUM, TRIMETHYLSILANE AND DIMETHYLMERCURY[1]

BY BRICE G. HOBROCK AND ROBERT W. KISER

Kansas State University, Department of Chemistry, Manhattan, Kansas

Received August 25, 1961

Electron impact data determined with a mass spectrometer are reported for tetramethylgermanium and two related organometallics, trimethylsilane and dimethylmercury. Probable ionization and dissociation processes are given and the heats of formation of the principal ions, consistent with the proposed processes, are calculated. Ionization potentials for the series of methyl-substituted silanes are calculated using the equivalent orbital treatment. The calculated values for the ionization potential of tetramethylgermanium and trimethylsilane are compared to the experimentally determined values of 9.2 ± 0.2 and 9.8 ± 0.3 e.v., respectively, and 8.90 ± 0.2 e.v. for dimethylmercury.

Introduction

Lampe and Field[2] have studied the electron impact spectroscopy of neopentane, and we have recently reported data for tetramethyl-silicon, -tin and -lead.[3] Electron impact data for the remaining member of the group IV tetramethyl compounds, tetramethylgermanium, is reported in this work. A study of two other related organometallics, trimethylsilane and dimethylmercury, also is included. From the previously reported data for tetramethylsilicon, and the present data for trimethylsilane, one may compare heats of formation for the ions and the dissociation processes in the two methyl-substituted silicon compounds. Molecular ionization potentials for the series of methyl-substituted silanes are calculated using the equivalent orbital treatment. Experimental values for the ionization potentials of trimethysilane and tetramethylgermanium are compared to calculated values.

Experimental

The mass spectra and appearance potentials reported here were obtained with a Bendix Model 12-100 time-of-flight mass spectrometer with an analog output system consisting of a monitor and scanner. This instrument has previously been described.[4]

Mass spectra for each of the compounds were obtained at nominal electron energies of 70 e.v.

Appearance potentials were calculated using the method of extrapolated voltage differences, described by Warren.[5] Krypton or xenon, mixed with the compound being investigated, was used to calibrate the ionizing voltage. Known spectroscopic values for the ionization potentials of krypton and xenon were used.[6]

Tetramethylgermanium was obtained from Chemicals Procurement Laboratories. No impurities were noted in the mass spectrum; hence, the sample was used as received. Gas chromatographic analysis was not attempted.

The sample of trimethylsilane was obtained from Peninsular Chem-research, Inc. The gaseous sample of trimethylsilane was received in compressed form and was transferred directly to sample bulbs on a vacuum line without the samples being exposed to air. No attempt was made to determine the purity of the sample by gas chromatography, although a small impurity was indicated by the presence of *m/e* 77, which was not identified further. This impurity was present in quantities of less than 1.0%.

Dimethylmercury was obtained from K and K Laboratories. Gas chromatographic analysis using a Fisher–Gulf model 160 Partitioner with a 14 foot column of tri-*n*-tolyl phosphate on Celite[3] revealed no impurities.

Results

The appearance potentials for the principal ions in the mass spectra of tetramethylgermanium, trimethylsilane and dimethylmercury are summarized in Tables I, II and III. The probable processes by which the various ions were formed are given, consistent with measured and extrapolated energetics. The calculated heats of formation are given in the last column.

The following heats of formation were used in the calculations with the measured appearance potentials: $GeMe_4$, −35 kcal./mole (see below); $SiHMe_3$, −54 kcal./mole[7]; $HgMe_2$, −47.5 kcal./mole[8]; CH_3, 32.0 kcal./mole[9]; CH_4, −17.8 kcal./mole[9]; C_2H_6, −20.2 kcal /mole[9]; C_2H_4, 12.5 kcal./mole[9]; H, 52.1 kcal./mole[9]; and C_2H_5, 24.5 kcal./mole.[10]

Mass Spectra.—The mass spectra of tetramethylgermanium and dimethylmercury are in essential agreement with those reported by Dibeler, *et al.*[11,12] To the best of our knowledge, the mass spectrum of trimethylsilane has not been reported previously.

Molecular Ionization Potentials.—Calculated and observed ionization potentials for the series of methyl-substituted silanes are listed in Table IV. An equivalent orbital treatment similar to that employed for the calculation of the ionization potentials of the group IV tetramethyl compounds was used. The parameter for methyl group–silicon atom interaction was calculated using the experimentally determined ionization potential of tetramethylsilicon.[3] The calculated value of 10.1 e.v. for the ionization potential of trimethylsilane compares favorably with the experimental value of 9.8 ± 0.3 e.v. The calculated ionization potential of tetramethylgermanium reported previously, 9.1

(1) This work was supported in part by the U. S. Atomic Energy Commission under Contract No. AT(11-1)-751 with Kansas State University. Taken in part from a thesis submitted by B. G. Hobrock to the Graduate School of Kansas State University in partial fulfillment of the requirements for the M.S. degree, August, 1961.

(2) F. W. Lampe and F. H. Field, *J. Am. Chem. Soc.*, **81**, 3238 (1959).

(3) B. G. Hobrock and R. W. Kiser, *J. Phys. Chem.*, **65**, 2186 (1961).

(4) E. J. Gallegos and R. W. Kiser, *J. Am. Chem. Soc.*, **83**, 773 (1961); *J. Phys. Chem.*, **65**, 1177 (1961); *ibid.*, **66**, 136 (1962).

(5) J. W. Warren, *Nature*, **165**, 811 (1950).

(6) C. E. Moore, "Atomic Energy Levels," Natl. Bur. Standards Circ. 467, Vol. III, U. S. Government Printing Office, Washington, D. C., 1958.

(7) S. Tannenbaum, S. Kaye and G. F. Lewenz, *J. Am. Chem. Soc.*, **75**, 3753 (1953).

(8) L. H. Long and R. G. W. Norrish, *Trans. Roy. Soc.* (London), **A241**, 587 (1949).

(9) R. D. Rossini, D. D. Wagman, W. H. Evans, S. Levine and I. Jaffe, "Selected Values of Chemical Thermodynamic Properties," Natl. Bur. Standards Circ. 500, U. S. Government Printing Office, Washington, D. C., 1952.

(10) P. Gray and A. Williams, *Chem. Revs.*, **59**, 239 (1959).

(11) V. H. Dibeler and F. L. Mohler, *J. Research Natl. Bur. Standards*, **47**, 337 (1951).

(12) V. H. Dibeler, *ibid.*, **49**, 235 (1952).

TABLE I

APPEARANCE POTENTIALS AND HEATS OF FORMATION OF THE PRINCIPAL IONS OF TETRAMETHYLGERMANIUM

Ion	% Abundance (monoisotopic)	Appearance potential (e.v.)	Process	ΔH_f^+ (kcal./mole)
CH_3^+		20.1 ± 0.5	$Ge(CH_3)_4 \longrightarrow CH_3^+ + Ge + 3CH_3$	254
Ge^+	3.8	19.2 ± .5	$\longrightarrow Ge^+ + 4CH_3$	279
$GeCH_3^+$	16.7	16.8 ± .4	$\longrightarrow GeCH_3^+ + 3CH_3$	245
$Ge(CH_3)_2^+$	3.3	14.1 ± .2	$\longrightarrow Ge(CH_3)_2^+ + 2CH_3$	226
$Ge(CH_3)_3^+$	74.8	10.2 ± .1	$\longrightarrow Ge(CH_3)_3^+ + CH_3$	168
$Ge(CH_3)_4^+$	1.4	9.2 ± .2	$\longrightarrow Ge(CH_3)_4^+$	177

TABLE II

APPEARANCE POTENTIALS AND HEATS OF FORMATION OF THE PRINCIPAL IONS OF TRIMETHYLSILANE

m/e	Relative abundance	Appearance potential (e.v.)	Process	ΔH_f^+ (kcal./mole)
15	31.1	14.8 ± 0.5	$SiH(CH_3)_3 \longrightarrow CH_3^+ + SiH(CH_3)_2$	(25)[a]
27	7.6	15.3 ± .5	$\longrightarrow C_2H_3^+ + SiCH_3 + 2H_2$	(73)[a]
			$\longrightarrow C_2H_3^+ + SiHCH_3 + H_2 + H$	(21)[a]
28	59.8	13.7 ± .3	$\longrightarrow Si^+ + CH_4 + C_2H_6$	300
29	17.2	14.2 ± .2	$\longrightarrow SiH^+ + C_2H_6 + CH_3$	262
			$\longrightarrow SiH^+ + C_2H_5 + CH_4$	267
31	10.4	14.3 ± .5	$\longrightarrow SiH_3^+ + CH_3 + C_2H_4$	231
41	11.4	11.7 ± .5	$\longrightarrow SiCH^+ + H + C_2H_6 + H_2$	186
			$\longrightarrow SiCH^+ + C_2H_5 + 2H_2$	194
42	12.1	10.6 ± .3	$\longrightarrow SiCH_2^+ + C_2H_6 + H_2$	211
			$\longrightarrow SiCH_2^+ + 2CH_4$	226
43	42.8	12.4 ± .3	$\longrightarrow Si(CH_3)^+ + CH_4 + CH_3$	218
44	11.0	11.0 ± .3	$\longrightarrow SiHCH_3^+ + C_2H_6$	220
45	14.7	12.8 ± .5	$\longrightarrow SiH_2CH_3^+ + C_2H_5$	216
58	27.9	10.3 ± .2	$\longrightarrow Si(CH_3)_2^+ + CH_4$	201
59	100	11.9 ± .3[b]	$\longrightarrow SiH(CH_3)_2^+ + CH_3$	188
73	53.8	10.9 ± .2[b]	$\longrightarrow Si(CH_3)_3^+ + H$	146
74	7.1	9.8 ± .3	$\longrightarrow SiH(CH_3)_3^+$	172

[a] Heat of formation of the radical. [b] Values of 11.82 e.v. for A.P. (59^+) and 11.02 e.v. for A.P. (73^+) have been determined by F. W. Lampe and G. Hess, private communication.

TABLE III

APPEARANCE POTENTIALS AND HEATS OF FORMATION OF THE PRINCIPAL IONS OF DIMETHYLMERCURY

Ion	% Abundance (monoisotopic)	Appearance potential (e.v.)	Process	ΔH_f^+ (kcal./mole)
Hg^+	22.4		$Hg(CH_3)_2 \longrightarrow Hg^+ + 2CH_3(?)$	(257)[a]
$HgCH_3^+$	54.2	10.4 ± 0.2	$\longrightarrow HgCH_3^+ + CH_3$	160
$Hg(CH_3)_2^+$	23.4	8.90 ± 0.2	$\longrightarrow Hg(CH_3)_2^+$	158

[a] See ref. 9.

TABLE IV

CALCULATED AND OBSERVED IONIZATION POTENTIALS OF THE METHYL-SUBSTITUTED SILANES

Compound	b, parameter[a]	Calcd. IP (e.v.)	Obsd. IP (e.v.)
$Si(CH_3)_4$	1.5	(9.8)	9.8[a]
$SiH(CH_3)_3$	1.5	10.1	9.8[b]
$SiH_2(CH_3)_2$	1.5	10.5	
SiH_3CH_3	1.5	11.1	

[a] See ref. 3. [b] This work.

e.v.,[3] is in good agreement with the experimental value of 9.2 ± 0.2 e.v.

Discussion

Tetramethylgermanium.—The heat of formation for tetramethylgermanium has not, to our knowledge, been reported in the literature. The calculations of the heats of formation for the ions produced from tetramethylgermanium are based upon an estimated value of −35 kcal./mole. This estimation was made on the basis of interpolation between the experimentally determined heats of formation for tetramethylsilicon, -tin and -lead, and by calculations using the method due to Franklin.[13] Calculations of heats of formation of ions based upon the estimated value of $\Delta H_f(GeMe_4)$ are found to be reasonable. Appearance potential measurements were made using the germanium isotope of mass 70 in order to minimize the effect of hydride formation. Hydride formation is quite apparent in the mass spectrum but no significant effects were noted in the measurement of appearance potentials of any ion using either the isotopes of *m/e* 70 or 74. The appearance potential of the parent molecule-ion was determined using the isotope of mass 74, exclusively, in order to obtain greater detection sensitivity.

m/e **15.**—The heat of formation calculated for CH_3^+, with the accompanying fragments of Ge and $3CH_3$, is 254 kcal./mole, only slightly lower than the value of $\Delta H_f^+(CH_3) = 262$ kcal./mole, given by Field and Franklin.[14]

(13) J. L. Franklin, *Ind. Eng. Chem.*, **41**, 1070 (1949).

m/e **70.**—This ion can be only Ge^+. The calculation of its heat of formation gave a value of 279 kcal./mole considering the neutral fragments formed to be four CH_3 groups. This is in fair agreement with the literature value for $\Delta H_f^+(Ge) = 267$ kcal./mole.[9]

m/e **85.**—The heat of formation for this ion, $GeCH_3^+$, is 245 kcal./mole considering the formation of three CH_3 groups as neutral fragments. If the neutral fragments were $C_2H_6 + CH_3$, $\Delta H_f^+(GeCH_3) = 328$ kcal./mole, a value considered to be unreasonably large.

m/e **100.**—This ion is $Ge(CH_3)_2^+$. The process is believed to involve the formation of two CH_3 groups as neutral fragments. The heat of formation of the ion then is 226 kcal./mole. Considerations of approximate energies needed to remove subsequent methyl groups and interpolation between the heats of formation of the other ions also lead to the conclusion that two CH_3 groups are the neutral fragments. Hydrides were apparent in the mass spectrum in this region, but it is believed they did not interfere with the determination of the appearance potential of this ion.

m/e **134.**—Good reproducibility (for repetitive determinations) was obtained for the ionization potential of tetramethylgermanium in spite of the low abundance of the ion. The experimentally determined ionization potential, 9.2 ± 0.2 e.v., is in good agreement with the value of 9.1 e.v. calculated using the modified equivalent orbital treatment.[3]

Dimethylmercury.—The heat of formation for dimethylmercury has been reported as −47.5 kcal./mole by Long and Norrish.[8] The heats of formation for the ions $Hg(CH_3)_2^+$ and $HgCH_3^+$ are based upon this value. All determinations were made on ions containing the mercury isotope of mass 200; hydride formation is not considered significant.

The ionization potential for this molecule, 8.90 ± 0.2 e.v., is similar to the ionization potentials of the other molecules reported here and agrees with the value of 9.02 ± 0.2 e.v. determined by Reese and Dibeler.[15]

Trimethysilane.—The heat of formation for trimethylsilane, −54 kcal./mole, as determined by Tannenbaum, Kaye and Lewenz,[7] was utilized in the calculation of the heats of formation for the principal ions in its mass spectrum. Heats of formation for various ions calculated using $\Delta H_f(SiHMe_3) = -54$ kcal./mole compare very favorably with literature values[14] that are available, and with the heats of formation for the ions from tetramethylsilicon.[3] The values for the heats of formation for the series of silanes reported by Tannenbaum, *et al.*,[7], −36, −54 and −63 kcal./mole for SiH_2Me_2, $SiHMe_3$ and $SiMe_4$, respectively, appear to fall into a regular series corresponding to relative stabilities of these compounds and are believed to be quite reliable.

Appearance potentials were measured for a number of hydrides that are formed as well as for the principal ions that appeared in the tetramethylsilicon spectrum. In several cases, the precision was not as good as was desired; the ionization efficiency curves for some of the hydrides tailed off as if two or more processes were occurring. This made it difficult to obtain accurate determinations.

m/e **15.**—This ion can be only CH_3^+, and is probably formed by a process involving the formation of $SiHMe_2$ as the neutral fragment. The heat of formation for the $SiHMe_2$ radical is not available, thus the heat of formation of CH_3^+ cannot be calculated. Using a value of 262 kcal./mole[14] for the heat of formation of CH_3^+, however, the heat of formation of the $SiHMe_2$ radical is calculated to be approximately 25 kcal./mole.

m/e **27.**—The absence of heats of formation for neutral fragments containing silicon again prevents the calculation of the heat of formation of this ion, which is $C_2H_3^+$. A possible process for the formation of this ion involves the formation of $SiCH_3 + 2H_2$ as neutral fragments. Also possible is the formation of $SiHCH_3 + H_2 + H$. Taking the heat of formation of $C_2H_3^+$ as 280 kcal./mole,[14] either the heat of formation for the $SiCH_3$ radical would be 73 kcal./mole or the heat of formation of the $SiHCH_3$ radical would be 21 kcal./mole. We cannot differentiate between these two values, although we believe the latter is more reasonable.

m/e **28.**—The energetics indicate the process to be that given in Table II; the calculated heat of formation of Si^+, 300 kcal./mole, compares fairly well with the literature value of 278 kcal./mole.[14] Any other process is incompatible with the energetics.

m/e **29.**—The process in which CH_3 and C_2H_6 are the neutral fragments leads to a heat of formation of $SiH^+ = 262$ kcal./mole, which compares favorably with the value of 267 kcal./mole for $\Delta H_f^+(SiH)$ as determined in a study of SiH_4.[14] However, the reaction $SiMe_3H \rightarrow SiH^+ + CH_4 + C_2H_5$ leads to $\Delta H_f^+(SiH) = 267$ kcal./mole.

m/e **31.**—The heat of formation of SiH_3^+ is calculated from the energetics to be 231 kcal./mole, in fair agreement with the value 214 kcal./mole.[14]

m/e **42.**—This ion could be only $SiCH_2^+$ and has a heat of formation of 210 kcal./mole, if its formation is accompanied by the formation of $C_2H_6 + H_2$ as neutral fragments. The process for the formation of two methane molecules also is possible, giving a heat of formation for $SiCH_2^+ = 226$ kcal./mole.

m/e **43.**—The shapes of the ionization efficiency curves obtained in the determinations of the appearance potential of this ion indicate that two or more processes are occurring. We did not, however, separate the processes. The appearance potential determined was 12.4 ± 0.3 e.v. Since this ion can be only $SiCH_3^+$, it is believed that the formation of this ion involves the production of neutral fragments of $CH_4 + CH_3$. $\Delta H_f^+(SiCH_3)$ then is calculated to be 218 kcal./mole, in fair agreement with the value of 234 kcal./mole.[3]

m/e **44.**—The heat of formation calculated for $SiHCH_3^+$, considering the accompanying formation of the neutral fragment C_2H_6, is 220 kcal./mole. This process is selected on the basis of interpolation

(14) F. H. Field and J. L. Franklin, "Electron Impact Phenomena and the Properties of Gaseous Ions," Academic Press, Inc., New York, N. Y., 1957.

(15) R. M. Reese and V. H. Dibeler, private communication.

between the heats of formation of Si^+, SiH^+, $SiH(CH_3)_2^+$ and $SiH(CH)_3^+$, which are established by other evidence in this work.

m/e **58.**—The heat of formation of $Si(CH_3)_2^+$ is calculated to be 201 kcal./mole, in good agreement with the value of 193 kcal./mole calculated from the tetramethylsilicon study.[3]

m/e **73.**—The heat of formation for this ion is calculated to be 146 kcal./mole, assuming the neutral fragment to be a hydrogen atom. This can be the only process for formation of this ion, but the value of 146 kcal./mole for $\Delta H_f^+(SiMe_3)$ appears low compared to the heat of formation of $Si(CH_3)_3$ = 165 kcal./mole calculated from the tetramethylsilicon study.[3]

m/e **74.**—The small abundance of the parent molecule-ion in the mass spectrum of trimethylsilane undoubtedly contains significant contributions made by $Si^{29}(CH_3)_3^+$ and $Si^{28}(C^{13}H_3)(CH_3)_2^+$. Several determinations of the ionization potential, using *m/e* 74, and in one case *m/e* 75, gave good agreement. The ionization potential for trimethylsilane has not been reported previously. The ionization potential of 9.8 ± 0.3 e.v. is essentially the same as that of tetramethylsilicon, as might be expected, and is in good agreement with the calculated value of 10.1 e.v. (see Table IV). The ionization potentials of the series of methyl-substituted silanes is expected on the basis of the equivalent-orbital treatment to fall into a series, where $I_{SiH_4} > I_{SiH_3Me} > I_{SiH_2Me_2} > I_{SiHMe_3} > I_{SiMe_4}$.

Acknowledgments.—We wish to acknowledge valuable discussions of portions of this work with Professor F. W. Lampe.

ELECTRIC MOMENTS OF METRAZOLE AND SOME RELATED TETRAZOLES

BY ALEXANDER I. POPOV[1] AND ROGER D. HOLM

Department of Chemistry, State University of Iowa, Iowa City, Iowa

Received August 30, 1961

As part of a general investigation of the physical properties of certain central nervous system stimulants, the electric moments of metrazole, 8-*t*-butylmetrazole, 8-*sec*-butylmetrazole and 1-cyclohexyl-5-methyltetrazole have been measured in benzene solution, values of 6.14, 6.20, 6.18 and 6.00 *D*, respectively, being obtained.

Introduction

In the process of screening various tetrazoles for convulsant activity, it was observed[2] that those substituted tetrazoles possessing aromatic substituents generally tended to exhibit depressant activity upon the central nervous system, while aliphatic substituents generally conferred convulsant activity to the compound. One of these aliphatically substituted tetrazoles, 1,5-pentamethylenetetrazole, hereafter referred to as metrazole, has found clinical application as a stimulant, and much information has been published on its physiological

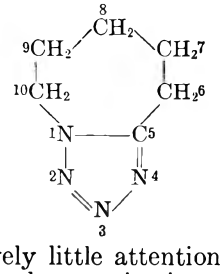

effects. Relatively little attention has been paid, however, to the characterization of the physical-chemical properties of metrazole, and even less information exists concerning the physical-chemical properties of various metrazole derivatives. Only the halogen[3] and silver[4] complexes of metrazole have been investigated with any degree of thoroughness.

Since it has been shown by Featherstone, *et al.*,[2] that the presence of substituents can greatly affect the convulsant strength of the metrazole derivative, an investigation of certain physical-chemical properties of metrazole and related compounds was begun as part of a broader study of the relations between physiological activity and physical properties. Since convulsant activity seems to be related to those tetrazoles in which the central ring is "electron-rich" it was felt desirable to initiate a study of the dipole moments of a series of metrazoles which vary considerably in convulsant activity but which exhibit relatively minor structural differences.

A few dipole moment investigations of various tetrazoles have been carried out. Jensen and Friediger,[5] in 1943, measured the moments of tetrazole, 5-aminotetrazole and 1-methyltetrazole, attributing the fairly large moments of 5.11 and 5.71 *D* in dioxane and 5.38 *D* in benzene, respectively, to the contributions of various charge-separated structures. In 1956, Kaufman, Ernsberger and McEwan[6] published the electric moments of 12 substituted tetrazoles and discussed the origins of these moments in terms of the resonance contributions of a number of charge-separated structures to the meso-ionic ring. A more analytical treatment of tetrazole moments was made by Kaufman and Woodman,[7] who applied the method of Hill and Sutton[8] to a discussion of 1-phenyl-5-

(1) Department of Chemistry, Northern Illinois University, DeKalb, Illinois.

(2) F. W. Schueler, S. C. Wang, R. M. Featherstone and E. G. Gross, *J. Pharmacol. Exptl. Therap.*, **97**, 266 (1949), and references listed therein.

(3) A. I. Popov, C. Castellani-Bisi and M. Craft, *J. Am. Chem. Soc.*, **80**, 6513 (1958).

(4) A. I. Popov and R. D. Holm, *ibid.*, **81**, 3250 (1959).

(5) K. A. Jensen and A. Friediger, *Kgl. Danske Videnskab. Selskab Mat.-fys. Medd.*, **20**, No. 20, 1 (1943); *Chem. Zentr.*, I, 416 (1944).

(6) M. H. Kaufman, F. M. Ernsberger and W. S. McEwan, *J. Am. Chem. Soc.*, **78**, 4197 (1956).

(7) M. H. Kaufman and A. L. Woodman, *J. Phys. Chem.*, **62**, 508 (1958).

(8) R. A. Hill and L. S. Sutton, *J. Chem. Soc.*, 746 (1949).

methyltetrazole and 1-methyl-5-phenyltetrazole. Yet the origin and nature of the tetrazole ring moment still is incompletely understood, and this study was begun in order to provide more information concerning the dipole moments of several tetrazole derivatives.

Experimental Part

Reagents.—The purification and physical constants of the cyclohexane reference liquid and benzene solvent have been described previously.[9]

Metrazole (Knoll Pharmaceutical Co.) was purified by filtering a saturated solution in warm, distilled ether, and then stirring in an ice-bath to obtain the product in small crystalline form. The metrazole then was filtered and dried *in vacuo* over P_2O_5 for a week; m.p. 60.3–60.9°, literature[3] value 61°.

Anal. Calcd. for $C_6H_{10}N_4$: C, 52.16; H, 7.30. Found: C, 52.02; H, 7.08.

The 8-*t*-butylmetrazole was prepared according to the procedure of Harvill, Roberts and Herbst.[10] The metrazole derivative was recrystallized five times from isopropyl alcohol and, after drying *in vacuo* over P_2O_5 for two days, exhibited a melting point of 129.6–130.4° (uncor.); lit.[10] 132.5–133°.

Anal. Calcd. for $C_{10}H_{18}N_4$: C, 61.82; H, 9.34; N, 28.84. Found: C, 61.71; H, 9.11; N, 27.89.

The 8-*sec*-butylmetrazole (Knoll Pharmaceutical Co.) was recrystallized from Skellysolve C and dried for two days *in vacuo* over P_2O_5; m.p. 69.8–69.9°, lit.[10] 70–71°.

Anal. Calcd. for $C_{10}H_{18}N_4$: C, 61.82; H, 9.34. Found: C, 61.80; H, 9.29.

The 1-cyclohexyl-5-methyltetrazole (Knoll Pharmaceutical Co.) was purified by recrystallization from absolute ethanol twice, followed by sublimation at 115° and 3 mm. pressure; m.p. 123.8–124.6° (cor.); lit.[11] 124–124.5°.

Anal. Calcd. for $C_8H_{14}N_4$: C, 57.80; H, 8.49. Found: C, 57.38; H, 8.09.

m-Dinitrobenzene was recrystallized three times from absolute ethanol; m.p. 89–90°, lit.[12] 89.57°.

Preparation of *p*-nitro-N,N-dimethylaniline followed the procedure of Bogoslovskii[13]; m.p. 163.4–164.3° (cor.), lit.[14] 164°.

Apparatus and Procedure.—The heterodyne-type instrument employed in measuring the dielectric constants of benzene–metrazole solutions, and the procedure for obtaining the electric moments utilizing the method of Halverstadt and Kumler[15] have been described in a previous paper.[9] Extrapolations were fitted to the data by the method of least squares.

Results

In order to evaluate the apparatus and the experimental procedure used in this investigation the dipole moments of *m*-dinitrobenzene and *p*-nitro-N,N-dimethylaniline were measured in benzene solution at 25°. The values of 3.88 and 6.93 *D* obtained, respectively, for those two compounds are in good agreement with literature values. Littlejohn and Smith[12] who have surveyed the reported values for the dipole moment of *m*-dinitrobenzene found that these ranged from 3.78 to 3.96 *D*. Marsden and Sutton[14] gave 6.91 *D* for the dipole moment of *p*-nitro-N,N-dimethylaniline, while later studies report 6.95[16] and 6.84 *D*.[17] The dielectric constant data furnished by the heterodyne instrument, a war surplus radio frequency calibrator, thus was felt to be sufficiently accurate for further work.

The results of the dielectric constant, specific volume and refractive index measurements for benzene solutions of metrazole, 8-*t*-butylmetrazole, 8-*sec*-butylmetrazole and 1-cyclohexyl-5-methyltetrazole are summarized in Table I. Distortion polarizations were calculated by extrapolation of the molar refraction to infinite wave length ($P_D = 1.05R$) which differed from the sodium-D line polarization by only 1.11 cc. In view of the fact that the orientation polarization is about 763 cc., this difference is negligible, and the molar refraction was henceforth measured for the sodium-D line. It is likely that the atomic polarization is reasonably constant in view of the similarities between the molecular structures studied.

In addition to the three metrazoles, the moment of 1-cyclohexyl-5-methyltetrazole was measured because this dialkyl tetrazole should not be subject to any tetrazole ring deformation which might be caused by the pentamethylene chain.

Discussion

Comparison of the dipole moments of tetrazoles investigated in this study shows that there is no simple correlation between the physiological activity of the compounds and their dipole moments. For example, 8-*t*-butylmetrazole has a minimum convulsant dose of 3 mg./kg. of body weight[18] and a dipole moment of 6.20 *D*, while 8-*sec*-butylmetrazole has a minimum convulsant dose of 750 mg./kg. and a dipole moment of 6.18 *D*. Whether the high dipole moment is a necessary (but certainly not sufficient) condition for convulsant action is, of course, a matter of conjecture. Since, however, it has been fairly well established that the convulsant action is associated with some unbalance in the passage of Na^+ and K^+ ions through the nerve membranes, it may be possible that a compound with a high dipole moment, which is fairly certain to produce an ion–dipole interaction, may affect the passage of the sodium and potassium ions through the membranes.

With dipole moments of the order of 6.1 to 6.2 *D* for the metrazoles, it is not surprising that the 1-cyclohexyl-5-methyltetrazole has a moment of 6.0 *D*. The moments of the metrazoles in this study are somewhat larger than some simple alkyltetrazoles reported earlier,[5,6] while other tetrazoles, *e.g.*, 1-alkyl-5-alkylaminotetrazoles, were found to have moments in excess of 7 *D*. Thus, the metrazole moments appear to form an intermediate case between 1,5-dimethyltetrazole and the 1-alkyl-5-aminotetrazoles.

The fact that the moments of the 8-butylmetrazoles are a little larger than the metrazole moment is of some interest, but there does not appear any obvious reason to account for this increase. The main source of charge separation giving rise to the dipole moment resides in the tetrazole ring, and any structural changes at position 8 are separated from the ring by essentially three carbon atoms.

(9) A. I. Popov and R. D. Holm, *J. Phys. Chem.*, **65**, 774 (1961).

(10) E. K. Harvill, C. W. Roberts and R. M. Herbst, *J. Org. Chem.*, **15**, 58 (1950).

(11) E. K. Harvill, R. M. Herbst, E. C. Schreiner and C. W. Roberts, *ibid.*, **15**, 662 (1950).

(12) A. C. Littlejohn and J. W. Smith, *J. Chem. Soc.*, 2476 (1957).

(13) B. M. Bogoslovskii, *Zhur. Obshchei Khim.*, **24**, 922 (1954).

(14) R. J. B. Marsden and L. E. Sutton, *J. Chem. Soc.*, 599 (1936).

(15) I. F. Halverstadt and W. D. Kumler, *J. Am. Chem. Soc.*, **64**, 2988 (1942).

(16) E. Hertel and H. Lubrman, *Z. physik. Chem.*, **B44**, 261 (1939).

(17) F. Moll and E. Lippert, *Z. Elektrochem.*, **58**, 853 (1954).

(18) E. G. Gross and R. M. Featherstone, *J. Pharmacol. Exptl. Therap.*, **87**, 291 (1946).

TABLE I
DIPOLE MOMENT DATA

	ϵ_1	α	n_1	β	n_1^2	γ	$P_{2\infty}$ (cc.)	P_D (cc.)	μ
m-Dinitrobenzene	2.2692	9.919	1.1425	−0.430	2.2432	0.196	349.2	41.5	3.88
p-Nitro-N,N-dimethylaniline	2.2762	32.01	1.14482	− .318	....	....	1040	59	6.93
Metrazole	2.2771	29.77	1.14470	− .3370	2.24415	.101	805.5	35.4	6.14
8-*t*-Butylmetrazole	2.2783	21.53	1.14452	− .2186	2.24540	.01391	838.4	53.3	6.20
8-*sec*-Butylmetrazole	2.2775	21.41	1.14470	− .2253	2.24408	.04486	834.1	54.0	6.18
1-Cyclohexyl-5-methyltetrazole	2.2760	23.56	1.14490	− .285	2.24386	.0181	778.4	42.5	6.00

The spatial configuration of the pentamethylene chain and 1-nitrogen relative to the plane of the tetrazole ring has not been established. It may be that the sterically bound pentamethylene chain which is attached at the 1- and 5-positions in metrazole might cause a small deviation from the most stable bonding direction of the alkyl groups directly attached to the tetrazole ring. However, if this is actually the case, there is evidently little effect upon the tetrazole ring moment, and there is certainly no loss in molecular stability.[19]

Acknowledgment.—The support of this work by the Research Grant B-1095 from the National Institute of Neurological Diseases and Blindness, Public Health Service, is gratefully acknowledged. The authors also are indebted to Dr. R. O. Hauck and Dr. C. R. Jacobson of the Knoll Pharmaceutical Company for the substituted metrazole derivatives.

(19) A. Dister, *J. pharm. Belg.*, **3**, 190 (1948).

THE USE OF A CATION-EXCHANGE RESIN TO STUDY THE CEROUS AND SULFATE ION COMPLEXES[1]

BY L. A. BLATZ

University of California, Los Alamos Scientific Laboratory, Los Alamos, New Mexico

Received September 5, 1961

It was desired to develop a precise method of using cation-exchange resins to study ionic equilibria in water solutions especially for the more difficult +3 metal ion systems. The sodium form of the cation-exchange resin Dowex-50 was used to obtain the complexing constants of cerous and sulfate ions at 25.04° and an ionic strength of 0.502$_0$ *M*. The values obtained for the association constants of $CeSO_4^+$ and $Ce(SO_4)_2^-$ are 56 ± 1 and 800 ± 40. There was no evidence for a third complex ion. During equilibration a constant cerous-ion concentration was maintained in the resin. A considerable study was made of the precision obtainable with this method. Two methods of extrapolation to zero sulfate-ion concentration are discussed.

Introduction

A critical review of and references to previous papers on the association constants of cerous and sulfate ions has been published elsewhere.[2] Since some of these studies are not in general agreement,[2] a new study seemed necessary in order to understand this system. Also, it was desired to explore the use of cation-exchange resins as a precision method for such studies.

In this work the sodium form of a sulfonated, cross-linked, polystyrene resin (Dowex-50) was used. The exchange equilibria of cerous ions between resin and aqueous phases before and after the addition of sodium sulfate were studied in such a way as to permit results to be obtained at constant cerium concentration in the resin phase.

Theory

The following is a summary of definitions and of equations derived elsewhere.[2] In the following, γ's and m's refer to activity coefficients and molalities (moles/kg.) in the resin phase while y's and C's (also M is used, moles/liter) refer to activity coefficients and molarities in the aqueous phase. Primed and unprimed quantities denote the presence and absence, respectively, of sodium sulfate in the aqueous phase. In the absence of sodium sulfate, the ionic strength, μ, is defined mainly by the sodium perchlorate concentration plus a small contribution from perchloric acid added to repress the hydrolysis of cerous ion.

The exchange equilibrium is represented by

$$Ce_w^{+3} + 3Na_R^+ = Ce_R^{+3} + 3Na_w^+ \qquad (1)$$

where R and W refer to resin and water solution phases. In addition the following equilibria are considered

$$Ce^{+3} + SO_4^= = CeSO_4^+$$

$$K_1 = \frac{C'_{CeSO_4^+}}{C'_{Ce^{+3}}C'_{SO_4^=}} \frac{y'_{CeSO_4^+}}{y'_{Ce^{+3}}y'_{SO_4^=}} = \beta_1 \frac{y'_{CeSO_4^+}}{y'_{Ce^{+3}}y'_{SO_4^=}} \qquad (2)$$

$$Ce^{+3} + 2SO_4^= = Ce(SO_4)_2^-$$

$$K_2 = \frac{C'_{Ce(SO_4)_2^-}}{C'_{Ce^{+3}}C'^2_{SO_4^=}} \frac{y'_{CeSO_4^+}}{y'_{Ce^{+3}}y'^2_{SO_4^=}} = \beta_2 \frac{y'_{Ce(SO_4)_2^-}}{y'_{Ce^{+3}}y'^2_{SO_4^=}} \qquad (3)$$

If exchange of the first complex with the resin is ignored, by application of the law of mass action and some manipulation, one obtains

(1) (a) This work was performed under the auspices of the U. S. Atomic Energy Commission. (b) Originally received July 11, 1960, and received in revised form September 5, 1961.

(2) L. A. Blatz, Los Alamos Scientific Laboratory Report, LA-2513, Office of Technical Services, U. S. Department of Commerce, Washington 25, D. C.

$$\frac{\dfrac{m^3_{Ce^{+3}} C^3_{Na^+}}{C_{Ce^{+3}} m^3_{Na^+}} \dfrac{\gamma_{Ce^{+3}} y^3_{Na^+}}{y_{Ce^{+3}} \gamma^3_{Na^+}}}{\dfrac{m'_{Ce^{+3}} C'^3_{Na^+}}{\Sigma C'_{Ce(III)}} \dfrac{\gamma'_{Ce^{+3}} y'^3_{Na^+}}{m'^3_{Na^+} y'_{Ce^{+3}} \gamma'^3_{Na^+}}} - 1}{C'_{SO_4^=}} =$$

$$K_1 \frac{y'_{Ce^{+3}} y'_{SO_4^=}}{y'_{Ce(SO_4)^+}} + K_2 C'_{SO_4^=} \frac{y'_{Ce^{+3}} y'^2_{SO_4^=}}{y'_{Ce(SO_4)_2^-}} \quad (4)$$

In equation 4, $\Sigma C'_{Ce(III)} = C'_{Ce^{+3}} + C'_{CeSO_4^+} + C'_{Ce(SO_4)_2^-}$ is the experimentally observed total cerium concentration in the water solution with sodium sulfate present, and $m'_{Ce^{+3}}$ is calculated from the difference between initial cerium(III) and $\Sigma C_{Ce(III)}$. The other two quantities are calculated from $C'_{Na^+} = C'(NaClO_4) + 2C'(Na_2SO_4) + 3m'_{Ce^{+3}}$ $(V/10^3$ g) and $m'_{Na^+} = C - 3m'_{Ce^{+3}}$, where C is the capacity of the resin in moles/kg. Throughout this work, 0.2000 liter (V) of solution per 0.2100 g. (g) of resin were used.

At constant cerium concentration in the resin and at constant ionic strength in the aqueous phase (for a limited trade-out of sodium perchlorate for sodium sulfate), it is assumed that all activity coefficients are constant or change negligibly. Therefore, the activity coefficients in the left member of equation 4 cancel, and the terms on the right side, except for $C'_{SO_4^=}$, are constant. If Q_0 and Q are substituted for the concentration quotients on the left and β_1 and $\beta_2 C'_{SO_4^=}$ for the terms on the right, equation 4 becomes

$$\frac{(Q_0/Q) - 1}{C'_{SO_4^=}} = \beta_1 + \beta_2 C'_{SO_4^=} \equiv Q_r \quad (5)$$

Hence, a plot of Q_r (Table II) *versus* $C'_{SO_4^=}$ gives a straight line with a slope of β_2 and an intercept of β_1. It has been shown elsewhere[2] that variations in hydrogen-ion concentration as $C'_{SO_4^=}$ varies had only a negligible effect on Q_0/Q in this study.

Since variations in electrolyte uptake[3,4] as sodium perchlorate is traded for sodium sulfate at constant ionic strength might seriously affect the Q_0/Q ratios, an independent extrapolation at different ratios of these two salts was undertaken. This was done by varying the sodium sulfate concentration at constant sodium perchlorate concentration (Table IV). Since the Q_0 values vary with the resulting variation in ionic strength, they were determined over a range of ionic strengths and compared with the Q values obtained at the same ionic strength and same cerium concentration in the resin. Under these conditions, it is assumed that the activity coefficients in the left member of equation 4 cancel again, and because the media are different for Q_0 and Q, this imposes the restriction that only a limited ionic strength range be considered.

Various expressions[2] were considered for the activity coefficient ratios on the right side of equation 4. The resulting empirical expression for equation 4 at 25° and a limited ionic strength range, $(\mu - \mu_0)$, is

$$Q_r(\mu) = K_1\, 10^{\left(-\exp\left[\frac{(\Delta Z_1)^2(0.5092)\mu^{1/2}}{1 + 0.3286\, \mathring{a}_1\mu^{1/2}}\right]\right)} + K_2\, 10^{\left(-\exp\left[\frac{(\Delta Z_2)^2(0.5092)\mu^{1/2}}{1 + 0.3286\, \mathring{a}_2\mu^{1/2}}\right]\right)^{\left(\frac{\mu - \mu_0}{3}\right)}} \quad (6)$$

(3) E. W. Baumann and W. J. Argersinger, Jr., *J. Am. Chem. Soc.*, **78**, 1130 (1956).

(4) D. H. Freeman, *J. Phys. Chem.*, **64**, 1048 (1960).

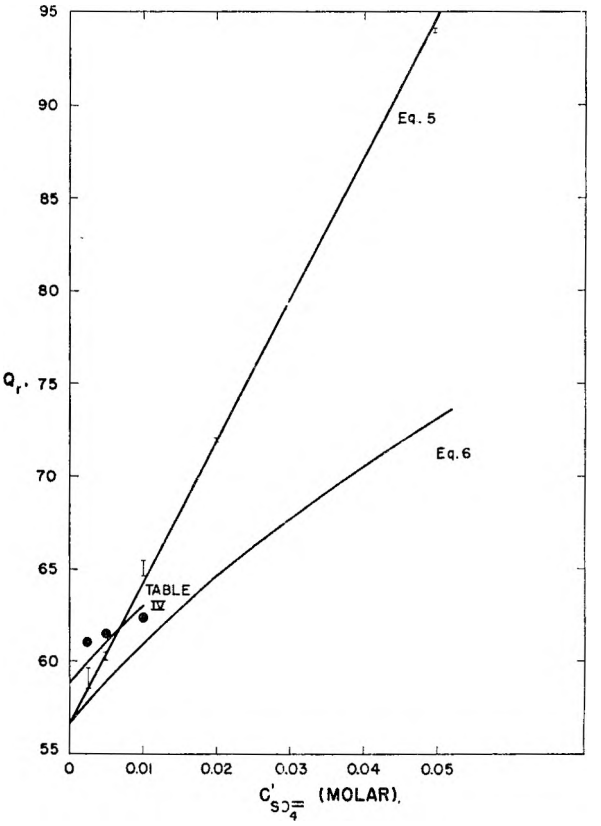

Fig. 1.—Plots of Q_r *versus* $C'_{SO_4^=}$. Equation 5, data of Table II, $\beta_1 = 56.7$, $\beta_2 = 767$, vertical lines represent $Q_r \pm \sigma$. Equation 6 (calculated) using $1/K_1 = 2.6 \times 10^{-4}$, $1/K_2 = 4.8 \times 10^{-6}$, $\mathring{a} = 5.9$. Q_r data of Table IV, diameter of points arbitrary.

where $C'_{SO_4^=} = (\mu - \mu_0)/3$, very nearly, and $\mu_0 = 0.502_0\, M$ for this paper. For equation 2, ΔZ_1^2, the algebraic sum of the squares of the charges, is 12, and similarly for equation 3, $\Delta Z_2^2 = 16$. From the work of Spedding and Jaffe,[5] $1/K_1 = 2.6 \pm 0.25 \times 10^{-4}$, and the $\mathring{a}_1$ is evaluated from the β_1 of this work. For lack of experimental information, the $\mathring{a}_2$ of the second term is taken as having the same value as $\mathring{a}_1$. K_2 then is calculated, and Fig. 1 shows a graph of equation 6 for $\mathring{a}_1 = 5.9 = \mathring{a}_2$. The intercept of equation 6 is β_1 (at μ_0), but the relation between β_2 (at μ_0) and the slopes of equation 6 is, in general, very complex. However, the limiting slope, which does not involve K_2 or its corresponding $\mathring{a}_2$, is given by

$$\left[\frac{dQ_r(\mu)}{dC'_{SO_4^=}}\right] = -\frac{21.11}{\mu_0^{1/2}(1 + 0.3286\, \mathring{a}_1\mu_0^{1/2})^2}\beta_1(\text{at } \mu_0) + \beta_2(\text{at } \mu_0) \quad (7)$$

$C'_{SO_4^=} \longrightarrow 0$

For $\mathring{a}_1 = 5.9$, the coefficient of β_1 (at μ_0) is -5.29 (-5.39 if $\mathring{a}_1 = 5.8$) and the whole term has a value around -300. Hence, equation 6 was used as an extrapolation guide for the data at varying ionic strength (Table IV), and β_2 (at μ_0) was evaluated from equation 7 and the experimental value of the limiting slope. The uncertainty[2] in β_2 (at μ_0), as evaluated with the aid of equation 7, was about $\pm 10\%$ for the data of Table IV.

(5) F. H. Spedding and S. Jaffe, *J. Am. Chem. Soc.*, **76**, 882 (1954).

Experimental

Procedure.—The Dowex-50 was purchased from the Dow Chemical Co. in about 1949. It was converted to the sodium form by five successive equilibrations with 5% sodium chloride. After standing overnight with a *p*H 8 solution of sodium hydroxide, it was swirled repeatedly with distilled water to wash out fine particles, foreign matter, and whatever sodium chloride remained in the resin. Obviously defective particles of larger sizes were removed with tweezers. The resin particles were 40 to 80 mesh. The nominal divinylbenzene content was unknown but was probably 8 to 10%.

The main part of the resin and approximately 200-mg. samples were stored at 98% relative humidity in desiccators over saturated lead nitrate solution.[6] Samples from such humidistats gave a water content of 35.27% after drying 6.5 months at 23° over anhydrous magnesium perchlorate, and a sodium form capacity of 2.97 equivalents per kilogram or 4.59 equivalents per kilogram of dry resin. Hence, the water content of resin samples was never more than perhaps 5%[7] different from the final equilibrium value.

A 1-g. standard sample, weighed 11 times over a period of 2 years at 21 to 25°, gave average and maximum deviations from the mean of ±0.04 and 0.12%, respectively. This same sample and even empty weighing bottles failed to give reproducible weights after storage in a humidistat over distilled water.

The equilibrating phases were stirred continuously at 25.04 ± 0.04° for not less than 5 days. After the solutions settled for three or more hours in the thermostat, samples from the top of the aqueous phase were analyzed for cerium by a spectrophotometric difference technique described elsewhere.[8] The resin molalities were calculated on the basis of the 98% relative humidity weights.

The preparation and treatment of the stock sodium perchlorate have been described elsewhere.[8] Its weight per cent was 44.651, its density, determined pycnometrically at 25.08 ± 0.005°, was 1.37296 g. per ml. (5.006 *M*), and the volume increased about 0.06 or 0.07%/°C. in the 22–25° range. Volumes of this solution were measured at 23 ± 1.5° with 50 or 100 ml. Precision Normax pipets (as for Q_0 values) and a Teflon stoppered buret. After data for Q_0 values had been obtained, a very careful and extensive re-check revealed that volumes of this stock solution were consistently too large by +0.1% relative to other volume measurements. An analytical method of adequate speed and precision to check the solutions used was not known, and some had been discarded. Since a 0.1% difference in sodium concentration changes Q_0 by 0.3% and Q_r by 3.4 and 2.1% at 0.0025 and 0.005 *M* sodium sulfate, respectively, a precision of ±0.05% in sodium concentration would have been desirable. This affects absolute but not relative values so that concentrations are reported to four numbers.

"Baker Analyzed" reagent grade sodium sulfate was recrystallized three times and then treated with the carbon[8] Spheron-6. It was dried at 450°, stored over anhydrous magnesium perchlorate, and dried at 150° previous to each weighing.

The preparations of cerous perchlorate and perchloric acid are discussed elsewhere.[8]

Attempts to approach equilibrium starting with about a 5% initial excess of cerium in the resin revealed that even after 23 days $C_{Ce(III)}$ was 2.1% below the equilibrium value, and that as much as several months time was required. Since absorption of cerium into the resin was comparatively fast at temperatures significantly greater than 25.04°, careful temperature control was required.

Two samples were equilibrated in the presence of enough glass beads to give an eight-fold increase of glass surface area. No evidence for adsorption of cerium on glass was observed.

Five *Q* numbers were rejected (51 were retained) when $C_{Ce(III)}$ was, for each number, around +2% different from the mean of its set. The reasons for these deviations are not known. Högfeldt[9] found equilibrium quotients for the silver–hydrogen ion exchange on Dowex-50-X4 to vary as much as 260% from one bead to another of the same batch of resin. Although this may be a partial explanation, the precision of the data of this work seems to indicate that these "heterogeneity effects" did tend to average out for the 1 or 2×10^4 beads used for each sample.

(6) N. A. Lange, "Handbook of Chemistry," 5th ed., Handbook Publishers, Inc., Sandusky, Ohio, 1944, p. 1412.

(7) B. R. Sundheim, M. H. Waxman and H. P. Gregor, *J. Phys. Chem.*, **57**, 969, 974 (1953).

(8) L. A. Blatz, *Anal. Chem.*, **33**, 249 (1961).

(9) E. Högfeldt, *Science*, **128**, [No. 3336], 1435 (1958).

Results

The following values were obtained for solutions initially 1.000×10^{-4} *M* in $Ce(ClO_4)_3$, 1.0×10^{-3} *M* in $HClO_4$ (except as noted), and the remainder of the ionic strength was defined by the *M* of $NaClO_4$.

Seven different solutions each yielded a pair of equilibrations at 25.04° and a molar ionic strength of 0.502_0. These fourteen samples gave an average $C_{Ce(III)}$ (Table II) of 1.938×10^{-5} *M* with average and maximum deviations from the arithmetic mean of ±0.6 and 1.2%, respectively. The standard deviation from the mean, σ, and the probable error of a single result, P.E., of this average $C_{Ce(III)}$ were ±0.19 and 0.48%, respectively. ($\sigma = [\Sigma(\Delta x)^2/n(n-1)]^{1/2}$; P.E. $= 0.6745\ [\Sigma(\Delta x)^2/(n-1)]^{1/2}$, where the Δx's are the deviations from the arithmetic mean and $n = 14$ is the number of samples.) These numbers gave an average Q_0 of 24.21 (Table II) with $\sigma = \pm 0.24\%$.

Six of the above fourteen samples were stirred continuously for over four months. Two of these six gave an average $C_{Ce(III)}$ of 1.922×10^{-5} *M*. The other four, which were made to approach equilibrium from an initial excess of cerium in the resin of 0.081 molal (calculated) gave an average $C_{Ce(III)}$ of 1.939×10^{-5} *M* as compared with the grand average of 1.938×10^{-5} *M*.

Two samples at $\mu = 0.442_0$ *M* gave cerium concentrations of 1.419×10^{-5} *M* and 0.08172 molal and a Q_0 of 24.41.

Seven samples at $\mu = 0.532_0$ (Table IV) gave an average $C_{Ce(III)}$ of 2.230×10^{-5} *M* with $\sigma = \pm 0.45\%$ and P.E. = ±0.80%, and a Q_0 of 23.92 with a σ of ±0.58%.

Hence Q_0 was somewhat insensitive to variations in μ in this region.

Two samples for which the $HClO_4$ was increased from 10^{-3} to 10^{-2} *M* at $\mu = 0.502_0$ gave averages of 1.958×10^{-5} *M* and 0.07659 molal; hence slight changes in acid concentrations were not significant.

TABLE I

EQUILIBRIUM DATA AND CALCULATED QUANTITIES FOR SOLUTIONS 0.01000 *M* IN Na_2SO_4 AND IONIC STRENGTH 0.502_0 *M*

No. of detns.	Initial $C_{Ce(III)}$, $M \times 10^4$	$\Sigma C'_{Ce(III)}$, $M \times 10^5$	$\Sigma m'_{Ce(III)}$, m	Q	Q_r
2	1.060	2.855	0.07377	14.71	64.5
2	1.090	2.961	.07561	14.64	65.4
4	1.106	2.994	.07682	14.75	64.1
2	1.115	3.020	.07743	14.78	63.8

Two samples, $\mu(25°) = 0.502_0$ stirred for 10 days at 8 ± 0.5° averaged 2.802×10^{-5} *M* and 0.06855 molal for an average change in $C_{Ce(III)}$ of 2.6%/°C.

Tables I, II and IV list the data and calculated quantities for solutions initially 1.0×10^{-3} *M* $HClO_4$. In Tables II and IV, the values in parentheses were interpolated or extrapolated from the experimental numbers nearest above and below each parenthesis. The data of these tables show

TABLE II

SUMMARY OF EQUILIBRIUM DATA AND CALCULATED QUANTITIES AT CONSTANT IONIC STRENGTH 0.502$_0$ M

No. of detns.	Initial $C_{Na_2SO_4}$, M	Initial $C_{Ce(III)}$, $M \times 10^4$	Equilibrium $\Sigma C_{Ce(III)}$, $M \times 10^5$	Equilibrium $\Sigma m_{Ce(III)}$, m	C_{NaClO_4}, M	Q	Q_r, eq. 5	Q_r, cor.
14	0	1.000	1.938	0.07678	0.5006	24.21		
7	0.002500	1.024	2.185	.07672	.4931	21.13	58.3	59.1
7	.005000	1.050	2.439	.07677	.4856	18.66	59.5	60.3
8	.01000	1.106	2.996	.07680	.4706	14.74	64.3	65.0
2	.02000	1.220	4.146	.07671	.4406	10.00	71.0	
(4)			(4.154)	(.07678)		(9.992)	(71.1)	(71.9)
2	.02000	1.230	4.187	.07727	.4406	9.975	71.3	
2	.05000	1.580	7.850	.07571	.3506	4.283	93.0	
(4)			(7.998)	(.07678)		(4.277)	(93.2)	(94.0)
2	.05000	1.616	8.055	.07719	.3506	4.269	93.4	

TABLE III

PRECISION INDICES FOR TABLE II

C_{SO_4}, M	$\Sigma C'_{Ce(III)}$ Av. dev., %	$\Sigma C'_{Ce(III)}$ Max. dev., %	Q_r Av. dev., %	Q_r Max. dev., %	Q_r Std. dev., %
0.002466	0.20	0.36	2.2	4.06	1.09
.004933	.11	.18	0.72	1.14	0.32
.009889	.39	.67	1.51	2.60	.61
.01980	.15	.30	0.28	0.57	.21
.04957	.11	.21	.15	.27	.11

that this linear interpolation or extrapolation could be made with negligible error. In Table II the eight values at 0.01000 M Na_2SO_4 were obtained from Table I excluding the two values at 1.060 $\times 10^{-5}$ M $C_{Ce(III)}$. The Q_r corrected column lists numbers corrected for sulfate ion tied up in HSO_4^- (K_A = 0.075 at 25° and μ = 0.5 M) and in $CeSO_4^+$ and $Ce(SO_4)_2^-$.

The listed deviations (Table III) in Q_r were calculated from the deviations in the Q numbers. Experimentally, this includes deviations in the $C'_{SO_4^-}$ term. Hence these numbers give a measure of relative precision. It would make little difference in the probable errors of β_1 and β_2 discussed below if the σ of Q_0 were combined with the σ's of the Q's.[10]

The Q_r values from Table II have been plotted as a function of $C'_{SO_4^-}$ in Fig. 1. The equation of the straight line was obtained by the method of least squares. The point at 0.04957 sulfate-ion concentration was omitted from this calculation. If the four points are weighted inversely proportional to the squares of their standard deviations from the mean, the values obtained for β_1 and β_2 and their probable errors, respectively, are 56.7 $\pm$ 0.2$_5$ and 767 $\pm$ 16. If, as mentioned earlier, a systematic error of +0.3% in Q_0 is assumed, and again using unequal weights for the four points, the values become 55.2 $\pm$ 0.1 and 820 $\pm$ 6.

TABLE IV

SUMMARY OF EQUILIBRIUM DATA AND CALCULATED QUANTITIES FOR IONIC STRENGTHS 0.502$_0$ TO 0.532$_0$ M

No. of detns.	Initial $C_{Na_2SO_4}$ M	μ	Initial $C_{Ce(III)}$, $M \times 10^4$	$\Sigma C_{Ce(III)}$, $M \times 10^5$	$\Sigma m_{Ce(III)}$, m	Q_0	Q	Q_r corr.	Std. dev. of Q_0, %
14	0	0.502$_0$	1.000	1.938	0.07678	24.21			0.24
...	0	.509$_3$	1.000	(2.011)	(.07609)	(24.13)			
...	0	.516$_8$	1.000	(2.084)	(.07539)	(24.06)			
7	0	.532$_0$	1.000	2.230	.07400	23.92			0.58 of Q_r
4	0.002500	.509$_3$	1.028	2.281	.07618		20.98		
(8)					(.07609)		(20.97)	61.1	1.4
4	.002500	.509$_3$	1.032	2.290	.07647		21.00		
2	.005000	.516$_8$	1.060	2.652	.07596		18.44		
(4)					(.07539)		(18.46)	61.5	1.6
2	.005000	.516$_8$	1.070	2.685	.07633		18.40		
4	.01000	.532$_0$	1.126	3.429	.07458		14.84		
(7)					(.07400)		(14.79)	62.4	0.9
3	.01000	.532$_0$	1.160	3.518	.07697		15.04		

The values of Q_r (Table IV) as a function of $C'_{SO_4^-}$ were plotted (see Fig. 1). The data were fitted with a curve which was made to parallel roughly the graph of equation 6, Fig. 1, using a value of $\mathring{a}$ = 5.9. This curve gives a value of β_1 = 59 $\pm$ 1 and a limiting slope of about 400. Substitution of these values into equation 7 gives a value of 720 $\pm$ 80 for β_2. If corrections for the error in Q_0 (use $Q_r(\mu)$ = 59.2, 60.3, and 61.7) values are made, values of β_1 = 58 $\pm$ 1 and $\beta_2 \backsimeq$ 780 $\pm$ 80 are obtained. The uncertainties[2] are estimates.

Newton and Arcand[11] showed (Table II) that polynuclear complexes are not significant even at cerous-ion concentrations about one-hundred-fold greater than used here.

Discussion

The agreement between results at constant and varying μ alleviates concern about the effects of uptake of electrolytes by the resin.

(10) A. E. Worthing and J. Geffner, "Treatment of Experimental Data," John Wiley and Sons, Inc., New York, N. Y., 1943, pp. 201, 207, 240, 243 and 249.

(11) T. W. Newton and G. M. Arcand, *J. Am. Chem. Soc.*, **75**, 2449 (1953).

It has been shown elsewhere[2] that if the Q_0 of the first complex ion has the expected value for a +1 ion of about 1, the effects on β_1 and β_2 are negligible; and that even if this Q_0 were much larger, the resulting curvature would be so slight as to be indectable from data with the precision indices of Table III.

Since the data of Table II are fitted precisely by a straight line, there is no evidence for a third complex even at 0.05 M Na_2SO_4. However, nothing meaningful can oe said about assumed β_3 values of less than 2 to 3 $\times$ 10^3, and perhaps even larger.

In view of the error in Q_0, the recommended values of β_1 and β_2 (and their subjectively estimated uncertainties) at 25° and μ = 0.502$_0$ M are 56 ± 1 and 800 ± 40, respectively. An attempt[2] has been made to correlate these values with values (some of which were corrected) from other studies at various ionic strengths.

Acknowledgment.—The author wishes to acknowledge the helpful interest and criticisms of Dr. J. F. Lemons under whose general direction this work was done. He also is grateful to Prof. R. E. Connick of the University of California for his helpful comments and encouragement, and to Prof. G. Scatchard of the Massachusetts Institute of Technology for his helpful criticisms.

ELECTRODE POTENTIALS IN MOLTEN LITHIUM SULFATE–POTASSIUM SULFATE EUTECTIC[1]

BY C. H. LIU[2]

Brookhaven National Laboratory, Upton, L. I., N. Y.

Received September 5, 1961

The lithium sulfate–potassium sulfate eutectic (80% lithium sulfate by mole; melting point 535°) was shown to be an adequate molten solvent for electrochemical investigations at 625°. A procedure for preparing the eutectic melt was established. The silver(I)–silver(0) system was found to be a satisfactory reference electrode in this melt. The electrode systems, whose standard potentials were measured by direct potentiometry against the silver reference, are: copper(I)–copper(0), copper(II)–copper(I), palladium(II)–palladium(0), and rhodium(III)–rhodium(0). The Nernst equation was applicable in all cases.

Interest in molten salt electrochemistry has been increasing and advances in this field have been rapid in recent years. Numerous attempts have been made to evaluate electrode potentials in fused solvents; however, experimental results are difficult to correlate because of the widely different molten solvents and experimental conditions employed by different workers. Comprehensive literature surveys on potentiometric measurements are available.[3] A systematic compilation of electrode potentials in molten lithium chloride–potassium chloride has been made by Laitinen and coworkers.[4] Flengas and Ingraham have made a similar investigation in molten potassium chloride–sodium chloride.[5] The potentials of a number of metal electrode systems were measured and compared in fused potassium fluoride–sodium fluoride by Grjotheim.[6] Very little has been reported in the published literature regarding chemical and electrochemical phenomena in molten sulfates. The oxygen–oxide potential on platinum was used to estimate the formation potentials of various metal oxides in lithium sulfate–potassium sulfate at temperatures up to 750°[7]; the results, however, were not definitive. In a series of articles,[8] Lux reported the use of an oxygen electrode on platinum to measure the oxide activities in molten potassium sulfate–sodium sulfate at 950°. The volatility loss of metal oxides was found to be rapid, and it was necessary to extrapolate the measured potentials to zero time to obtain reasonable results. The objectives of the present study are an evaluation of the oxidation–reduction potentials of various electrode systems in molten lithium sulfate–potassium sulfate eutectic at 625° and an examination of the electrolytic decomposition of this melt.

Apparatus and Chemicals

Furnace. Hevi-Duty crucible furnace, Type M-506, Hevi-Duty Electric Co., Milwaukee, Wisconsin.

Temperature Controller. Wheelco indicating controller Model 403 (Barber-Coleman Co., Rockford, Illinois).

Constant Current Generator. An all electronic current regulator built by the Instrumentation Division, Brookhaven National Laboratory. It is capable of delivering constant currents from 0.001 to 100 milliamp. with a precision of ± 0.5%.

Electrolytic Cell.—The main cell consisted of a quartz beaker placed in an outer Vycor jacket (3 in. o.d. and 13 in. long with a sealed flat bottom) the lower 8 in. of which were placed in the heating chamber of the furnace. The furnace then was insulated with asbestos plates and refractory insulating bricks. The outer Vycor jacket was equipped with a ground glass flange. Ground glass joints, sealed vertically to a borosilicate glass top with a similar ground flange, permitted the insertion of an argon inlet tube, a thermocouple tube, and various electrodes. Addition and removal of materials into and from the main cell also could be accomplished through these joints. A stopcock sealed to the side of the top served as the argon outlet and the

(1) This work was done under the auspices of the United States Atomic Energy Commission.

(2) Department of Chemistry, Polytechnic Institute of Brooklyn, 333 Jay Street, Brooklyn 1, New York.

(3) (a) C. H. Liu, Ph.D. thesis, University of Illinois, 1957; (b) J. W. Pankey, Ph.D. thesis, University of Illinois, 1958.

(4) (a) H. A. Laitinen and C. H. Liu, *J. Am. Chem. Soc.*, **80**, 1015 (1958); (b) H. A. Laitinen and J. W. Pankey, *ibid.*, **81**, 1053 (1959).

(5) S. N. Flengas and T. R. Ingraham, *J. Electrochem. Soc.*, **106**, 714 (1959).

(6) K. Grjotheim, *Z. physik. Chem.* (Frankfurt), **11**, 180 (1957).

(7) D. G. Hill, B. Porter and R. S. Gillespie, Jr., *J. Electrochem. Soc.*, **105**, 408 (1958).

(8) H. Lux, *Z. Elektrochem.*, **45**, 303 (1939); **52**, 220 (1948); **52**, 224 (1948); **53**, 41 (1949); **53**, 43 (1949); **53**, 45 (1949).

vacuum connection. The main cell was compartmented with small quartz tubes with sealed-in quartz fritted discs for bottoms. In this fashion, each preparation of the eutectic sulfate melt could be used in several separate experiments; the fritted discs also acted as salt bridges. The cell was evacuated at the start of each molten salt experiment to facilitate the filling of these fritted compartments. A dry argon atmosphere was maintained during each experiment; tank argon was passed through a heated Vycor column containing copper screens to remove oxygen and then through a column of anhydrous magnesium perchlorate to remove moisture before use.

Salt Filtration Assembly.—The eutectic melt was filtered into a quartz beaker placed in a Vycor outer jacket similar to the main electrolytic cell. The filter consisted of a fritted quartz disc, sealed to one end of a quartz tube which in turn was ring-sealed to a flanged quartz top. The eutectic was added to the fritted tube through a standard taper joint sealed vertically to the center of the top. An argon inlet tube was introduced through the same joint by means of an O-ring seal, and an argon vent also was provided. A stopcock sealed to the side of the top permitted connection to vacuum during filtration. This assembly was a modification of the type used by Van Norman.[9]

Chemicals.—All chemicals used were reagent grade.

Metal Electrodes.—All metal electrodes used were chemically pure and were in either foil or wire form.

Experimental Results and Discussion

Preparation and Analysis of the Melt.—Lithium sulfate monohydrate was mixed with potassium sulfate in the correct proportions (80% lithium sulfate by mole) and gradually heated to 200°. This temperature was maintained for a few hours to complete the preliminary drying. The dehydrated eutectic (melting point 535°) was melted in the filtration assembly under a dry argon atmosphere and filtered by vacuum suction through the quartz frit at approximately 625°. In this manner, solid particles, presumably carbonaceous and siliceous materials, were removed, and a clear melt resulted. After cooling, the filtered eutectic was crushed and stored in a desiccator to be used in molten salt experiments.

In order to make quantitative measurements, it was essential to know the amounts of salt present in the fritted compartments. The sulfate content of each compartment was determined by argentometric titrations after the sulfate had been converted to chloride by ion exchange, Dowex 1 being the anion exchanger used.

Electrode Potential Measurements. Nernst Equation[10] and Standard State.—When molality, m, is used as the reference function in the eutectic melt at 625°, the Nernst equation is

$$E = E^0 + \frac{0.1782}{n} \log \frac{m_{ox}}{m_{red}}$$

where

E is the electrode potential in volts
E^0 is the standard potential in volts
n is the no. of electrons in the electrode process, and ox and red designate the oxidized form and reduced form, respectively

The activity coefficients within the concentration limits to be reported are shown to be either unity or constant. Thus, either the concentration is identical with the activity or the activity coefficient can be incorporated as a constant term into the standard potential. An electrode system is said to be in its standard state when the ratio m_{ox}/m_{red} is equal to unity. For a pure metal, the standard state is defined as its physical state at 625° under one atmosphere of pressure. The standard state for a metal ion in a metal ion–metal system is unit molality.

Reference Electrode.—The silver(I)-silver(0) electrode at various concentrations of silver(I) was examined in detail. In most cases, silver(I) was produced by anodizing a silver coil electrode in a fritted compartment at a constant current for a measured period of time against a platinum working cathode. The current density was about five milliamperes per square centimeter. One hundred per cent. current efficiency was established by the weight loss of a silver wire after the passage of a known number of faradays of electricity in a coulometric measurement of the "n" value of the electrode reaction. In some cases, weighed portions of silver sulfate were added to the melt. The exact silver(I) concentration was calculated at the end of each experiment after the determination of the sulfate content of each compartment. The applicability of the Nernst equation to the silver(I)–silver(0) system is shown by curve 4 in the figure. The line is theoretical, based upon the standard potential 0.000 volt and a one-electron Nernst slope of 0.1782; the circles are experimental points from concentration cells of silver(I), one of which was the reference electrode. The experimental standard potential calculated from each potential measurement by the use of the Nernst equation showed an average deviation of ± 0.002 volts for 40 measurements over the concentration range from 0.0016 to 0.25 molal. At lower concentrations, positive deviations were observed. One possible cause for this deviation was the presence of oxidizing impurities in the melt which would react to yield silver(I). Several experiments were performed to check the validity of the silver(I)–silver(0) system as a reference electrode. Replicates of this electrode were constructed in each experiment. The drift of the potential between any two of these electrodes was never greater than two millivolts for observation periods up to 15 hr. Furthermore, the potential of the electrode at sufficiently high silver(I) concentrations was not shifted by the passage of a small current except for the iR correction. Thus, the silver(I)–silver(0) electrode was established as a satisfactory reference electrode in the eutectic sulfate melt. The potential of this electrode in the standard state is arbitrarily assigned the value 0.000 volt to be used as the reference point in the standard potential measurements.

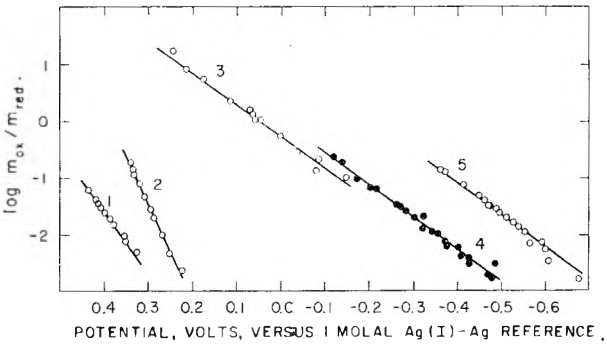

Fig. 1.—Nernst equation plots: 1, Pd(II)–Pd(0), 2, Rh(III)–Rh(0), 3, Cu(II)–Cu(I), 4, Ag(I)–Ag(0), 5, Cu(I)–Cu(0).

In each experiment, a fresh reference electrode was made by anodizing a silver coil of approximately two square centimeters in area in the manner described. The silver(I) concentration was made approximately 0.05 m with the exact concentration calculated at the end of the experiment.

Limiting Electrode Processes of the Melt.—When the melt was electrolyzed with two platinum electrodes, the electrode reaction at the anode appeared to be

$$SO_4^{-2} \longrightarrow {}^1/_2O_2 + SO_3 + 2e^-$$

Continuous and vigorous gas evolution occurred at the electrode with no observable solid deposits during an electrolysis at a current density of approximately ten milliamperes per square centimeter. The potential at the electrode at the beginning of electrolysis was about 0.7 v. after iR correction *vs.* the standard reference one molal silver(I)–silver(0) electrode and drifted to a stable value of 0.9 v. after fifteen minutes. In the cathode compartment, both sulfite and sulfide were found by chemical analysis, accounting for over 95% of the electricity passed. The cathode process was complicated and probably involved the total reactions

$$SO_4^{-2} + 2e^- \longrightarrow SO_3^{-2} + O^{-2}$$
$$SO_4^{-2} + 6e^- \longrightarrow S + 4O^{-2}$$

and

$$SO_4^{-2} + 8e^- \longrightarrow S^{-2} + 4O^{-2}$$

(9) J. D. Van Norman, Ph.D. thesis, Rensselaer Polytechnic Institute, 1959.

(10) The sign convention recommended by the IUPAC in the compt. rend. of the XVIIth Conference, Stockholm, 1953, is used.

However, elemental sulfur, if present at all, appeared to be a minor product. The cathode potential at the start was about −1.6 v. after *iR* correction *vs.* one molal silver(I)–silver(0) and drifted to a final stable value of −2.0 v. after 35 minutes.

Standard Potentials.—For the metal ion–metal electrodes, which included palladium(II)–palladium(0), rhodium(III)–rhodium(0), and copper(I)–copper(0), the metal ions were formed by anodizing a coil (or foil) electrode of the respective metal in an isolated compartment of the melt in a manner analogous to that described for the silver electrode. The "*n*" value of the electrode reaction was checked in each case by the weight loss of the metal electrode and the number of faradays of electricity passed. The potentials at the electrode after successive measured periods of anodization were measured against a silver(I)–silver(0) reference electrode. The molal concentrations of the metal ion for each potential measurement were calculated from the number of faradays of electricity passed, the "*n*" value, and the weight of melt present after the determination of the melt content of each compartment at the end of the experiment.

The copper(II)–copper(I) potential was evaluated by first anodizing a copper foil to form a known amount of copper(I) in a fritted compartment. After the removal of the copper foil, a platinum or palladium coil (or foil) electrode was lowered into the solution and anodized at a lower current density (approximately two milliamperes per square centimeter) to convert some of the copper(I) to copper(II). The potentials at the electrode after successive periods of electrolysis were measured against a silver(I)–silver(0) reference. The copper(I) and copper(II) concentrations were in the range from 0.005 to 0.1 *m*, and the same potential values were observed on platinum as on palladium.

All measured potentials were corrected to values *vs.* one molal silver(I)–silver(0) by the use of the Nernst equation in order to facilitate comparison and correlation of the results from different experiments. Extrapolation of these values to potentials of the electrode systems in the standard state yielded the standard potentials, which were computed as the averages of all measurements. The experimental results are presented as curves 1, 2, 3 and 5. The lines are based upon the experimental standard potentials and the theoretical Nernst slopes. The circles are experimental points.

The Nernst equation is obeyed in all cases. The experimental standard potentials, which are averages of large numbers of replicate measurements, are reproducible to within ± 0.002 to 0.003 v. These values are tabulated below

Electrode system	Standard potentials, v.
Pd(II)–Pd(0)	0.541
Rh(III)–Rh(0)	.387
Cu(II)–Cu(I)	.051
Ag(I)–Ag(0)	.000
Cu(I)–Cu(0)	− .202

Conclusions

The lithium sulfate–potassium sulfate eutectic at 625° may be used as a molten solvent for electrochemical investigations. It is easy to prepare and convenient to handle compared with the halide melts in the same temperature range. However, its potential span is much shorter than the alkali chloride melts.[3,5] The more active metal electrodes cannot be studied conveniently because of chemical reduction of sulfate. For example, nickel was observed to react with the melt to form nickel sulfide. Some metal ions tend to precipitate as their oxides, releasing sulfur trioxide. Bismuth(III) was observed to behave in this manner. A similar reaction between aluminum(III) and molten sodium sulfate has been reported.[11] Thus, competing acid–base equilibria also play an important role in molten sulfates.

Displacement of potential values and reversal in order in the electromotive force series are observed between the sulfate and chloride melts.[3,5] Apparently, stabilization of some valence states of metals by interaction with the solvent anions is the main cause for this phenomenon.

Acknowledgment.—The author wishes to acknowledge Drs. H. L. Finston, C. Auerbach, J. D. Van Norman and L. Newman for their helpful suggestions, discussions and encouragement. He also would like to thank Mr. G. Kissel for his assistance in the experimental part of the work.

(11) K. Grjotheim, T. Halvorsen and S. Urnes, *Can. J. Chem.*, **37**, 1170 (1959).

CORRELATION OF THE RELATIVE PULSE HEIGHT OF ORGANIC SCINTILLATORS WITH POLARITY AND RESONANCE EFFECTS[1]

BY STANLEY R. SANDLER, PAUL J. MCGONIGAL AND K. C. TSOU

The Central Research Laboratory of The Borden Chemical Company, Philadelphia, Pennsylvania

Received September 8, 1961

A linear correlation has been found between relative pulse height of plastic scintillators and the ionization potential and Hammett or Taft substituent constants (σ and σ_I, respectively) of the solvent and fluor that were used in the present work. Some aspects of the scintillation mechanism are discussed.

Introduction

In the previous papers[2−4] a correlation was found between the relative pulse heights (r.p.h.) of organic scintillators and the Hammett[5] or Taft[6] sigma (σ) values for the aromatic substituents of the solvent and fluor. The object of the present work was to extend the σ–r.p.h. correlation to new solvent and fluor systems and to show that the r.p.h. values also correlate well with the ionization potentials of the scintillation solvent.

(1) This work was supported by the U. S. Atomic Energy Commission under Contract No. AT-(30-1)-1931.

(2) S. R. Sandler and S. Loshaek, *J. Chem. Phys.*, **34**, 439 (1961).

(3) S. R. Sandler and S. Loshaek, *ibid.*, **34**, 445 (1961).

(4) S. R. Sandler, S. Loshaek, E. Broderick and P. Bernstein, *Nucleonics*, **18**, 102 (1960).

(5) L. P. Hammett, *Chem. Revs.*, **17**, 125 (1935).

(6) (a) R. W. Taft, Jr., "Steric Effects in Organic Chemistry," Edited by M. S. Newman, John Wiley and Sons, Inc., New York, N. Y., 1956, pp. 556–675; (b) R. W. Taft, Jr., N. C. Deno and P. S. Skell, *Ann. Rev. Phys. Chem.*, **9**, 287 (1958).

The mechanism[7-10] by which scintillations are produced in plastic and organic liquids when ionizing irradiation is absorbed is

Energy absorption by the solvent and excitation	$S + E/w_0 \longrightarrow S^*$	(1)
Fluorescence emission from the solvent	$S^* \xrightarrow{p_{es}} S + h\nu_1$	(2)
Solvent self-quenching	$S^* + S \xrightarrow{p_{ss}} S + S$	(3)
Energy transfer from solvent to solvent	$S^* + S \xrightarrow{p_{es}} S + S^*$	(4)
Energy transfer to fluor	$S^* + F \xrightarrow{p_t} S + F^*$	(5)
Fluorescence emission from fluor	$F^* \xrightarrow{p_{ef}} F + h\nu_2$	(6)
Fluor self-quenching	$F^* + F \xrightarrow{p_{ff}} F + F$	(7)
Fluor internal quenching by solvent interaction	$F^* + S \xrightarrow{p_i} F + S$	(8)
Fluor internal quenching	$F^* \xrightarrow{p_i} F$	(9)

In these equations S and F represent the solvent and flour concentrations, respectively, the p's are the probabilities of the various processes and E is the absorbed particle energy required to produce one fluorescent excitation in the solvent.

A semi-empirical pulse height equation is given by many researchers[7-10] and all are mathematically equivalent to the equation

$$\text{P.H.} = \left(\frac{E}{w_0}\right) q_1 \delta \left(\frac{q_0 + kc}{1 + kc}\right)\left(\frac{1}{1 + mc}\right) \qquad (10)$$

where $kc = p_t/(p_{ss} + p_{es})$; $mc = p_{ff}/p_{ef} + p_i)$; $q_1 = p_{ef}/(p_{ef} + p_i)$ is the quantum yield of the fluor exclusive of fluor self-quenching; c is the concentration of the fluor; p_t, p_{ss}, p_{es}, $p_{ff} = \beta_c$, p_{ef} and p_i are, respectively, the probabilities of transfer from the solvent to the fluor, solvent-quenching, direct emission by the solvent (very small), self-quenching of the fluor, emission by the fluor and internal quenching by the fluor; β is a constant; E is the particle energy which is completely absorbed by the scintillator; w_0 is the average dissipated particle energy required to produce one fluorescent excitation in the solvent; q_0 is the quantum yield of the solvent (very small in comparison to kc) and δ is a factor (includes photo cathode efficiency, instrument factors, etc.) which converts the number of emitted quanta from the scintillator to an observed pulse height.

Most of the investigations concerning the mechanism of scintillation have not been concerned with the molecular structure of the fluor[2-3] or solvent.[2-4] The present work as in the previous reports[2,3] is concerned with relating the molecular structure of the fluor with pulse height in plastic scintillators.

In the energy absorption step the aromatic solvent may be excited by ionization or by chemical bond excitation. It is reasonable to expect that a suitable parameter which characterizes electron density distribution in a solvent molecule or the ability of a solvent to ionize would bear some relation to the observed pulse height.

With the aromatic liquids and plastics it is possible to assign a numerical value for the energy to ionize it. This value is called the ionization potential and is given in electron volts. It also is possible to place a relative numerical value on the extent to which substituents either donate or withdraw electrons from the benzene ring as compared to hydrogen. These are the Hammett[5] sigma (σ) values and Taft's[6] inductive substituent constants (σ_I).

The application of the Hammett and Taft substituent constants and ionization potentials to pulse height will be considered in the discussion of results.

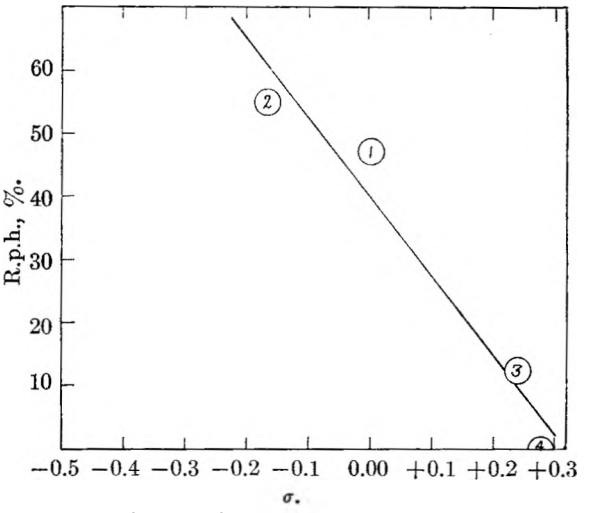

Fig. 1.—Relative pulse heights of polyvinyl toluene plastic scintillators containing 4-substituted p-terphenyls *vs.* σ: (1) p-terphenyl; (2) 4-methyl-p-terphenyl; (3) 4-bromo-p-terphenyl; (4) 4-iodo-p-terphenyl.

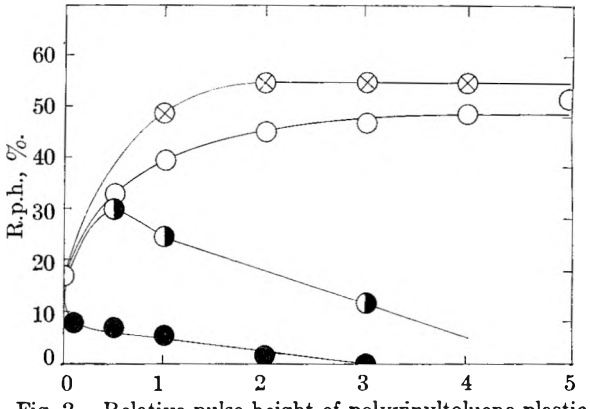

Fig. 2.—Relative pulse height of polyvinyltoluene plastic scintillators with varying concentrations of 4-substituted p-terphenyls as fluor: ○, p-terphenyl; ⊗, 4-methyl-p-terphenyl; ◑, 4-bromo-p-terphenyl; ●, 4-iodo-p-terphenyl.

Results

A. Correlation of the Electronegativity of the 4-Substituted p-Terphenyls with their Ability to Act as Fluors.—Plastic scintillators were prepared from vinyl toluene and a series of 4-substituted p-terphenyls whose substituent groups differed con-

(7) R. K. Swank and W. L. Buck, *Phys. Rev.*, **91**, 927 (1953).
(8) H. Kallmann and M. Furst, *ibid.*, **79**, 857 (1950).
(9) M. Furst and H. Kallmann, *ibid.*, **85**, 816 (1952).
(10) G. T. Reynolds, *Nucleonics*, **10**, 46 (1952).

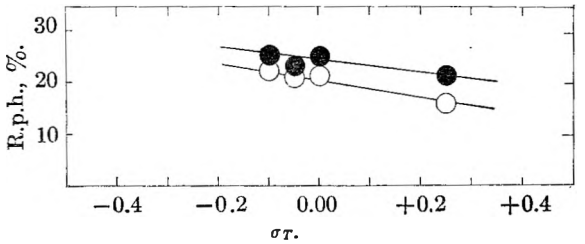

Fig. 3.—Relative pulse heights of substituted styrene scintillators containing naphthalene or 1-methoxynaphthalene as fluor: ○, naphthalene; ●, 1-methoxynaphthalene, (1) 2,5-dimethylstyrene; (2) vinyltoluene; (3) styrene; (4) *p*-methoxystyrene.

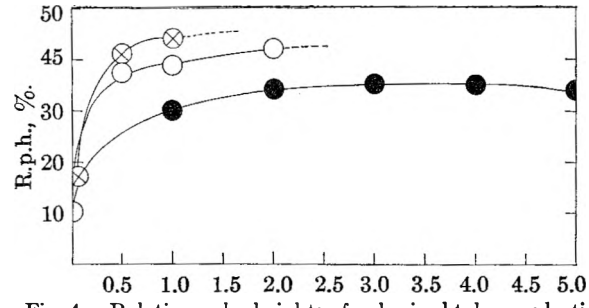

Fig. 4.—Relative pulse heights of polyvinyl toluene plastic scintillators containing 4-phenylstilbene, 4,4′-diphenylstilbene or *p*-terphenyl as fluor: ○, 4-phenylstilbene; ⊗, 4,4′-diphenylstilbene; ●, *p*-terphenyl.

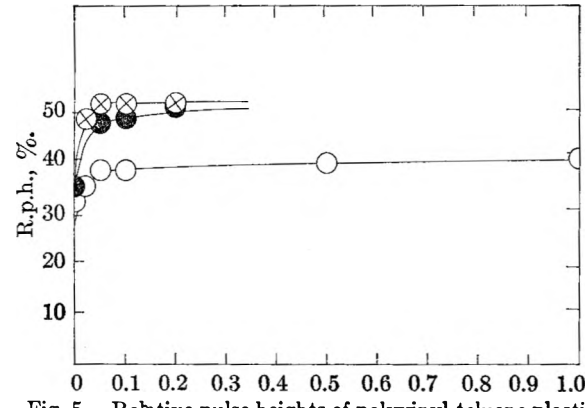

Fig. 5.—Relative pulse heights of polyvinyl toluene plastic scintillators with varying concentrations of wave-shifters: ⊗, 4% *p*-terphenyl with varying concentrations of 4,4′-diphenylstilbene as wave-shifter; ●, POPOP; ○, 4-phenylstilbene.

siderably in electronegativity. The 4-substituted *p*-terphenyls at 3% by weight and 0.05% POPOP (1,4-di-(2-(5-phenyloxazolyl))-benzene) were used throughout as the primary fluor and wave-shifter, respectively. The purity of the fluors was determined from their infrared and ultraviolet spectra. The pulse heights values were determined relative to an anthracene crystal of the same dimensions as previously described[7] (Pa^{234} β 0.01 mc., 2.32 mev.). The results are plotted in Fig. 1 *vs.* σ.

In Fig. 2 are plotted the results for r.p.h. *vs.* concentration data of *p*-terphenyl, 4-methyl-*p*-terphenyl, 4-bromo-*p*-terphenyl and 4-iodo-*p*-terphenyl. The concentration data were obtained in order to determine at what concentration the pulse height is maximum.

B. Pulse Heights of Substituted Styrene Scintillators Containing Substituted 1-Naphthalenes as Fluors.—Plastic scintillators were prepared from a series of substituted styrenes whose substituent groups differed considerably in electronegativity. Naphthalene or 1-methoxynaphthalene at 3% by weight and 0.05% POPOP were used throughout as the primary fluor and wave-shifter, respectively. Monomer purity was determined by infrared spectral analysis and by vapor phase chromatography. Relative pulse heights were determined as described in the previous section. The results are plotted in Fig. 3 where $\sigma = 0.00$ for unsubstituted naphthalene and $\sigma = -0.27$ for the 1-methoxy group on naphthalene.

C. Wave-shifters.—It is known[11] that 4,4′-diphenylstilbene is a good wave-shifter and also a good fluor. It was of interest to determine whether 4-phenylstilbene also would be a good wave-shifter and fluor. In order to test this compound on an equal basis with 4,4′-diphenylstilbene, a series of plastic scintillators was prepared with polyvinyltoluene and either 4-phenylstilbene or 4,4′-diphenylstilbene at various concentrations. The data are plotted on Fig. 4. The results for *p*-terphenyl[11] are included in Fig. 4 for comparison.

The wave-shifter efficiency of 4-phenylstilbene was evaluated in polyvinyltoluene and the results are plotted in Fig. 5 with data for 4,4′-diphenylstilbene from the literature[11] and also for POPOP, which were determined and are shown for comparison.

D. Correlation of Polarity and Resonance of Substituted Aromatic Compounds with Ionization Potentials.—Recently the ionization potentials (I_{ev}) of some aromatic liquids have been published and are listed in Table I with their appropriate

TABLE I

THE IONIZATION POTENTIAL AND SIGMA VALUES OF SOME AROMATIC LIQUIDS

No. in Fig. 6	Substituent	σ^{ab}	I_{ev}[12]	log I_s/I_0
(1)	None	0	9.52	.....
(2)	CH_3	−0.13	9.23	−0.0135
(3)	*p*-$(CH_3)_2$	− .23	8.88	− .0304
(4)	*m*-$(CH_3)_2$	− .28	9.02	− .0235
(5)	*o*-$(CH_3)_2$	− .23	8.97	− .0260
(6)	1,2,3-$(CH_3)_3$	− .36	8.75	− .0366
(7)	Cl	+ .28	9.42	− .0046
(8)	CH_3O	− .15	8.56	− .0459
(9)	OH	− .21	9.04	− .0235
(10)	NH_2	− .49	8.23	− .0632

[a] The average sigma value was calculated by holding one position fixed and obtaining the contribution of *m*,*p* and *o*-effects. For example

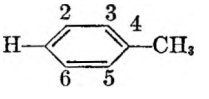

σ-values. The results are plotted in Fig. 6 as log (I_s, for the substituted benzene $/I_0$ for benzene) *vs.* the Hammett substituent constant σ. Position 1 is fixed and the methyl can be either *ortho*, *meta* or *para* to it. The average $\sigma = -0.13$. The σ-value for the *ortho* group is taken equal to that of

(11) L. J. Basile, *J. Chem. Phys.*, **27**, 801 (1957).

(12) Summarized in A. Streitwieser, Jr., *J. Am. Chem. Soc.*, **82**, 4129 (1960).

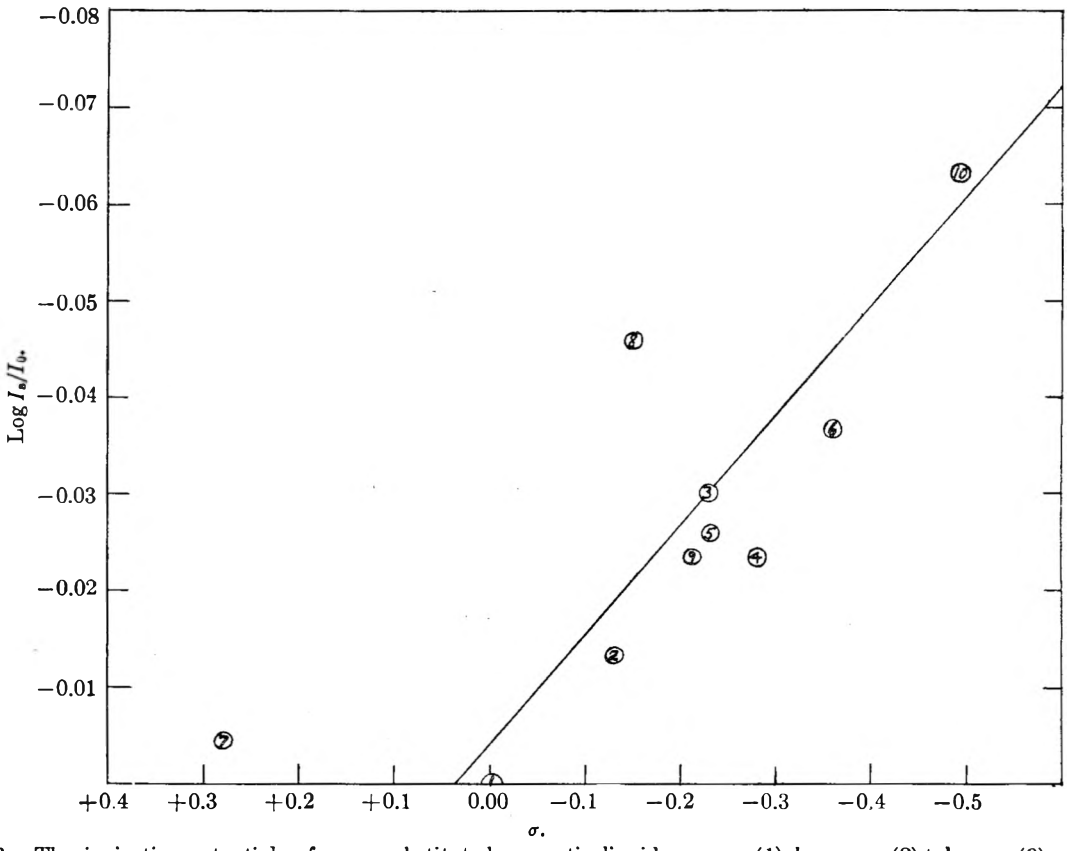

Fig. 6.—The ionization potentials of some substituted aromatic liquids *vs.* σ: (1) benzene; (2) toluene; (3) *p*-xylene; (4) *m*-xylene; (5) *o*-xylene; (6) 1,2,3-trimethylbenzene; (7) chlorobenzene; (8) methoxybenzene; (9) hydroxybenzene; (10) aniline.

the *para* group since the steric effect between the substituent and the aromatic hydrogen probably is small. Table II is a list of the ionization constants of the aromatic liquids and their σ-values relative to toluene. These results are plotted in Fig. 7.

TABLE II

THE IONIZATION CONSTANTS AND SIGMA VALUES[a] OF SOME ALKYL SUBSTITUTED AROMATIC LIQUIDS

No. in Fig. 7	Substituent	σ[a,b]	I_{ev}[12]
(1)	CH_3	0	9.23
(2)	*m*-$(CH_3)_2$	−0.07	9.02
(3)	*p*-$(CH_3)_2$	− .16	8.88
(4)	*o*-$(CH_3)_2$	− .16	8.97
(5)	1,2,3-$(CH_3)_3$	− .23	8.75

[a] Relative to toluene as zero.

E. Ionization Potentials and Relative Pulse Height of Plastic Scintillators.—In Fig. 8 is a plot of the r.p.h. values of some substituted styrene plastic scintillators and the ionization potential (I_{er}) of a similarly substituted benzene compound (relative to the tertiary carbon atom of the polystyrene backbone chain).

Discussion

A. Dependence of Scintillation Fluor and Wave-shifter Efficiency on Polarity and Resonance of its Substituents.—A strong dependence of pulse height on group electronegativity is shown in the plot of r.p.h. *vs.* σ for the substituents in Fig. 1. The more electron donating the substituent, *i.e.*, the more negative σ, the greater the pulse height. A similar strong dependence of r.p.h. on σ of the aromatic substituents also is found for the solvent, which was reported earlier.[1,2] The fact that both solvent and fluor show the same trend with substituent electronegativity suggests that electron density and mobility in the solvent and fluor are important in the scintillation process.

Electron mobility in a particular fluor system is an important factor which determines whether it will be a good fluor. *para*-Terphenyl probably is a good fluor because it is a highly resonating system with extended conjugation. Phenylstilbene can be considered similar to *p*-terphenyl since only a carbon double bond separates benzene from a biphenyl group. However, it would be slightly more resonating since it has an extra double bond. Furthermore, 4,4′-diphenylstilbene should be the best. These conclusions were verified and the data are shown as a plot of r.p.h. *vs.* fluor concentration in polyvinyltoluene in Fig. 4. It is interesting to note that 4,4′-diphenylstilbene is also a wave-shifter. This attribute is due to its fluorescence emission spectra having a strong peak at 4.050 Å., which is at the wave length of maximum sensitivity of most photomultiplier tubes. Thus 4,4′-diphenylstilbene can act efficiently as a secondary fluor by shifting the light output to a region where the photomultiplier tube is most sensitive. 4,4′-Diphenylstilbene is slightly more efficient than POPOP.

Earlier[2] it was suggested that the ionization of the tertiary hydrogen in the polystyrene backbone

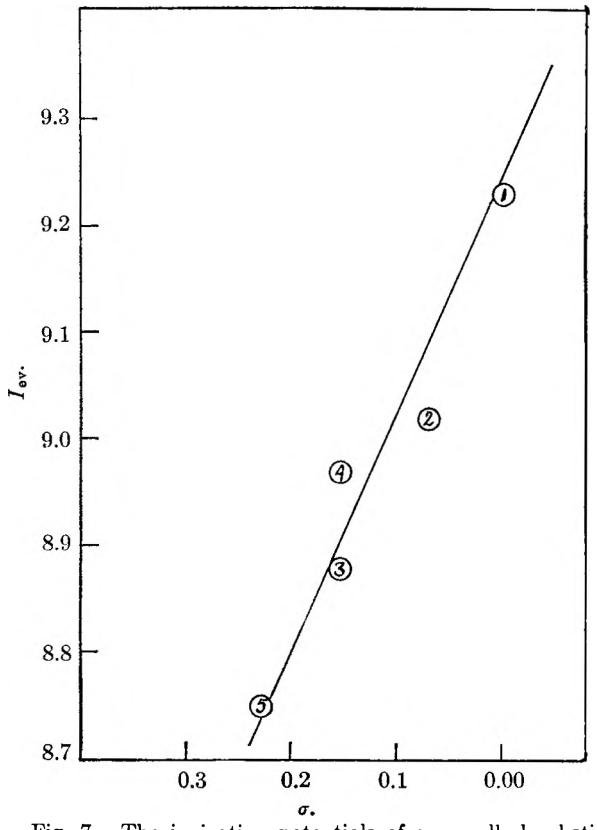

Fig. 7.—The ionization potentials of some alkyl substituted benzene compounds *vs.* σ: (1) toluene; (2) *m*-xylene; (3) *p*-xylene; (4) *o*-xylene; (5) 1,2,3-trimethylbenzene.

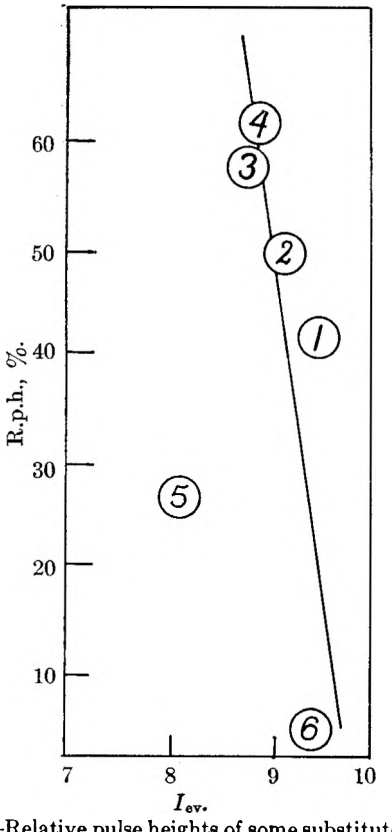

Fig. 8.—Relative pulse heights of some substituted styrene plastic scintillators *vs.* the ionization potentials: (1) styrene; (2) vinyltoluene; (3) 2,5-dimethylstyrene; (4) 3,4-dimethylstyrene; (5) *p*-methoxystyrene; (6) *p*-chlorostyrene.

chain during the energy absorption process is facilitated by substituents which donate electrons. It also is possible that electron donating groups on the fluor facilitate its being excited either by chemical bond excitation or ionization in the solvent–fluor energy transfer process (equation 5). The fact that as poor a fluor as 1-methoxynaphthalene is slightly more efficient than naphthalene indicates that the inductive effect may not be important in this system. However, since the differences are very small, as seen in Fig. 3 (within experimental error in most cases), no conclusions can be made with any degree of assurance. However, the r.p.h. values of the 4-substituted *p*-terphenyls differ significantly and the conclusion that can be made here is that electron donating groups probably facilitate the energy transfer between solvent and fluor (see p_t in equation 5).

B. Dependence of Scintillation Solvent Efficiency on Ionization Potentials.—The importance of the solvent in the energy absorption process (w_0 in equation 1) has been stressed in previous papers.[2-4] The solvents may absorb a quantum of energy either by ionization or by chemical bond excitation. If ionization is an important mode of excitation, as has been stressed also by other investigators,[13,14] then one would expect that the ionization potential of the solvent would bear some relationship to the observed efficiency of a scintillation system. In Figs. 6 and 7 are found correlations of the ionization potential of some substituted aromatic liquids with the Hammett substituent constant (σ) for the substituents. Since it has been shown[2-4] that the r.p.h. correlates with σ or σ_I of the substituent on the solvent or fluor molecule one also would expect that the r.p.h. would correlate well with the ionization potential of the substituent. Figure 8 illustrates a plot of the r.p.h. *vs.* the ionization potential for some substituted polystyrene plastic scintillators. It is seen that a good correlation also exists here for the substituted polystyrene systems. In the latter case the ionization potentials of the substituted polystyrene systems were taken equal to similarly substituted benzene compounds. However, the ionization potentials for the polystyrene systems are not the same as for the substituted benzene compounds, but their relative values would be. The ionization potential thus provides a good means of assessing a plastic or liquid medium for its ability to act as an efficient scintillation medium and also suggests that ionization probably is the dominant process by which energy is absorbed by the solvent.

Since it has been shown in this work and previous works,[2,3] that the relative pulse height is related to the Hammett or Taft substituent constant σ or σ_I, respectively, and since σ is related to the ionization potential (I_{ev}) the following relations can be written for organic scintillation systems

$$\text{r.p.h.} = k\sigma \text{ (or } \sigma_I) = k'(I_{ev})$$

where k and k' are proportionality constants.

(13) W. L. Buck, *I.R.E. Trans. on Nuclear Sci.*, **NS-7**, 11 (1960).
(14) J. B. Birks, *ibid.*, **NS-7**, 2 (1960).

Experimental

Synthesis of Monomers.—The general methods of preparing the alkyl styrenes have been described.[15] The purity of all the monomers was determined by vapor phase chromatography and infrared spectroscopy.

Synthesis of Fluors—4-Bromo-*p*-terphenyl.—This was synthesized in 26% yield according to the procedure of France, Heilbron and Hey[16] by adding bromine to a solution of *p*-terphenyl in hot glacial acetic acid in the presence of a trace of iodine and heating until the brown color faded. The product had a melting point of 229–230°. The infrared spectrum taken by means of a potassium bromide pellet showed absorption for *para* substitution at 12.25 μ (strong) and at 13.90 μ (weak) and only a trace of absorption at 12.92 μ (a peak which is present in *p*-terphenyl). The ultraviolet spectrum of this compound showed a $\lambda_{max}^{CHCl_3}$ at 280 mμ (ϵ_{max} 38,500).

4-Iodo-*p*-terphenyl.[17]—To a mixture of *p*-terphenyl in 3400 ml. of glacial acetic acid at 80° was added approximately 1 ml. of water. The reaction mixture was cooled to room temperature and then 31.6 g. (0.402 *M*) of iodine, 15.2 g. of potassium iodate, 33.8 cc. of concd. sulfuric acid and 42.2 cc. of CCl_4 were added. The reaction mixture was heated to 80° and stirred for 48 hr. at that temperature until the iodine color faded. The product precipitated on cooling and was recrystallized from benzene to yield 77.3 g. (50% yield) of 4-iodo-*p*-terphenyl, m.p. 245–247° (lit.[17] 246–247°), $\lambda_{max}^{CHCl_3}$ 281 mμ (ϵ_{max} 40,200).

4-Methyl-*p*-terphenyl.—To a solution (0.426 *M*) of 4-bromo-*p*-terphenyl in ether was added a solution of *n*-butyllithium (0.554 *M*). When the reaction was complete methyl sulfate was added in sufficient quantity to react with all the *p*-terphenyllithium. The product was obtained in 38% yield; m.p. 206–208° (lit.[18] m.p. 208°). The infrared spectrum of this compound was identical to that of an authentic sample supplied to us by Prof. Guido Daub of the University of New Mexico. The ultraviolet spectrum of this compound showed a $\lambda_{max}^{CHCl_3}$ 282 mμ (ϵ_{max} 29,700).

4-Phenylstilbene.—To an ethereal suspension of 20.9 g. of magnesium (0.88 *M*) was added 194 g. of 4-bromobiphenyl (0.833 *M*) in ether. When the reaction was complete freshly distilled 97.6 g. of phenylacetaldehyde (0.833 *M*) was added dropwise to yield 45 g. of 2-phenyl-1-biphenyl-1-ethanol which then was dehydrated over alumina at 300° under vacuum to 4-phenylstilbene, m.p. 221–222° (lit.[19,20] m.p. 221–222°; $\lambda_{max}^{CHCl_3}$ 325 mμ (ϵ_{max} 34,300).

Sources of Other Fluors.—Naphthalene was recrystallized three times from methanol, m.p. 80–81. 1-Methoxynaphthalene was obtained from Eastman Distillation Products and redistilled, b.p. 122° (5 min.), $n^{23}D$ 1.6222. *p*-Terphenyl—Dajac Laboratory—was scintillation grade, m.p. 212–213°; $\lambda_{max}^{CHCl_3}$ 279 mμ (ϵ_{max} 29,600). 4,4′-Diphenylstilbene was obtained from Pilot Chemical Co. and used without further purification; $\lambda_{max}^{CHCl_3}$ 340 mμ (ϵ_{max} 53,700). POPOP, scintillation grade, was obtained from Tracerlab and recrystallized from benzene.

Preparation of Plastic Scintillators.—The plastic scintillators were prepared as cylindrical discs $^1/_2$ in. high by $^{13}/_{16}$ in. in diameter by polymerizing the substituted styrenes in glass vials of the right diameter (degassed under vacuum) and machining to the desired height.

Determination of Pulse Height.—The method and apparatus for determining the relative pulse heights has been described.[7] For β-irradiation, a Pa^{234} (0.01 mc., 2,3-mev.) source was used. All pulse heights are relative to an anthracene crystal of the same dimensions.

Acknowledgment.—We are grateful to Mr. Heinz Gunter Dickens for his help in carrying out some of the experiments and to Drs. S. Loshaek and B. D. Halpern for their encouragement and helpful suggestions.

(15) D. T. Mowry, M. Renoll and W. F. Huber, *J. Am. Chem. Soc.*, **68**, 1105 (1946).

(16) H. France, I. M. Heilbron and D. H. Hey, *J. Chem. Soc.*, 1364 (1938).

(17) W. Kern, W. Gruber and H. O. Wirth, *Macromol. Chem.*, B37H3, 210 (1960).

(18) H. Gilman and E. A. Weipert, *J. Org. Chem.*, **22**, 446 (1957).

(19) F. Bergmann and J. Weizmann, *ibid.*, **9**, 408 (1944).

(20) R. Kuhn and T. Wagner-Jauregg, *Helv. Chim. Acta*, **13**, 9 (1930).

THE IONIZATION CONSTANT OF *p*-NITROPHENOL FROM 0 TO 60°

BY G. F. ALLEN, R. A. ROBINSON AND V. E. BOWER

National Bureau of Standards, Washington 25, D. C.

Received September 5, 1961

The spectrophotometric method has been used to measure the ionization constant of *p*-nitrophenol in aqueous solution from 0 to 60°. The ionization constant is 6.98×10^{-8} at 25°. It is given as a function of the absolute temperature (T) by $-\log K = 2150.69/T - 3.8133 + 0.01260T$.

Some spectrophotometric measurements already have been made to determine ionization constants over a temperature range; thus, Sager and Siewers[1] determined the ionization constant of 4-aminobenzophenone from 10 to 40° and Sager and Byers[2] that of 4-chloro-4′-aminodiphenylsulfone from 15 to 35°.

In order to determine changes in enthalpy and heat capacity occurring in the ionization of a weak acid, a knowledge of the ionization constant over a wide range of temperature is desirable. To see if the range could be extended, spectrophotometric measurements in the near-ultraviolet now have been made with *p*-nitrophenol between 0 and 60°.

The earlier measurements of Robinson and Biggs[3] at 25° were repeated but the data were treated by a somewhat different method due to Bates and Schwarzenbach.[4] E.m.f. measurements[5] of cells containing phosphate buffers yield unequivocal values of the quantity $-\log (m_H \gamma_H \gamma_{Cl})$. This was formerly called pwH but the symbolism is not consistent with that recommended recently.[6] The results of spectrophotometric measurements give the ionization constant of *p*-nitrophenol as

$$pK = -\log (m_H \gamma_H) - \log \alpha/(1 - \alpha) - \log \gamma_N/\gamma_{HN}$$

where α, the fraction of phenol ionized, is given by $(D - D_1)/(D_2 - D_1)$; D_1, D_2 and D being the optical densities of acid, alkaline and buffer solutions con-

(1) E. E. Sager and I. J. Siewers, *J. Research Natl. Bur. Standards*, **45**, 489 (1950).

(2) E. E. Sager and F. C. Byers, *ibid.*, **59**, 245 (1957).

(3) R. A. Robinson and A. I. Biggs, *Trans. Faraday Soc.*, **51**, 901 (1955).

(4) R. G. Bates and G. Schwarzenbach, *Helv. Chim. Acta*, **37**, 1069 (1954).

(5) R. G. Bates and S. F. Acree, *J. Research Natl. Bur. Standards*, **34**, 373 (1945); R. G. Bates, *ibid.*, **39**, 411 (1947).

(6) R. G. Bates and E. A. Guggenheim, *Pure Appl. Chem.*, **1**, 163 (1960).

taining *p*-nitrophenol and γ_N and γ_{HN} the activity coefficients of the nitrophenolate ion and the nitrophenol molecule, respectively. Thus,

$$pK = -\log(m_H\gamma_H\gamma_{Cl}) - \log \alpha/(1-\alpha) - \log(\gamma_N/\gamma_{Cl}\gamma_{HN})$$

The last term should be negligible at low ionic strength.

Some measurements of optical density at a wave length of 406 mμ were made in phosphate buffers at 25° and values of $\alpha/(1-\alpha)$ calculated; these, combined with $-\log(m_H\,\gamma_H\,\gamma_{Cl})$ data,[7] and with the last term in the above equation neglected, gave the following pK values

Solution	1	2	3	4	5
$-\log(m_H\gamma_H\gamma_{Cl})$	6.912	6.974	6.992	7.040	7.080
α	0.354	0.397	0.407	0.436	0.454
pK	7.17_3	7.15_6	7.15_5	7.15_2	7.16_0

Solutions 1 to 5 contained equimolal KH_2PO_4 and Na_2HPO_4 at total ionic strengths of 0.2, 0.1, 0.08, 0.04 and 0.02 mole/kg., respectively. They were prepared from Standard Samples of the National Bureau of Standards. *p*-Nitrophenol was Fisher's Reagent material, recrystallized from water.

It is evident that four solutions give concordant values of pK and it is justifiable to equate the $\gamma_N/(\gamma_{HN}\gamma_{Cl})$ term to unity. One solution gave a high pK value but, as it had a total ionic strength of 0.2, it is not surprising that the assumption is no longer valid. The mean of the four concordant results is 7.15_5; other determinations have given 7.14,[8] 7.14_9,[3] 7.15.[4]

Measurements were made over a temperature range 0 to 60° using a Beckman Model DU instrument. The cell compartment was fitted with jackets through which water could be circulated from a thermostat. A thermometer, inserted into the cell compartment and allowed to come to temperature equilibrium, showed a variation of less than 0.05° over periods of time much longer than those needed to make measurements of optical density.

The maximum in the absorption spectrum of alkaline solutions of *p*-nitrophenol shows some change with temperature of both the wave length at which the maximum is found and the extinction coefficient at that wave length (2°, 397 mμ, 17,700; 25°, 402 mμ, 17,900; 50°, 404 mμ, 18,200).

Using the equimolar phosphate buffer of total ionic strength 0.1, measurements of optical density were made at three wave lengths, 396, 406 and 416 mμ; from a large scale plot of optical density *vs.* temperature, values of optical density were read at round values of the temperature and the degree of ionization calculated. For brevity, only the average of the three α-values at each temperature is recorded. The following results were obtained

°C.	0	5	10	15	20
$-\log(m_H\gamma_H\gamma_{Cl})$	7.091	7.057	7.029	7.006	6.988
α	0.280	0.300	0.323	0.347	0.371
pK	7.50_1	7.42_5	7.35_0	7.28_1	7.21_6
°C.	25	30	35	40	45
$-\log(m_H\gamma_H\gamma_{Cl})$	6.974	6.964	6.956	6.951	6.949
α	0.397	0.422	0.449	0.471	0.495
pK	7.15_6	7.10_1	7.04_6	7.00_1	6.95_8
°C.	50	55	60		
$-\log(m_H\gamma_H\gamma_{Cl})$	6.948	6.950	6.954		
α	0.520	0.543	0.566		
pK	6.914	6.87_5	6.83_9		

The pK values can be represented by the equation

$$pK = 2150.69/T - 3.8133 + 0.01260T$$

The corresponding change of entropy on ionization is calculated to be 71 j. deg.$^{-1}$ mole^{-1}. The change of enthalpy is 19,730 j. mole^{-1} at 25°, compared with 19,660 j. mole^{-1} (4,700 cal. mole^{-1}) from the calorimetric measurements of Fernandez and Hepler.[9] We hope to improve the temperature control of the cell; at present, it is difficult to assess the accuracy of our results but the agreement with this direct measurement of the enthalpy change is encouraging.

For phenol itself Laidler, *et al.*,[10] found $\Delta\bar{H}^0$ = 23,430 j. mole^{-1} (5,600 cal. mole^{-1}) and $\Delta\bar{H}^0$ = 22,430 j. mole^{-1} can be calculated from the data of Binns.[11] Similarly, 22,260 j. mole^{-1} can be calculated for *o*-cresol.[12] For *p*-phenolsulfonic acid[13] in its second stage, where the ionization is of a different charge type, $\Delta\bar{H}^0$ = 16,883 j. mole^{-1}. Thus all of these phenolic acids, in contrast to the aliphatic acids, have large $\Delta\bar{H}^0$ values at 25° and their ionization constants are, therefore, markedly temperature-sensitive.

(7) Recalculated recently from the original data by R. G. Bates and R. Gary, *J. Research Natl. Bur. Standards*, **65A**, 495 (1961).

(8) C. M. Judson and M. Kilpatrick, *J. Am. Chem. Soc.*, **71**, 3110 (1949).

(9) L. P. Fernandez and L. G. Hepler, *ibid.*, **81**, 1783 (1959).

(10) H. M. Papée, W. J. Canady, T. W. Zawidski and K. J. Laidler, *Trans. Faraday Soc.*, **55**, 1734 (1959).

(11) E. H. Binns, *ibid.*, **55**, 1900 (1959).

(12) K. D. Louise, *ibid.*, **56**, 1633 (1960).

(13) R. G. Bates, G. L. Siegel and S. F. Acree, *J. Research Natl. Bur. Standards*, **31**, 205 (1945).

NOTES

A REFERENCE ELECTRODE FOR CERTAIN MOLTEN SALT SOLUTIONS

By George W. Harrington and H. T. Tien

Department of Chemistry, Temple University, Philadelphia, Pa.

Received May 29, 1961

Potentiometric investigations of molten salt systems have become increasingly popular because useful thermodynamic data can be obtained by these methods. The success of any potentiometric study depends on finding a suitable reference electrode. Several types of reference electrodes have been developed to meet this need. These electrodes may be divided into two groups. The first group consists of electrodes with liquid junctions such as the silver–silver nitrate electrode of Flengas and Rideal,[1] the silver–silver chloride electrode of Senderoff and Brenner,[2] and the Pt electrode of Laitinen and Liu.[3] The second group involves a glass barrier or bulb. Notable among these are Delimarskii's glass electrode,[4,5] filled with either sodium amalgam or Na–Sn alloy, and the glass membrane type filled with molten electrolyte as devised by Bockris, *et al.*[6]

A very simple reference electrode composed of Pyrex glass has been developed in this Laboratory which is similar to the electrode of Delimarskii. It differs, however, in that sodium is not necessary inside the bulb and the applicability is not limited to melts containing sodium ions. This is true provided the electrode has been equilibrated in the melt in which the measurements are to be carried out. A particular advantage of this electrode, apart from simplicity of construction, is that it can be used in different molten salt systems.

Experimental

Materials.—All chemicals were of reagent grade and were used directly without further purification except oven drying at 115°. $CoCl_2$ was obtained as the hexahydrate and was dehydrated before use by oven drying at 115°. Cobalt wire was 99.5% Co and B & S gage 18. The mercury in all electrodes was triply distilled.

Preparation of Electrodes.—The cobalt indicator electrode was simply cobalt wire. The wire was polished electrolytically in 50% HCl, in absolute ethanol, rinsed and dried. Cobalt amalgam also was used successfully as the indicator electrode but because of ease of handling the wire was preferred in most cases.

Construction of the reference electrode was very simple. A bulb of approximately 15-mm. diameter was blown on one end of a short length of 5-mm. o.d. Pyrex tubing. The bulb then was filled with either pure mercury, cobalt amalgam or Li–K nitrate eutectic containing 0.8 mole % $CoCl_2$. A platinum or tungsten wire then was inserted down the tube into the liquid in the bulb in order to establish contact with the measuring circuit.

Apparatus.—Using usual notation the cell may be written as: Co; Li–K nitrate or KSCN; glass; Hg. The cell consisted of a 600-ml. tall form Pyrex beaker, which was immersed in a salt-bath of stainless steel containing Li–K nitrate eutectic. The cell was covered with an asbestos pad with holes provided for electrodes, nitrogen gas inlet, thermowell and a port through which increments of $CoCl_2$ could be added. The assembly was heated in a resistance furnace and the temperature controlled by means of a Powerstat. Temperature was measured by a Chromel–Alumel thermocouple and was kept constant during the course of a run to ±1° of the initial value. Cell e.m.f. was measured by a Cary Vibrating-Reed Electrometer (Model 31) and was recorded by a Varian G-10 recorder. The readings were accurate within 1% of scale setting.

Procedure.—Five hundred grams of freshly prepared $LiNO_3$–KNO_3 eutectic was placed in the cell and the temperature was raised slowly to the desired value. Dry nitrogen was bubbled through the melt continuously to provide an inert atmosphere and to agitate the solution. Increments of $CoCl_2$, weighed to within 0.1 mg., were added and voltage readings taken after thermal equilibrium was re-established. The procedure was the same when pure potassium thiocyanate was used as the solvent, in which case this salt was substituted for the eutectic.

Results and Discussion

The results presented below are based on observations made using Li–K nitrate eutectic with pure mercury inside the glass bulb. Exactly analogous results were obtained when KSCN was the solvent. The glass bulb filled with pure mercury gave the best precision compared to bulbs filled with either cobalt amalgam or Li–K nitrate. The temperatures of the runs discussed were within the range 168–180°, held to the limits mentioned above.

Table I

E.m.f.(±1 mv.), mv. Initial	Final	Log Co concn.
290	255	−3.10
249	231	−2.77
228	210	−2.44
207	198	−2.15
180	171	−1.91
153	141	−1.63

Table I is a presentation of data obtained with a typical electrode. Identical results were found for each of eight other glass electrodes except, of course, for shifting of the base line. The initial and final values refer to the e.m.f. just prior to and just after an addition of $CoCl_2$. When either the initial or final values are plotted *vs.* log Co concentration straight lines are obtained. Neither of these lines, however, has a slope that agrees with the value predicted by the Nernst equation. It may be seen in Table I that when the initial value of any particular addition is compared to the final value for the preceding addition considerable drift has occurred. Approximately ten minutes elapsed between increments.

However, when the difference between initial and final values is plotted cumulatively *vs.* log

(1) S. N. Flengas and E. Rideal, *Proc. Roy. Soc.* (London), **A233**, 443 (1956).

(2) S. Senderoff and A. Brenner, *J. Electrochem. Soc.*, **101**, 31 (1954).

(3) H. A. Laitinen and C. H. Liu, *J. Am. Chem. Soc.*, **80**, 1015 (1958).

(4) Yu. K. Delimarskii and R. S. Khaimovkick, *Khim. Zhur.*, **15**, 77 (1949).

(5) Yu. K. Delimarskii and A. A. Kolott, *ibid.*, **16**, 438 (1950).

(6) J. O'M. Bockris, G. J. Hills, D. Inman and L. Young, *J. Sci. Instr.*, **33**, 438 (1956).

Co concentration a straight line is obtained having exactly the slope predicted by the Nernst equation for the cell involved.

Thus it is seen that the cell containing the glass electrode is behaving in the proper fashion once the effect of drift is removed. In order to be a useful reference, however, the electrode must be stable. It was observed that the drift decreased slowly with time, suggesting that an "aging" process was occurring. In order to study this effect the following experiment was set up. Three bulbs, selected at random, were prepared as above and placed in the molten solvent. One of these was arbitrarily selected as reference and the other two measured against it over a period of several days. Voltage readings were taken periodically over each eight-hour working day. For the first two days the voltages changed at rates greater than 50 mv./hr. On the third day one bulb showed a change of 2.5 and the other 6.5 mv./hr. On the fourth and fifth days the rates for each had fallen to less than 0.5 mv./hr. Beyond this time period the e.m.f. showed no further change. Thus five days aging yields a reference electrode that is stable for direct potentiometric measurements. Removal from the melt, washing and drying had no effect on this stability.

Several electrodes were selected at random and aged for one week in Li–K nitrate eutectic. Each then was placed in a cell of the type described earlier and the e.m.f. measured as a function of $CoCl_2$ concentration. Each cell yielded a linear Nernst plot having exactly the predicted slope. No drift was observed in any of these measurements.

On the basis of the information presented above it is not feasible to attempt a complete explanation for the mechanism occurring at this electrode. Certain observations may be made, however. The fact that the material inside the bulb made little difference suggests that this material serves only to establish electrical contact. The glass does not act as a membrane separating electrode compartments. Equilibration seems to follow an exponential rate suggesting a diffusion-controlled process. Once equilibration is established, however, it is apparently quite stable since random agitation (*i.e.*, N_2 bubbling) or complete removal appears to have no effect. Additional investigations are being conducted to answer these questions more fully. It should be pointed out, however, that this investigation, while establishing a useful reference electrode, also has shown the ideal behavior of Co(II) in the solvents studied. The maximum concentration used was 0.1 mole % and to this concentration the solutions behaved ideally. The presence of chloride ion added as $CoCl_2$ apparently has no effect at these concentrations.

H. T. Tien wishes to express his thanks to Dr. D. O. Rudkin, Eastern Psychiatric Institute, for his kind permission to use some of the facilities of the Institute.

NUCLEAR MAGNETIC RESONANCE STUDY OF BORON COÖRDINATION IN POTASSIUM BORATE GLASSES[1]

By S.-E. Svanson, E. Forslind and

Research Group for NMR, Division of Physical Chemistry, The Royal Institute of Technology, Stockholm, Sweden

J. Krogh-Moe

Swedish Institute of Silicate Research, Gothenburg, Sweden

Received June 5, 1961

The coördination of boron in the alkali borate glasses has been studied earlier with n.m.r. by Silver and Bray.[2,3] The B^{11}-resonance indicates that the boron nuclei in these glasses have two different local environments. Due to an anisotropic distribution of electronic charge around the boron nucleus, the resonance line in vitreous boron oxide shows a second-order broadening effect of nuclear quadrupole interaction, and this broad line is assigned to boron in threefold oxygen coördination. By addition of alkali oxide a sharp resonance line is produced which is attributed to the appearance of boron in fourfold coördination belonging to BO_4 tetrahedra with low quadrupole interaction. It would in principle be possible to calculate the amounts of threefold and fourfold coördinated boron in the sample after separation of the overlapping resonance lines and evaluation of the areas under each line. The results of Silver and Bray, however, were evaluated in a very simplified manner from the observed signal amplitudes. As pointed out by the authors themselves their method is likely to overestimate the fraction of fourfold coördinated boron at high alkali content, since the width of the broad line increases with increasing alkali content and, indeed, their measurements (filled circles in Fig. 1) lead to a fraction of fourfold coördinated boron definitely higher than that assumed by Warren[4] and the one observed in some crystalline borates investigated by Krogh-Moe.[5,6]

Warren assumed that boron changes from threefold to fourfold coördination as alkali oxide is added to the glass, supposing each oxygen bonded to two borons at low alkali content, all oxygens being engaged in boron–oxygen bonds. Krogh-Moe[6] has shown that the boron–oxygen networks of crystalline potassium pentaborate,[5] cesium triborate[6] and lithium diborate[7] are built in agreement with the following rule regarding the coördination of boron and oxygen: each "molecule" of alkali oxide added to boron oxide converts two boron atoms from threefold to fourfold coördination. This corresponds to a fraction of boron in fourfold coördination $N_4 = S/(1 - S)$ (shown by the solid line in Fig. 1), where S is the molar alkali concentration. The above rule and expression for N_4 follows from

(1) The Swedish Natural Science Research Council and the State Council of Technical Research have provided financial support and the n.m.r. apparatus cost has been defrayed by grants from the Knut and Alice Wallenberg Foundation.

(2) A. H. Silver and P. J. Bray, *J. Chem. Phys.*, **29**, 984 (1958).

(3) J. D. Mackenzie, "Modern Aspects of the Vitreous State," Vol. 1, Butterworths, London, 1960.

(4) B. E. Warren, *J. Am. Ceram. Soc.*, **24**, 256 (1941).

(5) J. Krogh-Moe, *Arkiv Kemi*, **14**, 439 (1959).

(6) J. Krogh-Moe, *Acta Cryst.*, **13**, 889 (1960).

(7) J. Krogh-Moe, to be published.

the Warren scheme for the region of low alkali oxide content (< 15 mole %). At higher alkali content, however, Warren assumes that some oxygens are bonded only to one boron, in which case the fraction of fourfold coördinated boron should be less than that given by the ratio $S/(1 - S)$. The dashed line in Fig. 1 indicates the values expected by Warren.

In order to investigate further the discrepancy between experimental and theoretical data we have repeated and extended some of Silver and Bray's measurements. During this work we made the observation that there is a close agreement between the spectra of crystalline boron oxide and vitreous boron oxide, from which we infer that the similarity of the spectra is based on a corresponding similarity of the two states with regard to the boron coördination. These findings, on the other hand, suggest the existence of corresponding relationships between other crystalline and vitreous boron compounds. Since the crystalline compounds so far investigated all lie on the theoretical $N_4(S)$ curve, the corresponding vitreous states are expected to yield N_4-values in the close vicinity of the theoretical line, an assumption which actually is borne out by experiment.

In particular, we may refer to a study of potassium borate glass at room temperature. The samples were prepared by melting boric acid and potassium carbonate in a platinum crucible. After solidification, the samples were coated with a plastic to be protected against moisture. The cylinders prepared were 16 mm. in diameter and of 70 mm. length. The compositions were determined by analyses within 0.1%. Spectra were recorded with a Varian-4250 wide line spectrometer at 13.0 Mc./sec. and three different settings of the radiofrequency field. Our recorded spectra were in agreement with those reported by Silver and Bray.[2] A rigorous calculation of the fraction of fourfold coördinated boron based on a detailed analysis of the two lines would, however, require considerable work, while still yielding values of limited accuracy because of the poor signal-to-noise ratio of the recorded broad line spectrum. As the signal-to-noise ratio of the sharp line much exceeds that of the broad one, we have therefore, to a first approximation, chosen to calculate only the area under the sharp absorption line as a measure of the changes in the amount of four-coördinated boron. The area is estimated to be of the magnitude $y'_m \cdot x^{2'}_m$, where y'_m is the ordinate and x_m the abscissa of the maximum of the experimental sharp line derivative, taking the center of the line as origin. For absorption curves of Gaussian or Lorentz line shapes, the area is proportional to this quantity. As y'_m and x_m refer to the central part of the sharp line, the influence on these quantities from the superposition of the broad line could be neglected. The calculated absorption line area is taken to be proportional to the fraction of fourfold coördinated boron and to the volume density of boron atoms in the sample. In this way it was possible to calculate the ratio between N_4-values for samples of different K_2O-content. The method, of course, does not allow an absolute determination of N_4. Our values, shown in Fig. 1 by open circles, therefore have been fitted to the theoretical line $N_4 = S/(1 - S)$ by the method of least squares, yielding a standard deviation from the theoretical value of 3%. A significance test of the deviation indicates that the boron–oxygen coordination in the potassium borate glass is in agreement with the $S/(1 - S)$-rule, in contradiction to the results obtained by Silver and Bray.[2,3]

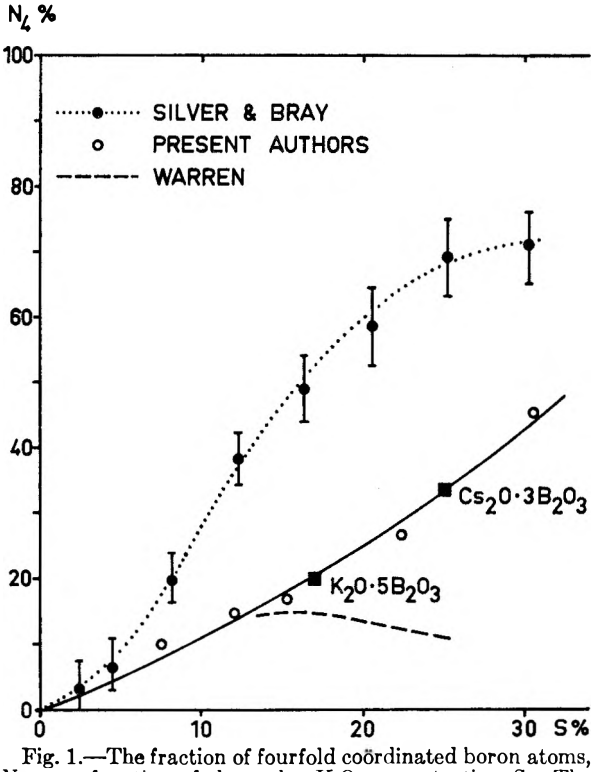

Fig. 1.—The fraction of fourfold coördinated boron atoms, N_4, as a function of the molar K_2O concentration S. The solid line represents the theoretical curve $N_4 = S/(1 - S)$.

THE KINETICS OF THE HYDROLYSIS OF POLYETHYLENE TEREPHTHALATE FILM

BY T. DAVIES, P. L. GOLDSMITH, D. A. S. RAVENS AND I. M. WARD

Research Department, Imperial Chemical Industries Limited, Fibres Division, Hookstone Road, Harrogate, Yorkshire, England

Received June 20, 1961

In a recent paper,[1] Golike and Lasoski have reported results for the hydrolysis of polyethylene terephthalate film. The problem of polyethylene terephthalate degradation has received considerable attention in these Laboratories and a recent account of this work has been given.[2] As our conclusions differ materially from those drawn by Golike and Lasoski, we feel that it is worth considering the experimental evidence of both investigations. We shall show that although the experimental results of Golike and Lasoski are in good agreement with our own, a very different interpretation of these results can be obtained. The principal conclusion of Golike and Lasoski is that the reaction rate is controlled by diffusion of water into the sample. We

(1) R. C. Golike and S. W. Lasoski, *J. Phys. Chem.*, **64**, 895 (1960).
(2) D. A. S. Ravens and I. M. Ward, *Trans. Faraday Soc.*, **57**, 150 (1961).

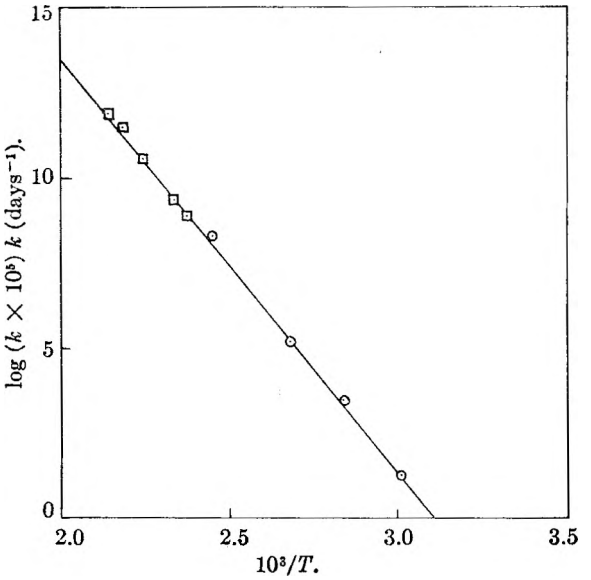

Fig. 1.—O, Golike and Lasoski[1]; □, Ravens and Ward.[2]

believe that this is incorrect, for reasons set out in detail below. First, it is incorrect to ignore the reverse reaction of esterification at low vapor pressures and secondly, at high vapor pressures it can be shown that the diffusion rate is orders of magnitude greater than the reaction rate.

From our results,[2] the rate of end group changes at 150° at 100 and 0.5% relative humidity (r.h.) (Table III[1]) can be calculated. Thus

$$\frac{r_p}{r_h} = K_c \frac{[OH][COOH]}{[EL][H_2O]}$$

where r_p and r_h are the rates of change of [COOH] for esterification and hydrolysis, respectively, and $K_c \simeq 12$. An intrinsic viscosity of 0.56 is equivalent to a total end group concentration[2] of 110×10^{-6} mole/g. of which for this sample[3] [COOH] = 20 and [OH] = 90. Thus at 100% r.h. $r_h \simeq 100\, r_p$ and hence esterification is negligible whereas at 0.5% r.h., $r_p \simeq r_h$.

We also have been able to compare the half-life time (t_R) for the reaction calculated from our results with the half-life time (t_D) for water diffusion using the unpublished results of Small.[4] Small's results also have been confirmed by measurement of the rate of deuteration of the end groups when polyethylene terephthalate is immersed in D_2O, this rate also being diffusion controlled.[5] At 149° under 100% r.h. ([H_2O] in polymer = 400×10^{-6} mole/g.) $t_R = 5.4 \times 10^4$ sec. and from Small's results the diffusion constant $D_{149} = 2.5 \times 10^{-6}$ cm.^{2} sec.$^{-1}$, giving a value for $t_D = 40$ sec. for a film thickness of 0.045 cm.

Further confirmation of our conclusions is shown by a direct comparison of Golike and Lasoski's results at 100% r.h. for 0.0025 cm. film with our results (recalculated using the intrinsic viscosity–molecular weight relationship given[1]) for 0.045 cm. film. This is shown in Fig. 1 and it can be seen that although there is an 18-fold increase in film thickness the agreement is satisfactory. This gives an over-all activation energy of 25 kcal. for hydrolysis, which compares reasonably well with 26 kcal. by McMahon[6] and our own value[2] of 27 kcal. The activation energy for diffusion[4,5] is 14 kcal. The evidence presented here would seem to confirm that diffusion does not control the hydrolysis rate.

In conclusion, there are errors in the mathematics of the diffusion calculations.[1] The approximation $\tanh x/x = 1 - x^2/3$ is only valid for $x < \pi/2$, *i.e.*, $\sqrt{kA/D}\cdot l < 1.57$. Hence in Table III[1] when $\sqrt{kA/D}$ is 625 or 740 the approximation cannot apply when $2l = 0.0075 - 0.0187$ cm. and when $\sqrt{kA/D}$ is 171 it cannot apply when $2l = 0.0187$ cm. It follows that all the derived quantities at 60° are incorrect and, in general, errors ranging from 10–70% have been introduced by the use of this approximation.

We have constructed curves for $\tanh \theta l/\theta l$ (where $\theta = \sqrt{kA/D}$) for values of θ from 50–1000 and compared them with the plots of each row of k' in Table II[1] against "l." Table I gives examples of this comparison for results where the experimental curve is of similar shape to the theoretical curve. Furthermore, there are some conditions where no value of θ gives a good fit, *e.g.*, 130° at 100% r.h. and this leaves doubt as to the adequacy of the theory.

TABLE I

Conditions	$\sqrt{\frac{kA}{D}}$ Golike and Lasoski	Estimated θ
150° 18 mm.	112	90
100° 51% r.h.	132	170
80° 100% r.h.	131	90
80° 51% r.h.	155	70

In view of the incorrect basis of the curves in Fig. 1 of the original paper it may seem surprising that the plot of log k *vs.* $1/T$ is a straight line. The reason for this is that the part of the argument which gives C_0 probably is valid. In addition, the extrapolation from the thinnest film to $l = 0$ is very short and provided that the derivative of the curve of k' *vs.* l is small a reasonable value of kC_0 is given by the calculated values of k' when $l = 0.0025$ cm. Thus the rate constants used in Fig. 2[1] are almost wholly derived from the thinnest film where, on the theory of Golike and Lasoski, diffusion can be most nearly neglected.

(3) R. C. Golike, private communication.
(4) K. W. Small, unpublished results.
(5) I. M. Ward, unpublished results.
(6) H. A. McMahon, *et al.*, *Chem. Eng. Data Ser.*, **4**, 57 (1959).

CONCERNING A SO-CALLED CHECK ON THE INITIAL DEVIATION FROM NEWTONIAN FLOW OF POLYMER SOLUTIONS

BY JOHN F. VOEKS

The Dow Chemical Company, Western Division, Pittsburg, California

Received July 17, 1961

The viscosity of a polymer solution or of a polymeric melt is, in general, non-Newtonian. As has been observed frequently (see for example Oldroyd[1]), the viscosity must be a positive even func-

tion of shear stress or shear rate. This requirement is fundamental so that any valid experimental evidence to the contrary must be of considerable concern and any claim of such data deserves critical examination.

Recently Philippoff and Gaskins[2] have presented data which they claim shows the initial deviation from Newtonian behavior of an essentially monodisperse (with respect to molecular weight), random coil polymer to be an odd function of shear rate. Their data are presented in a graph where the ordinate appears[3] to be $(\eta - \eta_s)/(\eta_0 - \eta_s)$ *vs.* log $\dot{\gamma}$ where η is the viscosity of the solution at the shear rate $\dot{\gamma}$, η_0 is the so-called zero shear viscosity, and η_s is the viscosity of the solvent. In the same figure they plot functions labeled $\eta_{sp}/(1 + x)$ and $\eta_{sp}/(1 + x^2)$. The functions appear to be $1/(1 + b\dot{\gamma})$ and $1/(1 + a\dot{\gamma}^2)$ *vs.* log $\dot{\gamma}$, respectively, where the parameters a and b have been selected to make the agreement between the function and the experimental data as good as possible. On the basis of their figure it is claimed, and indeed it appears true, that the function $(1 + b\dot{\gamma})^{-1}$ gives the best initial fit.

Unfortunately, this test lacks real significance. To show this one need only note, as Philippoff and Gaskins have, that the data corresponding to $(\eta - \eta_s)/(\eta_0 - \eta_s) > 0.90$ scatter so badly as to preclude analysis and then to show that "data" calculated from a suitable even function also appear to be better fit by $(1 + b\dot{\gamma})^{-1}$ than by $(1 + a\dot{\gamma}^2)^{-1}$ over a range comparable to that of the experimental data. Such a comparison is made in Fig. 1. Here, as with the experimental data of Philippoff and Gaskins, the best fit appears to be given by $(1 + b\dot{\gamma})^{-1}$, but in this example it is known that the correct function is positive and even. The difficulty apparently lies with a tendency to confuse the two distinctly different criteria: (1) goodness of fit over an appreciable range at low rates of shear, and (2) goodness of initial fit. The confusion is perhaps unavoidable because of the relatively large experimental errors at low rates of shear and the necessity for estimating initial curvature. In any case, it is apparent that such a test is unreliable.

As a matter of incidental interest, the positive even function plotted in Fig. 1 is the familiar[4,5]

$$\eta = \eta_N + \frac{\chi\beta}{\alpha}\frac{\sinh^{-1}\beta\dot{\gamma}}{\beta\dot{\gamma}}$$

recast for the present purpose as

$$\frac{\eta - \eta_s}{\eta_0 - \eta_s} = \frac{\eta_N - \eta_s}{\eta_0 - \eta_s} + \frac{\chi\beta}{\alpha(\eta_0 - \eta_s)}\frac{\sin^{-1}\beta\dot{\gamma}}{\beta\dot{\gamma}}$$

The constants have been chosen so that

$$(\eta_N - \eta_s)/(\eta_0 - \eta_s) = 0.45$$
$$\chi\beta/\alpha(\eta_0 - \eta_s) = 0.55$$
$$\beta = 10^{-4}$$

The reason for this choice was simply that this combination gives a reasonable fit to the data of Philippoff and Gaskins as the reader easily may verify for himself. One may note that these constants are also in fair agreement with the constants chosen by Kim, *et al.*,[6] to represent the data of Yang[7] on the same polymer under similar conditions. This correspondence is trivial to the present argument except as it shows that the positive even function in Fig. 1 is not some strange thing concocted for the present purpose. The essential point of interest here has not been what even function to choose. It has been to point out that results such as those of Philippoff and Gaskins do not provide a valid test of the form of the initial deviation from Newtonian flow, as has been alleged.

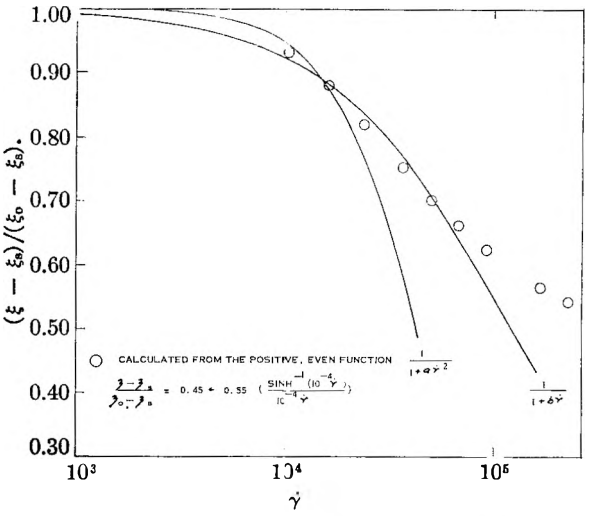

Fig. 1.—Comparison of a positive even function of viscosity *vs.* shear rate with $(1 + a\dot{\gamma}^2)^{-1}$ and $(1 + b\dot{\gamma})^{-1}$.

(1) F. R. Eirich, "Rheology—Theory and Applications," Vol. I, Academic Press, Inc., New York, N. Y., 1956, Chapter 16, J. G. Oldroyd.

(2) W. Philippoff and F. H. Gaskins, *J. Phys. Chem.*, **63**, 985 (1959).

(3) The ordinate axis is denoted by "Specific Viscosity, η_{sp} (Reduced)."

(4) T. Ree and H. Eyring, *J. Appl. Phys.*, **26**, 793 (1955).

(5) T. Ree and H. Eyring, *ibid.*, **26**, 800 (1955).

(6) W. K. Kim, N. Hirai, T. Ree and H. Eyring, *ibid.*, **31**, 358 (1960).

(7) J. T. Yang, *J. Am. Chem. Soc.*, **80**, 1783 (1958).

THE APPARENT MOLAR VOLUME OF SODIUM HYDROXIDE AT INFINITE DILUTION AND THE VOLUME CHANGE ACCOMPANYING THE IONIZATION OF WATER[1]

BY AGNES BODANSZKY AND WALTER KAUZMANN

Frick Chemical Laboratory, Princeton University, Princeton, N. J.

Received July 20, 1961

According to Owen and Brinkley[2] the volume change accompanying the reaction

$$H^+(\infty\ aq.) + OH^-(\infty\ aq.) \longrightarrow H_2O \qquad (1)$$

is 23.4 ml. at 25°. This result was derived from the best available data on apparent molar volumes of the common mineral acids, alkali hydroxides and their salts, extrapolated to infinite dilution. Direct measurements of the volume change of this reaction at finite concentrations using dilatometers give, however, considerably smaller values. Weber and Nachmannsohn[3] observed values of 21.0 ml. when

(1) This work was supported by a grant from the National Science Foundation.

(2) B. B. Owen and S. R. Brinkley, *Chem. Revs.*, **29**, 461 (1941).

(3) H. H. Weber and D. Nachmannsohn, *Biochem. Z.*, **204**, 215 (1929).

0.1 N nitric acid is added to 0.1 N sodium hydroxide and 20.7 ml. when 0.1 N HCl is added to 0.24 N sodium hydroxide. Measurements by one of us[4] give a volume change of 20.8 ml. when equal volumes of 0.1 N hydrochloric acid and 0.1 N sodium hydroxide are mixed to form 0.05 N sodium chloride. It is difficult to believe that the changes in apparent molar volumes that would accompany the infinite dilution of these electrolytes would amount to several ml. We therefore have re-examined the volume changes on dilution of the substances that are involved in this reaction.

Redlich and Bigeleisen[5] found that at 25° in the concentration range 0.0035 to 0.19 M[6] the apparent molar volume of hydrochloric acid is given by

$$\phi = 17.830 + 1.86\sqrt{M} - 1.15M \qquad (2)$$

For sodium chloride at 25° Wirth[7] found between 0.04 and 4 M

$$\phi = 16.435 + 2.010\sqrt{M} + 0.052M \qquad (3)$$

The molar volume of water at 25° is 18.069 ml. Studies of the apparent molar volume of sodium hydroxide have been made only at much higher concentrations, and the extrapolations to infinite dilution are therefore less reliable. Gucker[8] concluded from a survey of data in the literature that

$$\phi = -6.7 + 4.18\sqrt{M} \qquad (4)$$

but the measurements on which this result is based appear to have been made almost entirely in solutions more concentrated than 1 M. Owen and Brinkley[2] concluded that a value of -6.8 for the apparent molar volume of sodium hydroxide at infinite dilution is consistent with values obtained from the ionic volumes deduced from measurements of other hydroxides and salts. None of the volumes of these other hydroxides was obtained from data with solutions more dilute than 0.5 to 1 M. Akerlof and Kegeles[9] measured the apparent molar volumes of sodium hydroxide between 1 and 25 m at temperatures between 0 and 70°. At 25° and between 1 and 3.7 m their equations give

$$\phi = -5.944 + 3.9830\sqrt{m} \qquad (5)$$

Lanman and Mair[10] give apparent molar volumes of sodium hydroxide at 25° at three concentrations between 0.55 and 2.22 m, and their points give

$$\phi = -6.48 + 4.00\sqrt{m} \qquad (6)$$

in fair agreement with the measurements of Akerlof and Kegeles.

We have used dilatometers to measure the volume changes at 30° when water is added to sodium hydroxide solutions. The dilatometers were of the Carlsberg type.[11] The relative amounts of water and alkali solutions used ranged from 6:1 to 1:2, the initial concentration of alkali being in the range 0.125 to 1 M, and the final concentrations in the range 0.65 to 0.06 M.

Let us assume that the apparent molar volume can be expressed by the empirical equation

$$\phi = \phi_0 + S\sqrt{M} + TM \qquad (7)$$

where ϕ_0, S and T are constants. On changing the concentration from M_1 to M_2 we will find

$$\Delta\phi = S(\sqrt{M_2} - \sqrt{M_1}) + T(M_2 - M_1)$$

If we write $\Delta\sqrt{M} = \sqrt{M_2} - \sqrt{M_1}$ and $(\sqrt{M})_{av} = {}^1/_2(\sqrt{M_1} + \sqrt{M_2})$ we obtain[12]

$$\frac{\Delta\phi}{\Delta\sqrt{M}} = S + 2T(\sqrt{M})_{av} \qquad (8)$$

A plot of our measured values of $\Delta\phi/\Delta\sqrt{M}$ against $(\sqrt{M})_{av}$ is shown in Fig. 1. Included on the same graph are points obtained from the measurements of Akerlof and Kegeles at 30° (each point corresponds to a pair of directly measured values of ϕ at two concentrations differing by 20 to 50%, molalities having been converted to molarities). Within the experimental error it is seen that $\Delta\phi/\Delta\sqrt{M}$ is linear with respect to $(\sqrt{M})_{av}$ up to $(\sqrt{M})_{av} \cong 1.6$. Our results are consistent with those of Akerlof and Kegeles. Furthermore, extrapolation to $(\sqrt{M})_{av} = 0$ gives an intercept for $\Delta\phi/\Delta\sqrt{M}$ between 1.8 and 2.0, which is consistent with the slope of the ϕ *vs.* $\Delta\sqrt{M}$ curve at low concentrations predicted by the Debye–Hückel theory.[13,14] The results of measurements on other electrolytes by other workers also are plotted in the same way in Fig. 1. A linear variation of $\Delta\phi/\Delta\sqrt{M}$ with $(\sqrt{M})_{av}$ is found in general at low concentrations, tending to the Debye–Hückel value at infinite dilution, but it is interesting that for hydrochloric acid a marked deviation from linearity sets in at much lower concentrations than for other electrolytes.

The data for sodium hydroxide in Fig. 1 are expressed within the experimental error below $M = 2.5$ by the equation

$$d\phi/d\sqrt{M} = 1.86 + 1.56\sqrt{M} \qquad (9)$$

which on integration gives

$$\phi = \phi_0 + 1.86\sqrt{M} + 0.78M \qquad (10)$$

The magnitude of ϕ_0 may be determined from the observed value of ϕ at a concentration of 1 M, as measured by Akerlof and Kegeles (their concentration units first having been converted to molarities). It is found that when $m = 1$, $M = 1.0016$ and $\phi = -1.63$ at 30°. This gives

$$\phi_0 = -4.27\ (30°) \qquad (10a)$$

which is less negative by 2.4 ml. than the value arrived at by Gucker at 25°. The measurements of Akerlof and Kegeles indicate that at 25°, when $M = 1$, $\phi = -1.96$ ml. If equation 10 remains valid at 25° this gives

(4) W. Kauzmann, unpublished results.

(5) O. Redlich and J. Bigeleisen, *J. Am. Chem. Soc.*, **64**, 758 (1942).

(6) We shall use the symbol M when concentrations are in moles per liter of solution, and the symbol m when they are in moles per 1000 g. of water.

(7) H. E. Wirth, *J. Am. Chem. Soc.*, **62**, 1128 (1940).

(8) F. T. Gucker, *Chem. Revs.*, **13**, 111 (1933).

(9) G. Akerlof and G. Kegeles, *J. Am. Chem. Soc.*, **61**, 1027 (1939).

(10) E. H. Lanman and B. J. Mair, *ibid.*, **61**, 1027 (1939).

(11) K. Linderstrom-Lang and H. Lanz, *Compt. rend. trav. lab. Carlsberg, Ser. Chim.*, **21**, 315 (1938).

(12) *Cf.* the "Chord-area method" of T. F. Young and O. G. Vogel, *J. Am. Chem. Soc.*, **54**, 3030 (1932).

(13) H. S. Harned and B. B. Owen, "The Physical Chemistry of Electrolyte Solutions," Reinhold Publ. Corp., New York, N. Y., 3rd ed., 1958, Chap. 8.

(14) O. Redlich, *J. Phys. Chem.*, **44**, 619 (1940).

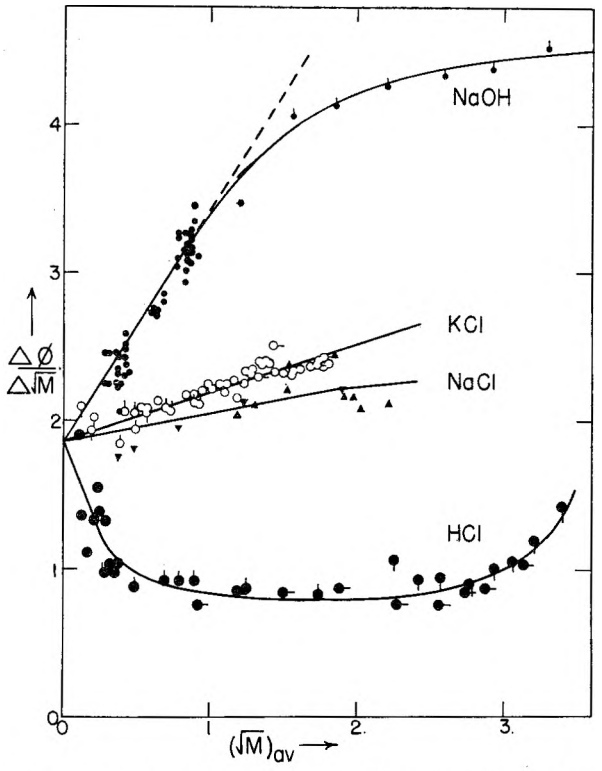

Fig. 1.—Dependence of $\Delta\phi/\Delta\sqrt{M}$ on $(\sqrt{M})_{av}$, where $\Delta\phi$ = change in the apparent molar volume of solute on changing the molarity from M_1 to M_2, $\Delta\sqrt{M} = \sqrt{M_2} - \sqrt{M_1}$, $(\sqrt{M})_{av} = (\sqrt{M_1} + \sqrt{M_2})/2$. NaOH (small filled circles): ●, our measurements; ●, Akerlof and Kegeles.[9] KCl: ○, Kruis[15]; ◔, Wirth[16]; ○, Geffcken[17]; ♀, Geffcken and Price.[18] NaCl: ▲, Geffcken[17]; ▼, Wirth.[7] HCl (large filled circles): ●, Redlich and Bigeleisen[5]; ●, Wirth[7]; ●, Geffcken[17]; ●, Akerlof and Teare.[19]

$$\phi_0 = -4.60\ (25°) \qquad (10b)$$

On combining the above value of ϕ_0 for sodium hydroxide with the values for hydrochloric acid and sodium chloride given in equations 2 and 3, and with the molar volume of water, 18.069 at 25°, we find that the volume change accompanying reaction 1 is 21.28 ml. Furthermore, equations 2, 3 and 10 may be used to calculate the volume change that takes place when equal volumes of hydrochloric acid and sodium hydroxide at molarity M are mixed

$$HCl(M) + NaOH(M) \longrightarrow NaCl(M/2) + H_2O \qquad (11)$$

It is found that for reaction 11

$$\Delta V = 21.28 - 2.30\sqrt{M} + 0.40M \qquad (12)$$

When $M = 0.1$, $\Delta V = 20.56$ ml., which is in good agreement with the value obtained in the dilatometric measurements mentioned above.

Thus it would appear that the apparent molar volumes of alkalies at infinite dilution as well as the volume change of reaction 1, as widely quoted in the literature, are in error by more than two ml.

(15) A. Kruis, *Z. physik. Chem.*, **B34**, 1 (1936).
(16) H. E. Wirth, *J. Am. Chem. Soc.*, **59**, 2552 (1937).
(17) W. Geffcken, *Z. physik. Chem.*, **A155**, 1 (1931).
(18) W. Geffcken and D. Price, *Z. physik. Chem.*, **B26**, 81 (1934).
(19) G. Akerlof and J. Teare, *J. Am. Chem. Soc.*, **60**, 1226 (1838).

MICROWAVE SPECTRUM OF FORMALDOXIME[1]

BY M. G. KRISHNA PILLAI

Department of Chemistry, Rice University, Houston, Texas

Received July 24, 1961

The microwave spectrum of formaldoxime has been studied and the rotational constants have been determined. The molecular dipole moment has been obtained from Stark effect measurements.

Formaldoxime was prepared by mixing an aqueous solution of formaldehyde with a solution of hydroxylamine hydrochloride to which sufficient sodium carbonate had been added to liberate the hydroxylamine.[2] From the mixture formaldoxime was extracted with ether. The polymer of formaldoxime, obtained by the evaporation of the ethereal solution, gives out the monomer when heated.

Zumwalt and Badger[3] have studied the infrared

TABLE I

ROTATIONAL CONSTANTS AND ROTATIONAL TRANSITIONS IN MC.

Rotational constants	Moments of inertia in A.M.U.A.[2]
A = 67,678.5	I_a = 7.4696
B = 11,589.1	I_b = 42.6281
C = 10,080.1	I_c = 50.1514
	Δ = +0.0537

Transition Frequencies

a-type	Obsd.	Calcd.
$0_{00} \rightarrow 1_{01}$	21939.15	21939.2
$1_{01} \rightarrow 2_{02}$	43836.7	43836.5
$1_{11} \rightarrow 2_{12}$	42099.2	42099.4
$1_{10} \rightarrow 2_{11}$	45657.4	45657.4
$3_{12} \rightarrow 3_{13}$	10674.8	10673.4
$4_{13} \rightarrow 4_{14}$	17786.2	17785.7
b-type		
$2_{02} \rightarrow 1_{11}$	11982.6	11983.0
$2_{12} \rightarrow 3_{03}$	11567.0	11567.4
$3_{13} \rightarrow 4_{04}$	35782.3	35782.2

TABLE II

STARK COEFFICIENTS OF CH_2NOH

Lobe		Obsd.	Calcd.
$0_{00} \rightarrow 1_{01}$	$M = 0$	0.086	0.087
$1_{11} \rightarrow 2_{12}$	$M = 0$	.460	.469
$1_{01} \rightarrow 2_{02}$	$M = 0$	− .0308	− .0308
	$M = 1$	.0183	.0176

$\mu_a^2 = 0.152\ D.^2$ $\mu_b^2 = 0.056\ D.^2$

spectrum of this molecule. Of the two possible positions of hydroxyl hydrogen, they prefer the one in which the hydrogen is far away from the carbon atom. They have estimated from infrared fine structure the mean of the larger moments of inertia of the molecule to be between the limits 73.3 × 10^{-40} and 76.8 × 10^{-40} g. cm.^{2}. This estimate was used in searching for the $0_{00} \rightarrow 1_{01}$ transition. In the present investigation it is found that the mean of the two large moments of inertia is 76.49 × 10^{-40} g. cm.^{2}, which is nearer to the upper limit.

A conventional Stark effect microwave spectrometer with a modulation frequency of 100 kc. was

(1) This work was supported by a grant from the Robert A. Welch Foundation.
(2) W. R. Dustan and A. L. Bossi, *J. Chem. Soc.*, **73**, 353 (1898).
(3) L. R. Zumwalt and R. M. Badger, *J. Chem. Phys.*, **7**, 235 (1939).

used in this work. The frequencies of the measured rotational transitions and the rotational constants are given in Table I together with the calculated frequencies using these constants. The rotational constants B and C were fitted to $0_{00} \rightarrow 1_{01}$, $1_{01} \rightarrow 2_{02}$, $1_{10} \rightarrow 2_{11}$ and $1_{11} \rightarrow 2_{12}$ transitions. The rotational constant A was obtained from b-type transitions.[4]

The Stark measurements are listed in Table II. The dipole moment components were calculated from the measurements by the method of Golden and Wilson[5] using the line strength tables of Schwendeman and Laurie.[6] The dipole moment of the molecule is 0.46 D.

The author gives sincere thanks to Dr. R. F. Curl, Jr., for the help received during the course of this work.

(4) The b-type assignment was made after learning from Mr. Ira Levine that it is possible to observe b-type transitions.

(5) S. Golden and E. B. Wilson, Jr., *J. Chem. Phys.*, **16**, 669 (1948).

(6) R. H. Schwendeman and V. W. Laurie, "Line Strengths for Rotational Transitions," Pergamon Press, London, 1958.

A CALORIMETRIC DETERMINATION OF THE OXIDATION YIELD OF THE FRICKE DOSIMETER AT HIGH DOSE RATES OF ELECTRONS[1a]

BY A. R. ANDERSON[1b]

Chemistry Division, Argonne National Laboratory, Argonne, Ill.

Received November 17, 1961

Accurate chemical dosimetry of ionizing radiation has not been established firmly at the very high instantaneous dose rates produced by pulsed electron accelerators. Measurements previously reported by Keene,[2a] by Rotblat and Sutton[2b] and by Glazunov and Pikayev[3] with aerated ferrous sulfate solutions in 0.8 N H_2SO_4 have shown a marked variation in the yield at comparable dose rates. As part of the continuing investigations of radical diffusion kinetics at this laboratory, the radiation chemistry of simple aqueous systems has been studied at high dose rates of electrons[4] requiring an accurate and consistent method of chemical dosimetry. Consequently we have made a calorimetric determination of $G(Fe^{3+})$ for the Fricke dosimeter (0.001 M $FeSO_4$, 0.001 M NaCl, 0.8 N H_2SO_4, aerated), not as a comprehensive study of dosimetry problems at very high dose rates but specifically to provide dosimetry for the irradiation conditions applicable to our chemical studies.

Experimental

All irradiations were carried out with the Argonne Linear Electron Accelerator (Applied Physics Corporation) which generates electrons in pulses from 1.4 μsec. to 5.5 μsec. duration. Our measurements have been made with ~15 Mev. electrons at a pulse length of ~1.4 μsec. which has a rise time of 0.2 μsec. and a decay time of 0.4 μsec. The area of the beam emerging from the exit window is 1 cm.^{2}, the peak current in the pulse is ~0.1 amp. for electron energies from 8 to 15 Mev. and the energy spectrum is constant within 0.5 Mev. of the peak energy. By lowering the current through the filament in the accelerator the dose rate can be reduced at any electron energy but with a reduction by a factor >50 the electron spectrum cannot be determined accurately.

Calorimetry.—The calorimetric measurements have been carried out under geometrical conditions identical with those for the purely chemical measurements,[4] and were designed so that measurements of energy input and chemical change could be made successively on the same irradiation cell without changing the geometry. The ferrous sulfate solution was contained in a cylindrical Pyrex sample cell (3.5 cm. diam., 3.5 cm. long containing about 25 ml. of solution) which is an analog of the irradiated part of the syringe used in the chemical studies.[4] This cell was suspended horizontally by Nylon threads inside an aluminum heating jacket, wound with a copper heating element, which in its turn was mounted inside a container of polystyrene foam to provide a thermal insulation barrier. Copper–constantan thermocouples were attached to various parts of the irradiation cell and located in grooves cut in the aluminum heating jacket.

The calorimeter was used adiabatically with prior electrical calibration over the range of energy input anticipated in the radiation measurements. Adiabatic control was maintained by placing a thermocouple from the sample in opposition to a jacket thermocouple across a sensitive potentiometer and the electrical energy supplied to the jacket adjusted continuously to maintain a temperature difference within the limits ± 1 μvolt ($\pm 0.025°$ with copper–constantan thermocouples). None of the thermocouples was calibrated absolutely as the method of comparative measurements requires only reproducibility of thermocouples during calibration and subsequent measurements. The temperature rise of ~100 μvolts in each case was recorded continuously by feeding the output from each of four thermocouples through a d.c. amplifier (Honeywell, model 2 HLA-7) to a multipoint Honeywell recorder. One of the thermocouples measured the temperature rise of the jacket, which should be equal to that of the sample if adiabatic conditions are maintained. In the electrical calibration, energy was supplied continuously through a tightly wound copper spiral immersed in water in the sample cell while the radiation energy was supplied in short bursts with a frequency ranging from 0.2 to 20 pulses per second depending on the instantaneous dose rate. With good adiabatic control it was assumed that the two methods of heating would give comparable thermal responses for the same energy input.

For measurements at the accelerator the electron beam first was degraded by passage through a polystyrene disc, 9.5 mm. thick,[4] and entered the sample cell *via* holes cut in the front of the outer container and in the heating jacket. A second hole cut in the aluminum jacket directly opposite the first, together with a detachable rear section of the outer container, permitted the visual positioning of the calorimeter by viewing the discoloration spot produced in a watch glass by intense electron bombardment. Once the calorimeter had been centered with respect to the beam it was fixed rigidly and access to the sample cell for pipetting solutions was provided by a detachable cover on the outer container and by a tightly fitting removable lid on the aluminum heating jacket. In this way a series of consecutive calorimetric and ferrous sulfate oxidation measurements was made without changing the fixed geometrical conditions.

Analysis.—Ferric ion concentrations were determined spectrophotometrically at a wave length of 3040 Å., where the molar extinction coefficient is 2225 at 25° and the temperature coefficient 0.7% per degree.

Definition of Dose Rate.—We have used the energy averaged mean intensity as given by Rotblat and Sutton[2b] to define our mean instantaneous dose rate. The contours of the irradiated volume were determined from the color imparted to a block of Plexiglas (density 1.2 g. ml.$^{-1}$) by the electron

(1) (a) Work performed under the auspices of the U.S. Atomic Energy Commission; (b) Chemistry Division, A.E.R.E. Harwell, Nr. Didcot, Berks., England.

(2) (a) J. P. Keene, *Radiation Research*, **6**, 424 (1957); (b) J. Rotblat and H. C. Sutton, *Proc. Roy. Soc.* (London), **A255**, 490 (1960).

(3) P. Ya. Glazunov and A. K. Pikayev, *Doklady Akad. Nauk*, **130**, (5) 1051 (1960).

(4) A. R. Anderson and Edwin J. Hart, *J. Phys. Chem.*, **66**, 70 (1962).

TABLE I

OPTICAL DENSITY DATA FROM IRRADIATED PLEXIGLAS

Wavelength, 3900 Å., r is radial distance from center of disc; Z is distance from point of entry of the beam.

	Optical Density				
	Z(cm.)				
r(cm.)	0.00	0.732	1.524	2.36	3.14
0.00	1.138	1.160	1.117	1.007	0.683
.20	1.112	1.148	1.105	1.000	.677
.40	1.045	1.046	1.068	0.975	.655
.60	.912	1.013	1.000	.928	.609
.80	.604	0.813	0.889	.840	.537
1.00	.276	.503	.663	.710	.460
1.20	.102	.250	.398	.555	.377
1.40	.036	.128	.225	.395	.297
1.60	.017	.078	.129	.260	.221

beam, cutting the irradiated block into thin slabs (0.50 cm. thick) and measuring the radial distribution of optical density at 3900 Å. with a Beckman spectrophotometer. Some of the optical density data are given in Table I. These and other data were programmed on an IBM computer to determine a mean optical density D_m for the irradiated volume of

$$D_m = \int(D\ dv)D / \int D\ dv$$

which leads to an effective irradiated volume $V_{Eff.}$ (as distinct from the total volume[2b]) defined by

$$V_{Eff.} = (\int D\ dv)^2 / \int D^2\ dv$$

From two independent determinations the effective irradiated volume was computed to be 15.3 ± 1.6 ml. Thus the energy averaged mean instantaneous dose rates are given by

$$\frac{\text{total energy absorbed per pulse (ev.)}}{\text{effective irradiated volume (ml.)} \times \text{duration of pulse (sec.)}},$$

and are those pertaining to a pulse assumed to be rectangular.

Results and Discussion.—Linear temperature *vs.* time curves were obtained both during electrical calibration and electron bombardment. In both cases the rate of temperature rise was independent of the thermocouples used for adiabatic control or for temperature rise measurement and was the same for measurements made on the sample cell and on the heating jacket. These observations show that adiabatic conditions were being maintained with both continuous and pulsed energy input. The results of all calorimetric measurements at the accelerator are given in Table II. At each mean instantaneous dose rate the rate of temperature rise was measured at different pulse rates. With constant machine conditions and reproducible adiabatic control the relationship between rate of energy absorption and pulse rate at each instantaneous dose rate should be constant as is shown in Table II, column 4. As the ferrous sulfate oxidation measurements required only about 1 to 2% of the number of pulses needed to achieve a temperature rise of 100 μvolts, they were made alternate to the calorimetric measurements, but only the mean values are quoted in Table II. The rate of energy absorption in the solution is calculated from the measured temperature rise, the experimentally determined calibration value, and the assumption that the total energy is distributed between the solution and glass walls in ratio of their electron stopping powers. As a check on the calorimetric techniques used and the assumptions inherent in the calculations, $G(Fe^{3+})$ was determined in a region of dose rate where there is general agreement that the oxidation yield of the

TABLE II

CALORIMETRY MEASUREMENTS AND FERRIC YIELDS

Measurement	No. of pulses per min.	Rate of temp. rise (μv. min.$^{-1}$)	Energy abs. in 0.8 N H_2SO_4 (ev. ml.$^{-1}$ per pulse × 10^{-13})	μequiv. of Fe^{3+} per pulse	Mean $G(Fe^{3+})$	Mean instantaneous dose rate (ev. ml.$^{-1}$ sec.$^{-1}$ 10^{-22})
Cal.[a]	600	4.81	0.49			
Cal.[a]	900	7.80	0.53			
Cal.[a]	1200	10.15	0.515		15.2 ± 0.4	0.57
Fe^{2+}[b]				0.033 ± 0.005		
Cal.[a]	75	4.57	3.74			
Cal.[a]	100	6.54	4.00			
Cal.[a]	150	9.41	3.83		14.5 ± 0.4	4.31
Fe^{2+}[b]				0.253 ± 0.006		
Cal.[a]	30	9.45	12.1			
Cal.[a]	60	20.6	13.2		11.3 ± 0.5	14.1
Fe^{2+}[b]				0.607 ± 0.009		
Cal.[a]	14.6	3.90	16.8			
Cal.[a]	20	5.24	16.6			
Cal.[a]	30.2	7.90	16.5		12.2 ± 0.5	18.2
Fe^{2+}[b]				0.877 ± 0.012		

[a] Calorimetry measurement. [b] Mean of from 5 to 8 ferrous oxidation measurements.

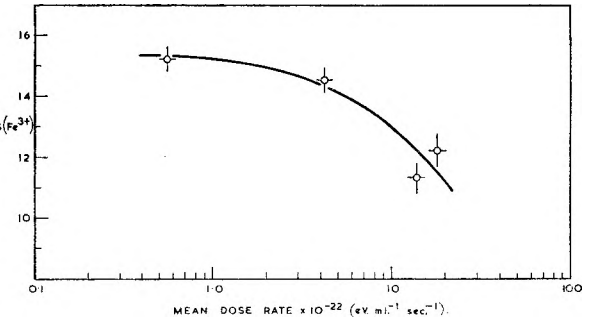

Fig. 1.—Variation of $G(Fe^{3+})$ with mean instantaneous dose rate.

Fricke dosimeter is constant. Our value of $G(Fe^{3+}) = 15.2 \pm 0.4$ at an instantaneous dose rate of 5.7×10^{21} ev. ml.$^{-1}$ sec.$^{-1}$ agrees with the accepted value of 15.6 ± 0.3[5] within the limits of experimental error and lends confidence to the calorimetric techniques used throughout this work.

The ferric yields determined at different instantaneous dose rates are plotted in Fig. 1, where it is seen that at dose rates $> 3 \times 10^{22}$ ev. ml.$^{-1}$ sec.$^{-1}$, $G(Fe^{3+})$ decreases rapidly with increasing dose rate while below 10^{22} ev. ml.$^{-1}$ sec.$^{-1}$ $G(Fe^{3+})$ is almost constant and approaches the accepted value for γ and electron irradiations at much lower dose rates. Other evidence from our chemical studies[4] supports the implication from the ferrous sulfate measurements that at dose rates $> 10^{22}$ ev. ml.$^{-1}$ sec.$^{-1}$, the homogeneous concentration of radicals throughout the solution is high enough for radical–radical reactions to compete with radical–solute reactions. The data from the present work are intermediate between those given by Glazunov and Pikayev[3] and by Keene[2a] and by Rotblat and Sutton.[2b] In the dose rate region where we have carried out most of our chemical studies,[4] *i.e.*, from 1.3 to 2.2×10^{23} ev. ml.$^{-1}$ sec.$^{-1}$, our calorimetric data indicate that the oxidation yield of the Fricke dosimeter can be represented adequately as 11.4 ± 0.5 ions per 100 ev. While these calorimetric data are adequate for our relevant chemical studies it must be emphasized that they are valid only for the particular beam and sample geometry used in this work. More work is required to establish unequivocal radiation dosimetry at dose rates greater than 10^{22} ev. ml.$^{-1}$ sec.$^{-1}$.

Acknowledgments.—It is a pleasure to acknowledge helpful discussions with Drs. E. J. Hart and S. Gordon and experimental assistance from Miss V. Meyers. The author also thanks the U.K.A.E.A. for support on an exchange scheme during the course of this work.

(5) C. J. Hochanadel and J. A. Ghormley, *J. Chem. Phys.*, **21**, 880 (1953).

USE OF KRYPTON FOR SURFACE AREA MEASUREMENTS

BY J. M. HAYNES*

Research Department, English Clays Lovering Pochin & Co. Ltd., St. Austell, Cornwall, England

Received July 28, 1961

The BET treatment of krypton adsorption data has been examined by several authors recently.[1-4] In particular, Gaines and Cannon[2] point out that to bring monolayer volumes of krypton into agreement with those obtained with other adsorbates, values of σ_{Kr}, the molecular area of krypton, ranging between 17.7 and 22.0 Å.[2] have been adopted.

We wish to draw attention to the importance of the value selected for p_0, the saturation vapor pressure of krypton at the adsorption temperature. Although krypton is a solid at 90 and 78°K., the two most commonly used adsorption temperatures, early users of this adsorbate[5,6] recommended that the extrapolated liquid vapor pressure be adopted. It is shown in Table I that the two values differ considerably, and also that agreement between different measurements is not always good.

The value of p_0 used influences the slope (and linearity) of a BET plot, and hence affects both the value of v_m and the ease with which it is obtained. This can be demonstrated by calculating an isotherm according to the BET equation, using a "correct" value p_0 for the saturation vapor pressure, and then replotting the calculated data using an "incorrect" value p_0'. By suitable choice of p_0', BET plots curving in either direction are obtainable.

Malden and Marsh[1] derived v_m values from curved BET plots by drawing a tangent to the curve in the region where v_m occurred. It is our purpose to show that although v_m values derived in this way satisfy the "internal consistency check" used by Gaines and Cannon,[2] they are dependent on the value chosen for p_0, and the extent of this dependence varies inversely as the magnitude of the BET c-constant.

Theory

If a set of adsorption data obeys the BET equation,[7] the volume v of gas adsorbed per gram is related to the pressure p of non-adsorbed gas by the equation

$$y = \frac{x}{v(1-x)} = Ax + B \qquad \text{(i)}$$

where x is the relative pressure p/p_0, and A and B are constants

$$A = \frac{c-1}{v_m c}; \quad B = \frac{1}{v_m c}$$

When x is changed to $x' = \phi x$, the originally straight BET plot becomes curved, the equation to the curve being given by

$$y_2 = \frac{x'}{v(1-x')} = y \times \frac{x'(1-x)}{x(1-x')} = \frac{Ax' + B\phi}{\phi} \times \frac{\phi - x'}{1-x'} \qquad \text{(ii)}$$

A straight line on this graph is of the form

$$y' = \frac{x'}{v'(1-x')} = A'x' + B' \qquad \text{(iii)}$$

where A' and B' are new values of the constants

$$A' = \frac{c'-1}{v_m' c'}; \quad B' = \frac{1}{v_m' c'}$$

If the straight line (iii) is to be tangential to the curve (ii) at the monolayer point defined by (iii), three conditions must be met

I. $y' = y_2$

II. $dy'/dx' = dy_2/dx'$

III. $v = v' = v_m'$

From condition I and equations ii and iii

$$A' = \frac{Ax' + B\phi}{\phi x'} \times \frac{\phi - x'}{1-x'} - \frac{B'}{x'} \qquad \text{(iv)}$$

* Department of Physical and Inorganic Chemistry, The University, Woodlane Road, Bristol 8, England.

(1) P. J. Malden and J. D. F. Marsh, *J. Phys. Chem.*, **63**, 1309 (1959).

(2) G. L. Gaines, Jr., and P. Cannon, *ibid.*, **64**, 997 (1960).

(3) J. M. Thomas, *Nature*, **189**, 134 (1961).

(4) P. Cannon and G. L. Gaines, Jr., *ibid.*, **190**, 340 (1961).

(5) R. A. Beebe, J. B. Beckwith and J. M. Honig, *J. Am. Chem. Soc.*, **67**, 1554 (1945).

(6) A. J. Rosenberg, *ibid.*, **78**, 2929 (1956).

(7) S. Brunauer, P. H. Emmett and E. Teller, *ibid.*, **60**, 309 (1938).

Differentiating equations ii and iii to meet condition II

$$A' = \frac{A}{\phi} \times \frac{\phi - x'}{1 - x'} - \frac{Ax' + B\phi}{(1 - x')^2} \times \frac{1 - \phi}{\phi} \qquad \text{(v)}$$

For condition III, we put $v' = v_m'$ in (iii), and obtain

$$\frac{A' + B'}{B'} = \left(\frac{1 - x'}{x'}\right)^2 \qquad \text{(vi)}$$

Equation vi is another form of the "internal consistency check" used by Gaines and Cannon[2]; its function is merely to ensure that the monolayer point (v_m', x_m'), which must necessarily be on the straight line (iii), is also on the curve (ii). It thus ensures that the data have been fitted in the monolayer region, as recommended by many workers, *e.g.*, MacIver and Emmett.[8]

Eliminating A' and B' between equations iv–vi and arranging as a quadratic in ϕ, we obtain

$$\alpha\phi^2 + \beta\phi + \gamma = 0$$

where

$$\alpha = B(1 - 3x')$$

$$\beta = 2x'^2(B - A)$$

and

$$\gamma = Ax'^2(1 + x') \qquad \text{(vii)}$$

By assigning arbitrary values to v_m and c, the "original" BET constants A and B are fixed. The coefficients in equation vii then can be evaluated for any particular x'. Relevant values of x' can be obtained by trial and error; they will lie close to, but not equal to, the values satisfying equation vi with $A' = A$ and $B' = B$. A series of values of ϕ (in pairs) thus will be obtained, corresponding to a series of values of x'. Equations iv and v then can be solved as a pair of simultaneous equations in A' and B', using each value of x' with its corresponding value of ϕ in turn. Hence the "new" values of v_m' and c' can be expressed in terms of the "original" values for a series of values of ϕ, which is a measure of the extent to which the "new" saturation vapor pressure p_0' of the adsorbate differs from the "original" value p_0. Thus, by an algebraic procedure equivalent to drawing a tangent at the monolayer point, v_m' and c' have been evaluated from a curved BET plot, where the curvature arises from the use of an inappropriate value of p_0'.

In this work, v_m always was given the value unity, and the calculation was performed for "original" values of c of 3, 10, 30 and 100. The results, shown in Fig. 1, demonstrate that the choice of p_0' affects the measured values of v_m' and c' to an extent which varies inversely with the "original" value of c. The maximum in c' corresponds to the condition $\beta^2 = 4\alpha\gamma$ in equation vii, and pairs of roots of this equation give equal values of c' symmetrically disposed about the maximum.

Discussion

At the high pressure end of a krypton adsorption isotherm measured below 115.6°K. it obviously is appropriate to use the vapor pressure of the solid; for example, Cosgrove[9] found that this was necessary in order to obtain reasonable Kelvin pore radii. This vapor pressure is measured readily by taking

(8) D. S. MacIver and P. H. Emmett, *J. Phys. Chem.*, **60**, 824 (1956).

(9) L. A. Cosgrove, *ibid.*, **60**, 385 (1956).

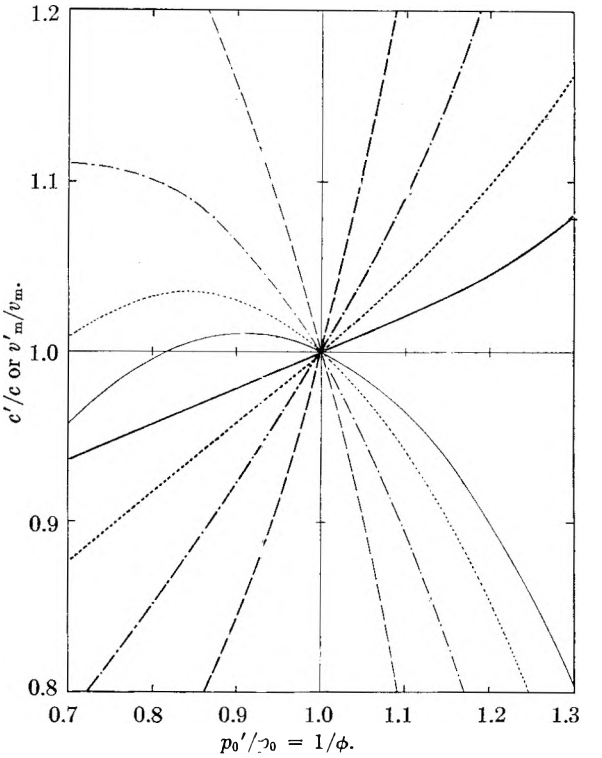

Fig. 1.—Variation of v_m'/v_m (thick lines) and c'/c (thin lines) with p_0'/p_0, for several original values of c: – – – –, c = 3; –·–·–, c = 10; ———, c = 30; ———, c = 100.

TABLE I

RECORDED VALUES OF VAPOR PRESSURE OF KRYPTON

p_0 (mm.) at 77.8°K.	90.1°K.	Ref.	Notes
		(a) Solid	
2.893	20.06	[a]	Interpolated from results at several temp.
1.972	20.50	[b]	
1.926	20.14	[c]	
2.630	22.00	[c]	Extrapolation at lower temp.
1.950	21.48	[b]	Extrapolation at higher temp.
1.753 ± 0.002	...	[e]	Measured at 77.60 ± 0.01° K.
1.754 ± 0.002	...	[f]	Measured at 77.3 ± 0.5°K.
		(b) Liquid	
2.748	27.13	[g]	Extrapolated from results at higher temp.
3.822	32.05	[h]	
4.753	33.22	[i]	
4.608	33.62	[g]	
2.63	27.1	[j]	Quoted without source
..	27.5	[k]	

[a] E. Justi, *Physik. Z.*, **35**, 571 (1935). [b] M. P. Freeman and G. D. Halsey, text ref 11. [c] W. H. Keesom, J. Mazur and J. J. Meihuizen, *Physica*, **2**, 669 (1935). [d] N. A. Lange, "Handbook of Chemistry," Handbook Publishers Inc., Sandusky, Ohio, 8th Ed., 1952, p. 1459. [e] G. L. Kington and J. M. Holmes, *Trans. Faraday Soc.*, **49**, 417 (1953). [f] S. Chu Liang, *J. Appl. Phys.*, **22**, 148 (1951). [g] J. J. Meihuizen and C. A. Crommelin, *Proc. Acad. Sci. Amsterdam* **39**, 1088 (1936). [h] A. Michels, T. Wassenaar and Th. G. Zweitering, *Physica*, **18**, 63 (1952). [i] G. L. Gaines, Jr., and C. P. Rutkowski, text. ref. 10. [j] R. Rudham and F. S. Stone, *Trans. Faraday Soc.*, **54**, 420 (1958). [k] B. B. Fisher and W. G. McMillan, *J. Phys. Chem.*, **62**, 494 (1958).

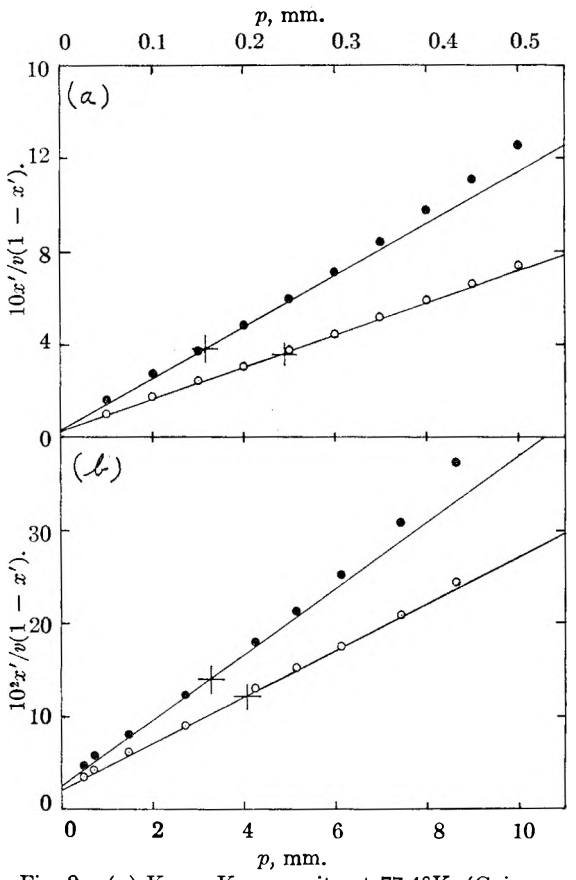

Fig. 2.—(a) Kr on K-muscovite at 77.4°K. (Gaines and Rutkowski[10]); (b) Kr on H-kaolinite at 90.1°K. Solid circles, solid vapor pressure; open circles, supercooled liquid vapor pressure. The BET constants of the straight lines are: (a) $p_0 = 1.753$ mm., $v_m = 0.257$, $c = 105.3$; $p_0 = 2.63$ mm., $v_m = 0.272$, $c = 96.4$; (b) $p_0 = 20.78$ mm., $v_m = 1.31$, $c = 29.3$; $p_0 = 27.1$ mm., $v_m = 1.44$, $c = 31.9$.

the adsorption to saturation. Two such measurements (at 77.6°K.) are listed in Table I, and show excellent agreement.

By contrast, in the monolayer region, the use of the solid vapor pressure can lead to curved BET plots. This difficulty is largely overcome by following Beebe, Beckwith and Honig's original recommendation[5] that the extrapolated liquid vapor pressure should be used. For example, Fig. 2a shows Gaines and Rutkowski's data for krypton adsorption at 77.4°K. on 60–80 mesh muscovite,[10] calculated for $p_0' = 2.63$ mm. (the extrapolated liquid vapor pressure used by them), and $p_0 = 1.753$ mm., and plotted according to the BET equation. Figure 2b shows previously unpublished data from this Laboratory for krypton adsorption at 90.1°K. on a kaolinite sample, also plotted according to the BET equation, with $p_0' = 27.1$ mm. (again the extrapolated liquid value used by Gaines and Rutkowski) and $p_0 = 20.78$ mm. (a recently measured value for the solid).[11] In both cases, a curved BET plot results from the use of the solid vapor pressure, while the use of the higher values for p_0' reduces the curvature greatly, although still higher values are needed to eliminate it in the monolayer region.

It is noticeable that the isotherm with the lower BET c-constant is the more sensitive to choice of p_0'. This is in agreement with the foregoing calculations, which show that as c approaches infinity the value used for p_0' becomes immaterial as regards its effect on v_m' and c'.

Fisher and McMillan,[12] studying the adsorption of krypton on sodium bromide between 66 and 84°K., found that the use of the extrapolated liquid vapor pressure gave a wider linear BET range, more consistent values of c, and values of v_m in better agreement with those obtained with other adsorbates than if the true (solid) vapor pressure were used. Similarly, Daneš and Nováková[13] found that in the monolayer region argon isotherms measured below the melting point agreed better with those measured above the melting point if plotted on a relative pressure scale using the extrapolated liquid vapor pressure at the lower temperature.

It should be noted that the procedure of using a value p_0' not equal to the true value p_0 obtaining at saturation, established by long practice in the case of krypton, is not compatible with the original BET assumption that the evaporation–condensation properties of the second and all subsequent layers are the same as those of the bulk adsorbate. In the derivation of the BET equation, quantities $g_i = (a_i/b_i)\exp(E_i/RT)$ are introduced, where a_i and b_i are, respectively, the condensation and evaporation coefficients in the i-th adsorbed layer, and E_i is the heat of adsorption in that layer. It then is assumed (i) that $g_2 = g_3 = \ldots = g_\infty = g$, (*i.e.*, that the evaporation–condensation properties of the second and higher layers are identical); and (ii) that $g = 1/p_0$, (*i.e.*, that these properties are those of the bulk adsorbate *at the adsorption temperature*).

Dole[14] has investigated the effects of variable heats of adsorption beyond the second layer, and both Fergusson and Barrer[15] and Theimer[16] have shown that if simple assumptions can be made concerning the decay of heats of adsorption with increasing coverage, an isotherm equation similar to that of BET can be obtained, containing additional constants to define the physical conditions imposed. Clearly, the simple form of the BET equation can have no absolute validity when used in conjunction with an incorrect value p_0' in place of p_0.

Since, however, the BET equation normally is expected to fit data in the monolayer region only, it may happen that the use of a particular value p_0' (being approximately equal to $1/g_2$) will give a satisfactory BET plot. Gaines and Cannon's considerations[2] of the energetics of adsorption suggest that such a procedure may be possible with krypton in particular, since multilayer formation is delayed until formation of the first monolayer is almost complete.

One would expect to find that $g_1 > g_2 \geqslant g_\infty$, and hence $p_0' \leqslant p_0$. In fact it is found that for krypton below its melting point a p_0' of the order of 50%

(10) G. L. Gaines, Jr., and C. P. Rutkowski, *J. Phys. Chem.* **62**, 1521 (1958).

(11) M. P. Freeman and G. D. Halsey, *ibid.*, **60**, 1119 (1956).

(12) B. B. Fisher and W. G. McMillan, *J. Chem. Phys.*, **28**, 549 (1958).

(13) V. Daneš and J. Nováková, *Chem. listy*, **52**, 382 (1958).

(14) M. Dole, *J. Chem. Phys.*, **16**, 25 (1948).

(15) R. R. Fergusson and R. M. Barrer, *Trans. Faraday Soc.*, **46**, 400 (1950).

(16) O. Theimer, *ibid.*, **48**, 326 (1952).

greater than p_0 gives linear BET plots in the region of monolayer coverage. This implies that the second adsorbed layer is considerably more disordered than the bulk adsorbate, and that as further adsorbed layers are built up, the decay of adsorption forces originating from the solid is offset by an increasing degree of order in the adsorbate layers. Anderson[17] also found that the range of linearity of BET plots was increased by using a value of p_0' higher than p_0.

The object of plotting adsorption data according to the BET equation is to obtain repeatable values of the constant v_m, for the purpose of comparing, not necessarily on an absolute basis, the surface areas of various adsorbent samples. For this reason, it seems justifiable to adopt a value of p_0' which will give, in as many cases as possible, straight BET plots from which v_m' may be obtained. It is not suggested that the BET equation is sufficiently well-founded to enable its use as a criterion for the selection of the correct value of a physical constant such as the saturation vapor pressure of krypton. On the contrary, the empirical nature of the BET theory when applied in conjunction with a value of the saturation vapor pressure other than the true one at the adsorption temperature is regarded as justification for a wholly empirical choice of p_0'; this procedure seems in any case to be necessitated by the scatter in the recorded vapor pressure data. The choice of the supercooled liquid vapor pressure to represent p_0' appears to have no more theoretical validity, and less practical value, than the choice of a p_0' which will give a straight BET plot.

The selection of the best value of p_0' is best made by examination of adsorption data on surfaces giving low c-constants, since these are more sensitive to such choice. On the basis of a number of isotherms on various clay minerals, similar to that in Fig. 1, our preliminary conclusion that p_0' = 30 cm. at 90.1°K. gives the most linear BET plots, and, when used in conjunction with a molecular area σ_{Kr} of 18.5 Å.,[2] consistent agreement is obtained with nitrogen monolayer volumes. However, the c-constants used all lie between 30 and 100, and the examination of isotherms with lower c-constants may well yield a better choice of p_0'.

An alternative, avoiding this difficulty altogether, would be to plot krypton adsorption data according to the Harkins–Jura relative equation.[18,19] The specific surface is determined from the slope of such a plot without reference to the value of p_0, by application of an empirical constant derived from measurements on a solid of known area. The BET method also requires such a calibration to obtain the value of σ_{Kr}; however, σ_{Kr} is dependent on p_0', whilst the Harkins–Jura constant is not.

Referred to a solid vapor pressure of 21 mm. at 90.1°K., our value of p_0' gives $\phi = 0.70$, whereas Gaines' value[10] gives $\phi = 0.77$. Other values of the extrapolated liquid vapor pressure quoted in Table I give ϕ as low as 0.62. Figure 1 shows that considerable variation in v_m' is to be expected from the use of these various values of p_0', especially on surfaces giving low c-constants. Since σ_{Kr} is evaluated by comparison of krypton monolayer volumes with those obtained with other adsorbates, it is clear that this quantity cannot be determined reliably without standardizing the choice of p_0', and the variability in the reported value of σ_{Kr}, mentioned by Gaines and Cannon,[2] easily could have arisen from this cause alone. Similarly, the reasons for the existence of curvature in BET plots cannot be discussed without reference to the value of p_0' used in obtaining them, except in cases where c is high enough to render the BET plot relatively insensitive to the choice of p_0'.

Acknowledgments.—This note is published by permission of the Research Director of English Clays Lovering Pochin & Co. Ltd. The author is indebted to Mr. P. J. Malden for invaluable discussions.

(17) R. B. Anderson, *J. Am. Chem. Soc.*, **68**, 686 (1946).
(18) W. D. Harkins and G. Jura, *J. Chem. Phys.*, **11**, 431 (1943).
(19) W. D. Harkins and G. Jura, *J. Am. Chem. Soc.*, **66**, 1366 (1944).

CUBIC CADMIUM SULFIDE

BY H. AHLBURG AND R. CAINES

Research Division, Raytheon Company, Waltham, Massachusetts

Received August 3, 1961

Cadmium sulfide crystals of large size have been grown only in the hexagonal form (α-CdS) no matter whether the crystals were grown from solution,[1,2] from the vapor phase,[3,4] or from the melt under pressure.[5-7] Using X-ray diffraction methods, Bohm and Niclassen[8] showed that CdS precipitated under certain conditions can have the cubic (β-) or zincblende structure; this result was confirmed by Ulrich and Zachariasen.[9] Milligan[10] investigated the structure of CdS precipitated from salt solutions at different temperatures. Stuckert[11] described conversion from α- to β-CdS, while Rittner and Schulman[12] reported essentially the opposite result. Traill and Boyle[13] found that a mineral of very small grain size hitherto assumed to be greenockite (α-CdS) was actually β-CdS. Sato[14] reported growth of both α- and β-CdS from solution on a lead sulfide substrate. Drickamer[15] assumed that a discontinuity in the optical absorption edge shift at 27,500 atm. implies transformation to the cubic phase at this pressure.

Experiments on Crystal Growth.—Our attempts to prepare macroscopic β-CdS crystals will now be described. Although our objective of growing such crystals was not

(1) E. T. Allen, J. L. Crenshaw and H. E. Merwin, *Am. J. Sci.*, [4] **34**, 341 (1912).
(2) A. Krembeller, A. K. Levine and G. Gasburov, *J. Electrochem. Soc.*, **107**, 12 (1960).
(3) D. R. Hamilton, *Brit. J. Appl. Phys.*, **9**, 104 (1958).
(4) L. C. Greene, D. C. Reynolds, S. J. Czyzak and W. M. Baker, *J. Chem. Phys.*, **29**, 1375 (1958).
(5) A. Fischer, *Z. Naturforsch.*, **13a**, 105 (1958).
(6) A. Addamiano and M. Aven, *J. Appl. Phys.*, **31**, 36 (1960).
(7) J. Medcalf and R. Fahrig, *J. Electrochem. Soc.*, **105**, 719 (1958).
(8) Bohm and Niclassen, *Z. anorg. u. allgem. Chem.*, **132**, 7 (1923).
(9) F. Ulrich and W. Zachariasen, *Z. Krist.*, **62**, 260 (1925).
(10) W. O. Milligan, *J. Phys. Chem.*, **38**, 797 (1934).
(11) L. Stuckert, *Die Glashuette*, **39**, 611 (1935).
(12) E. S. Rittner and J. H. Schulman, *J. Phys. Chem.*, **47**, 537 (1943).
(13) R. J. Traill and R. W. Boyle, *Am. Mineralogist*, **40**, 555 (1955).
(14) R. Sato, *Nature*, **184**, 2005 (1959).
(15) A. L. Edwards, T. E. Slykhouse and H. G. Drickamer, *J. Phys. and Chem. Solids*, **11**, 140 (1959); A. L. Edwards and H. G. Drickamer, *Phys. Rev.*, **122**, 1149 (1961).

achieved, we believe the information collected may be of interest. Since it is known that α-CdS is the stable form at temperatures above 800°, growth from the melt was ruled out. Growth from the vapor phase and many chemical transport methods furthermore cannot be used at low enough temperatures.

Cadmium sulfide exhibits very low solubility at normal temperature and pressure in all non-reacting solvents. In pure water at 25° its solubility is 1.5×10^{-10} mole/l.[16] Preparation of CdS from solution leads to high supersaturation which gives rise to spontaneous nucleation and hence minute crystallites. We tried to avoid excessive supersaturation in order to favor the growth of fewer nuclei into larger crystallites.

Some of Allen and Crenshaw's[1] experiments using salt solutions therefore were repeated and extended. Following Milligan,[10] we varied the temperature (0 to 100°), pressure (10 to 800 mm. of H_2S), Cd^{++} concentration (1 to 120 mg./ml.), and *p*H (H_2SO_4 or HNO_3, *p*H 2.5 to 0.5) of the nutrient solution. In some experiments we used alkaline Na_2S solutions. In others we added a wetting agent, sodium lauryl sulfate. Sulfur compounds such as thiourea $(NH_2)_2CS$, thioacetamide CH_3CSNH_2, and sodium thiosulfate $Na_2S_2O_3$ were employed as sources that would release sulfur ions slowly. In all these experiments, the particle size of the resultant precipitate did not exceed 1 or 2 μ.

In agreement with Milligan, the best cubic X-ray pattern and the coarsest grains were obtained when CdS was precipitated by bubbling H_2S through a boiling solution of $CdSO_4$ (10 g. Cd^{++} per liter) in dilute H_2SO_4 (20 ml. per liter).

Electron microscope examination[17] showed powder prepared this way consisted of spherical particles with an average diameter of 0.8 to 1 μ; no crystal faces were evident. On the other hand, when a Cd^{++} solution at 0° was mixed with water which had been saturated with H_2S near 0°, the resulting fine powder consisted of roughly spherical fragments 0.15 μ in diameter, but exhibiting cube corners and edges. This material thus showed better, although minute, crystals but its X-ray pattern indicated the presence of some hexagonal CdS.

Hydrothermal growth was attempted at seed temperatures between 120 and 250°, well below the 350° where hydrothermal treatment reported by Kremheller, *et al.*,[2] had yielded α-CdS. Seeds of cubic ZnS, HgS,[18] or mica were used. Precipitated β-CdS powder served as nutrient. Practically no growth was observed, yet the temperature was high enough to turn the nutrient CdS into the hexagonal modification. This result ruled out the hydrothermal method. Other growth methods which proved to be unsuitable included an aqueous circulation method, Allen and Crenshaw's double tube method, dissolving CdS in molten sulfur, and ion diffusion in water. In no case was significant cubic growth observed. Schneider's[19] method of growth also appeared useless because of the temperature necessary.

Transition Temperature.—According to Ulrich and Zachariasen,[9] β-CdS is transformed into the hexagonal form between 700 and 800°. If the transformation rate is high enough, one observes conversion of the thermodynamically unstable form into the one which is stable at that temperature, but never the reverse. (See ref. 1, 3, 5 on ZnS.) Samples of both α-[20] and β-material were heated *in vacuo* from 200 to 700° in steps of approximately 100° for five days at each temperature. These runs gave evidence of the conversion of the β- to α-material, the α-modification being completely stable. Conversion occurred at temperatures between 400 and 450°, the rate increasing with temperature.

Several differential thermal analysis runs supported these findings in general. The smallness of the effect, however, limited interpretation of the curves to general aspects.

Solvents facilitated conversion. The X-ray patterns of samples of each polymorph, which had been sealed individually in tubes containing distilled water and heated for several days at 220°, showed transformation of β- to α-CdS. At 130°, this transformation was not noticeable.

In another experiment, we checked the work of Stuckert[11] on the room temperature conversion of α-CdS to β-CdS in strong acid solution (50 ml. H_2SO_4 per liter). Samples of both α- and β-material were each immersed for one week in small stoppered tubes of this solution. No evidence of conversion in either direction could be observed from X-ray patterns of the resulting dried powders. If heated between 150 and 200°, conversion of the β-CdS to α-CdS was observed.

In order to check the results of Rittner and Schulman[12] cubic and hexagonal powder was immersed in a highly concentrated solution of ammonium hydrogen sulfide NH_4HS, and left at room temperature for three days. Transformation from β- to α-CdS occurred but not the reverse, confirming Rittner and Schulman's statements. At 5°, no transformation from β- to α-CdS could be detected after 5 days.

In agreement with Rittner and Schulman, we find the hexagonal modification of CdS is stable above 20°. If the cubic modification is stable at atmospheric pressure, it can only be below 20°. Identification of the exact transition temperature is limited by the infinitesimal reaction rate at low temperature.

Acknowledgments.—We wish to thank Dr. O. J. Guentert, Mr. W. R. Bekebrede and Mr. R. Hawkes for X-ray measurements and interpretation, Dr. J. Van Hook and Mr. C. Snider for taking differential thermal analysis curves, and Mr. R. C. Ellis, Jr., and Dr. D. M. Warschauer for many discussions and suggestions.

(16) S. F. Ravitz, *J. Phys. Chem.*, **40**, 61 (1936).

(17) Kindly done by Professor P. Dorain, Brandeis University, Waltham, Mass.

(18) Kindly supplied by Professor C. Frondell, Mineralogy Department, Harvard University, Cambridge, Mass.

(19) R. Schneider, *J. prakt. Chem.*, [2] **8**, 38 (1873).

(20) Luminescent grade CdS from the General Electric Co., Lamp Division, Cleveland, Ohio.

THE DIELECTRIC CONSTANT AND LOSS OF IRON PENTACARBONYL AT MICROWAVE FREQUENCIES

W. D. HORROCKS, JR., AND E. N. DICARLO

Department of Chemistry, Princeton University, Princeton, N. J.

Received August 2, 1961

The structure of iron pentacarbonyl has been the subject of considerable controversy. Some time ago Bergmann and Engel[1] and Graffunder and Heymann[2] found dipole moment values of 0.62 and 0.81 *D* for $Fe(CO)_5$ in benzene solution. The atom polarization was taken as zero in the above work, so these values can be considered only upper limits for a permanent dipole moment. More recently Weiss[3] measured the dipole moment of $Fe(CO)_5$ in benzene solution at radiofrequencies and found a value of $\mu = 0.63 \pm 0.06$ *D*, assuming zero atom polarization. In order to make the static dipole moment vanish it was necessary to assume an atom polarization equal to 20% of the electronic polarization, P^E. For $Ni(CO)_4$[4] an atom polarization of 5% of the P^E yields a zero dipole moment.

Evans and Lister[5] interpret their electron diffraction data in terms of a trigonal bipyramidal (D_{3h}) structure which would have no dipole moment. On the other hand, O'Dwyer[6] analyzed his infrared data in terms of a tetragonal pyramidal (C_{4v}) configuration. More recently

(1) E. Bergmann and L. Engel, *Z. physik. Chem.*, **13B**, 232 (1931).

(2) W. Graffunder and E. Heymann, *ibid.*, **15B**, 377 (1932).

(3) E. Weiss, *Z. anorg. u. allgem. Chem.*, **287**, 223 (1956).

(4) L. E. Sutton, R. G. New and J. B. Bentley, *J. Chem. Soc.*, 652 (1933).

(5) R. V. G. Evans and M. L. Lister, *Trans. Faraday Soc.*, **35**, 681 (1939).

(6) M. F. O'Dwyer, *J. Mol. Spectroscopy*, **2**, 144 (1958).

Cotton, *et al.*,[7] have re-examined the infrared spectrum of $Fe(CO)_5$ and failed to observe two bands crucial to O'Dwyer's argument. Other infrared investigations[8,9] and several normal coordinate analyses[10-12] support the D_{3h} structure. The Raman shifts observed recently by Stammreich, *et al.*,[13] also are consistent only with the non-polar structure.

In the present investigation the dielectric constant, ϵ', and dielectric loss, ϵ'', of pure liquid $Fe(CO)_5$ were measured at wave lengths of 1.25 and 3.22 cm. with an apparatus described elsewhere.[14] The dielectric constant also was measured at radiofrequencies. The results are shown in Table I.

TABLE I

Wave length, cm.	ϵ'	ϵ''	τ, sec.	μ, D
1.25	2.6209	0.00986	3.35×10^{-12}	0.15
3.22	2.6178	0.00465	28.5×10^{-12}	0.10
577 m.	2.6257	.....	.....	..

All measurements were taken at 20° on a triply-distilled sample of iron pentacarbonyl and all operations were carried out in subdued light. Using the data of Table I, estimates of the magnitude of the dipole moment were made from the equation[15]

$$\mu^2 = \frac{27kT(1 + \omega^2\tau^2)\epsilon''}{(\epsilon' + 2)^2 4\pi cN\omega\tau} \qquad (I)$$

The values of the relaxation time, τ, were determined in a somewhat approximate manner from the linear plot of ϵ' *vs.* $\epsilon''\omega$,[16] assuming a Debye line shape. Dipole moments of 0.15 and 0.10 D were calculated from the 1.25 and 3.22 cm. data, respectively. Although there is a large discrepancy in the calculated relaxation times, τ, for the two sets of data, it was found that using values of τ between the two calculated values tended to alter the calculated dipole moment, μ, only to a small extent (0.01 to 0.03 D) in both cases. Equation I yields a value of $\mu = 0.04$ D for benzene.[15] The values found for the dielectric loss of $Fe(CO)_5$ are considerably larger than those noted for some other non-polar molecules. Bleaney[17] measured some typical non-polar substances. The loss values for these are shown in Table II.

TABLE II

LOSS VALUES OF NON-POLAR SUBSTANCES

Wave length, cm.	1.35	3.2
Benzene	0.0012	0.00050
Carbon tetrachloride	0.00175	0.00069

Whiffen[18] has suggested that the losses in non-polar substances arise from the relaxation of small instantaneous dipole moments induced in the molecules by inter-molecular collisions in the liquid state. It is probable that a similar mechanism will account for the loss found in iron pentacarbonyl. This molecule possesses three infrared active fundamental vibrations between 90 and 110 cm.$^{-1}$.[7] It is these low-lying fundamentals which contribute heavily to the atom polarization and make the molecule easily susceptible to collision-induced dipole moments. Nickel tetracarbonyl has only two infrared active low-lying fundamentals and might be expected to have a smaller atom polarization than the iron compound. The limited data available[4] seem to confirm this. In $Fe(CO)_5$ the measured loss at 1.25 cm. is higher than the loss at 3.22 cm., which is consistent with the variation of loss with frequency observed by Whiffen[18] in several non-polar compounds. The findings of the present work are consistent with the D_{3h} structure of the undeformed $Fe(CO)_5$ molecule, the discrepancy between the total polarization and the electron polarization being due to a large atom polarization contribution and the presence of collision-induced instantaneous dipoles.

Acknowledgment.—We wish to thank Professor C. P. Smyth and Dr. W. E. Vaughan for their encouragement and many helpful discussions. One of us (E. N. DiC.) is indebted to the Esso Foundation for financial assistance in the form of a fellowship.

(7) F. A. Cotton, A. Danti, J. S. Waugh and R. W. Fessenden, *J. Chem. Phys.*, **29**, 1427 (1958).

(8) R. K. Sheline and K. S. Pitzer, *J. Am. Chem. Soc.*, **72**, 1107 (1950).

(9) W. F. Edgell (private communication quoted in ref. 7).

(10) W. G. Fateley and E. R. Lippincott, *Spectrochim. Acta*, **10**, 8 (1957).

(11) H. Murata and K. Kawai, *J. Chem. Phys.*, **28**, 516 (1958).

(12) C. W. F. T. Pistorius and P. C. Haarhoff, *ibid.*, **31**, 1439 (1959).

(13) H. Stammreich, O. Sala and Y. Tavares, *ibid.*, **30**, 856 (1958).

(14) W. M. Heston, Jr., A. D. Franklin, E. J. Hennelly and C. P. Smyth, *J. Am. Chem. Soc.*, **72**, 3443 (1950).

(15) W. M. Heston, Jr., and C. P. Smyth, *ibid.*, **72**, 99 (1950).

(16) R. H. Cole, *J. Chem. Phys.*, **23**, 493 (1955).

(17) B. Bleaney, J. H. N. Loubser and R. P. Penrose, *Proc. Phys. Soc.* (London), **59**, 185 (1947).

(18) D. H. Whiffen, *Trans. Faraday Soc.*, **46**, 124 (1950).

THE FORMATION CONSTANTS OF THE TANTALUM FLUORIDE SYSTEM. II. TANTALUM ELECTRODE POTENTIAL STUDIES[1]

BY LOUIS P. VARGA AND HARRY FREUND

Contribution from the Department of Chemistry, Oregon State University Corvallis, Oregon and the U. S. Bureau of Mines, Albany, Oregon

Received August 9, 1961

In a previous report[2] it was demonstrated that potentiometric hydrogen ion measurements and anion exchange distribution studies in perchloric acid solutions of Ta(V) and fluoride ion yielded the formation function between fluoride ligand numbers 4 and 9. This paper describes tantalum electrode–hydrogen electrode potential measurements made in 1 molal perchloric acid over the same fluoride ion concentration range covered in the previous studies. Apparent reversible behavior was found at fluoride ion concentrations above 4×10^{-4} molar in agreement with Haissinsky and coworkers.[3]

Since several tantalum fluoride species exist at

(1) Abstracted in part from the Ph.D. thesis of Louis P. Varga, Oregon State University, June, 1960. Presented at the 139th National Meeting, Am. Chem. Soc., St. Louis, Mo., March 30, 1961.

(2) L. P. Varga and H. Freund, *J. Phys. Chem.*, **66**, 21 (1962).

(3) M. Haissinsky, *Comite itern. thermodynam. et cinet. electrochim. Compt. rend. reunion*, 222 (1951); M. Haissinsky, A. Coche and M. Cottin, *J. chim. phys.*, **44**, 234 (1947).

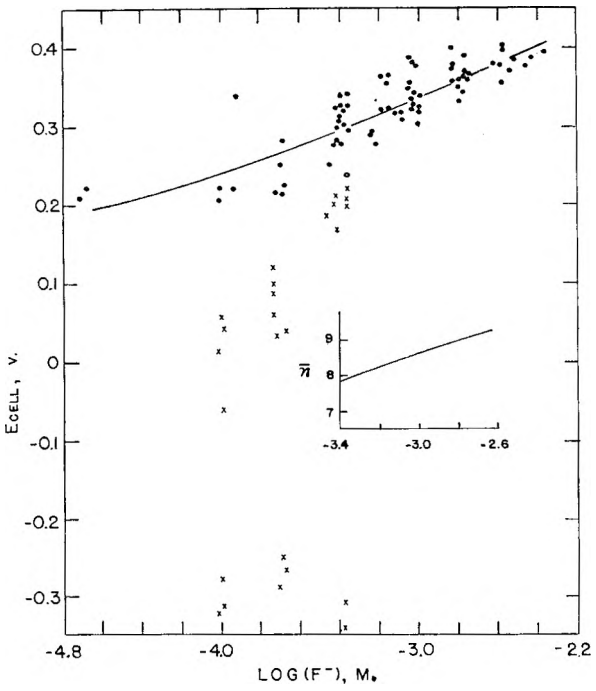

Fig. 1.—● Reversible or normal; × irreversible. Tantalum electrode cell potentials and the average tantalum fluoride ligand number as a function of log (F^-). The least squares quadratic equation for the potential curve drawn is $E_{cell} = 0.769 + 0.182 \log (F^-) + 0.013[\log (F^-)]^2$. Interpretation of the potential data beyond the limits of the insert is not justified using a quadratic function.

equilibrium at the surface of the electrode, the cell reaction with the hydrogen electrode may be written

$$Ta^0 + 5H^+ + \bar{n}F^- = TaF_n^{5-\bar{n}} + 5/2\ H_2 \quad (1)$$

The corresponding Nernst equation at 25° is

$$E_{cell} = E^{0\prime} + \frac{0.0591}{5}\bar{n}\log(F^-) - \frac{0.0591}{5}\log\frac{(TaF_n^{5-\bar{n}})(H_2)^{5/2}}{(H^+)^5} \quad (2)$$

where $E^{0\prime}$ contains the activity coefficient quotient term. Partial differentiation of E_{cell} with respect to log (F^-) gives

$$\frac{\partial E_{cell}}{\partial \log(F^-)} = \bar{n} \times \frac{0.0591}{5} \quad (3)$$

where it is seen that the slope of the E_{cell} *vs.* log (F^-) plot at constant metal and acid concentration is a direct measure of $\bar{n}$.[4] It should be noted that the derivation of equation 3 requires no knowledge of the tantalum species reversible to the metal electrode and analysis of potential data by equation 3 will give no information as to the species measured.

Experimental Procedure.—Potential measurements were made between tantalum metal electrodes and a hydrogen electrode without liquid junction in a series of solutions containing 1 molal perchlorate ion and 0.02 to 12 molar hydrofluoric acid. Repeat potential measurements were made at 15 to 30 minute intervals until two or three measurements indicated the absence of drift. The average tantalum electrode potentials have been tabulated.[1]

(4) I. Leden, *Z. physik. Chem.*, **A188**, 160 (1941).

All solutions were analyzed for total fluoride content by titration with thorium nitrate. The tantalum concentration increased slowly due to solution of the tantalum electrode in the acid fluoride medium. The hydrogen ion concentration of each solution was determined from potential measurements of the hydrogen electrode against a normal calomel electrode with liquid junction as detailed in reference 1. The fluoride ion concentrations were calculated from the total HF and hydrogen ion concentrations as described previously.[2]

Hydrofluoric and perchloric acids used for solution make-up were analytical reagent grade. The tantalum metal electrodes were made from Fansteel thin dental sheeting and from rolled tantalum sheet produced at the U. S. Bureau of Mines, Albany, Oregon. Spectrographic analyses of both metal samples have been reported.[1] The potentiometer and associated equipment were the same as used previously.[2] The cell container was partially immersed in a water-bath at 25 ± 0.1°, as was the calomel electrode. Plastic equipment was used throughout for all fluoride-containing solutions.

Polarization Studies.—A potential of 3.0 to 4.5 volts applied between the tantalum electrode as cathode and an adjacent bright platinum electrode as anode was intended as an electropolishing device. Since we were not dealing with a uniform surface such as a mercury pool, it was anticipated that vigorous evolution of hydrogen gas or some similar mechanical or chemical action by electrolysis would condition the natural crystalline nature of the tantalum electrode so that its potential would be reproducible. With solutions of log (F^-) greater than −3.4, it was observed that after such treatment the tantalum electrode potential changed rapidly at first, finally reaching a steady value in the range considered reversible. In log (F^-) concentrations of −3.4 and below, erratic behavior was encountered suggesting that an oxide layer was dissolved at least partially at the higher fluoride concentration but not at the lower concentration. The data are shown plotted in Fig. 1.

After anodic polarization of the tantalum electrode for one minute periods up to 0.040 microampere, the electrode potential returned to the original steady-state value after a few seconds in solutions of the higher fluoride concentration. Again the tantalum electrode behaved as if an oxide coating were dissolved slowly by the aqueous acid fluoride to give a surface which behaved in a normal manner. Whether the tantalum electrode was ever behaving reversibly toward some tantalum species in solution generally could not be proved by polarization tests. The tests did show that immersion in acidic HF solutions of sufficient concentration caused the tantalum electrode to become active and approach a potential in a predictable range. It is doubtful whether the exchange current for deposition of tantalum metal from solution approached the magnitude of the reverse current but this mechanism for reversible behavior is clouded by the continued forward corrosion reaction of the tantalum metal in the acid fluoride solution. Assuming that the experimental potentials approached the reversible potentials, an analysis may be made.

Results and Conclusions—The experimental potentials of the cell Ta/Ta(V), HF(1 *m* ClO_4^-)/H_2Pt as a function of log (F^-) are plotted in Fig. 1. The vertical scatter of the potential is inherent in the behavior of solid metal electrodes, even at the higher fluoride concentrations. A least squares fit of the 78 data points considered to be in the reversible or normal range was made to a quadratic function. The resultant equation

$$E_{cell} = 0.769 + 0.182 \log (F^-) + 0.013[\log (F^-)]^2 \quad (4)$$

is shown as the curve plotted in Fig. 1. The first derivative of equation 4

$$d E_{cell}/d \log (F^-) = 0.182 + 0.026 \log (F^-) \quad (5)$$

yields an analytical expression for the slope which may be substituted directly into equation 3 to give values of $\bar{n}$ as a function of log (F^-). Such a formation curve is shown as an insert in Fig. 1 over the fluoride ion concentration range for which the data would appear to be most applicable. This formation curve for the tantalum fluoride system is seen to be about one-half of an $\bar{n}$ unit higher in this fluoride region than the formation curve found previously.[2] This agreement is satisfactory considering the difficulties of the system, and the assumption that the cell approaches reversible behavior appears justified. No new calculation of a set of formation constants was made, but the results did strengthen the evidence for the existence of the species TaF_9^{-4}, although in a statistical sense only.

The solubility of Ta_2O_5 may be inferred from the studies by assuming from Fig. 1 that E^0 for the reaction of equation 1 was near 0.35 v. at the higher fluoride concentrations. Upon subtracting the tantalum fluoride half-reaction of equation 1 from Latimer's[5] half-reaction for the oxidation of tantalum to the pentoxide one obtains

$$2TaF_n^{5-n} + 5H_2O = Ta_2O_5 + 2nF^- + 10H^+, \; E^0 \cong 0.4 \text{ v.} \quad (6)$$

The free energy change favors the reaction from left to right as written. This agrees with observation since the salt K_2TaF_7 when dissolved in pure water is hydrolyzed to give an acid solution. Very thin oxide films and freshly precipitated hydrated tantalum oxide dissolve in sufficiently strong hydrofluoric acid, but the massive crystalline oxide such as is formed after sintering the hydrate at 1000° for several hours is hardly affected by the cold acid.

This work was supported by a coöperative agreement between Oregon State University and the U. S. Bureau of Mines, Albany, Oregon.

(5) W. M. Latimer, "Oxidation Potentials," 2nd ed., Prentice Hall, Englewood Cliffs, N. J., 1952.

GASEOUS OXIDES OF RHENIUM[1]

BY MARTIN H. STUDIER

Argonne National Laboratory, Argonne, Illinois

Received August 14, 1961

Several gaseous rhenium oxides have been detected with a Bendix Time of Flight Mass Spectrometer.[2] During a study of surface ionization,[3] neutral species were volatilized (at temperatures below 500°) from rhenium surfaces on which samples in nitric acid had been evaporated. Ions produced by electron bombardment of the gaseous species were identified by their masses and corresponded to the empirical formulas

Monomers	Dimers
Re^+	Re_2^+
ReO^+	Re_2O^+
ReO_2^+	$Re_2O_2^+$
ReO_3^+	$Re_2O_3^+$
ReO_4^+	$Re_2O_4^+$
	$Re_2O_5^+$, $Re_2O_5^{++}$
	$Re_2O_6^+$
	$Re_2O_7^+$, $Re_2O_7^{++}$

Gaseous oxides still were observed after they had been evaporated from the filament and the source had cooled to room temperature. As the source was warmed gradually the intensity of the oxide ion beams increased and the oxides were observed to fractionate with respect to each other.

Since Re_2O_7 has the highest mass of any oxide observed, it must be a primary gaseous product. All the lower dimeric oxides are primarily fragmentation products of the ionizing electron beam. Relatively high electron energies are required to produce the lower mass dimeric ions. In addition, at a given electron energy the dimeric forms were found to remain in constant ratio to each other with large variations in time, temperature and vapor pressure.

The highest mass monomeric oxide, ReO_4, is also a primary gaseous product for it was frequently observed in the absence of oxides of greater mass.

Although both ReO_3^+ and ReO_2^+ are formed in abundance by fragmentation of higher oxides, marked fractionation of ReO_2^+, ReO_3^+ and ReO_4^+ with respect to each other and to the dimeric forms suggests that both ReO_2 and ReO_3 have an independent gaseous existence. ReO^+ and Re^+ were observed as fragmentation products only.

It is of interest to note that the oxide ion ReO_3^+ appears at masses 233 and 235. It is possible that it may interfere with uranium isotopic analyses when rhenium filaments are used in surface ionization sources.

(1) Based on work performed under the auspices of the U. S. Atomic Energy Commission. Presented in part at the Ninth Annual Meeting (June, 1961) of the A.S.T.M. Committee E14 on Mass Spectrometry.

(2) D. B. Harrington, "Encyclopedia of Spectroscopy," Reinhold Publ. Corp., New York, N. Y., 1960, pp. 628–647.

(3) M. H. Studier, E. N. Sloth and L. P. Moore, *J. Phys. Chem.*, **66**, 133 (1962).

COMMUNICATIONS TO THE EDITOR

ON THE "DIMPLING" DURING THE APPROACH OF TWO INTERFACES[1]

Sir:

It is well established[2-6] that when a drop or bubble approaches a surface, especially a solid one, it rapidly "dimples," *i.e.*, acquires a reverse curvature so that a central lens of liquid is entrapped by a thinner "barrier ring." Although a qualitative explanation was given with the first observation,[2] this behavior still is considered not well understood.[6] Furthermore, despite the fact that the existence of the dimple depends on the deformability of at least one surface, the slow changes occurring as the dimple gradually thins have been successfully interpreted[3,6] in terms of Reynolds' formula for the approach of two parallel rigid discs.

We now have developed a purely hydrodynamic theory of the stability and evolution of the dimple which does not require any rigidity of any surface involved (so that dimpling is to be expected also for small soap films[7,8] in the absence of marginal regeneration[9]) and is applicable provided that at least one of the surfaces involved does not dilate (*i.e.*, does not expand radially) under the stresses involved. The theory neglects double layer, structural and van der Waals effects which may give important corrections but shows that these are not essential for the existence of the dimple.

For the simplest case when the surface approached is a rigid plane and buoyancy is the only driving force, the radius r_0 of the barrier ring formed by a bubble or radius R, effective density ρ, and interfacial tension γ is given[2] by

$$r_0 = R^2(2\rho g/3\gamma)^{1/2}$$

In the approximation of nearly flat surfaces[9] the flow in the neighborhood of the barrier ring is determined by the radial pressure gradient represented by $-\gamma \mathrm{d}^3z/\mathrm{d}r^3$, where z is the distance separating the two surfaces and r the distance from the center of the area of contact.

The flow Q through the ring per unit length of periphery is then

$$Q = (\gamma/3n^2\eta)z^3\mathrm{d}^3z/\mathrm{d}r^3$$

where n, the number of non-dilating surfaces, is now unity if the bubble surface dilates freely, and equals two when it does not dilate.

After the dimple is formed, we may disregard the fractional variation in periphery and the difference between inflow and outflow of the entrapping barrier ring; thus we treat Q as independent of radius and are led to the differential equation

$$\mathrm{d}^3\left(\frac{z}{b}\right)\Big/\mathrm{d}\left(\frac{r-r_0}{a}\right)^3 = \left(\frac{b}{z}\right)^3$$

where $a = 3\eta Q n^2 r_0^4/16\gamma T^4$; $b = 2Ta/r_0$; T is the maximum thickness of the dimple and η the viscosity. The numerical solution of this equation having unit asymptotic slope on the left is shown in the figure and represents the barrier ring profile as determined by purely hydrodynamic forces. In this solution the ordinate of the minimum is 1.25, the asymptotic curvature at the right 1.22.

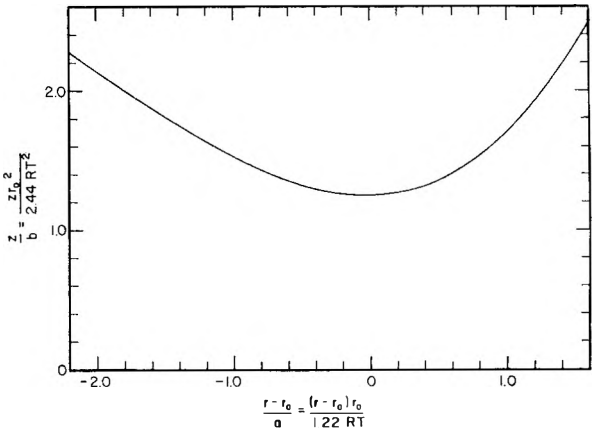

Fig. 1.

The thickness T in the middle of the dimple as a function of time t is given by

$$T = (0.0096 r_0^6 \eta n^2/\gamma R t)^{1/4}$$

The numerical factor is $3/1.22 \times 2^8$. The minimum thickness z_0 of the barrier ring is given by

$$z_0 = 3.05RT^2/r_0^2 = (0.060 n^2 R^5 \rho g \eta/\gamma^2 t)^{1/2}$$

The numerical factors are $1.25 \times 1.22 \times 2$ and $1.25^2 \times 1.22/2^5$, respectively.

This is dimensionally similar to the expression derived on the basis of Reynolds' formula for rigid parallel discs, and when neither surface dilates ($n = 2$), the numerical coefficients are within 2% ($4 \times 0.060 = 0.24$ *vs.* 0.25) of each other. On the other hand, Reynolds' formula is based on the assumption of uniform thickness in the entire area under pressure, hence requires $z_0 = T$, *i.e.*, there can be no dimple, while our result shows that $z_0/T \propto T$, *i.e.*, the dimpling persists at all times, becoming relatively more pronounced as the surfaces approach.

The same results apply as long as the total curvature in the dimple area is negligible, and the above argument can be modified readily to cover the case when pressure difference and flexibility of

(1) Supported in part by a grant from four oil companies (Mobil, Ohio, Shell, and California Research).

(2) B. V. Derjaguin and M. Kussakov, *Acta Physicochim. U. R. S. S.*, **10**, 25 (1939).
(3) G. A. H. Elton, *Proc. Roy. Soc.* (London), **A194**, 275 (1948).
(4) L. F. Evans, *Ind. Eng. Chem.*, **46**, 2420 (1954).
(5) P. S. Prokhorov, *Discussions Faraday Soc.*, **18**, 41 (1954).
(6) R. S. Allan, G. E. Charles, and S. G. Mason, *J. Colloid Sci.*, **16**, 150 (1961).
(7) B. V. Derjaguin and A. S. Titijevskaja, *Discussions Faraday Soc.*, **18**, 27 (1954).
(8) A. Scheludko, *Kolloid Z.*, **155**, 39 (1957).
(9) K. J. Mysels, K. Shinoda, and S. Frankel, "Soap Films," Pergamon Press, New York, N. Y., 1959

the surface combine to give the dimple a significant over-all curvature.[10]

4974 PALO DRIVE, TARZANA, CALIFORNIA
STANLEY P. FRANKEL
CHEMISTRY DEPARTMENT
KAROL J. MYSELS
UNIVERSITY OF SOUTHERN CALIFORNIA
LOS ANGELES 7, CALIFORNIA

RECEIVED NOVEMBER 8, 1961

(10) D. C. Chappelear, *J. Colloid Sci.*, **16**, 186 (1961); H. Princen, private communication.

ACTIVATION ENERGIES OF GAS-PHASE OXIDATIONS

Sir:

The over-all activation energies of oxidation reactions in the gas-phase sometimes can be used to calculate the activation energy of one of the elementary reactions occurring in the system.[1] However, not only, of course, must the mechanism postulated be substantially correct, but the over-all activation energy must also be a true measure of the variation of the reaction rate with temperature.

For the oxidation of propionaldehyde between 128 and 226° with a fixed aldehyde pressure of 50 mm. and oxygen pressures of 10, 15, 25 and 100 mm. the log maximum rate *versus* $1/T$ °K. plots, using rates from pressure–time data, showed deviations from linearity at the higher temperature (see the figure for typical results). The activation energies, calculated from the linear portions of the graphs, ranged from 9 kcal./mole at "low" oxygen pressures to 16.5 kcal./mole at "high" oxygen pressures. Under all conditions the rate became markedly less dependent on temperature between 180 and 226°. On the other hand the log maximum rate, measured from analytical data on the loss of oxygen in the system, *versus* reciprocal temperature plots were linear over the temperature range employed. The over-all activation energies were found to be larger than those derived from the pressure–time curves, and varied from approximately 12 kcal./mole with 10 mm. to 21 kcal./mole with 100 mm. oxygen pressure.

Similar results have been obtained for the oxidation of isobutene in the presence of hydrogen bromide. Over the temperature range 100–190° the log maximum rate (pressure–time data) *versus* $1/T$ °K. plot was distinctly curved (see figure), the over-all activation energy varying from 4.5 kcal./mole at low temperatures to 11.5 kcal./mole at high temperatures. However, the Arrhenius plot for the maximum rates, measured from data on the loss of oxygen, again was linear, the activation energy being 15.8 kcal./mole.

It is interesting to note that for both systems the over-all activation energy was higher when determined from data on oxygen loss than from pressure changes in the vessel. This is because the proportionality factor given by $(d\Delta P/dt)_{max}/(dP_{O_2}/dt)_{max}$, while independent of reactant pressures at any one temperature, decreased with increase of temperature. The results stress the care necessary in using pressure–time data as criteria of oxidation rates.

(1) *E.g.*, A. Combe, M. Niclause and M. Letort, *Revue Inst. Franç. du Petrole*, **10**, 786, 929 (1960).

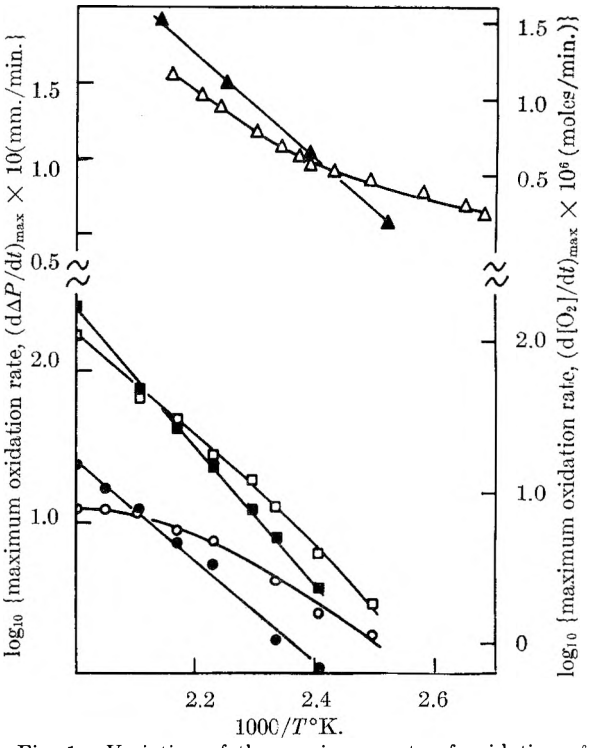

Fig. 1.—Variation of the maximum rate of oxidation of propionaldehyde and of isobutene in the presence of hydrogen bromide with temperature. Open symbols refer to results from pressure–time data; closed symbols refer to results from analytical data on loss of oxygen: △, isobutene and oxygen pressure, 140 mm., HBr pressure, 20 mm.; □, propionaldehyde pressure 50 mm., oxygen pressure, 100 mm.; ○, propionaldehyde pressure, 50 mm., oxygen pressure, 15 mm.

The decrease in the activation energy of propionaldehyde oxidation as the oxygen pressure is reduced can be explained in terms of the increased importance of the decomposition of the propionyl radical under oxygen deficient conditions. Attention has been drawn previously to the probability that carbonyl radical decomposition is the major source of carbon monoxide in many low temperature oxidations.[2]

DEPARTMENT OF INORGANIC AND PHYSICAL CHEMISTRY
THE UNIVERSITY
LIVERPOOL
GREAT BRITAIN
P. HURST
G. SKIRROW
C. F. H. TIPPER
B. P. WHIM

RECEIVED DECEMBER 12, 1961

(2) G. Skirrow and C. F. H. Tipper, Seventh Symposium on Combustion (1959), Butterworths, London, p. 134.

AN IMPROVED METHOD OF TRANSPORT NUMBER MEASUREMEMENT IN PURE FUSED SALTS

Sir:

We have developed a new method for measuring transport numbers in pure fused salts and have found it to have important advantages over other methods now in use. We describe it here briefly in anticipation of a fuller account at a later date.

The method devised by Duke and Laity[1] probably is the most reliable now in use for measurements on pure fused salts. A brief review of their technique provides a background against which to compare our method. In essence, Duke and Laity employ a cell comprising two electrode compartments connected by two tubes. The first tube contains an ultra-fine porosity plug designed for maximum hydraulic resistance and low electrical resistance. The second connecting tube is a horizontal capillary containing a gas bubble. This path, in the ideal case, is one of infinite electrical resistance and zero hydraulic resistance. When current is passed through the cell, the volume change which accompanies the ion-transport process and the electrode reaction is measured by observation of the bubble motion in the second connecting tube.

Matter transport during conduction in a fused salt creates a hydrostatic pressure difference between the two electrode compartments with a resulting hydraulic back flow. The Duke and Laity cell attempts to prevent this back flow by use of a plug of high hydraulic resistance and by use of the bubble-tube, which is intended to reduce the hydrostatic head to a small value and at the same time serve as an indicator of the volume change. Shortcomings of the method have been discussed by Lorenz and Janz,[2] who have shown that the bubble indicator possesses neither infinite electrical resistance nor zero hydraulic resistance. Frictional forces at the bubble interface can, in some cases, permit sizable build-up of hydrostatic pressure and consequent hydraulic leakage through the porous plug. A final criticism is that the excessive surface-to-volume ratio of the ultra-fine porous plugs, which must be used, may yield transport properties which are not the same as those of the bulk electrolyte.

The new method which we have developed substitutes a measurement of the mass transport during electrolysis for the volume measurement of Duke and Laity. Our cell consists of two electrode compartments connected by a tube containing a medium-porosity fritted Pyrex plug (pore diameter, 10–15 μ). The distance between the centers of the two compartments is equal to the length of the beam of an analytical recording balance, and the cell is suspended below the pans of the balance. The fine suspension wires also serve to carry the electrical current to the silver electrodes in each compartment. The cell is enclosed in a furnace capable of maintaining temperature to $\pm 1°$. To this point, our measurements have been confined to an electrolyte of molten silver nitrate.

When current is applied to the cell the balance records the motion of its center of mass. At the start of an experiment the hydrostatic pressure difference is zero and the change in mass results solely from the transport process. As matter moves from one side of the cell to the other a hydrostatic head is created, which, in turn, causes hydraulic back flow. The result is a weight-change *vs.* time recording which is very close to a straight line at the beginning, thereafter shows a decreasing slope, and finally reaches an asymptote when a steady state is reached between electrical transport and hydraulic flow.

Our medium porosity plug has a leakage rate of 1.8 g. of $AgNO_3$ per hour per centimeter of hydrostatic head—100 times greater leakage-rate than for plugs used by previous investigators.[3] Despite this, with currents of 25–50 ma. applied to our cell, the weight–time recordings are almost straight lines for times of one hour and more. Calculations show that, for these conditions, hydraulic leakage through the plug causes an error of only 3 parts in 1000 in the initial slope of the weight–time recording for a test of 30-minute duration. We use the initial slope of the recording to calculate the transport number of silver, and, in this calculation, the error in the slope causes an error only half as large (percentage-wise) in the transport number.

At present, the sensitivity of our measurements is about 1 mg., and we expect to improve on this by design alterations. This sensitivity corresponds to a volume change of about 2.5×10^{-4} ml. of molten silver nitrate—a much better precision than can be obtained by the Duke and Laity technique. It is this greatly increased sensitivity which is responsible for many of the advantages of our method. Since we require a much smaller amount of material transport to obtain an accurate measurement, the hydrostatic head which develops is correspondingly small. Thus the need of a bubble indicator is eliminated, with all of its attendant problems. Likewise, the ultra-fine porosity plug is not necessary. An additional advantage is that from the change in slope of the weight–time curve we can distinguish the flow of matter due to hydraulic backflow from that due to electro-migration in experiments of long duration or with plugs or capillaries of low hydraulic resistance.

With our present techniques we have definitely established a small temperature dependence for the transport number of silver in silver nitrate, as these reproducible results show:

at 219°, $T_{Ag} = 0.781 \pm 0.006$
at 281.5°, $T_{Ag} = 0.744 \pm 0.010$

These are to be compared with $T_{Ag} = 0.76 \pm 0.05$ at 225° and 275°, obtained by Duke and Laity,[4] and $T_{Ag} = 0.72 \pm 0.06$ at 350°, reported by Duke and Owens.[5] By improving the design of the apparatus, we expect a further increase in precision. This will permit more detailed investigation of the temperature dependence of the transport number, as well as secondary effects such as the presence of impurities in the melt and the nature of the material of the porous plug.

HENRY KRUMB SCHOOL OF MINES
DEPARTMENT OF MINERAL ENGINEERING
COLUMBIA UNIVERSITY HERBERT H. KELLOGG
NEW YORK 27, N. Y. PAUL DUBY

RECEIVED SEPTEMBER 5, 1961

(1) F. R. Duke and R. W. Laity, *J. Am. Chem. Soc.*, **76**, 4046 (1954); *J. Phys. Chem.*, **59**, 549 (1955).

(2) R. M. Lorenz and G. J. Janz, *ibid.* **61**, 1683 (1957).

(3) G. Harrington and B. S. Sundheim, *ibid.*, **62**, 1454 (1958).

(4) R. W. Laity and F. R. Duke, *J. Electrochem. Soc.*, **105**, 97 (1958).

(5) F. R. Duke and B. Owens, *ibid.*, **105**, 548 (1958).

THE RING INDEX *Second Edition*

A List of Ring Systems Used in Organic Chemistry

by Austin M. Patterson
Leonard T. Capell
Donald F. Walker

This index, published in 1960, provides a single source where structural formulas, names and numberings of the thousands of parent organic ring systems can be found. Since the first edition (1940) the number of ring systems has almost doubled.

features This new edition lists 7727 organic ring systems—almost a hundred percent increase over the first edition. It has been enlarged to 1425 pages to cover the abstracted literature through 1956. Each ring system contains: (1) a structural formula showing the standard numbering system in accord with the 1957 *Definitive Rules for the Nomenclature of Organic Chemistry* of the IUPAC; (2) other numberings that have appeared in the literature; (3) a serial number which identifies the system; (4) the preferred name and other names given to the system; (5) identifying references to the original literature.

arrangement The ring systems are arranged from the simplest to the most complex, beginning with single rings, then systems of two rings and so on up to twenty-two-ring complexes.

uses The Ring Index is an indispensable reference for organic chemists and for others who work with cyclic organic compounds. You can use it for determining accepted structure of a ring system . . . finding name or names of the system if structure is known . . . finding the numbering of a system . . . identifying a system if there are two or more isomeric forms . . . discovering what systems have been reported in the literature and where . . . naming and numbering a newly discovered ring system . . . as a reference book in teaching.

1425 pages. ***Cloth bound.*** ***Price: $20.00***

Order from:

Special Issues Sales / American Chemical Society / 1155 Sixteenth Street, N.W. / Washington 6, D.C.

14387